NUREG/CP-0051
CSNI Report No. 82

Proceedings of the

CSNI Specialist Meeting on Leak-Before-Break in Nuclear Reactor Piping

Held at
Monterey, California
September 1-2, 1983

Sponsored by
Office of Nuclear Regulatory Research

U.S. Nuclear Regulatory
Commission

Available from

GPO Sales Program
Division of Technical Information and Document Control
U.S. Nuclear Regulatory Commission
Washington, D.C. 20555

Printed copy price: $10.00

and

National Technical Information Service
Springfield, VA 22161

NUREG/CP-0051
CSNI Report No. 82

Proceedings of the

CSNI Specialist Meeting on Leak-Before-Break in Nuclear Reactor Piping

Held at
Monterey, California
September 1-2, 1983

Manuscript Completed: July 1984
Date Published: August 1984

Sponsored by
Division of Engineering Technology
Office of Nuclear Regulatory Research
U.S. Nuclear Regulatory Commission
Washington, D.C. 20555

TABLE OF CONTENTS

INTRODUCTION AND EXECUTIVE SUMMARY

J. Strosnider 1

KEYNOTE ADDRESS - U.S. NUCLEAR REGULATORY POSTION ON LEAK- BEFORE- BREAK

R. Vollmer 8

APPLICATION OF PIPING FRACTURE MECHANICS TO LEAK- BEFORE- BREAK

SESSION I

SESSION CHAIRMEN

DR. YOSHIO ANDO
UNIVERSITY OF TOKYO
JAPAN

DR. MARCEL BROEKHOVEN
DIENST U.H. STOOMWEZEN
NETHERLANDS

THEORETICAL ANALYSIS OF UNSTABLE FRACTURE IN TYPE 304 STAINLESS STEEL PIPE WITH A CIRCUMFERENTIAL PART-THROUGH CRACK UNDER TENSILE LOADING

K. Kashima and Y. Takahashi 19

STABLE AND UNSTABLE GROWTHS OF CIRCUMFERENTIAL CRACKS IN TYPE 304 STAINLESS STEEL PIPES UNDER TENSILE AND THERMAL LOADINGS

G. Yagawa, et al. 56

APPLICATION OF TEARING INSTABILITY ANALYSIS FOR COMPLEX CRACK GEOMETRIES IN NUCLEAR PIPING

J. Pan and G. Wilkowski 126

THE EFFECT OF LARGE CRACK EXTENSION ON THE TEARING RESISTANCE OF STAINLESS STEEL PIPING MATERIALS

P. C. Paris, J. V. Brunetti and K. H. Cotter 140

ASSESSMENTS OF LEAK AND BREAK MARGINS IN STAINLESS STEEL POWER PLANT PIPING

K. Hasegawa, et al. 163

LEAK-BEFORE-BREAK DIAGRAMS USING SIMPLE PLASTIC LIMIT LOAD CRITERIA FOR PIPES WITH CIRCUMFERENTIAL CRACKS

F. Gorner and D. Munz 180

MARGINS OF SAFETY BASED ON CIRCUMFERENTIAL CRACKED DEPTH USING THE NET-SECTION COLLAPSE ANALYSIS

G. M. Wilkowski 204

IMPLICIT SAFETY MARGINS IN THE ASME CODE ACCEPTANCE CRITERIA FOR FLAWS IN AUSTENITIC PIPING

S. Ranganath 264

SESSION II

LEAK RATE AND LEAK DETECTION

SESSION CHAIRMEN

MR. SPENCER BUSH
REVIEW AND SYNTHESIS ASSOCIATES, U.S.A.

DR. ROY NICHOLS
RISLEY NUCLEAR LABORATORY, U.K.

TWO-PHASE FLOW EXPERIMENTS THROUGH INTERGRANULAR STRESS CORROSION CRACKS

R. P. Collier and D. M. Norris 273

PREDICTION OF LEAK RATES THROUGH INTERGRANULAR STRESS CORROSION CRACKS

D. Abdollahian, B. Chexal and D. M. Norris 300

LEAK RATE MEASUREMENTS AND DETECTION SYSTEMS

D. Kupperman, W. J. Shack and T. Claytor 327

THE OPENING OF THROUGH-WALL CRACKS IN BWR COOLANT LINES DUE TO THE APPLICATION OF SEVERE OVERLOADS II: A SIMPLE APPROACH

E. Smith 342

LEAK-BEFORE-BREAK DUE TO FATIGUE CRACKS IN THE COLD LEG PIPING SYSTEM

M. E. Mayfield and R. P. Collier 359

SESSION III

LEAK-BEFORE-BREAK STUDIES, METHODS AND RESULTS

SESSION CHAIRMEN

DR. DOUGLAS M. NORRIS
ELECTRIC POWER RESEARCH
INSTITUTE, U.S.A.

DR. JOHANN BLAUEL
FRAUNHOFER-INSTITUT FUR
WERKSTOFFMECHANIC, FRG

SOME RESEARCH IN THE FIELD OF LEAK-BEFORE-BREAK CRITERIA FOR PIPING

L. Lazzeri 386

A PROBABILISTIC STUDY OF LEAK-BEFORE-BREAK CONCEPT

H. H. Woo 404

LEAK-BEFORE-BREAK DEMONSTRATION FOR A TYPICAL PWR MAIN STEAM PIPE

S. A. Swamy 422

THE CASE FOR ELIMINATING INSTANTANEOUS PIPE BREAK AS A DESIGN BASIS FOR WESTINGHOUSE MAIN COOLANT PIPING

W. H. Bamford, S. A. Swamy and E. R. Johnson 440

THE APPLICATION OF FRACTURE MECHANICS LEAK-BEFORE-BREAK ANALYSES FOR PROTECTION AGAINST PIPE RUPTURE IN SEP PLANTS

J. F. Copeland and P. C. Riccardella 468

SESSION IV

CURRENT AND PROPOSED POSITIONS ON LEAK-BEFORE-BREAK

SESSION CHAIRMEN

DR. C. K. CHOU
LAWRENCE LIVERMORE NATIONAL LABORATORY, U.S.A

MR. JACK STROSNIDER
U.S. NUCLEAR REGULATORY COMMISSION, U.S.A.

SOME CONSIDERATIONS IN THE APPLICATION OF FRACTURE MECHANICS TO DELIMIT LEAK-BEFORE-BREAK CONDITIONS IN NUCLEAR POWER PLANT PIPING

M. F. Kanninen 485

CURRENT POSITION AND ACTUAL LICENSING DECISIONS ON LEAK-BEFORE-BREAK IN THE FEDERAL REPUBLIC OF GERMANY

H. Schulz 505

PROPOSED CHANGES IN INTERMEDIATE PIPE BREAK CRITERIA

R. P. Schmitz 523

A PROBABILISTIC ASSESSMENT OF LEAK-BEFORE-BREAK

S. H. Bush 529

INTRODUCTION AND EXECUTIVE SUMMARY*

On September 1 and 2, 1983, the CSNI subcommittee on primary system integrity held a special meeting in Monterey, California, on the subject of leak-before-break in nuclear reactor piping systems. The purpose of the meeting was to provide an international forum for the exchange of ideas, positions, and research results; to identify areas requiring additional research and development; and to determine the general attitude toward acceptance of the leak-before-break concept. The importance of the leak-before-break issue was evidenced by excellent attendance at the meeting and through active participation by the meeting attendees. Approximately 125 people representing fifteen different nations attended the meeting. The meeting was divided into four technical sessions addressing the following areas:

- Application of Piping Fracture Mechanics to Leak-Before-Break
- Leak Rate and Leak Detection,
- Leak-Before-Break Studies, Methods and Results,
- Current and Proposed Positions on Leak-Before-Break

The keynote speaker for the meeting was Mr. Richard Vollmer, Director of the Division of Engineering, U.S. Nuclear Regulatory Commission. His opening presentation entitled, "U.S. Nuclear Regulatory Commission Position on Leak-Before-Break" dealt with the issue of BWR pipe cracking in the United States and the role of leak-before-break in the NRC evaluation of this issue. A total of twenty-nine presentations were made by authors from Japan, the United States, the Federal Republic of Germany, the United Kingdom, Italy, and Canada. Each technical session was concluded with an open discussion period. The highlights of the technical sessions are summarized below.

SESSION I: Application of Piping Fracture Mechanics to Leak-Before-Break

A variety of analysis techniques have been developed for evaluating the fracture behavior of cracked piping. These techniques range from simplified, closed form models to three dimensional, elastic-plastic finite element codes. Comparisons of the analytic techniques with experiments which have been conducted to date, have demonstrated the validity of analytic techniques such as net-section-collapse, critical crack tip opening angle, and tearing instability. However, the available relevant experimental data are limited and some questions still exist regarding practical application of the analyses techniques. For example, it was generally agreed that the concept of tearing instability has been validated in small scale tests, however, difficulties such as choosing the correct J-resistance curve or calculating the piping system compliance still exist when applying the method to an actual nuclear reactor piping system. Several large scale test programs are under development to experimentally validate the fracture mechanics analyses.

*This summary was prepared by J. Strosnider of the U.S. Nuclear Regulatory Commission based on input from the session chairmen.

New analyses and experimental data presented during this session indicate that the tearing resistance of stainless steel as characterized by the J-resistance curve may be much lower than previously assumed. Specifically, a complex crack geometry consisting of a throughwall flaw with a part through surface flaw around the remainder of the cross section was shown to reduce the value of J_{Ic} by a factor of 7 to 8 and to reduce the tearing modulus value by a factor of approximately 5 as compared to J-resistance curves generated from pipe specimens with simple through wall flaws. This reduction in tearing resistance is consistent with the observations in side grooved versus nonside grooved compact tension specimens. In addition to the effects of complex crack geometry on tearing resistance, data were presented which indicated that the tearing modulus values for stainless steel could be 50 or less at large crack extenions (2 to 3 inches). Data showing reduced fracture toughness in stainless steel weldments also was presented and discussions focused on the reduced fracture toughness of cost and aged cost stainless steels.

Another significant issue raised during this session was related to the factors of safety associated with the new flaw evaluation procedures for austenitic stainless steel piping to be incorporated in Section XI of the ASME Code. Information was presented which indicated that use of a lower value of flow stress than that assumed in developing the code acceptance criteria together with application of a correction factor for pipe ovalization resulted in lower factors of safety on load than reported in the code. Furthermore, for emergency and faulted conditions it was reported that a factor of safety less than 1.0 could exist for high stress ratios. A philosophical point that was raised relative to this issue dealt with the question of whether the factor of safety should be applied on load or on crack size. There seemed to be a consensus that the factor of safety was most appropriately applied on load. However, it was also pointed out that factors of safety based on crack size highlight the need for accurate nondestructive flaw sizing capabilities. The question of the adequacy of the Section XI flaw evaluation procedures is being evaluated by an ASME Section XI task force.

The final issue raised in Session I dealt with the type of loads which should be postulated for piping integrity assessments. In one suggested approach, it was assumed that all piping and equipment supports fail and the loads are displacement governed. The second approach was to define conservative but perhaps more realistic loads and displacements based on design conditions. Although either approach can be used, the former approach presents a more challenging set of conditions than the later and may make it more difficult to demonstrate piping integrity. This is particularly true in light of some of the data presented on low tearing resistance for stainless steel.

Specific recommendations and conclusions resulting from this session include:

1.1 Cooperation between various organizations in conducting large scale experimental programs is encouraged. This cooperation should be directed at minimizing duplication of effort and utilizing available resources throughout the world to conduct the most comprehensive program.

1.2 Cooperative efforts should be established to benchmark and validate analytic techniques against planned pipe fracture experiments.

1.3 A reevaluation of the ASME Section XI allowable flaw size criteria for stainless steel piping should be performed.

1.4 Additional efforts are necessary to better define the tearing resistance of piping materials in pipe geometries with real flaw configurations. Experimental and analytical efforts shall be closely coupled quantify the crack tip constraint and its influence on crack growth resistance. Environmental and aging effects on fracture toughness also need further evaluation.

1.5 Previous piping integrity analyses performed using tearing instability analysis should be reevaluated in light of the data presented on low tearing resistance for stainless steel pipes with complex crack geometries or postulated large crack extensions.

SESSION II: Leak Rate and Leak Detection

The conference developers found this area to be the most difficult to develop suggesting that a much lower level of effort currently exist in this field relative to that in piping fracture mechanics. This session consisted of five papers dealing with experimental measurements, analytic predictions of the leak rate from cracked pipes, and the ability to detect such leaks. Two of the papers dealt explicitly with the experimental leak rate testing results; one paper discussed the development of an analytic model based on experimental results; and two papers dealt with fracture mechanics calculations to predict crack opening areas. Two of the papers also addressed the use of acoustic emission monitoring to detect pipe leakage. Most of the work reported was completed some time ago and there is apparently very little ongoing effort in this area.

Experiments to determine leak rates through various forms of cracks are limited to date. Some discussions focused on the design of leak rate experiments with particular emphasis on the need for realistic cracks and water purity during the tests. Discussions suggested that the tightness of the cracks and impurities in the water which could clog the cracks could reduced predicted or measured leak rates by a factor of two to five. Parametric studies of these parameters have not been conducted.

Extensive discussions focused on the validity of the assumptions made in analytic leak rate models. Existing models assume homogeneous, nonequilibrium two phase critical flow based on a extension of Henry's two-phase critical flow model and on a modified Moody flow model. Simplifying assumptions regarding the crack shapes had to be made to apply the models.

The ability of acoustic emission to reliably detect small leakage under laboratory conditions was reported by two researchers. In addition, a demonstration program in which an acoustic emission monitoring system has been installed in an operating BWR was described.

Specific conclusions and recommendations resulting from this session included:

2.1 More experimental data on leak rates through various types of cracks, including stress corrision cracks and multiple cracks, and using various water purity levels are needed.

2.2 Analytic models for predicting crack opening areas and leak rates require additional validation against experimental leak rate test data.

2.3 Acoustic emission has been successfully demonstrated as a leak detection and monitoring technique under laboratory conditions and may be promising for field application.

2.4 Work is required on evaluating the reliability of leak detection systems as they exist in operating power plants.

SESSION III: Leak-Before-Break Studies, Methods, and Results

This session dealt with the integration of fracture mechanics, leak rate calculations, and leak detection, and loading assumptions in performing leak-before-break evaluations of real piping systems. Deterministic limit load and tearing instability analyses were used to demonstrate that postulated cracks detectable by leakage were subcritical. Piping systems considered included the primary reactor coolant system and secondary system piping. A model for estimating the probability of piping leaks and breaks was also presented. Calculations performed using the probabilistic code showed low probabilities of leak or break as a result of fatigue crack growth and normal operating and earthquake loads. Studies regarding leak-before-break in CANDU pressurized water reactors were discussed and a recent pressure tube failure in a CANDU reactor was described. Fracture mechanics arguments for elimination of postulated double-ended guillotine breaks was also presented.

Most of the studies presented were relatively straightforward utilizing generally accepted state-of-the-art fracture mechanics techniques. In general, the issues of leak rates, leak rate detection, and load definition, received much less attention than the fracture mechanics analyses. Reliably detectable leak rates were generally accepted as those established in plant's technical specifications. Similarly, loads were generally taken as the design basis loads with little attention given to loads outside the design basis envelope.

A significant amount of discussion was directed toward probabilistic modeling and its limitations. Items of particular interest were the initial crack size distribution and the time dependent nature of some of the random variables. The uncertainties related to these issues significantly reduce the confidence associated with the estimated failure probabilities.

Additional items which received attention during the discussion period included the need to take a second look at some of the analyses that were presented

in light of issues raised in Session I. These issues included reports of much lower tearing resistance for stainless steel than was previously believed, methods of computing piping system compliance when multiple cracks exist in the piping system, comparison of analyses with actual experience, and whether the need for further experimental verification of fracture mechanics techniques, particularly tearing instability analysis, is necessary. Regarding the last issue it was generally agreed that the tearing instability concept was on firm ground and that future experimentation should not be directed so much at verifying the theory as at determining how to effectively apply it to large piping systems.

Specific conclusions and recommendations resulting from this session included:

3.1 Investigations to date indicate large margins against failure and low probabilities of leak or break in the primary coolant system piping of pressurized water reactors.

3.2 Existing analyses rely on current estimates of leak rates which could be improved. In addition, the reliability of leak detection systems should be explicitly addressed.

3.3. Greater consideration of loads and stresses outside the design basis envelope, such as water hammer and residual stresses, is appropriate in conducting piping integrity analyses.

3.4 Probabilistic evaluations are useful but current uncertainties in input distributions and their time dependence suggest cautious use of the results.

3.5 A better job of integrating the elements of the leak-before-break analysis including identification of limitations and uncertainties in the analyses could be and should be done.

3.6 Additional experimental testing programs should be directed at demonstrating and developing the application of fracture mechanics techniques to piping systems rather than validating the analytic theory.

SESSION IV: Current and Proposed Positions on Leak-Before-Break

This session was intended to deal with statements of positions or philosophies on leak-before-break in nuclear reactor piping systems. Presentations were made on the safety significance of pipe cracking, the financial impacts of postulated design basis pipe breaks, approaches for eliminating postulated guillotine breaks, and existing positions on leak-before-break and postulated pipe break criteria.

The results of a risk assessment performed on pipe breaks provided a very interesting insight into the safety significance of pipe cracking. The conclusion of the study was that small to intermediate size pipe breaks dominate the risk from piping failures. This implies that demonstration of leak-before-break does not resolve all safety concerns; the magnitude of the leak is critical. Less than full guillotine breaks in pipes could result in leak rates of the magnitude that contribute most to the overall risk.

The financial impact of postulating and designing to accommodate double-ended guillotine breaks are enormous. A typical pressurized water reactor plant in the United States can have approximately 300 pipe whip restraints and the estimated cost for design and construction work associated with pipe break effects is 30 to 50 million dollars per plant. Studies which have concluded that these postulated pipe breaks are not necessary were referenced. Reference was also made to actual operating data which do not support the need for postulating pipe break at intermediate locations. Current pipe break design criteria in the United States was also stated to have adverse effects on personnel exposure and on the reliability of inservice inspection. Positions on this issue taken by other countries, specifically the Federal Republic of Germany, were reviewed. The Germans have adopted a basic safety concept in which they rely on, among other things, improved design, materials selection, and inservice inspection to assure piping integrity and less stringent pipe break criteria have been established for new plants designed, built, and operated in accordance with the basic safety concept.

The Sessior IV discussion period was opened to any subject covered during the 2-day meeting and conclusions and recommendations were solicited. Issues which continued to be brought up throughout the meeting and which resurfaced during the final discussion period included accurate determination of material properties, particularly tearing resistance data for specific piping geometries and for thermally aged cast stainless steel; accurate determination of loads and stresses to be used in the fracture mechanics anlaysis; the need for improved distributions of random variables for probabilistic assessments; improved leak rate models; and evaluation of leak detection reliability. There appeared to be a concensus that leak-before-break evaluations were more acceptable in piping systems for which fatigue crack growth is the dominant mode of degradation. There seemed to be less confidence in leak-before-break arguments for piping systems subject to corrosive mechanisms of degradation. The issue of the postulated crack shape and the potential for a uniform surface crack penetrating nearly through wall was raised. It was also pointed out that piping failures may be dominated by indirect causes such as design or fabrication errors. In general, it was concluded that leak-before-break is an important line of defense in the defense in depth concept but that there does not currently exist enough confidence in the leak-before-break argument to use it as a sole line of defense.

Specific conclusions and recommendations from this session include:

4.1 Risk to the public may be dominated by small and intermediate size breaks and that demonstration of leak-before-break is not a panacea.

4.2 Traditionally postulated design basis pipe breaks and resulting plant designs adversely affect personnel radiation exposure and reliability of piping inservice inspection and result in enormous financial costs.

4.3 The technology exists to design and build plants to less stringent pipe break criteria and to operate these plants without undue risk to the public health and safety.

4.4 Leak-before-break arguments are less convincing for piping systems subject to corrosive degradation mechanisms (e.g, intergranular stress corrosion cracking) than they are for systems where fatigue crack growth is the dominant degradation mechanism.

4.5 Piping failures may be dominated by errors in design or fabrication and these areas are difficult to treat analytically.

4.6 Leak-before-break is an important part of the defense in depth concept but not a panacea.

In summary, the subject meeting was very productive. There was a great deal of interaction between the meeting attendees and several critical issues and recommendations were identified. It is hopeful that the exchange of information and discussions sparked some new ideas and energies that will be brought to bear on the issues of evaluating and ensuring piping integrity.

On a final note, it seems appropriate to reiterate the benefits which could be derived from more extensive international cooperative efforts. A meeting of the type described herein brings attention to the large number of independent efforts planned or underway in the subject area. Well planned and organized cooperation between these efforts could avoid duplication and perhaps utilize resources in a more productive manner. Unfortunately, no well established vehicle for accomplishing such coordination exists. Development of such cooperation should be a principal objective of the international community.

KEYNOTE ADDRESS

U.S. NUCLEAR REGULATORY COMMISSION POSITION ON LEAK-BEFORE-BREAK

Richard H. Vollmer, Director
Division of Engineering
U.S. Nuclear Regulatory Commission

Ladies and Gentlemen:

It's an honor for me to present the opening remarks at this CSNI Conference on leak-before-break. The object of my presentation is to give you the current NPC thinking and direction on leak-before-break for nuclear piping systems and place these in perspective by describing a number of current issues and initiatives affecting nuclear piping systems and the integrity of the primary coolant pressure boundary. I do this with no pretences since I am by trade a reactor physisist who was knee deep in Three Mile Island and issues such as equipment qualification a few years ago. More recently, however, I have been heavily involved with steam generator problems, BWR pipe cracks, and of course leak-before-break.

Before I get into the primary topic of the day, I'd like to describe to you a recent initiative taken by the NRC's Executive Director for Operations. He has formed a Piping Review Committee with the following objective:

To review and evaluate the current regulatory requirements on piping systems for light water reactor designs, using currently available

domestic and foreign information, to provide recommendations on where and how current NRC requirements should be modified. In addition, this committee would give direction for work needed to respond to issues not currently amenable to resolution. The scope of the review covers all safety-related piping systems needed to assure the integrity of the reactor coolant system pressure boundary, to shut down the reactor and maintain it in a safe shutdown condition, and to mitigate the consequences of an accident. Finally, this effort is not to impact ongoing regulatory actions prior to acceptance of the committee's final report nor impede the resolution of specific piping problems. Dr. Larry Shao of NRC's Research Office and I will Co-Chair this activity and Dr. Spencer Bush will provide guidance as Vice Chairman.

He will form Task Groups composed of NRC staff and consultants to deal with these regulatory issues:

A. Pipe Cracking
   - IGSCC
   - NDE
   - Repair methodology
   - IHSI
   - Operation with existing cracks
   - Fatigue cracks and other cracking mechanisms

B. Seismic Design
   - Damping
   - Spectral broadening
   - Definition of OBE
   - Multiple supports

C. Pipe Break

- Leak-before-break and related issues which will be described shortly

D. Load Combinations

- LOCA plus SSE loads
- Water Hammer
- SRV discharge loads
- Vibration loads

The above items are included to be representative but not all inclusive of the topics that will be covered. The charter of this committee is quite broad.

Although all of these issues are quite important to the design of nuclear piping systems, some of this work will have to take the back seat to resolution of the current BWR cracking problems. You are all aware of the large number of cracks being found next to welds in austinetic stainless steal piping in the U.S. BWRs. On the average, about 25 percent of the welds have crack indications. Some plants are clear of indications but some plants have a 50 per cent crack frequency. Because of this we have an immediate menu dealing with:

- Resolution of cracks, repair or don't repair
- Inspection of remaining welds
- How long to operate with known cracks or temporary repairs
- Long term solutions including piping replacement

Although we believe that leak-before-break has a place in our regulatory philosophy and criteria, we believe that the BWR pipe cracks represent a safety issue upon which we cannot rely on leak-before-break alone. Rather strong actions on a number of fronts will be required to put this issue behind us.

Turning now to what the NRC is doing on leak-before-break, we are seriously pursuing the concept of leak-before-break (LBB), both technically and administratively, for any pipe or piping system for which it can be demonstrated by analysis, experimental evidence, operational experience or other means that this concept is viable and that the benefits to be gained clearly outweigh any possible increases in risk.

The Commission's regulations, as currently interpreted in the applicable Standard Review Plans and Regulatory Guides, postulate piping ruptures in high energy fluid systems, both inside and outside of containment as part of the design bases for structures, systems and components important to safety. These ruptures include circumferential and longitudinal

breaks up to and including double-ended guillotine breaks (DEGB) in piping which also encompasses the largest pipe in the reactor coolant system. The direct result of such postulated piping ruptures led to the establishment of the Unresolved Safety Issue A-2, "Asymmetric Blowdown Loads on PWR Primary Systems," and criteria to protect items important to safety against the consequences of pipe breaks in all other high energy fluid systems. Protective measures include physical isolation from postulated pipe rupture locations if feasible or the installation of pipe whip restraints, jet impingement shields or compartments.

Since these criteria were established, however, the fracture mechanics technology regarding the potential rupture of tough piping such as used in PWR primary coolant systems, has advanced considerably. The crack growth behavior in piping with flaws under normal and accident loads is now reasonably well understood.

In addition, we have recognized the various negative impacts of these criteria on plant design and inservice inspection. Therefore, we were receptive when advanced fracture mechanics technology was applied recently in topical reports submitted to the NRC on behalf of 11 licensees belonging to the A-2 Owners Group. The topical reports were intended to resolve the issue of asymmetric blowdown loads on the PWR primary systems for

those licensees' plants. In its evaluation of the topical reports, the NRC staff has concluded that large margins against unstable crack extension exist for certain stainless steel PWR primary coolant piping postulated to have large flaws and subject to the safe shutdown earthquake (SSE) in combination with the loads associated with normal plant conditions. However, as specified in the staff's evaluation of the topical report, the resolution of this issue is contingent upon satisfying the NRC staff's leakage detection criteria and, for two licensees under the Systematic Evaluation Program, the results of seismic reanalysis.

Without the application of the LBB concept, the 11 affected licensees of 16 plants would have to meet the provisions of NUREG-0609 resolution of generic task action plan A-2. This would involve postulating DEGBs at discrete pipe locations, performing analyses of resultant dynamic loads, and for each PWR, in varying degrees, adding piping restraints to prevent postulated large pipe ruptures from resulting in full double ended pipe break areas thus reducing the blowdown asymmetric pressure loads. This would also involve modifying component supports to withstand those loads as determined in plant specific analyses.

We have prepared a value/impact analysis supporting our technical review. In summary, the values (public risk and occupational exposure) show that the estimated reduction in public risk for installing additional pipe

restraints and modifying equipment supports as necessary to mitigate or withstand asymmetric pressure blowdown loads is only about 3 1/2 man-rem total for all 16 plants considered. Similarly, the reduction in occupational exposure associated with accident avoidance due to modifying the plants is estimated to total less than 1 man-rem. These small changes result from the small reduction in core-melt frequency that would result from modifying the plants. However, the occupational exposure estimated for installing and maintaining the plant modifications would increase by 11,000 man-rem.

The impacts are that the estimated industry costs to install plant modifications to withstand asymmetric pressure loads is about $50 million without even considering power replacement costs from excess downtime. Consequently the savings, both in terms of occupational radiation exposure and costs, far outweigh any potential benefits (e.g., decrease in public risk and avoided accident exposure) from plant modifications.

The value/impact, both in terms of costs and occupational radiation exposure discussed above, applies only to the primary coolant loop piping of a limited number of PWRs. However, significant cost and occupational radiation exposure benefits could accrue from elimination of pipe whip restraints and other protective measures against dynamic pipe break effects

in other high energy fluid piping systems. Removal and replacement of pipe whip restraints for inservice inspection purposes entail considerable accumulation of occupational radiation exposure plus the risks associated with either improper reinstallation of the restraints or damage to the restraints or adjacent components during reinstallation. Many restraints are massive and must be handled in severely restricted areas. An extension of evaluation criteria to other high energy fluid system piping, both within and outside of containment, is currently under further development by the staff.

The development and application of such criteria will take time. Ultimately, Rule changes will probably be necessary to put such changes fully into effect. Until then, we will consider case-by-case applications of LLB--where clear benefits can be shown--and where safety is clearly not affected. There are limitations to keep in mind, however, in any application of LLB:

1) for purposes of specifying design criteria for emergency core cooling system, containments, other engineered safety features, and for the evaluation of environmental effects on equipment, loss of coolant shall be assumed in accordance with existing regulations. That is, loss of coolant is based on an opening equivalent to twice the flow area of the largest diameter pipe in the system or that pipe which will result in the most limiting accident conditions.

2) For the present, these criteria shall not be considered applicable to high energy fluid system piping, or portions thereof, that operating experience has indicated particular susceptibility to failure from the effects of corrosion. For example, we will not apply these criteria to piping that has experienced intergranular stress corrosion cracking, water hammer or thermal fatigue.

In conclusion, our initial application of LBB is to the main PWR piping because sufficient information is, or can be, available for our reviews. Our immediate objective is to issue our safety evaluation for the facilities already reviewed. In the future, we plan to expand the leak-before-break concept to other piping systems and other facilities.

We will also propose to make appropriate changes to current Commission criteria to more clearly define our position, to put this activity on a generic basis, and to achieve public comment on revised criteria. We would also modify and/or augment the appropriate Standard Review Plans and Regulatory Guides to provide specific guidance to the industry and the staff reviewers.

The overall NRC leak-before-break program will require considerable time and effort. Continued support from the nuclear industry is needed to meet our mutual objectives. We also look for the experience and expertise of our foreign friends in the further development of leak-before-break technology. This conference and the activities of CSNI are key to the

overall success of these initiatives.

Thank you.

SESSION I

APPLICATION OF PIPING FRACTURE MECHANICS TO LEAK-BEFORE-BREAK

SESSION CHAIRMEN

DR. YOSHIO ANDO
UNIVERSITY OF TOKYO
JAPAN

DR. MARCEL BROEKHOVEN
DIENST U.H. STOOMWEZEN
NETHERLANDS

Theoretical Analysis of Unstable Fracture in Type 304 Stainless Steel Pipe with a Circumferential Part-Through Crack under Tensile Loading

K.Kashima & Y.Takahashi

Central Research Institute of Electric Power Industry (CRIEPI)

11-1, Iwato Kita 2-Chome Komae-shi, Tokyo, Japan

ABSTRACT

This paper presents the theoretical analysis of circumferential crack propagation in Type 304 stainless steel pipe under tensile loading. Finite element codes and a simplified analysis method are developed to predict the stable and unstable crack propagations. Leak-before-break condition of the pipe with a circumferential part-through crack is estimated based on the net stress criterion. The relatively good agreements are obtained between the numerical solutions and the experimental results.

OECD COMMITTEE ON THE SAFETY OF NUCLEAR INSTALLATIONS

SPECIAL ENLARGED MEETING ON
LEAK BEFORE BREAK IN NUCLEAR REACTOR PIPING SYSTEMS

1st-2nd September 1983
Monterey, California, USA

1. INTRODUCTION

The structural integrity of a nuclear power plant must be ensured by evaluating the margins of safety in the reactor components with respect to failure. In particular, studies on the structural strength of the nuclear piping systems in the presence of flaws have gained much importance since the discoveries of circumferential intergranular stress corrosion crackings (IGSCC) in several BWRs [1]. Most of the piping systems in nuclear power plants are made of ductile materials such as Type 304 stainless steel that has a high resistance to crack growth and is not normally vulnerable to fast fracture, being characterized rather by stable crack growth. Therefore, even if a flaw does exist in the piping system, structural safety can be maintained by leak before break (LBB) behavior, which permits coolant leakage to be detectable before a catastrophic pipe failure. It is important to demonstrate experimentally and theoretically that unstable pipe failure (tearing instability) can fully be prevented in the nuclear piping systems with IGSCC and that LBB behavior can be assured under the operating conditions of nuclear power plants.

As the theoretical investigations, a tearing instability criterion was proposed based on the J-integral approach in ductile material by Paris et al. [2] and Hutchinson and Paris [3] gave some conditions for J-controlled crack growth. Based on this criterion, some theoretical analyses were conducted for reactor piping systems [4, 5]. In order to study the applicability of the tearing instability criterion based on the J-integral approach, Wilkowski et al. [6] conducted bending tests on unstable fracture using circumferentially cracked stainless steel pipes. In relation to the flaw evaluation procedures in the ASME Boiler and Pressure Vessel Code, Section XI [7], acceptance criteria were proposed for the circumferential cracks in stainless steel piping by Norris et al. [8].

In Japan, a research project on the tearing instability for center-cracked plates and circumferentially cracked pipes subjected to tensile loading and leak before break for circumferentially cracked pipes under the cyclic tensile loading and the BWR environment is under way at the Nuclear Power Engineering Test Center under the sponsorship of the Ministry of International Trade and Industry (MITI) [9 ∿ 12].

This paper presents the numerical analysis of crack propagation in Type 304 stainless steel pipe. Two- and three- dimensional finite element codes are developed to study the criterion for stable crack growth. A simplified analysis model is also developed to predict the tearing instability for circumferentially cracked pipe. LBB condition in the pipe with a circumferential part-through crack is estimated by applying the theoretical results obtained in the simplified analysis. The numerical solutions are compared with some of the experimental results [9 ∿ 12] obtained in the above-mentioned project to examine the validity of the analysis method.

2. FINITE ELEMENT ANALYSIS OF THROUGH-WALL CRACK PROPAGATION

The prediction of circumferential crack propagation in a piping system requires the accurate evaluation of stress, strain and displacement in the vicinity of the crack. Extensive development of the plastic zone occurs near the crack tip because of the high ductility of Type 304 stainless steel pipe in which IGSCC have been discovered. Stress conditions during crack propagation can be obtained from elastic-plastic analysis. The finite element method (FEM) is considered to be one of the most powerful techniques applicable to this type of stress analysis in two- or three-dimensional complex structure.

Two-dimensional elastic-plastic finite element code, PLASTAN-II, is developed to establish the analysis method of crack propagation in Type 304 stainless steel plate as a preliminary study for three-dimensional analysis in the pipe structure.

Next, three-dimensional finite element code, PIPE-6, is developed to predict the propagation behavior of circumferential through-wall crack in Type 304 stainless steel pipe, based on the criterion obtained by two-dimensional analysis. Numerical solutions by PLASTAN-II and PIPE-6 are compared with the experimental results for plate and pipe specimens under room temperature [9, 10]. A good agreement is obtained between the numerical and the experimental results.

2.1 Analysis of Plate Specimen with a Center Crack

2.1.1 Description of the Problem

Figure 2-1 shows the shape and dimensions of the center-cracked plate specimen to be analyzed. The ratio of the original crack length ($2a_o$) to the specimen width ($2W$) takes three different values, $a_o/W=0.3$, 0.5 and 0.7. The width ($2W$) and thickness (B) of the specimen are 300 mm and 10 mm, respectively. As the boundary conditions, uniform displacement ($V_o/2$) is given at the top and the bottom of the specimen. Numerical solutions are compared with experimental results with respect to the crack opening displacement (COD) at the midpoint of the crack or the gauge point displacement (V_g) between two gauge points A and B, shown in the figure. Due to the geometrical symmetry, one-quarter portion of the specimen is cut out and modeled by the constant strain triangular element. Figure 2-2 shows one example of the finite element mesh pattern of a specimen with the original crack length of $a_o/W=0.5$ and the five integration paths for the J-integral calculations. The material properties of Type 304 stainless steel at room temperature used in the calculations are, as follows:

Young's modulus	$E = 185.1$ GPa
Poisson's ratio	$\nu = 0.3$
Yield stress	$\sigma_Y = 234.2$ MPa

Based on the experimental results, the relationship between the equivalent stress ($\bar{\sigma}$) and the equivalent plastic strain ($\bar{\varepsilon}_p$) can be represented as a bilinear expression. Hence, the strain hardening ratio ($H'=d\bar{\sigma}/d\bar{\varepsilon}_p$) is given as follows:

$$H' = \begin{cases} 2695 \text{ MPa for } \bar{\varepsilon}_p \leq 4\% \\ 2058 \text{ MPa for } \bar{\varepsilon}_p > 4\% \end{cases}$$

2.1.2 Calculation Methods

Table 2-1 describes some characteristics of the calculation method employed in the finite element code PLASTAN-II. Elastic-plastic calculation, being based on the J_2 flow theory, is performed by solving the elastic-plastic stiffness equations using the tangent modulus approach [13, 14]. The theory of small strain is assumed for geometric nonlinearity. A plane stress condition is adopted because the specimen is thin (10 mm). Using the elastic-plastic stress conditions, J-integral values are obtained by the path integral method [15].

As the crack extension method, the node releasing technique is adopted in the present analysis. As shown in Fig. 2-3, the reaction force (R_1) is calculated at the crack tip node. To cancel the reaction force at this node, a nodal force ($-R_1$) is applied in the reverse direction and the other reaction forces (R_2, R_3, ...) at the restrained nodes are redistributed under the equilibrium condition that the sum of the newly distributed nodal forces (R_2', R_3', ...) is equal to the externally applied load (P'). Crack extension is simulated by cancelling the reaction force and releasing the nodal restraint at the crack tip when the crack

opening displacement (COD) becomes equal to the critical value. This critical value of COD for crack extension can be determined from the experimental relationships between the crack opening displacement and the crack extension amount for three types of the plate specimens (a_o/W = 0.3, 0.5, 0.7).

2.1.3 Numerical Results

Figure 2-4 shows the calculated and experimental relationships between the load (P) and the gauge point displacement (V_g). The numerical solutions agree well over a wide range of displacement with the experimental results for three specimens having different crack lengths (a_o/W = 0.3, 0.5, 0.7) [9, 10]. The validity of the numerical solutions has been checked using these comparisons.

Next, several conditions for stable crack growth are examined by means of various parameters used in elastic plastic fracture mechanics [16, 17]. These were the J-integral and the crack tip opening angle (CTOA). Of the two, the J-integral approach assumes the resistance curve as the criterion for stable crack extension. Figure 2-5 shows the calculated relationship between the J-integral and crack extension, i.e., the J-integral resistance curve obtained for three specimens (a_o/W = 0.3, 0.5, 0.7). The crack extension property is well approximated by a single resistance curve without dependency on the original crack length (a_o). It can be predicted that the crack begins propagating at the J-integral value of about 1000-1500 N/mm and continues to extend stably in accordance with the single resistance curve shown in the figure.

The crack tip opening angle (CTOA) is proposed as the parameter describing the stable crack extension. In the criterion using CTOA, the crack is assumed to extend stably with the constant angle determined by the crack opening displacement. Figure 2-6 shows the calculated crack opening profiles for the specimen with the crack length of a_o/W = 0.3.

It can be observed that the crack angle denoted by "β" is almost constant during crack extension. From this fact, the constant crack opening angle can be considered as an effective criterion for stable crack extension.

Figure 2-7 shows the relationship between the crack tip opening angle (CTOA) and the crack extension amount (Δa). The CTOA is calculated as follows:

$$\text{CTOA} = 2\ell/s \qquad (2\text{-}1)$$

where s is a small fixed distance and 2ℓ is the crack opening displacement defined at the point of distance s behind the current crack tip. The value of CTOA becomes nearly equal to 0.2 with an increase in the crack extension amount. The CTOA criterion is represented as a single resistance curve because the CTOA is nearly independent of the original crack length (a_o). The CTOA is, therefore, considered to be an effective criterion for stable crack extension. It should be noted that this approach can be easily applied also to the analysis of stable crack extension in three-dimensional pipe structure.

2.2 Analysis of Pipe Specimen with a Circumferential Crack

2.2.1 Description of the Problem

The object of the present analysis is a Type 304 stainless steel pipe with a circumferential through-wall crack. Figure 2-8 shows the shape and dimension of a pipe to be analyzed. The initial crack length is $2a_o = 2R_m\alpha$, where R_m is the mean radius of the pipe and 2α ($=30°$) the initial crack angle. The axial tensile load (P) is applied through a compliance attached to the end of the specimen.

As shown in the figure, the axial length (2L) of the pipe specimen is too great (750 mm) to use the calculation model in its present form. A part of the pipe specimen is therefore taken with the length of $2L_o$ = 250 mm equal to the axial gauge length AB (A'B'), where A (A') and B (B') denote the gauge points in the experiment. Figure 2-9 shows a schematic generation of this partial-length model from the total-length model of the pipe specimen. Compared with the total-length model, the partial-length model shortens the calculation time by greatly reducing the number of the elements required in the analysis.

Due to its geometrical symmetry, only one-fourth of the pipe model is analyzed with three-dimensional finite elements. Figure 2-10 shows the 6-node isoparametric curved element used in the analysis. The finite element mesh is drawn in Figure 2-11 with 63 elements and 456 nodes.

As for the loading conditions, the measured gauge point displacements are applied on the edge plane of the partial-length model of the pipe specimen as the forced displacements in the axial direction.

The material properties used in the calculation are the same as those described in the case of two-dimensional analysis.

2.2.2 Calculation Methods

Calculation methods employed in PIPE-6 are described in Table 2-1.

Stable crack extension is simulated by releasing the nodal constraints at the crack tip and reducing the reaction force at the crack tip to zero through several iterative computations (Fig. 2-12). A constant crack tip opening angle (CTOA criterion) is assumed as the condition for stable crack growth. The CTOA values in the plate specimen approach about 0.2 with increases in the crack extension (Fig. 2-7). This tendency is nearly

independent of the initial crack length (a_o). A constant CTOA value of 0.2 is therefore adopted as the critical value for stable crack extension in the pipe specimen as well. An experimental load at crack initiation of P_i = 1240 kN is used in the present analysis as the condition for crack initiation.

2.2.3 Numerical Results

Crack propagation in a pipe is analyzed based on the numerical methods described in the preceding section. Numerical solutions are obtained as a relationship between the applied load and the crack opening displacement, as shown in Fig. 2-13. The applied load takes a maximum value after a given amount of stable crack growth. This maximum load was 1274 kN and 1392 kN, respectively, for the experiment and the numerical analysis. The applied load calculated by FEM is somewhat higher than that measured in the experiment, as shown in the figure.

Figure 2-14 and 2-15 show the variations in the applied load and displacement with crack extension. A maximum load value is obtained at small crack extensions of Δa=20 to 40 mm. This can be observed in both the experiments and numerical analysis (Fig. 2-14). The gauge point displacement (d_1) between A' and B' in Fig. 2-9 increases almost linearly with crack extension amount in both the experiment and the analysis, as shown in Fig. 2-15. Numerical solutions during crack extension show a relatively good agreement with the experimental results [9, 11]. These indicate the validity of the constant CTOA value employed in this analysis as the criterion for stable crack extension.

Figure 2-16 shows the variance of crack opening profiles for several crack extensions ranging from Δa=0 to 91 mm. Crack opening profiles after crack initiation are similar to that before crack initiation (Δa=0 mm) within initially cracked parts, $2\alpha \leq 30°$ or $x \leq 20$ mm,

where x denotes the circumferential distance from the center of the crack. Conversely, the crack opening profiles in a newly cracked part ($x > 20$ mm) can be approximated as straight lines, the gradients of which are determined by the CTOA criterion.

Table 2-1 Calculation Methods

Program	PLASTAN-II	PIPE-6
Element Type	2-D, Constant Strain Triangle	3-D, 6-node Isoparametric
Plasticity	Flow Theory	
Elastic-Plastic Calculation	Tangent Modulus	
Hardening Law	Isotropic	
Geometrical Nonlinearity	Small Strain	
Stress-Strain Relation	Bilinear	
Crack Extension Method	Node Release	
J-integral Method	Path Integral	

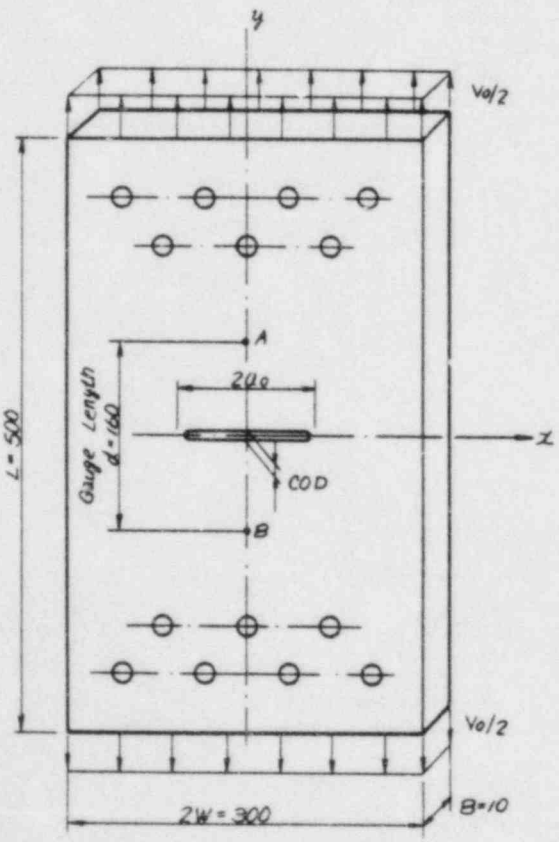

Fig. 2-1 Center Cracked Plate Subjected to Tension (Dimensions in mm)

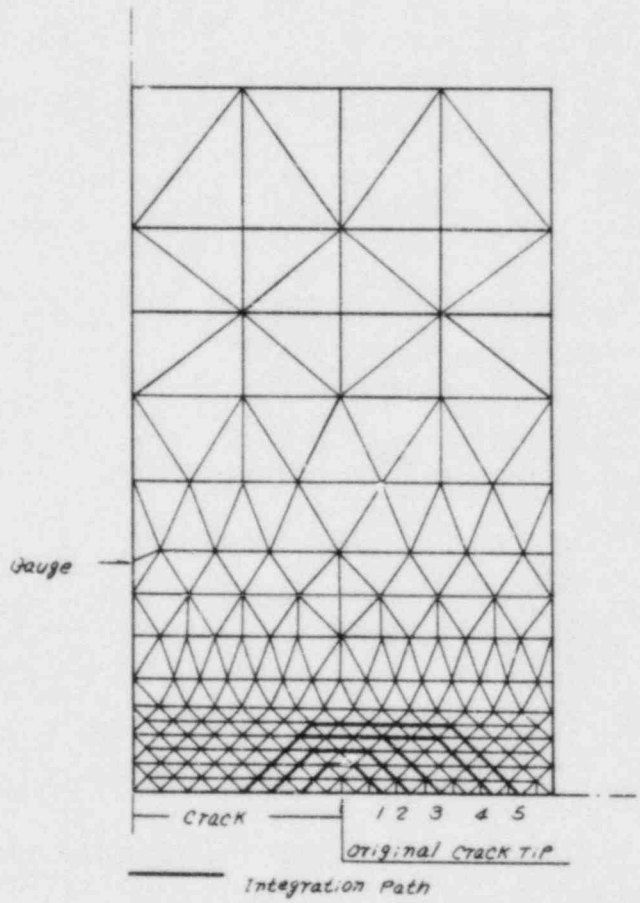

Fig. 2-2 Finite Element Mesh Pattern and J-integral Paths of Plate Specimen ($a_o/W = 0.5$)

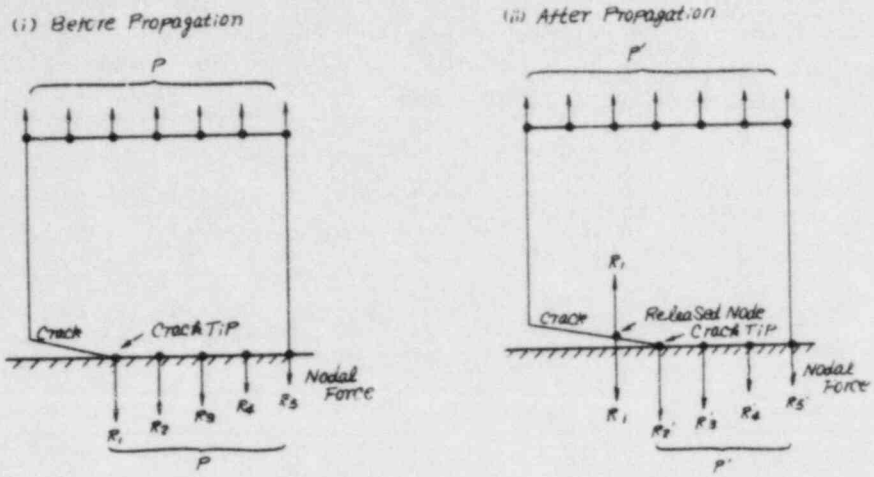

Fig. 2-3 Node Release at Crack Extension (Plate Specimen)

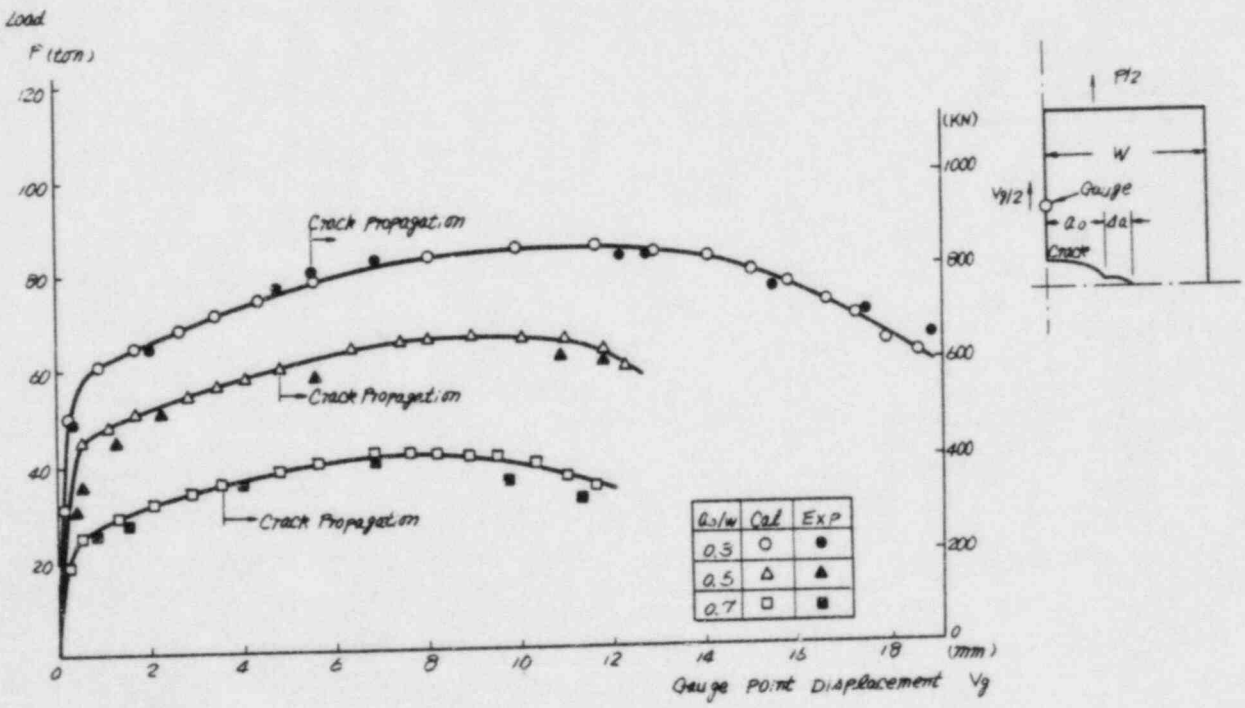

Fig. 2-4 Experimental and Calculated Relationships between Load and Gauge Point Displacement

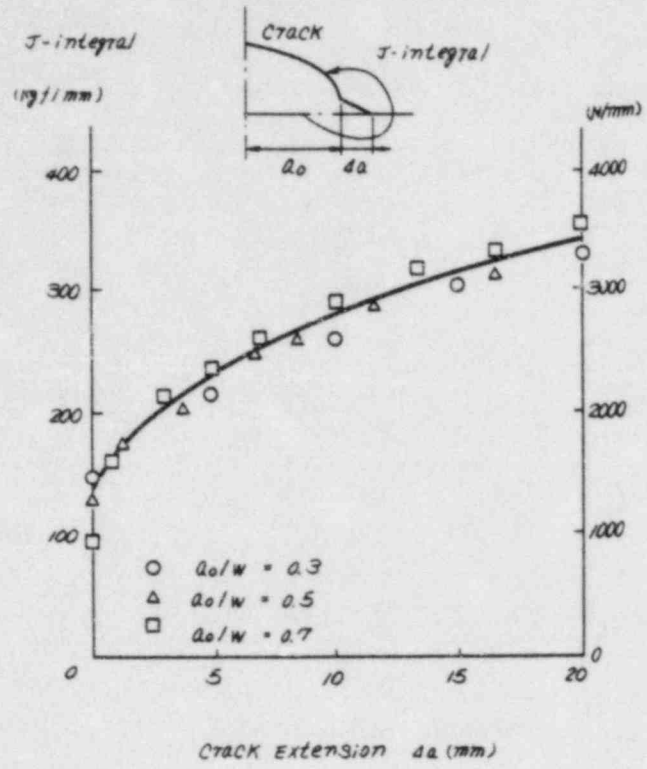

Fig. 2-5 Variation of J-integral with Crack Extension (Δa)

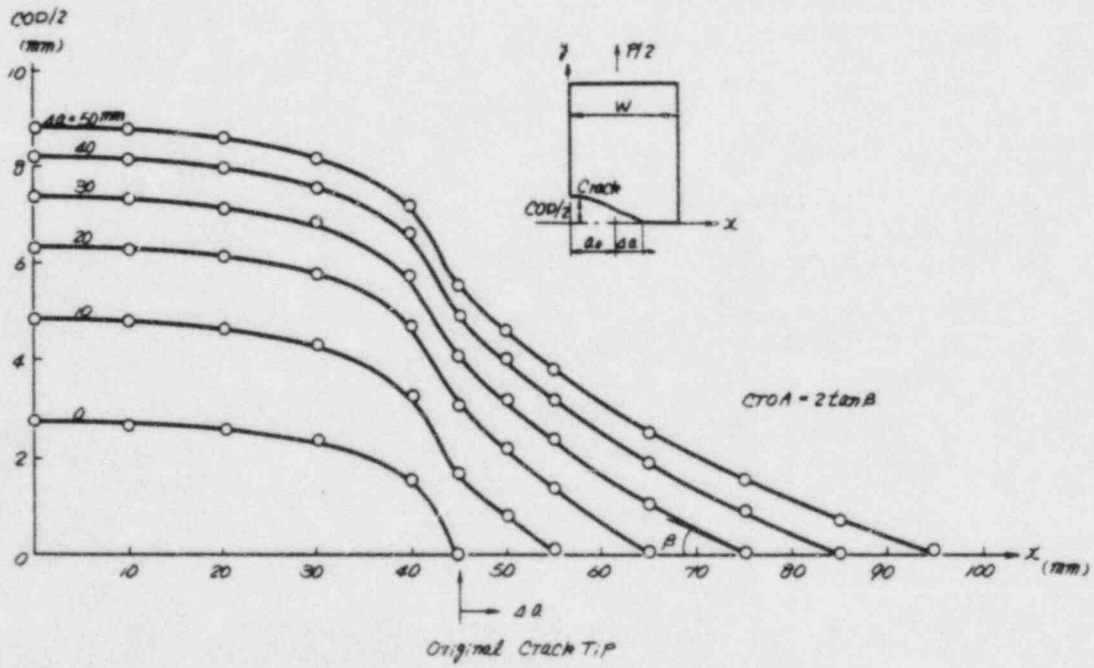

Fig. 2-6 Crack Opening Profiles for Various Crack Extensions in Plate Specimen ($a_o/W = 0.3$)

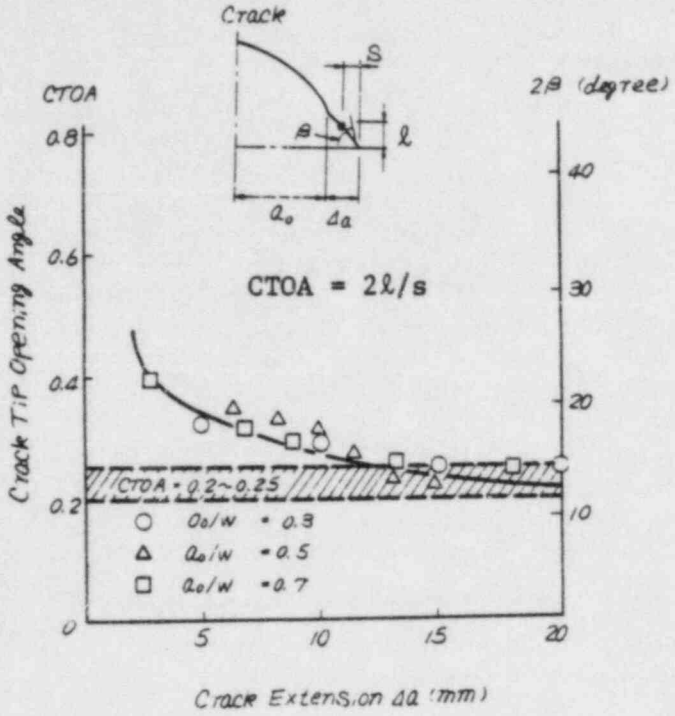

Fig. 2-7 **Variation of Crack Tip Opening Angle (CTOA) with Crack Extension (Δa)**

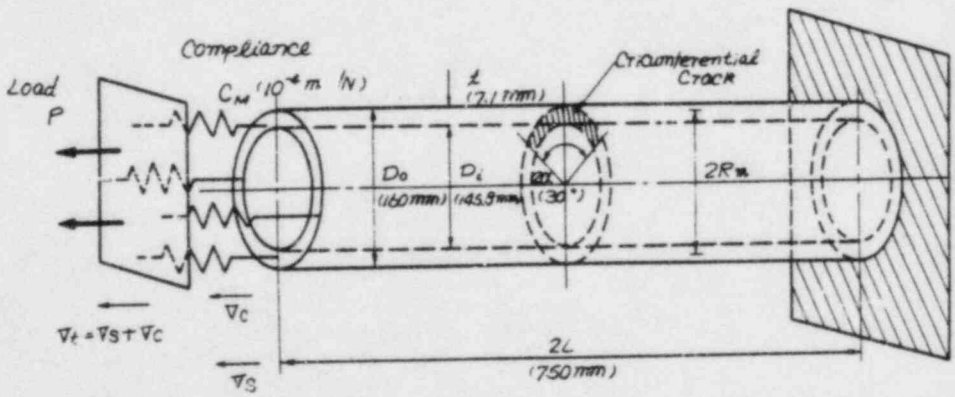

Fig. 2-8 **Circumferentially Cracked Pipe with Compliance Subjected to Tensile Load**

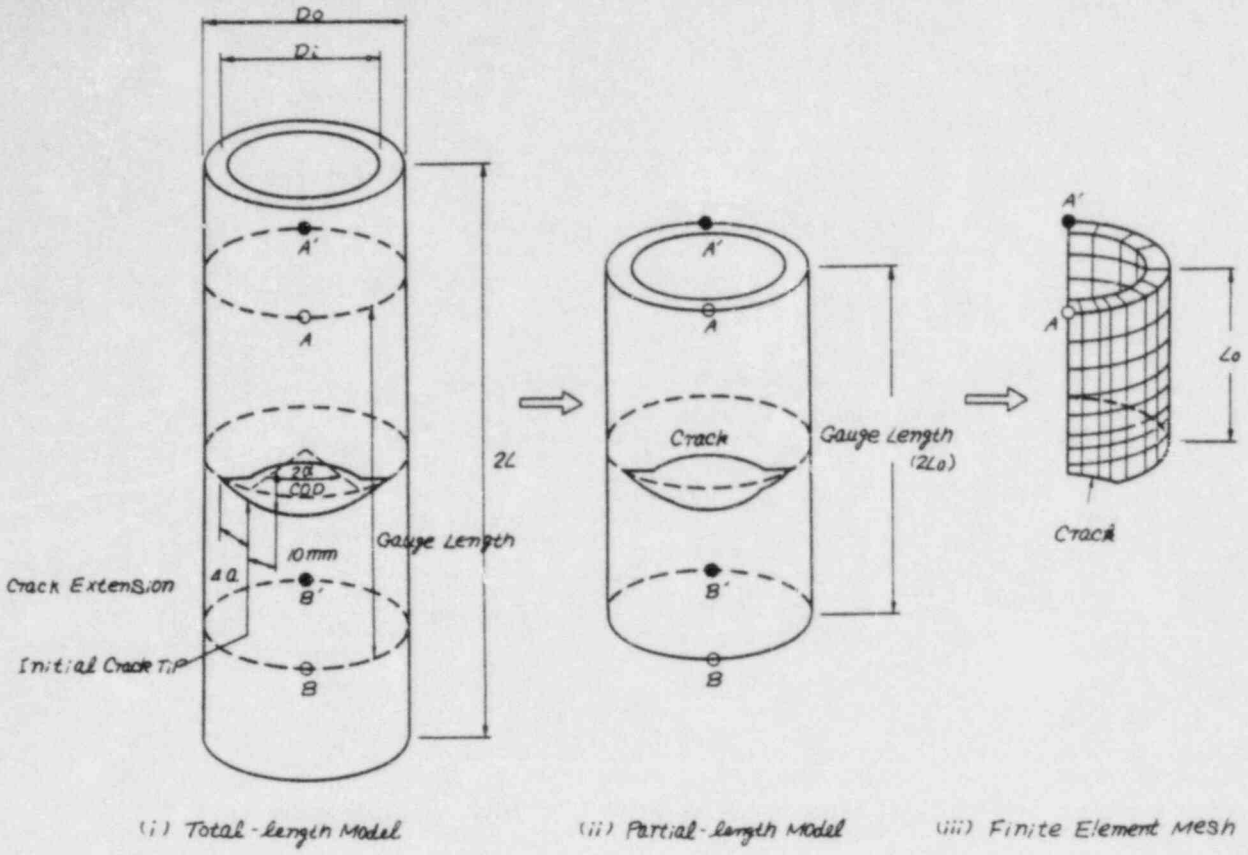

Fig. 2-9 Pipe Model for Finite Element Analysis

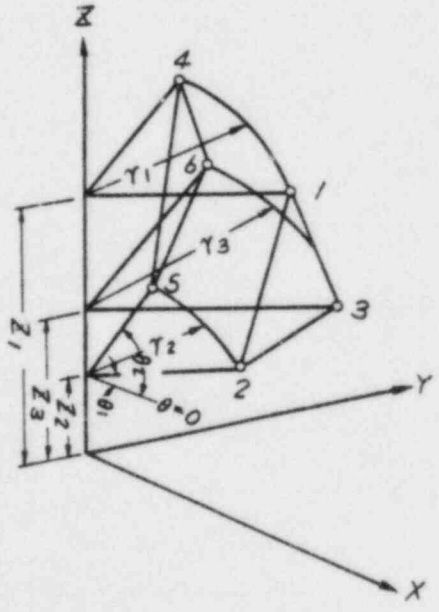

Fig. 2-10 6-Node Isoparametric Element

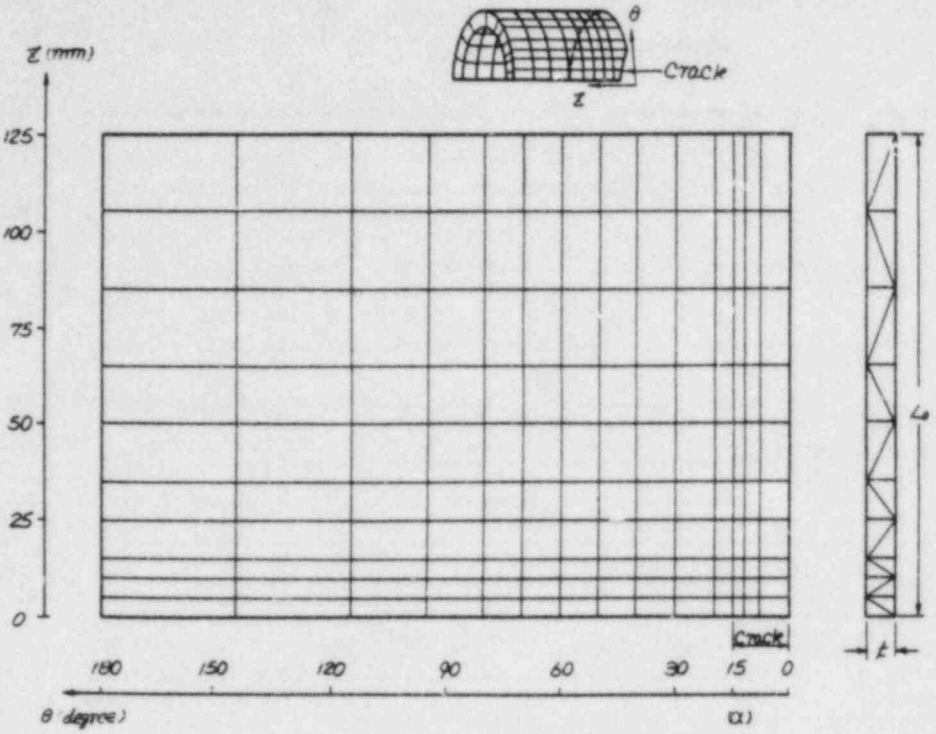

Fig. 2-11 Finite Element Mesh Pattern of Pipe Specimen (2α=30°)

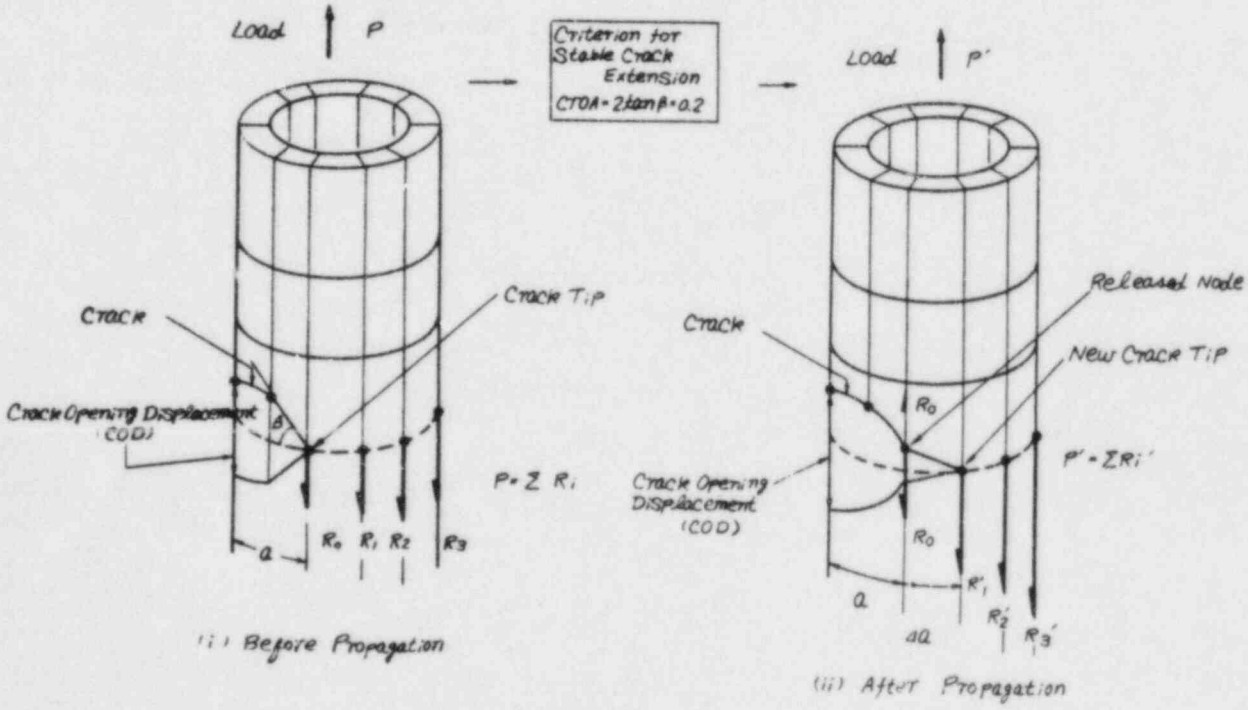

Fig. 2-12 Node Release at Crack Extension (Pipe Specimen)

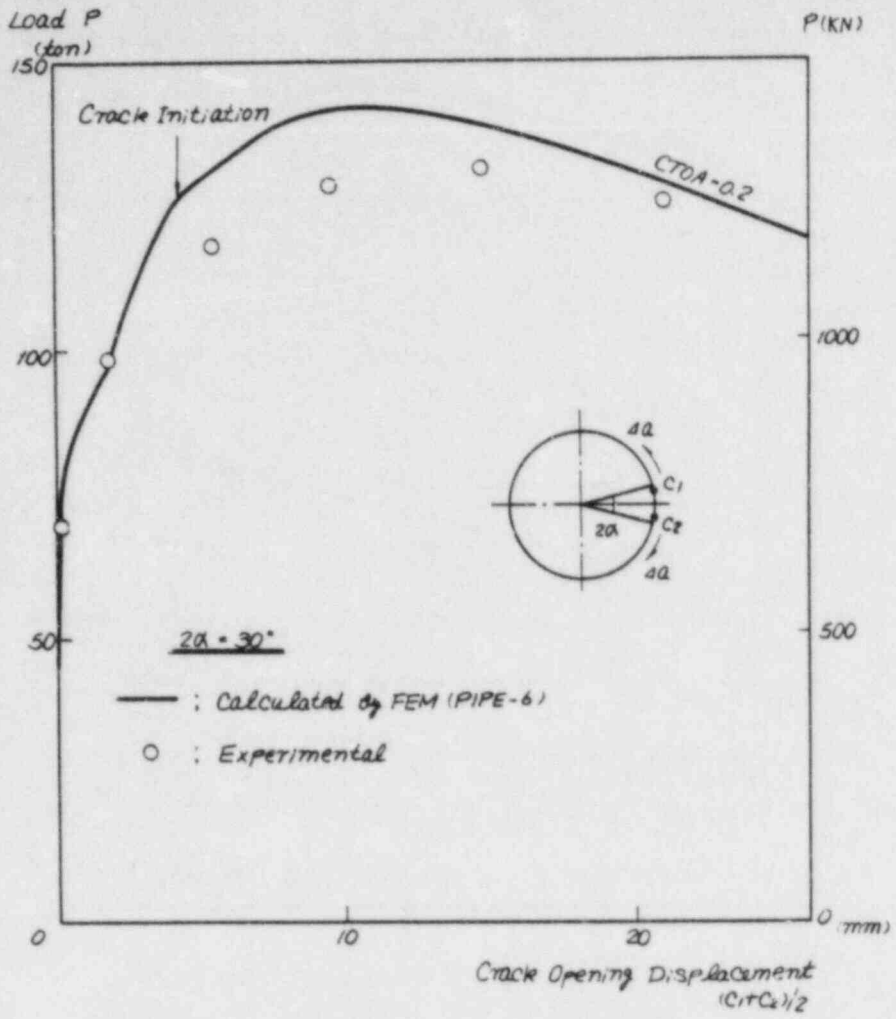

Fig. 2-13 Relationship between Load and Crack Opening Displacement

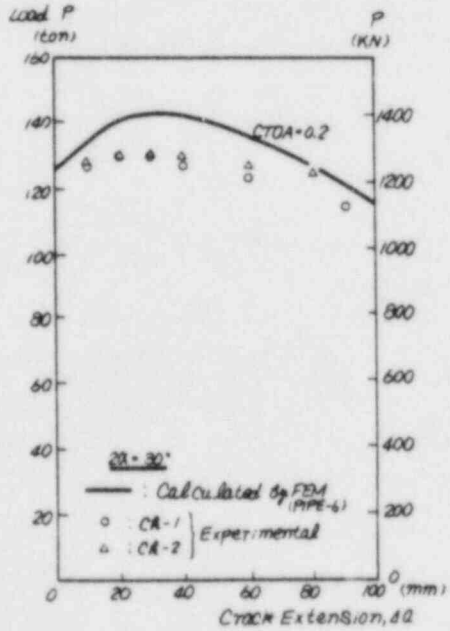

Fig. 2-14 Variation of Load (P) with Crack Extension (Δa)

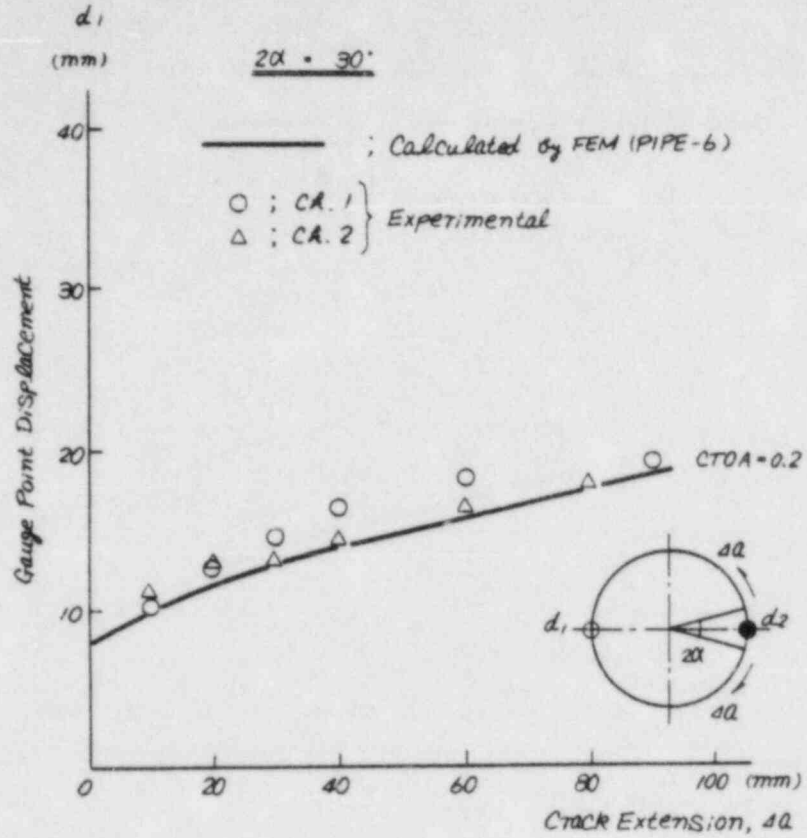

Fig. 2-15 Variation of Gauge Point Displacement (d_1) with Crack Extension (Δa)

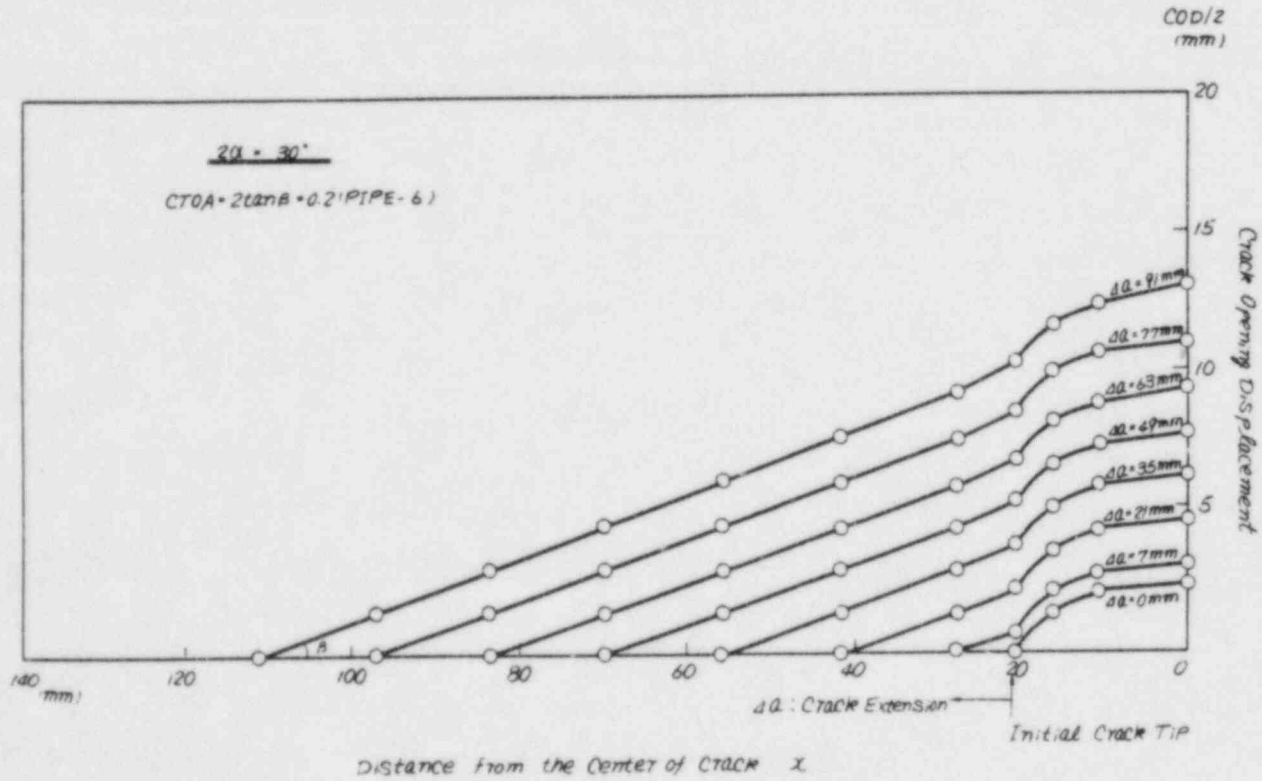

Fig. 2-16 Crack Opening Profiles for Various Crack Extensions in Pipe Specimen (2α=30°)

3. SIMPLIFIED ANALYSIS OF TEARING INSTABILITY FOR CRACKED PIPE

A simplified analysis model is developed to predict the unstable crack propagation in Type 304 stainless steel pipe. The criterion for stable crack growth is employed based on the numerical solutions by the finite element method. The crack instability is estimated using the load and deformation values calculated by the simplified analysis method. The theoretical solutions are then compared with the experimental results under high temperature (285°C) to examine the validity of the method. The effects of various parameters such as compliance and loading conditions on the crack instability are also discussed.

3.1 Stable Crack Propagation

Using the stable crack propagation condition (CTOA criterion) obtained from the finite element analysis, a simplified analysis method is developed to study the circumferential crack propagation. The shape of the pipe specimen with a circumferential through-wall crack to be analyzed is the same as that shown in Fig. 2-8.

Figure 3-1 shows a technique for estimating the load and deformation at crack propagation from the relationship between the load and the crack opening displacement obtained for two specimens having different crack length of 2a and 2(a+da). The load P(2a, COD) can be represented as a function of the crack length (2a) and the crack opening displacement (COD) by curve Ⓐ. The load P(2a+2da, COD) following the crack propagation is assumed to be approximated by curve Ⓑ with an initial crack length of 2(a+da). At crack propagation, the load is assumed to take the values at points ① through ⑤ because unloading ($-dP_1$) occurs at points ① → ② and loading (dP_2) occurs at points ② → ⑤ due to redistribution of the stress at the crack tip. Point ⑤ denotes the value after loading (dP_2) and is located on curve Ⓒ. Curve Ⓒ is obtained by moving curve Ⓑ leftwards by the distance d in order to continue

the displacement (COD) at Point ② after unloading. The variations of the load and displacement with the crack propagation (① → ⑤) are formulated by assuming the load equilibrium and using the criterion for the stable crack propagation.

The following equation represents the equilibrium between the load and the reaction force at the uncracked ligament for the unloading process ($-dP_1$) at crack propagation:

$$P - dP_1 = \sigma_N t \left\{ 2W - 2(a+da) \right\} + \sigma_N t \cdot da \qquad (3\text{-}1)$$

where the first term on the right side represents the reaction force at the ligament $\{2W-2(a+da)\}$ after crack propagation, and the second term represents the equivalent reaction force at the crack tip. The net stress at the ligament before crack propagation, σ_N, is

$$\sigma_N = P/(2W-2a)t \qquad (3\text{-}2)$$

where 2W and t are the pipe circumference (= $2\pi Rm$, Rm: mean radium of pipe) and the wall thickness, respectively. From Eqs. (3-1) and (3-2), the decrease in the load with crack propagation can be represented as follows:

$$dP_1 = da \cdot P/(2W-2a) \qquad (3\text{-}3)$$

Figure 3-2 shows a schematic deformation model at crack propagation, based on the CTOA criterion. Assuming from Fig. 3-2, that

$$CTOA = 2\tan\beta = 2(\ell/s) = 2(\ell'/s') = \text{const} \qquad (3\text{-}4)$$

holds during stable crack propagation, the increase in the crack opening displacement with the crack propagation can be represented as:

$$d(COD) = 2(\ell' - \ell) = CTOA(s'-s) = CTOA \cdot da \qquad (3\text{-}5)$$

Thus, assuming the gradient of the tangent at point ③ on curve Ⓑ in Figure 3-1 to be m, the increase in the load, dP_2, can be represented as follows:

$$dP_2 = m\,d(COD) = m \cdot CTOA \cdot da \tag{3-6}$$

Deriving the total load increment dP at the crack propagation from Eqs.(3-3) and (3-6),

$$dP = -dP_1 + dP_2 = \left\{ -P/(2W-2a) + m \cdot CTOA \right\} da \tag{3-7}$$

To obtain the gradient m, the relationship between the load (P) and deformation (COD) in the circumferentially cracked pipe is formulated as follows:

$$COD/(2W-2a) = f(\sigma_N) \tag{3-8}$$

This assumes that the displacement (COD) is dependent only on the length of the uncracked ligament (2W-2a) and the function f of the net stress σ_N. To define the shape of function $f(\sigma_N)$, the experimental results of the net stress (σ_N), and the ratio of the crack opening displacement to the ligament (COD/(2W-2a)) at the load level before crack initiation in the case of $2\alpha = 60°$ are used [9]. The function $f(\sigma_N)$ can be approximated by the power law for the net stress (σ_N) as follows:

$$f(\sigma_N) = A_o \sigma_N^n \quad (A_o = 2.07 \times 10^{-13}\,(MPa)^{-n},\ n = 4.56) \tag{3-9}$$

Although constants A_o and n in Eq. (3-9) are derived from the results for the cracked specimen with $2\alpha = 60°$, the function f is assumed to represent a "Key Curve" [18] independent of the initial crack angle (2α). Using Eqs. (3-8) and (3-9) to obtain the gradient m:

$$m^{-1} = \left\{ \frac{\partial (COD)}{\partial P} \right\}_{\substack{P-dP \\ 2(a+da)}} = \frac{A_o n P^{n-1}}{t^n (2W-2a)^{n-1}} \left\{ 1 + \frac{n-1}{2(2W-2a)} d(2a) \right\} \quad (3\text{-}10)$$

Substituting Eq. (3-10) into Eq. (3-7),

$$\frac{dP}{d(2a)} = - \frac{P}{2(2W-2a)} + \frac{(CTOA)\, t^n}{2A_o n} \left(\frac{2W-2a}{P} \right)^{n-1} \quad (3\text{-}11)$$

Solving this differential equation (3-11),

$$P = \left(\frac{CTOA}{A_o n} \right)^{1/n} t \sqrt{2W-2a} \left\{ C_o - (2W-2a)^{n/2} \right\}^{1/n} \quad (2a \geq 2a_o) \quad (3\text{-}12)$$

The constant C_o is defined using the load P_i at crack initiation ($2a=2a_o$):

$$C_o = \frac{A_o n}{CTOA} \left(\frac{P_i}{t \sqrt{2W-2a_o}} \right)^n + (2W-2a_o)^{n/2} \quad (3\text{-}13)$$

Figure 3-3 shows the results obtained by using these equations as the relationship between the load and the crack opening displacement for initial crack angle of $2\alpha = 60°$. As the criterion for stable crack propagation, CTOA value of 0.2 is selected for use, based on the results of the finite element analysis. In the analysis, a net stress of $(\sigma_N)_i = P_i/(2W-2a_o)t = 256$ (MPa) obtained from measurements is used as the crack initiation condition. The result of the simplified analysis is found to be in relatively good agreement with the experimental results for the load and deformation during stable crack propagation [9, 12].

3.2 Tearing Instability of Cracked Pipe

3.2.1 Crack Instability Condition

This section describes the analysis of crack instability using the load and deformation values during stable crack propagation. As the crack instability criteria, we adopt the stationary condition of the total dispacement of the loading system including the effect of compliance (C_M).

Total displacement (V_t) of the loading system is represented by the sum of the displacement (V_s) of the pipe specimen and the displacement (V_c) of the testing machine, as shown in Fig. 2-8. Approximating the displacement (V_s) of the pipe with the crack opening displacement (COD), and using the product of the compliance (C_M) and the load (P) to represent the displacement (V_c) of the testing machine, the total displacement (V_t) is obtained:

$$V_t = V_s + V_c \cong COD + C_M P \tag{3-14}$$

The instability condition is

$$dV_t/d(2a) = d(COD)/d(2a) + C_M dP/d(2a) = 0 \tag{3-15}$$

Substituting Eqs. (3-5) and (3-12) into Eq. (3-15), we get the following equation about the crack length ($2a_{inst}$) at the onset of the crack instability:

$$\left.\begin{aligned} g(x) &= x-2-K(x-1)^{1-1/n} = 0 \\ x &= C_o/(2W-2a_{inst})^{n/2} \\ K &= \frac{CTOA}{tC_M}\left(\frac{A_o n}{CTOA}\right)^{1/n} \end{aligned}\right\} \tag{3-16}$$

Assuming that the amount of stable crack extension at instability is Δa_{inst} ($=a_{inst}-a_o$), we get

$$\Delta a_{inst} = (\pi R_m - a_o)\left[1 - \left\{\frac{(A_o n/CTOA)\ (\sigma_N)_i^n + 1}{x}\right\}^{2/n}\right] \qquad (3\text{-}17)$$

Using this result, the critical amount of crack extension at instability (Δa_{inst}) can be obtained as a function of the compliance (C_M) and the initial crack angle (2α).

The specimen displacement (V_s) and testing machine displacement (V_c) are calculated for the specimen with an initial crack of $2\alpha = 60°$, and the critical amount of crack extension at instability is estimated from the stationary condition of the total displacement of the loading system ($dV_t/d(2a) = 0$). Those results are shown in Fig. 3-4. The critical amount of crack extension at instability (Δa_{inst}) is calculated to be the value of 78 mm (CTOA= 0.2) under a compliance of 10^{-4} mm/N, which is in fairly good agreement with the measured result of 70 mm [9].

3.2.2 Effects of Various Parameters on Crack Instability

This section studies some effects on the crack instability of various parameters, such as the compliance (C_M) and the net stress (σ_N).

Figure 3-5 shows the effect of the compliance (C_M) on the critical crack extension amount at instability (Δa_{inst}). Eq.(3-17) indicated that the non-dimensional critical crack extension amount, $\Delta a_{inst}/(\pi R_m - a_o)$, can be expressed as a function of the compliance and the CTOA for constant values of A_o, n, $(\sigma_N)_i$ and t. As shown in the figure, the larger compliance makes the critical crack extension smaller. When the compliance is as small as 10^{-6} mm/N, for example, the corresponding critical crack extension amount becomes nearly equal to $(\pi R_m - a_o)$, which means that the crack remains stable almost all through the uncracked ligament. On the other hand, when the compliance is as large as 10^{-2} mm/N, we may expect that $\Delta a_{inst} \simeq 0.13(\pi R_m - a_o)$.

This indicates that the crack propagation becomes unstable after the stable crack growth by only a very small length under the large compliance. The experimental result is obtained for the compliance (C_M) of 10^{-4} mm/N, agreeing reasonably well with the result of the simplified analysis.

Next, we shall examine the loading conditions that affect unstable cracking. Assuming the net section stress of the piping at crack instability to be $(\sigma_N)_{inst}$, from Eq. (3-12), we get

$$(\sigma_N)_{inst} = \left[\frac{CTOA}{A_o n} \{x - 1\} \right]^{1/n} \qquad (3\text{-}18)$$

Figure 3-6 shows the estimated relationships between the nominal applied stress (σ_g) and the crack length (2a) (CTOA=0.2). This plot shows that when a load is applied to the specimens having initial cracks (2α) of various sizes, stable crack propagation begins at the net stress $(\sigma_N)_i$ of $0.8\sigma_o$ (σ_o: flow stress), and the crack becomes unstable at the net stress $(\sigma_N)_{inst}$ of $1.24\sigma_o$ in the case of $C_M = 10^{-4}$ mm/N. The net stress at crack instability is calculated from Eq. (3-18) as $0.95\sigma_o$ under an infinite compliance ($C_M = \infty$) and $1.85\sigma_o$ under a small compliance ($C_M = 5 \times 10^{-5}$ mm/N).

Figure 3-7 shows the values of the net stress at crack instability $(\sigma_N)_{inst}$ as a function of the compliance (C_M) and pipe diameter ($2R_m$). As the compliance increases, the net stress at the onset of unstable crack propagation, $(\sigma_N)_{inst}$, decreases, making unstable pipe fracture take place more easily. The net stress at crack instability, $(\sigma_N)_{inst}$, becomes constant independently of pipe diameter and approaches to $0.95\sigma_o$ under a large compliance ($C_M \geq 10^{-2}$ mm/N). Employing the compliance condition of the safest side, $C_M = \infty$, the lowest limit of the net stress for unstable fracture of the cracked pipe can be estimated to be $0.95\sigma_o$.

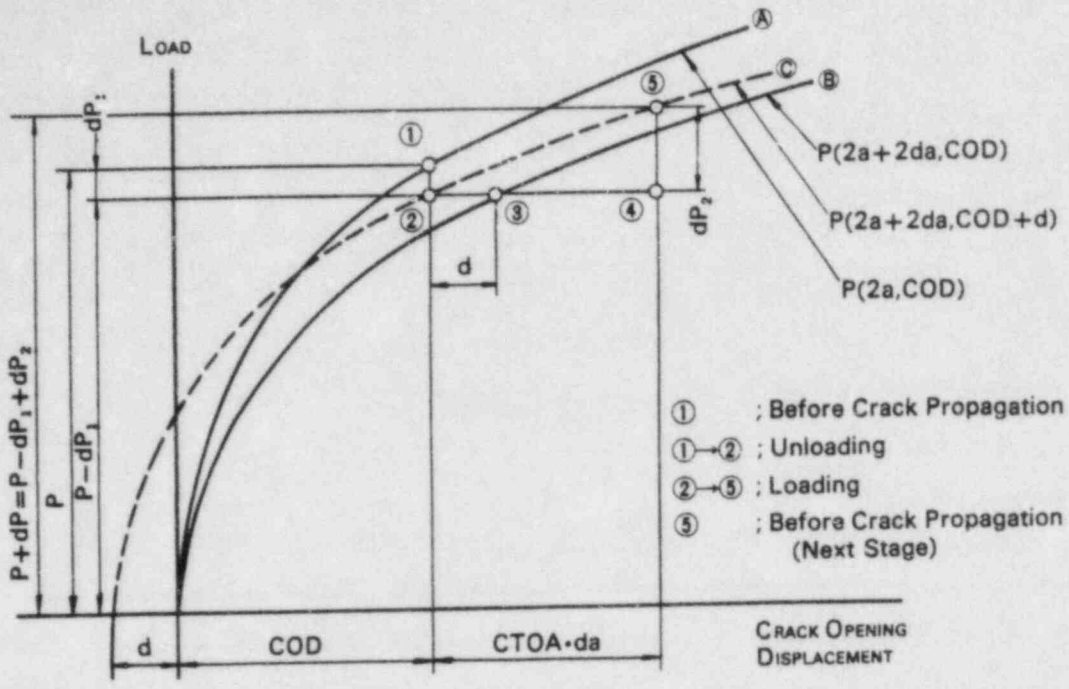

Fig. 3-1 Load vs. Crack Opening Displacement at Crack Propagation

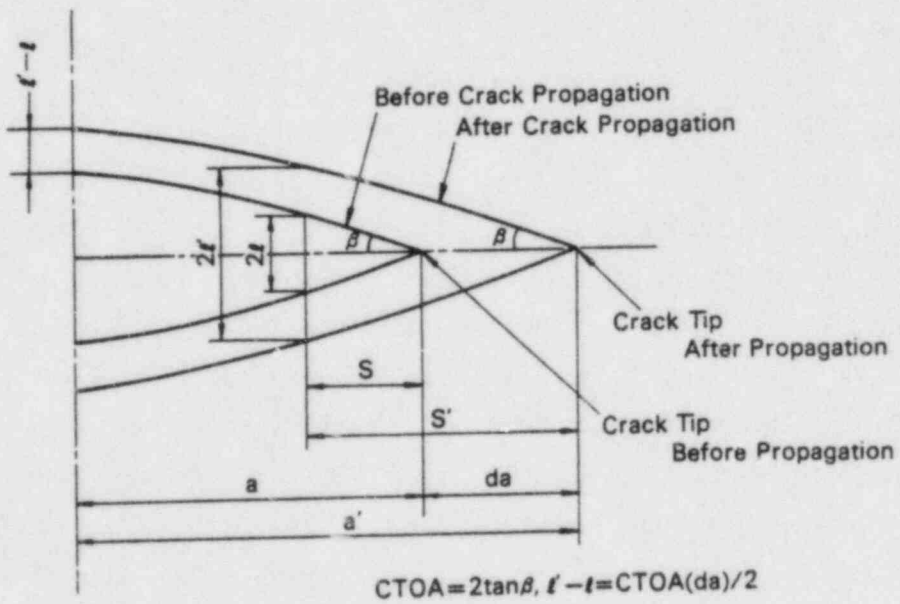

Fig. 3-2 Stable Crack Propagation under a Constant Crack Tip Opening Angle (CTOA)

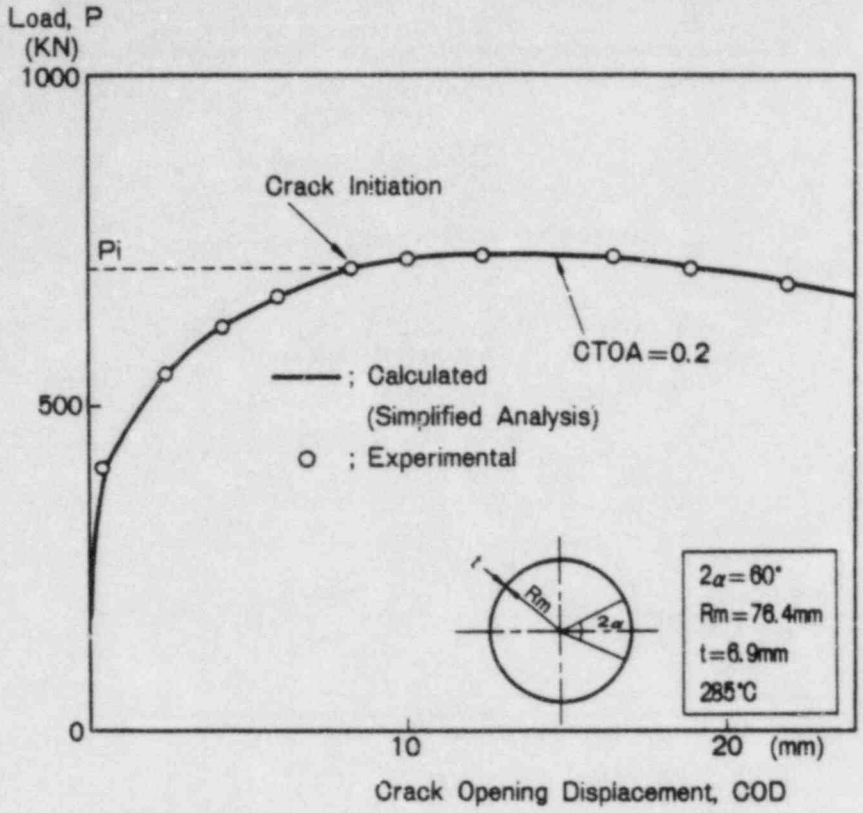

Fig. 3-3 Relationship between Load and Crack Opening Displacement

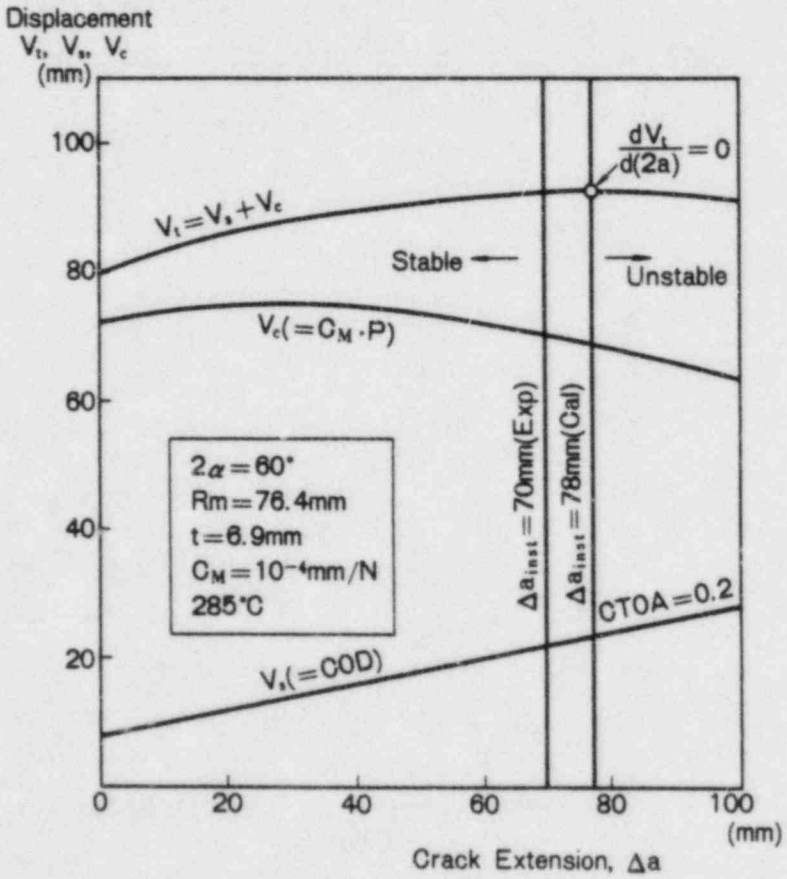

Fig. 3-4 Prediction of Crack Instability

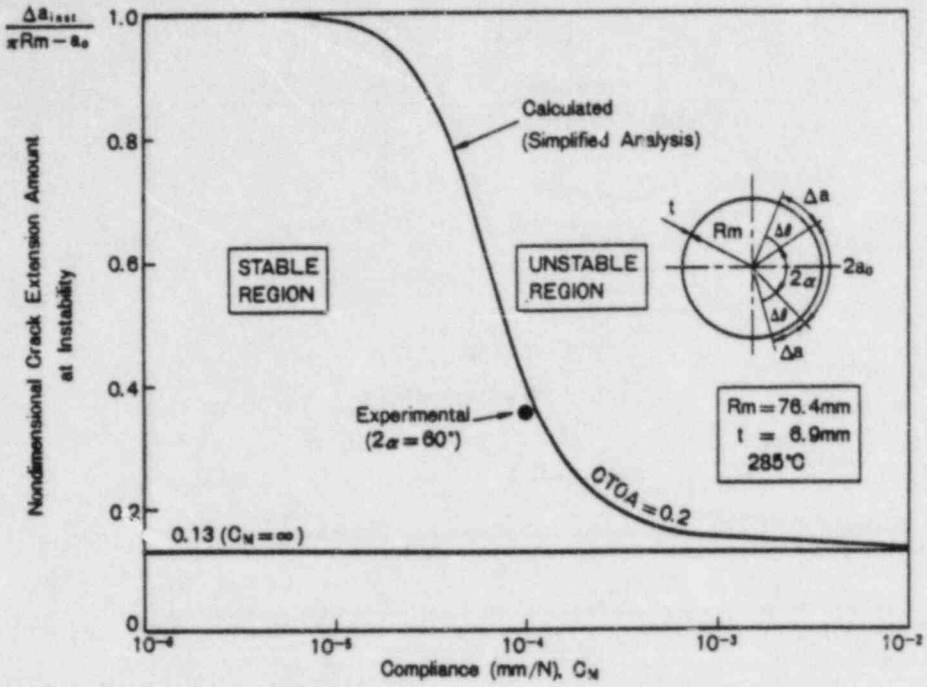

Fig. 3-5 Effect of Compliance (C_M) on Crack Extension Amount at Instability (Δa_{inst})

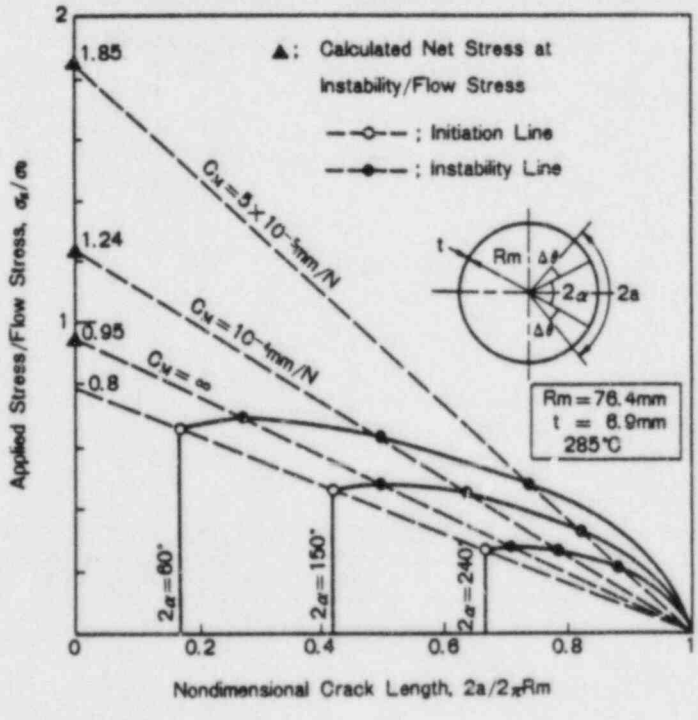

Fig. 3-6 Relationship between Applied Stress (σg) and Crack Length ($2a$)

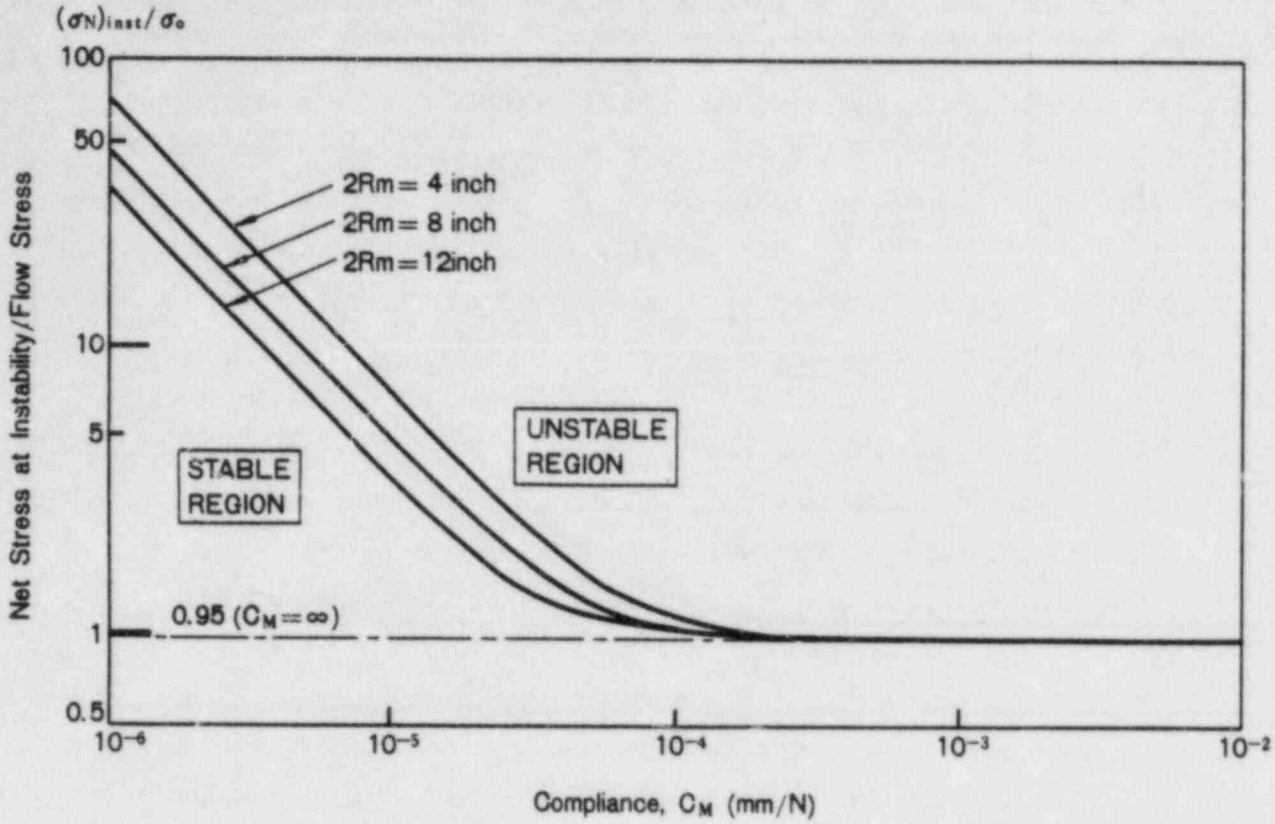

Fig. 3-7 **Relationship between Net Stress at Crack Instability $(\sigma_N)_{inst}$ and Compliance (C_M)**

4. LEAK BEFORE BREAK FOR CIRCUMFERENTIALLY CRACKED PIPE

In the preceding chapter, the fracture condition of the pipe with a circumferential through-wall crack was estimated using the net stress criterion, $\sigma_N = 0.95\sigma_o$, where σ_o is the flow stress of Type 304 stainless steel at high temperature (285°C). This net stress criterion can be applied to obtain the condition for unstable fracture of the pipe with a circumferential part-through crack.

Figure 4-1 shows the schematic variation of a crack shape during the propagation in the direction of pipe thickness from the stage of the initial part-through crack to the stage of the onset of pipe leakage under the constant applied stress (σ_g). The maximum depth of a part-through crack (c) is assumed to increase from the initial crack depth (c_o) to pipe thickness (t) with a constant crack angle (2α). The shape of a circumferential part-through crack is approximated by an arc of a circle. Pipe leakage is assumed to occur when the maximum crack depth becomes equal to pipe thickness (c/t = 1). Therefore, leak before break for the cracked pipe can be evaluated, as follows:

$\sigma_N/\sigma_o < 0.95$ (at c/t = 1) ..... LBB

$\sigma_N/\sigma_o \geq 0.95$ (at c/t = 1)..... NON LBB

Figure 4-2 shows the prediction of leak before break by the net stress criterion using the calculated relationships between the maximum crack depth (c)/pipe thickness(t) and the net stress (σ_N)/the flow stress (σ_o) for 4-inch diameter pipes with the various initial crack angles (2α). Experimental results about leak-before-break tests are obtained for the pipes with the crack angles of 2α = 150° and 240° and the initial crack depth of $c_o = 0.5t$, subjected to the cyclic applied stress equal to σ_Y (179 MPa), the 0.2% proof stress of the pipe at high temperature (285°C) and the internal pressure p (9 MPa) [9,12]. In the experiments, leak before break is confirmed in the specimen of 2α = 150°. On the contrary, fast fracture

is observed in the specimen of $2\alpha = 240°$. The axial applied stress, σ_g, is calculated as the sum of the tensile applied stress (σ_Y) and the axial stress ($pR_m/2t$) generated by the internal pressure (p). The analysis results corresponding to these experiments show that leak before break is established in the case of $2\alpha = 150°$ because the net stress at the time of pipe leakage ($c/t = 1$) is less than the critical value of $0.95\sigma_o$. On the other hand, the net stress at pipe leakage is greater than the critical value and leak before break may not be established under this applied stress in the case of $2\alpha = 240°$. These numerical results agree well with the experimental ones described above.

Next, leak before break for the pipes with various crack angles ($2\alpha = 60° \sim 360°$) and small initial crack depth ($c_o/t \simeq 0$) is estimated under the constant applied stress equal to the allowable design stress (S_m) for primary membrane stress [19]. It can be seen from the figure that the net stresses at pipe leakage ($c/t = 1$) are less than the critical value of $0.95\sigma_o$. Therefore, leak before break may be maintained, if a crack shape during the propagation in the direction of pipe thickness varies as shown in Fig. 4-1 under the constant applied stress equal to the allowable design stress (S_m).

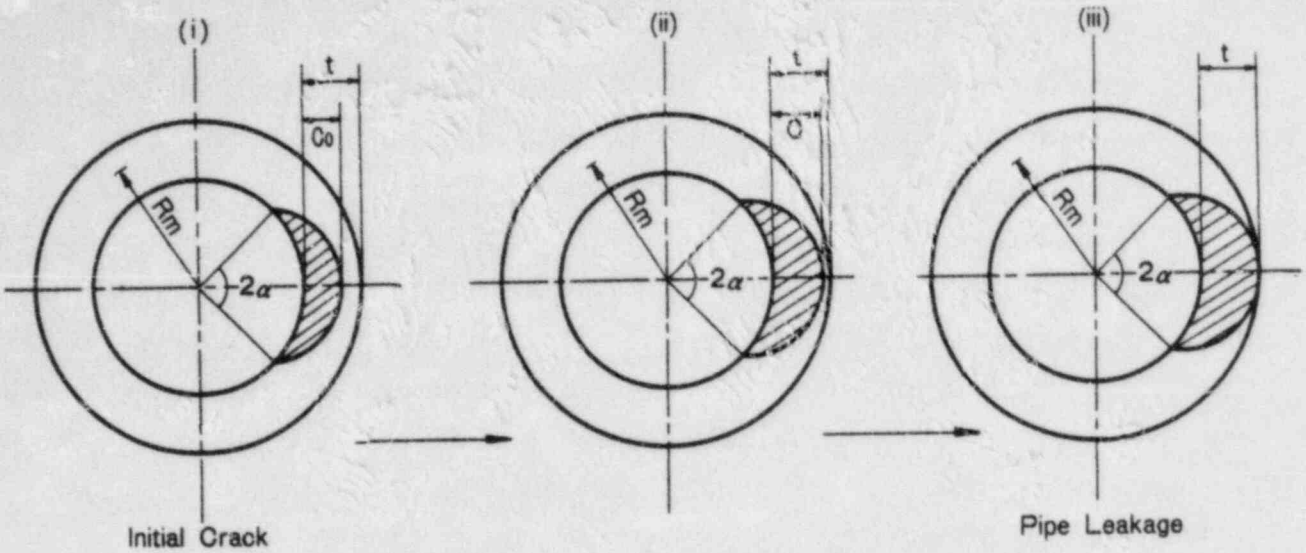

Fig. 4-1 Variation of Crack Shape during Propagation

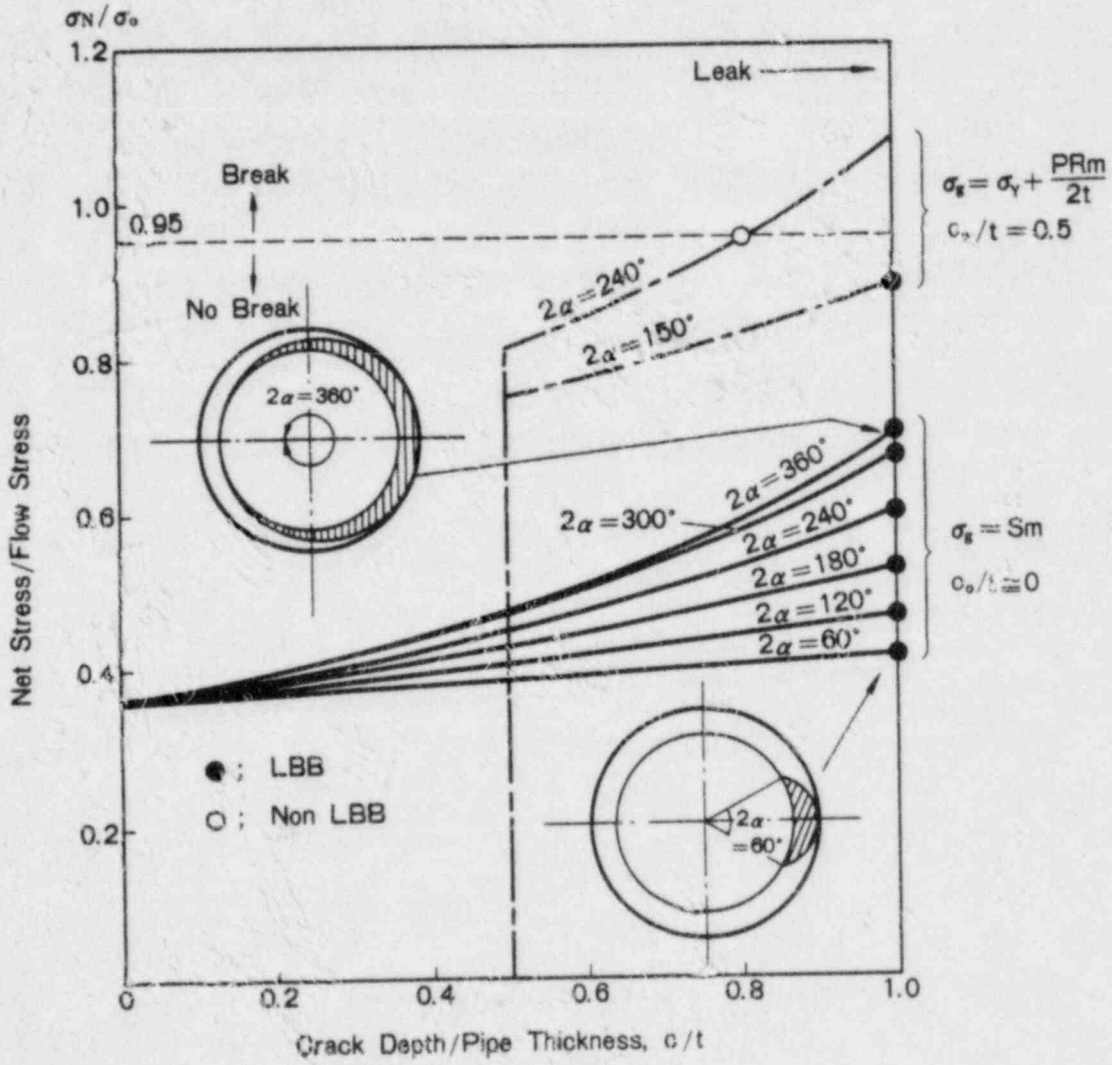

Fig. 4-2 Prediction of Leak before Break by Net Stress Criterion

5. CONCLUSIONS

In this paper, some numerical methods for the analysis of crack propagation in Type 304 stainless steel pipe under the axial tensile load were presented and applied to estimate the criteria of stable/unstable crack propagation and the leak before break condition for the circumferentially cracked pipe.

i) PLASTAN-II, an elastic plastic finite element code, was developed for the analysis of ductile crack extension in two-dimensional plate specimen.
Using this code, the onset of stable crack propagation could be predicted under the constant J-integral values (1000-1500 N/mm) for the center cracked plate specimen of Type 304 stainless steel. Crack propagation following the onset of stable crack extension was estimated in accordance with the resistance curve for the J-integral or the crack tip opening angle (CTOA). During stable crack propagation, a nearly constant CTOA (=0.2) was estimated.

The three-dimensional finite element code PIPE-6 was developed to evaluate the fracture behavior of circumferentially cracked Type 304 stainless steel pipe. Through-wall crack propagation under the axial tensile load could be simulated by the release of the nodal constraint at the crack tip while maintaining a constant crack tip opening angle (CTOA=0.2).
Numerical solutions for the applied load and displacement during crack propagation showed relatively good agreements with the experimental results.

ii) A simplified analysis model for the circumferential through-wall crack propagation was developed based on the CTOA criterion and the load-deformation relationship in the cracked pipe.
Using these conditions, the load and deformation during crack propagation were formulated. The crack instability condition was

estimated as the critical value of the net stress, $(\sigma_N)_{inst}$ $(=0.95\sigma_o)$. Some of the analysis results were in good agreements with the experimental ones.

iii) Leak before break condition for the pipe with a circumferential part-through crack was evaluated, based on the net stress at the time of pipe leakage. Leak before break may be maintained for the circumferentially cracked pipe subjected to the constant applied stress equal to the allowable design stress (S_m), if a crack shape was approximated by an arc of a circle with the constant crack angle during the propagation.

6. ACKNOWLEDGEMENTS

This paper was obtained during the investigations in the Crack Behavior Verification Test at the Nuclear Power Engineering Test Center. The authors would like to express their sincere gratitude to Dr. G. Yagawa, Chairman of the subcommittee for the Crack Behavior Verification Test and to all the members in this subcommittee for their assistance and valuable comments.

References

[1] USNRC Pipe Crack Study Group, "Investigation and Evaluation of Cracking in Austenitic Stainless Steel Piping of BWR Plants", NUREG - 75/067, 1975.

[2] Paris, P.C., Tada, H., Zahoor, A. and Ernst, H., "The Theory of Instability of the Tearing Mode of Elastic-Plastic Crack Growth", Elastic-Plastic Fracture, ASTM STP 668, p.5/36, 1979.

[3] Hutchinson, J.W. and Paris, P.C., "Stability Analysis of J-Controlled Crack Growth", Elastic-Plastic Fracture, ASTM STP 668, p.37/64, 1979.

[4] Tada, H., Paris, P.C. and Gamble, R., "Stability Analysis of Circumferential Cracks in Reactor Piping Systems", NRC, NUREG/CR-0838, 1979.

[5] Zahoor, A. and Kanninen, M.F., "A Plastic Fracture Mechanics Prediction of Fracture Instability in a Circumferentially Cracked Pipe in Bending-Part I. J-integral Analysis", ASME Journal of Pressure Vessel Technology, Vol. 103, No.4, p.352/358, 1981.

[6] Wilkowski, G.M., Zahoor, A. and Kanninen, M.F., "A Plastic Fracture Mechanics Prediction of Fracture Instability in a Circumferentially Cracked Pipe in Bending-Part II. Experimental Verification on a Type 304 Stainless Steel Pipe", ASME Journal of Pressure Vessel Technology, Vol. 103, No.4, p.359/365, 1981.

[7] ASME Boiler and Pressure Vessel Code, Section XI, Rules for Inservice Inspection of Nuclear Power Plant Components, ASME, 1980.

[8] Norris, D.M., Marston, T.U. and Tagart, Jr. S.W., "Acceptance Criteria for Circumferential Flaws in Stainless Steel Piping", Aspects of Fracture Mechanics in Pressure Vessels and Piping, ASME PVP-Vol. 58, p.185/199, 1982.

[9] Japan Power Plant Inspection Institute and Nuclear Power Engineering Test Center, "Summary Report of Proving Tests on Reliability for Nuclear Power Plant 1982 (Stress Corrosion Cracking Test in BWR)", 1982.

[10] Yagawa, G., Takahashi, Y. and Ando, Y., "Theoretical and Experimental Study of Unstable Fracture for Type 304 Stainless Steel Plates with a Soft Tensile Testing Machine", Engineering Fracture Mechanics, Vol. 16, No.5, p.721/731, 1982.

[11] Yagawa, G., Kashima, K., Takahashi, Y., Hasegawa, K., Saitoh, M., Umemoto, T., and Sasaki, N., "Stable Growth and Instability of Circumferential Crack in Type 304 Stainless Steel Pipes under Tensile Load", 7th International Conference on Structural Mechanics in Reactor Technology (SMIRT-7), G/F 4/1*, 1983.

[12] Yagawa, G., Kashima, K., Katoh, N., Hasegawa, K., Saitoh, M., and Umemoto, T., "Fracture Behaviors of Type 304 Stainless Steel Pipes with Circumferential Inner-Surface Crack under Cyclic Tension and BWR Environment", ASME, Pressure Vessels and Piping Conference, Portland, U.S.A, 1983.

[13] Yamada, Y., Yoshimura, N., and Sakurai, T., "Plastic Stress-Strain Matrix and its Application for the Solution of Elastic-Plastic Problems by the Finite Element Method", International Journal of Mechanical Science, Vol. 10, p.343/354, 1968.

[14] Marcal, P.V., and King, I.P., "Elastic-Plastic Analysis of Two Dimensional Stress Systems by the Finite Element Method", International Journal of Mechanical Sciences, Vol. 19, p.143, 1967.

[15] Rice, J.R., "A Path Independent Integral and the Approximate Analysis of Strain Concentration by Notches and Cracks", Transaction of the ASME, Series E., Vol. 35, No.2, p.379, 1968.

[16] EPRI, "Mechanical Fracture Predictions for Sensitized Stainless Steel Piping with Circumferential Cracks", EPRI NP-192, p.2-1/2-11, 1976.

[17] Zahoor, A. and Abou-Sayed, I.S., "Prediction of Stable Crack Growth in Type 304 Stainless Steel", Computers & Structures, Vol. 13, p.137/144, 1981.

[18] Ernst. H., Paris, P.C., Rossow, M. and Hutchinson, J.W., "Analysis of Load-Displacement Relationship to Determine J-R Curve and Tearing Instability Material Properties", Fracture Mechanics, ASTM STP 677, p.581/599, 1979.

[19] ASME Boiler and Pressure Vessel Code, Section III, Rules for Construction of Nuclear Power Plant Components, ASME, 1980.

Stable and Unstable Growths of Circumferential Cracks in Type 304 Stainless Steel Pipes under Tensile and Thermal Loadings

G. Yagawa: Department of Nuclear Engineering, University of Tokyo, 7-3-1 Hongo, Bunkyo-ku, Tokyo, 113 Japan

Y. Takahashi: Central Research Institute of Electric Power Industry, 2-11-1 Iwatokita, Komae-shi, Tokyo, 201 Japan

N. Kato: Nuclear Power Engineering Test Center, 3-6-2 Toranomon, Minato-ku, Tokyo, 105 Japan

H. Saito: Toshiba Corporation, 8 Shin-sugita, Isogo-ku, Yokohama-shi, 235 Japan

K. Hasegawa: Hitachi Ltd., 3-1-1 Saiwai-cho, Hitachi-shi, 317 Japan

T. Umemoto: Ishikawajima-Harima Heavy Industries Co. Ltd., 1 Nakahara-cho, Isogo-ku, Yokohama-shi, 235 Japan

1. Introduction

Since the discovery of the intergranular stress corrosion cracking (IGSCC) at the Dresden II reactor in 1974, the similar cracks have been found in the recirculation bypass lines as well as in the core spray lines of many Boiling Water Reactor (BWR) plants [1]. The IGSCCs have been found in the heat-affected zones of girth weld in Type 304 stainless steel pipes. No double-ended pipe rupture has occurred in BWR plants because these cracks have been detected by small steam leakage during operation or ultrasonic signals at the in-service inspection before they lead to the complete fracture of piping.

Type 304 stainless steel, which is used commonly as the pipe material, has so enough ductility and toughness that even when a flaw initiates and grows in a piping system, structural safety may be maintained by the leak-before-break (LBB) behavior, by which the unstable pipe rupture can be prevented. It is necessary, however, to demonstrate experimentally and theoretically that unstable pipe break without detectable leak of the coolant can thoroughly be prevented under all the conditions expected in the plants.

With this necessity, the researches on the fracture behavior of stainless steel pipes with cracks have been carried out in several countries. Since the linear elastic fracture mechanics can not be applied to this kind of problem because of high ductility of the material, the developments of new methodologies were required.

One of these methodologies is the so called net-section stress criterion proposed by the researchers at Battelle Columbus Laboratories [2]. This criterion with the assumption of fully plastic condition of cracked section was applied to plates as well as pipes subjected to tension and bending loads. It has an advantage that it requires no detailed numerical analysis but has some disadvantages. One of them is that it can not take into account the effect of system compliance on the pipe fracture instability.

On the other hand, Paris et al.[3] proposed the so called tearing instability criterion based on the J-integral resistance curve, which can take the effect of system compliance on fracture instability into consideration. Hutchinson and Paris [4] discussed the theoretical basis for the use of the J-integral in crack growth and gave some conditions for the J-controlled crack growth. Applications of the tearing instability criterion to circumferentially cracked pipes under the bending load were also made [5-6].

Several experiments were conducted to confirm the theoretical predictions. Paris et al. [7] performed the fracture experiments in which they employed three-point bend specimens of rotor steels with various compliances to observe the behavior of stable or unstable crack growth. Wilkowski et al.[8] made the fracture experiments on Type 304 stainless steel pipes subjected to four-point bending load through compliance to evaluate the applicability of the tearing instability criterion to the circumferentially cracked pipe. They predicted the instability points accurately with the criterion, but the geometry dependency of J-integral resistance curve was shown.

Besides, many numerical investigations were made using the elastic-plastic finite element methods and the validity of several parameters was studied [9-12]. Among others, the researchers in General Electric Company developed a simplified method of instability analysis using the fully plastic finite element solutions and gave the good estimates of crack propagation behaviors using the method [13].

In Japan, in order to demonstrate the structural integrity of the cracked pipes, Crack Behavior Verification Test Group at Nuclear Power Engineering Test Center (NUPEC) has conducted the extensive research on the fracture behaviors as well as leak-before-break behaviors of flawed pipes under the sponsorship of Ministry of International Trade and Industry. This paper is intended to give an overview of the results obtained so far, although some of them were published elsewhere [14-17].

The various experiments have been performed using the tension-type high-compliance apparatus specially developed for this project. The experiments consist of the following four tests.

1) Plate experiments under static or dynamic tension loading with and without "compliance" set in series (20 specimens tested).
2) Pipe experiments under static or dynamic tension loading with and without "compliance" set in series (20 specimens tested).
3) Pipe experiments under cyclic tension loading with "compliance" set in series superposed on constant internal pressure by the corrosive water of about 280°C with O_2 of 8 ppm (5 specimens tested).
4) Pipe experiments under transient thermal loading superposed on tension loading with and without "compliance" (4 specimens tested).

Moreover, the detailed analyses by the finite element method have been carried out regarding some of the experiments. Additionally, a simplified analytical method for the analysis of stable and unstable fractures has been applied to some pipes.

2. Plate Fracture Test under Tensile Load [14]

In this section, we present the result of the plate tests. As test specimens, we used twenty center cracked plates of Type 304 stainless steel with width of 300 mm and thickness of 10 or 5 mm. Using the high-compliance apparatus as well as the standard low-compliance machine, three types of loading were applied to these specimens.

Theoretical analyses were also carried out for several specimens to investigate the fracture behavior and the validity of Paris's tearing instability criterion [3]. At first, the J-integral resistance curve was generated from the experimental data of the low compliance tests. Then, with the tearing instability criterion based on the J-resistance curve, the points of fracture instability in the static high-compliance tests were predicted. In the analysis, three independent methods were employed. Finally, predictions of these analyses were compared with the experimental results.

2.1 Experiments

2.1.1 Specimens

The austenitic stainless steel (AISI Type 304) plates of 10 or 5 mm thickness were used for the test. The chemical composition and the mechanical properties are shown in Tables 2.1 and 2.2, respectively. Plate geometry and initial notch configuration are shown in Fig. 2.1. Twenty plates with a through-wall or surface notch were prepared. Notch geometry and test condition of these plates are summarized in Table 2.3.

The initial notches with width of 0.3 mm were introduced by electron discharge machining in the heat-affected zone of three plates with weld or in the plain base metal of the rest. The maximum depth of the surface notch denoted by c in Fig. 2.1 was 0.3t or 0.7t, where t represents the plate thickness.

2.1.2 Test Conditions and Measurements

As shown in Table 2.3, three types of loading were applied in order to study the compliance and the dynamic effects on fracture behavior. The first was the static low-compliance test in which the plates were loaded quasi-statically with the standard low-compliance testing apparatus. The second was the static high-compliance test using the high-compliance testing apparatus specially made for this project. The sketch of the apparatus is shown in Fig. 2.2. Here, the test plates were quasi-statically loaded through the compliance device, which is composed of many disk springs and has the compliance of 10^{-4} mm/N. Finally, in the third type of the experiment, six plates were loaded dynamically with the high-compliance apparatus, where the impact load was applied by releasing the stopper.

Applied load, gross elongation (gauge length : 160 mm) and crack opening displacement were continuously recorded in the test. Stable crack growth amount was measured by observing the plate surfaces in the static low-compliance test. Since unstable crack extension was expected in the high-compliance tests, crack gauges were attached on the specimen surfaces to obtain the crack propagation velocity.

2.1.3 Test Results

The fracture behaviors of the specimens were completely dependent on the loading types. In the static low-compliance tests, cracks never became unstable until they penetrated through the whole specimen width. In the static high-compliance tests, crack extension became unstable after some slow crack extension in all the cases.

From the fracture surface observation after the tests, the fracture surface of the low compliance test specimens was found to have macroscopically plane appearance, while in the surface of the static high-compliance test specimens, the changes from plane to slanting surfaces were observed. It became clear from the high speed photographs that the changes from plane to slanting surfaces were roughly corresponding to the transition from stable to unstable crack extensions. In the case of the dynamic high-compliance tests, negligible or very small plane surface was observed and almost all of the fracture surface was of slanting type.

The values of the maximum load for all the specimens are summarized in Table 2.3. It should be noted that these for the dynamic high-compliance test are the values of pre-load applied to the compliance device and set such that its displacement by pre-loading became to be about the maximum total displacement observed in the corresponding static high-compliance test.

It was observed from the break times of the crack gauges that the velocity of unstable crack growth increased with the crack extension and reached about 10 m/sec at penetration.

As for the surface notched specimens, the ductile crack seemed to penetrate first the plate wall, then extends in the direction of the plate width. Comparing with the specimens without weld, these with weld exhibited little difference concerning the fracture behavior including the instability point.

2.2 Theoretical Analyses

2.2.1 Outline of the Tearing Instability

We consider here a center cracked plate connected in series with a spring which has compliance C_M per unit thickness of the plate (see Fig. 2.3). The instability condition can be defined as follows

$$\frac{d\Delta_T}{da} \leq 0 \qquad (1)$$

where Δ_T is the total displacement and a is the half crack length. Δ_T can be written as follows

$$\Delta_T = \Delta + P\,C_M \qquad (2)$$

where P is the load per unit thickness of the plate and Δ is its displacement. Using eqs.(1) and (2), the instability condition can be rewritten as follows

$$C_M \geq -\frac{d\,\Delta}{d\,P} \qquad (3)$$

where $dP \leq 0$ is used as a necessary condition for instability. Therefore, if the relation of load and load point displacement of the cracked body is known, the point of instability will be estimated easily from eq.(3).

On the other hand, when we need to analyze the stability of crack extension in the structure whose deformation behavior is unknown, the material resistance curve is required. As the parameter characterizing the crack extension in the presence of large-scale plasticity, the J-integral and the crack tip opening angle are considered by many investigators to be most promising. If the J-controlled crack growth conditions [4] are satisfied, then the stable crack extension is controlled by the J-resistance curve as follows

$$J(a,P) = J_{mat}(\Delta a) \tag{4}$$

where J is the applied J-integral (crack driving force), J_{mat} is the value on the material J-resistance curve which represents the material resistance against the crack extension and Δa is the crack extension. In this equilibrium state, the Paris's instability criterion [3] is represented by

$$\left(\frac{\partial \omega}{\partial a}\right)_{\Delta_T} \geq \frac{dJ_{mat}}{da} \tag{5}$$

In the present work, the J-controlled crack growth was assumed and the stability of crack extension was analyzed based on eq.(5).

2.2.2 Numerical Analyses

(a) Three Parameter Method

At first, the J-resistance curves were generated from the record of the low compliance tests. Rice et al. [18] derived a formula to calculate the J-integral for center cracked specimens which is given by

$$J = G + \frac{1}{c}\left(\int_0^{\Delta_p} P\, d\Delta_p - \frac{1}{2} P\, \Delta_p\right)$$

$$= G + \frac{1}{c}\left(\int_0^{\Delta} P\, d\Delta - \frac{1}{2} P\, \Delta\right) \quad \left(\int_0^{\Delta_e} P\, d\Delta_e = \frac{1}{2} P\, \Delta_e\right) \tag{6}$$

where G is the linear elastic energy release rate, c is the remaining ligament length at each side, and Δ_e and Δ_p are respectively the elastic and the plastic contributions of the load point displacement. Equation (6) may be correct only for nongrowing cracks since the change of ligament length is not considered. Garwood et al. [19] proposed a formula for the J-integral value of growing cracks in bending specimens. Similarly as Garwood et al., a recurrence equation for a center cracked specimen is obtained as follows

$$J_{n+1} = \frac{1}{c_n}\left(J_n c_{n+1} + G_{n+1} c_{n+1} - G_n c_n + \frac{1}{2} P_n \Delta_{n+1} - \frac{1}{2} P_{n+1} \Delta_n\right) \tag{7}$$

where subscripts indicate the incremental step. Using eq.(7), the J-integral value can be calculated only from the relation of the load, the load point displacement and the ligament length. Thus the technique is often called as the three parameter method.

The J-resistance curves obtained from experimental data of the static low-compliance tests together with eq.(7) are shown in Fig. 2.4. From the figure, it can be seen that little difference exists between the four curves and the initial notch ratio and the plate thickness give relatively small influence on the relation within this test range. It should be noted that the crack length was measured at the surface of specimens so that no consideration for the crack tunneling was given. From the figure, the value

of J-integral at the crack initiation was found to be 0.95 - 1.63 MJ/m^2 and that of $\frac{dJ_{mat}}{da}$ 110 - 147 MJ/m^3 with the least square approximation. Thus, in the stability analysis described shortly, the values of $\frac{dJ_{mat}}{da}$ were assumed to be 136 MJ/m^3 and 110 MJ/m^3 for t = 10 mm and t = 5 mm, respectively.

For the applied $\frac{dJ}{da}$ under the condition Δ_T= constant, we used the equation derived by Hutchinson and Paris [4]. The variations of $(\frac{\partial J}{\partial a})_{\Delta_T}$ with crack extension for the static high-compliance tests are plotted in Figs. 2.5 - 2.8. In these figures, those of $\frac{dJ_{mat}}{da}$ are also shown. In these figures, the instability points are predicted as the intersection of two curves, which are indicated by the vertical lines in the figures. The lengths of the stable crack growth estimated from the fracture surfaces are also shown for comparison in these figures.

(b) Fully Plastic Solution Method

Shih and Hutchinson [20] proposed a simple estimation scheme for the J-integral value for plane stress center cracked plates using the fully plastic solutions together with the linear solutions. In the application of this method, the Kamberg-Osgood type uniaxial stress-strain relation are assumed as follows

$$\frac{\epsilon}{\epsilon_0} = \frac{\sigma}{\sigma_0} + \kappa(\frac{\sigma}{\sigma_0})^n \qquad (8)$$

where ϵ, ϵ_0 ,σ and σ_0 are the total strain, the reference strain, the uniaxial stress and the reference stress, respectively. κ and n are the material constants. For the material whose stress-strain relation is given by eq.(8), the J-integral and the residual load point displacement Δ^c are, rspectively, given by

$$J = J_{linear}(P,a) + J_{nonlinear}(P,a) \qquad (9)$$

$$\Delta^c = \Delta^c_{linear}(P,a) + \Delta^c_{nonlinear}(P,a) \qquad (10)$$

where subscripts 'linear' and 'nonlinear' represent the contributions of the elastic and plastic deformations to the total value, respectively. The nonlinear parts of these values were calculated using the fully plastic finite element solutions obtained by Shih and Hutchinson [20].

Using eqs.(9) and (10) with these solutions, $(\frac{\partial J}{\partial a})_{\Delta_T}$ is calculated as

$$(\frac{\partial J}{\partial a})_{\Delta_T} = (\frac{\partial J}{\partial a})_P - (\frac{\partial J}{\partial P})_a (\frac{\partial \Delta}{\partial a})_P / \{C_M + (\frac{\partial \Delta}{\partial P})_a\} \qquad (11)$$

In applying this method to the present material (Type 304 stainless steel), the material constants in eq.(8) are estimated as follows

σ_0=234MPa, ϵ_0=0.00126, κ=3.15, n=5

which give the best fit stress-strain relation in the range of $0<\varepsilon<0.1$.

Calculated values of $(\frac{\partial J}{\partial a})_{\Delta_T}$ for high compliance tests are shown in Figs. 2.5, 2.6 and 2.8 to compare with the results of the three parameter method. It can be seen from these figures that the values obtained by both methods are in good agreements with each other.

(c) Full Finite Element Analysis

Thirdly, the crack growth analysis by the full finite element method was made and the stability of crack growth was analyzed as well. The analysis was made for a rectangular panel shown in Fig. 2.9, which was modeled using the configuration of the specimen CB-3. Because of the geometrical symmetry, only a quarter part of the specimen was analyzed using 56 plane stress 8-noded isoparametric elements as shown in Fig. 2.10. As the boundary condition at the end of the specimen, uniform displacement in the direction of tension was given.

In the elastic-plastic calculation, von Mises yield condition, Prandtl-Reuss equation and the isotropic hardening rule were employed. As the algorithm of the elastic-plastic solution, partial stiffness method proposed by Marcal and King [21] was used.

The modulus of elasticity and Poisson's ratio were assumed to be 185.1 GPa and 0.3, respectively. In the yielded region, the multi-linear stress-strain approximation was used. As the criterion for crack extension, experimental relationship between the gauge displacement and crack extension amount was utilized.

The J-integral value was calculated according to the path integral definition at four contours as shown in Fig. 2.10. The variation of the J-integral calculated at each path with the crack extension is shown in Fig. 2.11. From this figure, it can be seen that the path dependency of the J-integral is increasing as the crack extends. One of the reasons for this may be due to the unloading accompanied with the crack extension. The J-resistance curve obtained by the three parameter technique explained above is also shown in this figure, which is seen to be somewhat higher than those by the full finite element method.

Next, the stability analysis of crack extension was made with the present finite element method with $(\frac{\partial J}{\partial a})_{\Delta_T}$ defined in eq.(11). Figure 2.12 shows the predicted points of instability for various compliance values which are given by the vertical arrow.

2.2.3 Comparison with the Experimental Data

Stability analysis of center cracked specimens was made by the above methods. Table 2.4 shows the comparison for the stable crack extension (i.e. the distance from the initial location of notch tip to the point of instability) between experimental and theoretical values. As the experimental date, two independent values are obtained for fracture instability; one is the length of crack extension up to the changing point of fracture surface (measured at the surface of specimens), and the other is the value estimated from the load-load point displacement relation using eq.(3). From this table, it can be seen that the predicted values given by the three

theories are closer to the experimental values estimated by eq.(3), than to those obtained from the observation of fracture surface.

2.3 Conclusions

Ductile crack extension experiment and stability analysis for center cracked plates of Type 304 stainless steel were made. From these, the following conclusions were obtained.

1) In the static high-compliance tests, unstable ductile crack growth was realized using the high-compliance testing machine.
2) With the record of static low-compliance tests, the J-integral resistance curves were calculated. The influences of initial notch ratio and thickness on the resistance curve were found to be rather small.
3) The points of fracture instability in the static high-compliance tests were estimated using the three independent methods. The predicted values coincided well with the experimental values, especially with those obtained from the load - load point displacement curves.

TABLE 2.1 CHEMICAL COMPOSITION (CHECK ANALYSIS)

(WT.%)

C	Si	Mn	P	S	Ni	Cr
0.06	0.63	0.92	0.028	0.006	9.00	18.27

TABLE 2.2 MECHANICAL PROPERTIES

ROOM TEMPERATURE		
0.2% PROOF STRENGTH (MPa)	TENSILE STRENGTH (MPa)	ELONGATION (%)
254	568	58

TABLE 2.3 TEST CONDITION AND MAXIMUM LOAD

TEST TYPE	TEST PLATE No.*1	PLATE THICKNESS (mm)	NOTCH GEOMETRY		MAXIMUM LOAD (kN)
			2a/2w*2	c/t*3	
STATIC LOW-COMPLIANCE TEST	CB-1	10	0.5	1	593
	CB-3	5	0.5	1	303
	CB-5	10	0.7	1	374
	CB-7	10	0.3	1	818
	CB-17	10	0.5	0.7	765
STATIC HIGH-COMPLIANCE TEST	CB-2	10	0.5	1	646
	CB-4	5	0.5	1	337
	CB-6	10	0.7	1	457
	CB-8	10	0.3	1	890
	CB-15	10	0.5	0.7	862
	CB-16	10	0.5	0.3	1294
	CBW-1	10	0.5	1	627
DYNAMIC HIGH-COMPLIANCE TEST	CB-9	10	0.5	0.7	1119
	CB-10	10	0.5	0.3	1862
	CB-11	10	0.5	1	851
	CB-12	5	0.5	1	540
	CB-13	10	0.7	1	699
	CB-14	10	0.3	1	1217
	CBW-2	10	0.5	1	846
	CBW-3	5	0.5	1	491

*1 W INDICATES WELD SPECIMEN

*2 2a: NOTCH LENGTH, 2w: PLATE WIDTH

*3 c: NOTCH DEPTH, t: PLATE THICKNESS

TABLE 2.4 COMPARISON BETWEEN EXPERIMENTAL AND THEORETICAL VALUES OF STABLE CRACK EXTENSION

TEST PLATE	STABLE CRACK EXTENSION (mm)				
	EXPERIMENTAL		THEORETICAL		
	FROM FRACTURE SURFACE	FROM EQ.(3)	THREE PARAMETER METHOD	FULLY PLASTIC SOLUTION	FULL FINITE ELEMENT METHOD
CB-2	25	17.0	21.4	18.3	15.8
CB-4	30	21.6	20.0	23.0	24.2
CB-6	10	7.6	5.6	-	-
CB-8	30	17.6	20.5	20.5	-

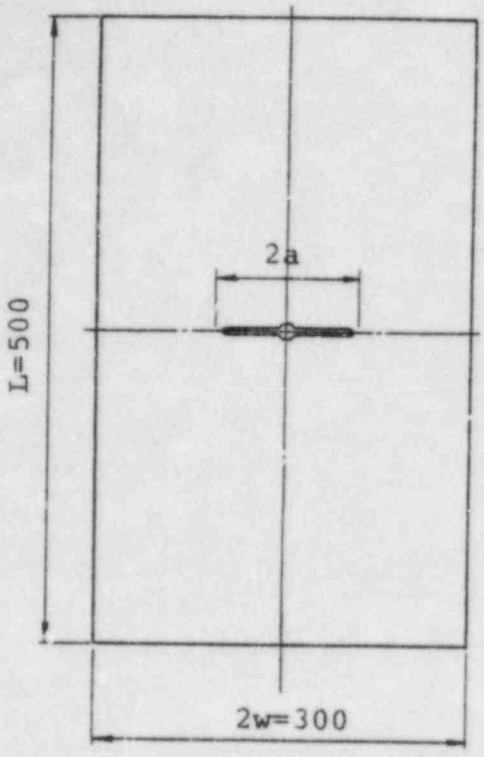

(A) NON-WELD TYPE TEST PLATE

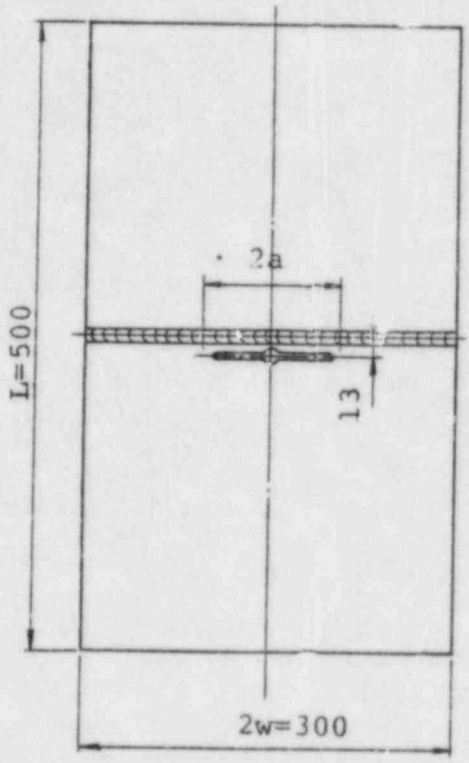

(B) WELD TYPE TEST PLATE

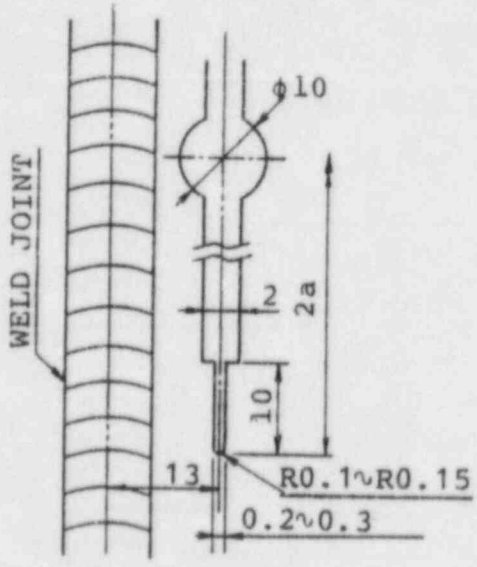

(C) DETAILS OF THROUGH-WALL NOTCH

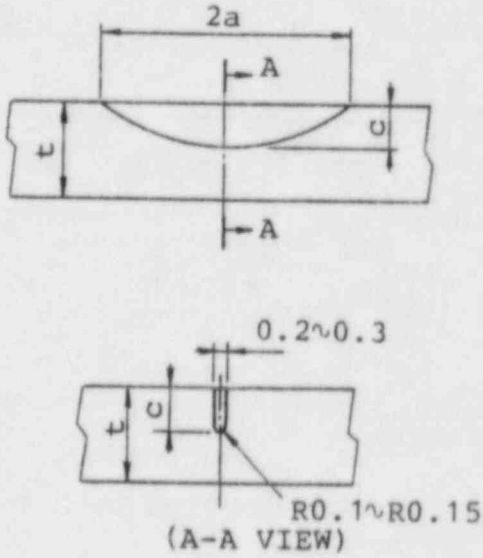

(D) DETAILS OF PART-THROUGH NOTCH

UNIT: mm

FIGURE 2.1 GEOMETRY OF TEST PLATE AND NOTCH

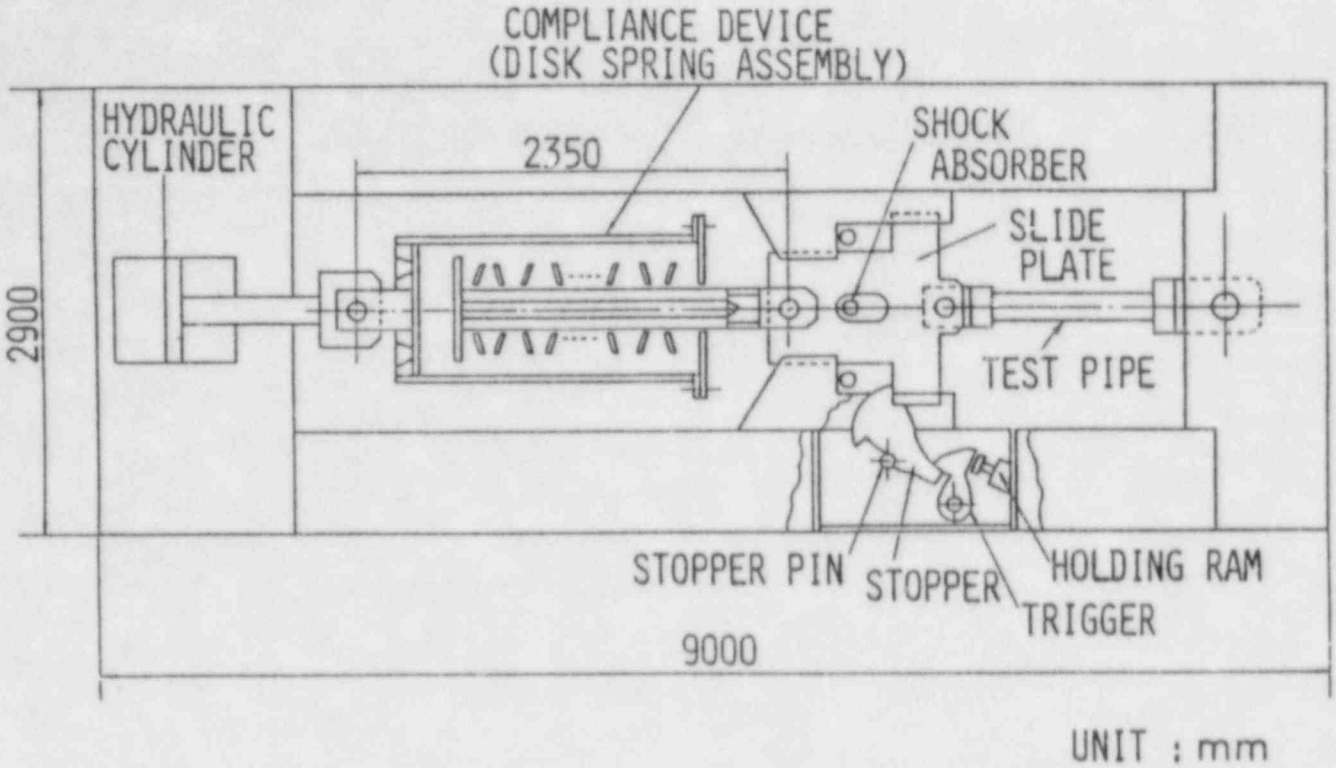

FIGURE 2.2 OUTLINE OF HIGH COMPLIANCE TEST APPARATUS

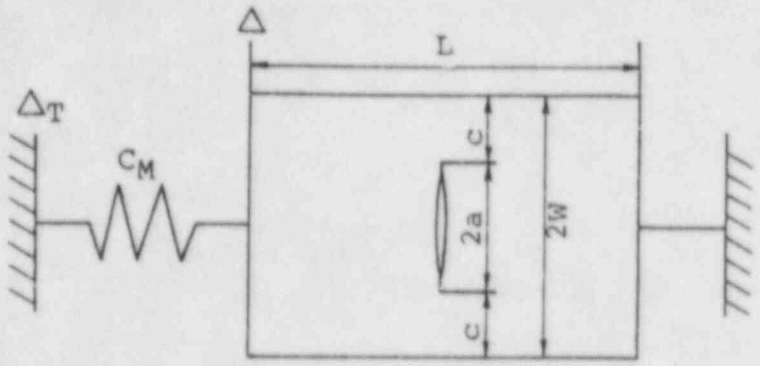

FIGURE 2.3 A CENTER CRACKED SPECIMEN CONNECTED IN SERIES WITH A LINEAR ELASTIC SPRING

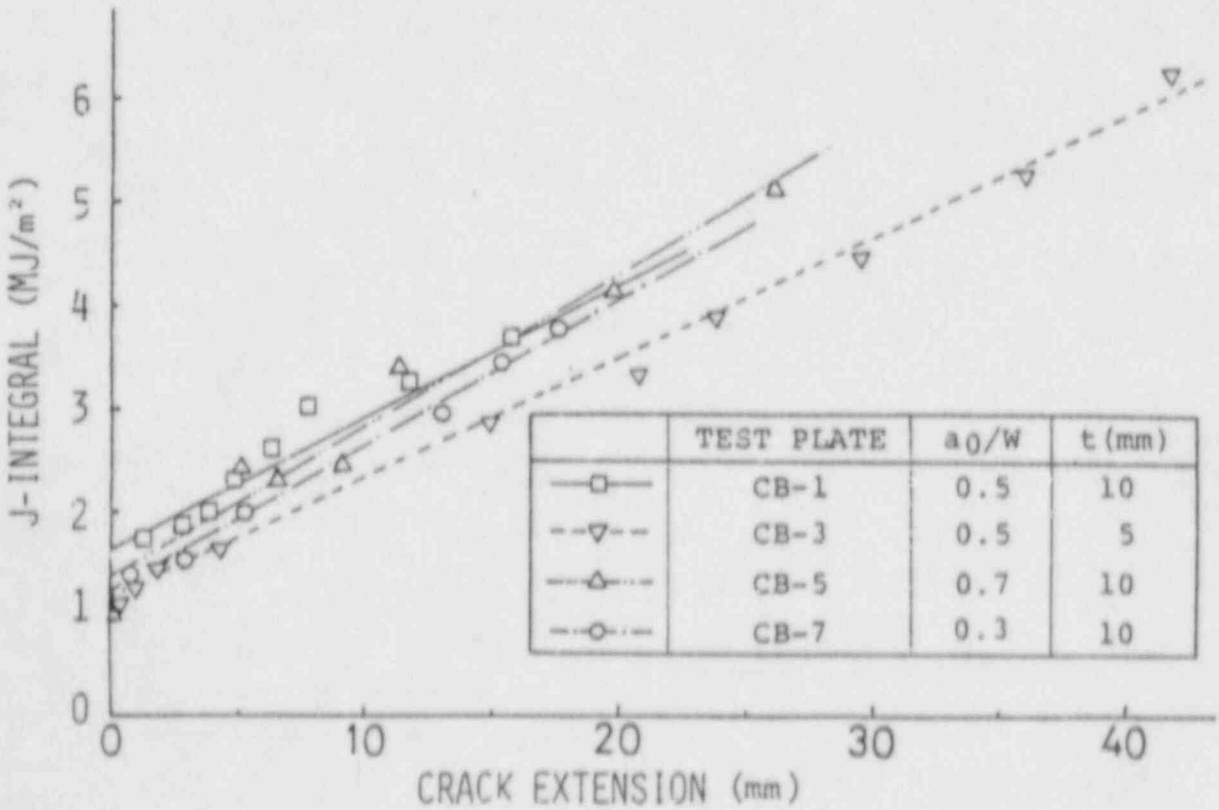

FIGURE 2.4 J-RESISTANCE CURVES DERIVED FROM THREE PARAMETER METHOD

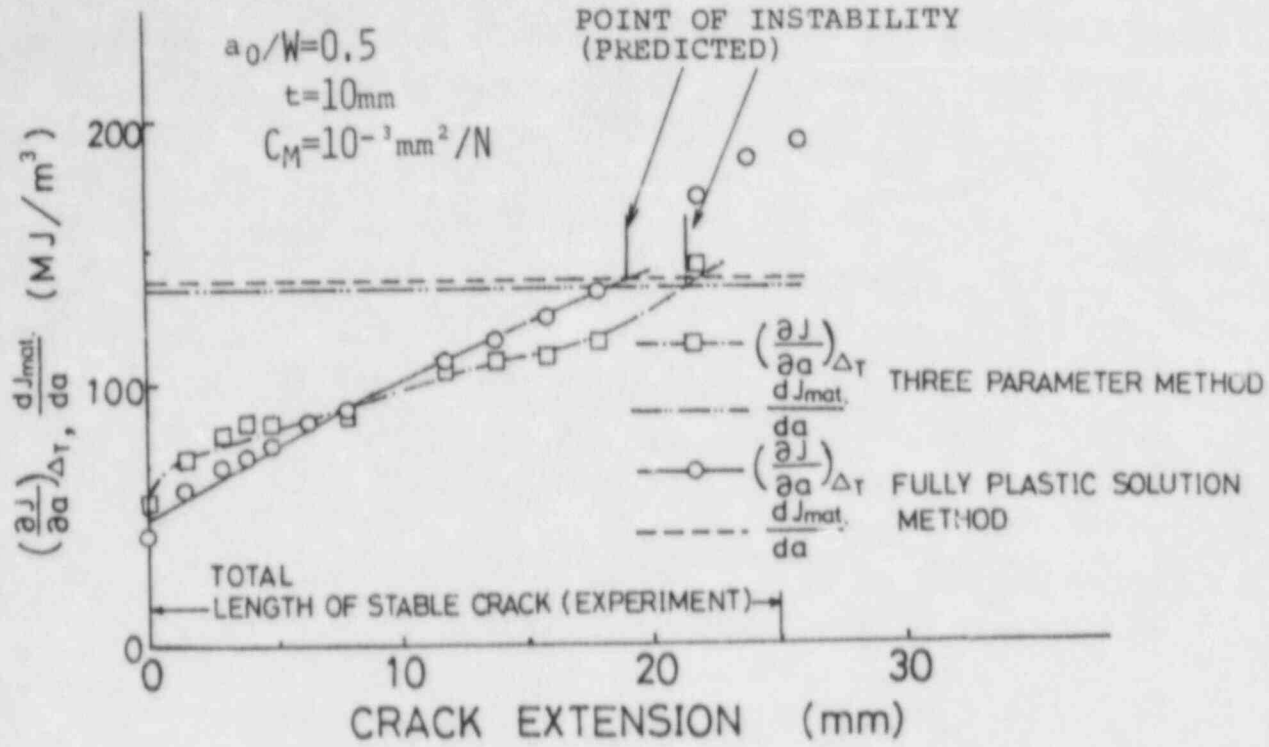

FIGURE 2.5 VARIATION OF $(\frac{\partial J}{\partial a})_{\Delta_T}$ WITH CRACK EXTENSION (CB-2)

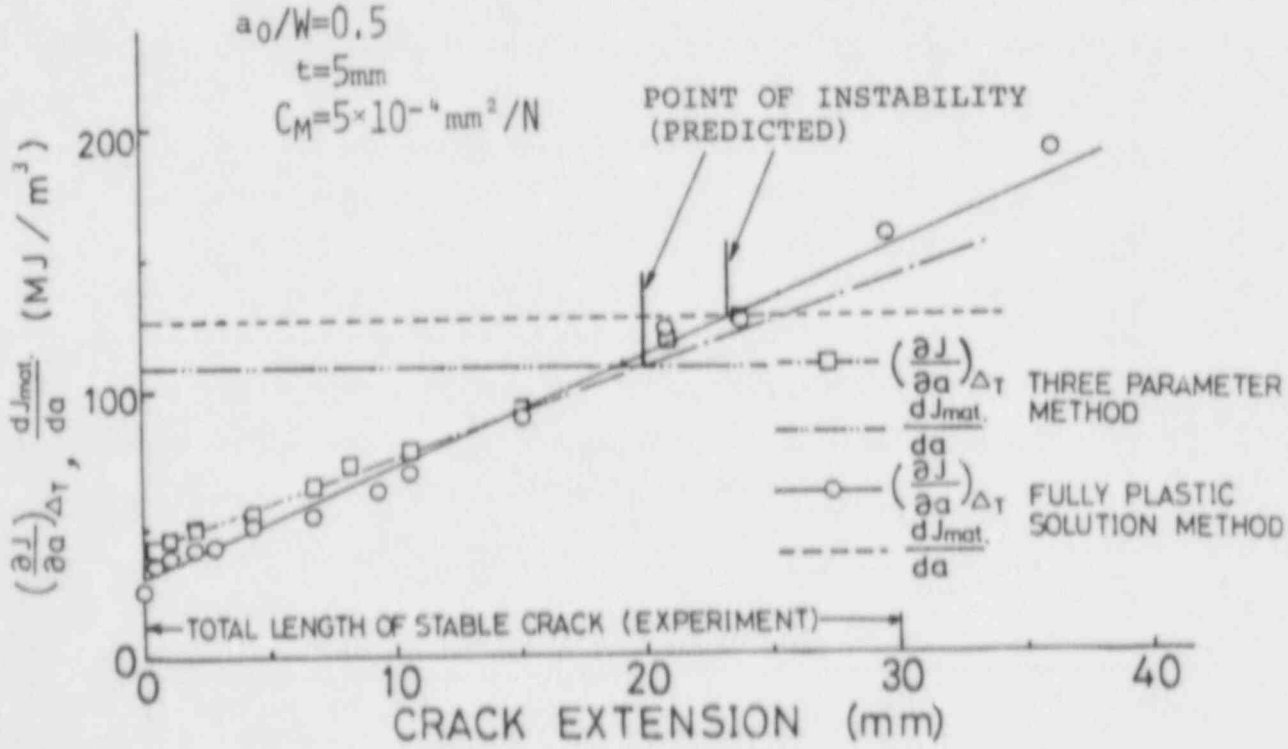

FIGURE 2.6 VARIATION OF $(\frac{\partial J}{\partial a})_{\Delta_T}$ WITH CRACK EXTENSION (CB-4)

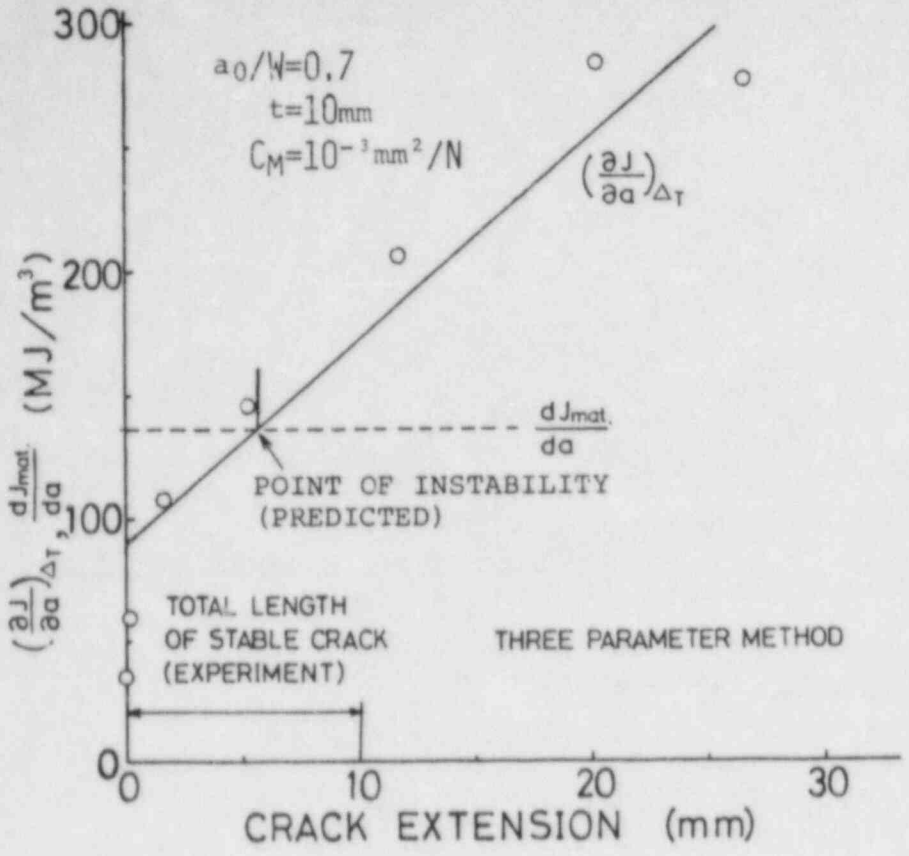

FIGURE 2.7 VARIATION OF $(\frac{\partial J}{\partial a})_{\Delta_T}$ WITH CRACK EXTENSION (CB-6)

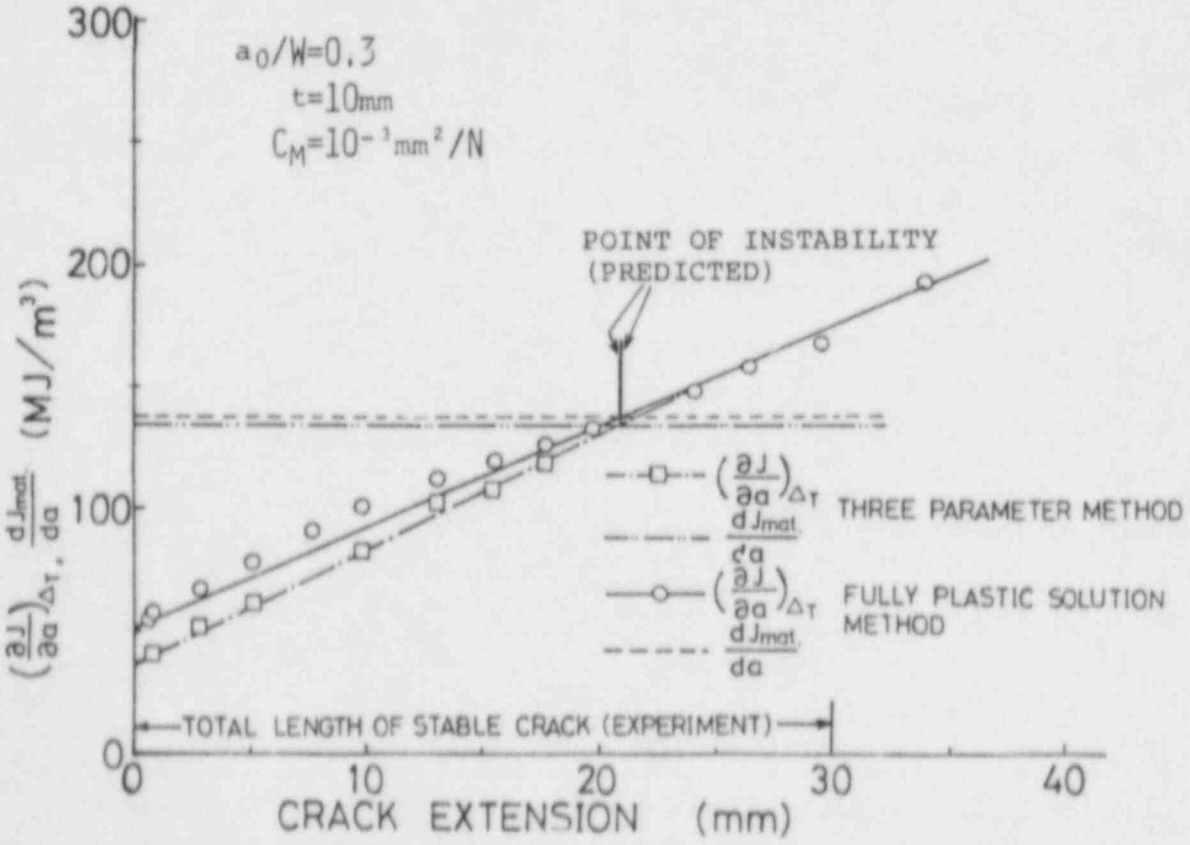

FIGURE 2.8 VARIATION OF $(\frac{\partial J}{\partial a})_{\Delta_T}$ WITH CRACK EXTENSION (CB-8)

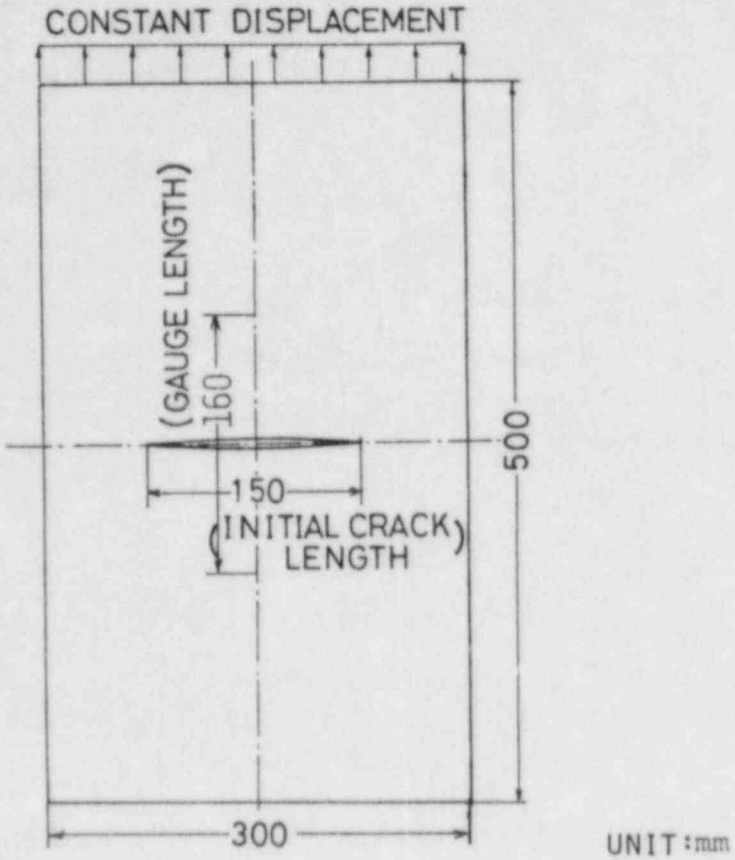

FIGURE 2.9 CRACKED PANEL USED FOR FULL FINITE ELEMENT ANALYSIS

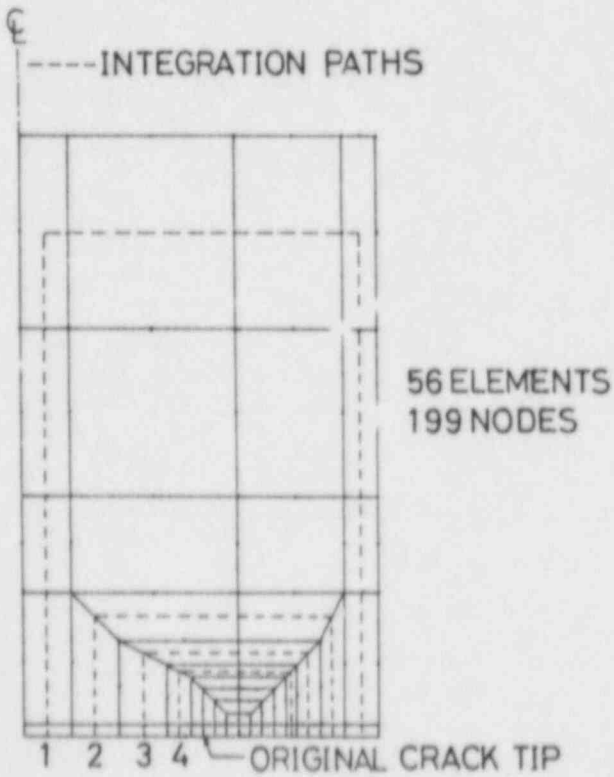

FIGURE 2.10 FINITE ELEMENT BREAKDOWN AND INTEGRATION PATHS FOR J-INTEGRAL

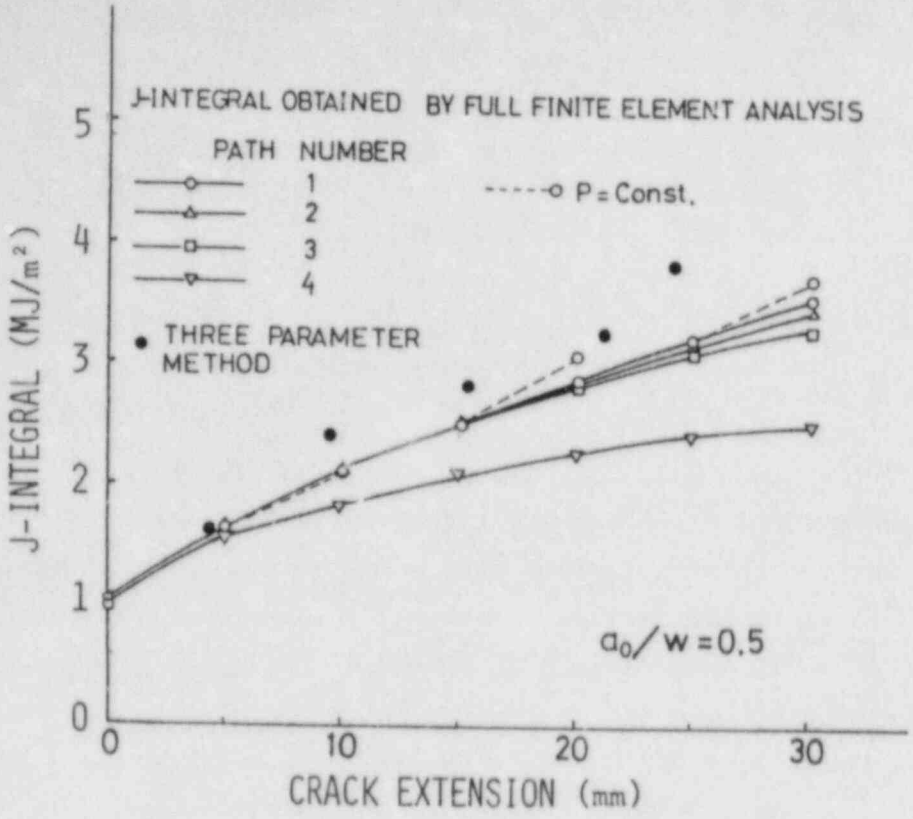

FIGURE 2.11 VARIATION OF J-INTEGRAL VALUE WITH CRACK EXTENSION

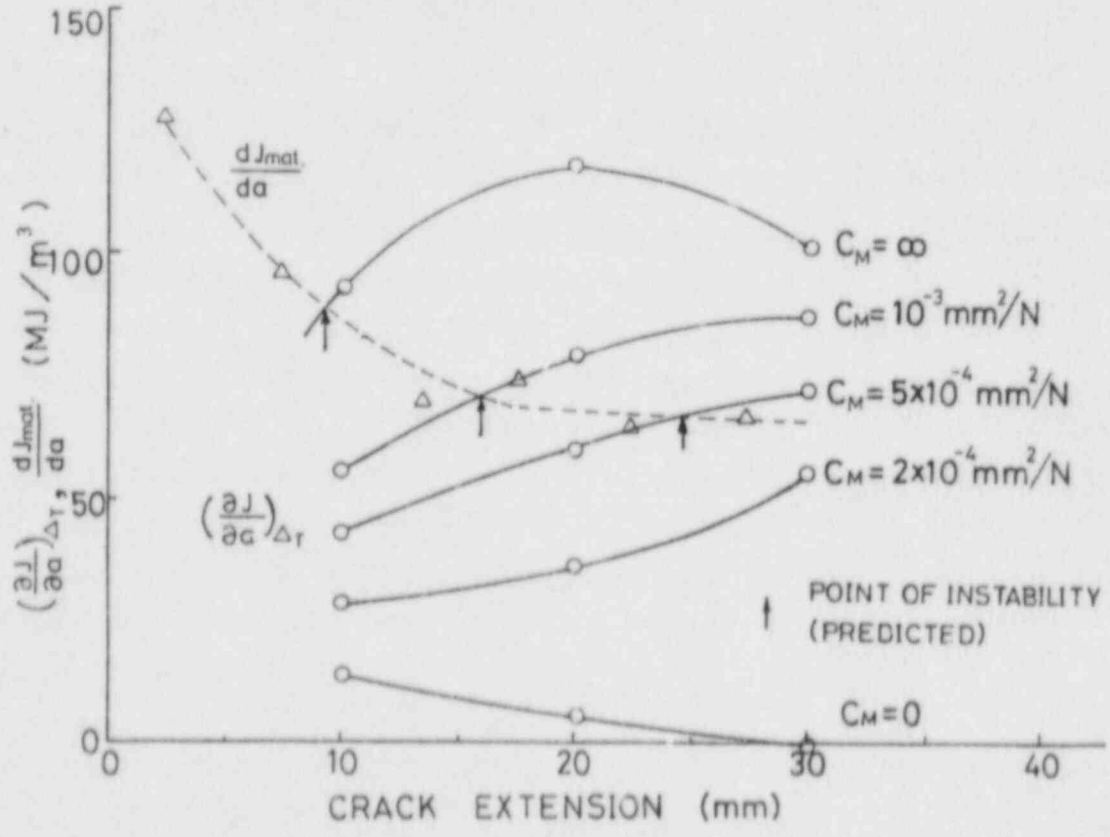

FIGURE 2.12 VARIATION OF $\left(\frac{\partial J}{\partial a}\right)_{\Delta_T}$ WITH CRACK EXTENSION ($a_0/W=0.5$, FULL FINITE ELEMENT METHOD)

3. Pipe Fracture Test under Tensile Load [16]

The results of the pipe fracture experiment under the low and high-compliance tensile loadings are given here. Twenty pipes with a through-wall or part-through initial notch were tested under three different types of loadings.

Theoretical considerations on stable crack growth and instability of the tested pipes are also shown in this section. Theoretical analyses utilized the three-dimensional finite element method as well as a simplified method.

3.1. Experiments

3.1.1 Specimens

The austenitic stainless steel (AISI Type 304) pipes of 6 inch and schedule 80 were used for the test. The chemical composition and the mechanical properties of the material are shown in Tables 3.1 and 3.2, respectively. Pipe geometry and initial notch configuration are shown in Fig. 3.1. Twenty pipes with an inner-surface or through-wall notch in the circumferential direction were prepared. Notch geometries and test conditions are summarized in Table 3.3.

The initial notches of 0.3 mm width were introduced by electron discharge machining in the heat-affected zone (HAZ) of three pipes with weld or in the plain base metal of the rest. The maximum depth of inner-surface notch, denoted by c in Fig. 3.1, is 0.3t or 0.7t, where t is the pipe thickness.

3.1.2 Test Conditions and Measurements

As shown in Table 3.3, three types of experiments were carried out in order to study the influence of compliance and dynamic effect on the fracture behaviors. The first was the static low-compliance test in which tensile load was applied quasi-statically with a standard low-compliance testing apparatus . The second was the static high-compliance test using the high-compliance apparatus shown in Fig. 2.2, in which the test pipes were quasi-statically loaded through a spring with the compliance of 10^{-4} mm/N. Finally, in the third type of the experiment, six pipes were loaded dynamically with the high compliance apparatus (the dynamic high-compliance test). These tests are conducted at room temperature or 285°C in air.

Applied load, gross elongations (gauge length : 250 mm) and crack opening displacement were continuously measured in the tests. Stable crack growth was measured by observing the pipe surface in the low-compliance test. Since unstable crack extension was expected in the high-compliance tests, crack gauges were attached on the pipe surface to measure the crack propagation velocity by their break time.

3.1.3 Test Results

Maximum loads for all the specimens are summarized in Table 3.3. The fracture behaviors of the specimens were found to be dependent on the loading types. Typical schematic drawings of the fracture surfaces for the three loading types are shown in Fig. 3.2.

In the static low-compliance tests, cracks never became unstable and fracture surfaces were flat in the entire regions. In the static high-compliance tests, both ductile flat and 45 degree shear parts were observed in the fracture surfaces. After stable ductile flat cracks of 50 to 70 mm length, the pipes exhibited rapid double-ended fracture. The reductions of wall thickness in the stable flat cracked area were about 50 % and those in the unstable shear cracked area were 25 %. In the case of the dynamic high-compliance tests, negligible or very small flat cracked surface was observed and almost all of the fracture surface was of shear fracture type.

The lengths of ductile flat crack for through-wall notched specimens are summarized in Fig. 3.3, which involves the static low-compliance test, the static high-compliance test and the dynamic high-compliance test, denoted respectively as ST, CM and DY. It can be seen from the figure that the difference between the non-weld and the weld type specimens is negligible.

Figure 3.4 shows the crack propagation velocity vs crack length in two pipes subjected to the static high-compliance loading which contain the through wall initial notches with circumferential angle of 30 and 120 degrees ,respectively. In this figure, CH-1 and CH-2 correspond to both sides of crack tip. Crack propagation velocities are seen to increase rapidly with the crack extension until about 10 m/sec.

3.2. Theoretical Analyses

3.2.1 Finite Element Analysis

Two three-dimensional elastic-plastic finite element codes named PIPE-6 and PIPE-16 have been developed to study the fracture behavior of the circumferentially cracked pipes tested.

(a) Models for Analysis

Taken as an example of calculation was the static high-compliance test specimen with a through-wall initial notch of 30 degrees. Figure 3.5 shows the finite element model for the calculation. To economize the computer cost, we modeled only the 1/12 part of the pipe, where the gross elongations between the points A and C and between A' and C' had been measured. Linearly interpolated along the circumferential direction, these elongation data were used to prescribe the displacement at the end of the model structure. The 6-noded and 16-noded isoparametric elements were used in PIPE-6 and PIPE-16, respectively. The finite element subdivisions for the both codes were, respectively, shown in Figs. 3.5(B) and 3.5(C).

The material properties used in the plate analyses were also utilized in this analysis.

(b) Methods for Analysis

Table 3.4 describes the theoretical backgrounds employed in the both codes. As can be seen in the table, the J-integral was calculated based on the virtual crack extension technique[22] in PIPE-16.

As a criterion for crack extension, the experimental relation between the gross elongations along the lines AB and A'B' indicated in Fig. 3.5 and the crack extension amount was utilized in PIPE-16 (i.e. Generation phase simulation). In PIPE-6, on the other hand, the constant Crack Tip Opening Angle (CTOA) criterion was used and the critical CTOA of 0.2 radian, which

had been obtained from the analysis for the center cracked plates, was employed (i.e. Application phase simulation). In the both calculations, the value of CTOA was evaluated from the crack opening displacement at the corner node nearest to the crack tip. The crack extension was realized by the nodal releasing technique in the both codes, in which the nodal reaction force was eliminated in several increments with the removal of nodal restraint.

(c) Numerical Results

Figure 3.6 shows the variations of the applied load and the crack opening displacement (COD) at the point 10 mm apart from the initial notch tip with the crack extension Δa. The applied load reached the maximum value after some stable crack growth and then decreased gradually with the stable crack growth. This maximum load was calculated to be 1303 kN (PIPE-16) or 1392 kN (PIPE-6), while the value of 1274 kN was obtained in the experiment. The values of the COD, increasing almost linearly with the crack extension, are shown in the figure with the experimental values.

Two fracture mechanics parameters, the J-integral and the CTOA, were obtained from the numerical solutions by PIPE-16, the code for generation phase simulation. The J-integral value, being about 1 MN/m at the crack initiation, increases remarkably with the stable crack growth as shown in Fig. 3.7. These characteristics in the J-resistance value for the pipe specimen are nearly the same as those of the center cracked plate specimens plotted in the figure. Figure 3.8 shows the CTOA resistance curve calculated using PIPE-16. As shown in the figure, the CTOA obtained by the present analysis is relatively close to the CTOA scattered band calculated for the center cracked plate specimens.

From these results, the J-integral and the CTOA approaches are considered to be effective criteria which can describe the crack initiation and stable crack extension, rather independent of the configuration of cracked specimens, within the scope of notched pipe and center notched plate under tension load.

Next, the instability point of the circumferential crack in the pipe specimen is predicted from the condition that the total displacement reaches the maximum value during the crack extension (see eq.(1)). The total displacement Δ_t is represented as the sum of the displacement of the pipe specimen Δ and that of the spring for high compliance itself Δ_c. Assuming the pipe displacement Δ to be nearly equal to the COD and using the relation $\Delta_c = C \cdot P$ with C being the compliance and P being the load, the total displacement Δ_t is obtained as a function of the crack extension amount Δa.

Figure 3.9 shows the variations of Δ_t, Δ and Δ_c with the crack extension obtained using the codes PIPE-6 and PIPE-16, respectively. Employing the instability condition of eq.(1), the stable crack extension amount up to the instability Δa_{inst} was predicted to be 48.9 and 51.3 mm by PIPE-6 and PIPE-16, respectively. Experimental measurement on the fracture surface showed that the unstable crack propagation began after the stable crack extension of 50 to 60 mm. Thus, the finite element solutions seem to predict the crack instability point with comparably good agreement with the experimental result, although the theories gave somewhat shorter stable crack extensions than the experiment.

3.2.2 Tearing Instability Analysis by the Simplified Method

Next, the fracture instability for the pipe with a circumferential through-wall crack was studied by the simplified method. This method utilizes the experimental relation between the net-section stress and the crack opening displacement. The net-section stress is used for the criterion of onset of the stable crack growth. The constancy of the CTOA and the stationariness of the total displacement are employed as the criteria of the stable crack propagation and the onset of the crack instability, respectively. The stable crack extension amount at the instability Δa_{inst} can be obtained as a function of the pipe dimensions (radius; R_m, thickness; t), the initial crack angle 2α or length $2a_0$, the material CTOA value and the compliance C_M. The detail of the analysis method was given in the reference [23].

Figure 3.10 shows the effects of the compliance on the nondimensional stable crack extension amount at the instability $\Delta a_{inst}/(\pi R_m - a_0)$, which is not dependent on the initial crack angle in this theory. As shown in the figure, the value of Δa_{inst} becomes smaller with the increase of the compliance. When the compliance is as small as $C_M = 10^{-6}$ mm/N, the crack propagation is almost stable within the whole region of the remaining ligament, i.e. $\Delta a_{inst} = (\pi R_m - a_0)$. On the other hand, the crack instability occurs after some amount of stable crack growth under the large compliance. For example, Δa_{inst} can be estimated to be about 12mm for the initial crack angle $2\alpha = 60°$ under the compliance of 10^{-2} mm/N. Experimental value of Δa_{inst} under the compliance of 10^{-4} mm/N is in good agreement with the calculated result. This figure also shows the accumulated frequency of compliance in the recirculation piping systems of a 1100 MWe BWR plant. The compliance of 10^{-4} mm/N used in the present pipe tests can be regarded as a relatively conservative value as compared with the compliances in the BWR piping system because about 80 per cent of the BWR piping system have the compliance less than 10^{-4} mm/N as shown in the figure.

3.3 Conclusions

The fracture behaviors of Type 304 stainless steel pipes with a circumferential crack were studied with the experiments and the numerical analyses. The following conclusions were obtained:

1) In the static low-compliance test, cracks extend stably showing the flat fracture surfaces. The changes from stable to unstable crack extension, which is characterized by the 45° shear fracture surfaces, are observed in the static high-compliance test as well as in the dynamic high-compliance test.
2) Maximum crack velocity in the unstable fracture region often exceeds 10 m/sec.
3) From the application and generation phase simulations by the finite element methods, it is found that the J-integral and the CTOA are

effective parameters for the crack initiation and the stable crack extension.

4) Crack instability is predicted from the stationariness condition of the controlled displacement, taking the effect of the compliance of the loading system into account, with either the detailed finite element analysis or the simplified method.

TABLE 3.1 CHEMICAL COMPOSITION (CHECK ANALYSIS)

(WT.%)

C	Si	Mn	P	S	Ni	Cr
0.05	0.50	1.51	0.026	0.003	9.30	18.30

TABLE 3.2 MECHANICAL PROPERTIES

ROOM TEMPERATURE			285°C		
0.2% PROOF STRENGTH (MPa)	TENSILE STRENGTH (MAa)	ELONGATION (%)	0.2% PROOF STRENGTH (MPa)	TENSILE STRENGTH (MPa)	ELONGATION (%)
284	588	67	167	431	38

TABLE 3.3 TEST CONDITION AND MAXIMUM LOAD

TEST TYPE	TEST PIPE No.*1	NOTCH GEOMETRY		MAXIMUM LOAD (kN)
		2α*2 (DEG)	c/t*3	
STATIC LOW-COMPLIANCE TEST	CP-1	30	1	1176
	CP-2	60	1	1039
	CP-3	90	1	909
	CP-12	60	0.7	1044
STATIC HIGH-COMPLIANCE TEST	CP-4	30	1	1278
	CP-5	60	1	1084
	CP-6	90	1	977
	CP-7	120	1	852
	CPW-1	60	1	1004
	CP-9H	60	1	725
	CP-10	60	0.7	1071
	CP-11	60	0.3	——
	CP-14H	60	0.7	840
	CPW-3H	60	1	753
DYNAMIC HIGH-COMPLIANCE TEST	CP-8	60	1	1115
	CPW-2	60	1	1107
	CP-13H	60	1	765
	CP-15	90	1	959
	CP-16	60	0.7	1143
	CP-17	60	0.3	1656

*1 W INDICATES WELD SPECIMEN
H INDICATES HIGH TEMPERATURE TEST (285°C)

*2 NOTCH ANGLE

*3 c: NOTCH DEPTH, t: PIPE THICKNESS

TABLE 3.4 METHOD FOR SOLUTION

COMPUTER CODE	PIPE-6	PIPE-16
ELEMENT TYPE	6-NODED ISOPARAMETRIC	16-NODED ISOPARAMETRIC
NUMBER OF NODES	330	456
NUMBER OF ELEMENTS	280	63
PLASTICITY THEORY	FLOW THEORY (ISOPARAMETRIC HARDENING)	
GEOMETRICAL NONLINEARITY	SMALL STRAIN	
CALCULATION SCHEME	TANGENT MODULUS (PARTIAL STIFFNESS)	
STRAIN HARDENING PROPERTY	BILINEAR APPROXIMATION	
J-INTEGRAL CALCULATION	———————	VIRTUAL CRACK EXTENSION METHOD
CRACK EXTENSION TECHNIQUE	NODAL RELEASING	
CRACK EXTENSION CRITERION	CRACK TIP OPENING ANGLE (CTOA)	GAUGE DISPLACEMENTS
SIMULATION TECHNIQUE FOR CRACK EXTENSION	APPLICATION PHASE	GENERATION PHASE

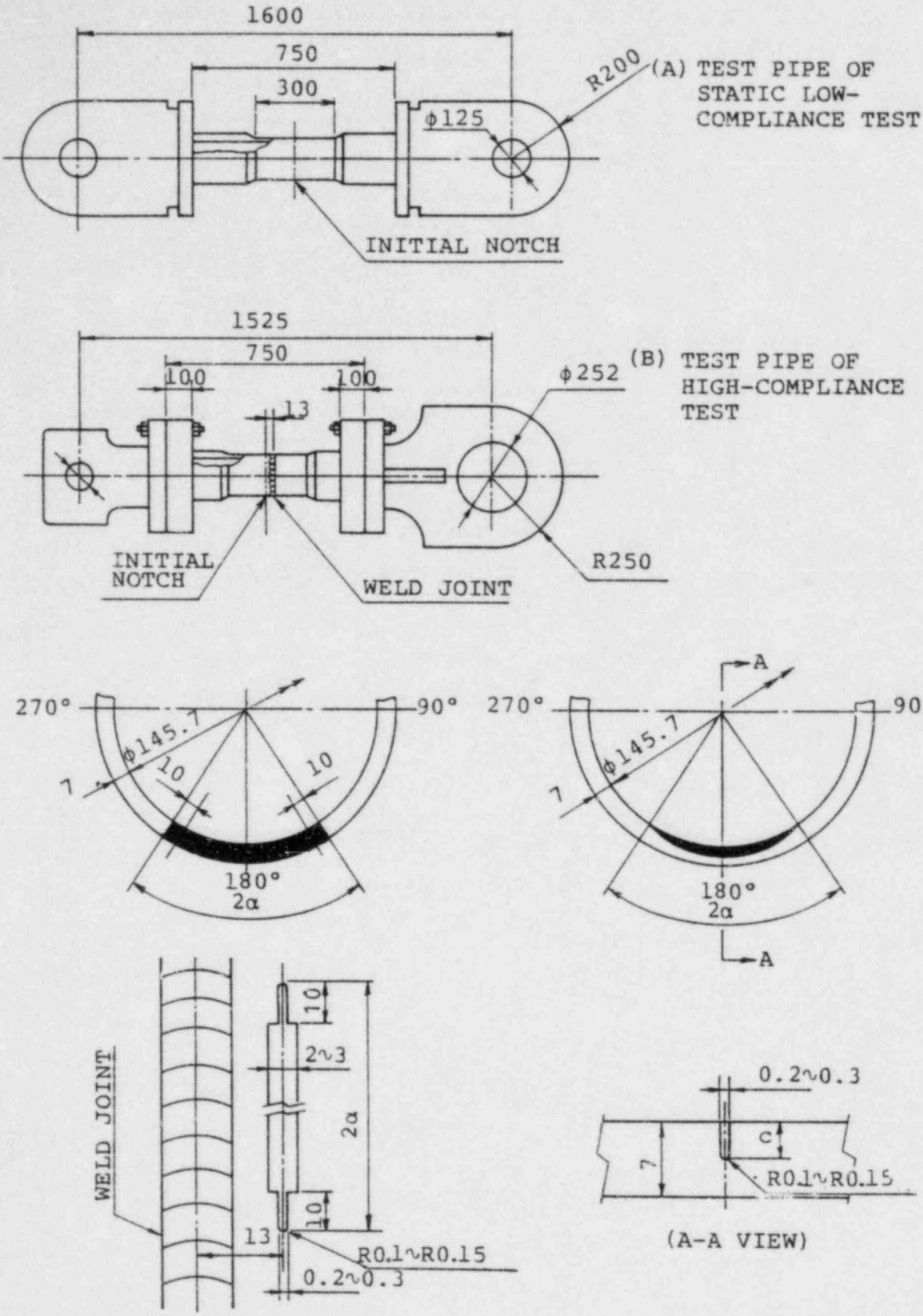

UNIT: mm

FIGURE 3.1 GEOMETRY OF TEST PIPE AND NOTCH

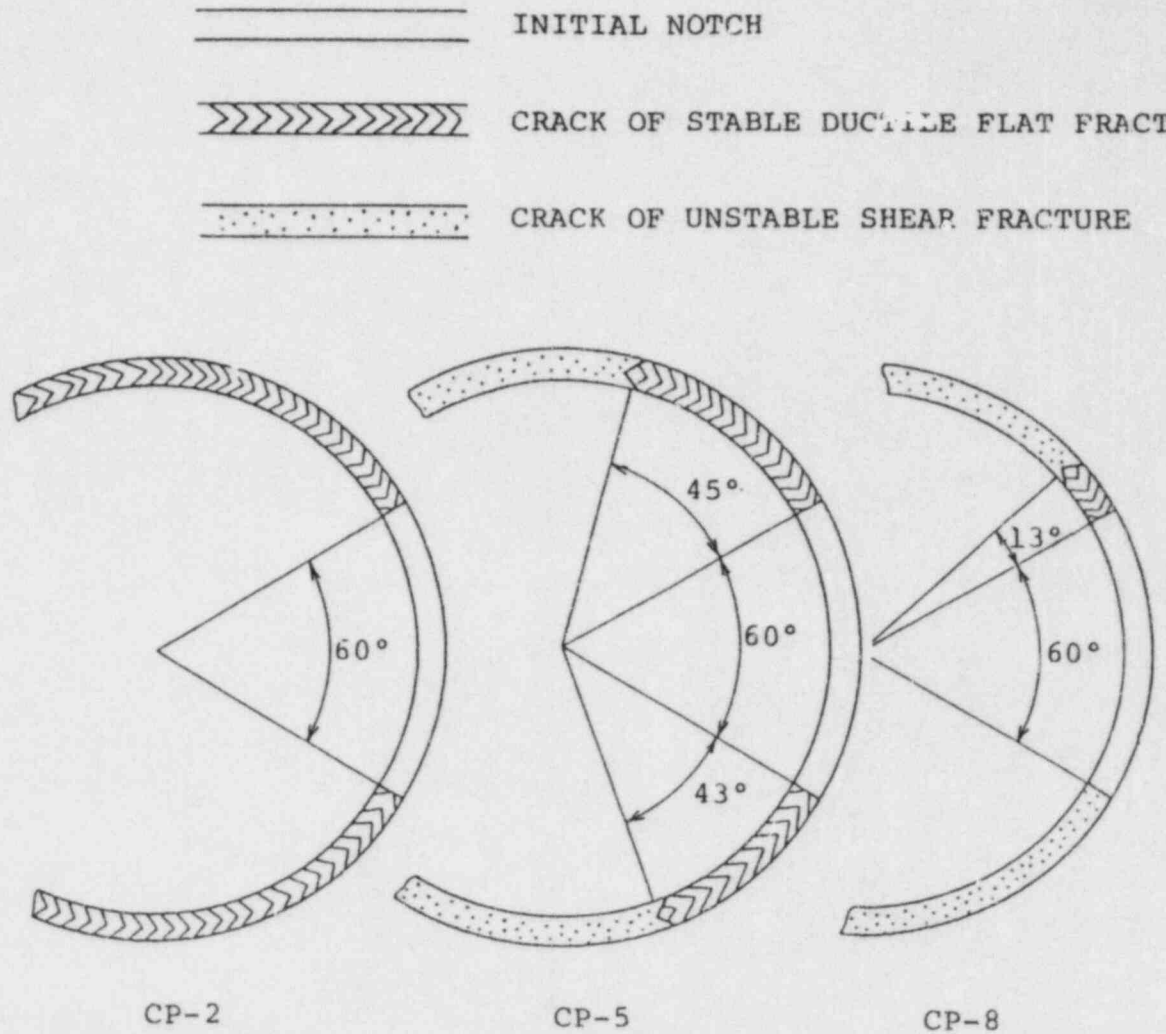

FIGURE 3.2 CROSS-SECTIONAL VIEW OF POST-FRACTURE SURFACE

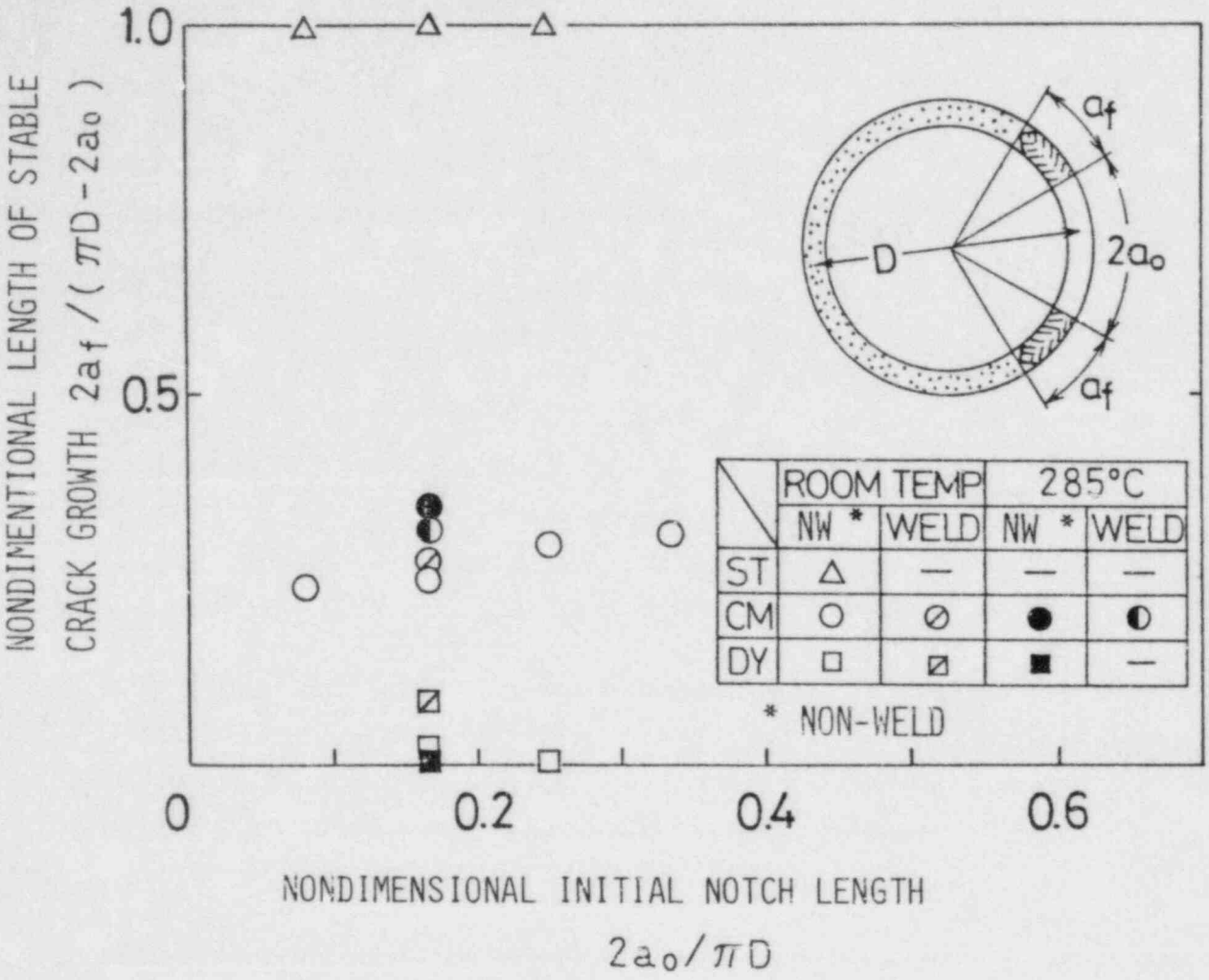

FIGURE 3.3 NONDIMENSIONAL LENGTH OF STABLE CRACK GROWTH VS. NONDIMENSIONAL INITIAL NOTCH LENGTH

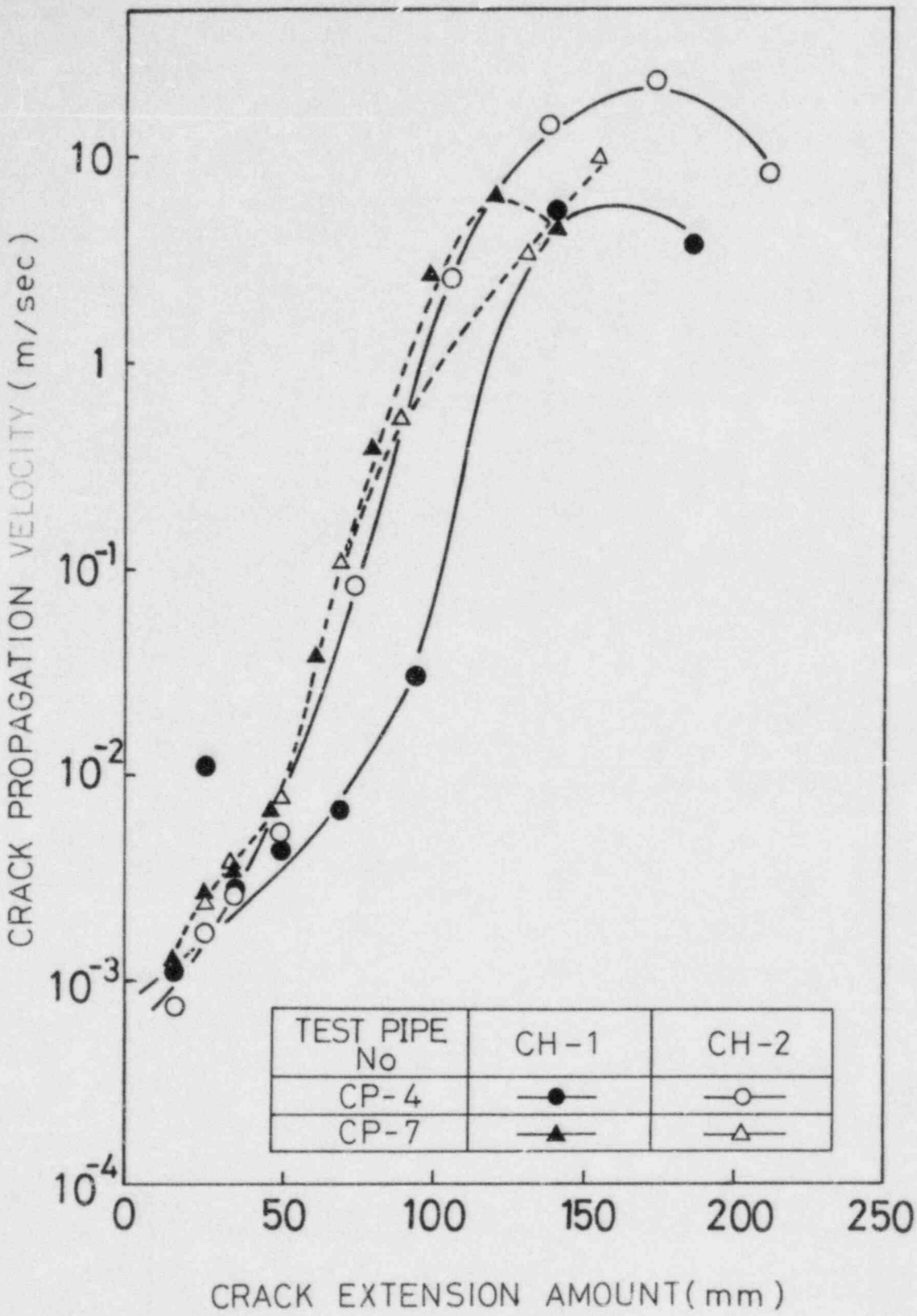

FIGURE 3.4 CRACK PROPAGATION VELOCITY OF TEST PIPE CP-4 AND CP-7

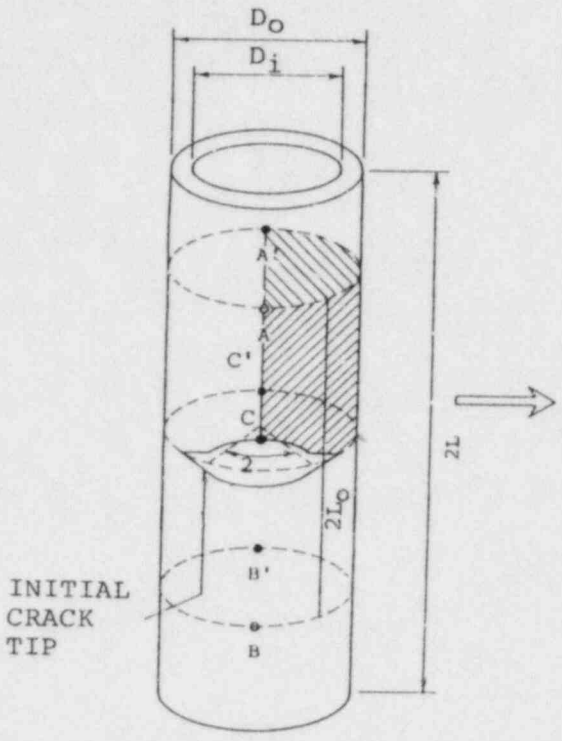

(A) PIPE MODEL FOR EXPERIMENT

D_i = 145.8 mm
D_o = 160 mm
L = 375 mm
L_o = 125 mm
α = 15 DEGREES

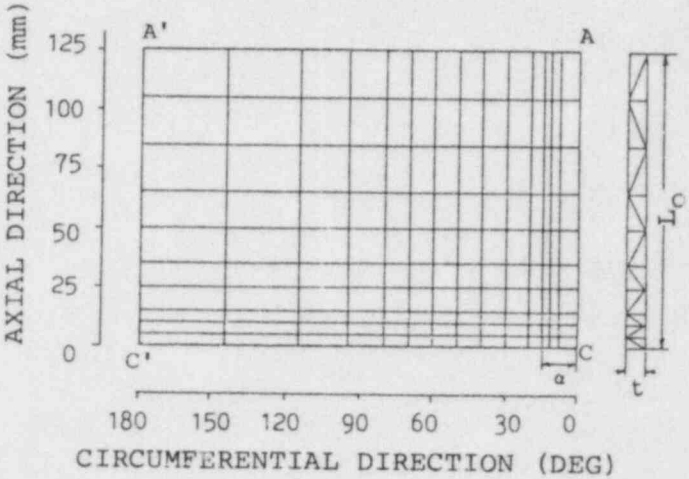

(B) FINITE ELEMENT SUBDIVISION FOR PIPE-6

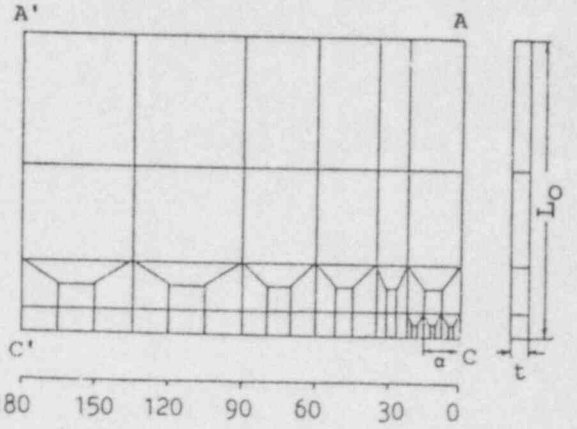

(C) FINITE ELEMENT SUBDIVISION FOR PIPE-16

FIGURE 3.5 FINITE ELEMENT FOR CRACKED PIPE

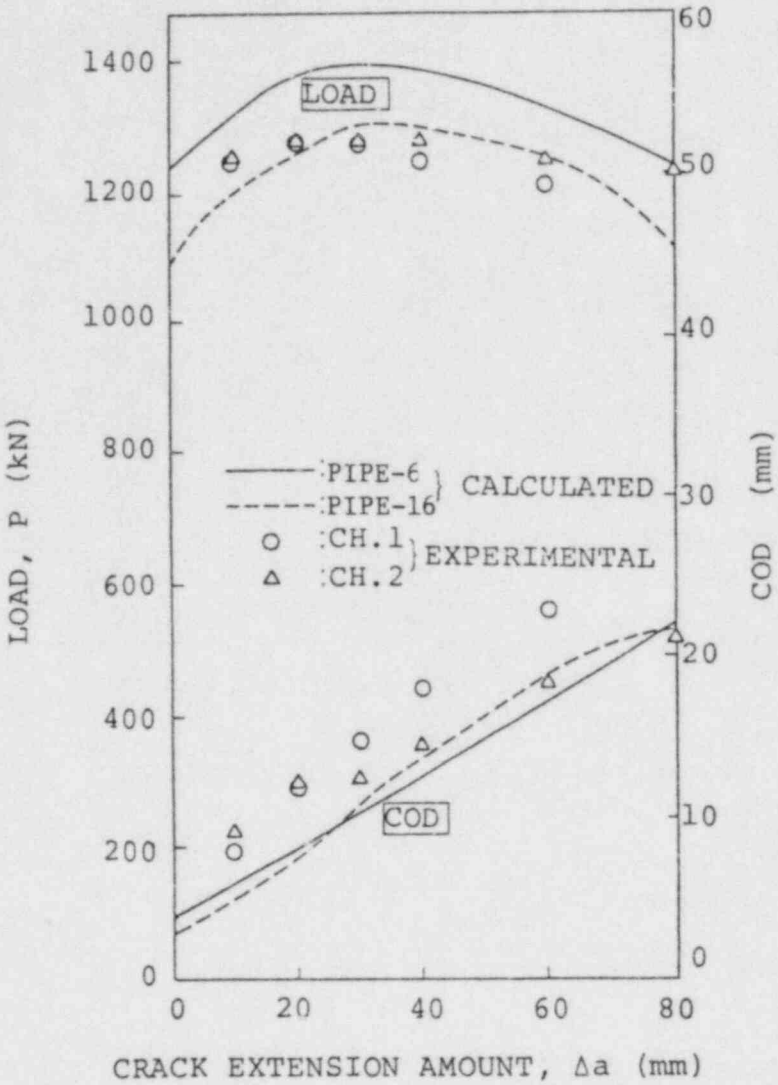

FIGURE 3.6 VARIATIONS OF LOAD AND CRACK OPENING DISPLACEMENT WITH CRACK EXTENSION (CP-4)

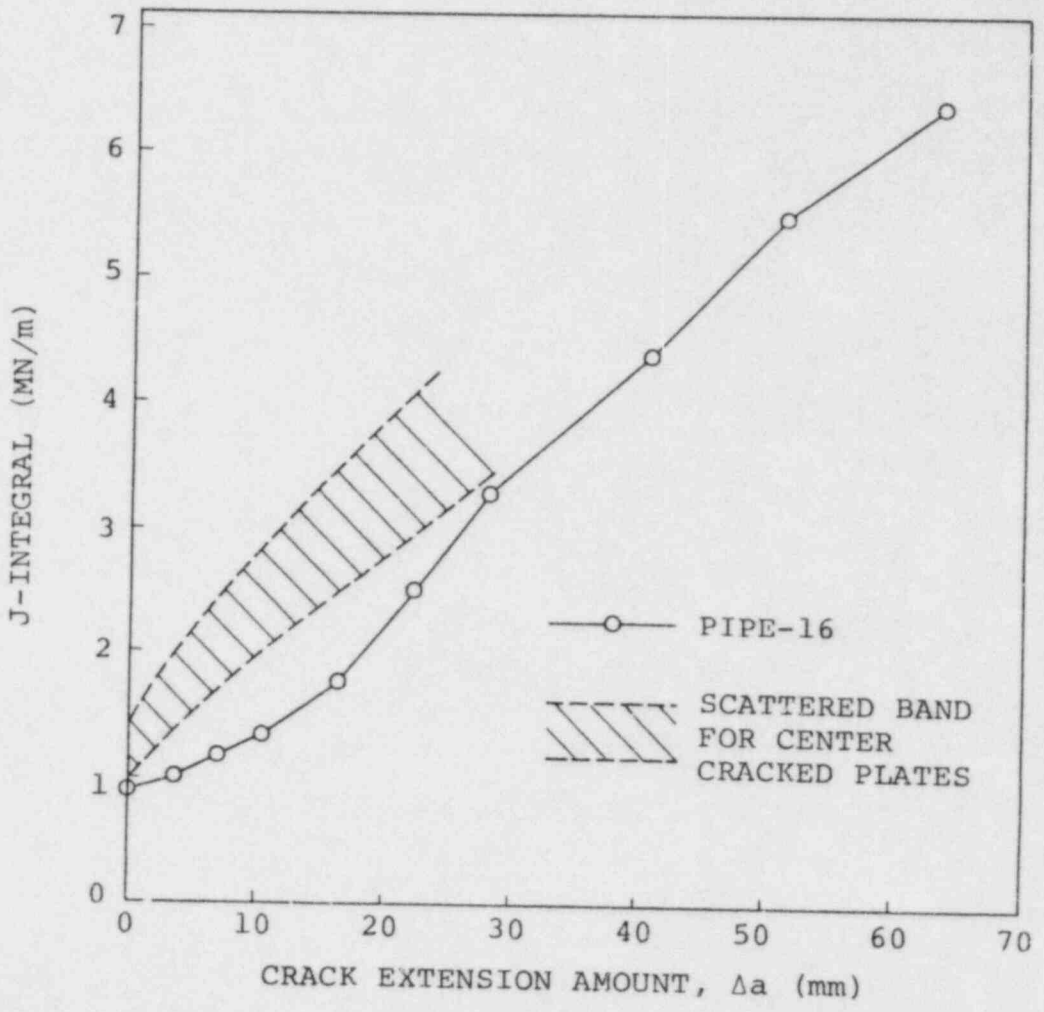

FIGURE 3.7 J-INTEGRAL VS. CRACK EXTENSION AMOUNT

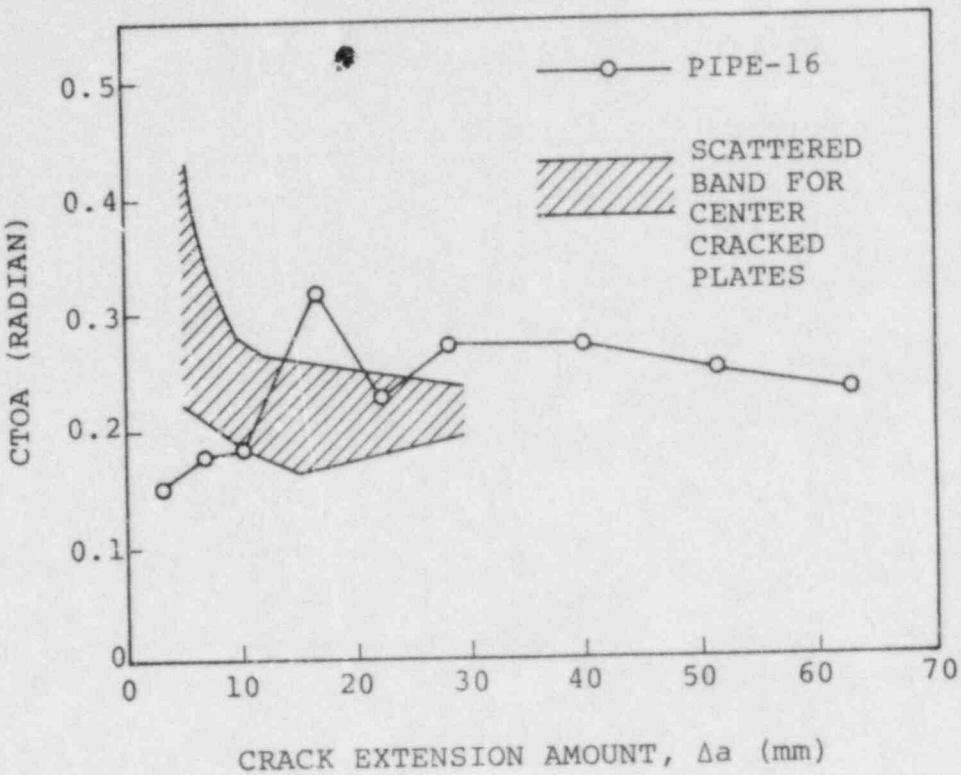

FIGURE 3.8 CTOA VS. CRACK EXTENSION AMOUNT

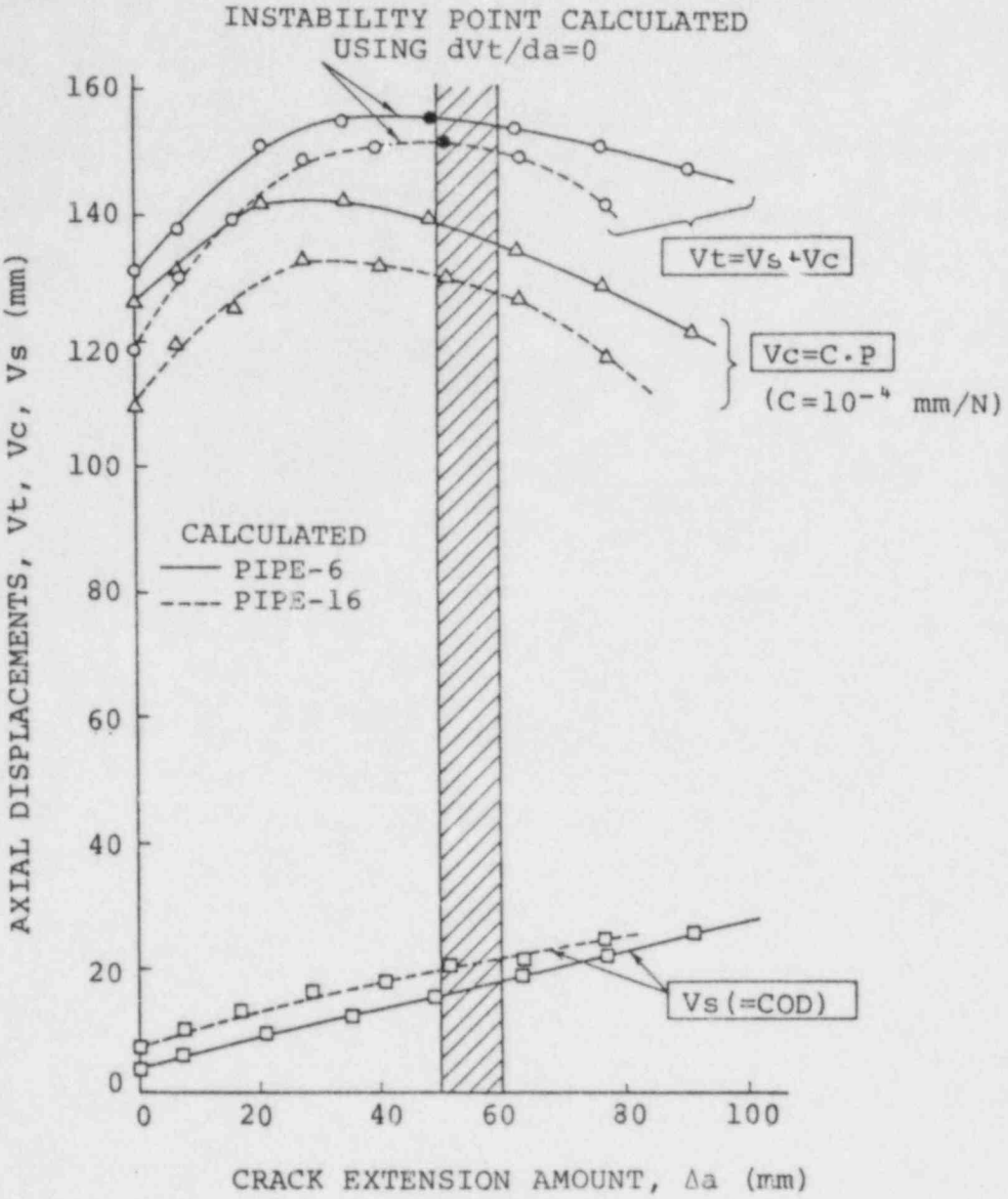

FIGURE 3.9 PREDICTION OF TEARING INSTABILITY (CP-4)

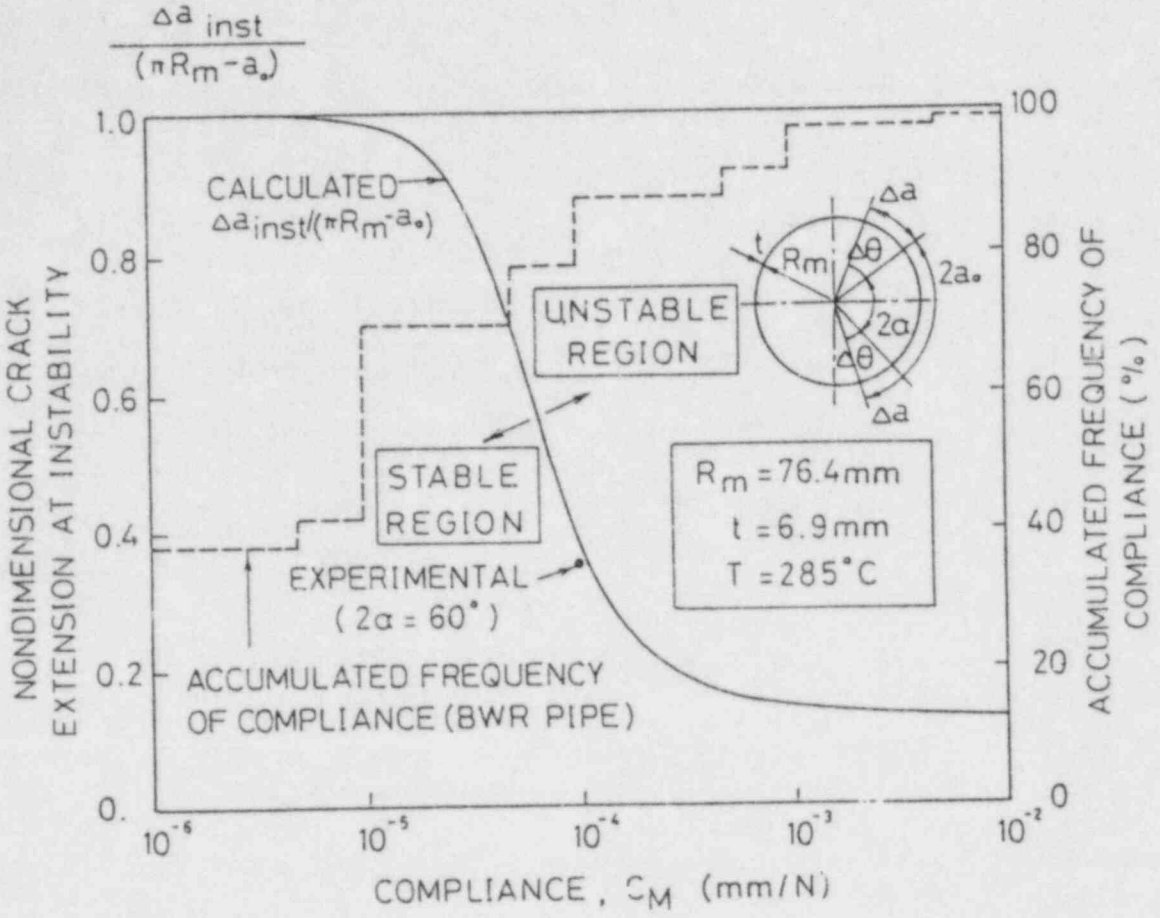

FIGURE 3.10 EFFECT OF COMPLIANCE ON CRACK INSTABILITY

4. Leak-Before-Break Test under High-compliance Loading Condition

In the preceding two sections, we presented the instability tests under the tensile load. However, to assess the leak before break condition with reality, the process of subcritical crack growth due to stress corrosion cracking combined with cyclic load must be considered. From this consideration, we performed the leak-before-break test for the part-through notched pipes under the presences of internal pressurized water and cyclic tensile load. From the tests, the bound for leak-before-break is clarified. In addition, the test results are used for the evaluation of margin for unstable fracture in the piping of various diameters.

4.1 Experiments

4.1.1 Specimens

The austenitic stainless steel (AISI Type 304) pipes of 4-inch schedule 80 were used as the test material. The chemical composition and mechanical properties of the steel are shown in Tables 4.1 and 4.2, respectively. Five test pipes with artificial inner-surface notches in the circumferential direction were prepared. A circular notch of 0.3 mm width was introduced in the heat affected zone of each welded pipe by electron discharge machining. Figure 4.1 shows the shape and dimensions of the test pipe in detail. The sizes of the initial notches are tabulated in Table 4.3.

4.1.2 Test Conditions and Measurements

Each pipe was set in the high-compliance testing machine shown in Fig. 2.2. The cyclic axial load shown in Fig. 4.2 was applied to the pipe in the BWR environment (the high temperature pure water of 285°C with 8 ppm dissolved oxygen and the internal pressure of 8.7 MPa). The axial load was cyclically applied until the leak was detected by the moisture detector installed near the test pipe or until the pipe fractured. The applied load and the oil pressure of the cylinder were monitored through the load cell and the pressure transformer, respectively. The nominal strains on the test pipe were measured with the high temperature strain gauges as shown in Fig. 4.1. Additionally, two crack gauges were used to estimate the time of crack penetration through the pipe wall.

4.1.3 Test Results

The leak-before-break behaviors were observed in the test pipes with the initial circumferential crack angles of 36°, 150° and 180°, i.e. the specimen numbers CPI-1, CPI-2 and CPI-3. The crack lengths along the outer surfaces were 4.5, 56 and 7 mm when the cracks penetrated through the pipe walls in the test pipes CPI-1, CPI-2 and CPI-3, respectively. The total load cycle numbers required before the leaks for these pipes were 187, 52 and 99, respectively. The steam leakages were detected at the increasing stage of the load for all these pipes.

On the other hand, in the test pipes with the initial circumferential crack angles of 240° and 360°, i.e. the specimen numbers CPR-1 and CPR-2, fast fracture occurred during the load holding. In other words, the leak-before-break was not realized in these pipes. The total load cycle numbers until fast fractures were 8 and 7 in the test pipes CPR-1 and CPR-2, respectively. Figure 4.3 shows the typical time records for the cases of the

leak-before-break and of fast fracture. As shown in Fig. 4.3(B), the instability was observed during the load holding.

After the test, dye penetrant examinations were performed to examine the crack growth along the inner surfaces of the pipes. In CPI-1, cracks of about 1 mm long were detected at the both initial notch tips in the pipe inner surface along the direction of notches. Another crack of about 6.5 mm long was also found near the notch tip region. A crack of about 2 mm was obserbed at one crack tip in the pipe inner surface of the test pipe CPI-3. No cracks were seen on the inner surface of the other pipes.

The cracked regions of all the test pipes were cut into small samples in order to assess the cracking mechanism. The macroscopic aspects of fracture surfaces are shown in Fig. 4.4. The IGSCC was observed throughout the initial crack front lines in the test pipes CPI-1 and CPI-2, while in the test pipe CPI-3 the IGSCC was partially seen at two isolated regions along the initial crack front line. This is maybe due to the nonuniformity of the degree of sensitization by welding along the notch front line.

Optical microscopic observations were carried out for small samples at the initial notch tip region of these pipes. Figure 4.5 shows the results for the test pipe CPI-3. Fracture surfaces of the test pipes CPR-1 and CPR-2 which fractured in unstable manner were examined by a scanning electron microscope. Figure 4.6 shows the results on the test pipe CPR-1.

These fractographic examinations revealed that the fracture surfaces of the test pipes CPI-1, CPI-2 and CPI-3 were of typical intergranular mode due to the IGSCC. As for the test pipes CPR-1 and CPR-2, dimple patterns due to the fast fractures were observed in the region near the outer surface, while the fracture surfaces between the initial notch and the ductile tearing crack seemed to be those of the IGSCC.

4.2 Theoretical Considerations on Leak-Before-Break

Of five specimens tested here, the test pipes CPI-1, CPI-2 and CPI-3 showed steam leakage from the cracks, while the test pipes CPR-1 and CPR-2 exhibited the unstable double-ended breaks. The experimental net-section stresses at the leaks or the breaks for all the specimens are shown in Fig. 4.7 as the function of the cracked area which includes both the initially notched area A_2 and the cracked area by the IGSCC A_3. Here A_1 indicates the uncracked area.

Figure 4.7 also contains the results of the static high-compliance tests of the pipe specimens described in Section 3. Plotted in the figure are the net-section stress values at the crack initiations, collapses (i.e. maximum load points) and instabilities for the through-wall notches and those at the crack penetrations, collapses and instabilities for the part-through notches. The open marks indicate the crack initiations or the crack penetrations, while the half and full solid marks indicate the collapses and instabilities, respectively. In the calculation of the net stresses, the crack-induced bending moment was not taken into account. It can be seen in the figure that the leak occurred at the nondimensional net-section stress σ_N/σ_0 (σ_N; net-section stress, σ_0; flow stress) being less than 0.92, while the collapse or instability occurred when σ_N/σ_0 is larger than 0.92, where σ_0 is taken to be the average value of 0.2 % proof strength and tensile strength.

The net-section stress under the tensile load condition corresponding to the design stress S_m of the ASME Code Section III is drawn by a broken line

in the figure. Similarly the net-section stress calculated from the internal pressure of 7 MPa as the typical loading condition in BWR piping is drawn by a solid line. From these, it is very unlikely that a cracked pipe breaks only by the working internal pressure. Moreover, it should be noted that the quite large initial cracked area is required until the pipe breaks satisfying σ_N/σ_0=0.92 under the design stress condition of S_m.

In order to demonstrate the leak-before-break, it is necessary to show that the crack with leak does not cause the subsequent unstable pipe break. Regarding this, it is assumed from the above consideration that if the nondimensional net-section stress σ_N/σ_0 reaches the value of 0.92, the pipe break takes place.

As for the critical crack lengths for the detectable leak, we assume that the leakage of five gallons per minute (5 gpm) can be detected and that the leak rate from the through-wall crack is estimated from the crack opening area A approximately given by

$$A = \frac{2\pi a^2 \sigma_N}{E} \sec\left(\frac{\pi\sigma_N}{2\sigma_0}\right) \qquad (12)$$

Multiplying the leak rate of 55 lb/sec.in^2 for the saturated water at the internal pressure of 7 MPa by the area calculated by eq.(12), the length of through-wall crack which gives the leak rate of 5 gpm can be calculated.

In Fig. 4.8, the variations of the critical crack lengths for detectable leak and break with the pipe diameter are shown. This figure also contains the critical crack lengths for instability for some finite compliance values, which were obtained by the simplified method described in Section 3. It should be emphasized from this figure that the crack length for 5 gpm leakage is considerebly smaller than the crack lengths for collapse or instability and that large diameter pipes have more margin for break than small diameter pipes.

4.3 Conclusions

The fracture behaviors of Type 304 stainless steel pipes with circumferential part-through cracks were studied with the pipe experiments performed in the BWR environments under the cyclic tension loading with high comliance. The following results were obtained from these experiments and the theoretical considerations.

1) The leak-before-breaks were confirmed in the test pipes with small initial notch angles of 30°, 150° and 180°. On the other hand, the fast fractures were observed in the specimens with the large initial notch angles of 240° and 360°.
2) Based on the net-section stress approach, the critical condition was obtained to determine the failure mode, i.e. leak or break, in the circumferentially cracked pipe.
3) It was found that the critical crack length for pipe break was much larger than that required for the leak detection at the applied load S_m.
4) Large diameter pipes have more margin for break than small diameter pipes.

TABLE 4.1 CHEMICAL COMPOSITION (CHECK ANALYSIS)

(WT.%)

C	Si	Mn	P	S	Ni	Cr
0.06	0.59	1.75	0.022	0.006	9.40	18.60

TABLE 4.2 MECHANICAL PROPERTIES

ROOM TEMPERATURE			285°C		
0.2% PROOF STRENGTH (MPa)	TENSILE STRENGTH (MPa)	ELONGATION (%)	0.2% PROOF STRENGTH (MPa)	TENSILE STRENGTH (MPa)	ELONGATION (%)
275	608	65	179	464	43.8

TABLE 4.3 TEST CONDITION AND RESULTS

TEST PIPE No.	NOTCH GEOMETRY		LTS*3	σ_{Max}*5	TEST RESULTS
	2α*1 (DEG)	c/t*2			
CPI-1	36	0.5	YES	σ_y*6	LEAK
CPI-2	150	0.5	NO	σ_y	LEAK
CPI-3	180	0.5	YES*4	σ_y	LEAK
CPR-1	240	0.5	YES	σ_y	BREAK
CPR-2	360	0.5	YES	$0.7\sigma_y$	BREAK

*1 NOTCH ANGLE

*2 c:NOTCH DEPTH, t:PIPE THICKNESS

*3 LOW TEMPERATURE SENSITIZATION (550°C × 24h)

*4 APPLIED AFTER 198TH LOADING CYCLE

*5 MAXIMUM APPLIED GROSS STRESS

*6 0.2% PROOF STRENGTH AT 285°C (=179 MPa)

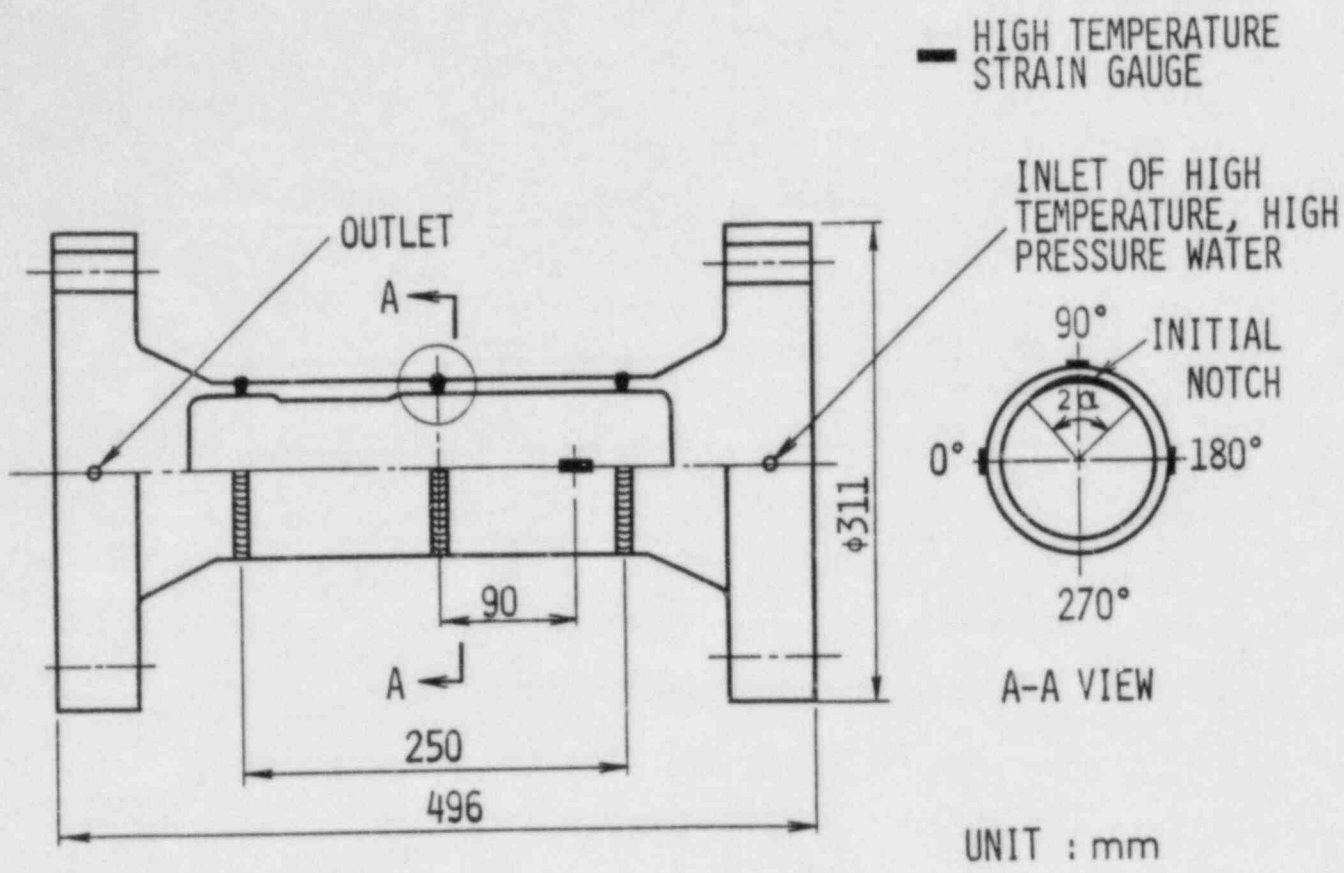

FIGURE 4.1 DETAILS OF TEST PIPE

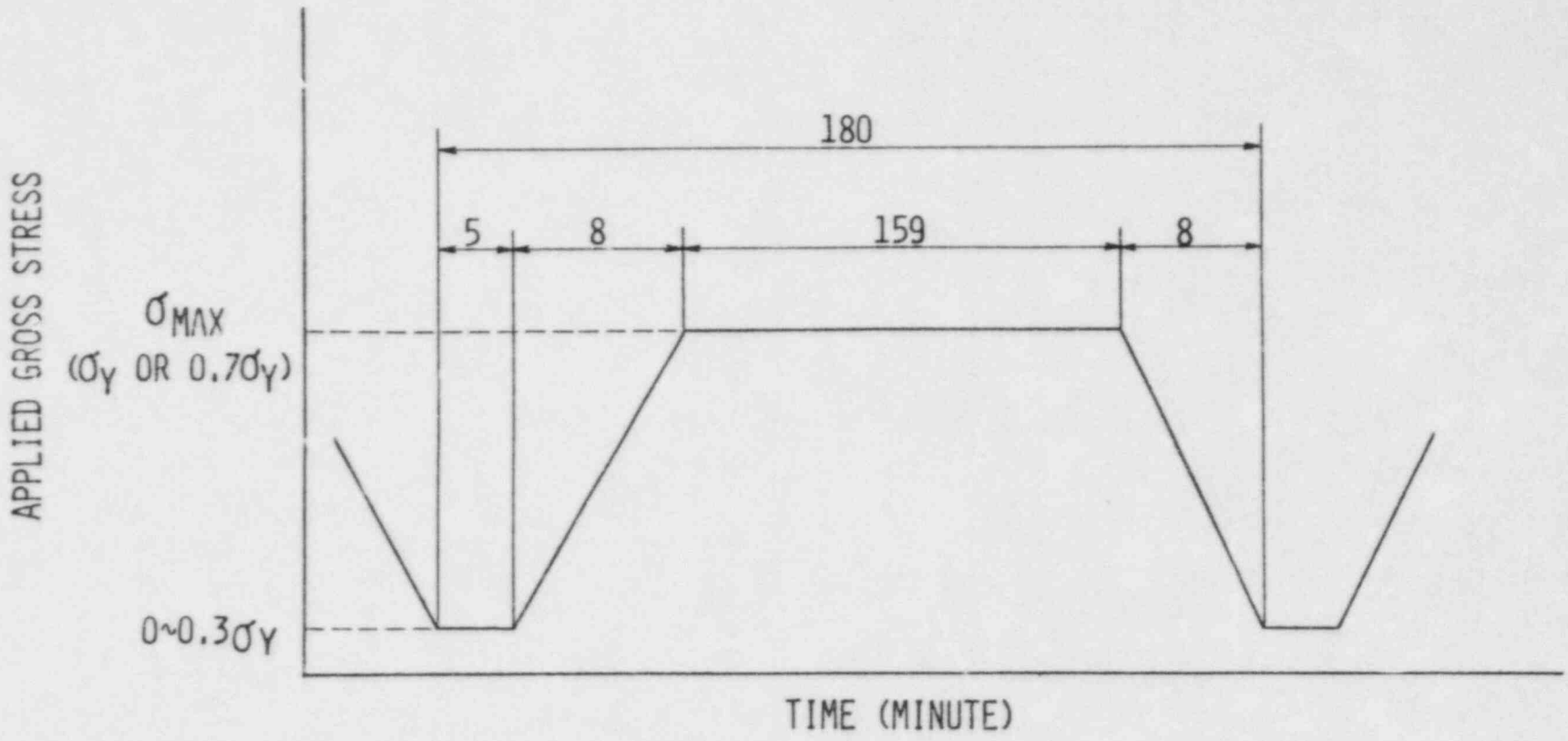

FIGURE 4.2 AXIAL LOADING CYCLE PATTERN

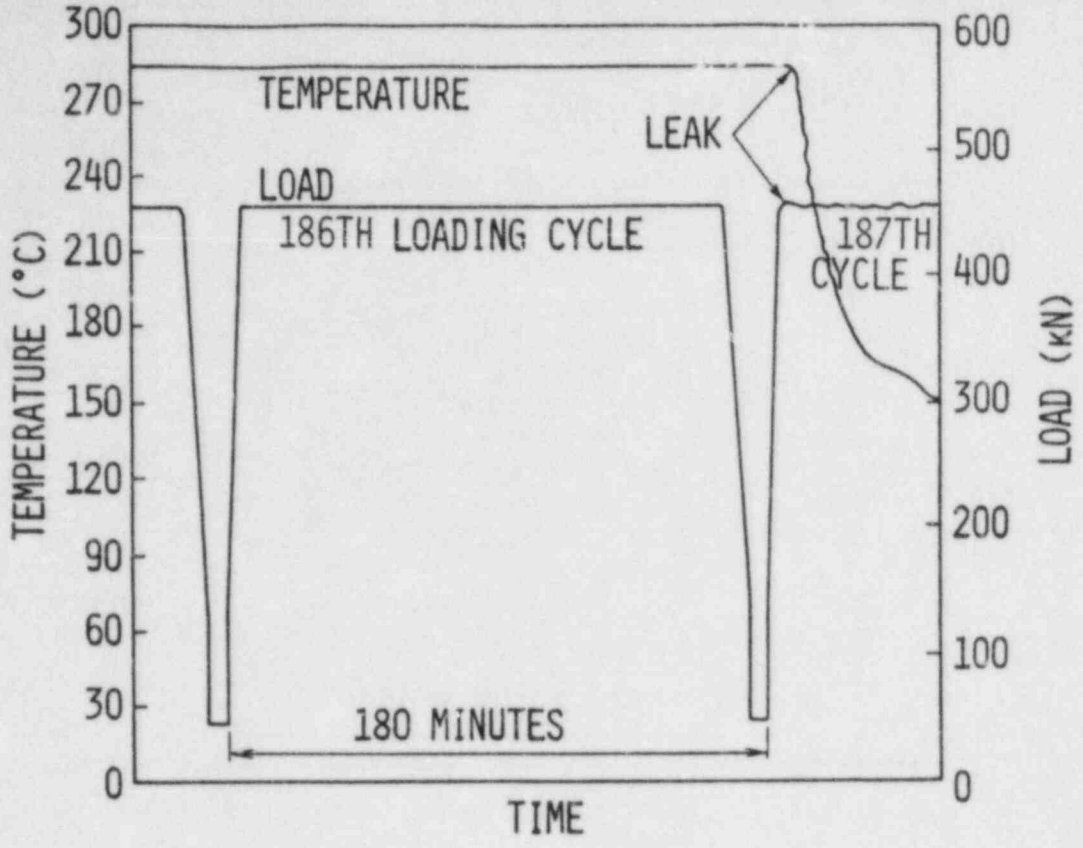

A) CPI-1

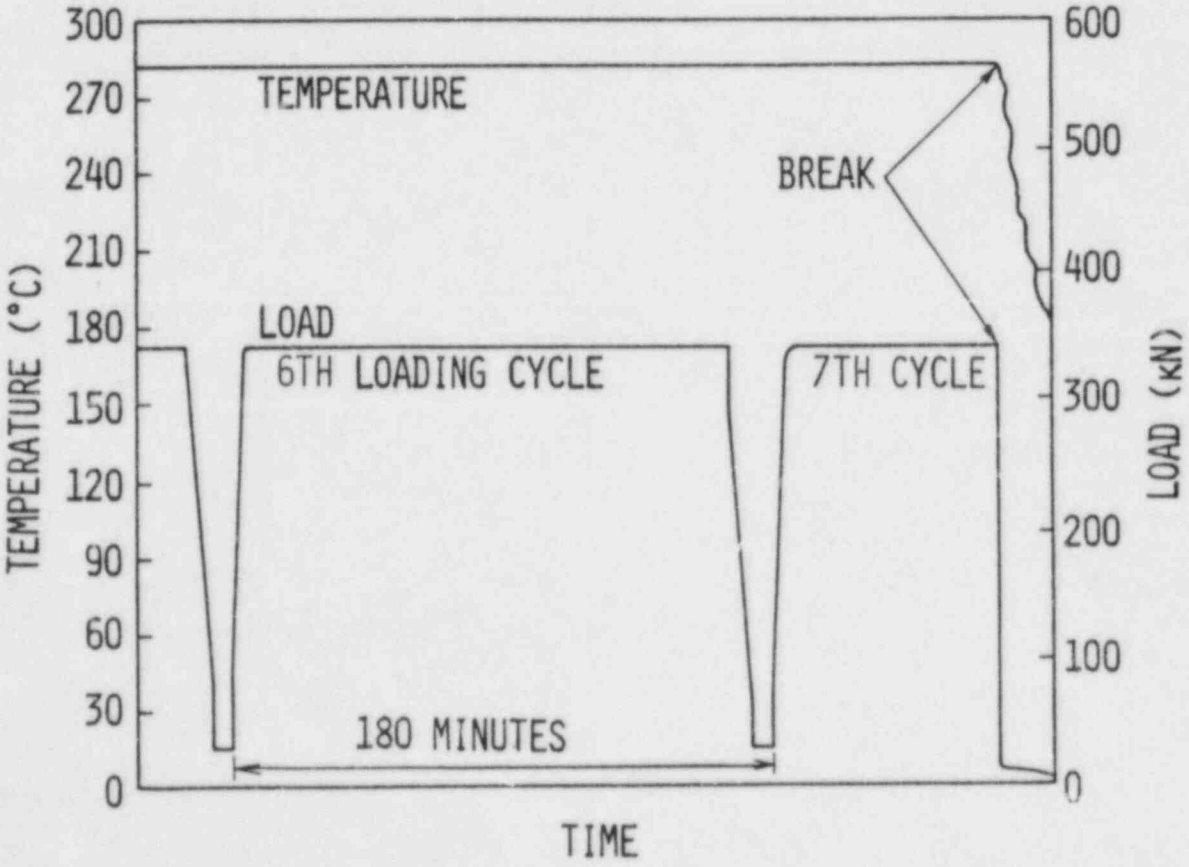

B) CPR-2

FIGURE 4.3 TYPICAL TEST DATA RECORD

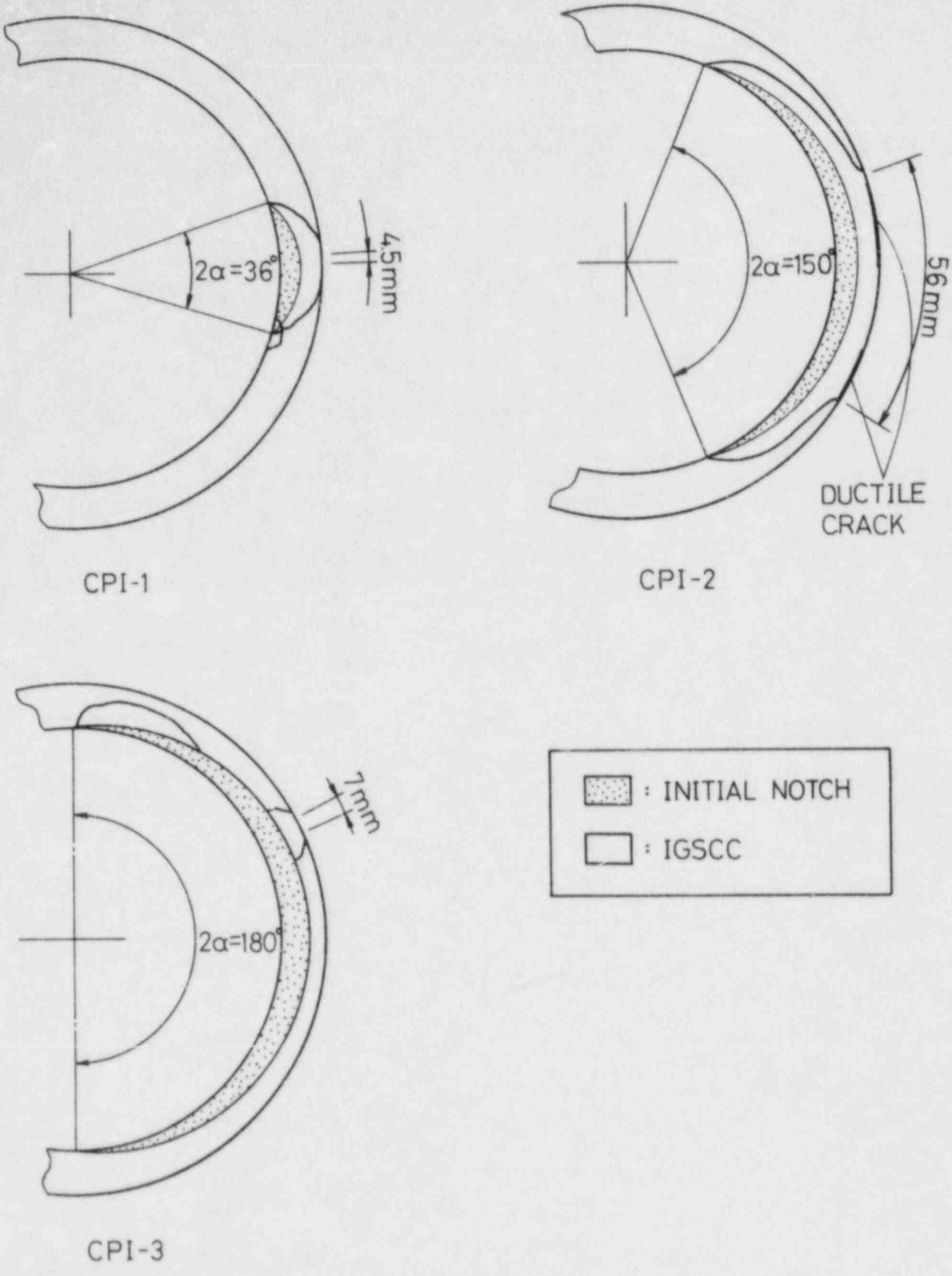

FIGURE 4.4 PROFILES OF FRACTURE SURFACE
(CPI-1,2,3)

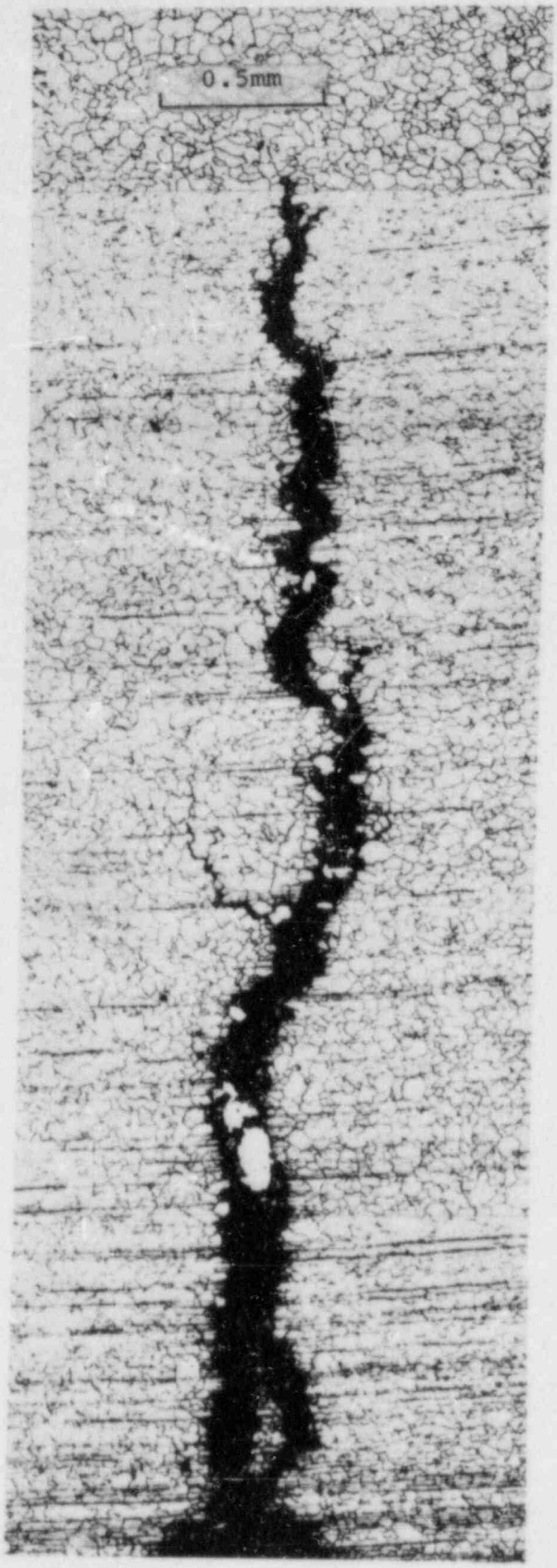

FIGURE 4.5 OPTICAL MICROGRAPH OF CRACK IN CPI-3

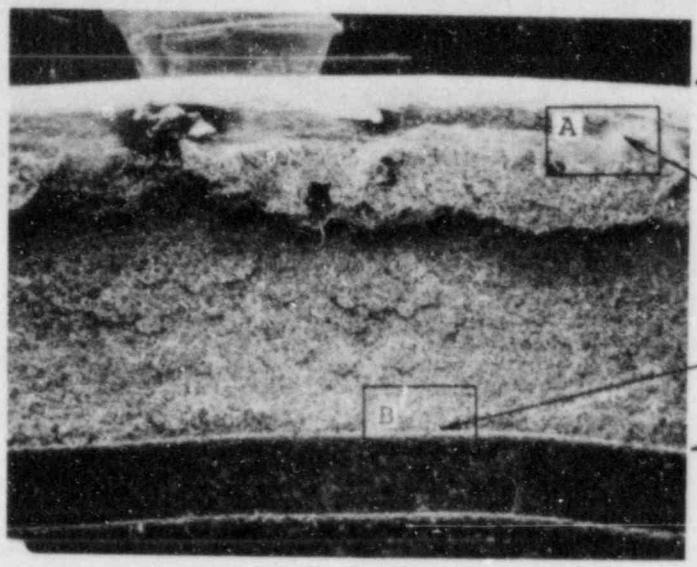

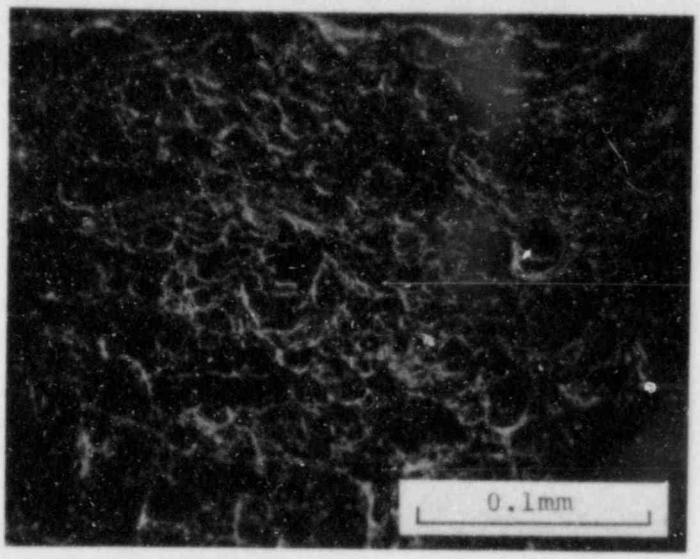

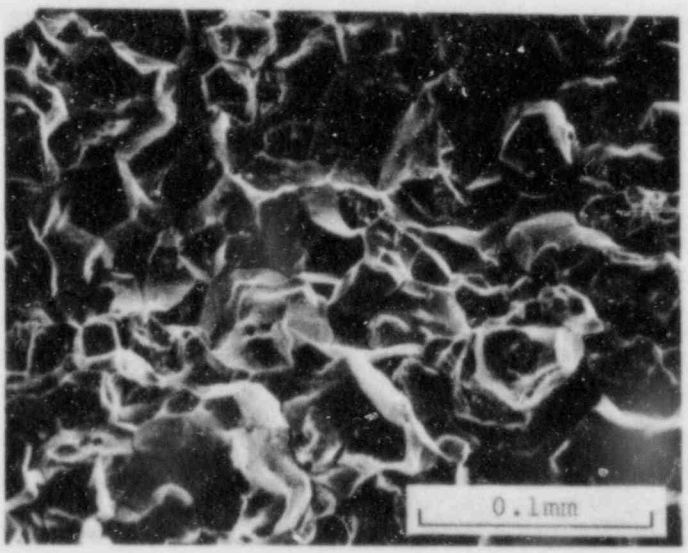

FIGURE 4.6 ELECTRON MICROGRAPHS OF THE FRACTURE SURFACES IN CPR-1

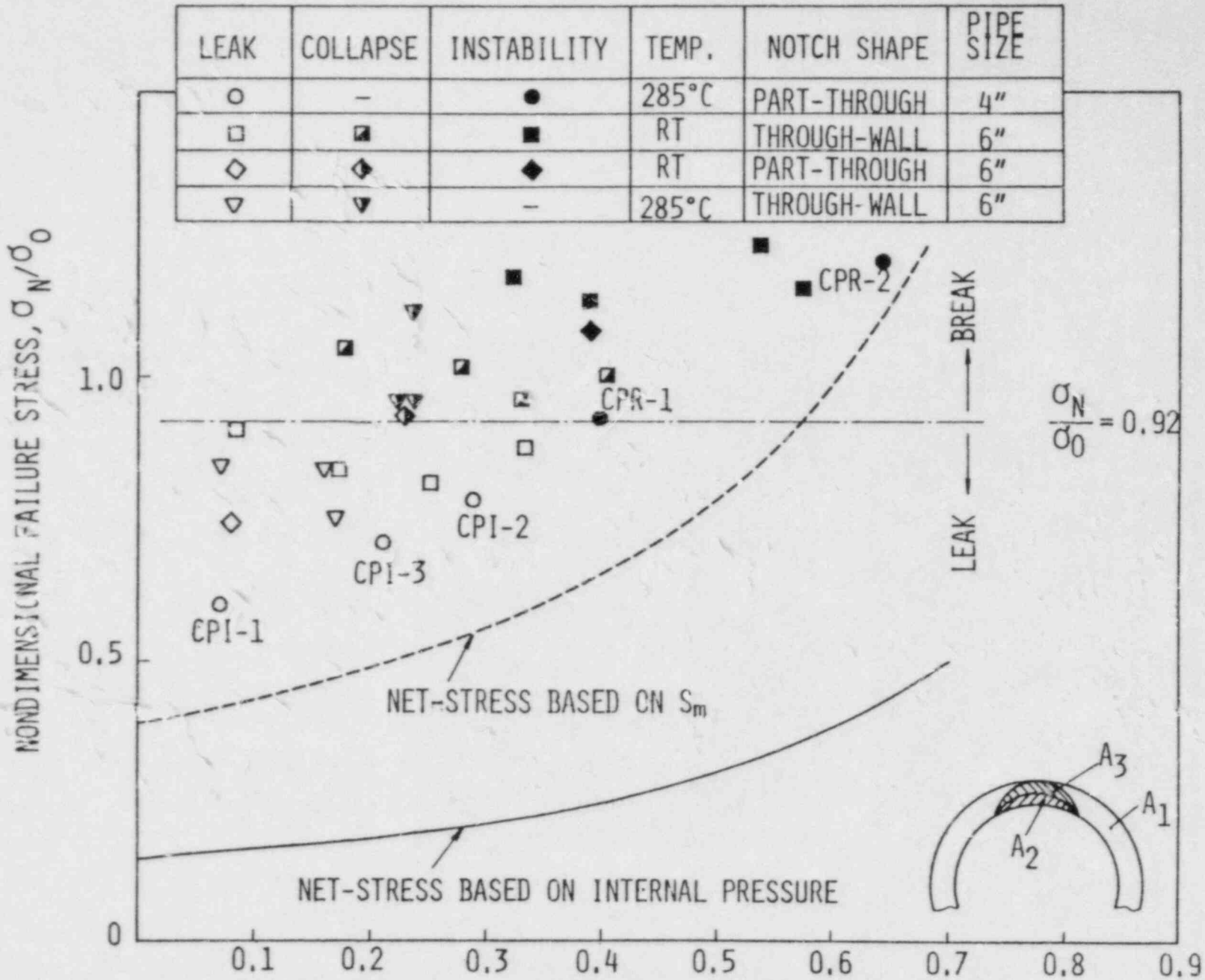

FIGURE 4.7 NET-STRESS FOR LEAK, COLLAPSE AND INSTABILITY

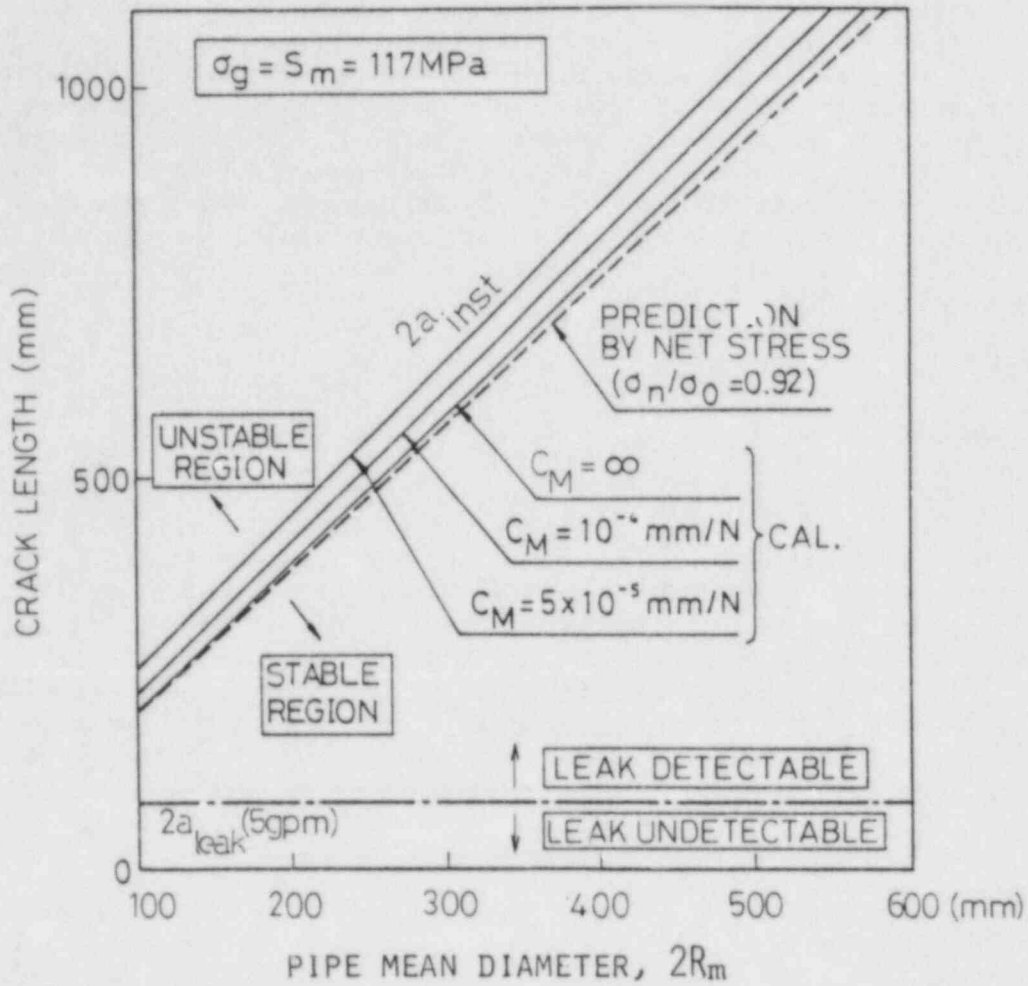

FIGURE 4.8 VARIATIONS OF CRITICAL CRACK LENGTHS FOR INSTABILITY AND LEAK WITH PIPE DIAMETER

5. Thermal Shock Test for Circumferentially Cracked Pipes

In core spray and recirculation piping systems of BWRs, the thermal transient might occur on the emergency core cooling. Type 304 stainless steel, which is used as the material of these piping system, has so enough ductility and toughness that crack propagation in this material is presumed to be stable.

However, it has never been demonstrated experimentally so far that the crack propagation and unstable pipe fracture can thoroughly be prevented in nuclear piping with quite large intergranular stress corrosion cracking (IGSCC) when the thermal transient such as the emergency core cooling occurs.

For this purpose, we conducted the experiments on the crack propagation from circumferential part-through notches in Type 304 stainless steel pipes to investigate crack behaviors under the thermal transient. This section describes the results of these experiments and the related preliminary theoretical considerations.

5.1 Experiments

5.1.1 Specimens

The austenitic stainless steel (AISI Type 304) pipes of 8-inch schedule 80 were used as the test specimens. The chemical composition and mechanical properties of the steel are shown in Table 5.1 and Table 5.2, respectively. Four test pipes, which were welded by tungsten arc welding (Heat input: 10 kJ/cm for 1st to 3rd layers and 23 kJ/cm for 4th to 7th layers), were prepared as shown in Fig. 5.1.

A part-through circumferential artificial notch of maximum 3mm width was introduced into the heat affected zone of each welded pipe by electron discharge machining. Table 5.3 shows the notch depth and its circumferential angle for each pipe. As can be seen in the table, two types of cracks, which have circumferential angles of 180 and 360 degrees respectively, were machined in this tests.

5.1.2 Test Conditions and Measurements

Two kinds of loading conditions were considered in the experiments. The first was the high compliance test using the high compliance apparatus shown in Fig. 2.2. The second was the low compliance test using the same testing machine but without the compliance device.

Figures 5.2 and 5.3 show the overall view of the test pipe set in the apparatus and the outline of the cooling water loop system for applying the thermal shock to the pipes, respectively. The temperature, the pressure and the flow rate of the cooling water were 20°C, 4kgf/cm^2 and 6.7m/s, respectively.

In all the tests, mechanical pre-load in the axial direction whose value is shown in Table 5.3 was applied to the specimen before the thermal shock. The values of the pre-load are determined such that the net-section stress at the cracked section of pipes were equal to $1.4\sigma_{0.2}$, where $\sigma_{0.2}$ is the 0.2% proof stress of the material at 285°C.

The test procedure was as follows.

1) Set the test pipe in the apparatus.
2) Heat the pipe up to nearly 285°C by using electric heater surrounding the pipe.

3) Apply the axial tensile pre-load up to the specified value shown in Table 5.3.
4) Shut the valve A and open the valves B and C.
5) Immediately after removing the air from the loop, open the valve D with shutting the valve C.
6) Then the cooling water rapidly flows into the test pipe and causes the thermal shock in the pipe.

The change in tensile load was monitored by using the strain gauges mounted on the loading arm. The temperature distribution through the pipe thickness was also measured by the thermocouples which were attached at 0.5, 8, 10 and 11.7mm depths from the outer surface near the notch in the pipe.

5.1.3 Test Results

Figure 5.4 shows the typical example of the time variations of the temperature at various depths and the tensile load measured in the low compliance test. From the figure, it can be observed that the temperature at the inner surface became below 30°C at about five seconds after the injection of cooling water, and that it took more than one minute for the outer surface to be cooled below 50°C.

Figure 5.5 illustrates the temperature distributions along the pipe wall for each pipe. From these tempetature distributions in the pipe thickness, it was expected that the thermal stress which occurred in the pipe changed from the bending type to the tensile type with time.

Shown in Table 5.3 are the total loads and the thermal loads occurred in the three pipes in the pipe longitudinal direction in the steady condition after the thermal transients, where the latters are obtained by subtracting the pre-loads from the total loads. Because of the rigid constraint, the higher thermal loads appeared in the zero compliance tests than in the high compliance tests.

In all the tests, no pipe fracture was observed. By the macroscopic observation after the tests, it was found that no ductile crack growth took place in all the pipes. As an example, Fig. 5.6 shows the photograph of the neighborhood of the notch after the thermal shock loading for CPII-3, which was the highest of all the tests. Although the notch seems to be blunted by the thermal loading to some extent, no ductile crack growth can be seen as shown in the photogragh.

5.2 Theoretical Analyses

5.2.1 Conditions of Analysis

The axisymmetrical elastic-plastic analyses for pipes with the high and the low compliances were conducted using the finite element program with the consideration of the large deformation effects. Here, CPII-2 and CPII-4 with a full circumferencial notch were analyzed.

Mesh breakdowns for these pipes are shown in Figs. 5.7 and 5.8. Due to the symmetry half lengths of the pipes were modeled as axisymmetrical bodies. The conditions of the calculations for both pipes are tabulated in Table 5.4.

For the analysis of CPII-2, the high compliance was replaced by the dead load condition for simplicity. In other words, the mechanical pre-load was applied at the end of the pipe, and then it was kept constant during the period of the thermal shock.

On the other hand, the specimen CPII-4 with the zero compliance was

simulated by the displacement constant condition. The pipe end after applying the specified pre-load was fixed during the thermal transient.

Table 5.5 gives the material properfies for the present calculations. The values between 25°C and 300°C were approximated by linear interpolation. To model the stress-strain relation, the multilinear and the bilinear approximations were used for CPII-2 and CPII-4, respectively. Von Mises's criterion and the associated flow rule was employed as the plasticity theory.

The temperature distributions in the wall thickness of the pipes were obtained experimentally as shown in Fig. 5.5. At the time of eight seconds after injecting cold water, the temperatures at the outer surface were unchanged, while the tempetatures at the inner surface were decreased nearly to the temperature of the injected cold water. The differences in temperatures between the inner and the outer surfaces are the largest at the time of about eight seconds. Therefore, the temperature distributions in the thickness direction at the time of eight seconds were utilized in the calculations for conservatism.

5.2.2 Calculated Results

Crack opening profiles under the dead load and the fixed displacement conditions are compared in Fig. 5.9. The profiles at t=0 are the values due to the mechanical pre-load.

The axial stress distributions at the pipe section far from the cracks at the time of eight seconds are shown in Fig 5.10. It should be noted that the stress distributions at this time are about the same for both dead load and displacement constant conditions.

5.3 Discussions

As mentioned above, no ductile crack growth was observed in all the tests. This was confirmed also by the finite element analyses. In other words, the maximum crack tip opening displacement obtained by the finite element analyses was 0.17mm, which is considerebly smaller than the value required for the ductile crack initiation in Type 304 stainless steel, i.e. about 1 mm [25].

Also found from the analyses was that no large difference appeared in the transient thermal stresses between with and without compliance loading conditions in the earlier stage of transient.

It should be noted that the pre-loading and the thermal transient conditions taken in the present experiments are much severer than those expected in the actual piping system. Moreover, considerebly large initial notches whose areas were nearly half of the pipe section were introduced in the present experiments.

Taking these factors into consideration, it can be considered that it is very unlikely for pipe rupture to occur under the possible thermal transient condition in the actual piping of Type 304 stainless steel.

5.4 Conclusions

The following conclusions were obtained from the present thermal shock tests for cracked pipes and the related finite element analyses.

1) Although initial notches were expanded by the thermal shock loading to some extent, neither stable nor unstable ductile crack growth was observed in the tests.

2) From the finite element analyses, it was found that the compliance does not have much influence on the thermal stress in the pipe under the thermal transient condition. The value of CTOD was found to be considerebly smaller than that required for the ductile crack initiation.
3) Considering the fact that no ductile crack growth took place and the severity of the experimental conditions employed in this tests, it can be concluded that the unstable rupture of Type 304 stainless steel pipe is very unlikely to occur under the thermal transient condition anticipated in the actual piping system.

TABLE 5.1 CHEMICAL COMPOSITION (CHECK ANALYSIS)

(WT.%)

C	Si	Mn	P	S	Ni	Cr
0.069	0.48	1.50	0.026	0.001	9.60	18.20

TABLE 5.2 MECHANICAL PROPERTIES

ROOM TEMPERATURE			285°C		
0.2% PROOF STRENGTH (MPa)	TENSILE STRENGTH (MPa)	ELONGATION %	0.2% PROOF STRENGTH (MPa)	TENSILE STRENGTH (MPa)	ELONGATION %
275	608	66	171	482	44

TABLE 5.3 TEST CONDITION AND RESULTS

TEST PIPE No.	NOTCH GEOMETRY		TEMPERATURE (°C)	COMPLIANCE OF DEVICE (mm/N)	PRE-LOAD (kN)	THERMAL LOAD (kN)	TOTAL LOAD (kN)
	2α *1 (DEG)	c/t *2					
CPII-1	180	0.53	276	10^{-4}	1458	35	1493
CPII-2	360	0.35	276	10^{-4}	1174	—	—
CPII-3	180	0.49	294	0	1485	383	1868
CPII-4	360	0.34	288	0	1152	282	1434

*1 NOTCH ANGLE

*2 c:NOTCH DEPTH, t:PIPE THICKNESS

TABLE 5.4 TWO DIMENSIONAL ELASTIC-PLASTIC FINITE ELEMENT CONDITIONS

MODEL	CPII-2	CPII-4
COMPLIANCE	HIGH	LOW
LOADING CONDITION	CONSTANT LOAD	CONSTANT DISPLACEMENT
ELEMENT TYPE	4 NODE ISPORAMETRIC AND TRIANGLE ELEMENTS	8 NODE ISOPARAMETRIC ELEMENT
NUMBER OF ELEMENT	223	30
NUMBER OF NODE	253	113

TABLE 5.5 MATERIAL CONSTANTS FOR FINITE ELEMENT ANALYSIS

TEMPERATURE	25°C	300°C
YIELD STRESS	274 MPa	147 MPa
YOUNG'S MODULUS	1.94×10^5 MPa	1.75×10^5 MPa
POISSON'S RATIO	0.260	0.284
COEFFICIENT OF THERMAL EXPANSION	1.64×10^{-6} /°C	18.6×10^{-6} /°C

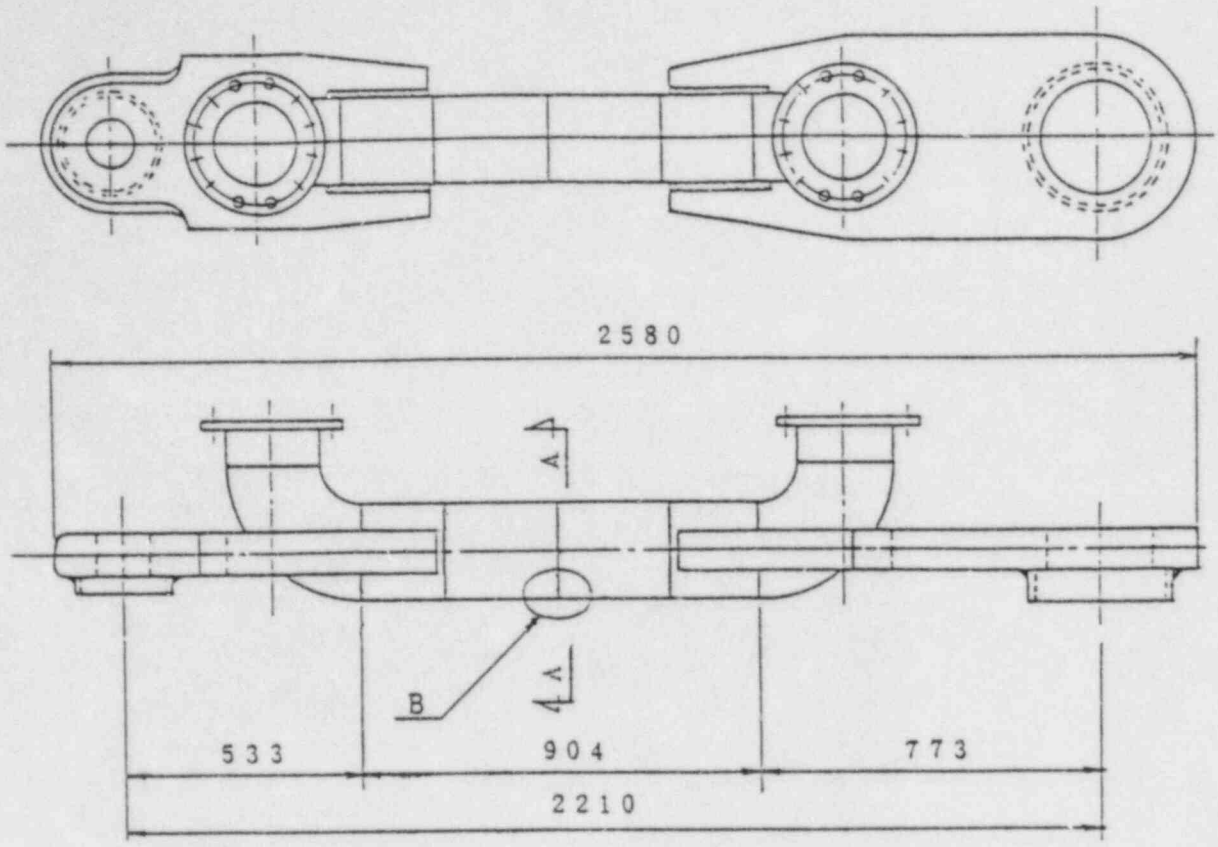

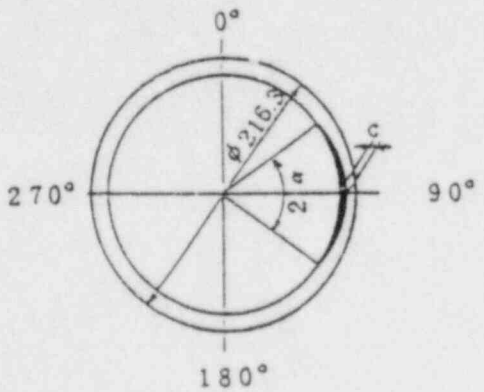

A-A VIEW

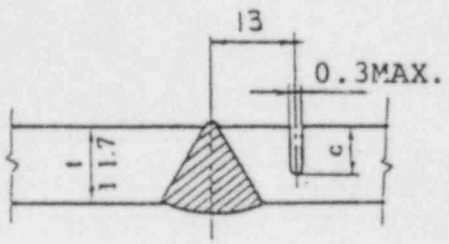

DETAILS OF B

UNIT:mm

FIGURE 5.1 DETAILS OF TEST PIPE

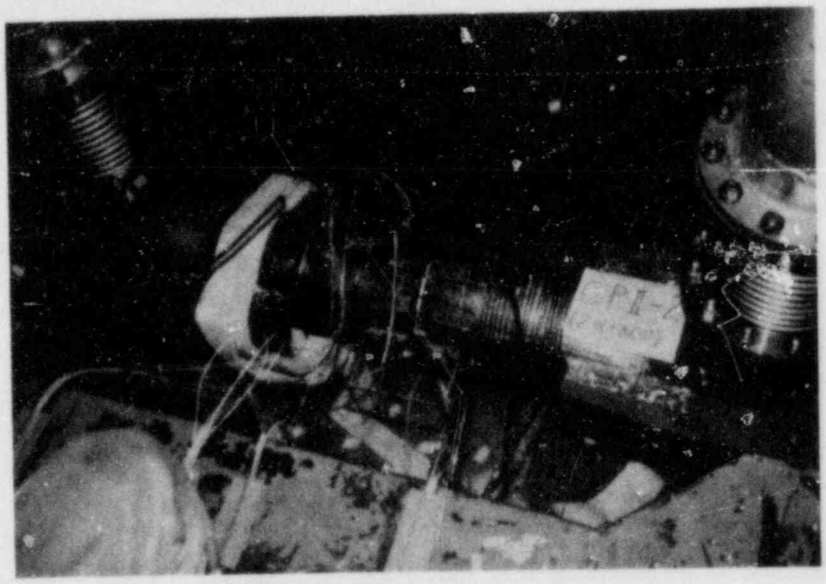

FIGURE 5.2 OVERVIEW OF TEST PIPE SET
IN THE APPARATUS WITH HEATER

FI: FLOW INDICATOR
PI: PRESSURE INDICATOR
TI: THERMO INDICATOR
AO: AIR OPERATED VALVE
P: PUMP

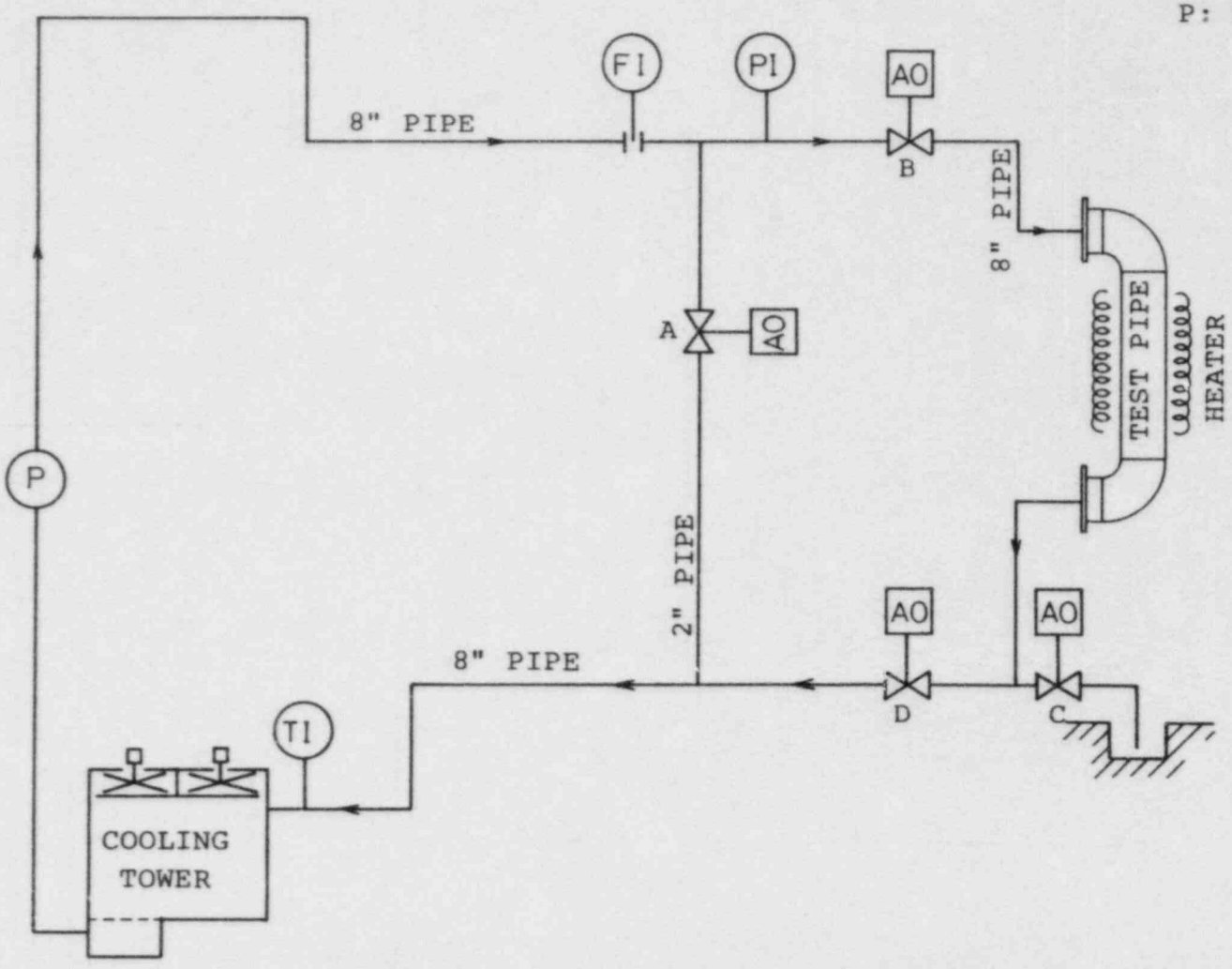

FIGURE 5.3 TESTING LOOP

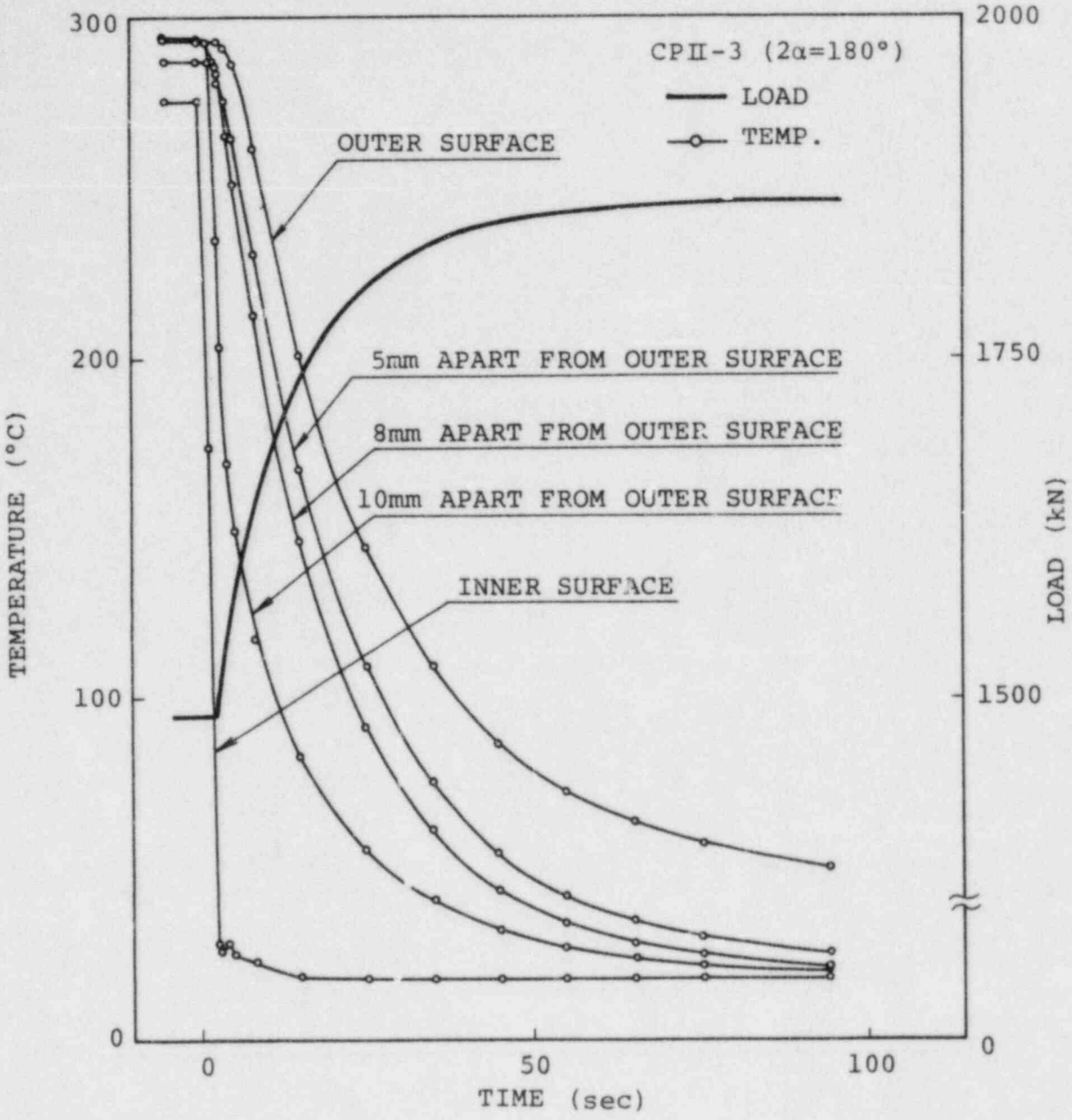

FIGURE 5.4 TYPICAL EXAMPLE OF TEMPERATURE AND LOAD VS. TIME RECORD

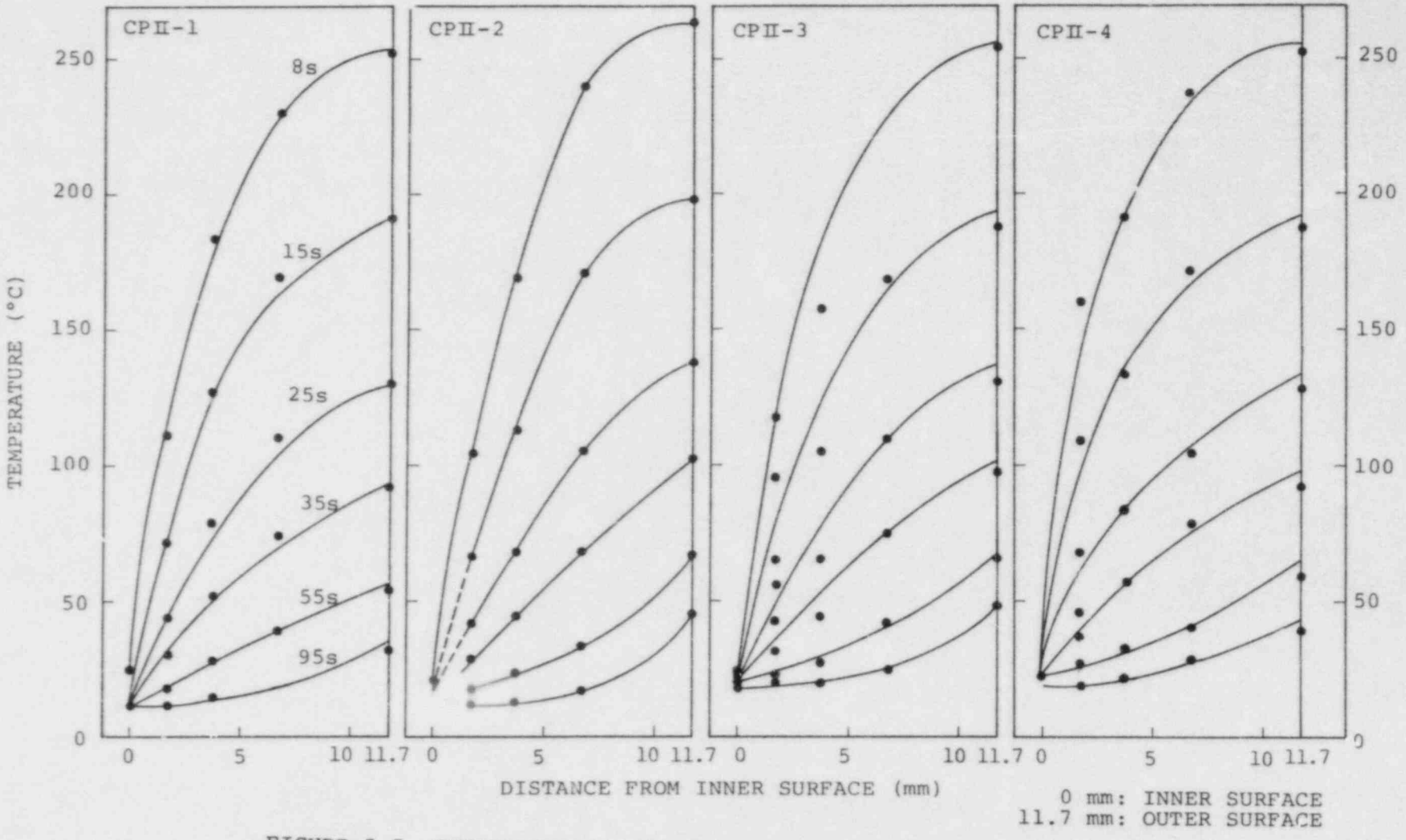

FIGURE 5.5 TEMPERATURE DISTRIBUTION OF THE PIPES

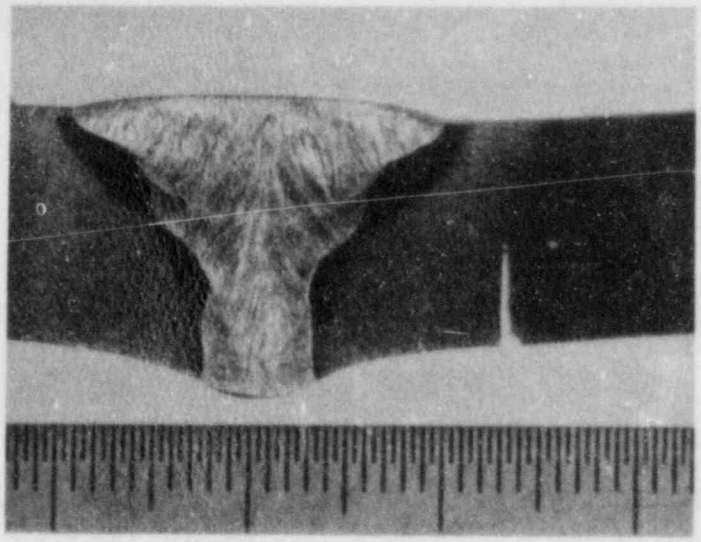

(A) CROSS SECTION AT WELDED REGION

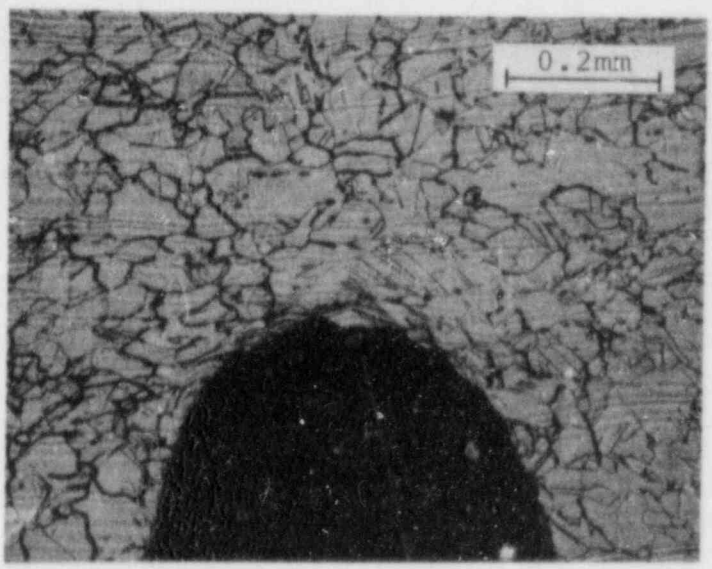

(B) DETAILS OF NOTCH TIP

FIGURE 5.6 THE VIEW OF THE NOTCH SHAPE AFTER THERMAL SCHOCK

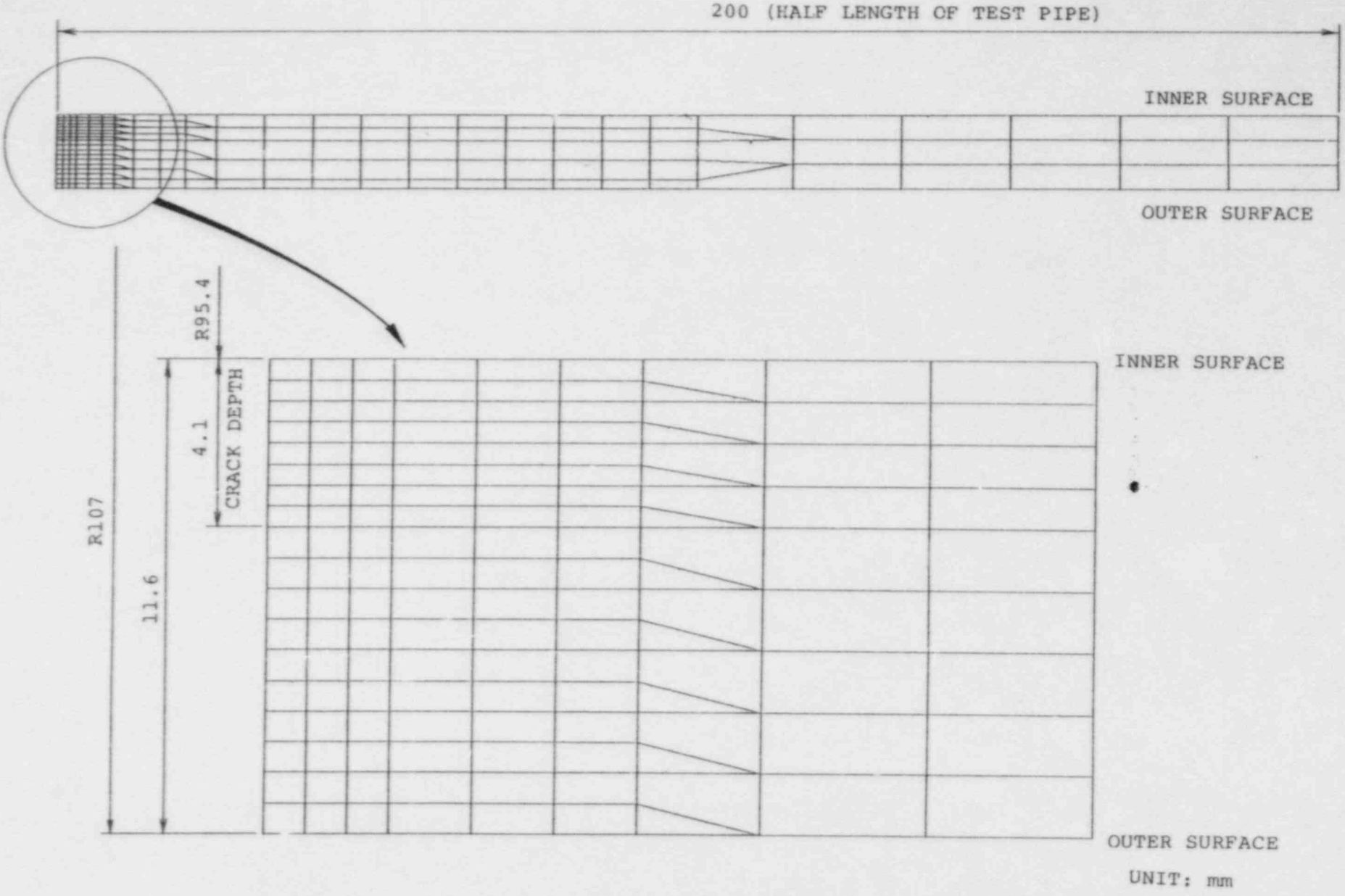

FIGURE 5.7 FINITE ELEMENT MESH MODEL OF CRACKED PIPE (CPII-2)

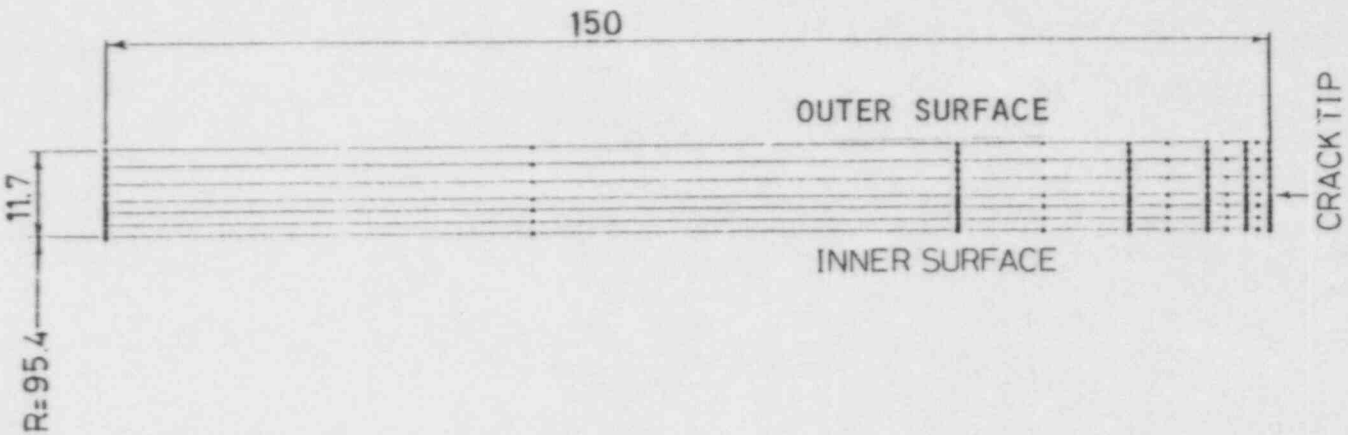

FIGURE 5.8 FINITE ELEMENT MESH MODEL OF CRACKED PIPE (CPII-4)

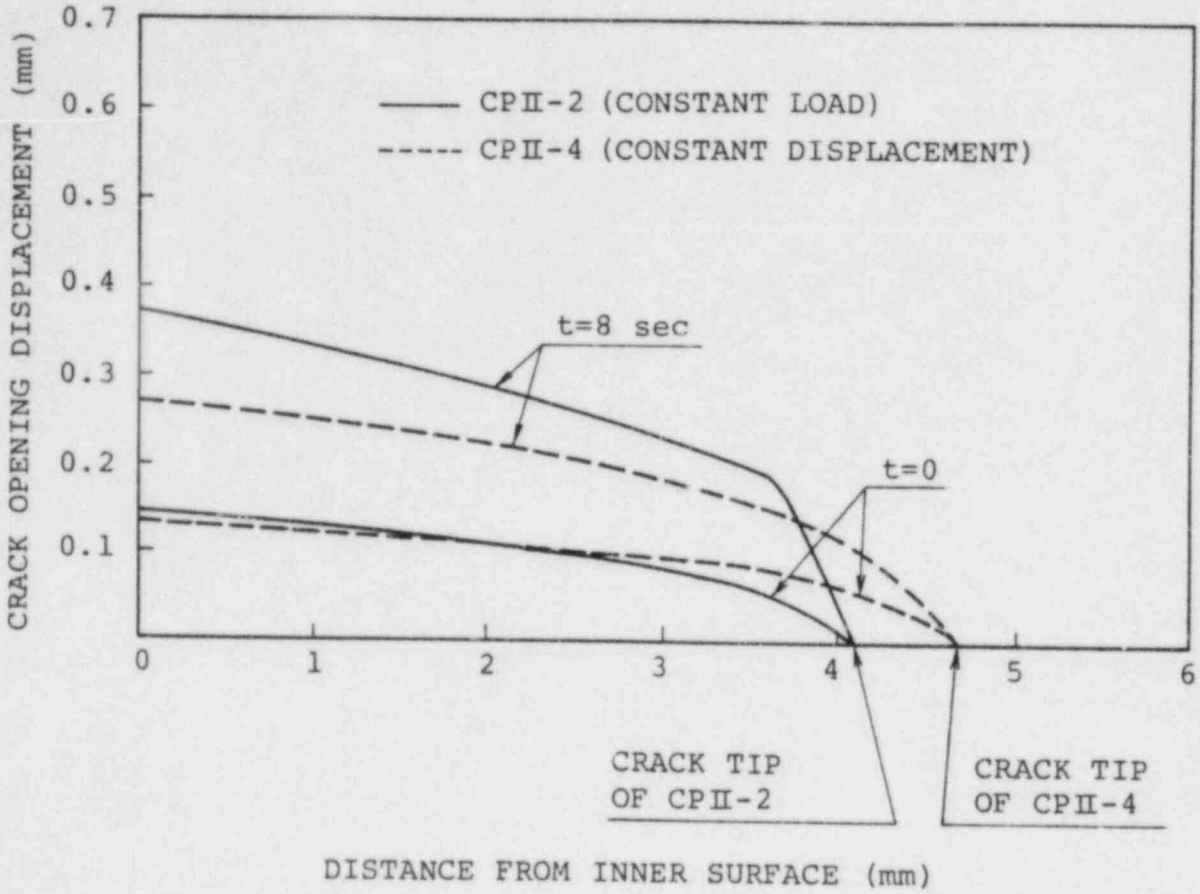

FIGURE 5.9 CALCULATED CRACK OPENING DISPLACEMENTS FOR CPII-2 AND CPII-4

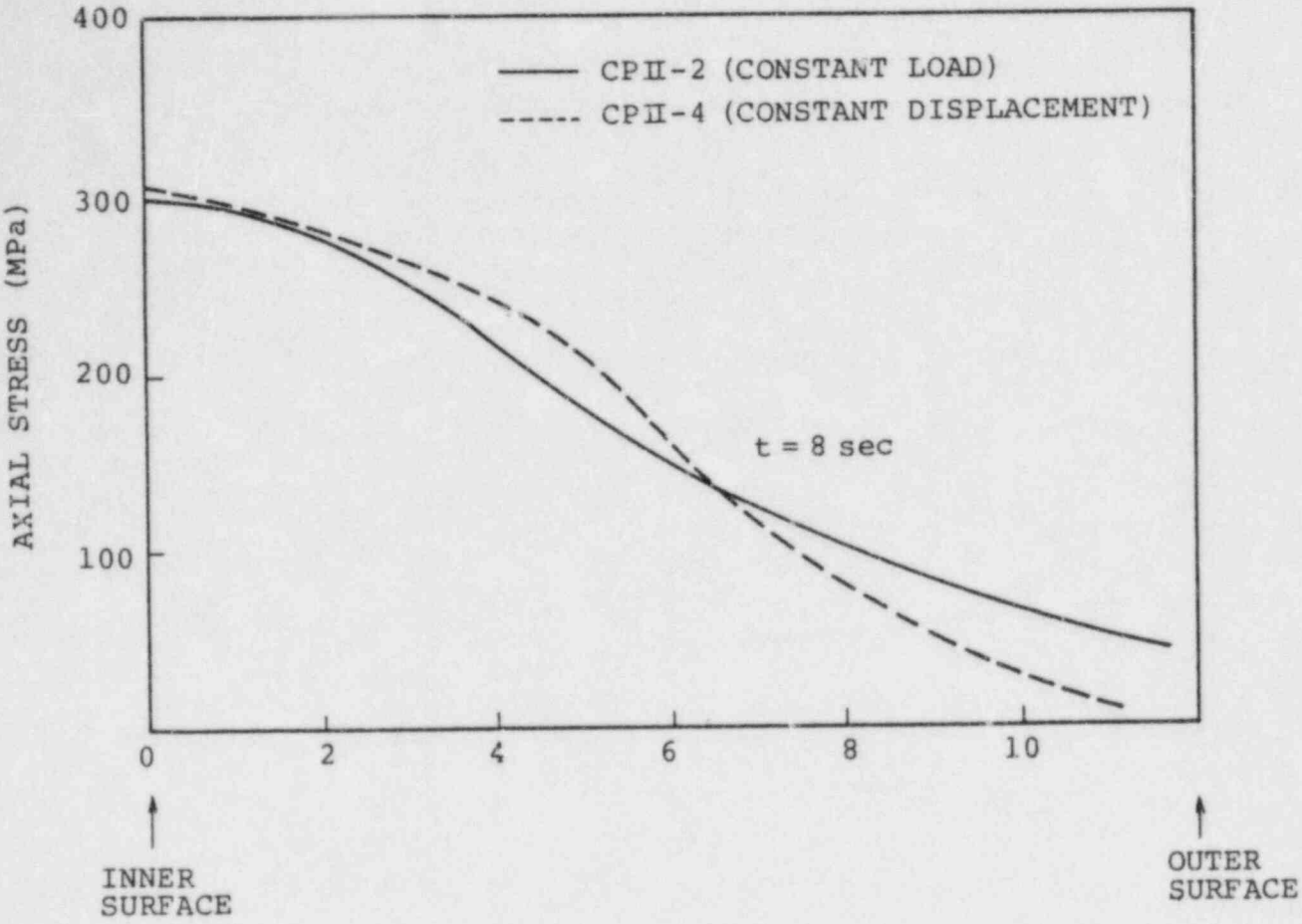

FIGURE 5.10 AXIAL STRESS DISTRIBUTION ALONG THE PIPE WALL THICKNESS AT 8 SECONDS AFTER CRAMMING COLD WATER

6. General Conclusions

From the above studies, the following general conclusions were derived.

1) The unstable fractures of the plates and pipes of Type 304 stainless steel were realized with the use of the tensile-type high-compliance testing device. The changes of the fracture surface were observed near the instability points.
2) With the finite element analyses, the stable crack growth was found to be well-characterized by the J-integral or the crack tip opening angle. The onset of the unstable crack growth was predicted by the T-criterion or the stationariness of the total displacement.
3) Under the cyclic high-compliance loading condition superposed on the interal pressure by the corrosive water, the two pipes with a part-through crack of circumferential angle larger than 180° exhibited unstable breaking, while the other three pipes showed the leak-before-break behavior. The boundary between the unstable breaking and the leak-before-break was found to be well represented by the net-section stress.
4) In the thermal shock tests under both with and without compliance loadings, no crack growth was observed in all the four pipes. It was found from the tests that the unstable fracture due to the thermal transient is very unlikely to occur in the actual pipes made of Type 304 stainless steel.

Acknowledgements

This work is a part of the Stress Corrosion Cracking Study for BWR piping sponsored by the Ministry of Internaitnal Trade and Industry. The research was managed by Nuclear Power Engineeing Test Center (NUPEC). The authors wish to express their appreciations to Prof. Emeritus Y. Ando, Prof. N. Ogura and members of Stress Corrosion Crackng Test Advisory Committee of NUPEC for their useful discussions. We also acknowledge Mr. K. Fujii of Ishikawajima-Harima Heavy Industries Co., Ltd, for his experimental work and Mr. K. Kashima of Central Research Institute of Electric Power Industry for his numerical analysis as well as theoretical discussions.

References

[1] Fox, A., Proceedings: Seminar on Countermeasures for Pipe Cracking in BWRs, Vol.1, Paper No.1, EPRI, 1980.
[2] Kanninen, M.F., Broek, D., Hahn, G.T, Marschall, C.W., Rybicki, E.F., Wilkowski, G.M., Nuclear Engineering and Design, Vol.48, 1978, p.117.
[3] Paris, P.C., Tada, H., Zahoor, A., Ernst, H., ASTM STP 668, 1979, p.5.
[4] Hutchinson, J.W., Paris, P.C., ASTM STP 668, 1979, p.37.
[5] Tada, H., Paris, P.C., Gamble, R., ASTM STP 700, 1980, p.296.
[6] Zahoor, A., Kanninen, M.F., Trans. ASME, Ser. J, Vol.103, 1981, p.352.
[7] Paris, P.C., Tada, H., Zahoor, A., Ernst, H., ASTM STP 668, 1979, p.251.
[8] Wilkowski, G.M., Zahoor, A., Kanninen, M.F., Trans. ASME, Ser. J, Vol. 103, 1981, p.359.
[9] Kanninen, M.F., Rybicki, E.F., Stonesifen, R.B., Broek, D., Rosenfield, A.R., Marschall, C.W., Hahn, G.T., ASTM STP 668, 1979, p.121.
[10] Zahoor, A., Abou-Sayed, I.S., Computers and Structures, Vol.13, 1981, p.136.
[11] Nakagaki, M., Chen, W.H., Atluri, S.N., ASTM STP 668, 1979, p.195.
[12] Shih, C.F., deLorenzi, H.G., Andrews, W.R., ASTM STP 668, 1979, P.65.
[13] Kumar, V., deLorenzi, H.G., Andrews, W.R., Shih, C.F., German, M.D., Mowbray, D.F., 4th Semianual Report, RP 1237-1, 1981.
[14] Yagawa, G., Takahashi, Y., Ando, Y., Engineering Fracture Mechanics, Vol.16, No.5, 1982, P.721.
[15] Yagawa, G., Kashima, K., Katoh, N., Hasegawa, K., Saitoh, M., Umemoto, T., paper presented at ASME 4th National Congress on Pressure Vessel and Piping Technology, June 1983, Portland, Ore., U.S.A.
[16] Yagawa, G., Kashima, K., Takahashi, Y., Hasegawa, K., Saitoh, M., Umemoto, T., Sasaki, N., Trans. 7th International Conference on Structural Mechanics in Reactor Technology, G/F 4/1*, 1983.
[17] Yagawa, G., Takahashi, Y., Kashima, K., Engineering Fracture Mechanics (to be published).
[18] Rice, J.R., Paris, P.C., Merkle, J.G., ASTM STP 536, 1973, p.231.
[19] Garwood, S.J., Robinson, J.N., Turner, C.E., International Journal of Fracture, Vol.11, No.3, 1975, p.528.
[20] Shih, C.F., Hutchinson, J.W., Trans. ASME, Ser. H, Vol.98, 1976, p.289.
[21] Marcal, P.V., King, I.P., International Journal of Mechanical Sciences, Vol.9, 1967, p.143.
[22] Parks, D.M., Proc. 1st International Conference on Numerical Methods in Fracture Mechanics, 1978, p.464.

[23] Kashima, K., paper presented at ASME 4th National Congress on Pressure Vessel and Piping Technology, June 1983, Portland, Ore, U.S.A.
[24] ASME Code Section III, Rules for Construction of Nuclear Power Plant Components, 1980.
[25] Kanninen, M.F., Zahoor, A., Wilkowski, G., Abou-Sayed, I., Marschall, C., Broek, D., Sampath, S., Rhee, H., Ahmad, J., EPRI NP-2347, Volume 2, Project T118-2, Final Report, 1982.

APPLICATION OF TEARING INSTABILITY ANALYSIS FOR COMPLEX CRACK GEOMETRIES IN NUCLEAR PIPING

Jwo Pan and Gery Wilkowski

BATTELLE
Columbus Laboratories
Columbus, Ohio 43201

ABSTRACT

The analysis of the experimental data of 304 stainless steel pipes using Zahoor and Kanninen's estimation scheme has shown that the J resistance curve of a circumferentially cracked pipe with a simulated internal surface crack around the remaining net section is much lower than the J resistance curve of pipes with a idealized through-wall crack (without a simulated internal surface crack). The implications of the low J at initiation and tearing modulus on the stability analysis of typical BWR piping systems are discussed on the condition that an internal circumferential surface crack is assumed to occur along with a circumferential through-wall crack due to stress corrosion. The results presented here show that the margin of safety is reduced and in some cases instability is predicted due to the low J resistance curve and tearing modulus.

1. INTRODUCTION

Ductile materials such as Type 304 stainless steel used in nuclear pipings exhibit high resistance to unstable crack growth even when structures contain large flaws. The global instability of the cracked structures can be analyzed via the tearing instability analysis proposed by Paris et al [1,2] under J-controlled crack growth conditions [3]. Within the context of the tearing instability analysis, the applied J, denoted as J_{app}, which can be expressed as a function of the load and the crack length a, is assumed to follow a material curve, J_{mat}, which is a function of the crack extension Δa only. It is

$$J_{app} = J_{mat}\ (\Delta a) \tag{1-1}$$

and unstable crack growth occurs when

$$\frac{dJ_{app}}{da} > \frac{dJ_{mat}}{da} \quad . \tag{1-2}$$

Paris et al [1,2] introduced the nondimensional parameters which are

$$T_{app} = \frac{E}{\sigma_o^2} \frac{dJ_{app}}{da} \tag{1-3}$$

and

$$T_{mat} = \frac{E}{\sigma_o^2} \frac{dJ_{mat}}{da}$$

where T_{app} is the applied tearing modulus, T_{mat} is the material tearing modulus, E is Young's modulus, and σ_o is the flow stress. The instability criterion of equation (1-2) becomes

$$T_{app} > T_{mat} \tag{1-4}$$

It should be noted that the J resistance curve of the material concerned is never measured. It can be obtained either by finite element computations or by estimation techniques using the experimental records of load, displacement, and crack length. Figure 1 shows the J resistance curves of Type 304 stainless steel obtained from different methods and test geometries. Curves 1 and 2 are obtained using Zahoor and Kanninen's estimation method [4] for four-inch diameter pipes with the idealized circumferential through-wall crack subjected to four-point bending [5]. Curves 3 and 4 are obtained from finite element computations using the experimental data as the input for the center-cracked panel and three-point bend specimen, respectively [6]. Curve 5 is obtained using Zahoor and Kanninen's estimation method for a four-inch diameter pipe with a circumferential through-wall crack and an internal side-groove around the remaining net section [7]. Curves 3 and 4 show the geometric dependent of the J resistance curve verified by the finite element computations. This might be due to the inherent different plastic flow patterns for center cracked panel and three-point bend specimen under large scale yielding conditions. However, the reasons for higher J resistance curves for pipes with the idealized circumferential through-wall crack are not clear since the estimation method are used to construct the

curves. It might be due to the inaccuracies of the J estimation method. Further verifications by finite element computations are needed.

Curve 5 represents the J resistance curve for the circumferentially cracked pipe with the internal side-groove around the remaining net section, and is much lower than curves 1 and 2 which represent the J resistance curve for the circumferentially cracked pipe without side-groove. The internal side-groove was used to simulate an internal surface crack. The circumferential crack length for curves 1, 2 and 5 are 22.9, 37.1 and 25 percent of the pipe circumference, respectively. The pipe corresponding to curve 5 had an internal side-groove of 75 percent of the pipe wall thickness completely around the circumference. The same estimation method are used to construct curves 1, 2 and 5. However, the values of J at initiation are 11330 in-lb/in^2 for curve 1 and 2750 in-lb/in^2 for curve 5. Note that the circumferential crack lengths corresponding to curves 1 and 5 are approximately same. This will give an approximate factor of 4 reduction of J at initiation due to the thickness reduction from the internal side-groove. Furthermore, the slope of the J resistance for the crack growth less than 0.4 inch also is reduced approximately by the same factor due to the existence of the side-groove. The implications of the reduction of J at initiation and $\frac{dJ_{mat}}{da}$ due to the internal side-groove on the stability analysis of nuclear piping systems when the internal surface flaw around the circumference is assumed to accompany with the circumferential through-wall crack will be discussed below.

2. NET THICKNESS EFFECTS

Tada et al [8] made a stability analysis of circumferentially cracked pipes subjected to pure bending. As shown in Figure 2, t represents the remaining thickness of the pipe wall, t_o represents the wall thickness of the pipe, R is the mean radius of the remaining wall thickness, 2θ represents the total circumferential crack angle. In the analysis of Tada et al, the cross section containing the crack is assumed to be fully yielded while the other part of the pipe is elastic. The material is assumed to be perfectly plastic. Therefore, as shown in Figure 2, ϕ_{cp} represents the plastic rotation of the pipe due to crack and ϕ_t represents the total rotation of the pipe.

The analysis of Tada et al will be summarized here. Since the material is assumed to be perfectly plastic, the limit moment M_o is

$$M_o = 4\sigma_o R^2 t F(\theta) \tag{2-1}$$

where σ_o is the flow stress, and $F(\theta)$ is

$$F(\theta) = \cos \frac{\theta}{2} - \frac{1}{2} \sin \theta \tag{2-2}$$

The J integral is

$$J = -2\sigma_o R F'(\theta) \phi_{cp} \tag{2-3}$$

where

$$F'(\theta) = -\frac{1}{2} \sin \frac{\theta}{2} - \frac{1}{2} \cos\theta \tag{2-4}$$

The total rotation ϕ_t consists of the plastic rotation due to crack, ϕ_{cp}, and the elastic rotation of the pipe without crack, ϕ_{nce}.

$$\phi_t = \phi_{nce} + \phi_{cp} \tag{2-5}$$

The elastic rotation has the form

$$\phi_{nce} = C_{nc} M \tag{2-6}$$

where C_{nc} represents the elastic compliance of the pipe, and M is equal to the limit moment M_o. The applied $\frac{dJ}{da}$ can be evaluated under constant total rotation conditions. It can be obtained as

$$\frac{\partial J}{\partial a}\Big)_{\phi_t} = \frac{J}{R} \frac{F''(\theta)}{F'(\theta)} + \frac{M_o^2}{2R^2 t} \left(\frac{F'(\theta)}{F(\theta)}\right)^2 C_{nc} \tag{2-7}$$

where a represents Rθ, and F"(θ) is

$$F''(\theta) = -\frac{1}{4}\cos\frac{\theta}{2} + \frac{1}{2}\sin\theta \qquad (2\text{-}8)$$

Substituting equation (2-1) into equation (2-7) gives

$$\left.\frac{dJ}{\partial a}\right)_{\phi_t} = \frac{J}{R}\frac{F''(\theta)}{F'(\theta)} + 8\sigma_o^2 R^2 t F'^2(\theta) C_{nc} \qquad (2\text{-}9)$$

Some simple calculations using the data given in [9] reveal that the compliance in the typical piping system is large enough so that the second term on the right hand side of equation (2-9) is the dominant term for $\left.\frac{\partial J}{\partial a}\right)_{\phi_t}$. In Figure 3, $F(\theta)$, $F'(\theta)$, $F'^2(\theta)$ and $\frac{F''(\theta)}{F'(\theta)}$ are plotted as a function of the half crack angle θ. The figure shows that $F''(\theta)$ is zero at $\theta = 29^o$. Therefore, for a fixed ϕ_{cp}, the J value will be maximum at $\theta = 29^o$. The maximum $\left.\frac{\partial J}{\partial a}\right)_{\phi_t}$ will occur in the neighborhood of and less than 29^o; the exact angle will depend upon the system compliance. Accordingly to the above analysis, it is recommended that the half crack angle θ for the worst case study should be around 25^o ~ 30^o.

The applied tearing modulus T_{app} is

$$T_{app} = \frac{E}{\sigma_o^2}\left.\frac{\partial J}{\partial a}\right)_{\phi_t}$$

$$= \frac{E}{\sigma_o^2}\frac{J}{R}\frac{F''(\theta)}{F'(\theta)} + 8 E R^2 t F'^2(\theta) C_{nc} \qquad (2\text{-}10)$$

Cotter et al [9] made a stability analysis of piping systems in BWR and PWR with the assumption that a circumferential through-wall crack with different crack angles occurs at various locations in the piping systems. They found that, at least for 304 stainless steel pipe in BWR piping systems, the margin of safety is acceptable using Tada et al's approach. Their results are summarized in Table 1. In this table, a simple parameter which measures the margin of safety is defined as T_{mat}/T_{app}. These values for the worst

locations are larger than unity. It should be noted that in the analysis of Cotter et al a maximum plastic rotation due to crack is assumed to be 1^o.

Here, we examine the case of a through-wall crack and an internal surface crack completely around the circumference. The assumed crack geometry is as shown in Figure 2 with the remaining thickness t equal to one quarter of the wall thickness t_o. From the table in [9], the flow stress σ_o, and the compliance C_{nc} can be calculated based on the information provided in [9]. Then, equation (2-10) can be used to calculate T_{app} which is reduced approximately by a factor of 4 due to the reduction of net thickness which can carry the load by a factor of 4. However, J_{app} increases slightly due to the slight increase of the mean radius R of the remaining thickness for 1^o of plastic rotation. The values of J_{app} and T_{app} for various worst locations are tabulated in Table 1.

According to curve 5 as shown in Figure 1 and accounting for the differences in flow stress, the estimated T_{mat} at 550^oF is 32. (The flow stress used is 52.95 ksi which corresponds to the ASME Code minimum anticipated yield and ultimate strength at 550^oF. The flow stress [6] is defined as 1.15 times the average of yield and ultimate strength.) If $T_{mat} = 32$ is adopted for stability analysis, two of the piping system are predicted to have tearing instability for the circumferential through-wall crack with the internal surface crack.

The other concern on the circumferentially cracked pipe with internal surface flaw is the reduction of the loading capacity due to the reduction of the net wall thickness which can support the load. Figure 4 shows the load-displacement curves corresponding to curves 1 and 5 in Figure 1. The upper curve is for the pipe with the idealized circumferential through-wall crack and the lower one is for the pipe with the circumferential through-wall crack and the internal side-groove. The cracked pipes have approximately same circumferential through-wall crack lengths. For the lower curve, the net thickness that can carry the load is reduced by a factor of 4 due to the internal side-groove. The experimental data show that the reduction of the maximum load is also by the approximate same factor. The plastic displacement due to crack, however, is reduced by the same factor. This was reflected in the reduction of a factor of 4 on the estimation of the

J values at initiation. If the low J resistance curve can apply to the large diameter pipe, the calculations for the 28 inch diameter pipe in Table 1 are unrealistic since J_{app} = 12,386 in-lb/in^2 is beyond being described by curve 5 in Figure 1.

3. DISCUSSION

The implications of the low J resistance curve for the circumferentially cracked pipe with the simulated internal surface crack on the tearing instability analysis of the piping system are discussed. These calculations predict that instability is possible at a few worst locations, whereas the prior analysis indicates the pipes were fracture proof. The lack of a rigorous analysis of the J resistance curve for cracked pipes leaves speculations on the validity of the J resistance curve obtained by estimation methods. Therefore, a finite element computation together with a well-designed experiment is needed to investigate the validity of the J estimation scheme for these more realistic flaw geometries.

A well-defined T_{mat} is also needed for tearing instability analysis of nuclear pipings at different temperatures. The variation of the flow stress and J resistance curve as a function of temperature is hence needed to be determined. Furthermore, the strain hardening effects should be included in the analysis. As in [5], the strain hardening analysis give a conservative prediction of instability compared to that of the limit load analysis with a high value of the flow stress. But, the limit load analysis with a low flow stress will predict no instability as shown in [5]. Therefore, the strain hardening effect is necessary to be included in the tearing instability analysis.

Another practical concern is the behavior of a surface crack in or close to the girth weld. The J resistance curves for stainless steel weld metals have been found to be lower [10] than these for the 304 stainless steel base metal examined in this paper. The combined effects of the lower toughness of the weld metal and of the constraint due to the complex crack geometry could result in even lower T_{mat} values than that presented in this work. These effects should be investigated further.

REFERENCES

1. Paris, P. C., Tada, H., Zahoor, A., and Ernst, H., "The Theory of Instability of the Tearing Mode of Elastic-Plastic Crack Growth", Elastic-Plastic Fracture, ASTM STP 668, J. D. Landes, J. A. Begley, and G. A. Clarke, Eds., American Society for Testing and Materials, 1979, pp 5-36.

2. Paris, P. C., "Tearing Instability Analysis and Applications", Proceedings of U.S.-Japan Cooperative Seminar, "Fracture Tolerance Evaluation", East-West Center, Honolulu, December 7-11, 1981.

3. Hutchinson, J. W. and Paris, P. C., "Stability Analysis of J-Controlled Crack Growth", Elastic-Plastic Fracture, ASTM STP 668, J. D. Landes, J. A. Begley, and G. A. Clarke, Eds., American Society for Testing and Materials, 1979, pp 37-64.

4. Zahoor, A. and Kanninen, M. F., "A Plastic Fracture Mechanics Prediction of Fracture Instability in a Circumferentially Cracked Pipe in Bending - Part I: J-Integral Analysis", Journal of Pressure Vessel Technology, Vol. 103, pp 352-358, 1981.

5. Pan, J., Ahmad, J., Kanninen, M. F., and Popelar, C. H., "Application of a Tearing Instability Analysis for Strain Hardening Materials to a Circumferentially Cracked Pipe in Bending", 15th ASTM National Symposium on Fracture Mechanics, College Park, Maryland, July 7-9, 1982.

6. Kanninen, M. F., et al, "Instability Predictions for Circumferentially Cracked Type 304 Stainless Steel Pipes Under Dynamic Loading", Vol. 1 and 2, Final Report, EPRI Project T118-2, April, 1982.

7. Wilkowski, G. M., Pan, J., Kanninen, M. F., "Effects of flaw shape on J-resistance curve of a circumferentially cracked pipe", to appear in PVP Volume, ASME, New York, 1983.

8. Tada, H., Paris, P. C., and Gamble, R. M., "A Stability Analysis of Circumferential Crack for Reactor Piping Systems", Fracture Mechanics: Twelfth Conference, ASTM STP 700, American Society for Testing and Materials, 1980, pp 296-313.

9. Cotter, K. H., Chang, H. T., and Zahoor, A., "Application of Tearing Modulus Stability Concepts to Nuclear Piping", EPRI Final Report, Project T118-9, February, 1982.

10. Gudas, J. P. and Anderson, D. R., "J-R Curve Characteristics of Pipe Materials and Welds", USNRC 9th Water Reactor Safety Research Meeting, October 1981.

TABLE 1. COMPARISON OF INSTABILITY ANALYSES FOR THE BWR PIPING SYSTEM

BWR System	Outside Diameter Inch	Thickness Inch	Leff/R	Idealized Through-Wall Crack				Complex Crack (Through-Wall Crack and Internal Surface Crack)			
				J_{app}	T_{app}	T_{mat}	T_{mat}/T_{app}	J_{app}	T_{app}	T_{mat}	T_{mat}/T_{app}
Isolation Condenser											
Supply Line	12.75	0.688	131	5352	105	230	2.19	5581	28	32	1.14
Supply Line	12.75	0.688	119	5352	[illegible]	230	2.40	5581	26	32	1.23
Return Line	8.63	0.500	203	4102	163	240	1.47	4291	44	32	0.73
Return Line	8.63	0.500	194	4102	156	240	1.54	4291	43	32	0.74
Core Spray	10.75	0.594	150	4102	120	240	2.00	4281	33	32	0.97
Recirculation	28.00	1.317	95	11944	75	210	2.80	12386	20	32	1.60

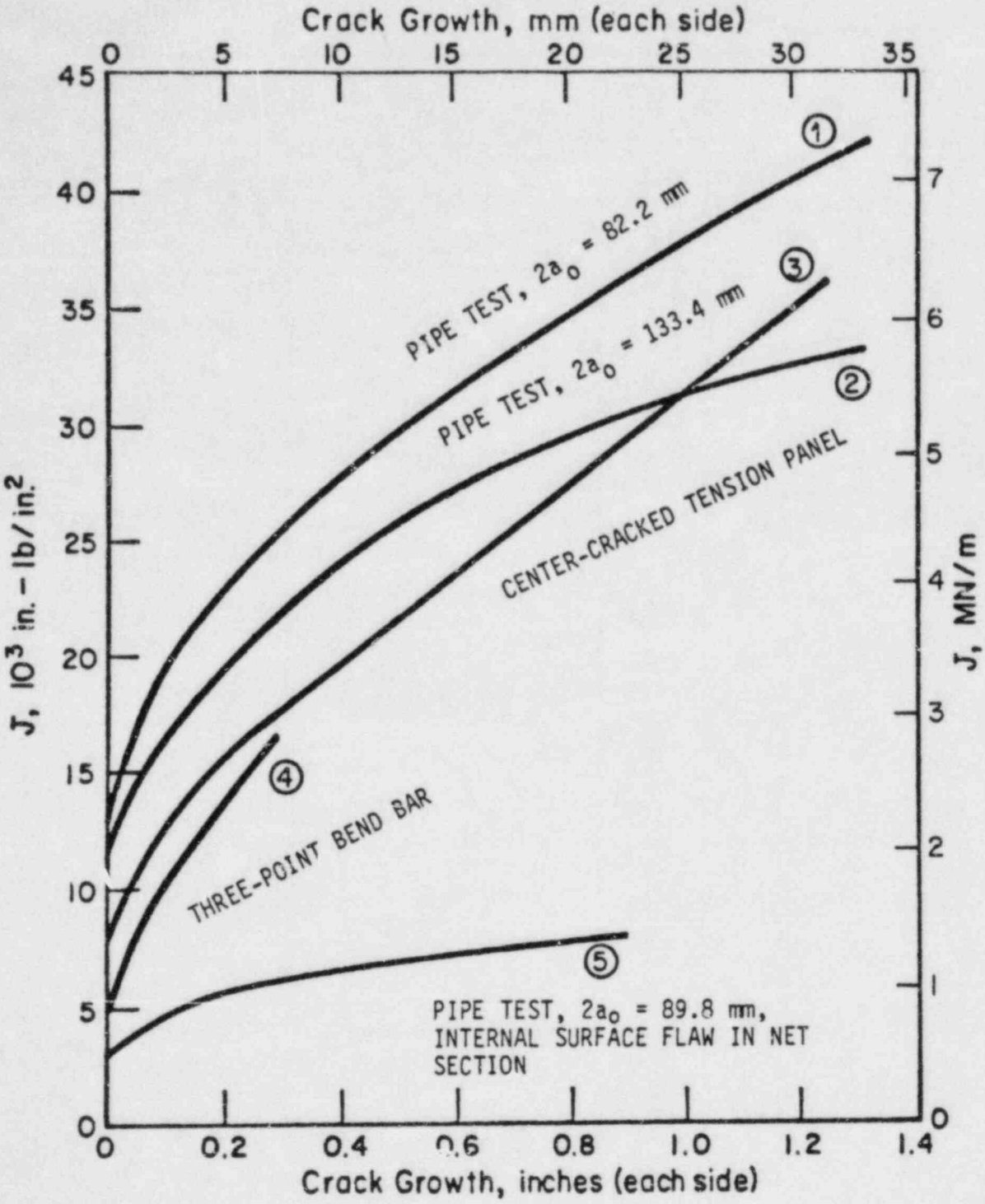

FIGURE 1. COMPARISON OF THE J RESISTANCE CURVES OBTAINED FROM DIFFERENT METHODS AND TEST GEOMETRIES FOR 304 STAINLESS STEEL

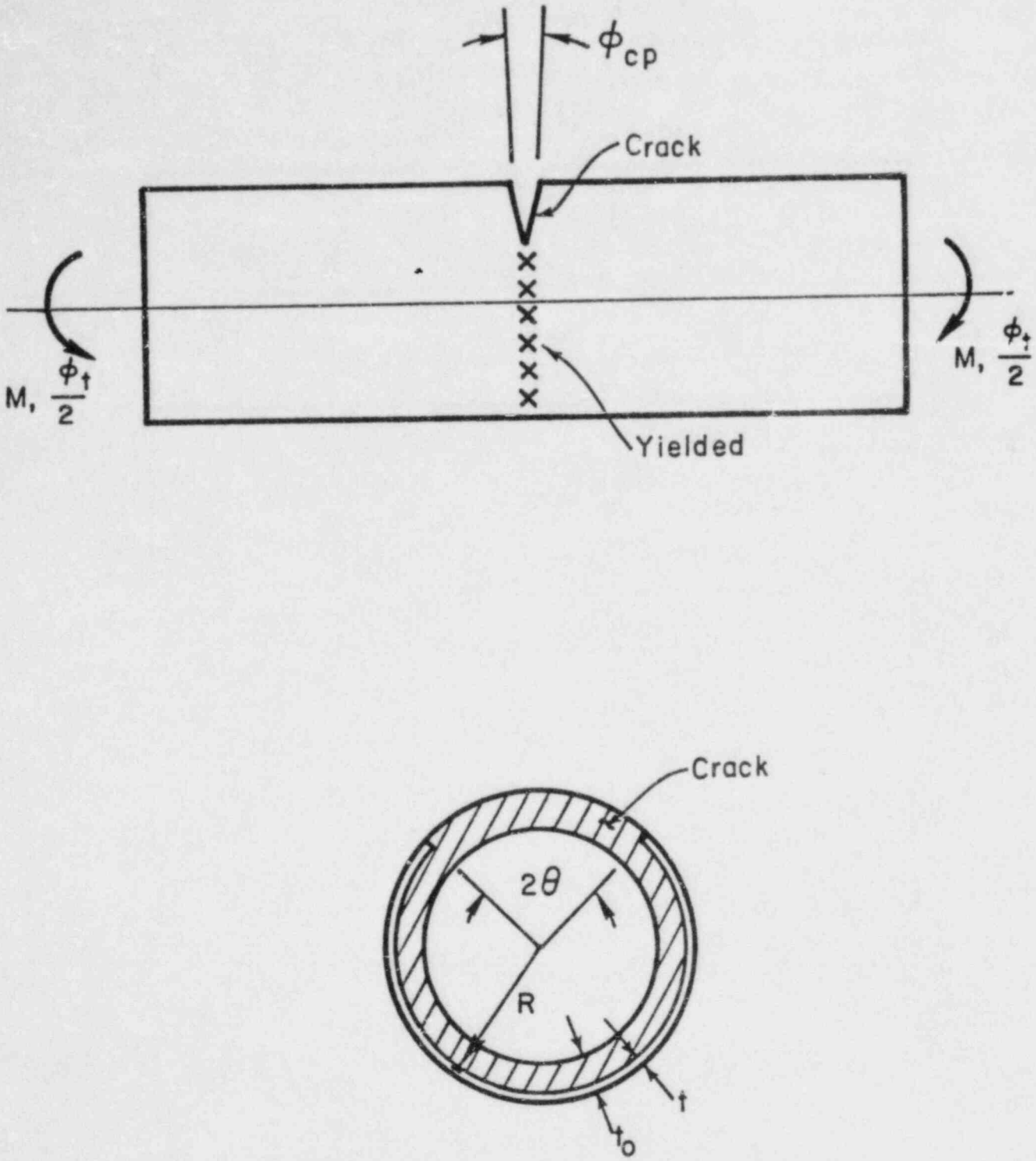

FIGURE 2. A CIRCUMFERENTIALLY CRACKED PIPE SUBJECTED TO BENDING

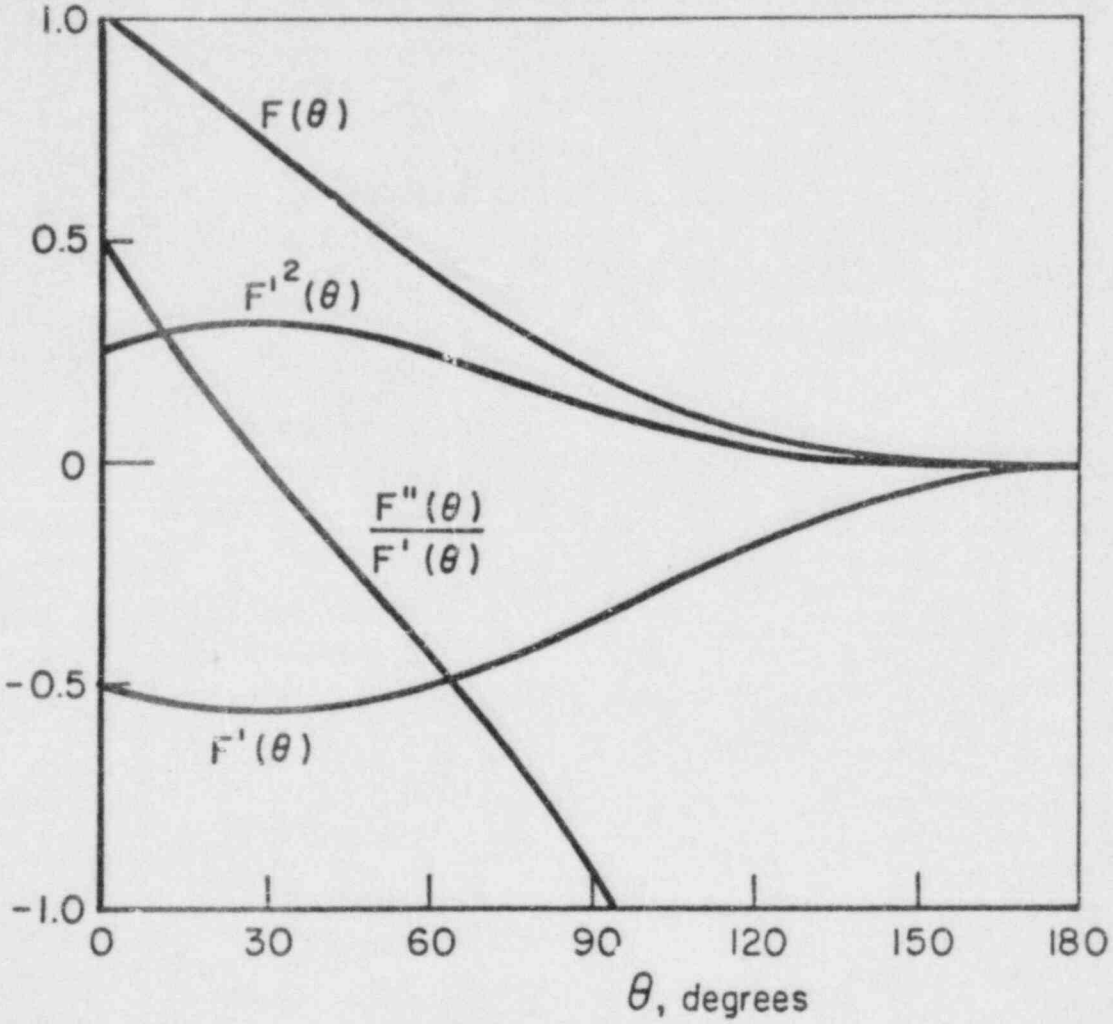

FIGURE 3. A PLOT OF THE FUNCTIONS USED FOR STABILITY ANALYSIS

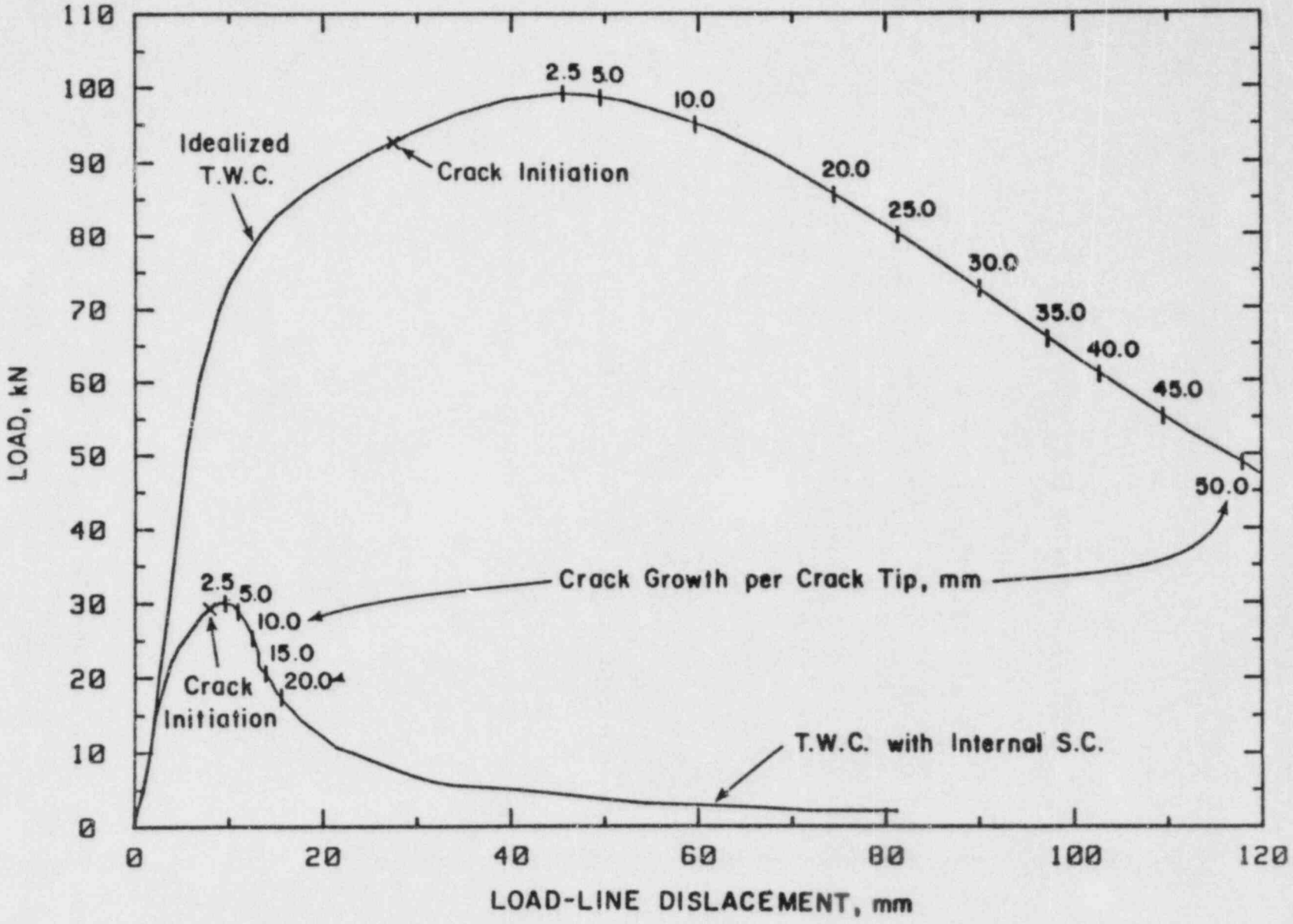

FIGURE 4. LOAD VERSUS LOAD-LINE DISPLACEMENT AND CRACK GROWTH RECORDS FOR 4-INCH SCHEDULE 80 TYPE 304 STAINLESS STEEL PIPE SUBJECTED TO FOUR-POINT BENDING

THE EFFECT OF LARGE CRACK EXTENSION ON THE TEARING RESISTANCE OF STAINLESS STEEL PIPING MATERIALS

by Paul C. Paris[1,3], James V. Brunetti[2] and Keyren H. Cotter[1]

Presented at the CSNI Specialist Meeting

on

"Leak-Before-Break in Nuclear Reactor Piping Systems"

September 1-2, 1983

Monterey, CA

[1] Fracture Proof Design Corporation, St. Louis, MO
[2] New York Power Authority, White Plains, NY
[3] Professor of Mechanics, Washington University, St. Louis, MO

ABSTRACT

For the past decade, tough materials have been characterized by the use of the J-integral crack growth resistance curve or J-R curve. Early J-R curve tests were limited to small crack extensions because the usual purpose of the tests was to determine the fracture toughness of the material, i.e., a J_{Ic} value. Such tests were valid for their intended purposes. After the development of plastic tearing stability concepts, the need for material characterization at values of J and crack extension, Δa, above J_{Ic} was obvious. In order to apply tearing stability methods to the analysis of cracks in nuclear reactor piping, data for very high values of J and large Δa are required. Furthermore, the tests must meet J-controlled growth criteria which was absent in a number of earlier tests.

In this paper, tests of typical stainless steels used in primary coolant system piping of PWR and BWR reactors are presented. The parameters considered in the test program included: temperature, 70F vs. 550F; side grooving; Inconel vs. stainless weld metal; cast vs. wrought product form; and, the location of the crack in either the base metal or in the weld metal. These parameters were evaluated in tests for values of J up to 50,000 in-lb/in^2 and Δa up to 5 inches.

The results are presented in the form of J vs. T stability curves. It was shown that the heretofore use of wrought stainless steel data based on small crack extensions and low J values is unconservative. The development of this new data suggests that certain of the analyses of nuclear piping that have been performed to date must be re-evaluated and, specifically, that the strong dependence of the material tearing resistance on the magnitude of the applied J must be taken into account.

INTRODUCTION

The objective of this study was to develop material property data in the form of tearing resistance curves or J_{mat} vs. T_{mat} J_{mat} values in the vicinity of 50-60,000 in-lb/in^2. Furthermore, the material property data had to be representative of forged stainless pipe, cast stainless elbows and several weld types over a temperature range from 70F to 550F as is found in typical BWR and PWR piping.

SPECIMEN DESIGN

Prior to the initiation of this program, the typical approach to developing J-R curves was to use a 1T or 2T compact tension (CTS) type of specimen design. The limitation in the utilization of a 1T or 2T specimen is that the maximum obtainable value of the J-integral tends to be considerably less than is required by this project. A further limitation stems from the requirement that the test data be within the allowable limits for J-controlled growth which is typically governed by the value of ω. The physical limitation imposed by the ω limits is that the crack extension, Δa, that is permitted for the 1T or 2T type specimen tends to be small. This follows from the ratio of the Δa to the remaining ligament, b. In order to

circumvent this problem, a modified CTS design was used with dimensions B = 1.0 and W = 20.0 inches. This specimen is basically a modification of the standard CTS design that permits achieving large crack extension Δa and high values of J.

Another feature of the specimen design was that the specimen could be reused for developing J-R curves for welds. This eliminated the need to fabricate additional specimens for weld material thereby keeping the test program costs as low as possible. The initial specimen design assumed that the test parameters would require the use of a/W = .6 to .7. Although it was not originally intended, it was decided early in the test program that buckling guides would be required because the deformation of the specimen induced out-of-plane bending moments that could result in buckling and thereby invalidate the test. The specimen was also selected so that the compliance method for determining Δa, that is used for the smaller CTS specimens, could be directly extended to this size specimen.

MATERIALS

A number of the PWR and BWR nuclear reactor primary cooling system (RCS) piping systems are fabricated from A376, TP316 forged sections and A351, Grade CF8M cast elbows. Thus, these materials were identified as being representative and could serve as the basis for this project. As no piping or elbow sections of actual piping were readily available at reasonable cost, suitable substitutes were required.

A240 Plate

Typical piping sizes range up to 36 inches in diameter with wall thickness up to 2.5 inches. Upon review of the material specifications for A376, TP316 piping, it was determined that a suitable substitute would be A240, TP316 plate. The one-inch thickness was selected based on cost considerations and to facilitate ease in handling the specimens. Based on a review of the existing (through 1981) literature, it was determined that data based on one-inch thick material would not be significantly different from the actual wall thicknesses found in the piping.

CF8M Cast Plate

The actual elbows found in the in RCS are cast CF8M, TP316 stainless steel. The ID's of the elbows range from 27.5 to 31 inches and have wall thicknesses that range from 2.56 to 2.88 inches. As with the piping, there were no elbows available at affordable prices and it was necessary to develop representative material for use in the specimens. One approach considered was that of making centrifugally or statically cast pipe sections, slitting the sections, and then rolling them flat to make a specimen suitable for testing. This was rejected in favor of a static cast flat plate. This casting design used simulated cooling rates that might be expected in the actual elbow castings.

The soundness requirement used for casting of the plate was that one of the four quadrants of the plate had to meet the radiography requirements of ASTM E-446, Severity Level 2. It was further mandated that the best quadrant meeting Level 2 or better should be identified as that would be the quadrant that would be used for developing material property data.

Welds

After testing the base metal specimens, the specimens were cut into two pieces along the plane of fracture. Thus, the specimens for welding were obtained by re-using these A240 and CF8M brace metal test specimens. Then, the outside edges of the plate (the edges parallel to the fracture plane) were bevelled in preparation for welding. Welds were then made using both E316L electrodes and Inconel weld metal. The following welds were made: E316L weld of A240 plate, E316L weld of CF8M cast plate, and Inconel weld of A240 plate.

It is important to note that the actual welding of the specimens was performed by welders that are qualified for fabrication at a nuclear plant construction site. Thus, the conditions surrounding the fabrication of the specimens were as close as possible to the typical conditions existing during the fabrication of a plant rather than that of a laboratory environment.

TEST PROCEDURE

The specimens were finish-machined followed by saw cutting to a pre-determined length to facilitate pre-cracking. A pre-cracking procedure following ASTM E813-81(1) was utilized to produce a crack having the desired initial length. The test was conducted following the procedures of ASTM E813-81(1) and periodic unloading slopes were produced following the usual procedures. The load was measured by a load cell and recorded both digitally and graphically. The displacement was computed based on the measured ram stroke and was recorded both digitally and graphically. Verification of crack extension, Δa, was achieved using optical observation of crack extension and fatigue marker bands. In addition, the final crack length was compared with the predicted crack length.

DATA REDUCTION

Preliminary data in the form of J vs. Δa was derived. But, data, in the form of J-Δa curves, cannot be readily adapted for use in analytical studies of crack stability. Accordingly, development of J-T curves is required. Because the preliminary data contained some scatter, smoothing was required. The procedures for smoothing of the data, plotting, correcting for errors in Δa based on observed vs. computed and correcting for displacement effects on J and Δa follow below.

Smoothing

As mentioned above, the raw laboratory data contained varying degrees of scatter, that is normally found, along with errors due to large displacement effects. The effects of large displacement were accounted for by introducing a correction due to Tada(2). Then, using a conservative procedure, the data was smoothed. The conservatisms in the approach included the developing of an adjusted or smoothed J-Δa curve wherein the value of J, as adjusted, and the slope of the smoothed J-Δa curve are always less than what is evident from the actual corrected experimental data. It must be emphasized that the purpose for this smoothing is simply to facilitate the numerical computation of dJ/da from the data by the computer codes. That is, data containing the usual amount of scatter does not lend itself readily to development of tearing modulus values.

Development of J_{mat}-T_{mat} Curves

The J-Δa curves, after smoothing, were used to develop J_{mat}-T_{mat} curves for each of the test conditions. The method used relied on fitting a second order polynomial through five points and taking the slope at the mid-point. This procedure and plotting of the data was achieved using the JTPLOT(4) program.

FRACTURE SURFACE MORPHOLOGY

Figure 1 compares the fracture surfaces of A240 plate tests. The specimens are numbered from left to right, starting with specimens SS4 and SS6 which were tested at 70F and followed by specimens SS3, SS7 and SS8 which were all tested at 550F. It is noted that there is considerably more shear on the specimens at 550F compared with those at 70F. However, this is not true for the specimen with side-grooving, SS8, where a very flat fracture surface is noted.

The cast CF8M material at the two temperatures is shown in Figure 2. On the left side of the figure, the 550F specimens C2 and C4 are shown followed by C3 and C1 at 70F. In comparing the cast fracture surfaces with those of the A240 plate, it is noted that the fracture surface is much more granular in appearance and that there is considerable deformation evident on the side of the specimen. It is further noted that the elevated temperature specimens tend to have slightly more shear on the fracture surface than at 70F.

The pronounced difference between the cast vs. wrought fracture surfaces can be seen in Figure 3. The specimens on the left are cast specimens C4 and C2 followed by wrought specimens SS3 and SS7 and all were tested at 550F.

The welded cast specimens are shown in Figure 4 wherein we read from left to right as follows: the first specimen is WC1, followed by WC4, WC3, WC2, then followed by the unwelded specimens, C4 and C2. All of these specimens were tested at 550F. We further note that specimen WC1 had been side-grooved and shows a much flatter fracture surface than the other specimens. As might be expected, the fracture surfaces of the welds are quite similar to that of the cast specimens.

The welded plate specimens, again from 550F tests, are shown in Figure 5. The side-grooved specimen, on the far left, is WSS4 and it shows a very flat fracture surface. This is followed by three other welded specimens, WSS7, WSS6 and WSS3. Lastly, the unwelded specimens SS3 and SS7 are shown on the right-hand side of Figure 5. It is noted that the fracture surface of welded plate specimens tends to be quite similar to that of the unwelded specimens. It is also noted, by comparing Figures 4 and 5, that the appearance of the fracture surface of the welded cast plate shows considerable difference from the welded plate.

Finally, in Figure 6 we compare the Inconel weld with the E316L weld. Reading from left to right, we have specimen WSS7 followed by WSS2, WSS4 and finally WSS1. The two specimens on the right are side-grooved and show a much flatter fracture surface than those which are not. Specimens WSS1 and WSS2 are from an Inconel weld while the others are from the E316L weld and all were tested at 550F.

TEARING RESISTANCE RESULTS

Base Metal

Figure 7 shows the crack growth resistance data developed for A240 plate. No predominant temperature effect can be seen upon comparing the 70F and 550F tests. However, the side-grooving naturally lowers the value of the tearing modulus for corresponding values of J.

On the contrary, a pronounced temperature effect is found to exist for cast CF8M as seen in Figure 8. This effect is consistent with the results of Bamford and Bush(3) and other investigators(5-7). In comparing the difference between cast and wrought type 316 stainless steel, as shown in Figures 9, it is noted that the cast material has lower tearing resistance at 550F than that for the A240 plate.

The actual effect of the side-groove can be idealized as follows. Since the actual pipe does not contain a side-groove, rather it is either smooth or has a weld, there is no need to use test data based on the side-groove for an application that does not involve a side-groove. It is noted that side-grooving may be a reasonable idealization of the behavior of cracks in the presence of IGSCC such as that found in BWR recirculation piping. However, PWR primary systems are not prone to IGSCC. Thus, it is felt that utilization of data based on side-grooving may be unduly conservative for applications not prone to IGSCC. Side-grooving, however, does serve to keep the crack growth along a well-defined plane as can be noted by observing the fracture surfaces. Therein it is readily apparent that the side-grooved specimens result in a very flat crack plane whereas the others tend to seek the path of least resistance.

Weld Metal

In Figure 10, welded A240 plate is compared with base metal. Therein it is readily apparent that the welds have properties that tend to be quite

similar to those of the base metal. This is noted by comparing specimens SS3 and SS7 with WSS3 and WSS7. We note that specimens SS8 and WSS4 are side-grooved which accounts for their lower tearing resistance. The results for specimen WSS6 were considered an anomaly. This conclusion can be drawn by observing Figure 5 wherein the crack surface morphology of specimen WSS6 is characteristically different from those of the other welded A240 specimens. Specimen WSS6 will be subjected to fractography and metallurgical evaluation in the future to attempt to isolate the causative metallurgical factors. The similarity of the crack surface morphology of the base metal specimens SS3 and SS7 with the welded specimens WSS3 and WSS7 should be noted. It is reasonable to use the same argument to disregard the side-grooved WSS4 data as was used for the SS8 side-grooved specimens.

In Figure 4, the similarity of the crack surface morphology of the welded CF8M with the base metal CF8M can be noted. This would lead to the expectation of similar resistance curves for the welded CF8M compared with the CF8M base metal. However, some noticeable difference occurs upon examining the values of the tearing modulus. The results shown in Figure 11 indicate that the tearing resistance of the weld specimens is less than the base metal. This can be attributed to the difference in flow stress between the weld and base metals.

Finally, in Figure 12, the results of the Inconel weld tests on specimens WSS1 and WSS2 are compared with those of the E316L welds. It is noted that very little difference exists between the two types of welds. The specimens without the side-grooves, WSS2, WSS3 and WSS7, have similar tearing resistance. For the specimens with the side-grooves, WSS1 and WSS4, the tearing resistances are quite similar with the Inconel data showing slightly greater resistance.

Lower Bound Data

The development of lower bound crack growth resistance data must be based on both the crack driving force, J_{mat}, and the value of the tearing modulus, T_{mat}. A complete set of all tests is shown in Figure 13. It is immediately apparent that the side-grooved welded specimens WSS4 and WC1 have the lowest values. As stated before, it is not felt that this data is representative of the conditions that are present in PWR's not prone to IGSCC. Upon further examination, the data evidenced by specimens WC4 and WSS7 appear to represent valid lower bounds for the cast and wrought material respectively in non-IGSCC environments.

CONCLUSIONS

It was shown that a definite temperature dependence exists for a wide range of J_{mat} values for cast CF8M stainless steel. It was also shown that welds have lower tearing resistance than base metal and that side-grooving can reduce the apparent crack growth resistance properties of both base metal and weld metal material. It was concluded that use of tearing modulus data based on cast CF8M at 550F is a reasonable lower bound for most stainless steel piping applications. This lower bound is strictly applicable only to welds of cast sections. Stability can be demonstrated for higher values of

applied tearing modulus in wrought than in cast TP316 stainless steels and similarly in base than in weld metals.

Based on the above results, we find an overall minimum expected value for tearing modulus to be approximately 20 at 550F in a CF8M weldment and at a value of J_{mat} equal to 28,000. Somewhat higher values of T_{mat} are found for other materials.

Such results suggest that previous analyses of stainless steel piping that were based on values of $T_{mat} = 200$ must be re-evaluated to insure structural safety is not impaired.

REFERENCES

1. ASTM Specification E813-81.

2. Tada, Hiroshi, Private Communication, April 1983.

3. "Fracture Behavior of Stainless Steel", Bamford, W. H. and Bush, A. J., ASTM STP 668, p. 553, 1979.

4. "JTPLOT" Computer Code, Version 2, Level 3, Fracture Proof Design Corporation, St. Louis, MO.

5. Private Communication, John Gudas, NSRDC, Annapolis, MD, July 1981.

6. "The Effect of Aging on Cast Stainless Steel", Bamford, W.H., Westinghouse Report dated June 1980.

7. "Interim Report on Fracture Toughness of Operating Reactor Internal Stress", James, L.A., HEDL Corr. No. 7950722, dated March 1, 1979.

Table 1, SUMMARY OF TEST PARAMETERS

Spec. No.	Material	a_i/W	Temp(F)	Side Grooved
SS4	A240 plate	.693	70	N
SS6	"	.604	70	N
SS3	"	.696	550	N
SS7	"	.603	550	N
SS8	"	.675	550	Y
C1	CF8M cast	.601	70	N
C3	"	.602	70	N
C2	"	.606	550	N
C4	"	.603	550	N
WSS1	Inconel weld (A240)	.600	550	Y
WSS2	"	.590	550	N
WSS3	E316 weld (A240)	.590	550	N
WSS4	"	.600	550	Y
WSS6	"	.600	550	N
WSS7	"	.585	550	N
WC1	E316L weld (CF8M)	.595	550	Y
WC2	"	.595	550	N
WC3	"	.600	550	N
WC4	"	.590	550	N

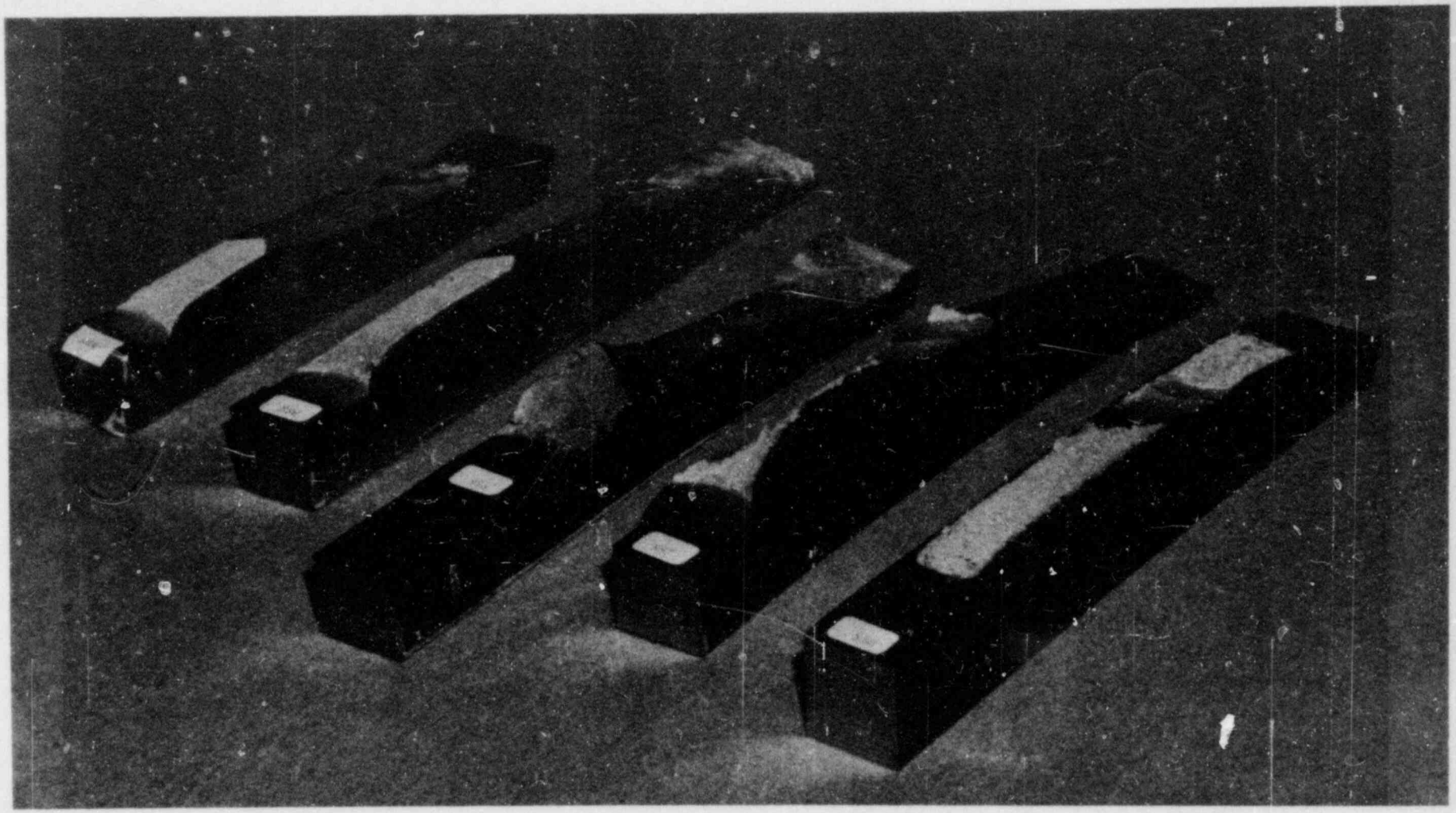

Figure 1 Fracture Surfaces of A240 Plate Test Specimens. Specimens Numbered Left to Right: SS4, SS6, SS3, SS7, SS8

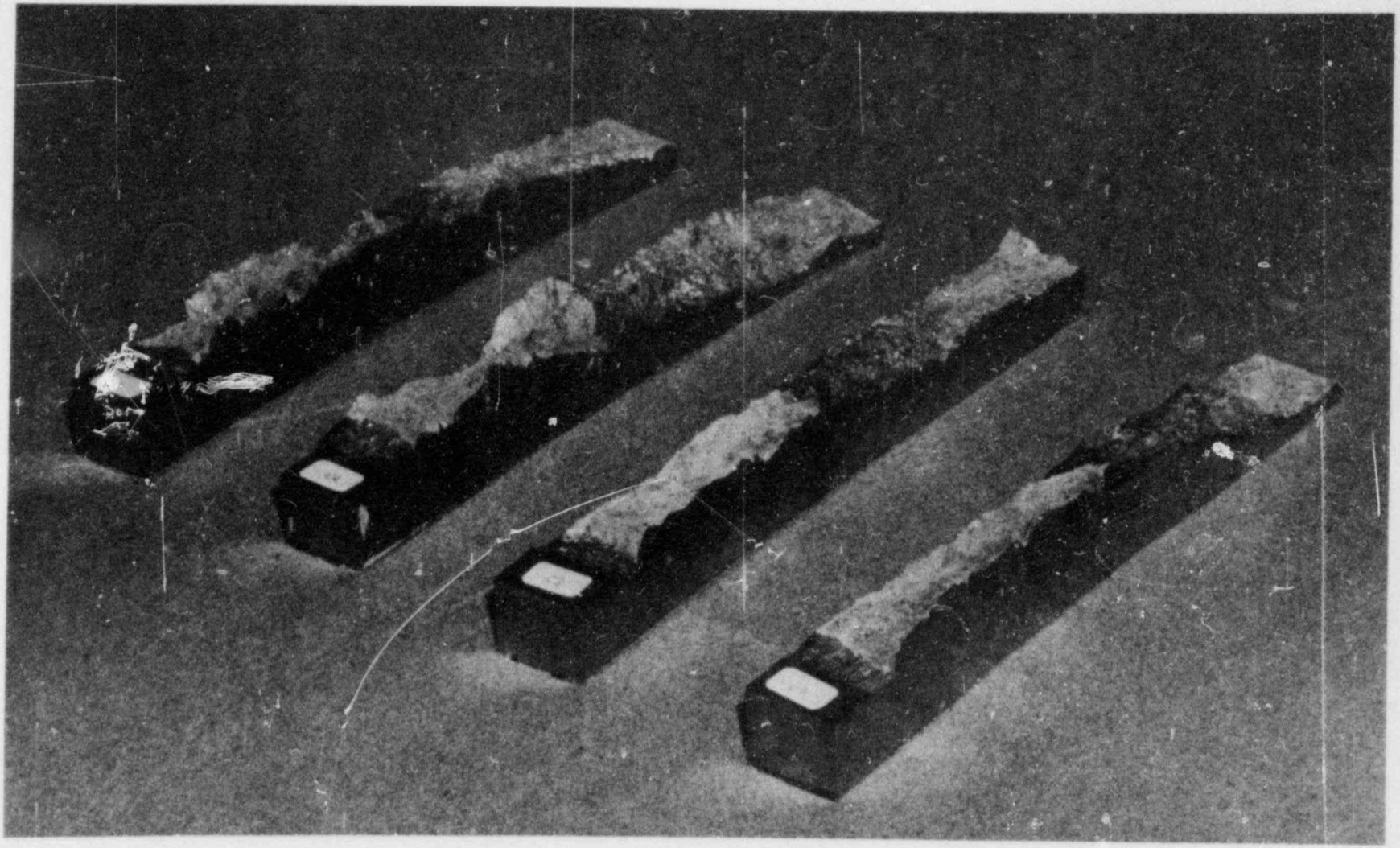

Figure 2 Cast CF8M Test Specimen Fracture Surfaces. Specimens Numbered Left to Right: C2, C4, C3, C1

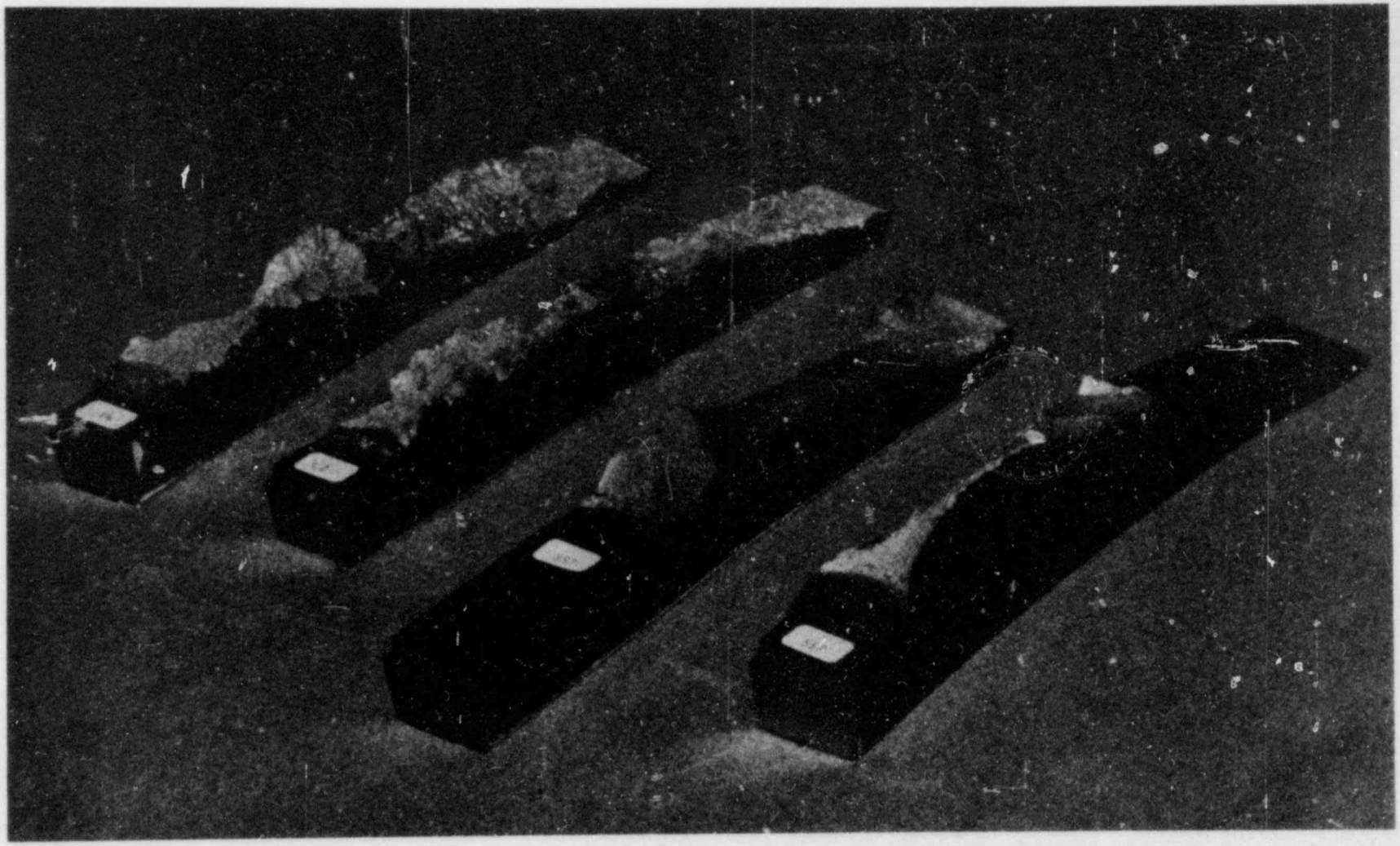

Figure 3 Comparison of Cast CF8M and Wrought A240 Plate Specimens at 550F. Specimens Numbered Left to Right: C4, C2, SS3, SS7

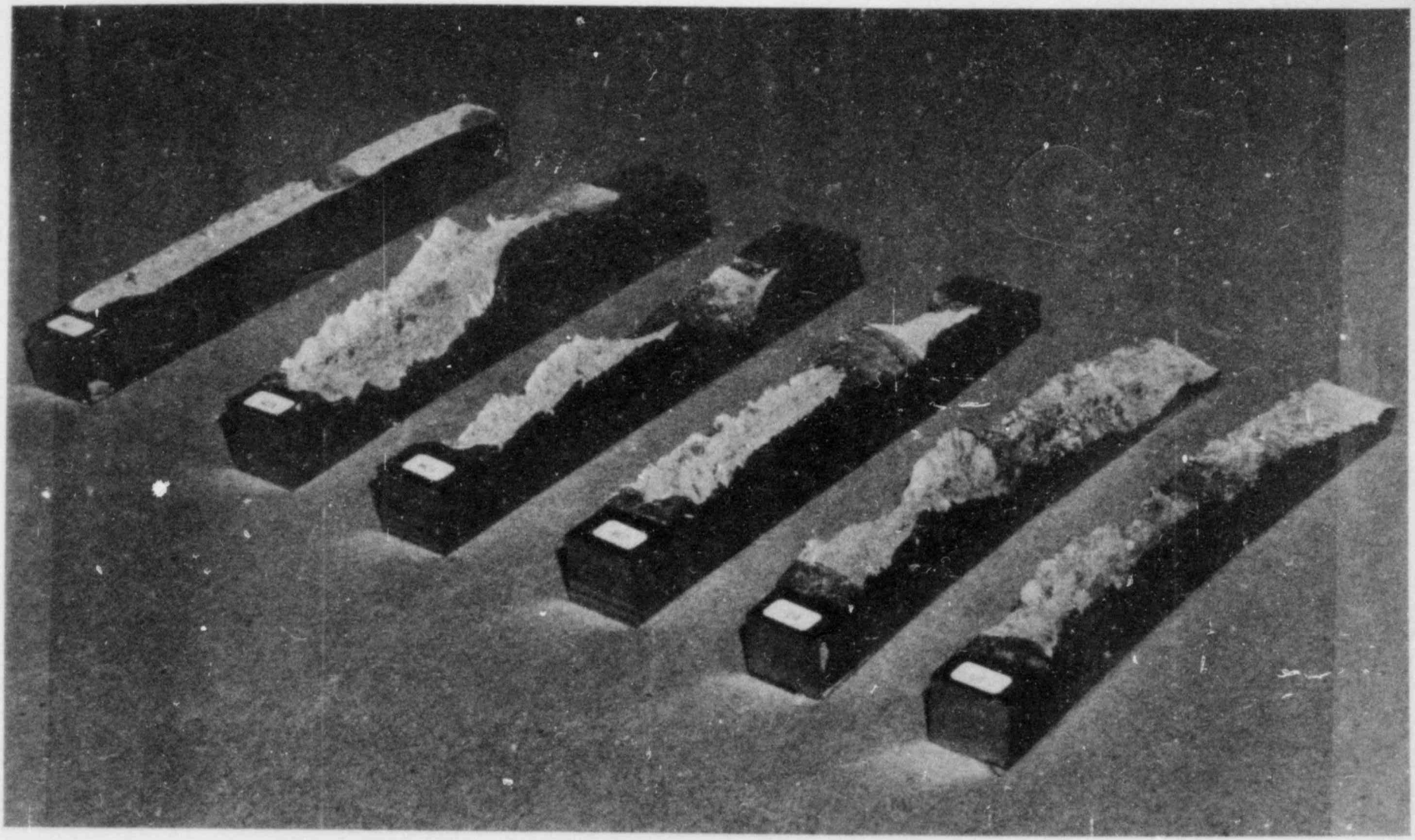

Figure 4 Comparisons of Fracture Surfaces of CF8M Casting Welded with E316L Weld Metal with Base Metal. All Specimens 550F. Specimens Numbered Left to Right: WC1, WC4, WC3, WC2, C4, C2

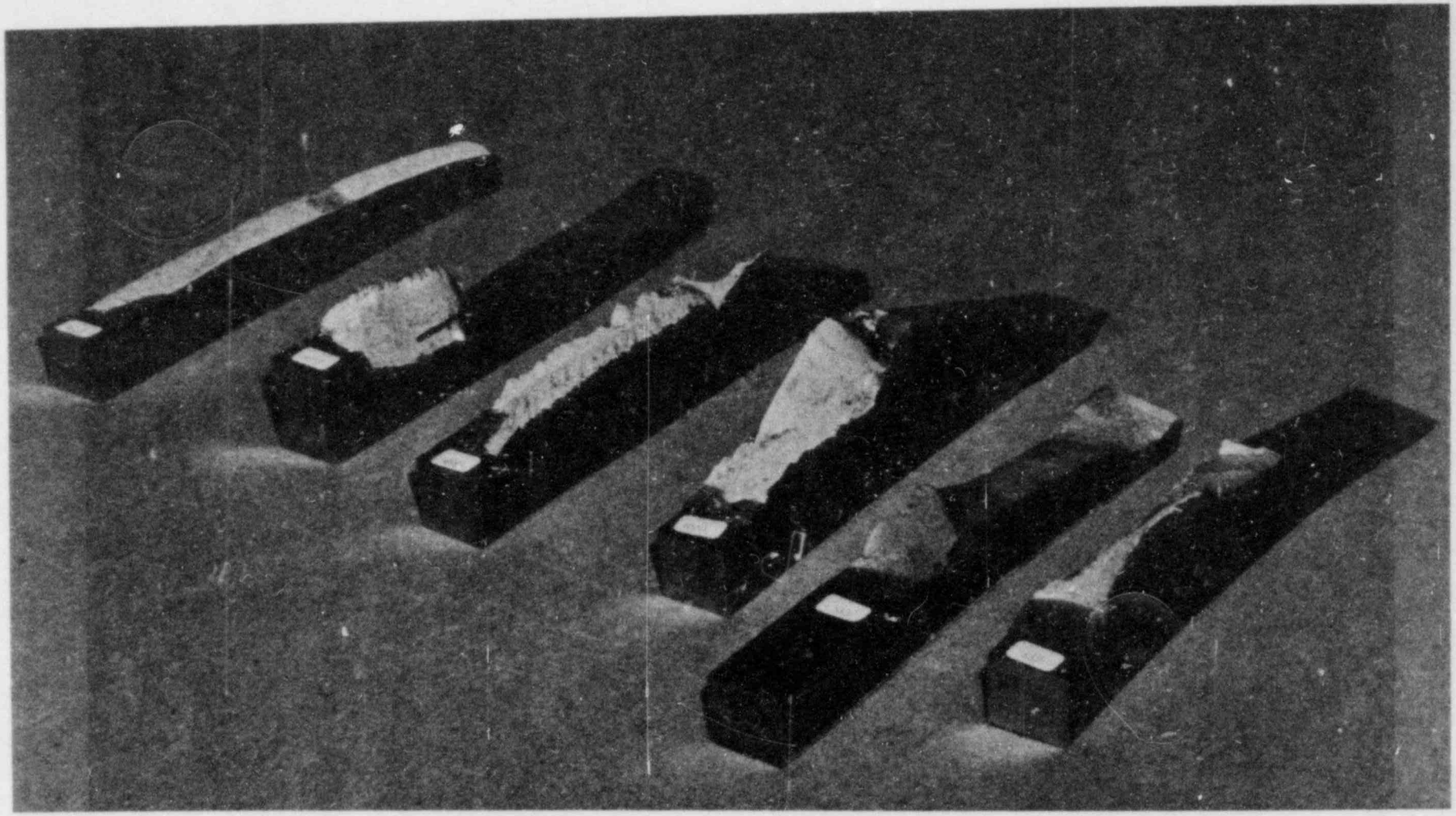

Figure 5 A240 Plate Welded with E316 Electrode Fracture Surfaces Compared with Base Plate for Tests at 550F. Specimens Numbered Left to Right: WSS4, WSS7, WSS6, WSS3, SS3, SS7

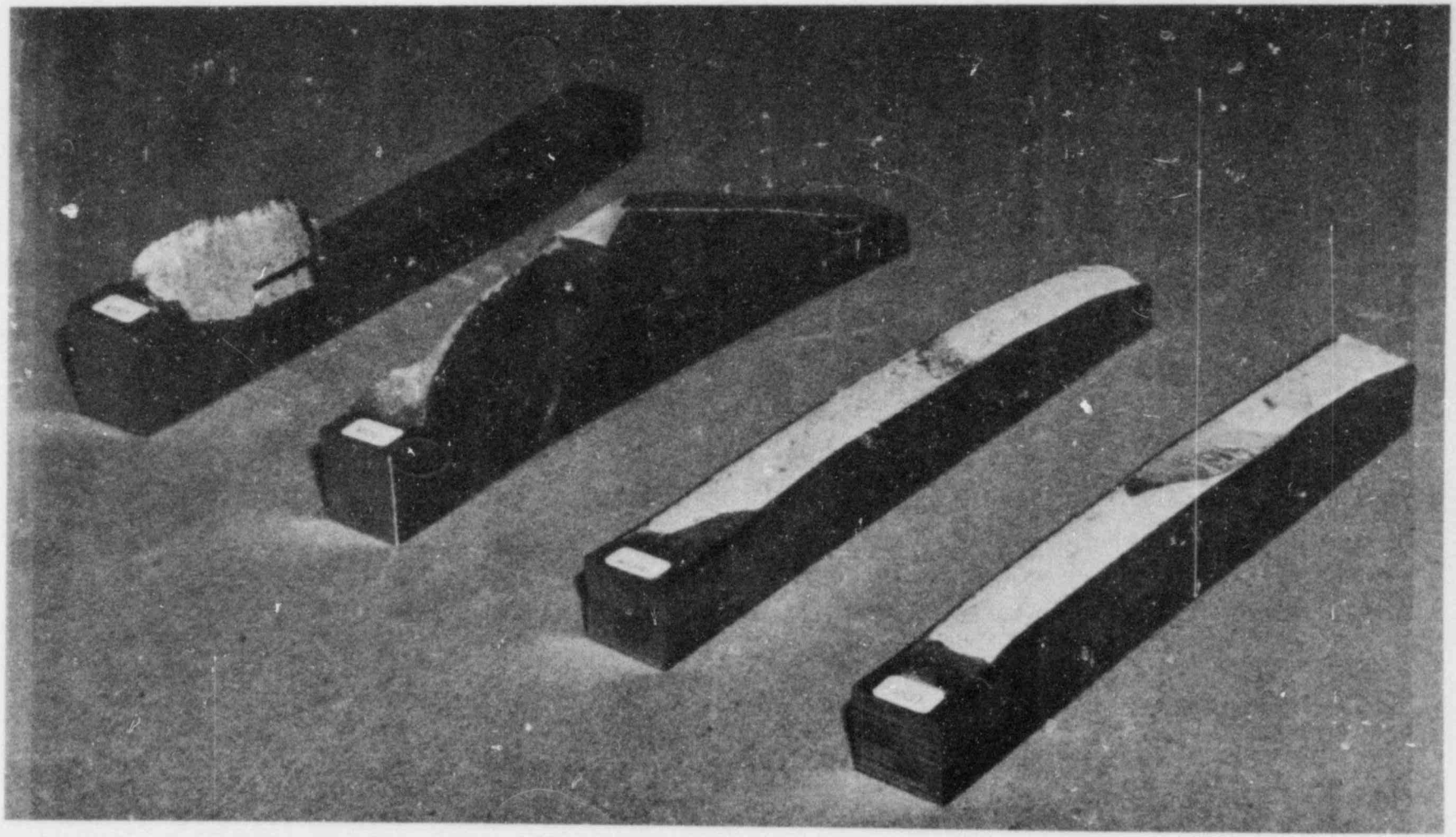

Figure 6 Comparison of the Fracture Surfaces of E316L and Inconel Weld Metal for Specimens Tested at 550F. Numbered Left to Right: WWS7, WSS2, WSS4, WSS1

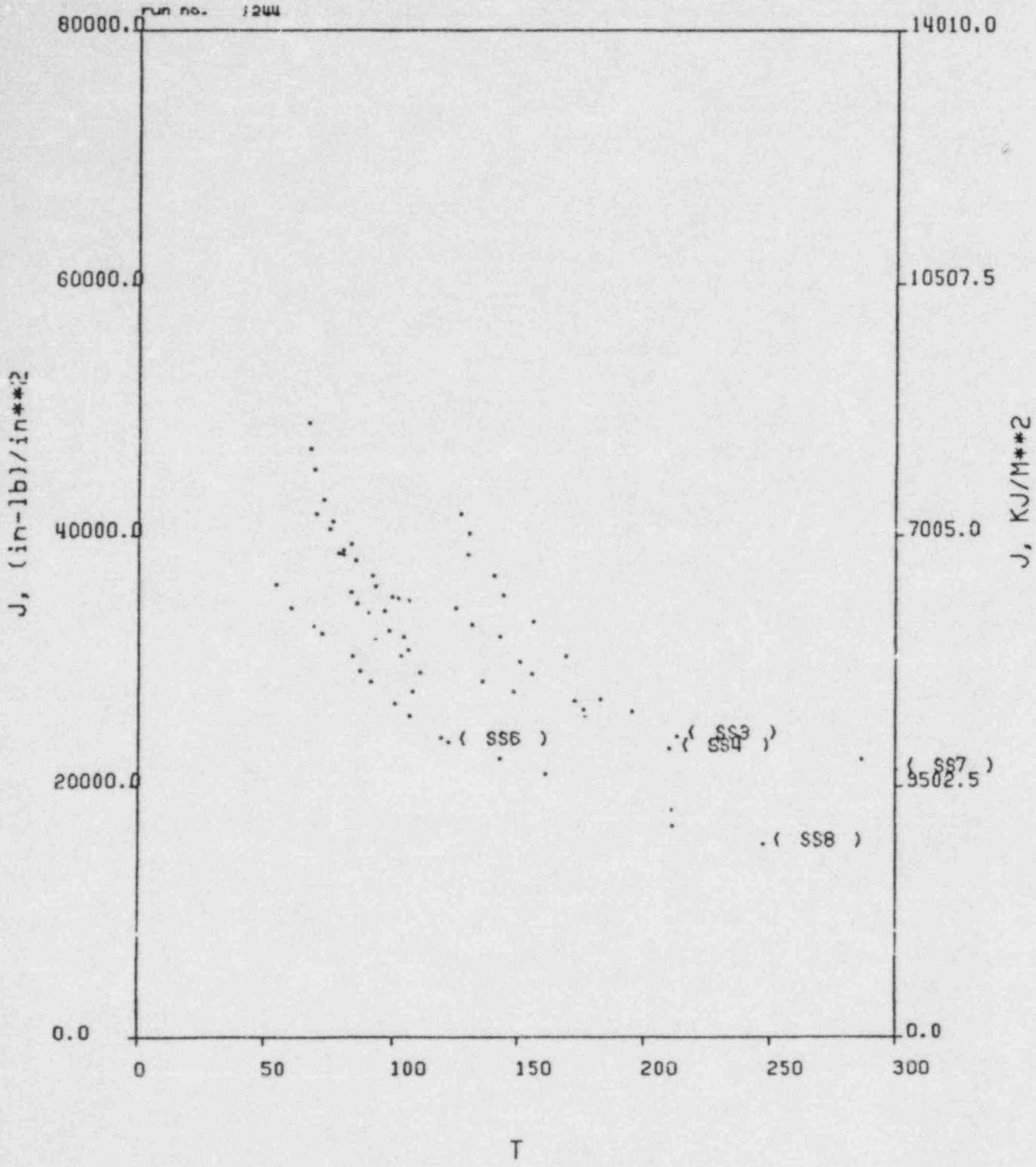

Figure 7 J vs. T Material Curves for A240 Plate at 70F and 550F

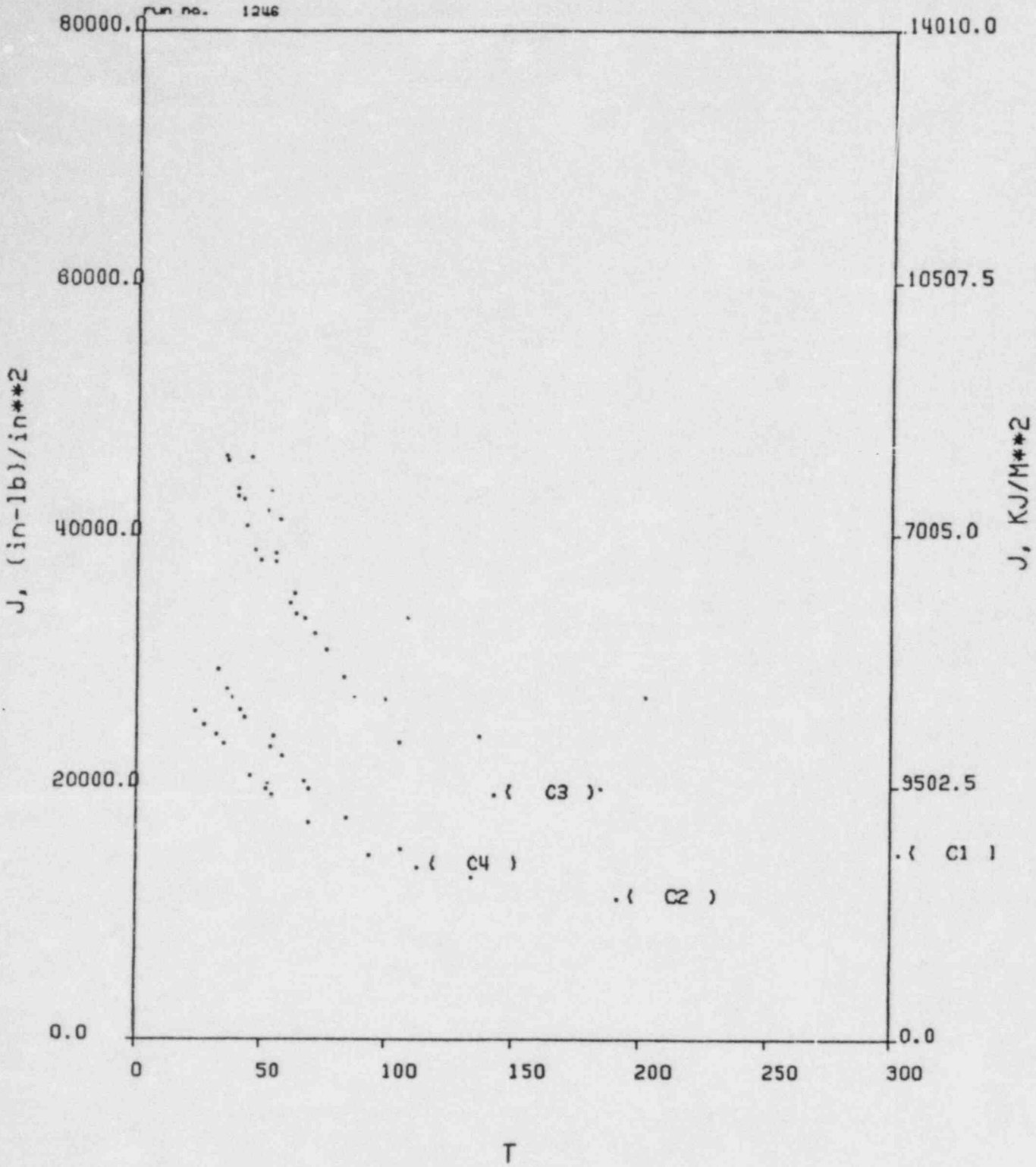

Figure 8 J vs. T Material Curves for CF8M Plate at 70F and 550F

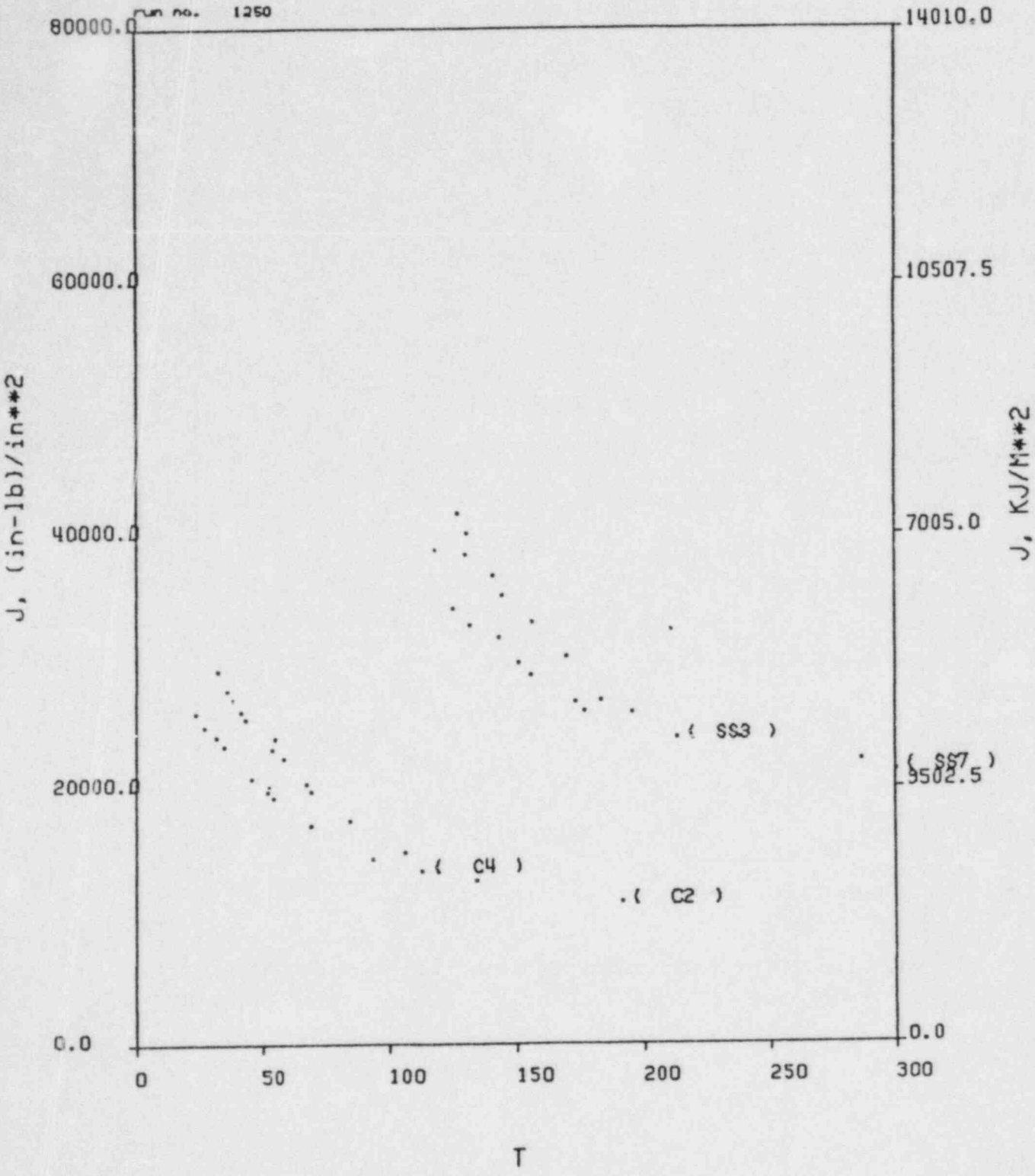

Figure 9 Comparison of J vs. T Material Curves for CF8M Casting with A240 Plate at 550F

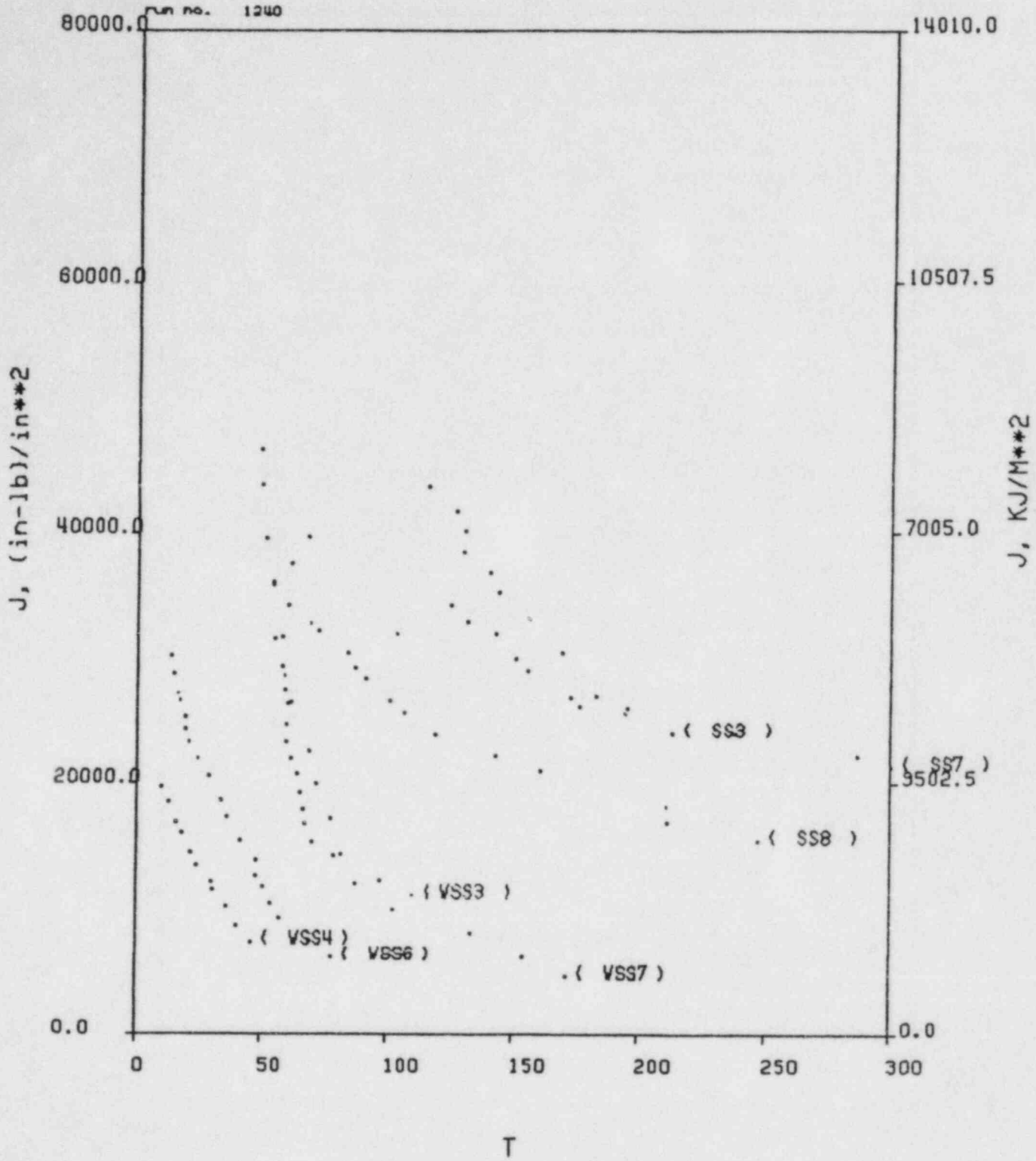

Figure 10 J vs. T Material Curves Comparing Welded A240 Plate with Base Metal at 550F

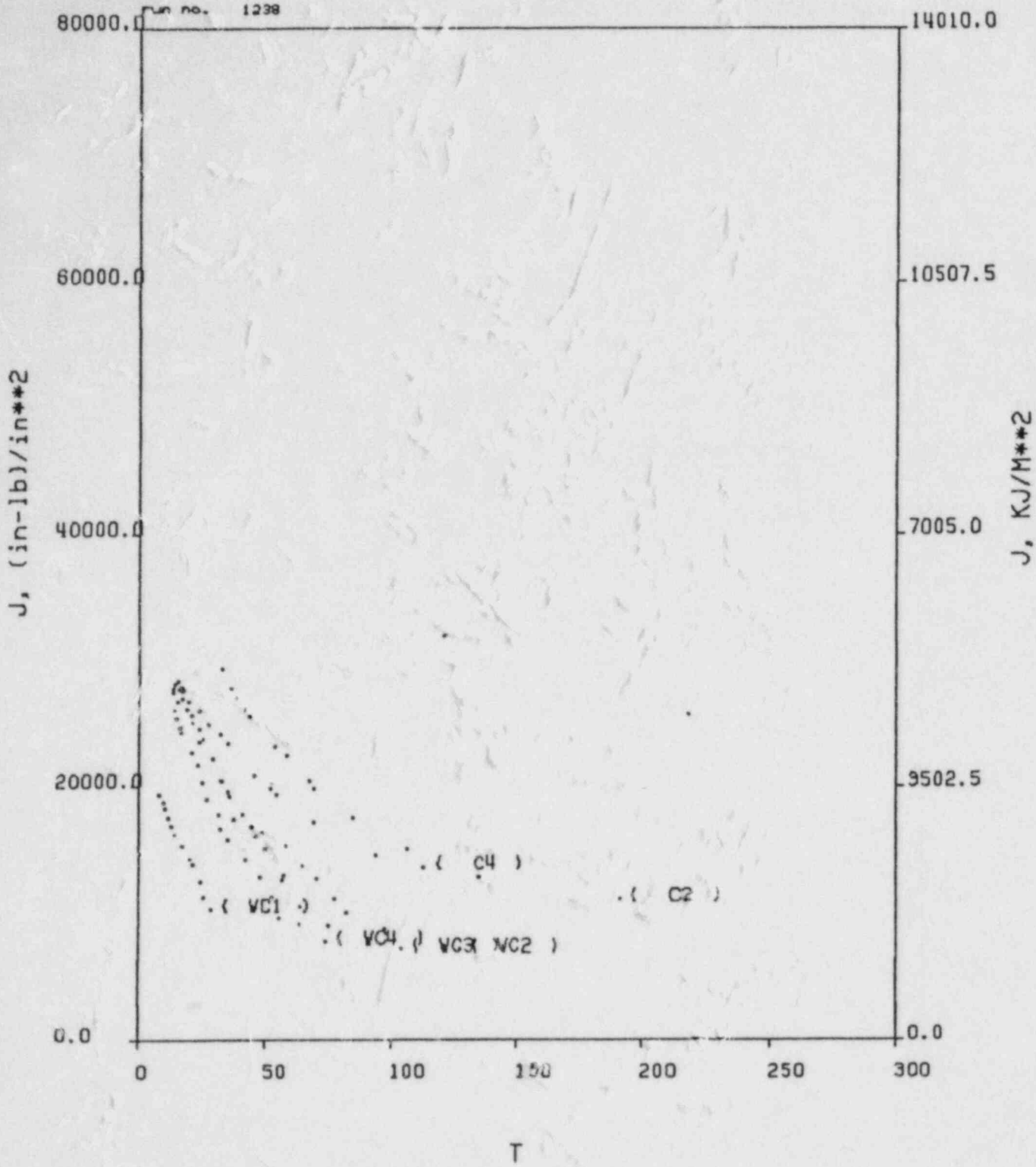

Figure 11 J vs. T Material Curves for E316 Welded CF8M Compared with Base Metal CF8M at 550F

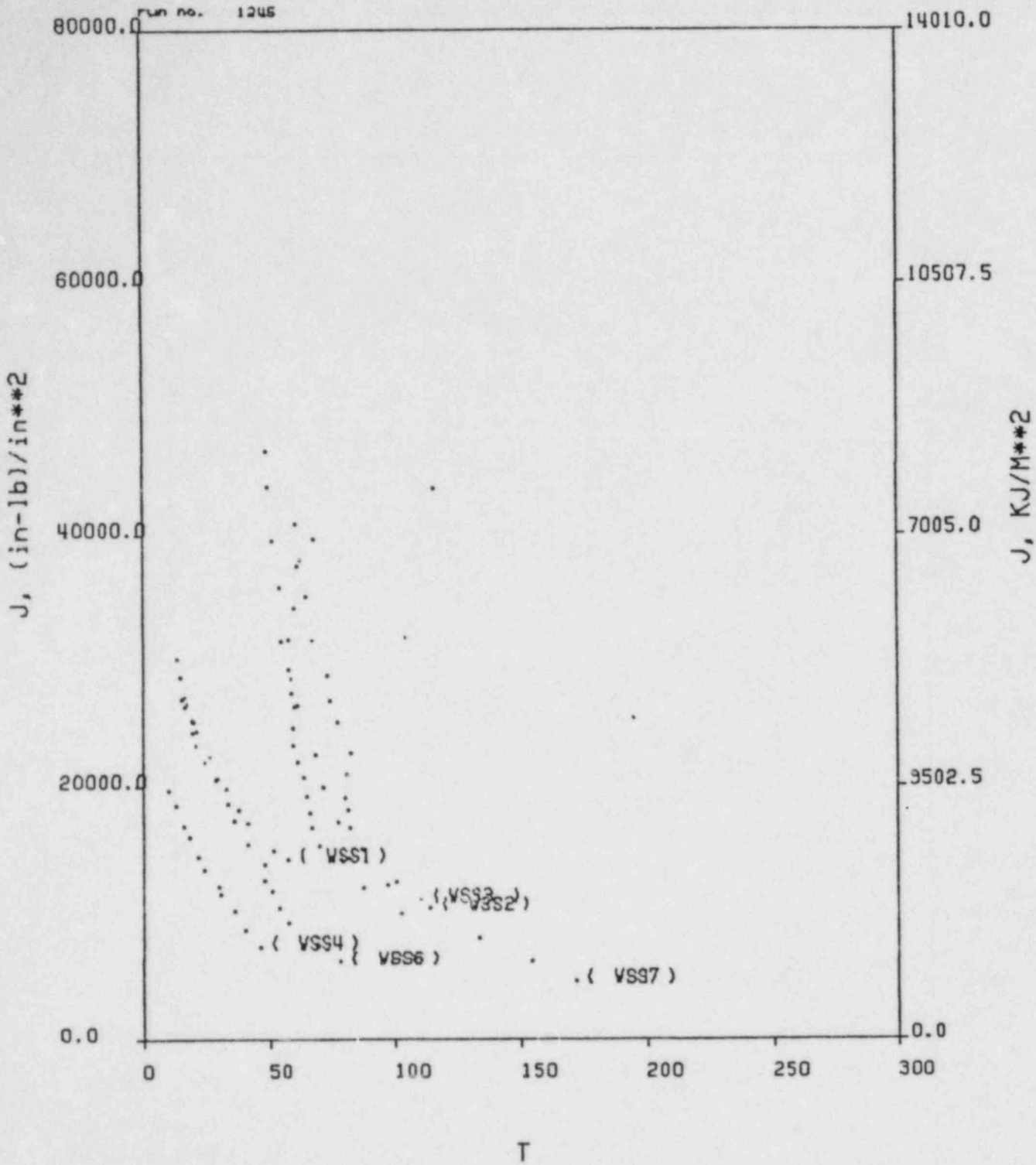

Figure 12 J vs. T Material Curves at 550F Showing Effect of Weld Metal Type and Side-Grooving on Tearing Resistance for Welded A240 Plate

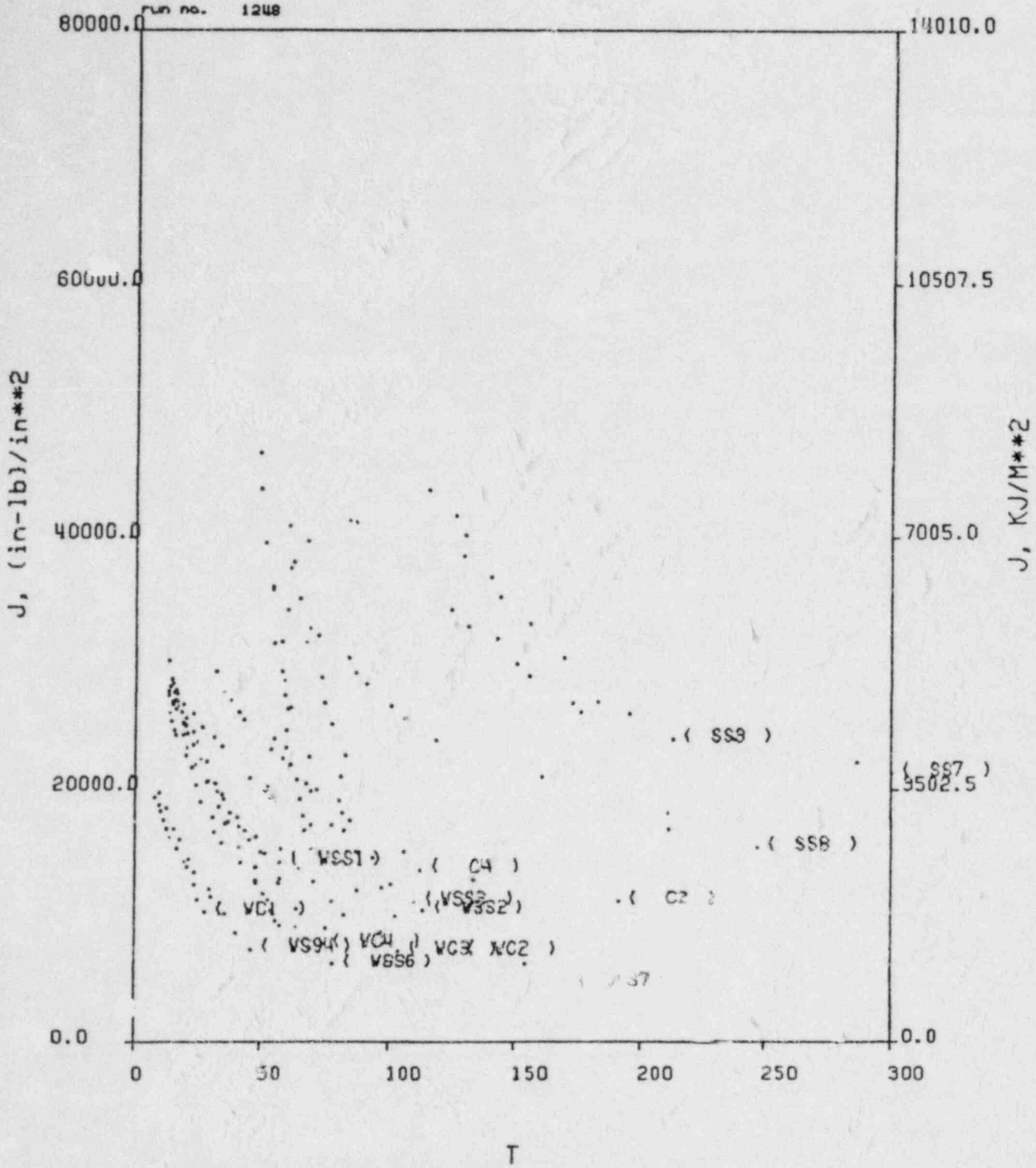

Figure 13 Summary of All J vs. T Data at 550F

Assessments of Leak and Break Margins in Stainless Steel Power Plant Piping

Kunio Hasegawa*
Tasuku Shimizu*
Shigeru Shida*
Tsutomu Hayashi**

Abstract

Leak and break loads for Type 304 stainless steel pipes containing circumferential part-through cracks are predicted by simple methods based on the net-section stress approach. Evaluation of critical sizes of the cracks is studied, and the allowable flaw sizes for pressurized pipes were discussed from the viewpoint of leaks and breaks.

* Mechanical Engineering Research Laboratory, Hitachi, Ltd., Saiwai-cho 3-1-1, Hitachi-shi, Ibaraki-ken, 317, Japan.

**Hitachi Works, Hitachi, Ltd., Saiwai-cho 3-1-1, Hitachi-shi, Ibaraki-ken, 317, Japan.

1. Introduction

Austenitic stainless steel is the principal structural material for light water reactor piping. The steel is a tough ductile material that exhibits considerable strength even when flaws such as stress corrosion cracks exist.

However, an accurate quantitative safety margin for the piping is required both to set inspection requirements and to guide replacement/repair decisions when cracks are actually detected. To assess the margin of safety for degraded piping, three items must be considered; the size of the load at which coolant leaks from a part-through crack, the size of the break load which is the maximum load following coolant leakage, and the possibility of unstable crack growth.

Attempts to account for the leak and break loads for pipes preceding fracture instability has led to the development of several fracture approaches. The net-section stress approach is convenient for estimating leak and break loads [1~3]. The J-integral tearing modulus criterion [4], which takes the effect of piping system compliance into account, can determine the point of an unstable fracture.

This paper is concerned with pipe leak and break criteria leading to the evolution of critical size of circumferential cracks in Type 304 stainless steel piping.

2. Leak and Break Criteria for Cracked Pipe

2.1 Crack Growth Behavior

It is important to ascertain a realistic mode of fracture in order to assess the safety margin for piping containing a crack. A schematic flow diagram of a pipe containing a circumferential part-through crack is illustrated in Fig. 1. As an applied load progressively increases, the crack begins to gradually open and to propagate stably in the thickness direction of the pipe. Local necking simultaneously grows on the outer surface of the pipe corresponding to the location of the part-through crack. When the part-through crack penetrates the wall thickness, it is called a "leak load". Crack penetration accompanies a drop in load, when the load drops until the crack penetrates the wall thickness completely, as shown in Fig. 1.

After crack penetration occurs, the applied load increases again, reaching "collapse" or "break load", which is the maximum load following crack penetration. The onset of stable crack growth in the circumferential direction is in the vicinity of the break load. Finally, the pipe experiences a double-ended fracture.

The transition from stable to unstable crack growth may occur during double-ended fracturing. Such a transition is controlled by varying the stiffness of the testing machine and the loading fixture. The occurrence of the manner of instability for a degraded pipe is evaluated by the tearing modulus criterion.

Circumferential part-through cracks in pipes grow in the wall-thickness direction prior to the circumferential direction. The sizes of the loads for pipe leaks and breaks depend on the initial crack depthes and lengths. Break loads can be estimated by the traditional Plastic Limit Load concept which is sometimes prone to be overly conservative. The Net-section Collapse Failure Criterion proposed by Kanninen, et al. [5] also estimates leak and break loads for stainless steel pipes. In relation to this method, a simple method for predicting leak and break loads for cracked pipes has been developed [6] based on the Net-section Collapse Failure Criterion. This newly developed method is briefly explained in the next section.

2.2 Prediction of Leak Load

Models of stress distributions at the leaks for circumferentially part-through cracked pipes subjected to tensile load and bending moment are assumed as shown in Fig. 2.

The external tensile load for the pipe leak shown in Fig. 2(1) is given by

$$P_L = \sigma_P A + (1 - \phi)\, \sigma_f A_L - P_S$$

$$= \sigma_P A + \sigma_{ef} A_L - P_S \qquad (1),$$

with

$$\sigma_P = \sigma_U - (\sigma_U - \sigma_y) d/t \qquad (2),$$

$$A = (D - t)(\pi - \theta)t \qquad (3),$$

$$A_L = (D - t + d)(t - d)\theta \qquad (4).$$

In Eq. 1, P_L is the leak load, ϕ is the reduction of a obtained from a smooth specimen, σ_f is the true fracture stress, and σ_{ef} is the engineering fracture stress which is equal to $(1-\phi)\sigma_f$.

Equation 2 was determined experimentally, and the stress σ_p is obtained from the ultimate tensile strength σ_U and the yield stress σ_y of the pipe material. The meanings of Eqs. 1 and 2 are as follows. For d/t=0.0, indicating an uncracked pipe, a pipe break occurs when the nominal stress reaches σ_U. For a deeply cracked pipe, where d/t=1.0, the crack penetrates the pipe wall thickness wher the net-stress reaches σ_y.

Pipes utilized in actual plant situations receive service loading such as internal pressure, dead weight, thermal expansion, vibration and so on. In Eq. 1, P_S is an axial force which depends on plant operating conditions, such that when axial force P_S is a force due to internal pressure Pr, Ps is expressed as

$$P_S = \pi\left(\frac{D}{2} - t\right)^2 Pr \qquad (5).$$

The external bending moment at the leak for circumferentially part-through cracked pipe is calculated, assuming the stress distribution as is shown in Fig. 2(2). From the equilibrium of axial forces and that of the bending moments, the leak moment M_L is given as

$$M_L = 2\sigma_{ef}R^2t(1-x)\sin\theta + 2\sigma_pR^2t(2\sin\beta_L - \sin\theta) \qquad (6),$$

where

$$\beta_L = \frac{\theta(1-x)\sigma_{ef}}{2\sigma_p} + \frac{\pi-\theta}{2} - \frac{\pi}{4}\frac{RPr}{t\sigma_p} \qquad (7)$$

for $\beta_L \leq \pi-\theta$, and

$$M_L = 2R^2t[(1-x)\sigma_{ef} + \sigma_p]\sin\beta_L \qquad (8),$$

where

$$\beta_L = \frac{\pi}{(1-x)\sigma_{ef} + \sigma_p}\left[(1-x)\sigma_{ef} - \frac{RPr}{2t}\right] \qquad (9)$$

for $\beta_L > \pi-\theta$. The neutral angle is expressed as β_L, the ratio of crack depth d/t by x, and σ_p is given by Eq. 2. For $\beta_L > \pi-\theta$, M_L is independent of crack angle θ.

2.3 Prediction of Break Load

The break load depends on the initial crack depth. Stress distribution models at the pipe breaks are shown in Fig. 3. The external tensile load at break P_B is expressed as

$$P_B = \sigma_b A - P_S \quad (10),$$

where σ_b is

$$\sigma_b = \frac{1}{(0.9)^2}(\sigma_U - \sigma_o)\left(1 - \frac{d}{t}\right)^2 + \sigma_o \quad (11)$$

for $0.1 \leq d/t \leq 1.0$, and

$$\sigma_b = \sigma_U \quad (12)$$

for $0 \leq d/t < 0.1$, where σ_o is the flow stress given by $(\sigma_U + \sigma_y)/2$.

Equations 11 and 12 were obtained from tensile tests of stainless steel. Through-wall cracked pipe, i.e., $d/t=1.0$, breaks when the net-stress reaches the flow stress σ_o of the pipe material. The break load P_B of the pipe coincides as a matter of course with that given by the Plastic Limit Load criterion [1]. For a shallow crack of less than $d/t=0.1$ depth, Equation 12 implies that the static tensile strength for high ductile material such as stainless steel is hardly influenced by the existence of the crack. Moreover, in accordance with ASME Code Section XI, small defects with less than an approximately 12% wall thickness depth are judged to be allowable defects not requiring flaw evaluation. if they were detected during an in-service examination. Such small defects are not considered to compromise nuclear components.

In order to predict the size of the moment at the instant of break for a cracked pipe subjected to a bending load, the internal stress distribution in the cracked section of the pipe wall is assumed to be as that shown in Fig. 3(2). The external bending moment M_B at the break is determined as

$$M_B = 2\sigma_b R^2 t(2\sin\beta_B - \sin\theta) \quad (13),$$

where

$$\beta_B = \frac{\pi-\theta}{2} - \frac{\pi}{4}\frac{R}{t}\frac{Pr}{\sigma_b} \quad (14).$$

The leak and break loads for circumferentially cracked pipes can be predicted simply by the above equations which represent the mechanical properties of the pipe materials.

2.4 Comparison with Experiments

Tensile and bending tests were performed on 2-inch diameter Type 304 stainless steel pipe containing circumferential part-through cracks at ambient temperature, with no internal pressure in the pipes. Leak and break loads obtained from the experiments are compared with those of the calculations designated above.

Nominal tensile stresses at the leaks and breaks for 2-inch diameter Type 304 stainless steel pipes are shown in Fig. 4, and bending stresses at these same leaks and breaks are shown in Fig. 5. Experiments and calculations excluded the effect of internal pressure. The stress of the ordinate in Fig. 5 is calculated from the bending moments at leak M_L and break M_B divided by the Section Modulus Z for a hollow cylinder. It can be seen from these figures that the experimental data are in good agreement with the results of the calculations and that the stresses at the leaks and breaks for pipes decrease with an increasing crack angle. It is also to be noted that the stress at the breaks becomes smaller than at the leaks when the crack angle of the pipe becomes larger.

3. Flaw Sizes for Leaks and Breaks

Flaw sizes requiring the occurrence of leaks and breaks can be expressed as a parameter of stress. The equilibrium flaw sizes for leaks or breaks at the same stress are illustrated in Figs. 6 and 7, where the pipes are 2-inch diameter Type 304 stainless steel. The calculations of these figures as indicated took the effect of an 7.8 MPa internal pressure into account. The design stress defined by ASME Code Section III is represented as Sm.

Figure 6 shows the equilibrium flaw sizes for leaks and breaks of the tensile stresses at Sm and 2Sm. The flaw sizes become smaller for leaks and breaks indicating that they occur under large tensile stress such as 2Sm. The flaw sizes at the same leak and break load values are shown as a solid line of $P_L=P_B$. The reason the solid line is discontin-

uous at the d/t=0.1 wall thickness stems directly from stress σ_b, because σ_b is independent of the crack depth of the pipe, as was shown in Eq. 12.

In the region above the $P_L = P_B$ solid line, the break load is larger than the leak load, indicating that a larger load is necessary to break the pipe when leaking. On the contrary, in the area below the $P_L=P_B$ line, the break load is less than the leak load, such that the pipe breaks easily following a pipe leak.

The equilibrium flaws sizes at the leak and break stresses of 1.5Sm and 3Sm are illustrated in Fig. 7. The line indicating flaw sizes at the same leak and break loads is shown as $M_L=M_B$, which is discontinuous at d/t=0.1. In the area above the solid line of $M_L=M_B$, the moment at the leak is less than that for the break for a circumferentially part-through cracked pipe. The leak moment is smaller than the break moment when the crack is deeper and exhibits a smaller angle.

Acceptance standards for defects are provided in ASME Code Section XI for austenitic piping. The allowable flaw depth is approximately 12% of the wall thickness, but essentially depends on the wall thickness and aspect ratio of the flaw. The flaw depth as seen in Figs. 6 and 7 may therefore be considered a quite conservative standard.

4. Allowable Flaw Considerations

Components that receive tensile load employ the design stress of 1.0Sm, i.e. $Pm \leq 1.0Sm$. For the bending moment, the components are designed such that $Pm + Pb \leq 1.5Sm$, where Pm is primary membrane stress and Pb is primary bending stress. Hereinafter, let 2Sm for pipe tension and 3Sm for pipe bending apply as critical safety values. Based on the 2Sm value in Fig. 6, allowable resultant flaw sizes in tensile loading are then shown in Fig. 8.

As bending stress in piping is a more general occurrence than tensile stress, acceptable flaw sizes are explained using Fig. 9. Allowable flaw sizes as illustrated for circumferentially part-through cracked pipe use the results of Fig. 7. The crack angle $2\theta/2\pi$ and its depth d/t at the leak and break 3Sm cross-point are approximately 0.15 and 0.56, respectively, as shown in Fig. 7. Pipe with crack sizes less than $2\theta/2\pi=0.15$ ($2\theta=54°$) and d/t=0.56 never leak or break at a stress less than 3Sm. When a crack of a less than 0.15 angle becomes deeper, although the leak and break stresses are reduced below 3Sm, the break

moment M_B is larger than the leak moment M_L, requiring a greater external moment to break the leaking pipe. For such a cracked pipe, leaks can be detected prior to the pipe breaking. Allowable flaw sizes for leaks prior to breaking are shown as the solid line in Fig. 9, and crack depth is truncated as d/t=0.75 as indicated in Reference [7].

When the depth of a circumferential part-through crack is defined by non-destructive examinations, the allowable flaw size area is bounded by the broken line at the lower left of the 3Sm leak stress curve. Although break stress is less than 3Sm for a crack angle greater than $2\theta/2\pi=0.15$, the pipe does not break because a leak prior to the break does not occur.

For more common cases of combined tensile and bending stresses, the allowable bending stress flaw sizes shown in Fig. 9 are used, as these flaw sizes are included in the tensile loading of Fig. 8 as well, also because they represent conservative evaluation.

5. Conclusion

Simple methods for predicting leak and break loads for pipes containing circumferential part-through cracks have been introduced. The methods are applied to ductile materials such as Type 304 stainless steel. Based on the calculated results from these methods, allowable flaw sizes for ductile pipes are determined from the viewpoint of leaks and breaks.

References

[1] Schulze, H.D., Togler, G., and Bodman, E., Nuclear Engineering and Design, Vol. 58, 1980, p.19.

[2] Iorio, A.F., and Crespi, J.C., Int. J. Pres. Ves. & Piping, Vol.9, 1981, p.241.

[3] Enrietto, J.F., Bamford, W.H., and White, D.F., Int. J. Press. Ves. & Piping, Vol.9, 1981, p.421.

[4] Paris, P.C., Tada, H., Zahoor, A., and Ernst, H., ASTM STP 668, 1979, p.5.

[5] Kanninen, M.F., Broek, D., Hahn, G.T., Marshall, C.W., Rybicki, E.F., and Wilkowski, G.M., Nuclear Engineering and Design, Vol. 48, 1978, p.117.

[6] Hasegawa, K., Sakata, S., Shimizu, T., and Shida, S., ASME 4th National Congress on PVP, Portland, USA, June 1983.

[7] Norris, D.M., Marston, T.U., and Tagart, Jr. S.W., ASME PVP Vol.58, 1982, p.185.

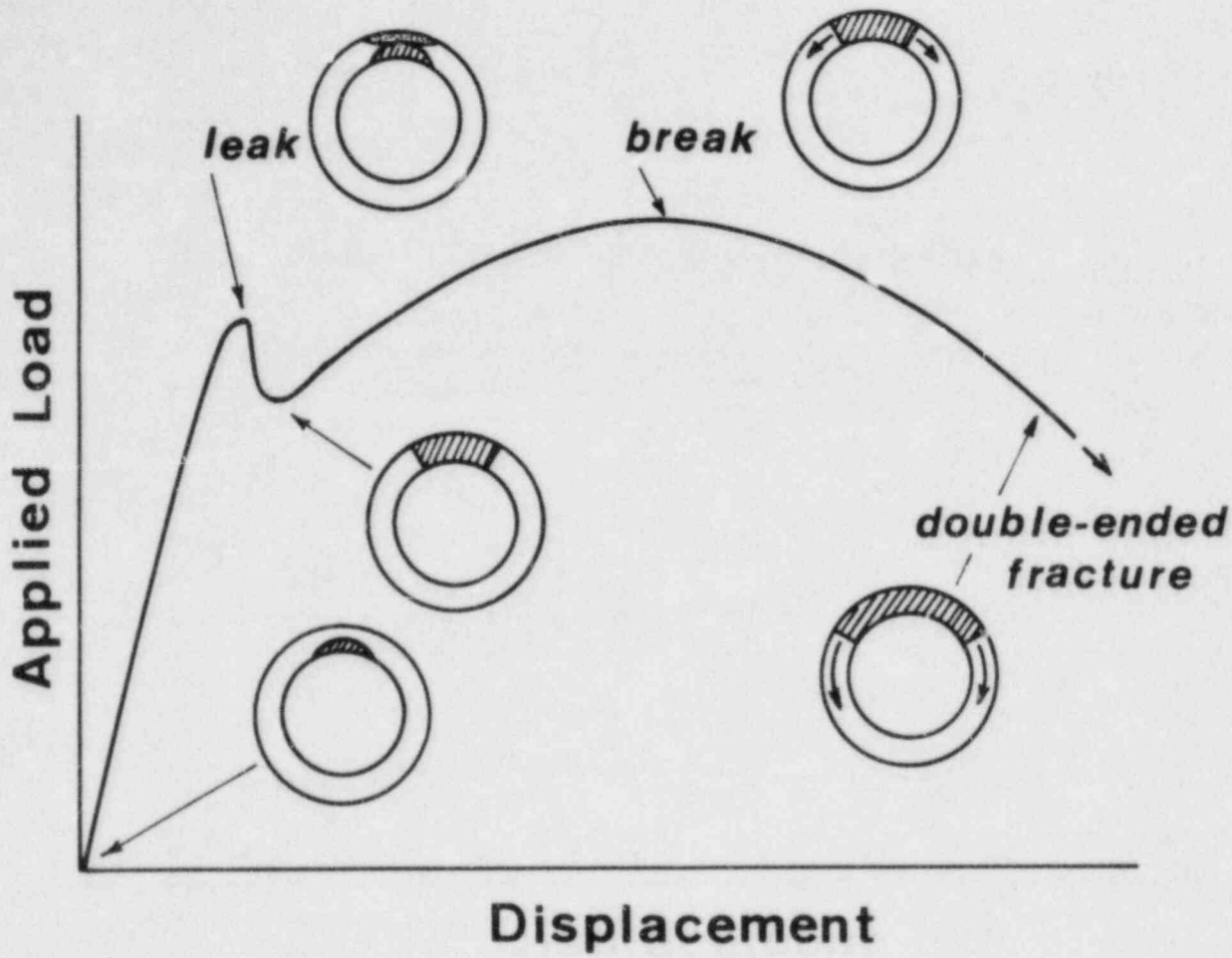

Fig. 1 Crack growth behavior of degraded pipe.

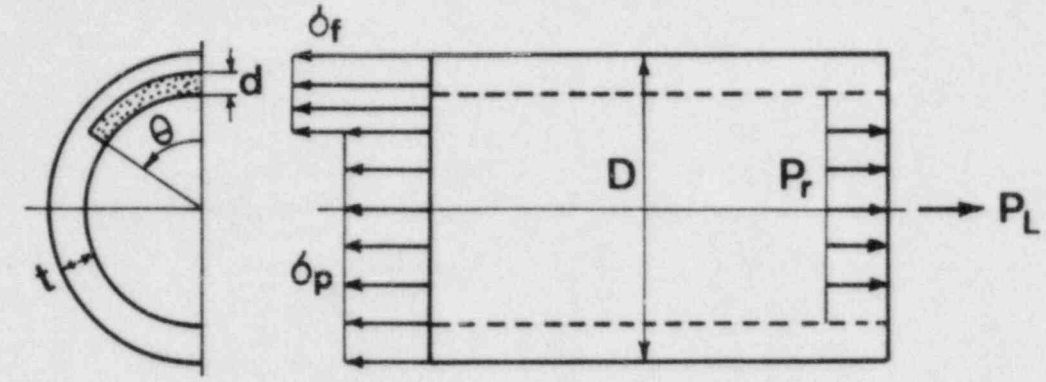

1) Cracked Pipe Subjected to Tensile Load

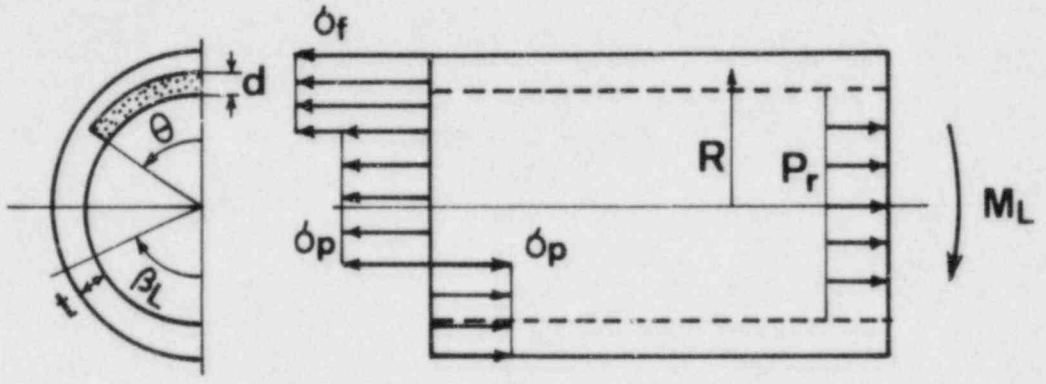

i) $\beta_L \leq \pi - \theta$

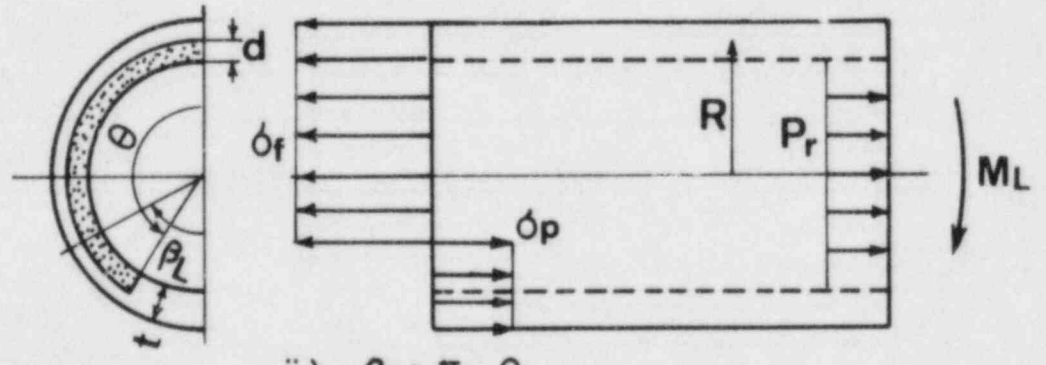

ii) $\beta_L > \pi - \theta$

2) Cracked Pipe Subjected to Bending Moment

Fig. 2 Stress distribution models for cracked pipe leaks.

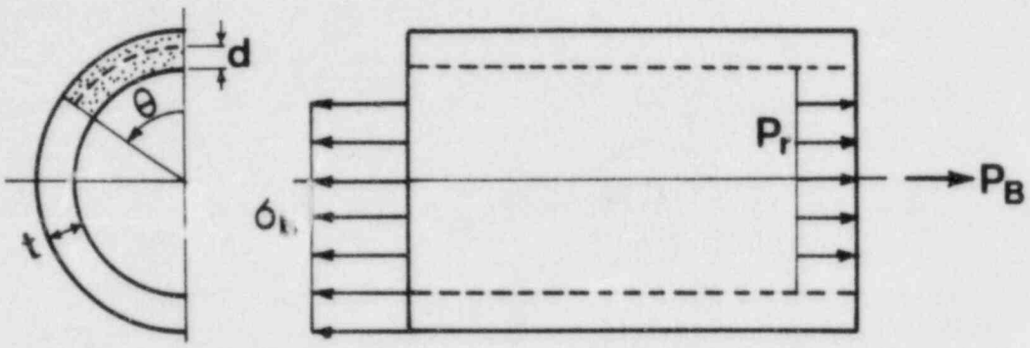

1) Cracked Pipe Subjected to Tensile Load

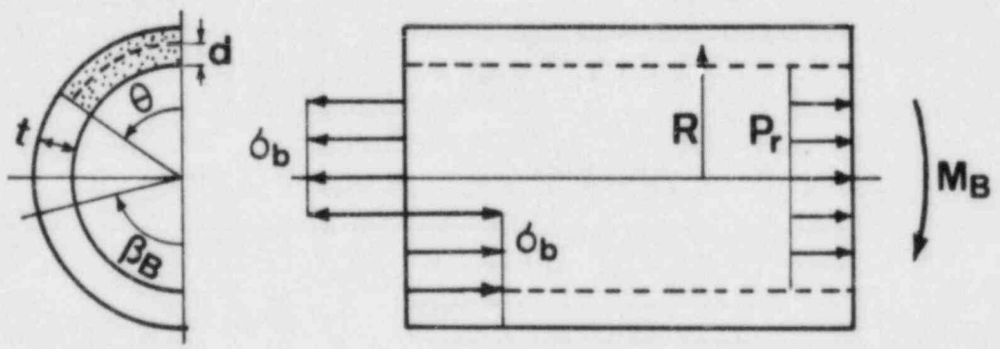

2) Cracked Pipe Subjected to Bending Moment

Fig. 3 Stress distribution models at the breaks for cracked pipes.

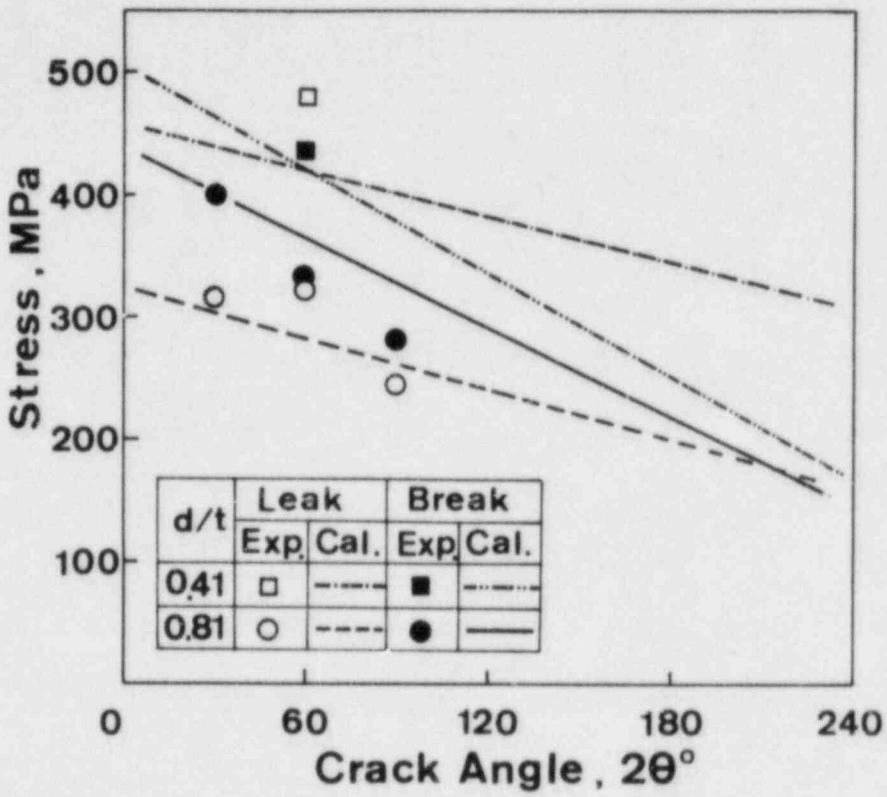

Fig. 4 Nominal tensile stresses at leaks and breaks for 2-inch diameter Type 304 stainless steel pipes.

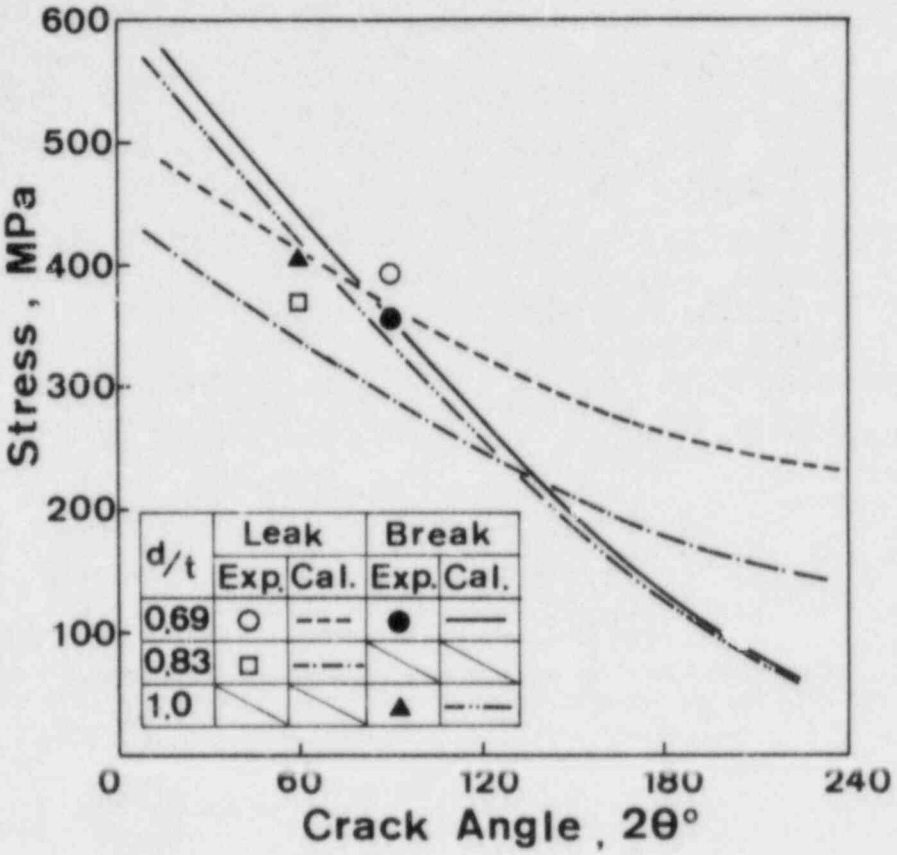

Fig. 5 Leak and break stresses for 2-inch diameter Type 304 stainless steel pipes subjected to bending moments.

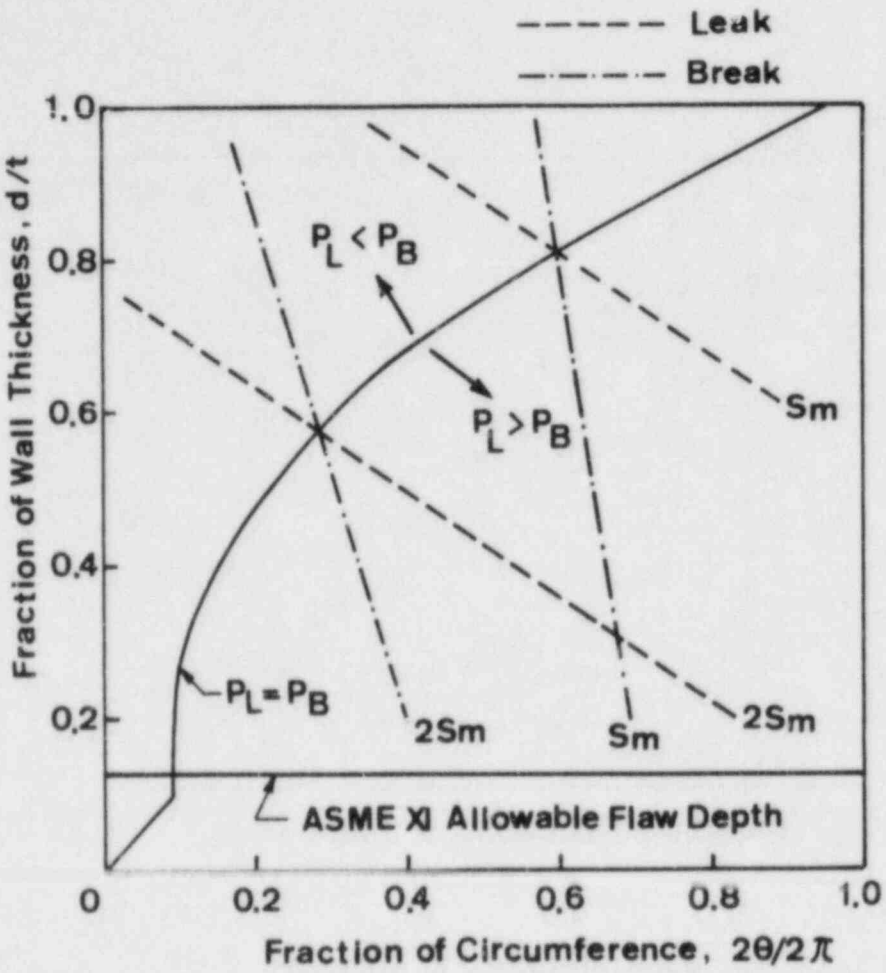

Fig. 6 Locus of the tensile leak and break loads for 2-inch diameter Type 304 stainless steel pipe with an internal pressure of 7.8 MPa.

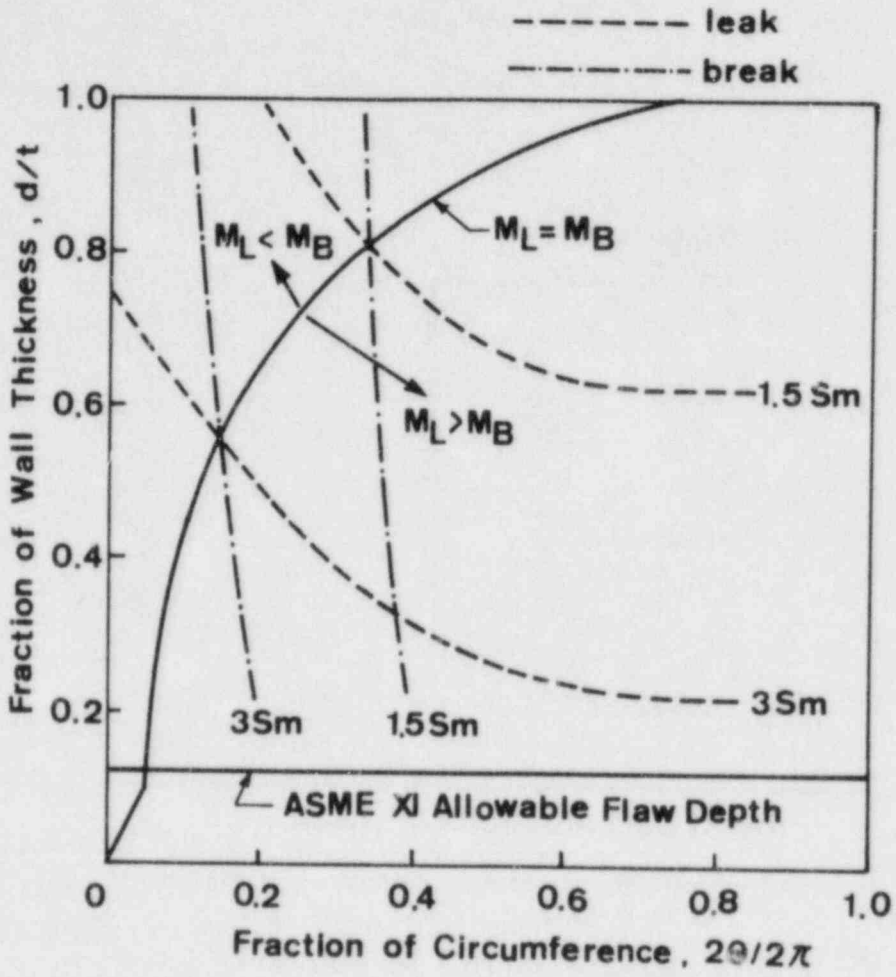

Fig. 7 Locus of the leak and break moments for 2-inch diameter Type 304 stainless steel pipes with an internal pressure of 7.8 MPa.

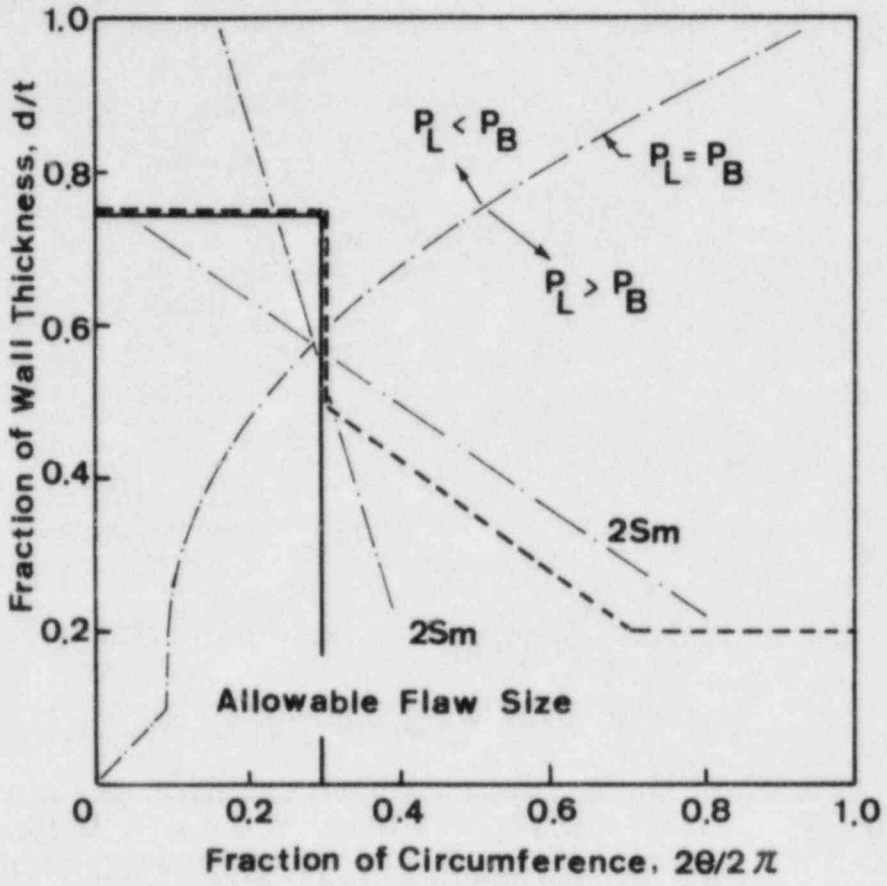

Fig. 8 Determination of allowable flaw sizes for Type 304 stainless pipe subjected to tensile loading.

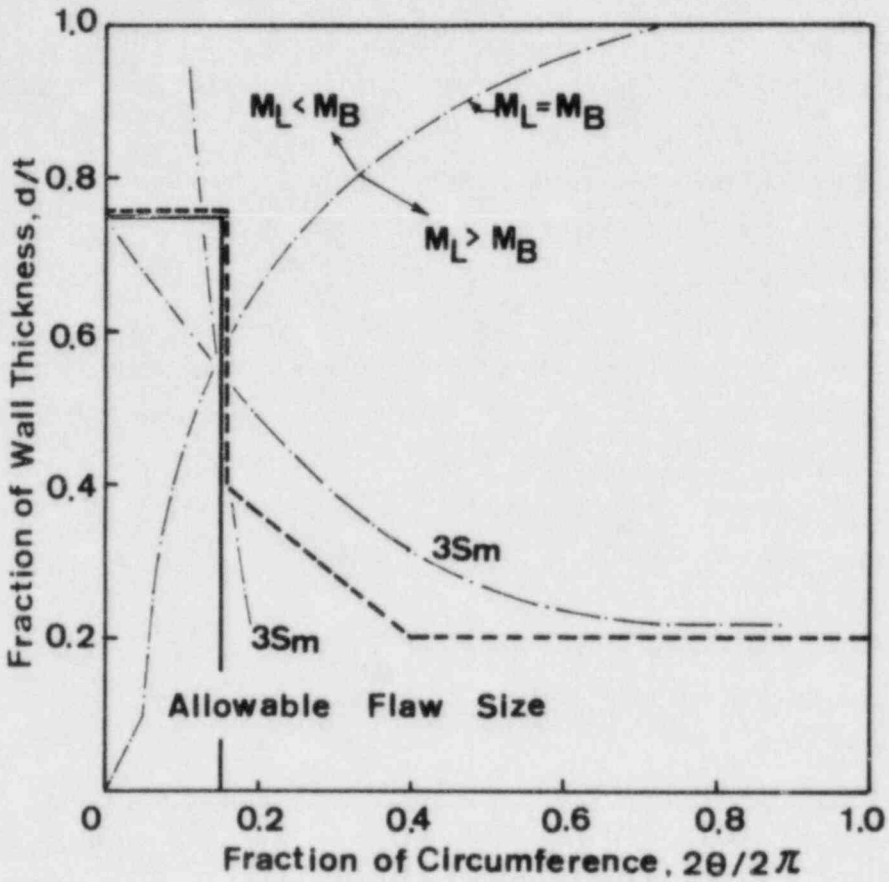

Fig. 9 Determination of allowable flaw sizes for Type 304 stainless steel pipe subjected to bending stress and combined tensile and bending stresses.

Leak-Before-Break Diagrams Using Simple Plastic Limit Load Criteria for Pipes with Circumferential Cracks

F. Görner, D. Munz*

1. Introduction

For the evaluation of the leak-before-break behaviour of pressurized components two critical loads have to be known:

- the critical load for wall penetration of a surface or an embedded flaw (local instability),
- the critical load for complete fracture (global instability).

These critical loads are dependent on the geometry of the component, the geometry of the crack, the material properties and the loading conditions.

In this paper simple criteria are used for circumferential cracks which can only be applied to very tough materials, for instance austenitic stainless steels. The criteria used are

- net section yielding, assuming an ideal plastic material. For strain hardening materials a mean flow stress has to be defined;
- relations proposed by Kiefner et al./1/ using the linear-elastic Foliasfactor. These relations had been proposed originally for longitudinal cracks. Later they were also used for circumferential cracks;
- relations proposed by Hasegawa et al. /2,3/.

All these relations are very simple. They may be too simple; however, they were used successfully in the past. At least trends in the leak-before-break behaviour can be deduced from these relations.

---

*) Kernforschungszentrum Karlsruhe
Institut für Reaktorbauelemente, Arbeitsgruppe Zuverlässigkeit und Schadenskunde, P.O. Box 3640, D-7500 Karlsruhe (West-Germany)

All calculations made in this paper are valid for load controlled conditions. It is assumed that at the calculated stress, if sustained, the crack will grow through the wall for local instability or through the cross section of the pipe for global instability. For displacement-controlled deformation the crack extension under decreasing load has to be considered. Then the compliance of the whole systems is an important factor for global instability. A component, which for a given crack does not show leak-before-break behaviour under conditions of load control, may leak before break in displacement control. Therefore, the relations given in this paper for load-controlled conditions are conservative for displacement-controlled loading.

The geometry of the considered crack is shown in fig. 1.
It is an internal surface flaw characterized by the crack angle 2α and the crack length 2c, respectively. The crack depth is a, the wall thickness t and the pipe radii are R_a and R_i. All relations given in this paper are for thin-walled pipes with

$$R = \frac{R_i + R_a}{2} \tag{1}$$

$$c = \alpha R \tag{2}$$

2. Internal pressure

2.1 Global instability

For longitudinal cracks it was shown that plastic instability of tough materials can be described using the linear-elastic stress intensity correction factor M_{FL} /1,4/. For circumferential cracks the same approach can be applied /5/. The stress intensity factor for a through-the-wall crack is given by

$$K = \frac{pR}{2t} \sqrt{\pi c} \cdot M_{FC} \tag{3}$$

M_{FC} is a function of the shell parameter

$$\lambda = \frac{c}{\sqrt{Rt}} \left[12\ (1 - \nu^2)\right]^{1/4} = \frac{\alpha}{\sqrt{t/R}} \left[12\ (1 - \nu^2)\right]^{1/4} \tag{4}$$

Instead of λ a reduced shell parameter λ^* is used

$$\lambda^* = \frac{c}{\sqrt{Rt}} = \frac{\lambda}{[12\ (1-\nu^2)]^{1/4}} \tag{5}$$

For $\nu = 1/3$ there is $\lambda^* = 0.533\lambda$.
Results of Delale and Erdogan /6/ for $c/t < 10$ can be described by a polynomial expression

$$M_{FC} = 1 + 0.0237\lambda^* + 0.1449\lambda^{*2} - 0.0344\lambda^{*3} + 0.00255\lambda^{*4} \tag{6}$$

Failure by plastic instability is assumed to occur for

$$P_L = \frac{2t}{R}\ \sigma_f \frac{1}{M_{FC}} \tag{7}$$

or

$$\frac{\sigma_L}{\sigma_f} = \frac{1}{M_{FC}} \tag{8}$$

σ_f is the flow stress and σ_L the instability stress in the longitudinal direction.
Alternatively to eq. (8) it can be assumed that plastic instability occurs, if the stress exceeds the flow stress in the net section.

If one assumes a pipe which is prevented from bending and therefore the stress in the net section is constant, the critical stress is given by

$$\frac{\sigma_L}{\sigma_f} = 1 - \frac{\alpha}{\pi} = 1 - \frac{\sqrt{t/R}\ \lambda^*}{\pi} \tag{9}$$

For a pipe without constraints compressive deformation will occur opposite to the crack. From the requirements of equilibrium for load and moment the critical pressure and tensile stress, respectively, are given by

$$\frac{\sigma_L}{\sigma_f} = \frac{2}{\pi}\ \left[\cos^{-1}\left(\frac{1}{2}\sin\alpha\right) - \frac{\alpha}{2}\right] \tag{10}$$

$$= \frac{2}{\pi}\ \left[\cos^{-1}\left(\frac{1}{2}\sin\sqrt{t/R}\,\lambda^*\right) - \frac{\sqrt{t/R}\ \lambda^*}{2}\right]$$

A comparison of eqs. (8), (9) and (10) is shown in fig.2. For the net-section yield criteria - eqs. (9) and (10) - the critical stress depends on the shell parameter and on t/R. It is interesting that the net-section yield criterion for the pipe without constraints leads to a considerably lower failure stress than the application of eq. (8) using the Folias factor M_{FC}.

2.2 Local instability

For the critical pressure in a pipe with a longitudinal surface crack Kiefner et al. /1/ presented an empirical relation which was verified also in further investigations /4/. A similar relation for circumferential cracks was applied by /5/:

$$P_L = \frac{2\sigma_f t}{R} \frac{1-a/t}{1-\frac{a}{M_{FC}t}} \qquad (11)$$

For the surface crack shown in fig.1 the shell parameter λ has to be calculated according to eq. (4). For semi-elliptical surface cracks the crack length parameter c has to replaced by /1/

$$c_{eq} = \frac{\pi}{4} c \qquad (12)$$

2.3 Leak-before-break-diagrams

A leak-before-break-diagrams is a crack depth (a/t) versus crack length (α)-diagram. A given point in such a diagram characterizes a given crack of length α (or 2c) and depth a. In an increasing pressure test the diagram has two regions- leak or fracture -, separated by a leak-before-break boundary curve. For a given pressure the diagram has three regions: no failure, leak and fracture. The leak-before-break boundary curve is calculated on the assumption that during the break-through of a surface crack (local instability) the crack angle and crack length 2c, respectively, do not change. Then, in an increasing pressure test, the leak-before-break boundary curve is given by:

$$P_{L,local}(a,\alpha) = P_{Lglobal}(\alpha) \qquad (13)$$

By combination of the three relations for global instability - eqs. (8), (9), (10) - with eq. (11) describing local instability, the curves in fig.3 are obtained. There is a small effect of the t/R-ratio and, as can be expected from fig.2, a larger effect of the relation chosen for global instability. For a given crack (a/t,α) fracture is expected if its location is below the relevant curve in fig.3. For a crack depth above the curve a leak before a complete fracture should occur.

More important are diagrams which include the failure line for local instability at a given pressure. This failure line is implicitly described by eq. (11) and is shown in fig.4 for a pressure corresponding to a longitudinal stress $\sigma/\sigma_f = 0.6$. All cracks on this curve extend through the wall at this stress. The intersection of the leak-before-break boundary curve and the failure line for local instability define a critical crack angle α_c and the three regions: no failure, leak and fracture. For $\alpha < \alpha_c$ no failure can occur, only a leak if a/t is above the boundary curve. In fig.5 the relation between α_c and the longitudinal stress is given for the three criteria governing global instability.

If the hoop stress is less than the flow stress, the longitudinal stress is less than $0.5\ \sigma_f$. Under this assumption no failure is expected for $\alpha < 47^o$, if the global fracture relation eq. (10) (net section yielding for a pipe without constraint) is correct or for $\alpha < 90^o$ if relations eq(8)or (9) is correct.

3. Combined tension and bending

Tensile loading may be caused by internal pressure or by an external force F. It is characterized here by the stress in the unflawed pipe:

$$\sigma_m = \frac{F}{2\pi Rt} + P\,\frac{R}{2t} \qquad (14)$$

The bending moment is characterized by the linear elastic outer fibre bending stress σ_b. It is assumed that the crack is located on the tensile side of the bending stress.

3.1 Global instability

For the global instability of the through-wall crack it is assumed that the net section has completely yielded. The assumed stress distribution is shown in fig.6. From the equilibrium of load and moment a relation between σ_{bL}, σ_{mL} and the crack angle α is obtained

$$\frac{\sigma_{bL}}{\sigma_f} = \frac{2}{\pi} (2 \cos\beta - \sin\alpha) \tag{15}$$

β is the angle of the neutral axis and is given by

$$\beta = \frac{\alpha}{2} + \frac{\sigma_{mL}}{\sigma_f} \cdot \frac{\pi}{2} \tag{16}$$

Figures 7, 8 and 9 show the relation between σ_{bL}, σ_{mL} and α.

3.2 Local instability

For the calculation of local instability simple assumptions have to be made. Figure 10 shows one possibility. It is assumed that the ligament area has yielded and that in the remaining cross-section the stress is elastic provided that the stress on the compressive side σ_u, is less than the flow stress.
For $\sigma_u < \sigma_f$ the stress distribution is given by

$$\sigma(y) = \sigma_f \text{ for } y > R\cos\alpha \tag{17}$$

$$\sigma(y) = \sigma_f + (\sigma_u - \sigma_f)\frac{\cos\alpha - y/R}{1 + \cos\alpha} \quad \text{for } y < R\cos\alpha$$

$$\sigma(\varphi) = \sigma_f + (\sigma_u - \sigma_f)\frac{\cos\alpha - \sin\varphi}{1 + \cos\alpha} \quad \text{for } -\frac{\pi}{2} < \varphi < \frac{\pi}{2} - \alpha$$

The equilibrium requirement of the force and moment leads to

$$\frac{\sigma_u}{\sigma_f} = 1 - \frac{\left[\pi\left(1 - \frac{\sigma_m}{\sigma_f}\right) - \alpha\frac{a}{t}\right]\left[1+\cos\alpha\right]}{(\pi - \alpha)\cos\alpha + \sin\alpha} \tag{18}$$

$$\frac{\sigma_{bL}}{\sigma_f} = \frac{2}{\pi} \left\{\left(1-\frac{\sigma_u}{\sigma_f}\right)\frac{\sin\alpha\cos\alpha + \frac{\pi-\alpha}{2} - \frac{\sin 2\alpha}{4}}{1+\cos\alpha} - \frac{a}{t}\sin\alpha\right\} \tag{19}$$

The restriction $\sigma_u < \sigma_f$ leads to a critical angle α^* which is a function of a/t and σ_m/σ_f:

$$\cos\alpha^* \left[\frac{\sigma_m}{\sigma_f} \cdot \pi - 2\alpha^* + \frac{\alpha^* a}{t} + \pi\right] + 2\sin\alpha^* - \pi + \frac{a}{t}\alpha^* + \frac{\sigma_m}{\sigma_f}\pi = 0 \qquad (20)$$

In fig.11 α^* is plotted versus a/t with σ_m/σ_f as the parameter. For $\alpha > \alpha^*$ the stress distribution is given by

$$\sigma = \sigma_f \qquad \text{for} \quad \frac{\pi}{2} - \alpha < \varphi < \frac{\pi}{2} \qquad (21)$$

$$\sigma = \sigma_f \frac{2\sin\varphi + \sin\gamma - \cos\alpha}{\cos\alpha + \sin\gamma} \quad \text{for} - \gamma < \varphi < \frac{\pi}{2} - \alpha$$

$$\sigma = -\sigma_f \qquad \text{for} - \frac{\pi}{2} < \varphi < -\gamma$$

From the equilibrium of forces the angle γ(fig.10) can be obtained as a function of a/t and α

$$(1 - \frac{a}{t})\alpha + \gamma - \frac{\pi}{2} + \frac{2(\cos\gamma - \sin\alpha) + (\frac{\pi}{2} - \alpha + \gamma)(\sin\gamma - \cos\alpha)}{\cos\alpha + \sin\gamma} \qquad (22)$$

$$= \pi \frac{\sigma_m}{\sigma_f}$$

From the equilibrium of moment the relation between σ_{bL}/σ_f, σ_{mL}/σ_f, a/t and α is obtained

$$\frac{\sigma_{bL}}{\sigma_f} = \frac{2}{\pi}\left\{(1 - \frac{a}{t})\sin\alpha + \cos\gamma \right. \qquad (23)$$

$$\left. + \frac{\frac{\pi}{2} - \alpha + \gamma - \frac{1}{2}(\sin 2\alpha + \sin 2\gamma) + (\cos\alpha - \sin\gamma)(\sin\alpha - \cos\gamma)}{\cos\alpha + \sin\gamma}\right\}$$

In fig. 12 the relation between σ_{mL}, σ_{bL}, α and a/t is shown.

3.3 Leak-before break-diagrams

The leak-before-break boundary curves for combined tension and bending loading are shown in fig.13, with σ_m/σ_f as the parameter. If the tensile stress is constant and the bending moment increases, a leak before break is expected, if the crack is located above the boundary curve for this tensile stress. For $0 < \sigma_{mL}/\sigma_f < 0.5$ all boundary curves are close together.

Figure 14 shows boundary curves for fixed bending stresses and increasing tensile stresses. The curve for $\sigma_{bL} = 0$ is similar to the curves in fig. 3. The difference results from a different criterion for local instability.

In fig. 15 the leak-before break boundary curves are shown for three different tensile stresses and the ligament failure curves for different bending stresses. From these diagrams for given σ_{bL}/σ_f and σ_{mL}/σ_f the three regions "no failure", "leak" and "fracture" can be obtained. The angle α_c below which no fracture can occur, is shown in fig.16.

3.4 Calculation according to Kanninen et al. /7/.

In an investigation by the Battelle, Columbus Laboratories on stainless steel pipes with circumferential cracks leak-before-break boundary curves were calculated. It was assumed that in case of local instability not only the ligament of the surface crack but also the whole cross-section has yielded. Based on experimental results for plates with surface cracks, different flow stresses for local and global instabilities were assumed. For the investigated austenitic stainless steel the ratio of the flow stress σ_i for local instability to the flow stress σ_f for global instability σ_f was found to be 0.85. The local instability is given by

$$\frac{\sigma_{bL}}{\sigma_i} = \frac{2}{\pi} \left[2 \cos \left(\frac{\alpha a}{2t} + \frac{\pi}{2} \frac{\sigma_m}{\sigma_i} \right) - \frac{a}{t} \sin\alpha \right] \qquad (24)$$

Using eq. 15 for global instability the leak-before-break boundary curve is given by

$$2\cos\left[\frac{\alpha}{2}+\frac{\sigma_m}{\sigma_f}\frac{\pi}{2}\right]-2\frac{\sigma_i}{\sigma_f}\cos\left[\frac{\alpha a}{2t}+\frac{\pi}{2}\frac{\sigma_m}{\sigma_f}\cdot\frac{\sigma_f}{\sigma_i}\right]-\sin\alpha+\frac{a}{t}\frac{\sigma_i}{\sigma_f}\sin\alpha=0 \qquad (25)$$

Results are shown in fig. 17. The boundary curve is nearly independent of the tensile stress. The angle α_c below which no fracture is possible is shown in fig. 18 together with the results of fig.16. The general behaviour is similar. the discrepancies are largest for small crack angles.

3.5 Calculations according to Hasegawa et al. /2,3/

Hasegawa et al. developed also simple relations for local and global instabilities based on results for surface cracks in plates. The stress distribution assumed in case of local instability for a plate is shown in fig.19. It is assumed that the stress at failure in the ligament is equal to the engineering fracture stress in a tensile test σ_{ef}. In the remaining cross-section a constant stress σ_p dependent on the strain hardening capacity is assumed. From experimental results

$$\sigma_p = \sigma_{UTS} - (\sigma_{UTS} - \sigma_y)\frac{a}{t} \qquad (26)$$

was found For pipes undergoing pure bending the stress distribution is shown in fig.19. From this diagram the critical bending stress σ_{bL} follows:

$$\frac{\sigma_{bL}}{\sigma_o} = \left[\frac{\sigma_{ef}}{\sigma_o}\left(1-\frac{a}{t}\right)\sin\alpha+\frac{\sigma_p}{\sigma_o}\left(2\cos\beta-\sin\alpha\right)\right] \qquad (27)$$

with

$$\beta = \frac{\alpha}{2}-\frac{\alpha(1-a/t)\sigma_{ef}}{2\sigma_p} \qquad (28)$$

σ_o is the average flow stress

$$\sigma_o = \frac{1}{2}\left(\sigma_{UTS}+\sigma_y\right) \qquad (29)$$

In tests of specimens with surface cracks, where global instability followed local instability a slight effect of the depth a/t of the surface crack on the stress was found for global instability. This effect was described by a net flow stress σ_f given by

$$\sigma_f = \frac{1}{(0,9)^2} (\sigma_{UTS} - \sigma_o) \left(1 - \frac{a}{t}\right)^2 + \sigma_o$$

for $0.1 \leq \frac{a}{t} \leq 1.0$ (30)

$\sigma_f = \sigma_{UTS}$ for $0 \leq a/t \leq 0.1$

From these relations a leak-before-crack boundary curve can be calculated, which is dependent on the stress-strain curve of a tensile test. For the material properties obtained by Hasegawa et al. for the stainless steel investigated

$$\sigma_y = 255 \text{ MPa}, \ \sigma_{UTS} = 578 \text{ MPa}, \ \sigma_{ef} = 471 \text{ MPa}$$

the curve shown in fig.20 is obtained. The relation between α_c and σ_{bL} is shown in fig.18. It is interesting to see the good agreement with the curves following from the different assumptions made in 3.3 and 3.4.

Conclusion

Simple criteria for local and global instabilities were used to calculate leak-before-break-diagrams for load-controlled deformations. Relations between the tension and bending stresses in the uncracked pipe and the critical crack angle α_c, below which complete fracture cannot occur, were developed for combined loading by internal pressure and external tension and bending. The different assumptions made for local and global instability lead to similar conclusions about the allowable crack length for leak-before-break behaviour.

It has not been the intention of this paper to compare the conclusions with experimental results available. This will be done in a separate study.

/1/ Kiefner, J. F., Maxey, W A., Eiber, J. J., Duffy, A. R., "Failure Stress Levels of Flaws in Pressurized Cylinders", ASTM STP 536 (1973) pp. 461-481.

/2/ Hasegawa, K.,Shimizu, T., Sakata, S., Shida, S., "Stable Crack Growth and Leak Predictions of Stainless Steel Pipes with Circumferential Cracks", Transactions of the 6th Conference on Structural Mechanics in Reactor Technology", Paper L 5/3.

/3/ Hasegawa, K., Sakata, S., Shimizu, T., Shida, S., "Prediction of Fracture Tolerances for Stainless Steel Pipes with Circumferential Cracks", 4th ASME Pressure Vessel and Pipe Conference, Portland 1983.

/4/ Schulze, H. D., Togler, G., Bodmann, E., "Fracture Mechanics Analysis on the Initation and Propagation of Circumferential and Longitudinal Cracks in Straight Pipes and Pipe Bends", Nuclear Engineering and Design 58 (1980), pp. 19-31.

/5/ Wilkowsi, G. M., Eiber, R. J., "Evaluation of Tensile Failure of Girth Weld Repair Grooves in Pipe Subjected to Offshore Laying Stresses", Journal of Energy Resources Technology 103 (1981)pp. 48-55.

/6/ Delale, F., Erdogan, F.; "Transverse Shear Effect in a Circumferentially Cracked Cylindrical Shell", Quaterly Applied Mathematics 37 (1979)239-258

/7/ Kanninen, M. F., Zahoor, A., Wilkowski, G., Abou-Sayed, I., Marshall, C., Broek, D., Sampath, S., Rhee, H., Ahmad, J.; "Instability Predictions for Circumferentially Cracked Type 304 Stainless Steel Pipes Under Dynamic Loading", Final Report, EPRI NP-2347, Volumes 1 and 2, April 1982.

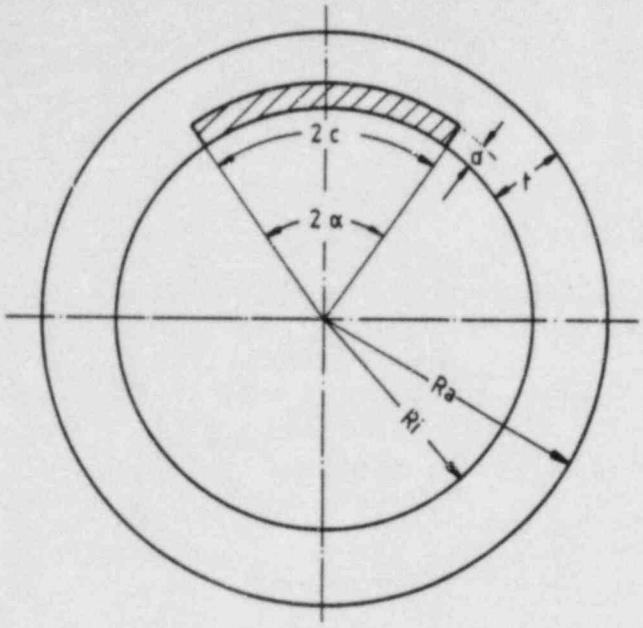

Fig. 1 Geometry of the cracked pipe

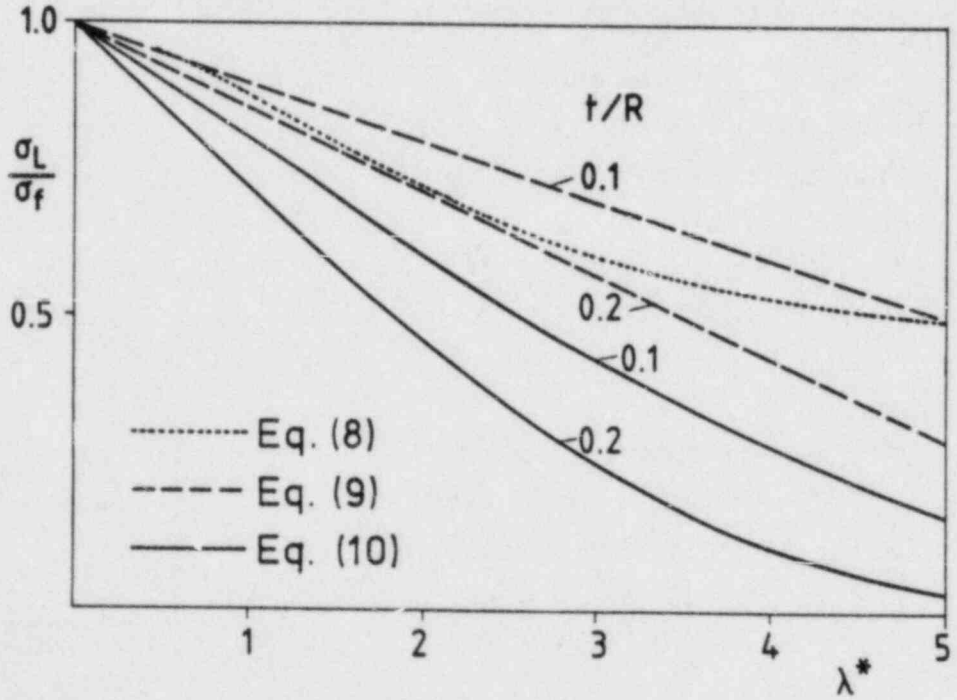

Fig. 2 Comparison of the calculated failure stresses for global instability under internal pressure

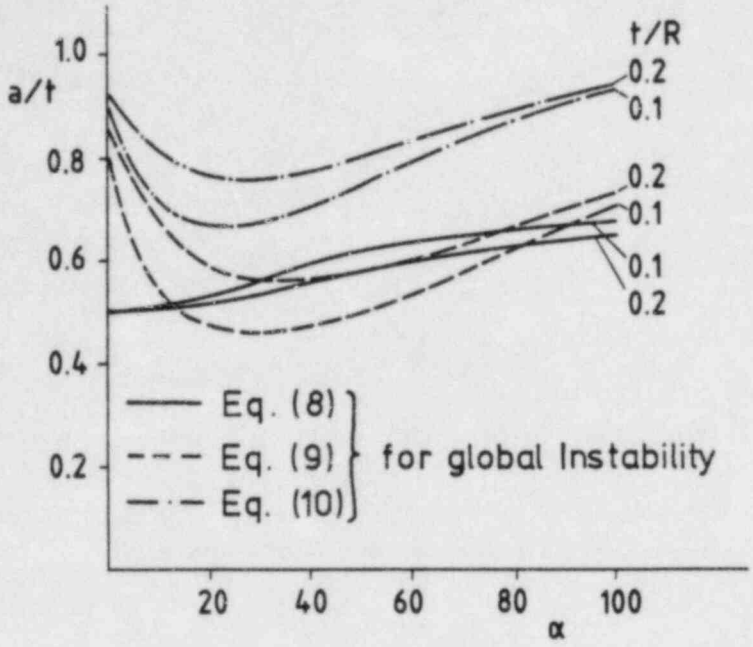

Fig. 3 Leak-before-break boundary curves for pressurized pipes calculated with different assumptions for global instability.

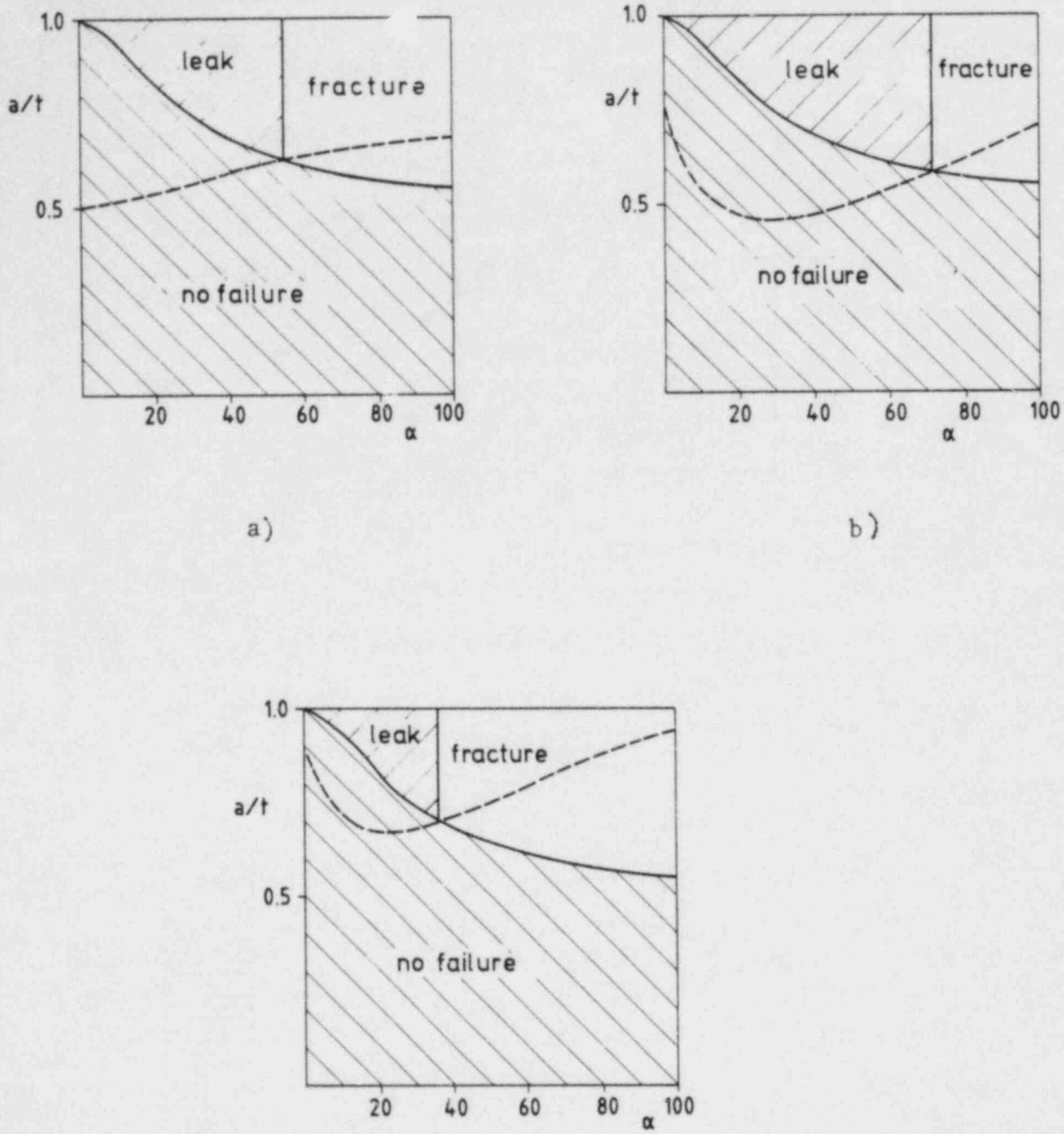

Fig. 4 Leak-before-break diagrams for pressurized pipes with $\sigma/\sigma_f = 0.6$.
Global instability after a) eq. (8), b) eq. (9), c) eq. (10).

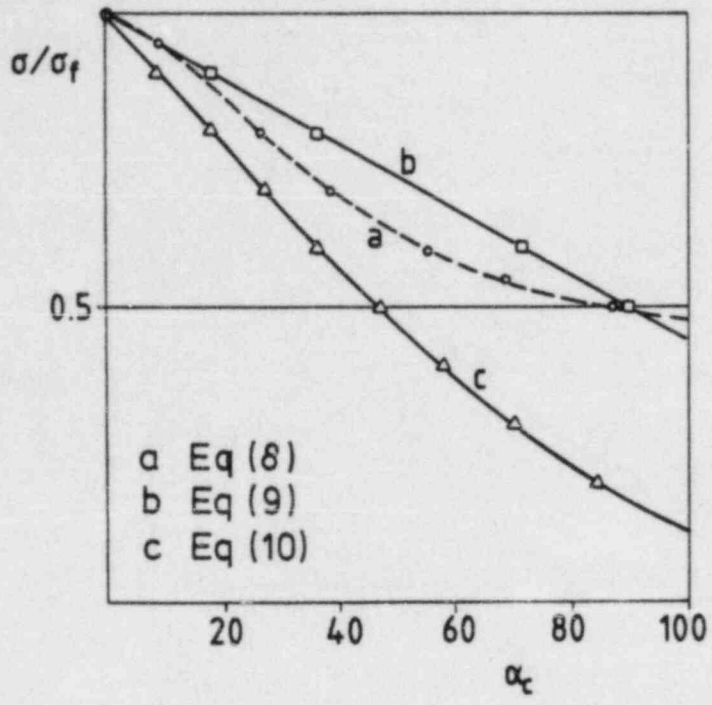

Fig. 5 Critical angle α_c for pressurized pipes.

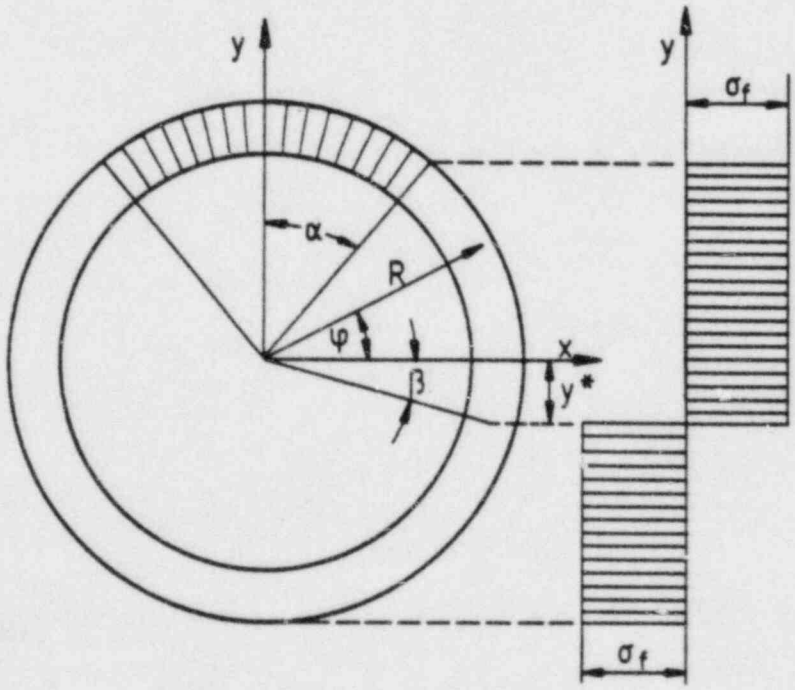

Fig. 6 Assumed stress distribution for a pipe under combined tension and bending loading in the case of global instability.

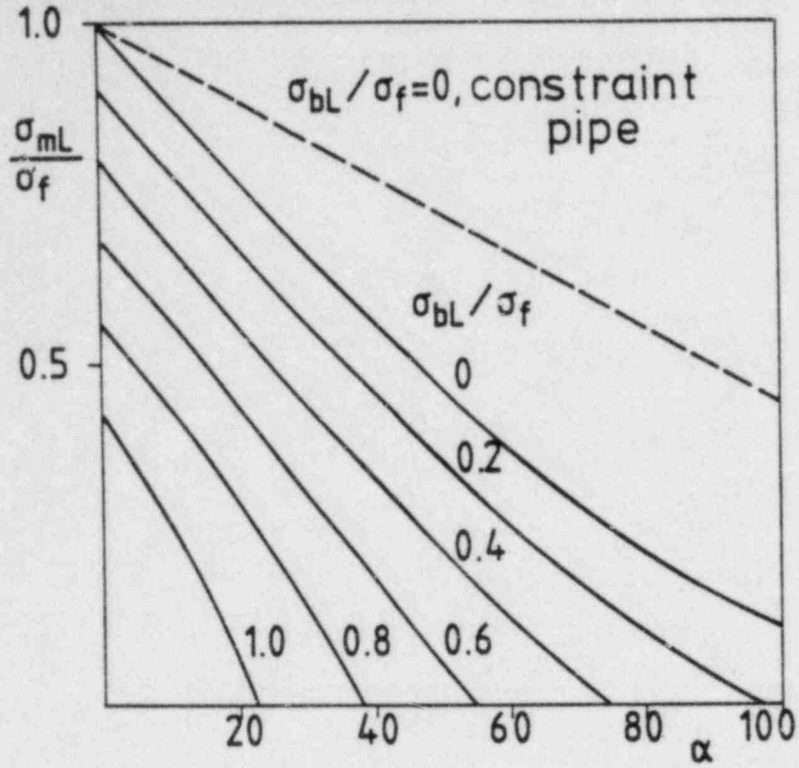

Fig. 7 σ_{mL}/σ_f versus α for circumferential through-cracks at plastic instability.

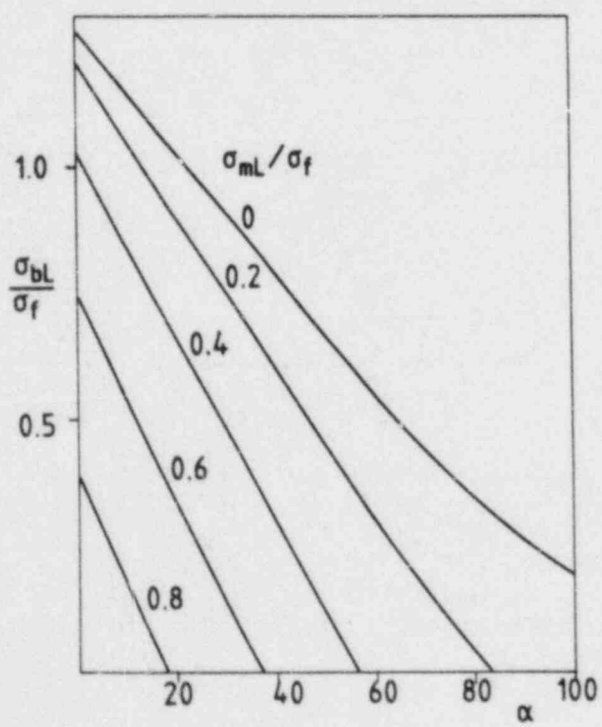

Fig. 8 σ_{bL}/σ_f versus α for circumferential through-cracks at plastic instability.

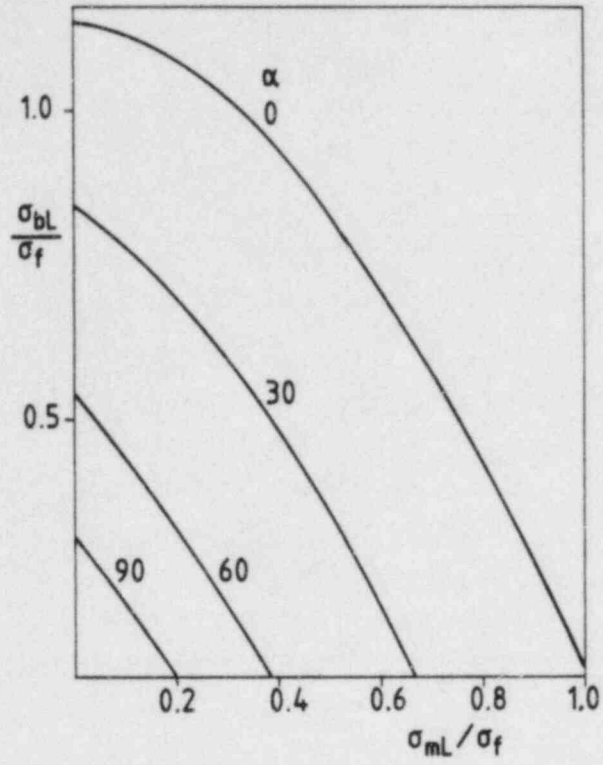

Fig. 9 σ_{bL}/σ_f versus σ_{mL}/σ_f for circumferential through-cracks at plastic instability.

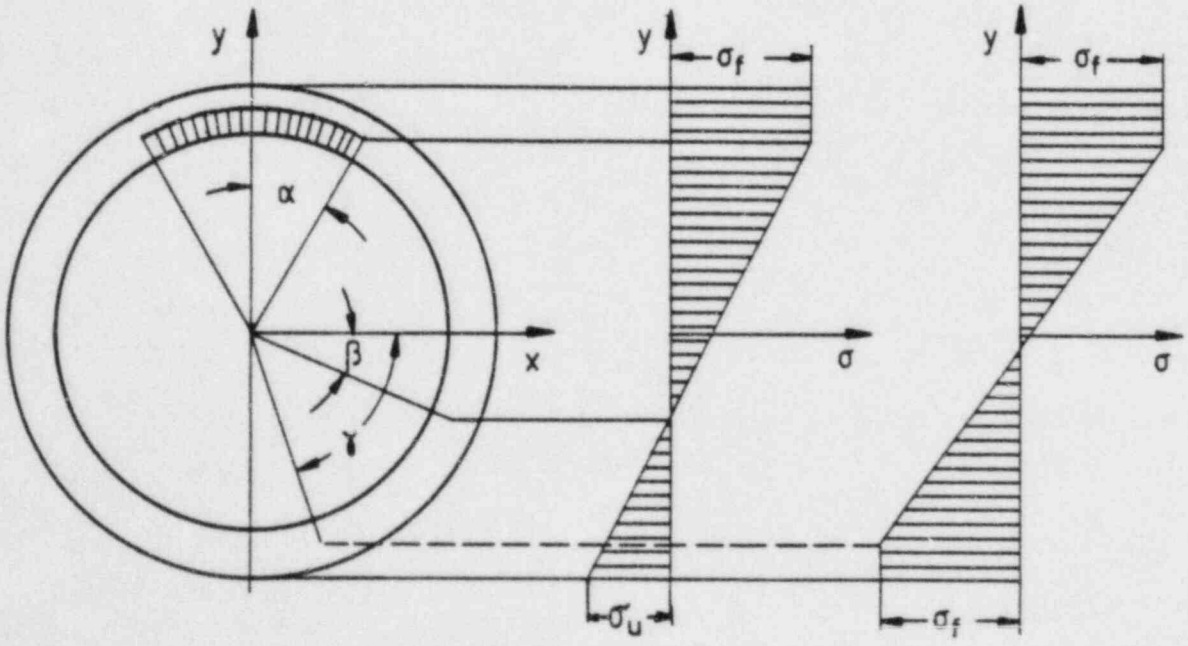

Fig. 10 Assumed stress distribution for a pipe under combined tension and bending loading in the case of local instability for part-through-cracks.

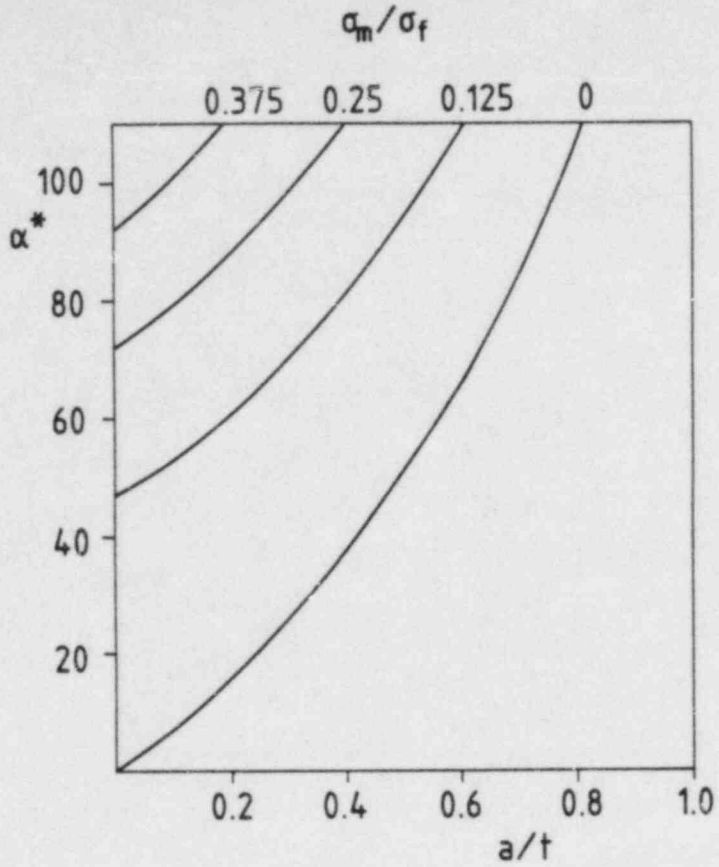

Fig. 11 Critical angle α^* for $\sigma_u = \sigma_f$ versus a/t.

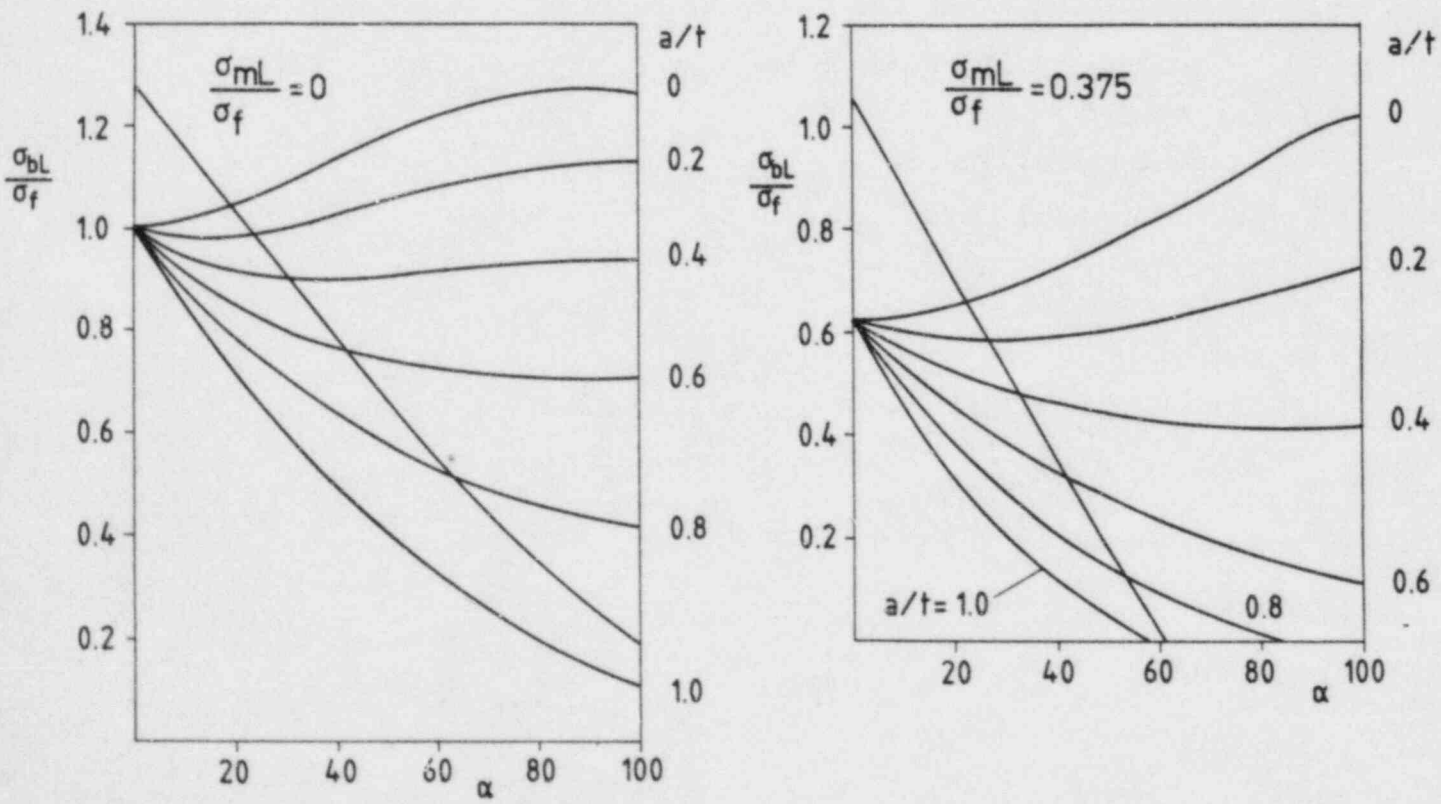

Fig. 12 σ_{bL}/σ_f versus α for local and global plastic instability.

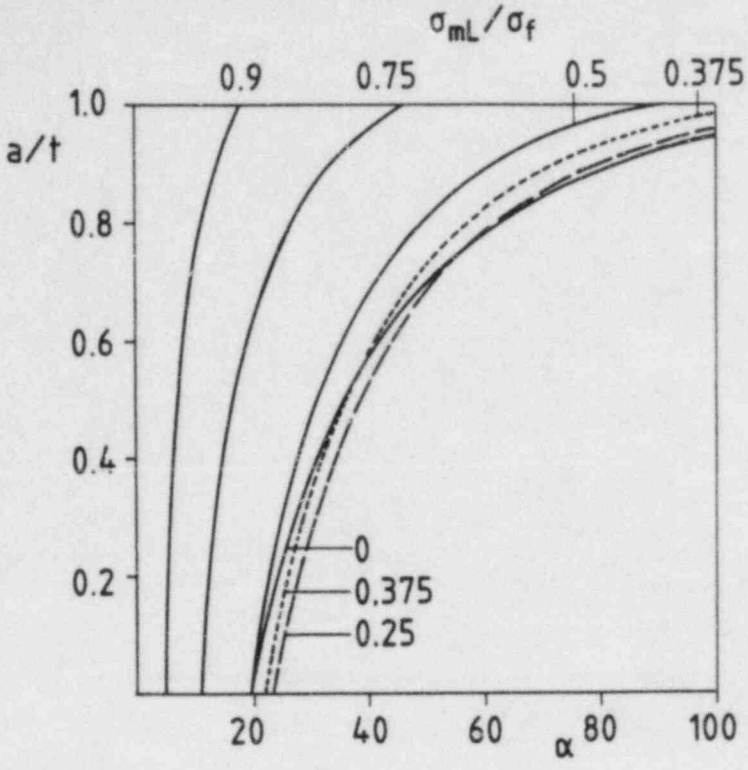

Fig. 13 Leak-before-break boundary curves for combined tension and bending loading and fixed tensile stresses.

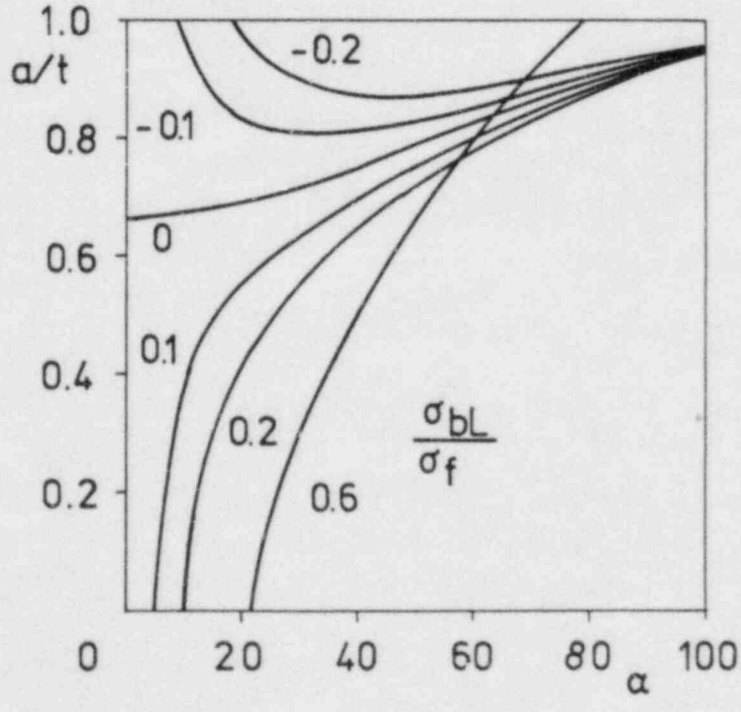

Fig. 14 Leak-before-break boundary curves for combined tension and bending loading and fixed bending stresses.

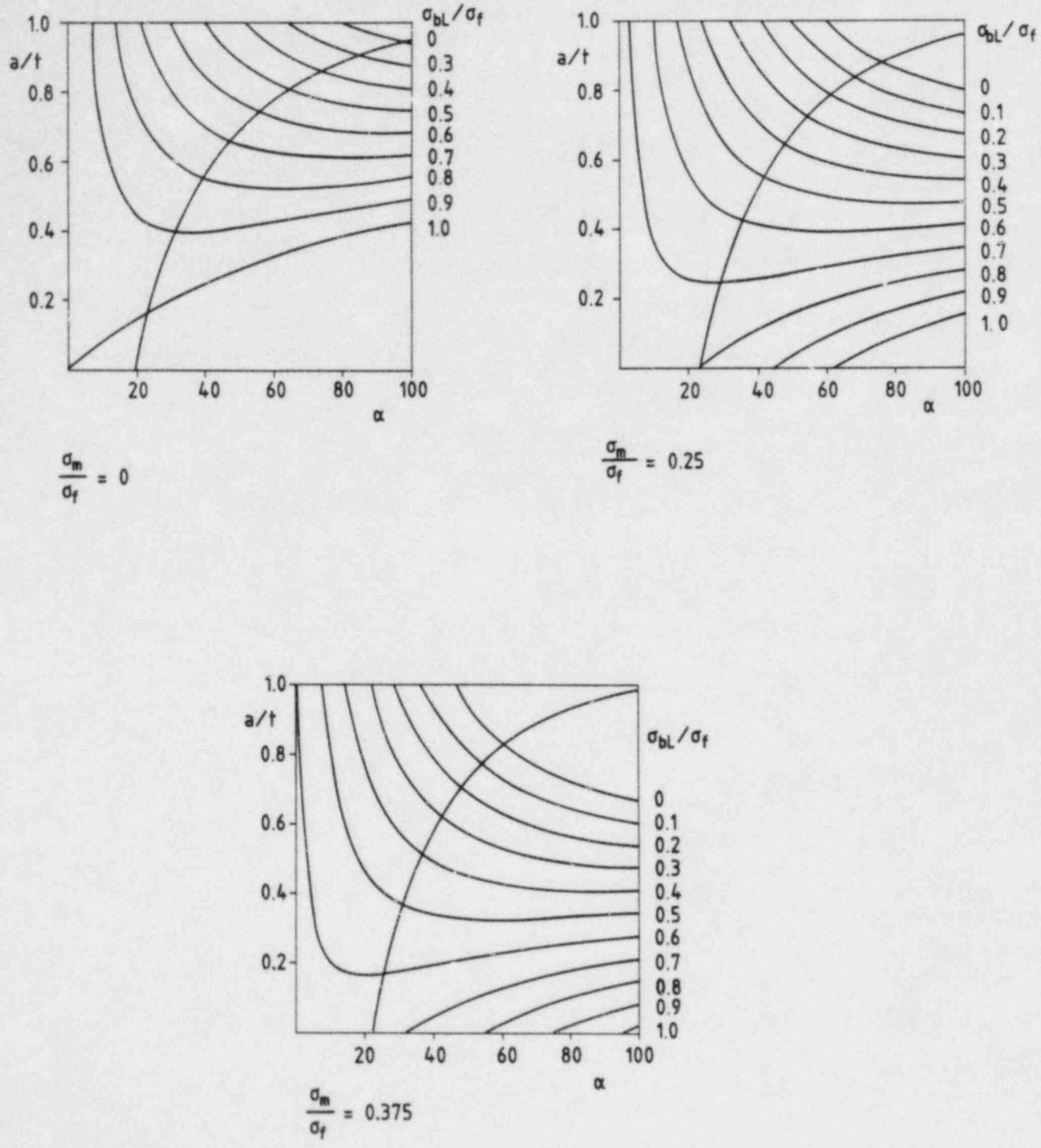

Fig. 15 Leak-before-break boundary curves and ligament-failure curves for different tensile stresses.

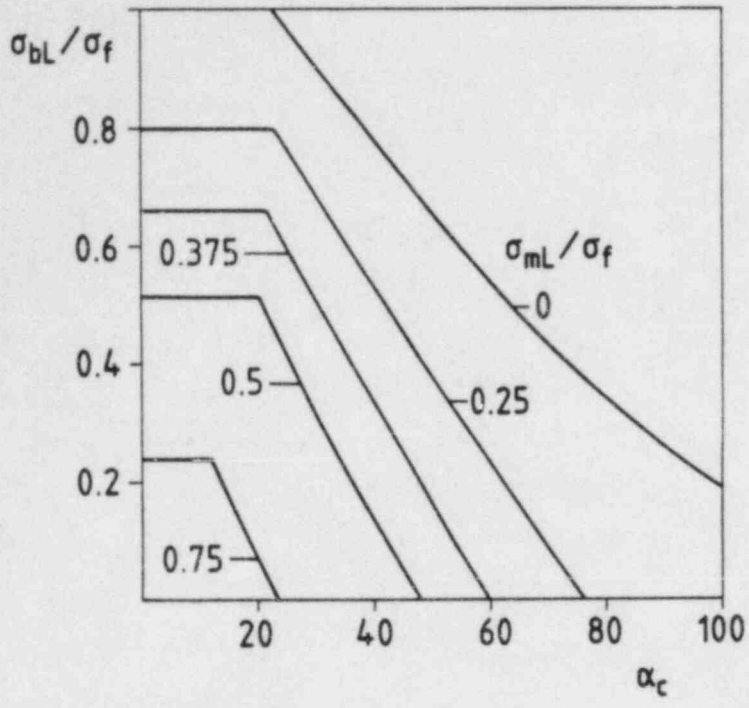

Fig. 16 Critical angle below which no fracture can occur for combined tension and bending loading

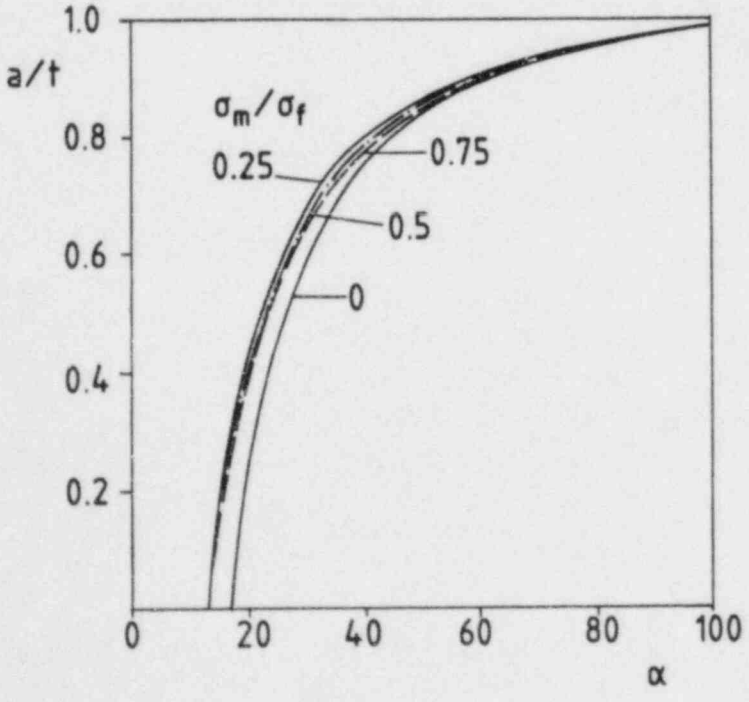

Fig. 17 Leak-before-break boundary curves for combined tension and bending loading after Kanninen et al. /7/.

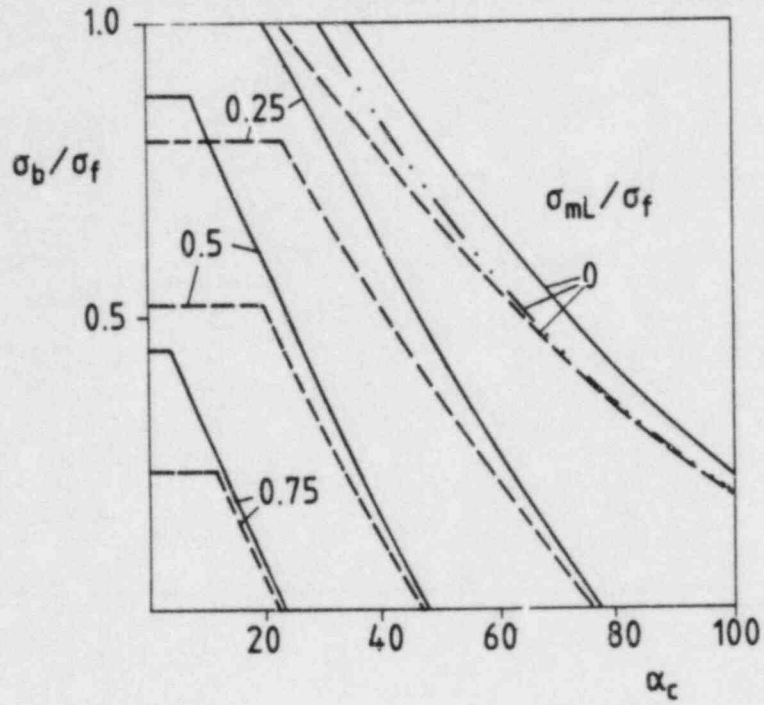

Fig. 18 Comparison of critical angles below which no fracture can occur

———— after chapter 3.3

--------- after chapter 3.4

—·—·—·— after chapter 3.5

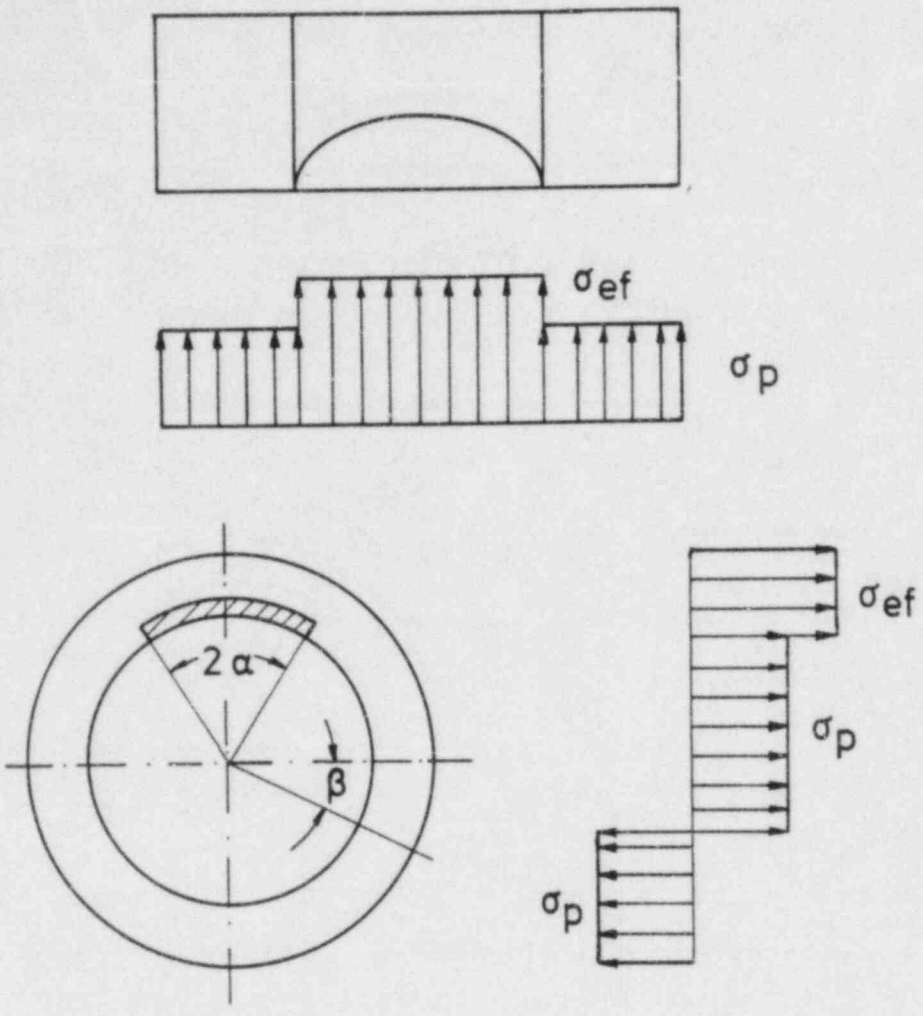

Fig. 19 Stress distribution at local instability after Hasegawa et al. /3/,

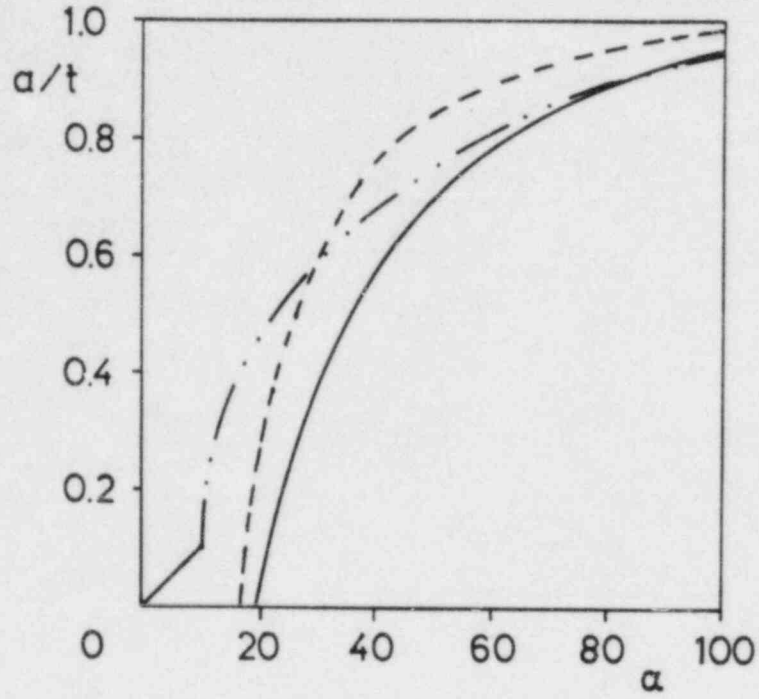

Fig. 20 Leak-before-break boundary curves for pure bending

———— after chapter 3.3
--------- after chapter 3.4
-·-·-·-·- after chapter 3.5

MARGINS OF SAFETY BASED ON CIRCUMFERENTIAL CRACKED DEPTH USING THE NET-SECTION COLLAPSE ANALYSIS

by

G. M. Wilkowski

BATTELLE
Columbus Laboratories
505 King Avenue
Columbus, Ohio 43201

September 23, 1983

Presented at the CSNI/NRC Meeting
on "Leak-Before-Break",
Monterey, California, September 1, 1983.

ABSTRACT

This paper involves an evaluation of the safety factors in the proposed ASME Section XI criterion (IWB 3640) for flaw acceptance in austenitic piping. In developing the end-of-life flaw sizes in IWB 3640 several simplifying assumptions were made in using the net-section collapse criterion. Safety factors on stress were used in developing the IWB 3640 end-of-life flaw sizes. This paper examines not only the safety factors on stress, but also the safety factors on flaw depth of the IWB 3640 values relative to a detailed net-section collapse analysis. Prior to making these comparisons, a review of the development of the net-section collapse analysis for circumferential cracks is given.

DEVELOPMENT OF THE NET-SECTION COLLAPSE ANALYSES

The net-section collapse concept for predicting the failure of a circumferentially cracked pipe was initially developed in EPRI Project RP585[1]*. One major assumption was that the material toughness is sufficiently high so that failure is governed by the strength of the material (i.e., flow stress or collapse stress) and is not sensitive to the materials toughness. The flow stress is a value between the material's yield strength and the ultimate strength and represents an average critical net-section stress reached throughout the flawed ligament of the structure, see Figure 1. Hence, for small cracks, the structure must be subjected to large plastic stresses in order for the crack to initiate. The following sections describe experimental results in verifying the net-section collapse analysis for center-cracked flat plates, through-wall circumferential cracks in pipes, and circumferential surface cracks in pipes.

Results of Center Cracked Flat Plate Experiments

In the initial developmental efforts[1], Type 304 stainless steel center cracked flat plate and circumferential through-wall cracked pipe experiments were conducted. The flat plate experiments were 12 inches wide and 0.35 inch thick. Experiments were conducted under a variety of conditions. Some of these conditions were; the cracks were located in either the base metal or sensitize base metal or HAZ of welds, the cracks were either sharp machine notches or fatigue precracked notches, loading was either monotonic load-controlled or displacement-controlled load or with simulated seismic loading[2]. In all cases, the crack initiation and maximum load stresses were consistent. Figure 2 shows an example of a few of the experiments showing the stresses at crack initiation and maximum load were independent of initial crack size. Here a net-section stress of 63 ksi (436 MPa) corresponded to crack initiation, and 73 ksi (498 MPa) corresponded to

---

* Numbers in parentheses denote references listed at the end of the paper.

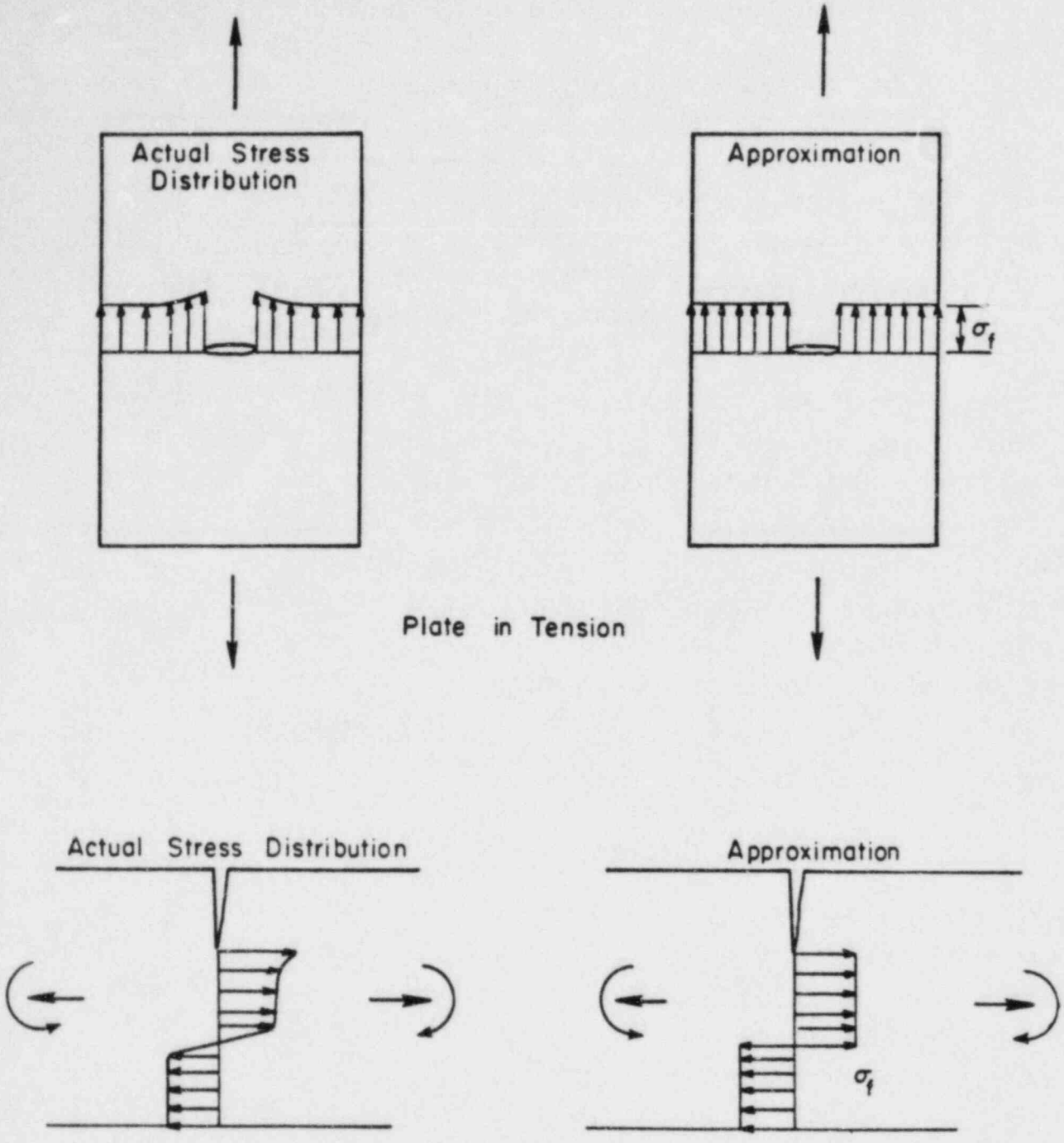

FIGURE 1. NET-SECTION COLLAPSE CRITERION

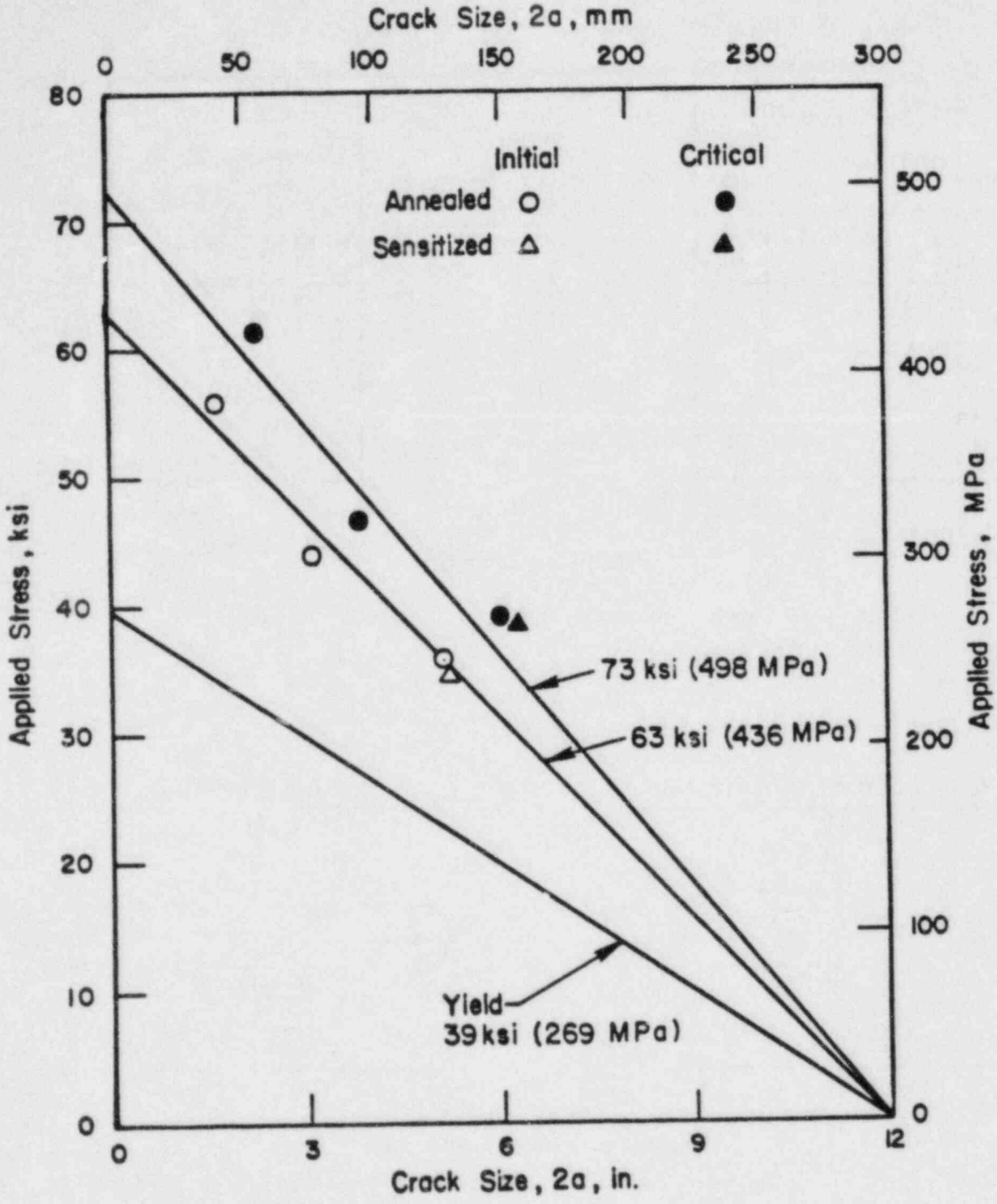

FIGURE 2. RESIDUAL STRENGTH OF 0.3125 INCH (9 MM) PLATE WITH THROUGH-WALL CRACKS AT ROOM TEMPERATURE AS A FUNCTION OF THE CRACK SIZE

maximum load, as well as the net-section stress during subsequent crack growth. These flat plate results provided the initial incentive for the development of the net-section collapse analysis.

Through-Wall Circumferential Cracked Pipe

Initial Net-Section Collapse Formulation - Through-Wall Circumferential Cracks

A pressurized pipe under pure bending was considered in the initial net-section collapse formulation[1]. An idealized bending stress was assumed in the plane of the crack as shown in Figure 3. At crack initiation or maximum load, this stress was assumed to reach a critical constant value of σ_i or σ_f, respectively. A free body analysis shows that the point of the stress inversion (angle β in Figure 3) is defined in Equation (1). (Nomenclature is defined in Figure 3.)

$$\beta = \frac{\pi-\alpha}{2} - \frac{\pi}{4}\frac{R_i^2 p}{Rt\sigma_f} \tag{1}$$

The bending moment can be determined by using Equation (2).

$$M = 2\sigma_f R^2 t\,(2 \sin\beta - \sin\alpha) \quad . \tag{2}$$

This relation was developed by integrating the forces around the pipe circumference and assuming the pipe retains a circular cross-section. The assumption of a circular cross-section within the fully plastic net section was a good, first approximation. The effects of pipe ovalization were subsequently investigated in Reference (2), and are discussed below.

Pipe Ovalization Corrections--Through-Wall Circumferential Cracks

Experimental observations in Reference (2) showed that pipes with short through-wall cracks under bending will ovalize in a similar manner to that of an uncracked pipe. Whereas, for long through-wall cracks, the pipe

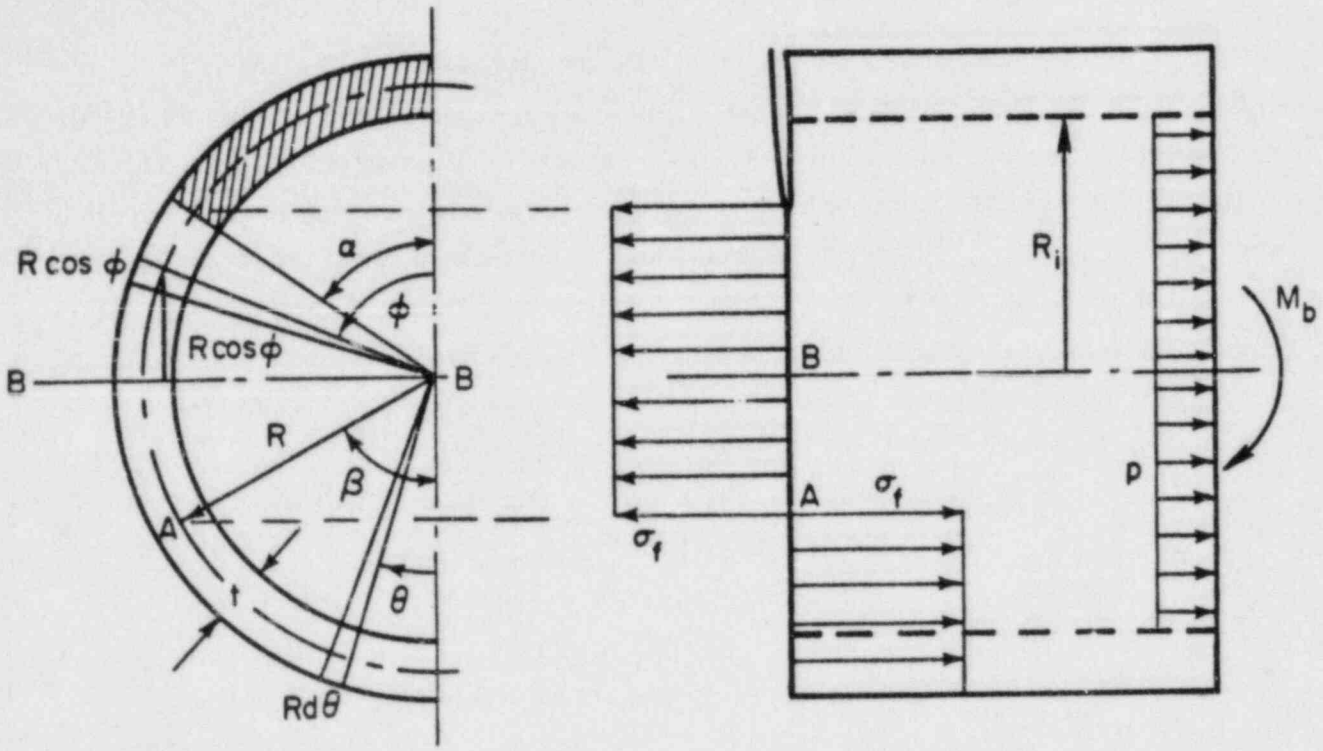

FIGURE 3. NOMENCLATURE AND LOADING SYSTEM FOR THE APPLICATION OF THE NET-SECTION COLLAPSE CRITERION TO A PIPE WITH A CIRCUMFERENTIAL CRACK

will ovalize in the opposite plane, see Figure 4. At some crack length the cross-section of the pipe would remain essentially circular. The short crack length ovalization effect reduces the moment carrying capacity the pipe can sustain relative to the circular cross-section predictions. Whereas, the ovalization for the long crack length increases the moment capacity of the pipe relative to the circular cross-section capacity. This is illustrated in comparing the net-section collapse predictions to the experimental through-wall cracked 4-inch (101.6-mm) diameter pipe data, see Figure 5.

A simple analysis was carried out to evaluate the effect of pipe ovalization to determine if the pipe diameter, or the pipe diameter-to-thickness ratio, was a significant factor. The calculations involved comparing the moment of inertia of a pipe with a circular cross-section to a pipe with an elliptical cross-section. These calculations involved the elliptical integral to relate the circular pipe diameter to the major and minor diameter of the elliptical pipe so that both pipes have the same circumference. Pipes with diameter-to-thickness ratios of 5, 10, 20, and 40 were evaluated. Within the degree of ovalization observed in these experiments, there is no significant effect of the pipe diameter-to-thickness ratio on the ratio of the moment at inertia of the circular to elliptical pipes, see Figure 6. Although this calculation was only performed on an uncracked pipe, the results imply that there is an ovalization correction factor that is independent of the pipe diameter-to-thickness ratio.

The ovalization function for the through-wall cracked pipe is, therefore, a function of the through-wall crack length and load applied to the pipe. Since stainless steel piping fails at a collapse stress slightly higher than the average of the yield and ultimate strength, the strain or deformation of the pipe will also be relatively constant. Hence, an ovalization function can be derived from the experiments for either crack initiation or maximum load conditions. These could also be analytically defined by 3-dimensional finite element calculations, but such calculations with large plasticity are very expensive. It is not expected that this function would be the same for lower toughness materials which fail at stresses below the net-section collapse condition, and hence would exhibit less ovalization.

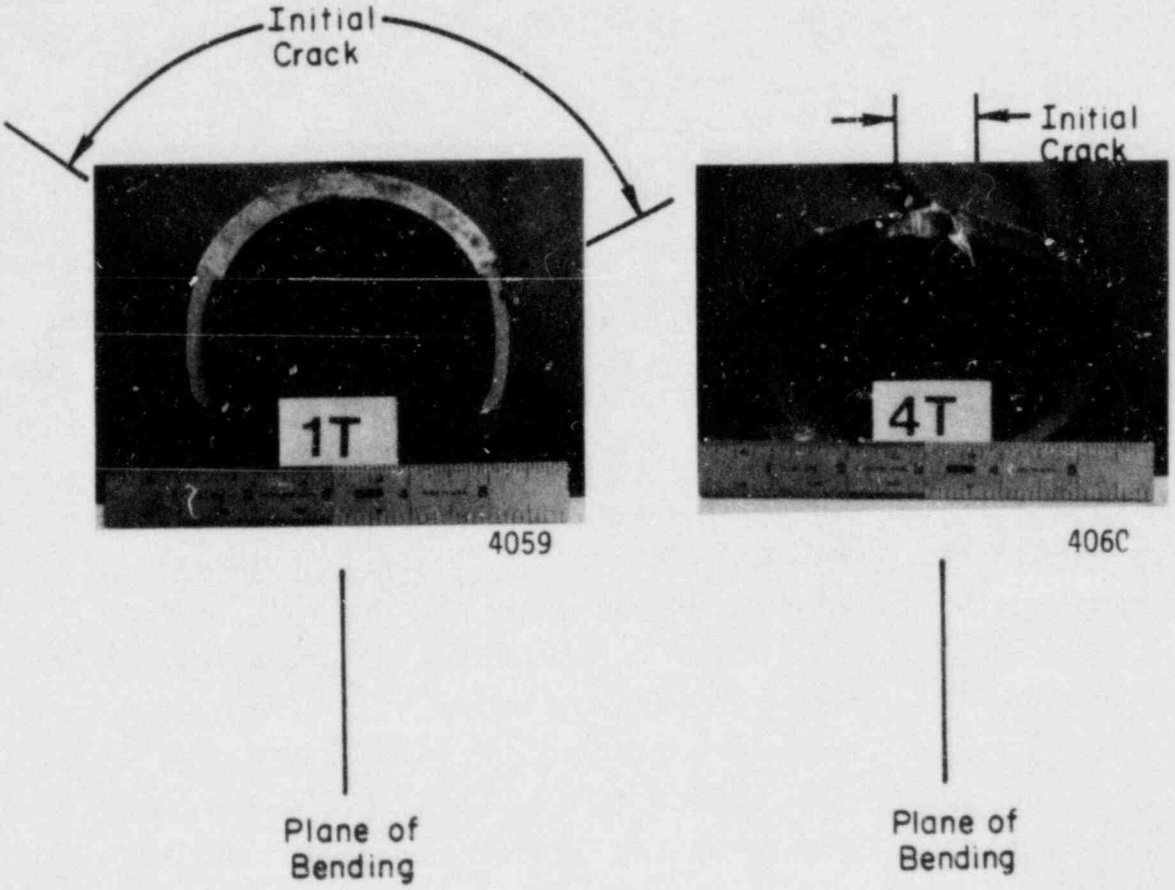

FIGURE 4. OVALIZATION OF 4-INCH (101.6-MM) DIAMETER PIPES WITH DIFFERENT INITIAL THROUGH-WALL CRACK LENGTHS FROM REFERENCE 2

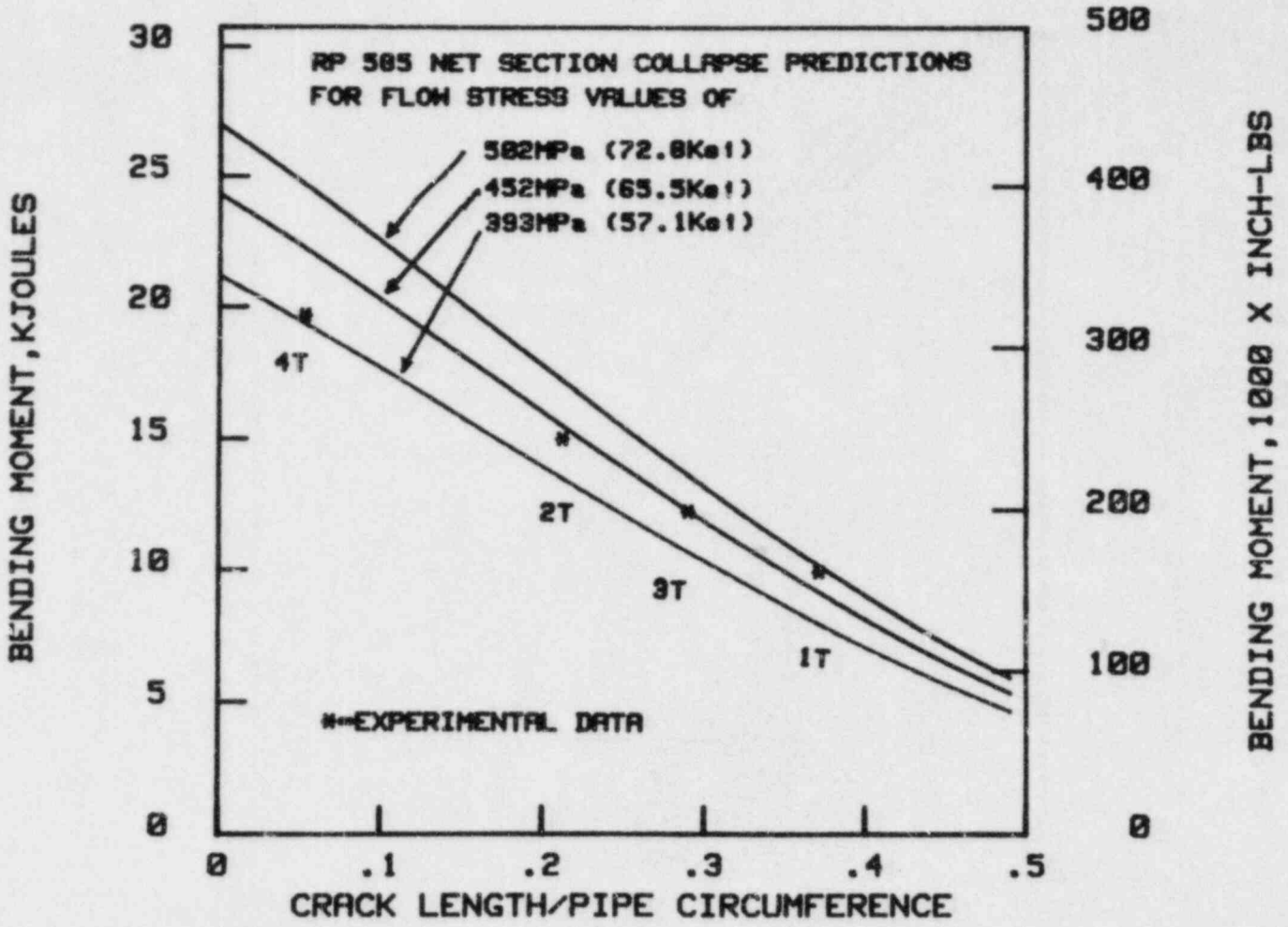

FIGURE 5. COMPARISON OF ORIGINAL NET-SECTION COLLAPSE FORMULATION TO EXPERIMENTAL MAXIMUM BENDING MOMENTS IN INITIAL THROUGH-WALL CIRCUMFERENTIAL CRACK LENGTHS

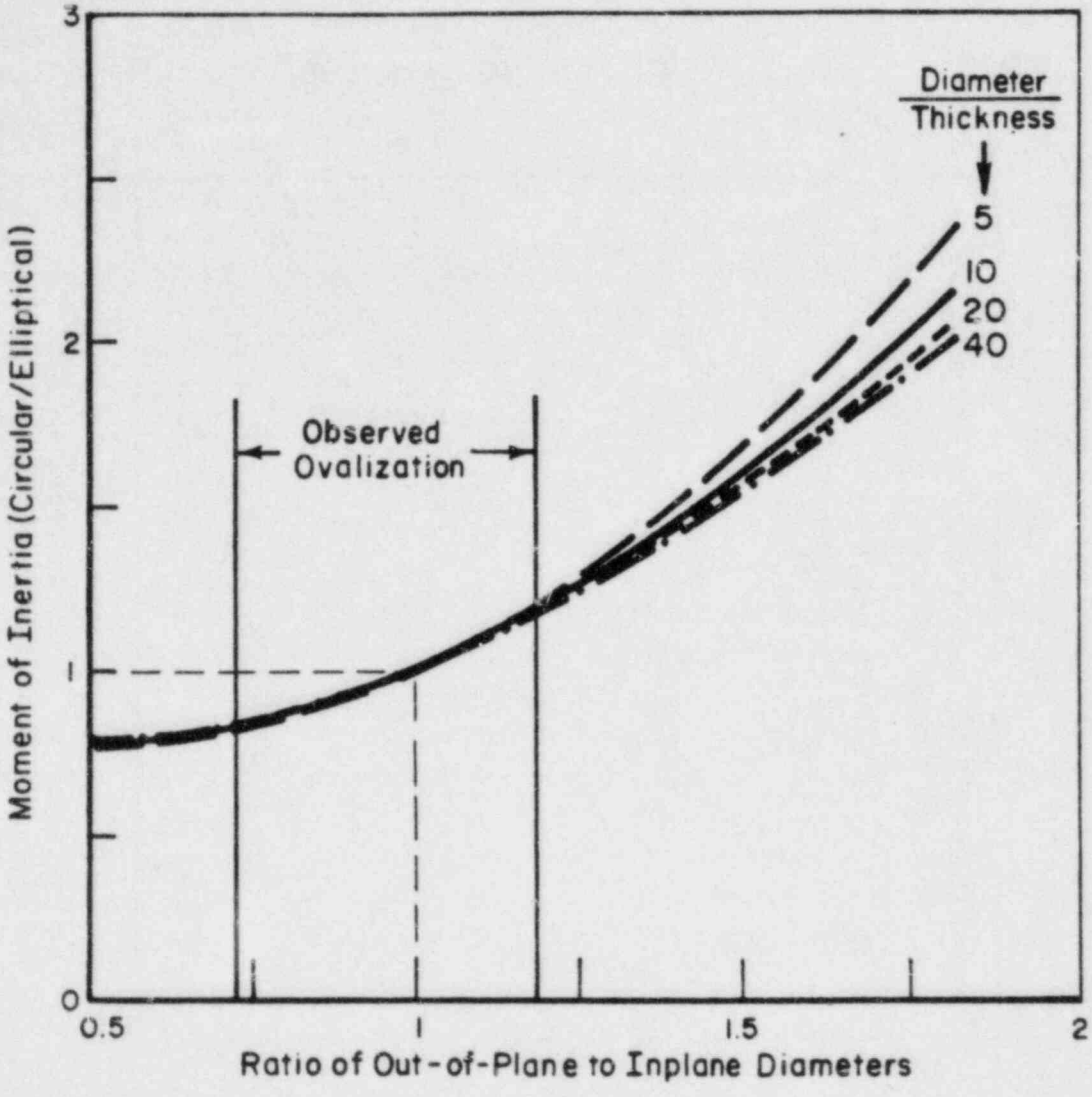

FIGURE 6. EFFECT OF PIPE OVALIZATION ON MOMENT OF INERTIA FROM REFERENCE 2

The experimentally derived ovalization correction function for through-wall circumferential cracks is given in Equation (3). This function was based on the difference of the results from Experiments 1T, 2T, 3T, and 4T (see Table 1) and the original net-section collapse predictions. These four experiments were performed on 4-inch (101.6-mm) diameter Schedule 80 Type 304 stainless steel pipe at room temperature.

$$V(\phi) = \frac{\pi}{4} \left[1 + 0.134\alpha + 0.00152\alpha^2 + 0.0696\alpha^3\right] \quad . \qquad (3)$$

The modified net-section collapse analysis for through-wall flaws including this ovalization function is given in Equation (4).

$$M = 2R_a^2 t\sigma_f \left[2 \sin(\beta) - \sin(\alpha)\right] V(\alpha) \quad , \qquad (4)$$

where;

M = bending moment
R_a = average pipe thickness
t = pipe thickness
σ_f = flow stress = $1.15(\sigma_y + \sigma_u)/2$
2α = total crack angle, radians
β = included angle for section of pipe in compression = $(\pi - \alpha)/2$.

To verify this through-wall crack net-section collapse formulation with the ovalization corrections, the calculated failure stresses were compared to all experimental pipe data. The comparisons using values calculated from Equation (4) and the experimental data included two experiments on 2-inch (50.8-mm) diameter pipe, one experiment on 16-inch (406.4-mm) diameter pipe, and one experiment on a 4-inch (101.6-mm) diameter Schedule 80 pipe having a 90 degree through-wall circumferential crack and a surface crack 75 percent of the depth around the remaining circumference. As seen in Figure 7, the through-wall crack experimental data points are within $\pm$ 5 percent of the calculated value from Equation (4). The flow stress used was 1.15 times the average of the yield plus ultimate. This flow stress relation for circumferentially cracked pipe was also observed in other circum-

TABLE 1. CIRCUMFERENTIAL THROUGH-WALL CRACKED PIPE FRACTURE DATA FROM REFERENCE (2)

Experiment	Length, % Circumference	Thickness, inch (mm)	Bending Moment, in-lb (kN-m) at Initiation	at Maximum Load	at Start of Instability	Internal Pressure, psig (MPa)
4-inch Diameter Schedule 80						
RP-585-1	0.371	0.343 (8.712)	--	153,500 (17.4)	--	1,050 (7.23)
RP-585-1	0.229	0.328 (8.330)	--	224,600 (25.3)	--	2,500 (17.21)
1T	0.371	0.354 (9.017)	152,600 (17.2)	153,300 (17.3)	--	0
2T	0.229	0.352 (8.950)	235,460 (26.6)	242,000 (27.4)	--	0
3T	0.290	0.350 (8.890)	199,330 (22.5)	204,600 (23.1)	186,270 (21.0)	0
4T	0.053	0.350 (8.890)	321,000 (36.3)	321,500 (36.3)	--	0
12IRS	Irregular[a]	(b)	61,050 (6.90)	65,675 (7.4)	--	0
2-Inch Diameter Schedule 80						
6T	0.229	0.237 (6.02)	43,410 (4.90)	43,880 (4.96)	--	0
7T	0.371	0.237 (6.02)	29,620 (3.34)	29,960 (3.38)	--	0
16-Inch Diameter Schedule 100						
8T	0.3675	1.036 (26.2)	6,609,000 (747)	6,957,000 (786)	--	0

(a) Through-wall crack for 25 percent of the circumference with approximately 75 percent deep surface crack around rest of circumference.

(b) Thicknesses at crack tips were 0.080 inch (2.03 mm) and 0.0875 inch (2.22 mm).

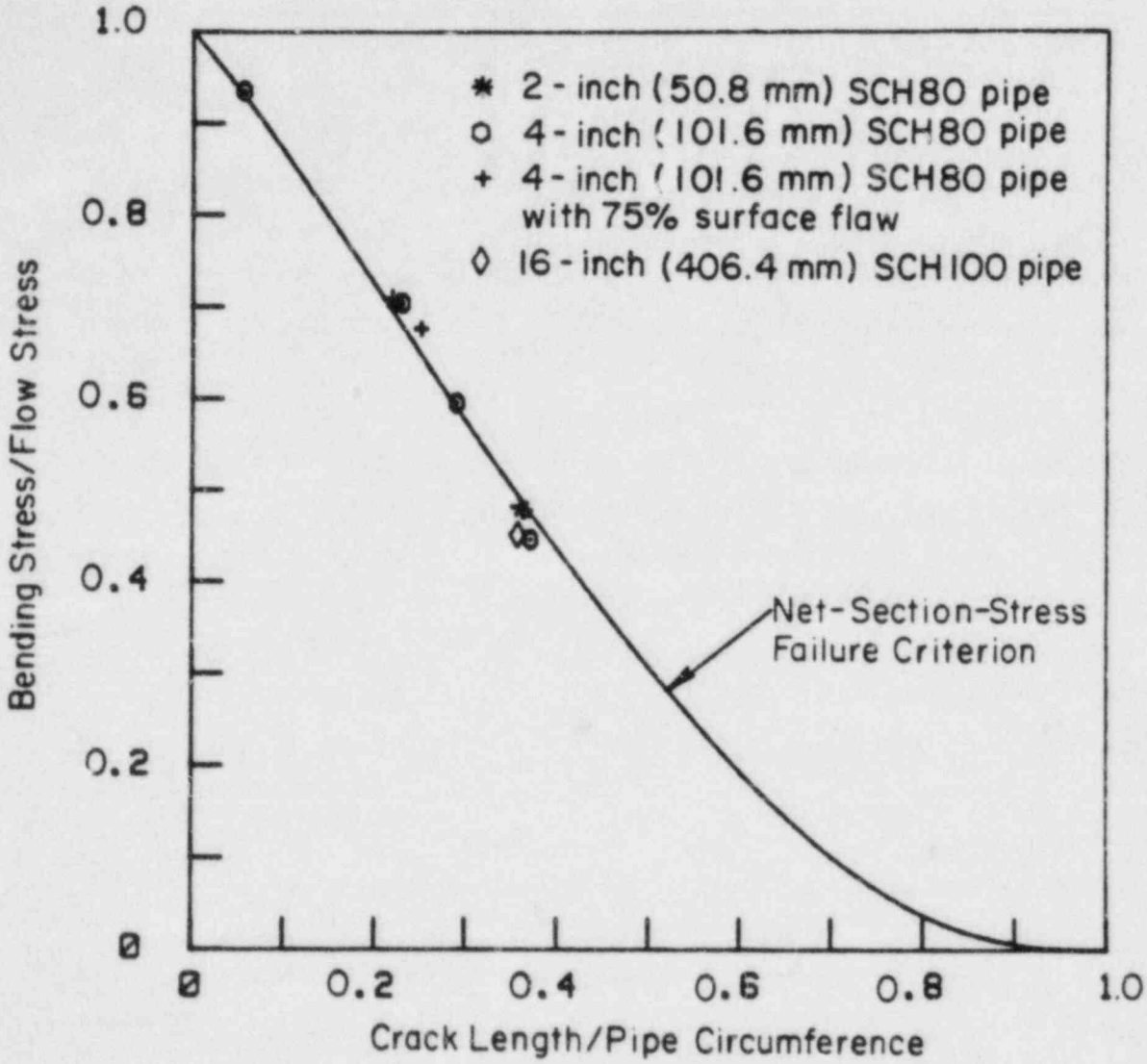

FIGURE 7. COMPARISON OF QUASI-STATICALLY LOADED THROUGH-WALL CIRCUMFERENTIALLY CRACKED TYPE 304 STAINLESS STEEL PIPE EXPERIMENTS TO THE PREDICTION OF THE NET-SECTION-STRESS-FAILURE CRITERION FROM REFERENCE 2

ferentially cracked pipe experiments conducted at Battelle[5], see Figure 8.

Effect of Pipe Diameter on
Through-Wall Circumferential Crack

The net-section collapse approach was compared[3,4,5] to a more rigorous analysis using the GE-CRDC J-integral estimation technique[6]. Smith[3] used the estimation technique for flat plates, and then used the flat plate analysis as being similar to a through-wall circumferentially cracked pipe under a uniform axial load. The flat plate analysis showed that for a fixed crack-length to plate-width-ratio, the failure stress should decrease with increasing plate width. This effect has not yet been demonstrated in plate experiments.

Using this analysis and assuming that the pipe circumference is equal to the plate width, the failure stress ratio (collapse stress/yield strength) was evaluated as a function of the pipe diameter for a 90 degree crack length. (The induced bending moment in the pipe due to the presence of the crack was neglected.) As shown in Figure 9, the predicted failure stress of a 16-inch (406.4-mm) diameter pipe is 80 percent of the 4-inch (101.6-mm) diameter pipe. The failure stress of the 2-inch (50.8-mm) diameter pipe is 113 percent of the 4-inch (101.6-mm) diameter pipe. This trend was not evident in the through-wall cracked pipe bending experiments. The experimental data indicated that the collapse stress from Equation (4) for through-wall cracks was approximately 1.15 times the average of the yield and ultimate strengths. Furthermore, for the 2-inch (50.8-mm) diameter pipe material, the yield strength was 38.6 ksi (266 MPa) and the ultimate strength was 90.2 ksi (621 MPa). However, the predicted collapse stress from Figure 9 would be 95.7 ksi (659 MPa), which is greater than the ultimate strength. Hence, the flat plate representation of a pipe using the estimation scheme is in error for pipes with through-wall circumferential cracks.

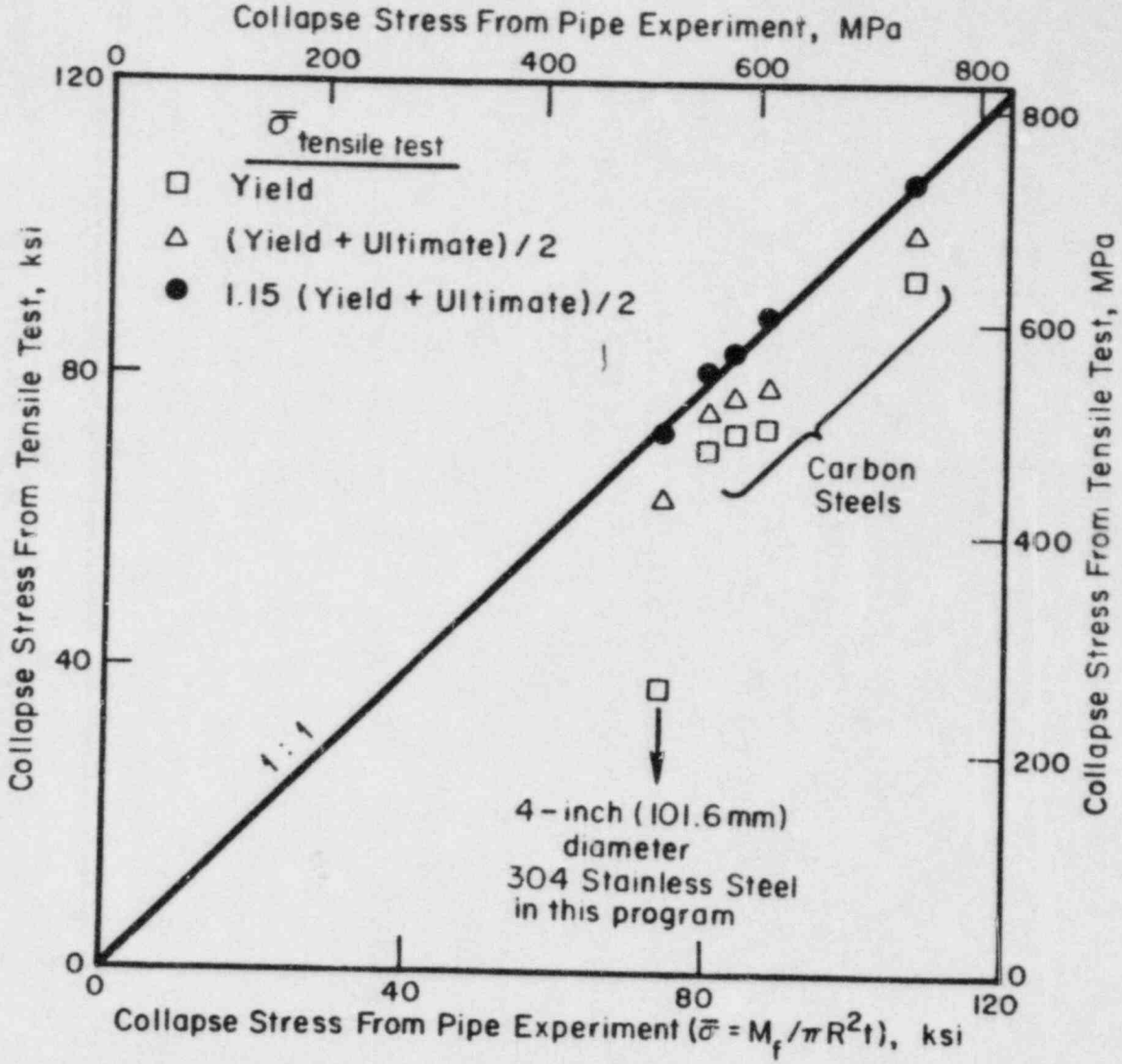

FIGURE 8. RELATION BETWEEN TENSILE TEST DATA AND FLOW STRESS FROM CIRCUMFERENTIALLY CRACKED PIPE EXPERIMENTS CONDUCTED AT BATTELLE

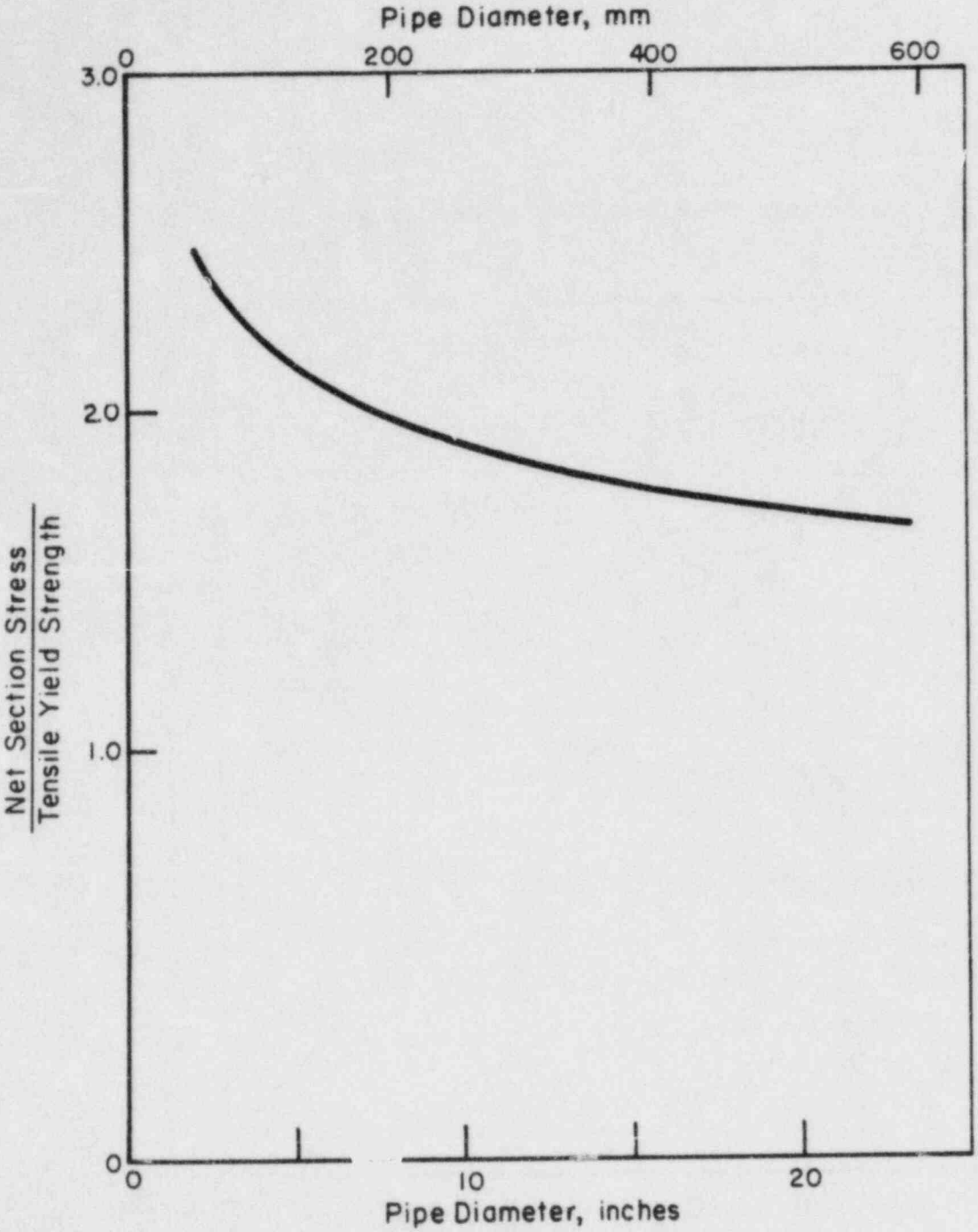

FIGURE 9. PREDICTED NET-SECTION STRESS VERSUS PIPE DIAMETER FOR A 90 DEGREE THROUGH-WALL CIRCUMFERENTIAL CRACK USING THE ANALYSIS IN REFERENCE (3)

Circumferential Surface Cracked Pipe

Initial Net-Section Collapse Formulation - Circumferential Surface Cracks

The net-section collapse relation for surface cracks from Reference[1] was developed from experimental observations during flat plate experiments. The hypothesis was that the exact shape of the surface crack was less important than knowing the area of the crack. From the flat plate results, a load-controlled leak-before-break criteria was developed. The center-cracked flat plate results showed that there was a critical collapse stress, σ_i, where the surface crack grew in a slow stable manner (through the thickness). Depending on the shape of the crack, the surface crack could penetrate the thickness prior to maximum load (a leak) or coincide with maximum load (a load-controlled break). This load-controlled leak-before-break behavior is illustrated in Figure 10.

For a surface flawed pipe, the analysis assumed a constant depth surface crack with a depth of "d". The crack is also assumed to be symmetrically oriented with respect to the bending plane. The stress inversion point β for plastic collapse is defined in Equation (5).

$$\beta = \frac{\pi-(d/t)\alpha}{2} \quad \frac{R_i^2 p}{4Rt\sigma_f} \quad . \tag{5}$$

This assumes the circumferential crack is short enough so that it does not extend into the compressively stressed side of the pipe. The bending moment is then determined from Equation (6).

$$M = 2\sigma_i R^2 t \left[2 \sin \beta - (d/t) \sin \alpha\right] \quad . \tag{6}$$

Although Reference (1) develops a parallel solution for surface cracks extending below the neutral axis, intuition suggests that the compressively loaded tight crack faces can transmit the compressive load. Hence, the long surface crack will behave the same as a circumferential crack length extending just to the neutral axis. Figure 11 shows a graph of the normalized bending moment at initiation versus circumferential crack

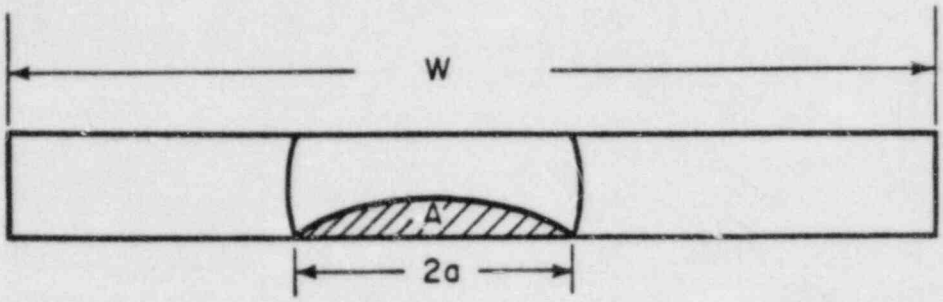

$P_i = \sigma_i (Wt - A)$

$P_f = \sigma_f t (W - 2a)$

Failure:

$P_i > P_f$

Slow Growth:

$P_i < P_f$

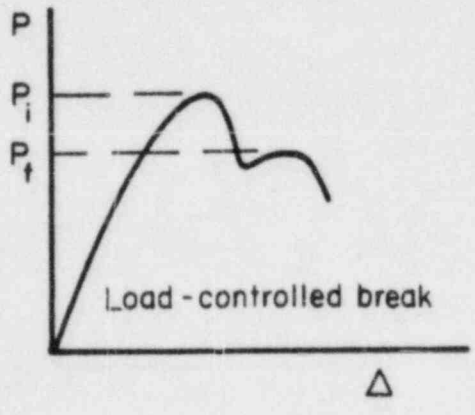

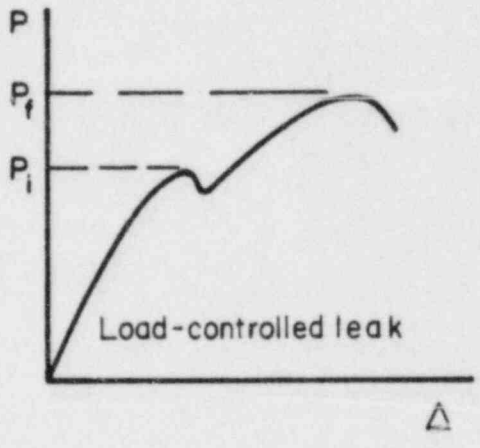

FIGURE 10. CONDITIONS AFTER BREAKTHROUGH OF SURFACE FLAWS FROM REFERENCE 1

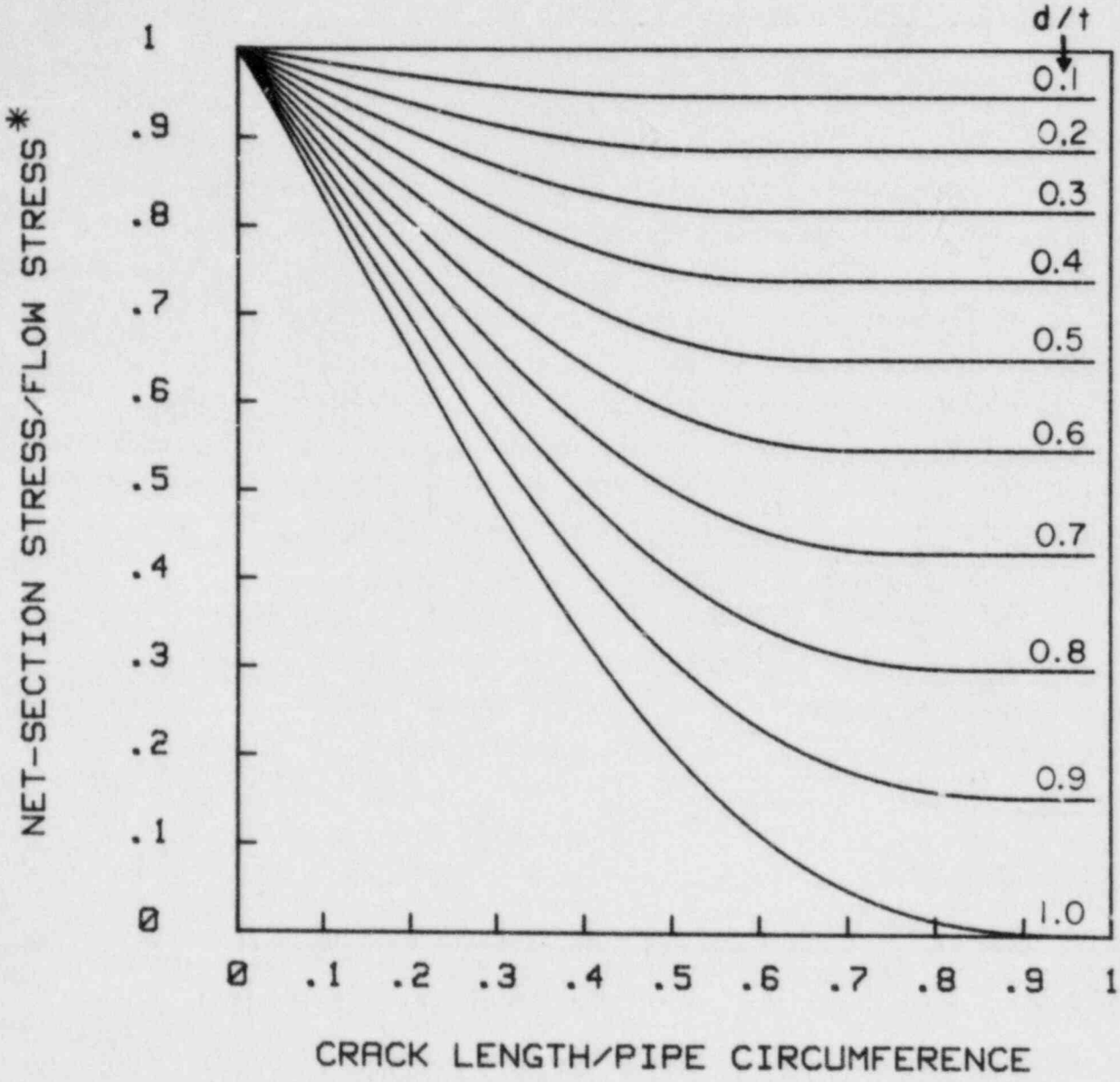

FIGURE 11. NORMALIZED NET-SECTION COLLAPSE PREDICTIONS FOR CIRCUMFERENTIALLY CRACKED PIPE IN PURE BENDING

* Nominal Bending Stress = $M/\pi R^2 t$.

length for various surface crack depth to thickness ratios as calculated from Equation (6), and keeping the failure stress constant for crack lengths extending below the neutral axis.

Circumferential Surface Cracked Pipe Experimental Observations

The through-wall cracked pipe experiments conducted in Reference (2) showed that there was a significant ovalization effect for short or long through-wall circumferential cracks in pipes. Similarly, there should be an ovalization effect for surface cracks. However, the circumferential surface crack ovalization function may differ from the through-wall circumferential crack ovalization relationship given in Equation (3). The following points relative to surface cracks will be discussed: (1) ovalization effect on the failure stresses compared to the predicted net-section collapse values, (2) effect of a variable depth surface crack versus a constant depth surface crack, (3) effect of the pipe diameter, and (4) instability behavior of surface cracks. Ten experiments were conducted and these data are in Table 2.

The typical data recorded were load versus displacement, crack mouth opening versus d-c electric potential across the crack, and load versus crack mouth opening. Figure 12 shows a typical load versus load-line displacement record for a displacement-controlled internal circumferential surface cracked pipe experiment. Crack initiation was detected by the crack mouth opening versus d-c electric potential record[7] in Figure 13. Several of the pipe specimens were heat-tinted to document the e.p. crack growth calibration, and the shape of the crack growth. Note in Table 2 that for the non-compliant long surface cracked pipe experiments, there were limited instabilities. These resulted in finite length through-wall flaws, or a displacement-controlled leak-before-break condition.

Comparisons of Net-Section-Collapse Predictions to Experimental Data and Ovalization Effects

The constant depth internal circumferential surface crack data were first compared to the net-section collapse predictions for the 4-inch

TABLE 2. CIRCUMFERENTIAL SURFACE CRACKED PIPE FRACTURE DATA

Experiment	Depth Thickness	Length, % Circumference	Thickness, inch (mm)	Bending Moment, in-lb (kN-m) at Initiation	Bending Moment, in-lb (kN-m) at Maximum Load	Bending Moment, in-lb (kN-m) at Start of Instability
4-Inch (101.6-mm) Diameter Schedule 80						
1S	0.10	0.500	--	--	--	--
2S	0.380	0.500	0.350 (8.890)	350,430 (40.7)	363,520 (41.1)	330,680 (37.0)
3S	0.594	0.500	0.355 (9.017)	283,870 (32.0)	292,050 (33.0)	255,200 (28.8)
4S	0.10	0.250	--	--	--	--
5S	0.387	0.250	0.336 (8.534)	329,700 (37.3)	333,850 (37.7)	--
6S	0.608	0.250	0.347 (8.814)	286,820 (32.4)	297,000 (33.5)	286,000 (32.3)
7S	0.116	0.750	0.345 (8.763)	Not Reached	360,750 (40.8)[b]	--
8S	0.413	0.750	0.346 (8.789)	328,160 (37.1)	331,650 (37.5)	296,450 (33.5)
9S	0.645	0.750	0.335 (8.509)	264,080 (29.8)	267,850 (30.2)	248,600 (28.1)
10S	0.575	0.500	0.365 (9.271)	275,050 (31.0)	286,000 (32.3)	253,000 (28.6)
11IRS	Irregular[c]		0.350 (8.890)	281,050 (31.7)	281,270 (31.8)	--
16-Inch (406.4-mm) Diameter Schedule 100						
13S	0.66	0.588	1.030 (26.2)	7,987,000 (902.)	10,441,000 (1,180)	10,388,000 (1,175)

Experiment	Depth Thickness	Length, % Circumference	Thickness, inch (mm)	Depth at Center of Surface Crack at, inches (mm) Initial	Maximum Load,[a]	Start of Instability,[a]	Comments
4-Inch (101.6-mm) Diameter Schedule 80							
1S	0.10	0.500	--	--	--	--	Deleted.
2S	0.380	0.500	0.350 (8.890)	0.133 (3.377)	0.190 (4.826)	0.255 (6.477)	Shorter Moment Arm.
3S	0.594	0.500	0.355 (9.017)	0.211 (5.359)	0.233 (5.918)	0.261 (6.629)	
4S	0.10	0.250	--	--	--	--	Deleted.
5S	0.387	0.250	0.336 (8.534)	0.130 (3.305)	0.200 (5.080)	0.266 (6.756)	Gradual load drop, no instability, several unloading cycles occurred prior to maximum load.
6S	0.608	0.250	0.347 (8.814)	0.211 (5.362)	0.236 (5.994)	0.275 (6.985)	Gradual load drop, no instability.
7S	0.116	0.750	0.345 (8.763)	0.039 (0.991)	--	--	Pipe buckled before breaking.
8S	0.413	0.750	0.346 (8.789)	0.143 (3.625)	0.194 (4.928)	0.262 (6.654)	Clip gage data bad.
9S	0.645	0.750	0.335 (8.509)	0.216 (5.510)	0.233 (5.918)	0.250 (6.350)	
10S	0.575	0.500	0.365 (9.271)	0.210 (5.280)	0.230 (5.842)	0.269 (6.833)	Used RP-585 pipe.
11IRS	Irregular[c]		0.350 (8.890)	0.224 (5.69)	0.235 (5.967)	--	Variable depth surface crack.
16-Inch (406.4-mm) Diameter Schedule 100							
13S	0.66	0.588	1.030 (26.2)	0.680 (17.27)	0.855 (21.7)	0.877 (22.2)	

(a) From Electric Potential Measurements.
(b) Pipe buckled before crack initiation.
(c) Maximum depth in center = 0.60 x thickness, length = 50 percent of circumference, see Figure A-58.

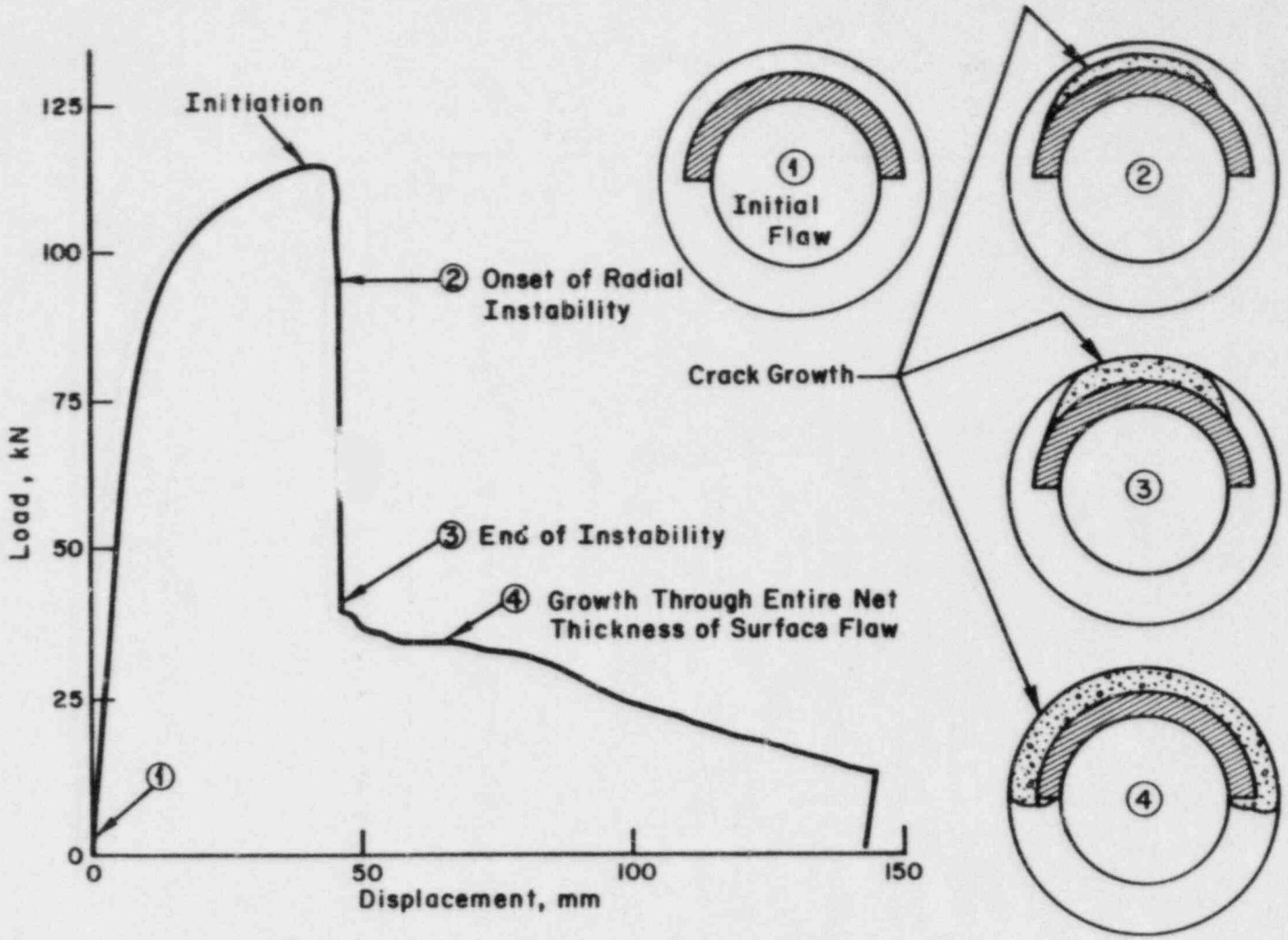

FIGURE 12. LOAD-DISPLACEMENT RECORD OF SURFACE CRACKED PIPE EXPERIMENT 10S FROM REFERENCE 2

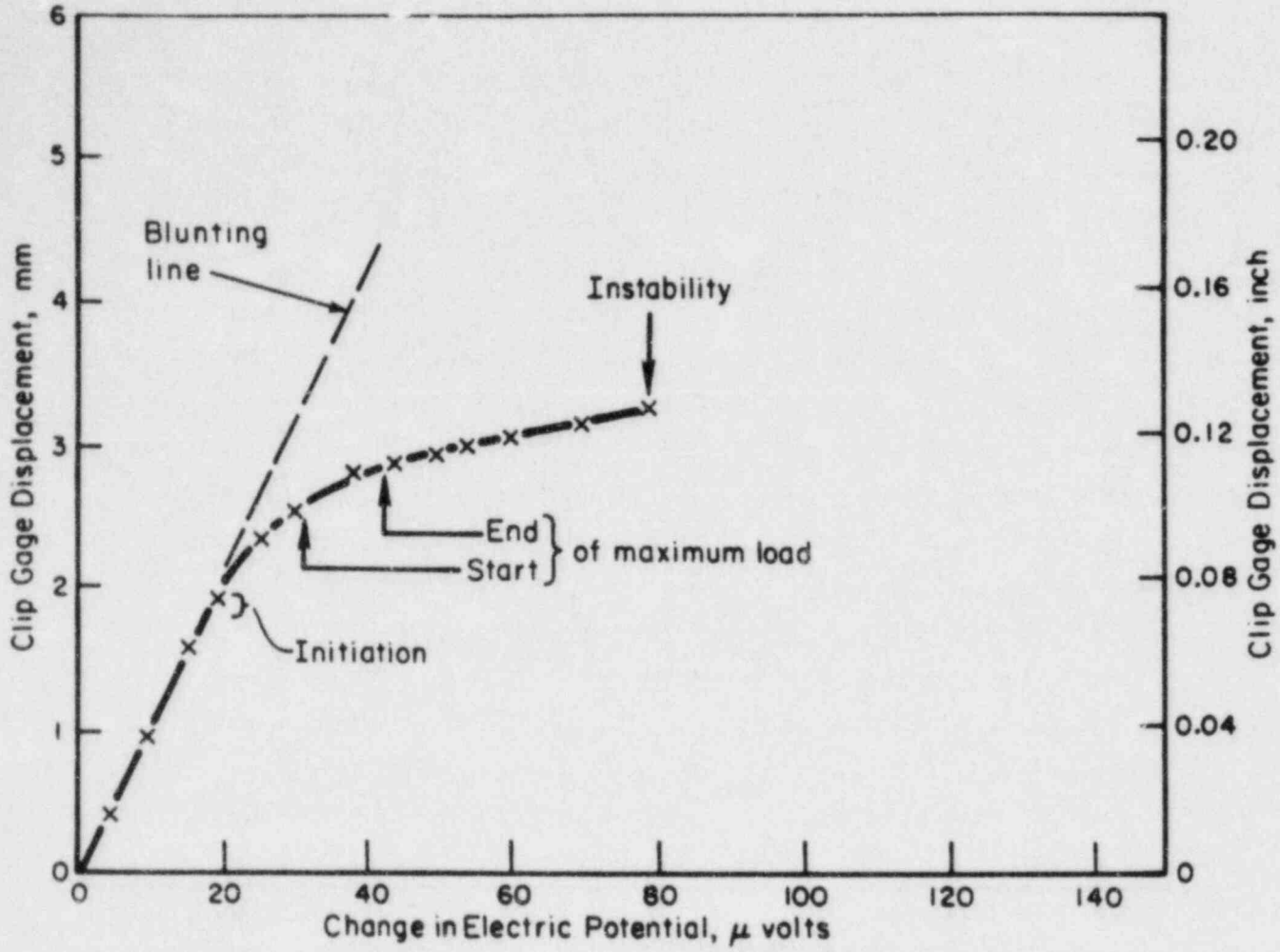

FIGURE 13. CRACK MOUTH OPENING DISPLACEMENT ACROSS THE CENTER OF THE SURFACE FLAW VERSUS ELECTRIC POTENTIAL ACROSS THE CENTER OF THE SURFACE FLAW FOR EXPERIMENT 10S FROM REFERENCE 2

(101.6-mm) diameter pipe experiments, see Figure 14. The electric potential data[7] for all the 4-inch (101.6-mm) diameter pipe experiments showed that the load at crack initiation was 98 percent (± 1 percent) of the maximum load. Hence, the value of σ_i, which arises in the RP-585 net-section collapse analysis, is approximately equal to σ_f. Consequently, leak-before-break behavior as predicted by the existing surface flaw net-section collapse analysis under load-controlled conditions would occur for surface cracks with extremely short lengths and large depths. All surface flawed pipe experiments had the surface crack break through the thickness, slightly past maximum load. Hence, under load-controlled conditions they would have been breaks. No surface cracks with extremely short lengths and large depths were tested. Therefore, load-controlled leak-before-break criteria were not experimentally determined for Type 304 stainless steel pipe within this program. Prior research at Battelle[8] on carbon steel pipes has shown that load-controlled leak-before-break conditions for circumferential surface cracks in carbon steel pipes under bending can occur, but only for short, deep surface cracks.

Figure 15 shows the experimental bending moments at crack initiation versus the predicted moments using Equation (4) for the 4-inch (101.6-mm) diameter Schedule 80 surface flawed pipe experiments. This figure shows the degree of conservatism (or nonconservatism) in the circumferential surface flawed pipe data. The agreement for the constant depth 4-inch (101.6-mm) diameter pipe surface flaw experiments was found to be within ± 12 percent. This shows a much larger scatter in the surface flaw data than in the through-wall flaw data, but may be satisfactory for conservative estimates of critical crack sizes. Note that the nonconservative data points are for shorter circumferential crack lengths. Figure 16 presents the same 4-inch (101.6-mm) diameter surface flaw data in the form of the ratio of the experimental bending moment to the predicted bending moment (using Equation 6) versus the circumferential crack length (normalized by the pipe circumference). A definite trend between the ratio of the experimental and the predicted moments is seen as a function of crack length. A curve is drawn through the data points so that for $2c/\pi D$ up to 0.5. For the long circumferential crack lengths, an upper limit is indicated. This is

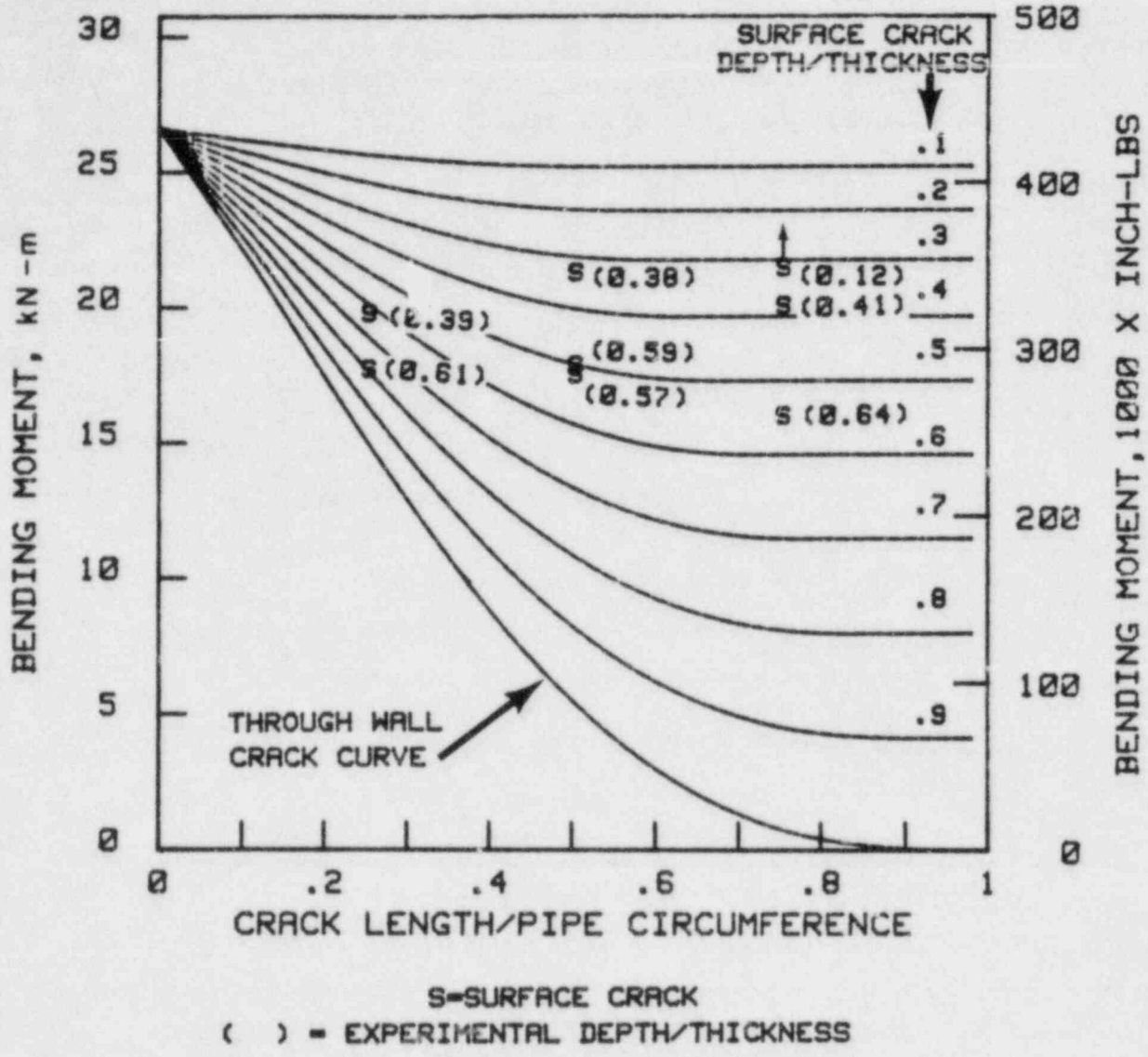

FIGURE 14. COMPARISON OF EXPERIMENTAL 4-INCH (101.6-MM) DIAMETER SCHEDULE 80 PIPE FRACTURE DATA TO PREDICTIONS USING RP585 SURFACE FLAW NET-SECTION COLLAPSE ANALYSIS MODIFIED FOR CRACK CLOSURE FROM REFERENCE 2 (σ_f = 72.8 KSI [501.6 MPA])

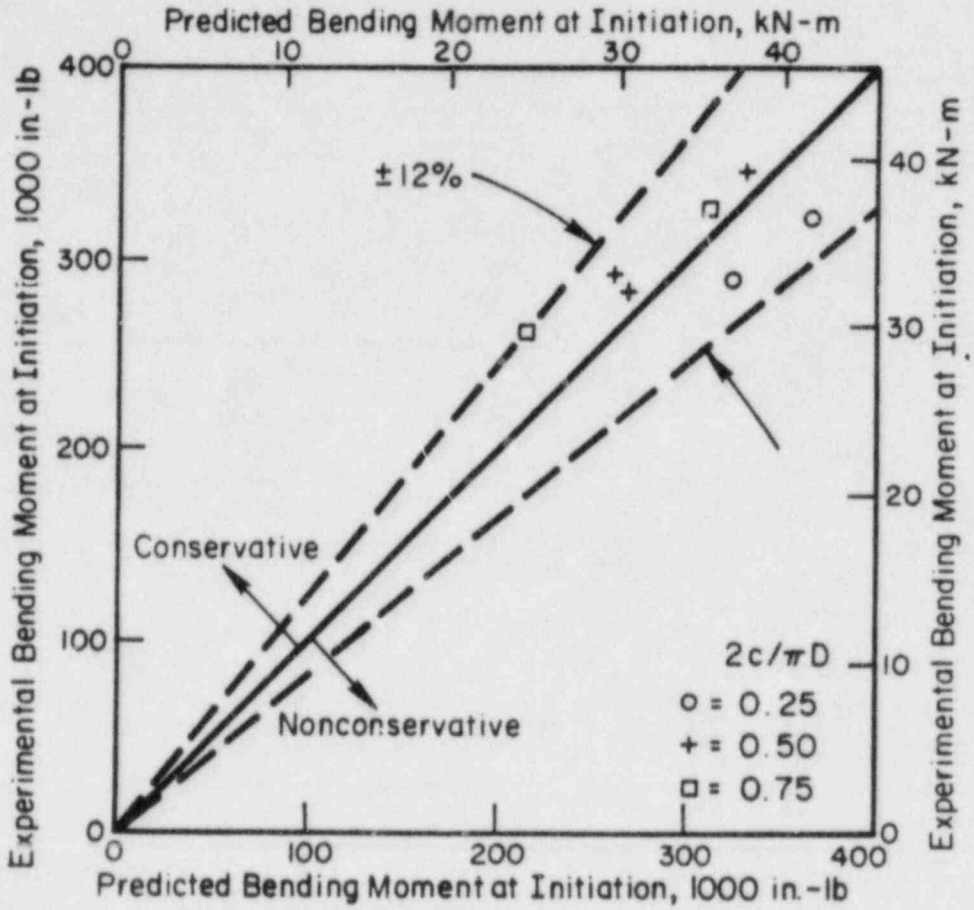

FIGURE 15. COMPARISON OF EXPERIMENTAL VERSUS PREDICTED MAXIMUM BENDING MOMENTS FOR 4-INCH (101.6-MM) DIAMETER TYPE 304 SEAMLESS STAINLESS STEEL PIPE EXPERIMENTS WITH CONSTANT DEPTH INTERNAL CIRCUMFERENTIAL SURFACE CRACKS FROM REFERENCE 2

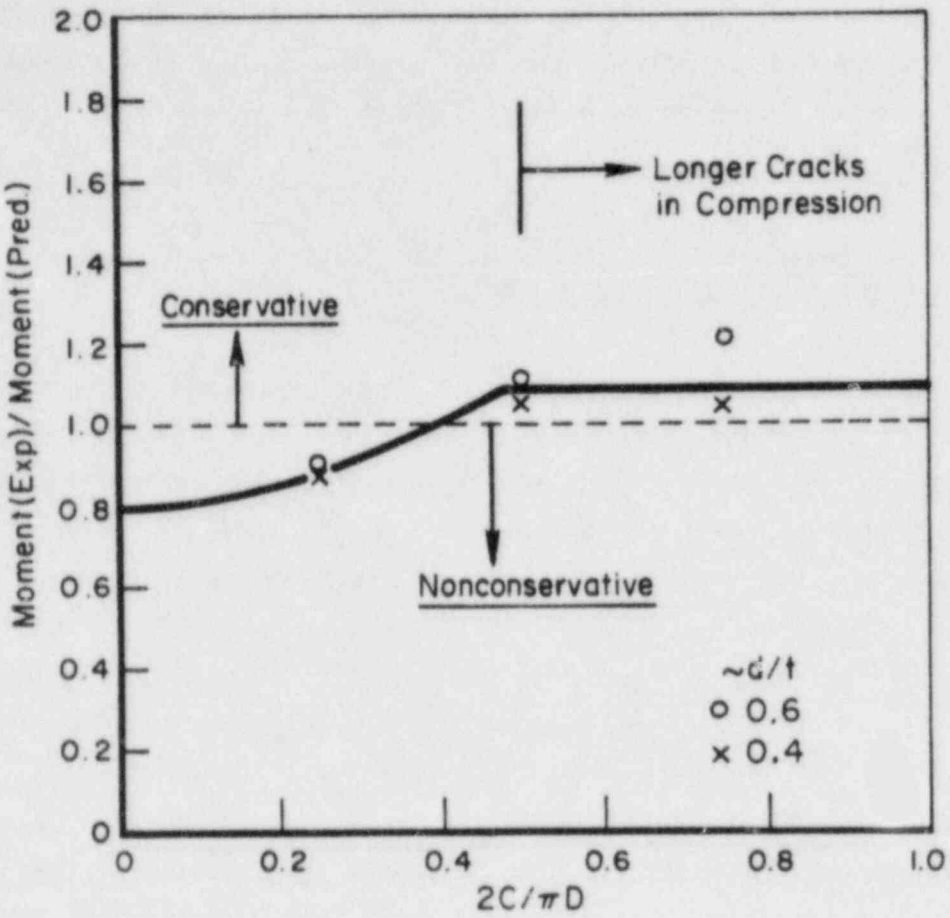

FIGURE 16. RATIO OF EXPERIMENTAL TO PREDICTED* MAXIMUM BENDING MOMENTS FOR 4-INCH (101.6-MM) DIAMETER SCHEDULE 80 CONSTANT DEPTH INTERNAL CIRCUMFERENTIAL SURFACE CRACKS VERSUS THE CIRCUMFERENTIAL LENGTH OF THE SURFACE CRACKS FROM REFERENCE 2

*PREDICTED BY INITIAL NET-SECTION COLLAPSE ANALYSIS

because at long circumferential surface crack lengths, part of the surface crack is below the neutral axis of the pipe in bending. The neutral axis for a surface crack with depth to thickness ratios of 0.4 to 0.6 is approximately at $2c/\pi D = 0.5$ (see Figure 14). Hence, the indicated limiting value occurs at approximately a crack length of $c/\pi D$. This is in good agreement with all but one of the data points which would be conservative by 9 percent. The zero crack length value is 0.8 which equals the difference due to ovalization in the through-wall circumferential crack relation (i.e., Equation 3).

Variable Depth Internal Circumferential Surface Crack on a 4-Inch (101.6-mm) Diameter Pipe

In Reference (2), a variable depth internal circumferential surface crack experiment, 11IRS, was conducted on a 4-inch (101.6-mm) diameter pipe, see Table 2. The maximum depth was 60 percent of the thickness and the length was 50 percent of the circumference. The objective of the experiment was to assess the effect of variable surface crack shape, specifically, whether the failure stresses are governed by the cross-sectional area of the flaw, or by the depth of the flaw. This flaw geometry was designed such that the average depth of the flaw was 40 percent of the thickness.

The result of the experiment showed that crack initiation was 96.7 percent of the maximum load. This is consistent with the other 4-inch (101.6-mm) diameter pipe fracture data. The failure stress of this flaw was in close agreement with the experimental data from the 60-percent deep constant depth surface cracked pipes. Hence, the failure stress was governed by the maximum depth of the surface cracks, not the average depth.

Behavior of a Circumferential Surface Cracked Large Diameter Pipe

In Reference (2), one experiment was conducted on 16-inch (406.4-mm) Schedule 100 Type 304 stainless steel pipe to evaluate the effect of larger diameter and thicker pipe, see Table 2. The pipe had a constant

depth internal circumferential surface crack with a depth of 66 percent of the thickness and a circumferential length of 47.5 percent of the circumference. The pipe was tested in four-point bending at 70 F (21 C). The details of the experiment are given in Reference (2).

One of the significant points observed during the experiment was that the crack initiated at 76.5 percent of the maximum bending moment. This is a significantly lower percent of the maximum load than in any other experiment.

The nominal bending moment at crack initiation was 7,987,000 in-lb (903 kN-m), which corresponded to an outer fiber bending stress of 43.1 ksi (297.2 MPa). This was 94 percent of the yield strength. The bending moment at the maximum load was 10,441,000 in-lb (1,180 kN-m) which corresponds to a nominal outer fiber bending stress of 56.3 ksi (388 MPa). This stress was 1.23 times the yield strength. The depth of the surface crack at the center was 85 percent of the thickness at the maximum moment.

The calculated bending moment was 11,956,000 in-lb (1,350 kN-m), using Equation (6) with σ_f* = 79.7 ksi (549 MPa), and with the initial flaw size. This was 50 percent greater than the experimental moment at crack initiation. With the initial flaw depth, the calculated moment is 14.5 percent greater than the maximum moment from the experiment. If the actual flaw depth at the maximum moment is used, then the predicted maximum moment is 8,112,000 in-lb (917 kN-m) which is conservative.

Figure 17 shows the ratio of the experimental bending moments to the net-section collapse calculated bending moment versus the surface crack depth. If no crack growth is assumed for the calculated moment, then the moment at crack initiation and the maximum moment are in the nonconservative area. The similar 4-inch (101.6-mm) diameter surface flawed pipe experiments were conservative by 5 to 11 percent. This indicates a slightly greater deviation in the fracture behavior during this experiment compared to the smaller pipe experiments. However, if the actual crack depth (from the experimental measurements) is used for the calculated bending moment, the bending moment at crack initiation is in the nonconservative region. As

---

* $\sigma_f = 1.15\ (\sigma_y + \sigma_u)/2$.

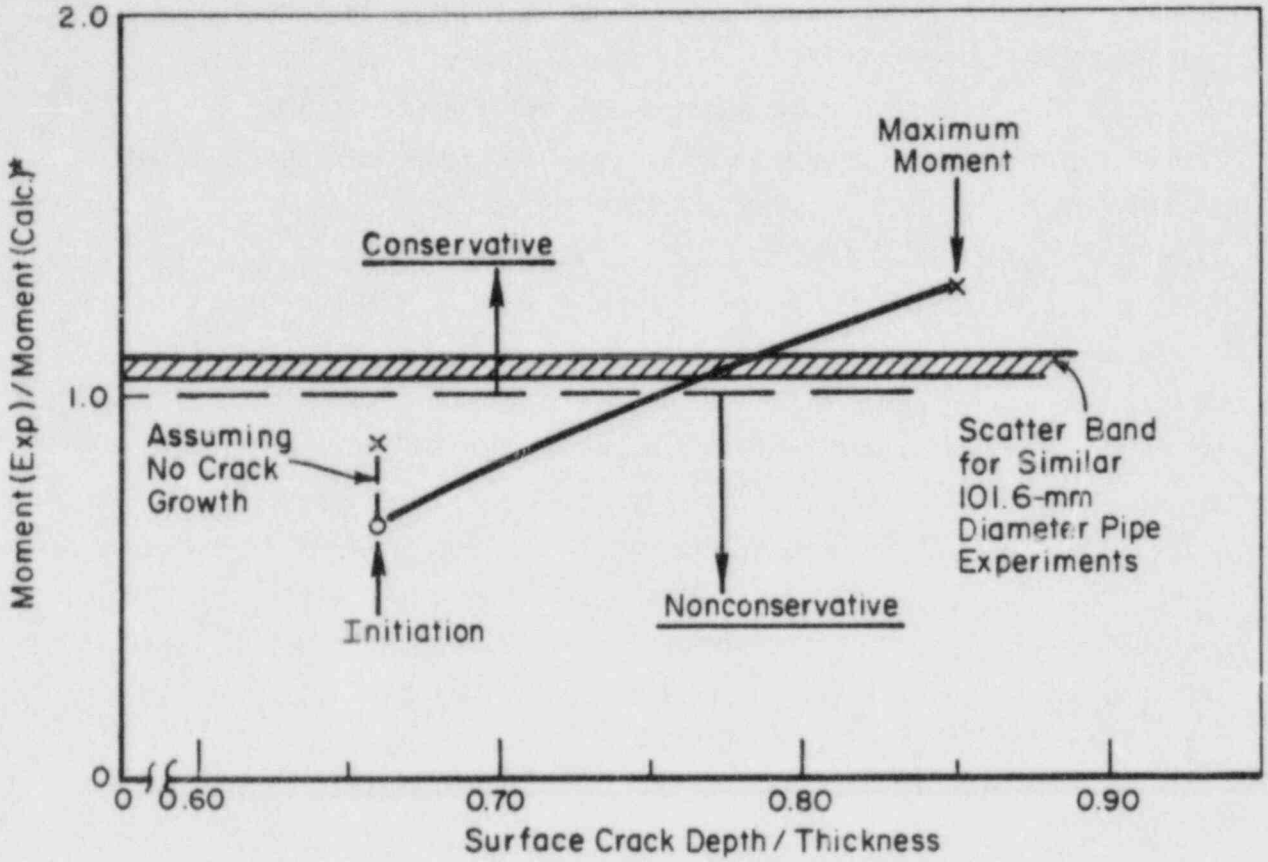

FIGURE 17. COMPARISON OF EXPERIMENTAL TO CALCULATED* BENDING MOMENTS FOR DATA FROM 16-INCH (406.4-MM) SCHEDULE 100 TYPE 304 STAINLESS STEEL PIPE EXPERIMENT

*USING EXPERIMENTAL CRACK GROWTH DATA AT THE CENTER OF THE SURFACE CRACK, EQ. 6, AND σ_f = 79.7 KSI (549 MPA)

the crack grows, the moment increases into the conservatively predicted region before the maximum moment is reached. This conservative prediction, however, can only be made if the crack growth can be predicted.

The results of this experiment as shown in Figure 17 indicate that net-section collapse conditions did not occur until there was significant crack growth. The violation of the net-section collapse condition may be due to the greater constraint of the surface flaw in the larger pipe, i.e., a lowering of the materials crack growth resistance. Further efforts on surface cracks in thick walled stainless steel pipe are needed to answer this concern.

EVALUATION OF SAFETY FACTORS IN IWB 3640

The safety factors for the IWB 3640 criteria were calculated both on stress level and on flaw depth. The safety factor on stress level, N_{Sm}, is defined in Equation (7).

$$N_{Sm} = (S_m)_{\text{net-section collapse}}/(S_m)_{\text{IWB 3640}}, \tag{7}$$

where d/t is constant.

The safety factor on flaw size, $N_{d/t}$, is defined in Equation (8).

$$N_{d/t} = (d/t)_{\text{net-section collapse}}/(d/t)_{\text{IWB 3640}}, \tag{8}$$

where S_m is constant.

A brief review of the IWB 3640 criteria[9] is first presented, followed by the safety factors on stress level, safety factors on flaw size, and then considerations of worst case conditions.

IWB 3640 End-of-Life Flaw Limits

The IWB 3640 end-of-life flaw limits for circumferentially crack pipe under normal conditions, Table I, and under faulted and emergency conditions, Table II, were based on allowable stress (P_m and P_b) where $P_m = S_m/2$ and the flow stress = 3 S_m. The allowable $P_m + P_b$ values in Tables I and II were then calculated using Equation (9).

$$P_b = \frac{2\sigma_f}{\pi}\left[2 \sin \beta - (d/t) \sin \alpha\right], \tag{9}$$

where

$$\beta = \left[\pi - \alpha(d/t) - (P_m/\sigma_f)\pi\right]/2$$

2α = total crack angle.

The safety factor on the allowable stress, $P_m + P_b$, at normal operating conditions was 2.77. This was the average of that for bending,

2.55, and axial tension, 3.00. For faulted conditions, the safety margin was said to be half of that at normal stresses, which would be 1.39.

Two additional modifications were made to these calculations. These are: (1) the maximum d/t is limited to 0.75, and (2) for flaws greater than 50 percent of the circumference, the d/t of a 50 percent long crack was used. Tables 3 and 4 of this text correspond to the IWB 3640 Tables I and II.

Safety Factors on Stress Level

The safety factors on stress levels first involved calculating the detailed net-section collapse relation in terms of S_m, and then making comparisons to the IWB 3640 S_m values for the same flaw sizes.

For Type 304 stainless steel pipe and centrifugally cast CF8m pipe, the code anticipated minimum yield and ultimate strengths* at 500 F were used. These values are given in Table 5. The S_m values were 0.9 Sy which were lower than Su/3. The flow stress was calculated using Equation (10).

$$\sigma_f = 1.15(\sigma_u + \sigma_y)/2 \quad . \tag{10}$$

Note that for these two materials that (σ_f/S_m) was very close to 2.8 S_m. Hence, 2.8 S_m was used as flow stress for the net-section collapse analysis. Figure 18 shows the circumferential crack relation in terms of S_m as well as stress normalized to flow stress. In this analysis the pipe ovalization was accounted for using the $\pi/4$ factor in Equation (4), hence the net-section stress is equal to the nominal bending stress used in the code. Note that for any stress level above 2.8 S_m, any size of flaw would cause the pipe to fail.

Another way of graphically illustrating the same relation is to plot d/t versus normalized circumferential crack length $(2c/\pi D)$ as a function of stress. This is shown in Figure 19 where stresses are given in terms of S_m. Note that for a stress of 2.8 S_m, the curves degenerate to the origin, i.e., no flaw sizes are safe.

A comparison of the net-section collapse analysis to the IWB 3640 Table I values for a stress of 1.0 S_m is shown in Figure 20. Note that the IWB

---

* 1983 ASME Boiler and Pressure Vessel Code, Section III, Division 1 Appendices, Tables I-2.2 and I-3.2.

TABLE 3. (IWB3640 TABLE 1) ALLOWABLE END-OF-EVALUATION PERIOD FLAW DEPTH[1]-TO-THICKNESS RATIO FOR CIRCUMFERENTIAL FLAWS, NORMAL OPERATING (INCLUDING UPSET AND TEST) CONDITIONS

$\frac{P_m + P_b}{S_m}$ [3]	Ratio of Flaw Length (ℓ_f) to Circumference[2]					
	0.0	0.1	0.2	0.3	0.4	0.5 or more
1.5	(4)	(4)	(4)	(4)	(4)	(4)
1.4	0.75	0.40	0.21	0.15	(4)	(4)
1.3	0.75	0.75	0.39	0.27	0.22	0.19
1.2	0.75	0.75	0.56	0.40	0.32	0.27
1.1	0.75	0.75	0.73	0.51	0.42	0.34
1.0	0.75	0.75	0.75	0.63	0.51	0.41
0.9	0.75	0.75	0.75	0.73	0.59	0.47
0.8	0.75	0.75	0.75	0.75	0.68	0.53
0.7	0.75	0.75	0.75	0.75	0.75	0.58
≤0.6	0.75	0.75	0.75	0.75	0.75	0.63

Notes:

(1) Flaw depth = a_n for a surface flaw
= $2a_n$ for a subsurface flaw
t = nominal thickness
linear interpolation is permisible

(2) Circumference based on nominal pipe diameter

(3) P_m = Primary Membrane Stress
P_b = Primary Bending Stress
S_m = ASME Code Allowable Design Intensity

(4) IWB-3514.3 allowable flaw standards shall be used

TABLE 4. (IWB3640 TABLE II) ALLOWABLE END-OF-EVALUATION PERIOD FLAW DEPTH(1)-TO-THICKNESS RATIO FOR CIRCUMFERENTIAL FLAWS - EMERGENCY AND FAULTED CONDITIONS

$\frac{P_m + P_b}{S_m}$ (3)	Ratio of Length (ℓ_f) to Circumference(2)					
	0.0	0.1	0.2	0.3	0.4	0.5 or more
3.0	(4)	(4)	(4)	(4)	(4)	(4)
2.8	0.75	0.40	0.21	0.15	(4)	(4)
2.6	0.75	0.75	0.39	0.27	0.22	0.19
2.4	0.75	0.66	0.56	0.40	0.32	0.27
2.2	0.75	0.73	0.73	0.51	0.42	0.34
2.0	0.75	0.75	0.75	0.63	0.51	0.41
1.8	0.75	0.75	0.75	0.73	0.59	0.47
1.6	0.75	0.75	0.75	0.75	0.68	0.53
1.4	0.75	0.75	0.75	0.75	0.75	0.58
<1.2	0.75	0.75	0.75	0.75	0.75	0.63

Notes:

(1) Flaw depth = a_n for a surface flaw
= $2a_n$ for a subsurface flaw
t = nominal thickness
linear interpolation is permisible

(2) Circumference based on nominal pipe diameter

(3) P_m = Primary Membrane Stress
P_b = Primary Bending Stress
S_m = ASME Code Allowable Design Intensity

(4) IWB-3514.3 allowable flaw standards shall be used

TABLE 5. PIPE PROPERTIES AT 500 F FOR NET-SECTION COLLAPSE ANALYSIS

Material Properties	Material	
	Type 304 Stainless Steel Pipe	CF8m Stainless Steel Pipe
σ_y, ksi	20.9	19.9
σ_u, ksi	71.2	67.0
Sm, ksi	18.81	17.91
σ_f, ksi	52.95	49.97
σ_f/Sm	2.82	2.79

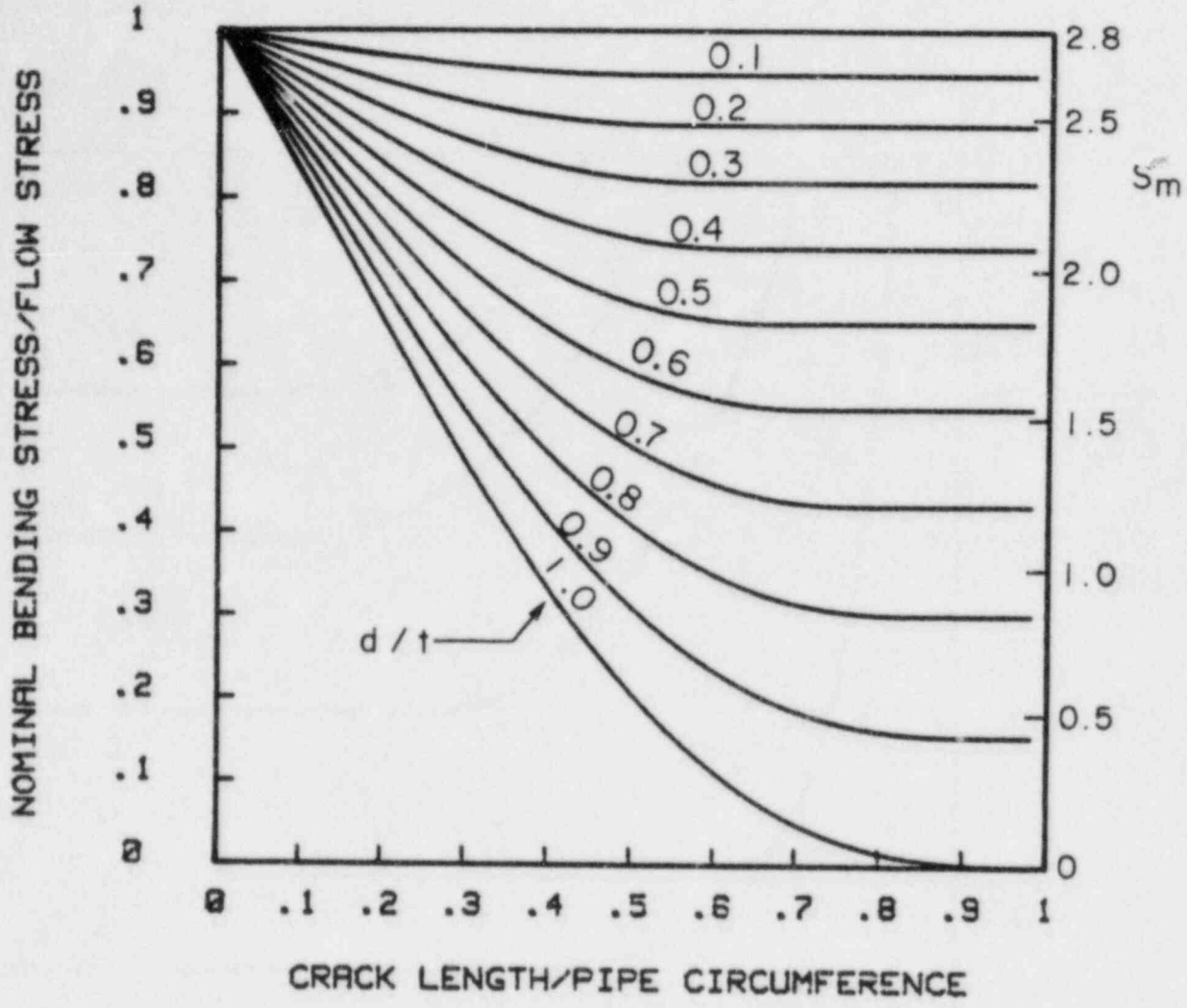

FIGURE 18. NET-SECTION COLLAPSE ANALYSIS FOR CIRCUMFERENTIALLY CRACKED PIPE IN PURE BENDING IN TERMS OF S_m WHERE 2.8 S_m = FLOW STRESS (OVALIZATION CORRECTION OF $\pi/4$ USED)

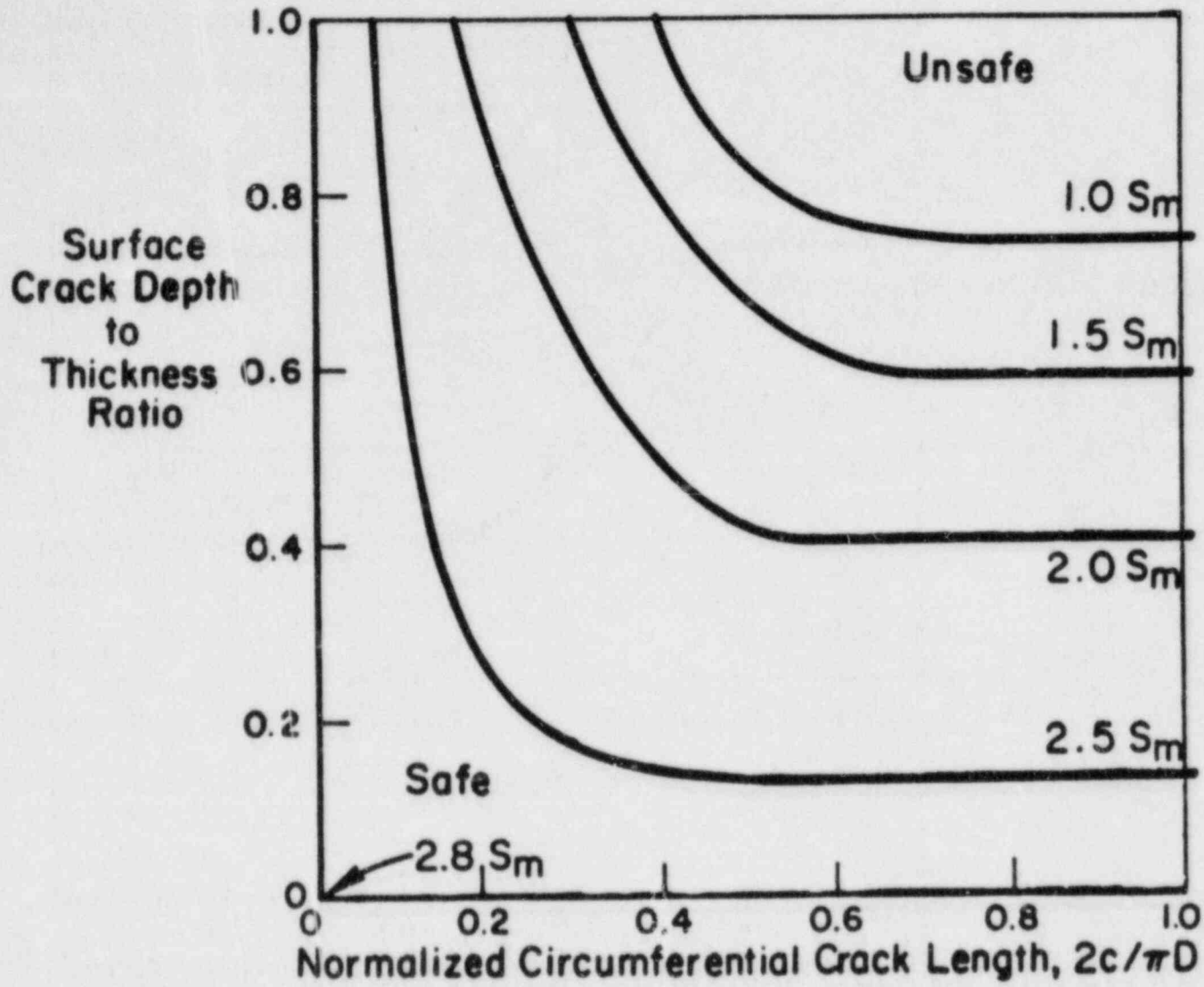

FIGURE 19. FAILURE ASSESSMENT DIAGRAM FOR SAME RELATION IN FIGURE 18

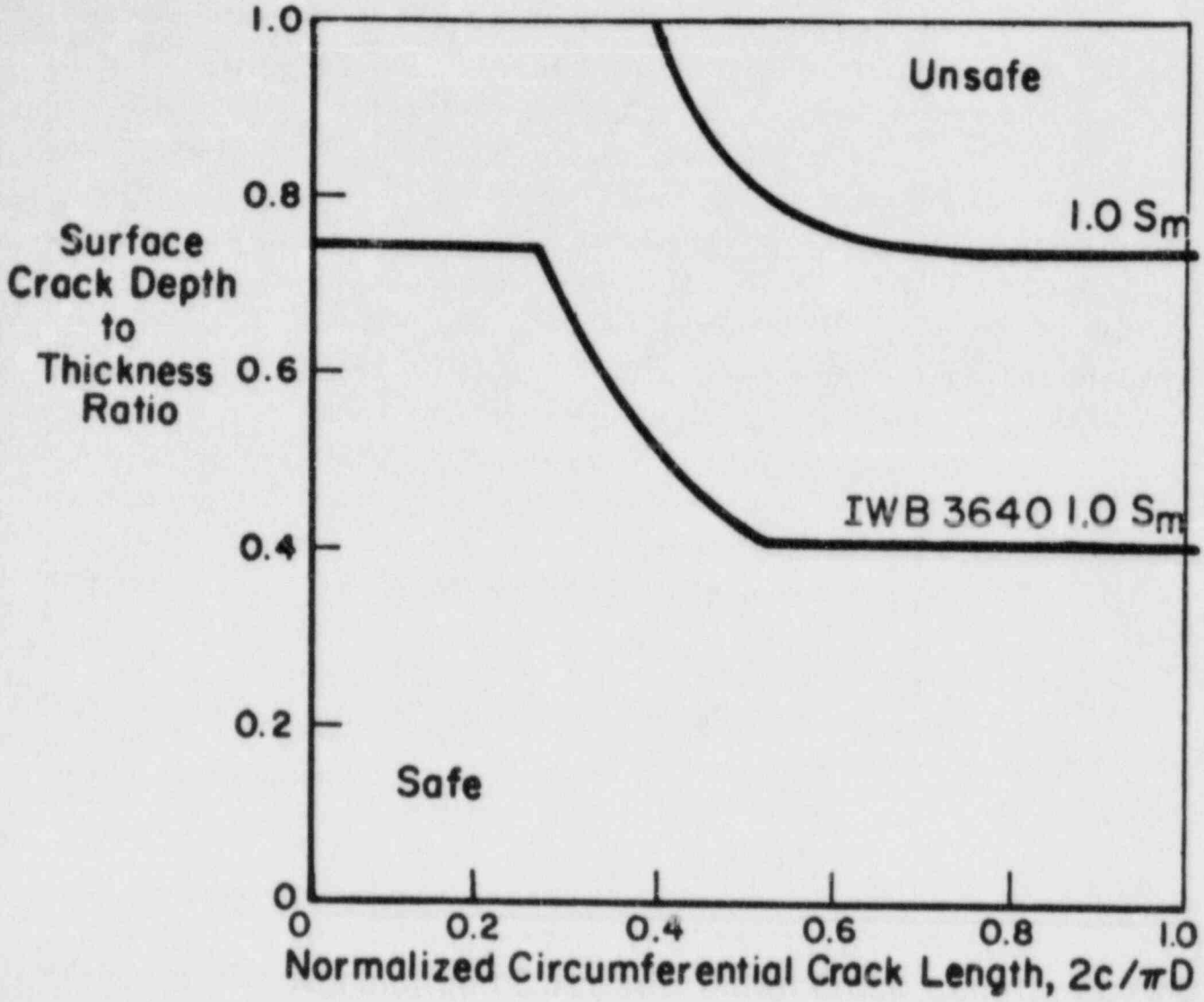

FIGURE 20. COMPARISON OF NET-SECTION COLLAPSE ANALYSIS TO VALUES IN IWB 3640 TABLE 1 FOR STRESS OF 1.0 S_m

3640 values have a maximum depth of 75 percent of the thickness, and the d/t ratio is constant for crack lengths greater than half the pipe circumference.

The safety factors on stress were calculated as a function of circumferential crack length for a stress level of 1.0 S_m in IWB 3640 Table I, see Figure 21. This safety factor was very close to 2.0 for crack lengths greater than 30 percent of the pipe circumference. For shorter crack lengths, the safety factor increased due to the 0.75 d/t limit in the IWB 3640 tables. Since there was so little difference in the safety factor for long crack lengths, the subsequent safety factors calculated were only for circumferential surface cracks completely around the circumference.

The safety factors on stress levels are shown in Figure 22. These are all for 360 degree circumferential crack lengths. The normal operation (including test and upset) conditions correspond to IWB 3640 Table I, and the emergency and faulted condition curve corresponds to Table II. The first observation is that the safety factor is not constant with stress. At normal conditions the safety factor varied from 2.6 to 1.9 as the stress increased from 0.6 to 1.4 S_m. These are slightly lower than the 2.77 values cited for IWB 3640. For stress levels below 0.6 S_m, the safety factors would continue to increase.

At emergency and faulted conditions the safety factors are much lower, and at stresses above 2.8 S_m, there is no safety factor. At a stress of 2.0 S_m the safety factor is 1.0.

Safety Factors on Flaw Size

The safety factors on flaw size were calculated using the values in Table 5 and the relationship shown in Figure 18. Here the procedure involved selecting a stress level and flaw geometry from IWB 3640 Tables I and II. Then the d/t can be determined from Figure 18 for the same stress level. The safety factor is the (d/t) from Figure 18 to the (d/t) from the IWB 3640 tables.

The initial calculations examined the change in the safety factor on the flaw depth to thickness ratio as a function of crack length. This was done for a stress level of 1.0 S_m, and is shown in Figure 23. Here leak-

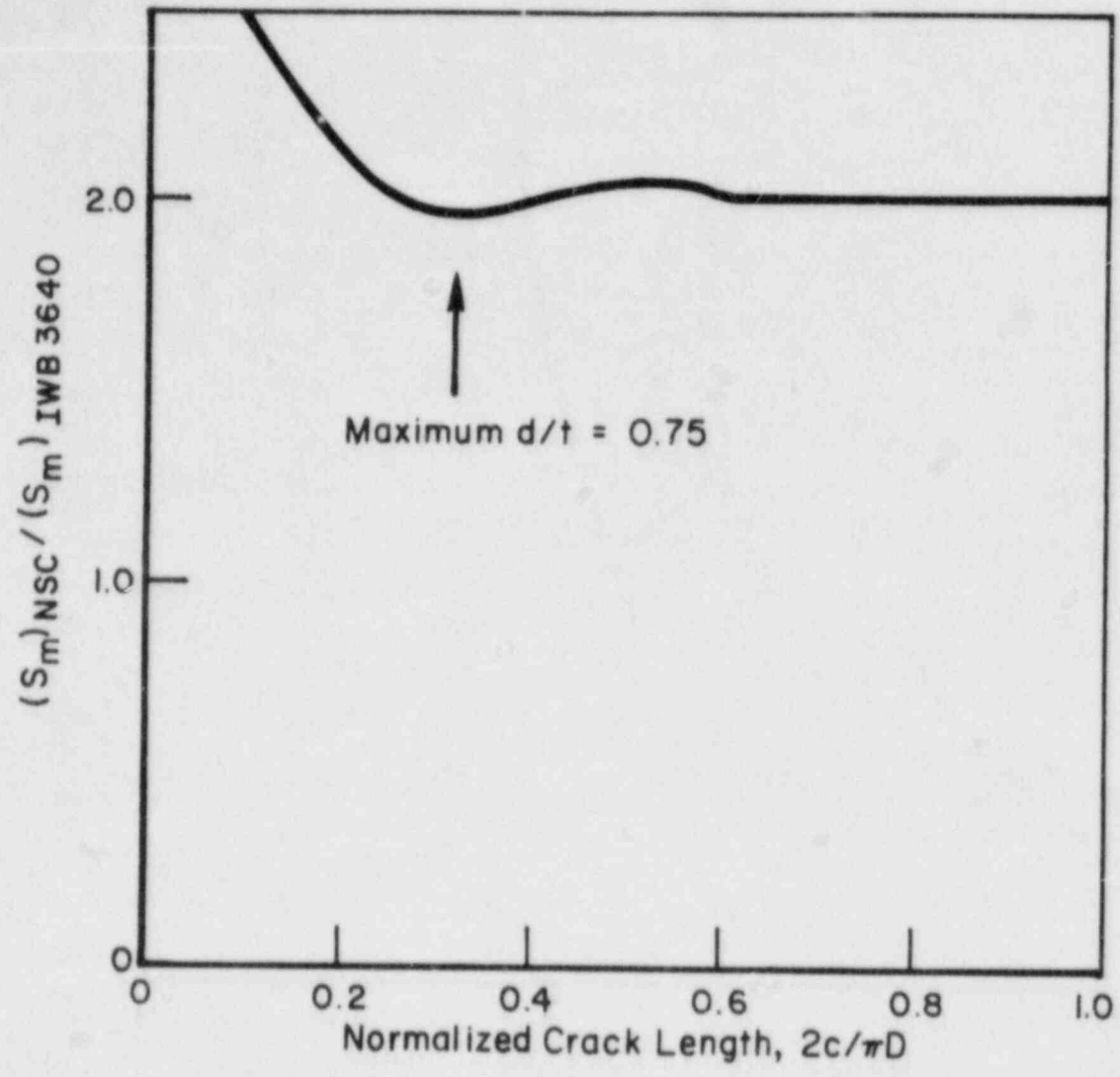

FIGURE 21. SAFETY FACTOR ON STRESS LEVEL FOR FLAW SIZES CORRESPONDING TO A STRESS OF 1.0 Sm IN IWB 3640 TABLE I

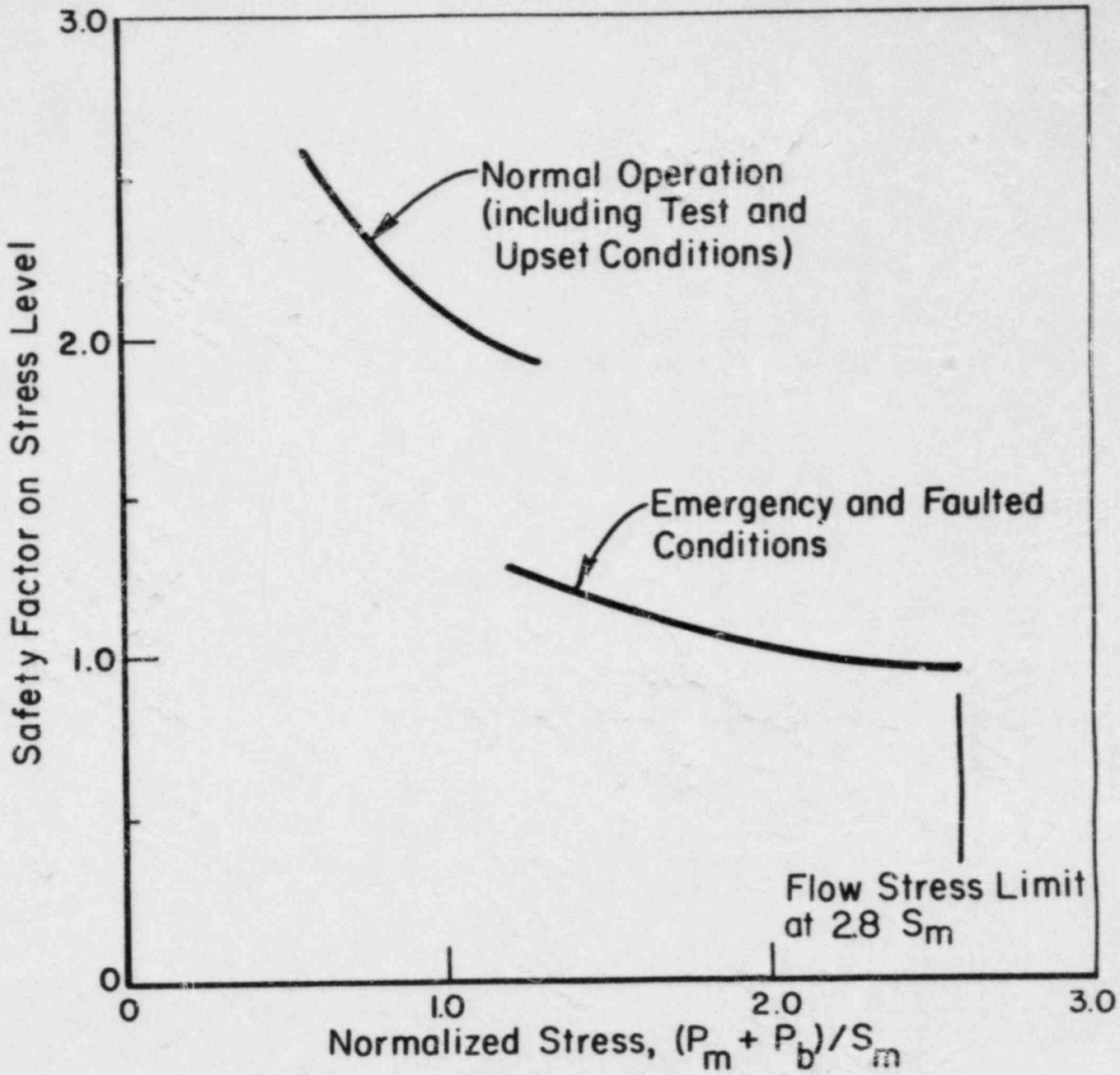

FIGURE 22. SAFETY FACTORS ON STRESS LEVEL FOR IWB3640 TABLES 1 AND 2 FOR CIRCUMFERENTIALLY CRACKED PIPE IN PURE BENDING

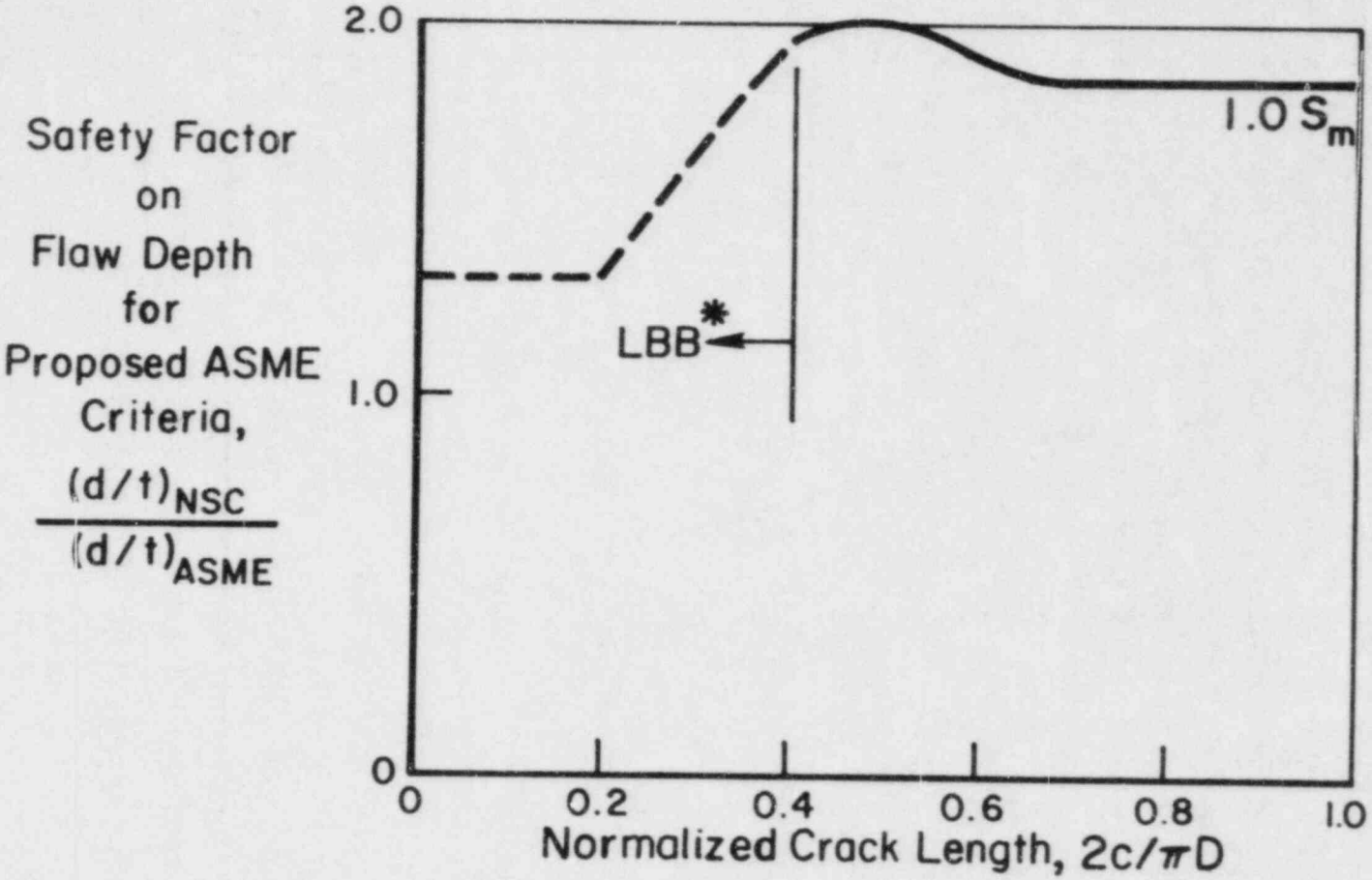

FIGURE 23. SAFETY FACTOR ON FLOW DEPTH/THICKNESS AS A FUNCTION OF CRACK LENGTH FOR AN APPLIED STRESS OF $1.0S_M$

*LBB is leak-before-break predicted on basis of circumferential crack length.

before-break is predicted on a basis of circumferential crack length, where the critical through-wall crack length at a stress of 1.0 S_m is equal to 0.38 times the circumference, see 1.0 S_m curve in Figure 19. Secondly, the minimum safety factor is for very long cracks, but there is very little difference from $0.4 < 2c/\pi D < 1.0$. Subsequent calculations therefore, only considered circumferential cracks completely around the circumference.

The safety factors on flaw depth-to-thickness ratio are shown in Figure 24 for normal conditions and emergency conditions. For normal conditions the safety factor on d/t increases from 1.3 to 5 as stress increased from 0.6 to 1.4 S_m. These are quite good safety factors, especially for stress from 1.0 to 1.4 S_m.

At emergency and faulted conditions, however, the safety factors are 1.1 to 0 as stress increases from 1.2 to 2.8 S_m. The safety factor is approximately 1.0 at a stress of 2.0 S_m. At 2.8 S_m or higher stresses, the stresses are equal to or larger than flow stress, so no flaws can be tolerated, hence the zero safety factor. As with the safety factors on stress level, the safety factors on d/t at emergency and faulted conditions are lower than desired.

Considerations of Worst Case Conditions

Two effects could cause the above calculated safety factors to decrease. First, limited data on thick-walled circumferential surface cracked Type 304 stainless steel pipe showed the actual failure stresses were 14 percent below the net-section collapse stress. As noted in a prior section in this paper, this effect is believed to be due to constraint effects from the surface crack on reducing the toughness. This would affect the safety factors at normal as well as at emergency conditions.

Secondly, limited existing data has shown that sustained loads can reduce the maximum load in pipe fracture experiments, as well as in laboratory specimens. The limited supporting technical data are discussed below.

Experimental Data on Sustained Loads

Sustained load effects have been evaluated for axially crack pipe for the gas and oil industries at Battelle[10]. Flaw growth during hydro-

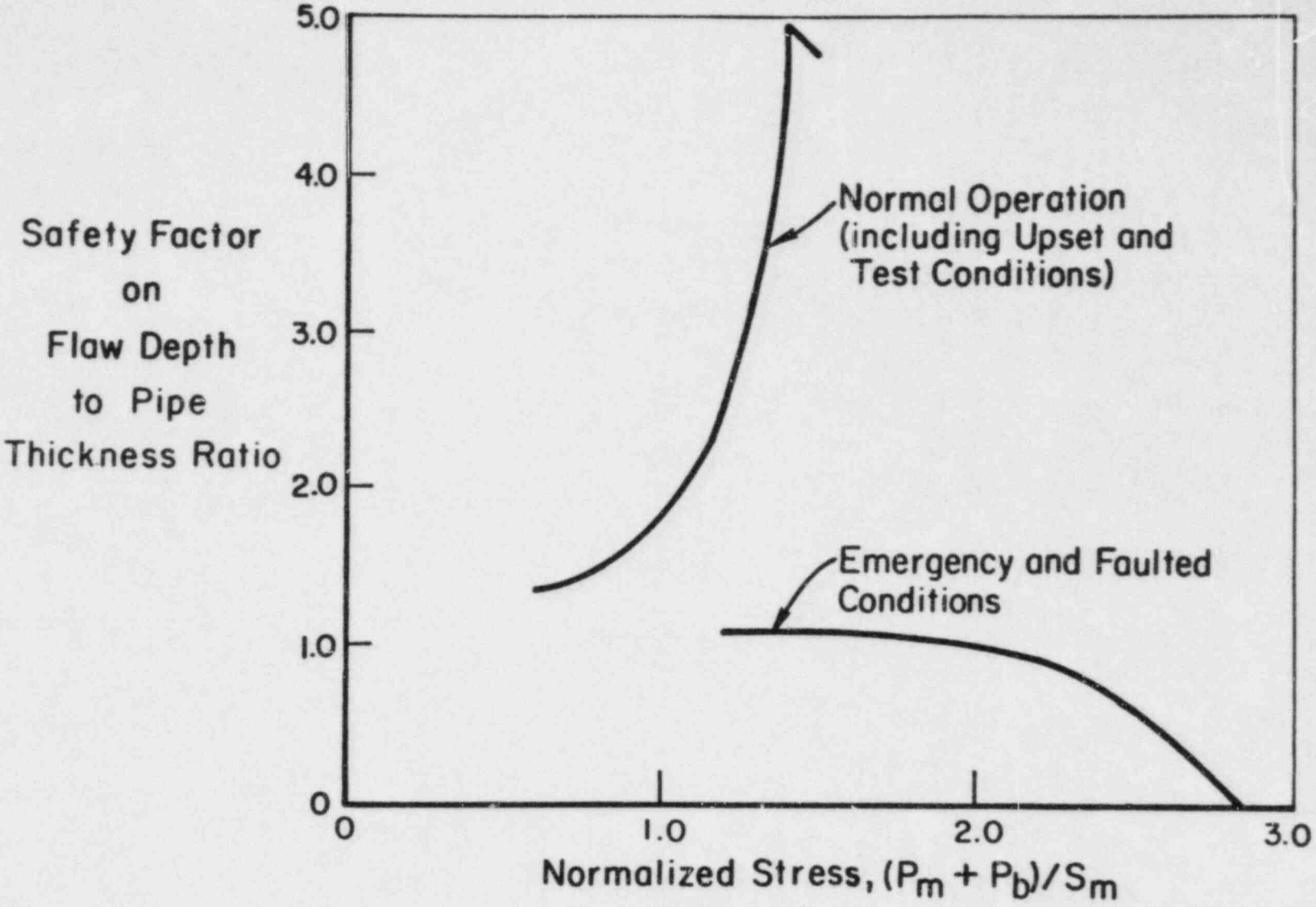

FIGURE 24. SAFETY FACTORS ON IWB3640 FLOW DEPTH TO PIPE THICKNESS RATIO FOR FULL CIRCUMFERENTIAL SURFACE CRACKS, AND PIPES IN PURE BENDING

static testing was the practical concern here[11]. In one series of experiments[10] 36-inch diameter by 0.390-inch API 5LX60 pipe with axial cracks was held at pressure levels below the failure pressure under monotonic pressurization to failure. The reduction of the failure pressure with time reached a low plateau, see Figure 25. This lower plateau varied from 7.9 to 9.5 percent of the monotonically increasing failure pressure. These experiments, however, were on carbon steel pipe at ambient temperature. Additional studies by Tsuru and Garwood[12] examined time dependent ductile tearing failure in three-point-bend-bar carbon steel specimens at room temperature. These results showed that the maximum load decreased by 15 percent. Finally, there are unpublished studies at JAERI which have evaluated the effect of slow strain rates and water at 98 C on the J_R curve of Type 304 stainless steel. At low strain rates J_{Ic} was found to decrease by a factor of ten, and dJ/da decreased by a factor of three. At 550 F local crack tip creep fracture interaction may be significant; however, no studies have been conducted to date. Consequently, a potential reduction in maximum loads of 15 percent below the net-section collapse stress was used in the following calculations. Only the normal operating condition values would be effected by sustained load effects.

Worst Case Safety Factors

The effect of a 14 percent decrease on stress due to thick-wall pipe constraint, and a 15 percent decrease in stresses due to constraint on the calculated safety factors are shown in Figures 26 and 27. For the safety factors on stress in Figure 26, the worst case condition at normal operating conditions is when both sustained load and thick-wall pipe constraint is assumed. Here the safety factors vary from 1.8 to 1.4 as the stress changes from 0.6 to 1.4 S_m. Table 6 summarizes the range of safety factors on stress levels as well as on flaw depth.

At emergency and faulted conditions, the thick-walled pipe correction decreased the safety factor on stress to a range of 1.1 to 0.8 for stress levels from 1.2 to 2.8 S_m. The safety factors for stress levels above 2.8 S_m

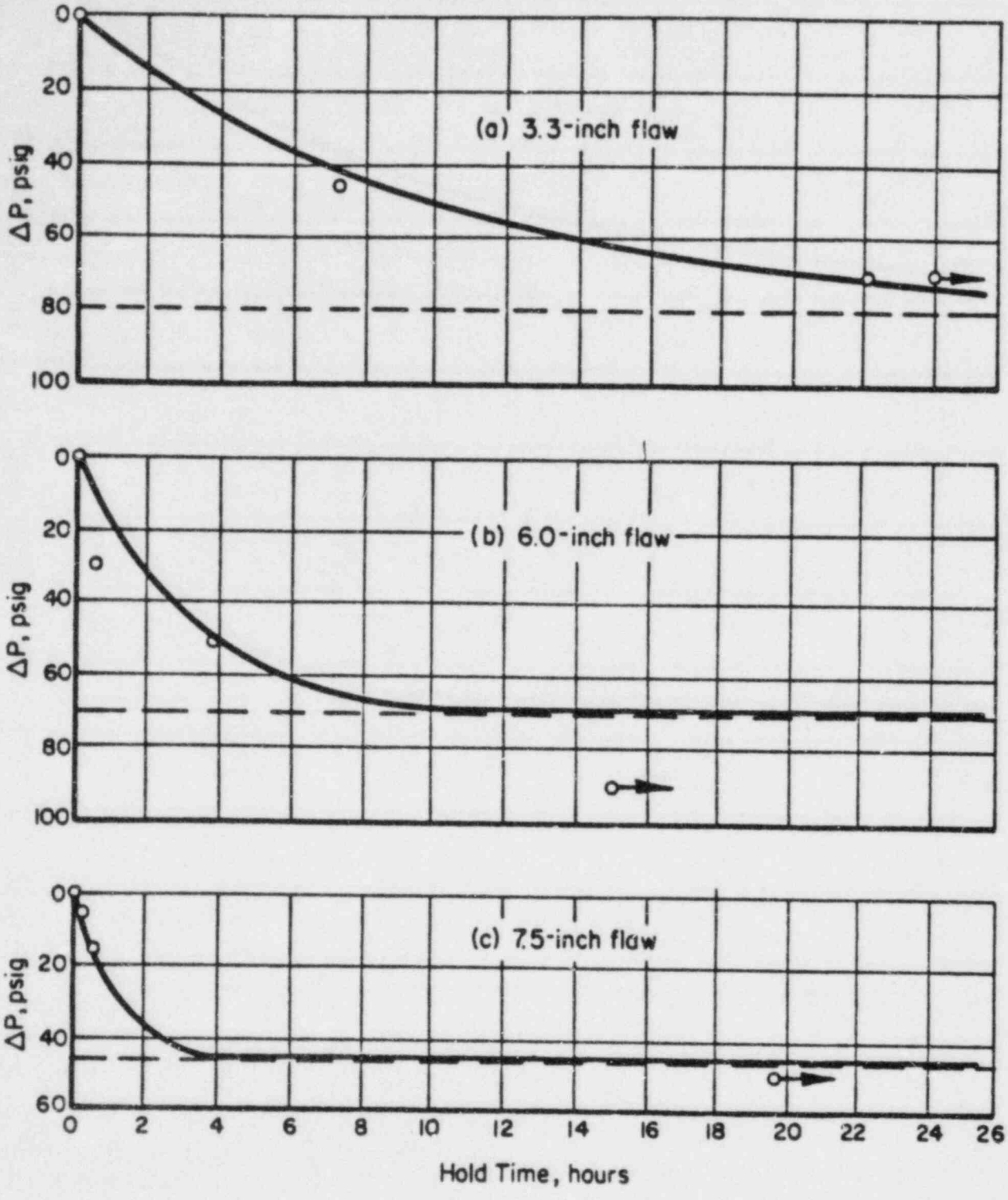

FIGURE 25. EFFECT OF SUSTAINED LOAD ON FAILURE PRESSURE OF AXIAL SURFACE CRACKS IN 30-INCH DIAMETER BY 0.390-INCH THICK API 5LX60 AT ROOM TEMPERATURE(10)

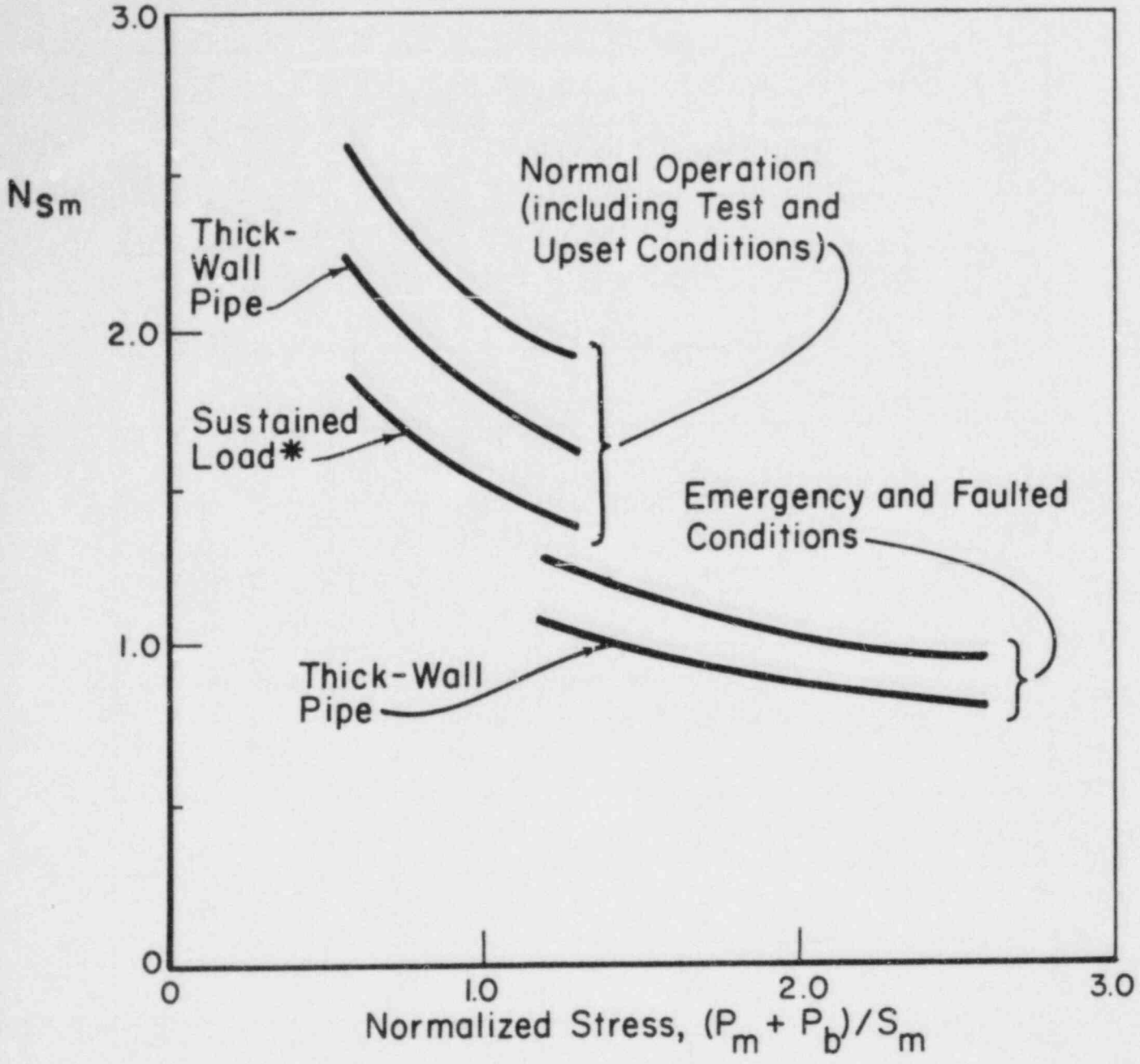

FIGURE 26. SAFETY FACTORS ON STRESS LEVEL FOR WORST CASE CONDITIONS

* SUSTAINED LOAD CURVE IS FOR BOTH THICK-WALLED PIPE AND SUSTAINED LOAD CORRECTIONS

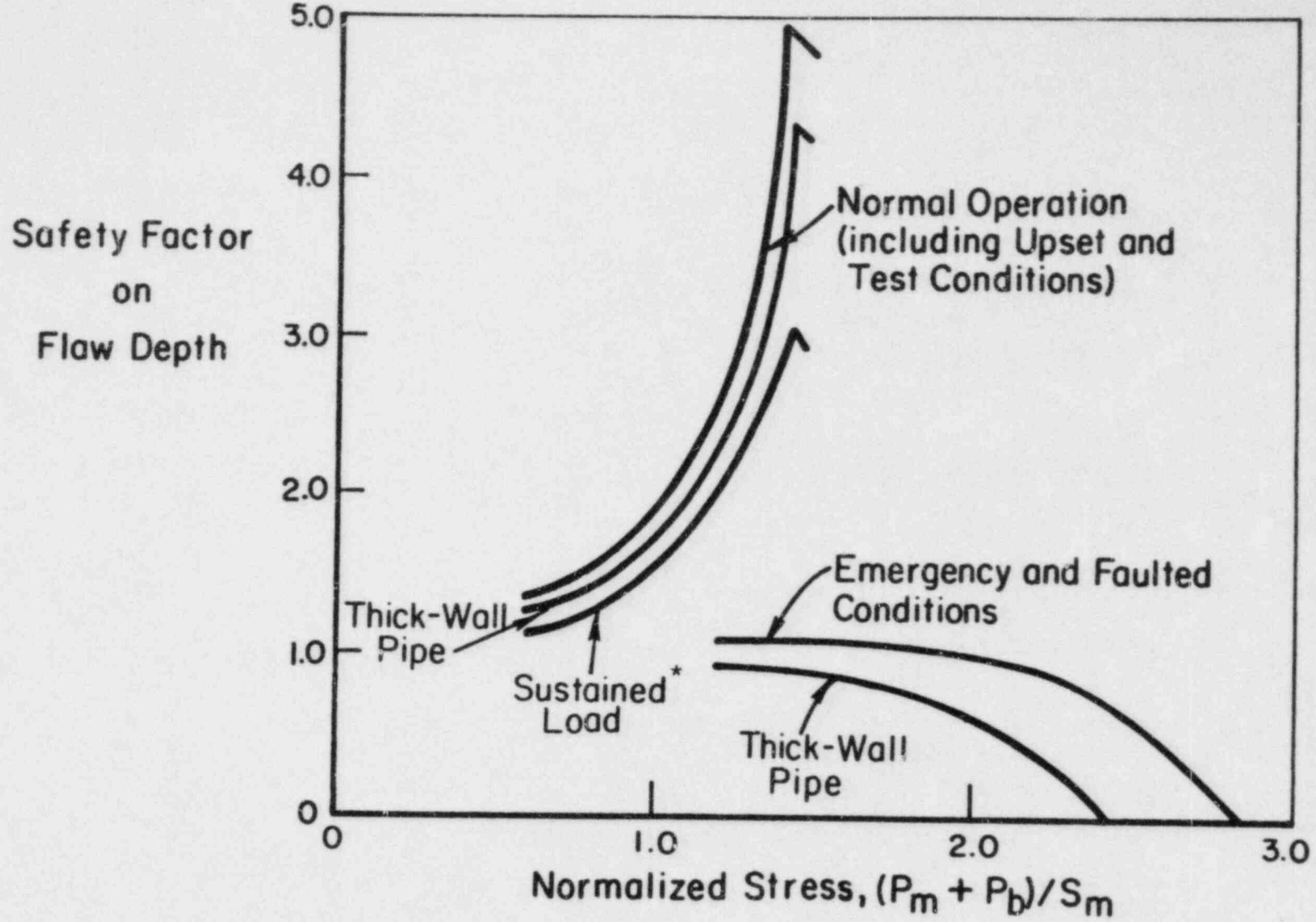

FIGURE 27. SAFETY FACTORS ON FLAW DEPTH FOR WORST CASE CONDITIONS

* SUSTAINED LOAD CURVE IS FOR BOTH THICK-WALLED PIPE AND SUSTAINED LOAD CORRECTIONS

TABLE 6. SUMMARY OF CALCULATED SAFETY FACTORS

CRITERIA	SAFETY FACTOR			
	NORMAL OPER.		EMERGENCY	
	N(Sm)	N(d/t)	N(Sm)	N(d/t)
IWB 3640	2.78	--	1.39	--
Net Section Collapse	1.9-2.6	1.3-4.9	0-1.3	0-1.1
Thick Wall Correction	1.6-2.2	1.2-4.2	0-1.1	0-0.9
Sustained Load	1.3-1.8	1.1-3.0	--	--

are zero since these stresses are above flow stress and cracks of any size would cause failure.

Safety factors on flaw depth to pipe thickness ratio are shown in Figure 27. At normal operating conditions, combined thick pipe and sustained load correction, the worst case safety factors vary from 1.1 to 3.0. At emergency and faulted conditions, the worst case safety factors vary from 0.9 to 0. The safety factor of zero applied for stress levels above 2.4 S_m.

DISCUSSION

The safety factors at emergency and faulted conditions appear to be of greatest concern; however, there are several factors which make the real life situation better than shown in the calculations previously presented. These points are discussed below.

(1) Stresses seldom get above 2.4 S_m, and in fact, the code limits the maximum stress to the lower of either 3.0 S_m or 2.0 Sy. A value of 2.0 Sy for the austenitic piping of concern in IWB 3640 is equal to a stress of approximately 2.22 S_m.

(2) The stresses in emergency and faulted conditions are short in duration, so that unloading would occur during the fracture event. This would promote leak-before-break behavior for ductile materials. This is a significant effect. In a past program conducted for EPRI at Battelle,[2] the safety factor for a single transient dynamic load was a factor of two over the static analysis for crack initiation.

(3) Dynamic loads are perhaps too conservatively calculated since plasticity is not accounted for. This effect is even larger when plasticity at the crack is considered in the dynamic calculations; however, such calculations are difficult to make.

(4) Dynamic loading increases the material's flow stress and toughness; however, from existing experimental data, these beneficial effects on the failure loads are relatively small.

(5) Actual pipe thickness and strengths will generally be greater than code minimum values.

However, there are also several points that may make the calculated safety factors appear non-conservative. These are:

(1) Sustained load effects at 550 F may be more significant than the 15 percent load decrease used. The higher temperature

would increase the crack tip creep interaction with ductile tearing.

(2) Thick pipe with IGSCC surface cracks extending into the weld metal may have lower failure stresses than the 14 percent reduction used.

(3) Cracks in the HAZ of centrifugally cast stainless steel pipe may be in a region of thermal degradation of the material as well as inducing constraint in heavy-wall pipe. Thermal aging in base metal of CF8m pipe have received little attention, and the degradation from combined welding and long term thermal aging from service temperatures, to our knowledge, has not been investigated to date.

A final point of issue is whether safety factors on flaw size should be incorporated into a code allowable defect tolerance criteria. On one hand it is extremely important to ensure that the NDE technique accurately sizes the flaw dimensions of concern. Techniques that are not sufficiently accurate on defect sizing, obviously are of concern especially if the accuracy of the technique is not accounted for in the code analysis of the defect acceptance. In accounting for the accuracy of the NDE technique, the potential error needs to be known in terms of either depth-to-thickness ratio, or if the accuracy depends on absolute flaw depth dimensions. For instance, for the case of circumferentially cracked austenitic pipes in bending, the safety factor on flaw depth can be easily determined using 360 degree crack length. Figure 28 shows the 360 degree crack depth-to-thickness ratio versus normalized stress, as a function of the safety factor on flaw depth ($N_{d/t}$). The lower level of d/t = 0.125 corresponds to IWB 3514.3 limits.

If the accuracy of the NDE technique was a function of the pipe thickness, then a different relation on allowable d/t would exist. Figure 29 shows such a relation, based on the assumption that the NDE accuracy is 0.1 times the pipe thickness. Here the maximum allowable stress at the IWB 3514.3 limit corresponds to that using a safety factor of 1.9 on depth-to-thickness ratio.

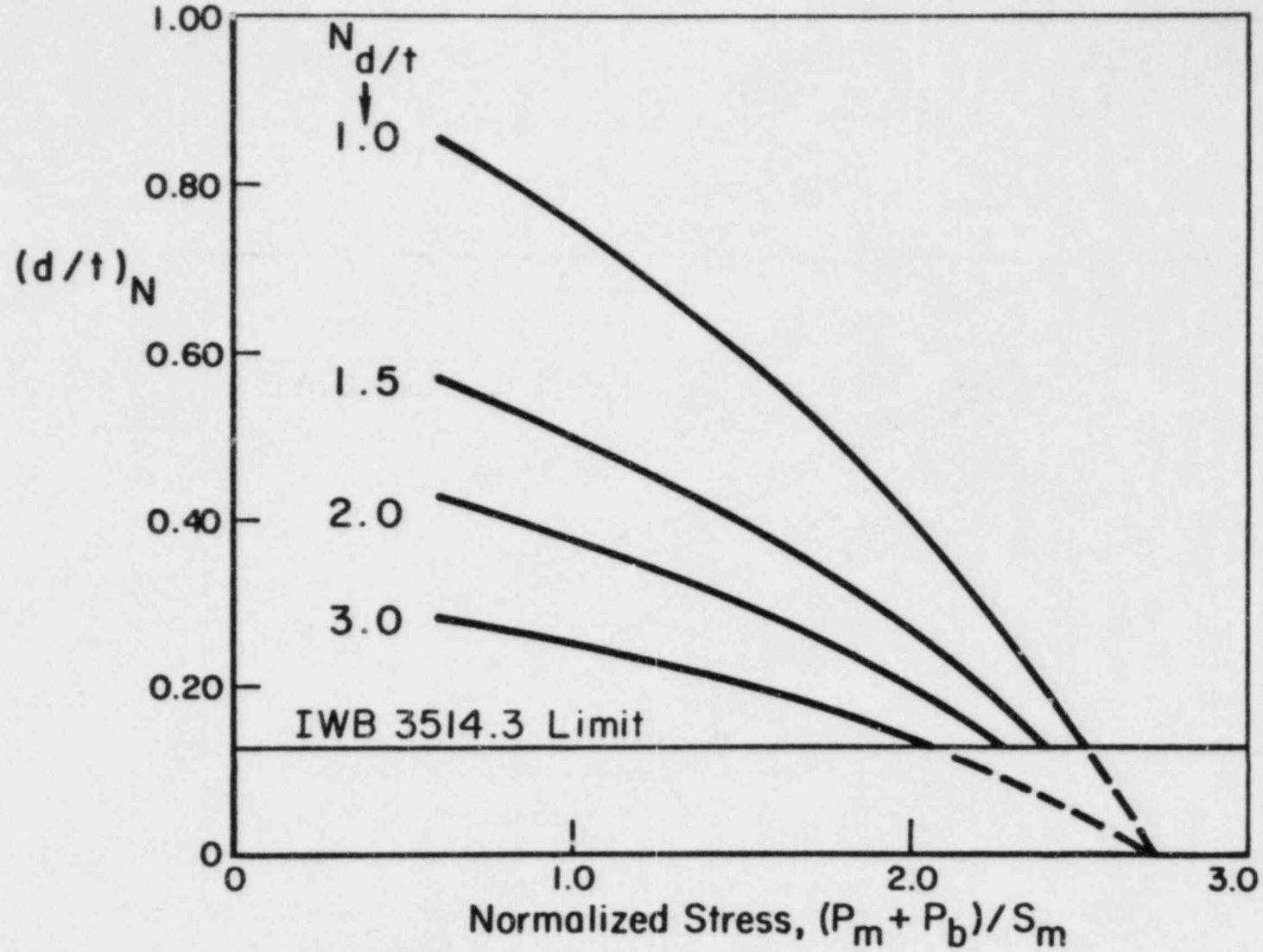

FIGURE 28. VARIATION IN FLAW DEPTH TO PIPE THICKNESS RATIO VERSUS APPLIED STRESS, AND A FUNCTION OF SAFETY FACTOR ON FLAW DEPTH-TO-THICKNESS RATIO

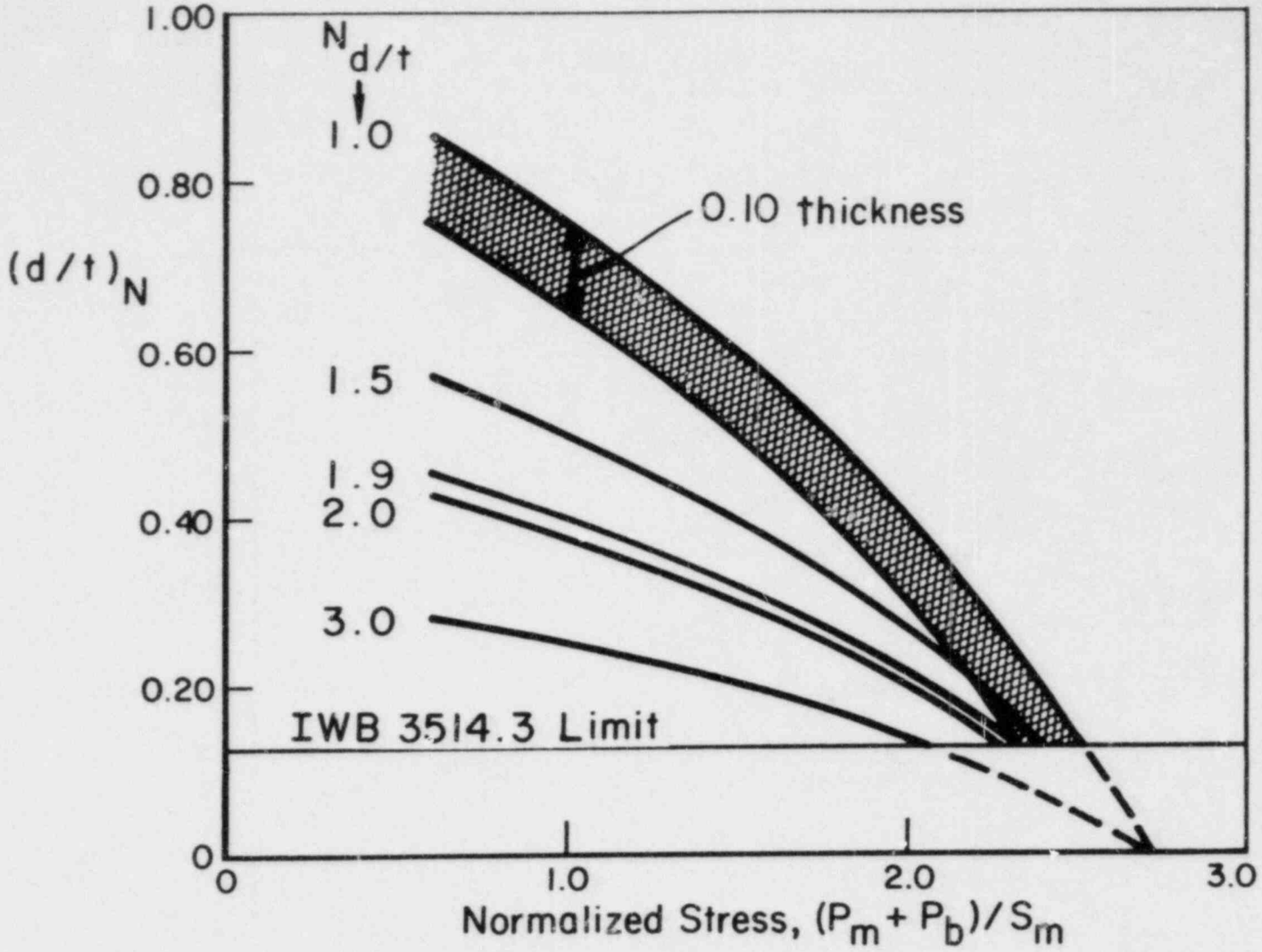

FIGURE 29. EFFECT OF NDE UNCERTAINITY ON ALLOWABLE FLAW SIZE BEING A FUNCTION OF PIPE THICKNESS RATHER THAN FLAW DEPTH-TO-THICKNESS RATIO

Arguements for not including safety factors on flaw depth-to-thickness are that the accuracy of the technique varies with different techniques and is material sensitive. Furthermore, future improvements in NDE techniques could significantly improve upon the accuracy of current techniques, requiring continuous updating of the code allowable flaw dimensions. Hence, engineering prudence would suggest that safety factors on stress level would be appropriate for a code criteria as long as the accuracy of the NDE method is accounted in the flaw dimensions of the code analysis.

CONCLUSIONS

The safety factors on the end-of-life flaw sizes in the IWB 3640 criteria for continued temporary operation was reviewed in detail. It was found that the safety factors on stress were not constant and varied with applied stress when pipe ovalization is accounted for. At normal conditions, the safety factors, although less than desired, were still close to or above 2.0.

The safety factors on stress for emergency and faulted conditions were significantly below the 1.39 value cited for IWB 3640 due to ovalization and the method of calculating the flow stress. The corresponding safety factors on flaw depth to pipe thickness ratio, hence, were also low at emergency and faulted conditions. These calculations imply that the values in IWB 3640 Table II should be reconsidered. Although the calculated safety factors were low, in reality the transient dynamic loading conditions would tend to promote leak-before-break behavior, hence the real safety factors will be much larger.

The use of safety factors on flaw depth for code application is complicated by the variability of different techniques used, sensitivity of the methods for different materials, and improvements of future NDE methods. Engineering prudence should be used in allowing for the accuracy of the NDE method used, and the subsequent flaw size used in engineering assessments.

REFERENCES

(1) Kanninen, M. F., Broek, D., Marschall, C. W., Rybicki, E. F., Sampath, S. G., Simonen, F. A., Wilkowski, G. M., "Mechanical Fracture Predictions for Sensitized Stainless Steel Piping with Circumferential Cracks", Final Report, EPRI NP-192, Sept. 1976.

(2) Kanninen, M. F., Zahoor, A., Wilkowski, G., Abou-Sayed, I., Marschall, C. Broek, D., Sampath, S., Rhee, H., and Ahmad, J., "Instability Predictions for Circumferentially Cracked Type 304 Stainless Steel Pipes Under Dynamic Loading", Final Report, EPRI NP-2347, Volumes 1 and 2, April, 1982.

(3) Smith, E., "The Net-Section Stress Approach for Predicting Pipe Failure"; an unpublished paper, Manchester University, United Kingdom.

(4) Shih, C. F., German, M. D., and Kumar, V., "An Engineering Approach for Examining Crack Growth and Stability in Flawed Structures", Int. J. Pres. Ves. and Piping, 9, 1981, pp 159-196.

(5) Smith, E., "Limitation of the Critical Stress Approach for Predicting the Onset of Crack Extension at a Crack Tip"; an unpublished paper, Manchester University, United Kingdom.

(6) Kumar, V., German, M. D., and Shih, C. F., "An Engineering Approach for Elastic Plastic Fracture Analysis", Topical Report, EPRI NP-1931, July 1981.

(7) Wilkowski, G. M., "Application of the Electric Potential Method for Measuring Crack Growth in Specimens, Flawed Pipes and Pressure Vessels", Presented at ASTM 14th National Symposium on Fracture Mechanics, June 30 - July 1, 1981.

(8) Wilkowski, G. M., and Eiber, R. J., "Evaluation of Tensile Failure of Girth Weld Repair Grooves in Pipe Subjected to Offshore Laying Stresses", Journal of Energy Resources Tech., 103, March 1981, pp 49-55.

(9) Ranganath, S. and Norris, D. M., "Evaluation Procedure and Acceptance Criteria for Flaws in Austenitic Steel Piping", (Technical Support Document for IWB 3640), Submitted to PVRC of WRC.

(10) Duffy, A. R., "Hydrostatic Testing", in 4th Symposium on Line Pipe Research, November, 1969, American Gas Association Catalogue Number L30075.

(11) Kiefner, J. F., et al, "A Study of the Causes of Failures That Have Survived a Prior Hydrostatic Test", 1981, American Gas Association Catalogue No. L51398.

(12) Tsuru, S. and Garwood, S. J., "Some Aspects of the Time Dependent Ductile Fracture of Line-Pipe Steels", ICM 3, Vol. 3, August, 1979, pp 519 to 528.

IMPLICIT SAFETY MARGINS IN THE ASME CODE ACCEPTANCE CRITERIA FOR FLAWS IN AUSTENITIC PIPING

S. Manganath
General Electric Company
San Jose, California

Introduction

The Main Committee of the ASME Code [1] recently approved evaluation procedures and acceptance criteria for flaws in austenitic piping. These revisions will appear in the Winter 1983 Addenda to Section XI of the ASME Code. The allowable flaw sizes were specified in IWB-364-1 as a function of applied stress and loading category (e.g., normal and upset, emergency and faulted conditions). The allowable flaw sizes were intended to provide a minimum safety margin of 2.77 for normal and upset conditions and 1.39 for emergency and faulted conditions. Recently, concerns [2] have been expressed on whether the Code allowable flaw sizes do indeed provide the intended safety margins. The purpose of this is to demonstrate the technical basis for the acceptance criteria and confirm the Code margins by considering selected examples.

Safety Margins for Circumferential Cracks

The use of the limit load concept to predict the load capability of austenitic piping has been justified by comparing the predicted failure load with experimental data as well as plastic fracture predictions based on the material J-R curve [3]. Using this method, the critical load corresponding to plastic instability can be calculated for a given combination of flaw depth and length. The allowable stress can then be determined by applying the appropriate safety factors. For a circumferential crack of length ℓ and depth

α (Figure 1) subjected to primary membrane stress P_m, the bending stress P_b corresponding to limit load is given by the following equations:

Case 1: Neutral axis located such that $\alpha + \beta < \pi$

$$\beta = \frac{(\pi - \alpha\, d/t) - (P_m/\sigma_f)\pi}{2}$$

$$P_b = \frac{2\sigma_f}{\pi} (2 \text{ Sin } \beta - d/t \text{ Sin } \alpha) \qquad (1)$$

Case 2: Neutral axis located such that $\alpha + \beta > \pi$ (assume crack takes compression)

$$\beta = \frac{\pi\,(1 - d/t - P_m/\sigma_f)}{2 - d/t}$$

$$P_b = \frac{2\sigma_f}{\pi} (2 - d/t) \text{ Sin } \beta \qquad (2)$$

Where σ_f = flow stress of the material
t = pipe thickness,
α = half the crack angle, and
β defines the location of the neutral axis as shown in Figure 1.

These equations assume thin shell approximation which is reasonable for most piping configurations.

In determining the allowable flaw, the following assumptions are made:

(i) the flow stress is assumed to equal to $3S_m$ where S_m is the ASME Code design stress intensity for the material. This is close to experimentally measured data and is based on code minimum properties.

(ii) In computing the stress levels corresponding to limit load it is assumed that for normal conditions the membrane stress $P_m = S_m/2$. This is reasonable in pipes which are sized such that the hoop stress is close to S_m. Parametric studies have shown that for a given $P_m + P_b$ value, the allowable flaw sizes are not significantly affected by the assumed membrane stress.

(iii) The safety factor of 2.77 for normal conditions is applied on the total stress $P_m + P_b$.

(iv) The procedure described above determines the allowable stress for a given flaw size. This was inverted to determine the allowable flaw size for a given stress level using linear interpolation.

Table 1 shows the Code allowable size for circumferential flaws. The safety margin in the Code allowable flaw sizes can be illustrated by considering two examples.

Case 1

$P_m + P_b = S_m$ (normal and upset conditions). For a 360° circumferential crack the allowable depth is 0.41t. Substituting in Equation 2, the angle β defining the neutral axis is given by

$$\beta = \frac{\pi (1 - 0.41 - 0.5/3)}{(2 - 0.41)}$$

$$= 0.84$$

The maximum bending stress is given by

$$P_b = \frac{2}{\pi} (3S_m)(2 - .41) \text{ Sin } (0.84)$$

$$= 2.26\ S_m$$

$$P_m + P_b \text{ corresponding to failure} = (2.26 + 0.5)\ S_m = 2.76\ S_m$$

Comparing this with the applied stress of 1.0 S_m, it is seen that the safety margin is 2.76. The minor difference between this and the stated Code margin of 2.77 is due to the roundoff in the allowable flaw size to two decimal places.

Case 2

$$P_m + P_b = 0.8\ S_m$$

$$\ell/2\pi R = 0.2$$

$$d/t = 0.75$$

Substituting in Equation 1

$$\beta = \frac{\pi - (0.2\pi)(0.75) - 0.5/3\pi}{2}$$

$$= 1.073$$

$$P_b = \frac{2}{\pi} (3S_m)(2 \text{ Sin } (1.073) - 0.75 \text{ Sin } (0.2\pi))$$

$$= 2.515\ S_m$$

$$P_m + P_b \text{ corresponding to failure} = (2.515 + 0.5) = 3.015\ S_m$$

Comparing this with the applied stress of 0.8 S_m, the safety margin is 3.76. In this case the safety margin is higher than the Code minimum value of 2.77 because of the cutoff in d/t values at 0.75.

The examples illustrated here confirm that the allowable flaw sizes in IWB-3674 do assure a minimum safety margin of 2.77 for normal and upset conditions. Similar analysis can be performed to show a safety margin of 1.39 for emergency and faulted conditions. In most realistic cases the criteria for normal conditions govern.

Discussion

The allowable flaw sizes for austenitic piping are based on providing safety factors on stress to failure predicted using limit load concepts. Failure is predicted using a flow stress equal to $3S_m$. This is close to experimentally measured values of flow stress and is conveniently expressed in terms of the design stress intensity S_m. Conservatism is provided by the fact that this is based on Code minimum properties. Also, actual mechanical strength near weld locations (where cracks are likely to occur) is likely to be higher than that of the base material due to work hardening. It should be noted that the safety margins apply for the final flaw size at the end of the inspection interval.

Safety margins based on flaw size [2] are not meaningful, since failure is governed by the remaining cross section, not the flaw size in itself. In fact, if one were to determine the safety margin on flaw size, it would be high for high stresses and low for low stresses. Since safety margin is of less concern for low stress conditions, the safety factor on flaw size is not a relevant parameter. A more important measure of safety factor is the margin on the remaining ligament area which is equivalent to the factor on stress.

Finally, the tables on allowable flaw sizes for faulted conditions included stresses up to $P_m + P_b = 3S_m$. Since the Winter 1981 Addenda, the allowable stress for faulted conditions has been revised to $3S_m$ or $2S_y$, whichever is

lesser. For stainless steel piping the $2S_y$ limit is controlling. In any case, this does not affect evaluations since actual stresses in piping are well below this limit; therefore, the allowable flaw sizes for normal conditions are more limiting.

References

1. American Society of Mechanical Engineers Boiler and Pressure Vessel Code.

2. G. Wilkowski, 'Margins of Safety Based on Circumferential Crack Depth Using the Net Section Collapse Analysis,' presented at the CSNI Special Meeting on Leak Before Break at Monterey, California, September 1-2, 1983.

3. Ranganath, S. and Mehta, H. S., 'Engineering Methods for the Assessment of Ductile Fracture Margin in Nuclear Power Plant Piping,' Elastic-Plastic Fracture: Second Symposium, Volume II--Fracture Resistance Curves and Engineering Applications, ASTM STP 803, C. F. Shih and J. P. Gudas, Eds., American Society for Testing and Materials, 1983 (to be issued).

SR73.da

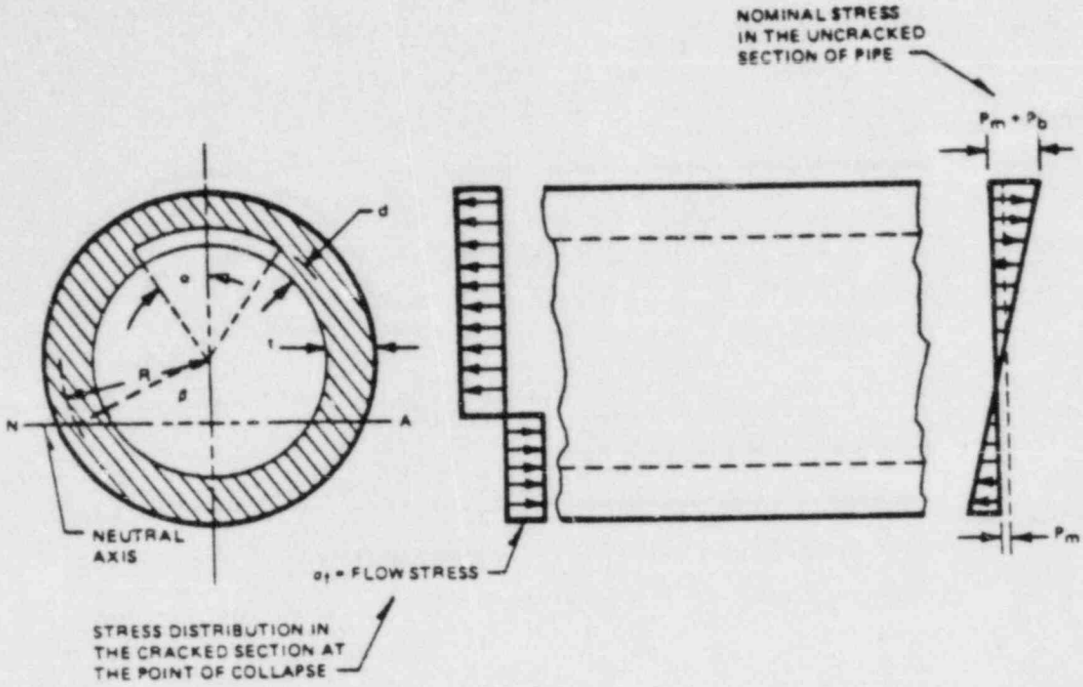

Figure 1 Schematic Showing Stress Distributed in a Cracked Pipe at the Point of Collapse

Table I

ALLOWABLE END-OF-EVALUATION PERIOD FLAW DEPTH[1]-TO-THICKNESS RATIO FOR CIRCUMFERENTIAL FLAWS, NORMAL OPERATING (INCLUDING UPSET AND TEST) CONDITIONS

$\frac{P_m + P_b}{S_m}$ [3]	Ratio of Flaw Length (ℓ_f) to Circumference[2]					
	0.0	0.1	0.2	0.3	0.4	0.5 or more
1.5	(4)	(4)	(4)	(4)	(4)	(4)
1.4	0.75	0.40	0.21	0.15	(4)	(4)
1.3	0.75	0.75	0.39	0.27	0.22	0.19
1.2	0.75	0.75	0.56	0.40	0.32	0.27
1.1	0.75	0.75	0.73	0.51	0.42	0.34
1.0	0.75	0.75	0.75	0.63	0.51	0.41
0.9	0.75	0.75	0.75	0.73	0.59	0.47
0.8	0.75	0.75	0.75	0.75	0.68	0.53
0.7	0.75	0.75	0.75	0.75	0.75	0.58
≤0.6	0.75	0.75	0.75	0.75	0.75	0.63

Notes:

(1) Flaw depth = a_n for a surface flaw
= $2a_n$ for a subsurface flaw
t = nominal thickness
linear interpolation is permisible

(2) Circumference based on nominal pipe diameter

(3) P_m = Primary Membrane Stress
P_b = Primary Bending Stress
S_m = ASME Code Allowable Design Intensity

(4) IWB-3514.3 allowable flaw standards shall be used

SESSION II

LEAK RATE AND LEAK DETECTION

SESSION CHAIRMEN

MR. SPENCER BUSH
REVIEW AND SYNTHESIS ASSOCIATES, U.S.A.

DR. ROY NICHOLS
RISLEY NUCLEAR LABORATORY, U.K.

TWO-PHASE FLOW EXPERIMENTS THROUGH INTERGRANULAR STRESS CORROSION CRACKS

R. P. Collier
Battelle's Columbus Laboratories
Columbus, Ohio

and

D. M. Norris
Electric Power Research Institute
Palo Alto, California

ABSTRACT

Experimental studies of critical two-phase water flow, through simulated and actual intergranular stress corrosion cracks, were performed to obtain data to evaluate a leak flow rate model and investigate acoustic transducer effectiveness in detecting and sizing leaks. The experimental program included a parametric study of the effects of crack geometry, fluid stagnation pressure and temperature, and crack surface roughness on leak flow rate.

In addition, leak detection, location, and leak size estimation capabilities of several different acoustic transducers were evaluated as functions of leak rate and transducer position.

This paper presents flow rate data for several different cracks and fluid conditions. It also presents the minimum flow rate detected with the acoustic sensors and a relationship between acoustic signal strength and leak flow rate.

INTRODUCTION

The presence of cracks in reactor piping has attracted considerable attention over the past several years. In particular, intergranular stress corrosion cracks (IGSCC's) in heat-affected zones near welds in Type 304 stainless steel piping have been the subject of considerable study. In the

mid-1970's, a number of cracks of this type were found in small diameter core spray and recirculation bypass lines in Boiling Water Reactors (BWR's). Recently, similar cracks have been found in larger diameter piping, including BWR main recirculation lines. The occurrence of these cracks is of concern because of their effect on plant availability and plant reliability, as well as their potential effect on safe plant operation.

In response to the problem, the Electric Power Research Institute and the BWR Owners Group have jointly sponsored an extensive research program designed to understand the resolve IGSCC problems in BWR's. This investigation is a part of that research effort.

One area of interest in the overall program has been the evaluation of acoustic emission (AE) techniques for leak detection, location, and sizing. In particular, determination of the minimum sensitivity of AE detection of very small two-phase leaks through IGSCC's has been given high priority. In this project, we evaluated the minimum leak detection, leak location, and leak size estimation capabilities of several AE systems. This was done by mounting several AE transducers on a test vessel with a leak through an IGSCC of known length. AE signals were measured for a variety of leak rates. A brief summary of key results is presented in this paper.

A second area of interest has been in relating the size of a through-wall crack to the critical two-phase leak rate through that crack. An analytical flow model has been developed to predict crack size if flow rate and fluid conditions are known. This information could be used in conjunction with a crack growth model to determine the maximum safe operating time before shutdown when a crack is discovered; and it could be used to evaluate the validity of the measurable leak-before-break philosophy for a range of pipe sizes, materials, and fluid operating conditions.

In this project, we carried out experimental studies of critical two-phase water flow through simulated and actual IGSCC's. The influences of crack geometry, fluid stagnation conditions, and crack surface roughness on leak flow rate were measured. This paper concentrates on the results of the flow rate experiments. The flow model and application to reactor piping are discussed in two related papers (1,2).

Review of Recent Work

Several recent reviews are available which summarize much of the important theoretical and experimental work in the field of critical two-phase flow (3-8). However, this research has concentrated on flow in pipes, nozzles and orifices, and there is little direct information available on the flow rate of two-phase fluids through tight cracks. Recently, Button, et al (9) investigated nitrogen gas flow through idealized cracks. They found that the surface roughness and crack geometry may play important roles in determining the flow rate. However, non-equilibrium critical two-phase flow would be very different from and more complex than single phase gas flow, which is generally regarded as in thermodynamic equilibrium. For example, the composition and phase distribution of the two-phase fluid would be determined, in part, by the flow rate. The flow rate, in turn, is a function of the fluid composition and phase distribution.

Agostinelli and Salemann (10) investigated flows of flashing water and steam through smooth annuli of fine clearance experimentally. Test data were obtained with stagnation conditions to 315 C and 20.7 MPa (600 F abd 3000 psia). Ryley and Parker (11) used a transparent test section 3.56 cm (140 in.) deep, 2.54 cm (1.0 in.) long, and 0.127 cm (0.05 in.) wide, and observed steam flow with water injection at the inlet. They found visual evidence of a free liquid jet at the inlet and separated flow throughout the channel. Simoneau (12) carried out an experimental study of two-phase nitrogen flow through a slit. He concluded that a uniform two-phase flow pattern existed in most of the test runs and that vaporization was occurring at or near the exit plane. He also compared his results with the Henry (13) model for critical flow of initially subcooled or saturated liquid through a long tube. In general, the agreement between the model and his experimental data was reasonably good. However, Simoneau suggested that frictional effects should be accounted for in the analysis.

We recently developed an analytical approach based on the theory suggested by Henry (13,14), to predict two-phase flow through cracks (1,15, 16). This model accounts for wall friction and flow area change.

EXPERIMENTAL STUDY

The experimental program was carried out in two phases. In the first phase, we used simulated cracks, or slots, in which the critical geometric parameters and surface roughness could be controlled easily. In the second phase, we used actual IGSCC's in stainless steel pipe. The geometry was characterized by the crack depth-over-hydraulic diameter ratio, L/D_h. For tight cracks, D_h is approximately equal to twice the crack opening displacement, COD.

Phase I - Simulated Cracks

Figure 1 is a schematic sketch of the facility used in the Phase I experiments. Briefly, the facility consisted of a supply vessel and three test vessels. Each test vessel contained a different simulated crack in which the L/D_h and surface roughness could be varied. The supply vessel was large enough so that several experiments could be conducted without refilling the vessel. The water was heated using electrical immersion heaters. The supply temperature was measured with thermocouples. System pressure was controlled with a high-pressure, high-flow capacity gas regulator and a nitrogen supply. The pressure could be pre-set or adjusted during each experiment.

The simulated cracks were machined from blind flanges attached to the top of the test vessels. The flanges were split and "crack faces" were machined in the center of each half. Various surface roughnesses were obtained by shot blasting the faces. The crack length dimension, 2C, was fixed at 6.35 cm (2.5 in.) and the crack depth dimension, L, was fixed at 5.72 cm (2.25 in.). The L/D_h ratio was set at the desired value by adjusting the crack opening displacement, COD, with spacer blocks between the halves. These blocks also provided a seal at the ends of the crack faces. Thus, the flow cross-section was rectangular, with fixed dimensions. Measurements

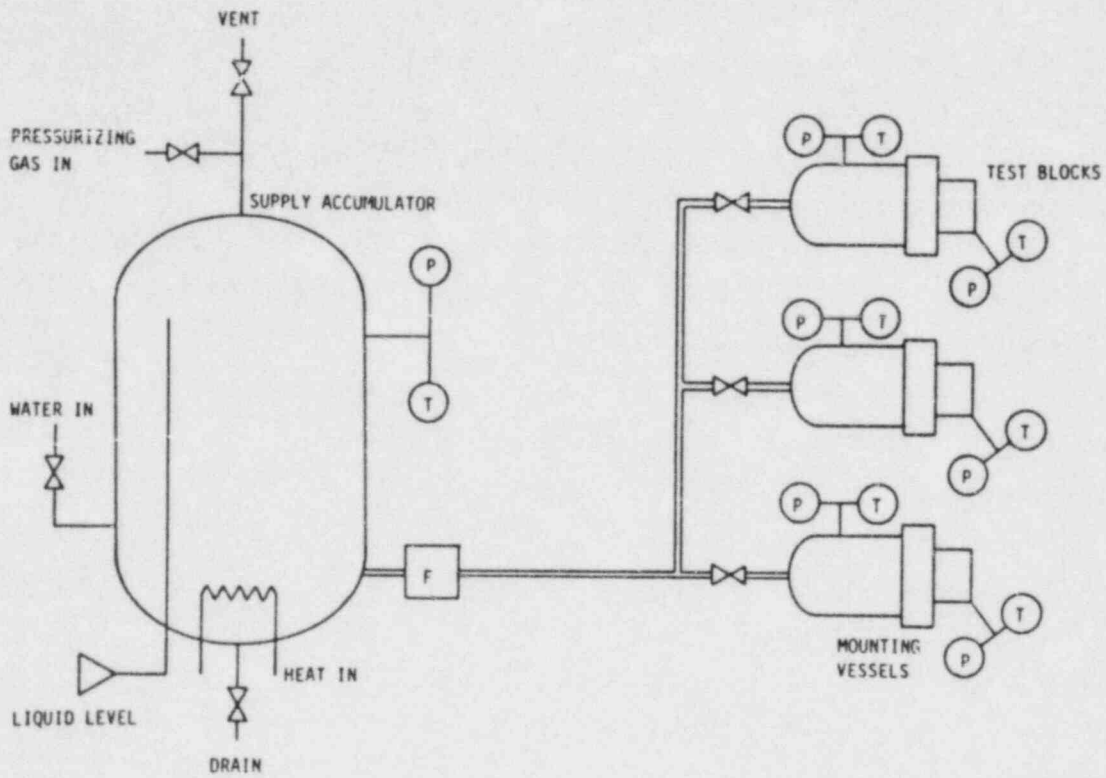

FIGURE 1. SCHEMATIC SKETCH OF EXPERIMENTAL FACILITY

made during the shakedown tests indicated that the COD did not change during the tests. The surface roughness was varied by machining the crack faces to the desired roughness. The crack faces were initially ground to an average surface roughness of 0.3 μm (1.18×10^{-5} in.), as measured by a surface profilometer. After completing the "smooth" tests, the test blocks were removed, disassembled, and the crack surfaces were roughened by shot blasting to an average roughness of 5.2 μm (2.05×10^{-4} in.). For the final set of tests, the crack faces were roughened to 10.2 μm (4.02×10^{-4} in.) average roughness. Figure 2 shows a simulated crack flange with instrumentation attached.

Test measurements included supply vessel temperature and pressure, liquid level in the supply vessel, flow rate from the supply vessel to the test vessel, pressure and temperature just upstream of the simulated crack, the pressure and temperature at three locations along the simulated crack flow path, and the acoustic emission spectra.

A test was initiated by opening the flow control valve for about 30 seconds to pre-heat the piping and test vessel. The valve was then closed, the water level in the supply vessel was measured, the data acquisition system was started, and the flow valve was re-opened for typically 30 to 120 seconds. At that time, the flow valve was closed and the supply vessel water level was again measured. The pre-heat flow allowed the test pressure to be set more accurately and allowed more nearly steady-state conditions. Thus, the change in liquid level served as a relatively accurate check on the flow rate determined from the orifice flow meters.

Phase II - Actual Cracks

The basic facility used in the Phase II experiments was similar to that used in the Phase I program. However, the simulated crack test vessels were replaced by a vessel containing an intergranular stress-corrosion crack.

Two test vessels were fabricated, using concentric pipes as shown in Figure 3. The outer pipe included a 61 cm (24 in.) length of stainless steel pipe with an outside diameter of 32.4 cm (12 in. Schedule

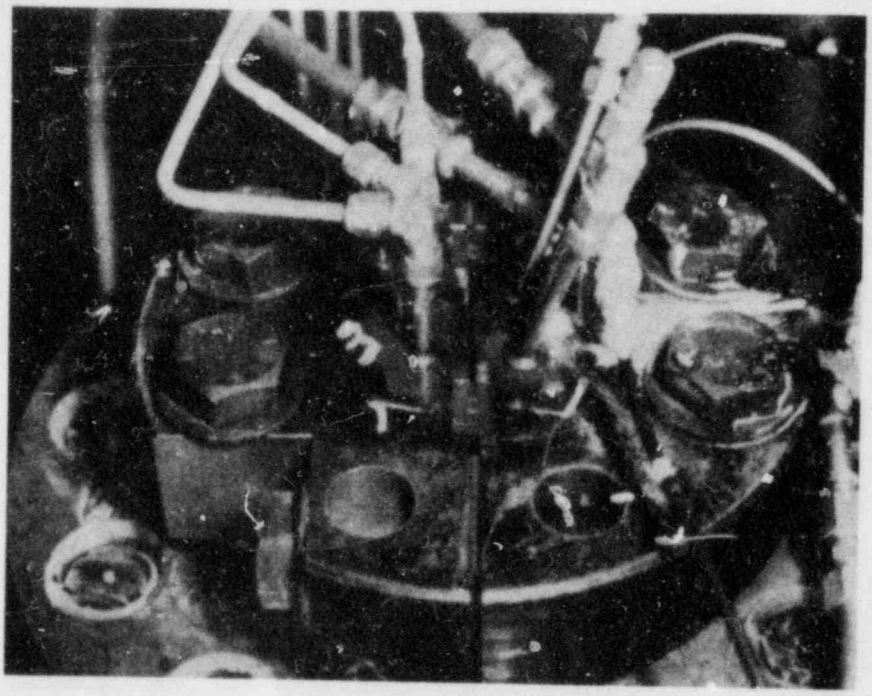

FIGURE 2. PHASE I SIMULATED CRACK FLOW FLANGE

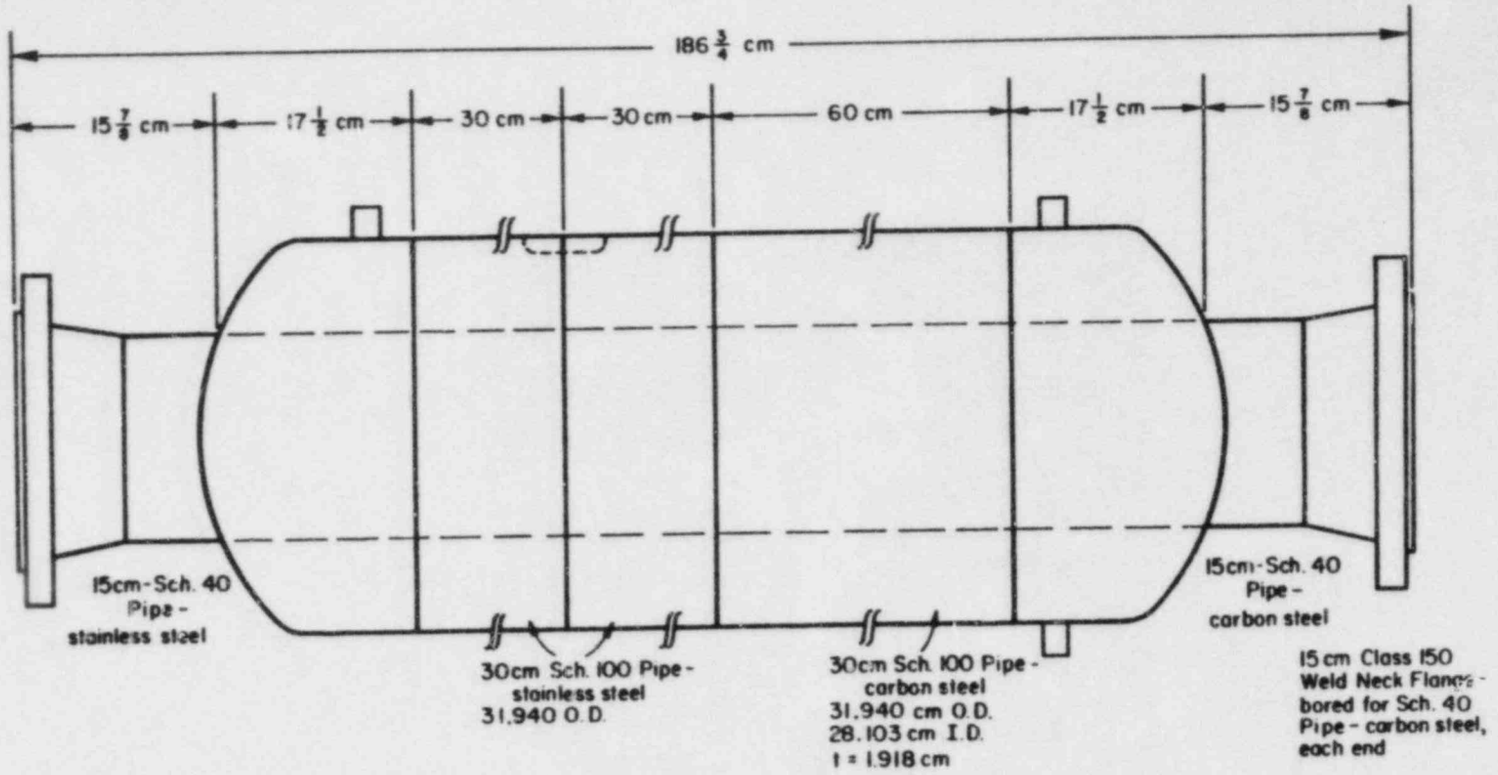

FIGURE 3. OVERALL VIEW OF PHASE II VESSEL ASSEMBLY

100) supplied to the program by EPRI. Each of these sections contained a girth butt weld at mid-length, with full circumferential stress-corrosion cracks in the vicinity of the welds.

To provide a longer vessel for acoustic attenuation measurements, the test pipe length was increased by welding another 61 cm (24 in.) length of carbon steel pipe to the cracked sections. The inner pipe was fabricated from both carbon and stainless steel so that the axial thermal expansion of the inner and outer pipes were matched. The inner pipe provided a mechanical restraint in the unlikely event that the cracked section fa'led.

The annular space between the two pipes provided a reservoir of water at the desired test conditions. A propane burner firing into the inner pipe was used to maintain the test temperatures. This was necessary due to the heat loss during the low flow rate experiments.

Figure 4 illustrates the way in which through cracks of varying lengths were obtained. The initial circumferential cracks were about 90 percent of the wall thickness. The pipe surface in the vicinity of the crack was carefully machined away until the tip of the resulting through crack could be identified using a microscope. The cutter was moved axially along the pipe so that varying the width of the cutter varied the crack length. The smallest crack length attained was about 0.74 mm (0.029 in.), and the longest crack length was 27.89 mm (1.098 in.). For longer crack lengths, the cutter width was increased, however, the depth of cut was maintained. Thus, the flow path length, L, was held constant.

As in Phase I, a number of measurements were made during each test. The Phase II measurements included supply vessel pressure and temperature, flow rate from the supply vessel to the test vessel, test vessel pressure and water temperature just upstream of the crack, crack-opening displacement, and a variety of acoustic emission signals from several transducers mounted on the pipe.

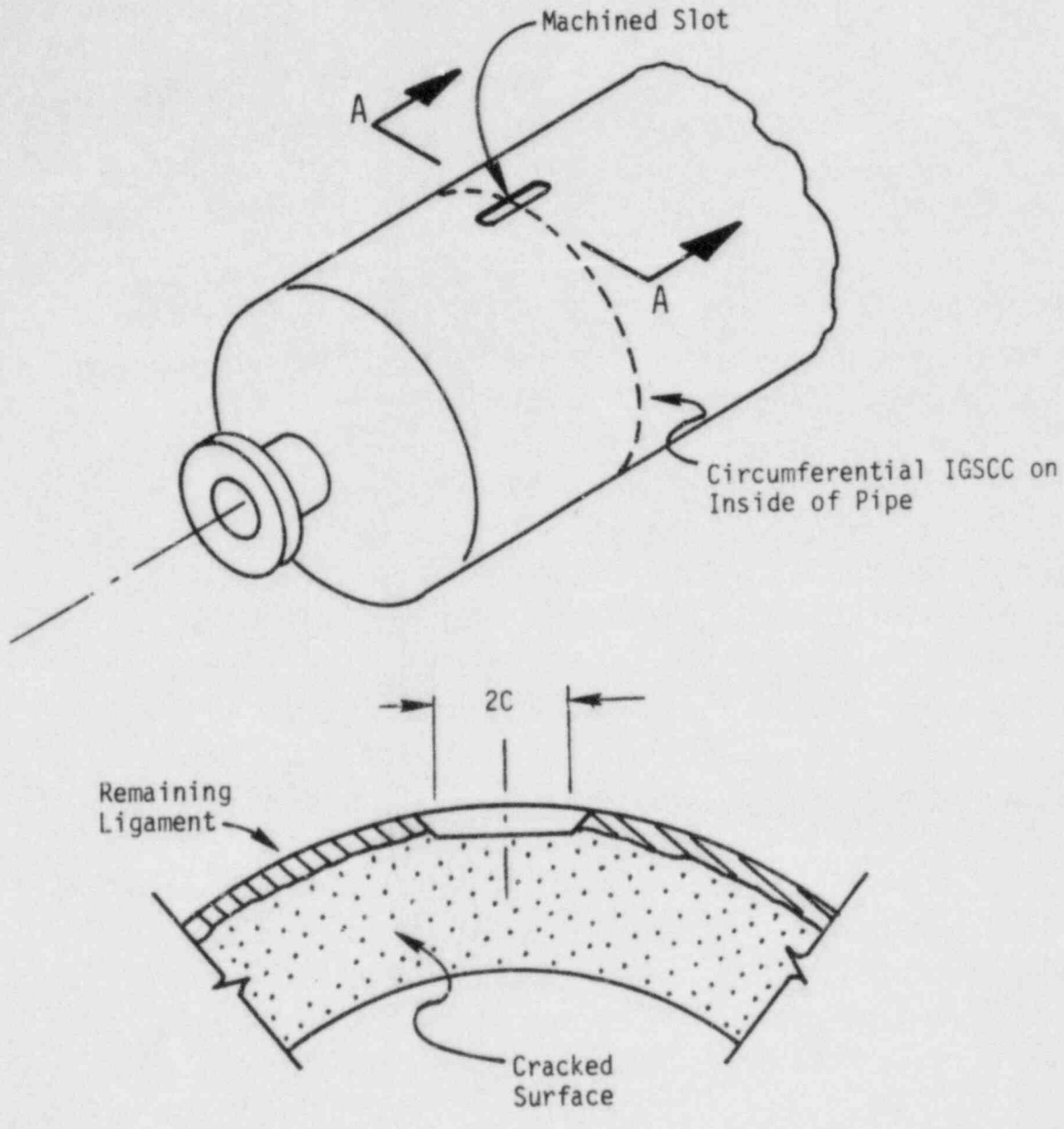

SECTION A-A

FIGURE 4. SKETCH OF CRACK DETAILS

EXPERIMENTAL RESULTS

Acoustic Emission Leak Detection

The first priority of a leak detection system is reliable detection of the signal produced by a leak in the presence of background noise. The determining factor for detection of the smallest possible leak is the signal-to-background-noise ratio. For the reasonably quiet facility used in these experiments (no pumps running during testing), we were able to detect leak flow rates of about 1×10^{-4} kg/s (about 0.02 gpm at 1000 psia and 500 F) with signal-to-noise ratio of about 2, with commercially-available AE transducers located about 180 mm (about 7 in.) from a 0.74 mm (0.029 in.) long IGSCC.

We found the transmission of the acoustic emission from a leaking crack was strongly directional, with signal strength strongest directly along the axis from the crack and weakest directly around the pipe circumference from the crack. This result could complicate the use of AE systems for detailed leak location since most leak location schemes depend on comparison of signals received at two or more transducers.

A key result of this study was the delineation of two types of behavior for AE signal as a function of leak rate. Figure 5 illustrates the difference in the two types. When the crack length was fixed and the leak flow rate was controlled by varying the fluid stagnation pressure and temperature, the AE signal strength varied by about an order of magnitude as the leak flow rate varied by an order of magnitude. When the leak flow rate was varied by maintaining fluid conditions and changing crack length, the AE signal varied about one order of magnitude, while the leak flow rate varied over approximately four orders of magnitude.

Flow Rate Results - Phase I

The flow rate data obtained during the Phase I experiments are summarized in Table 1. Tabulated data include the stagnation pressure and temperature, P_o and T_o; the initial subcooling, ΔT; the surface

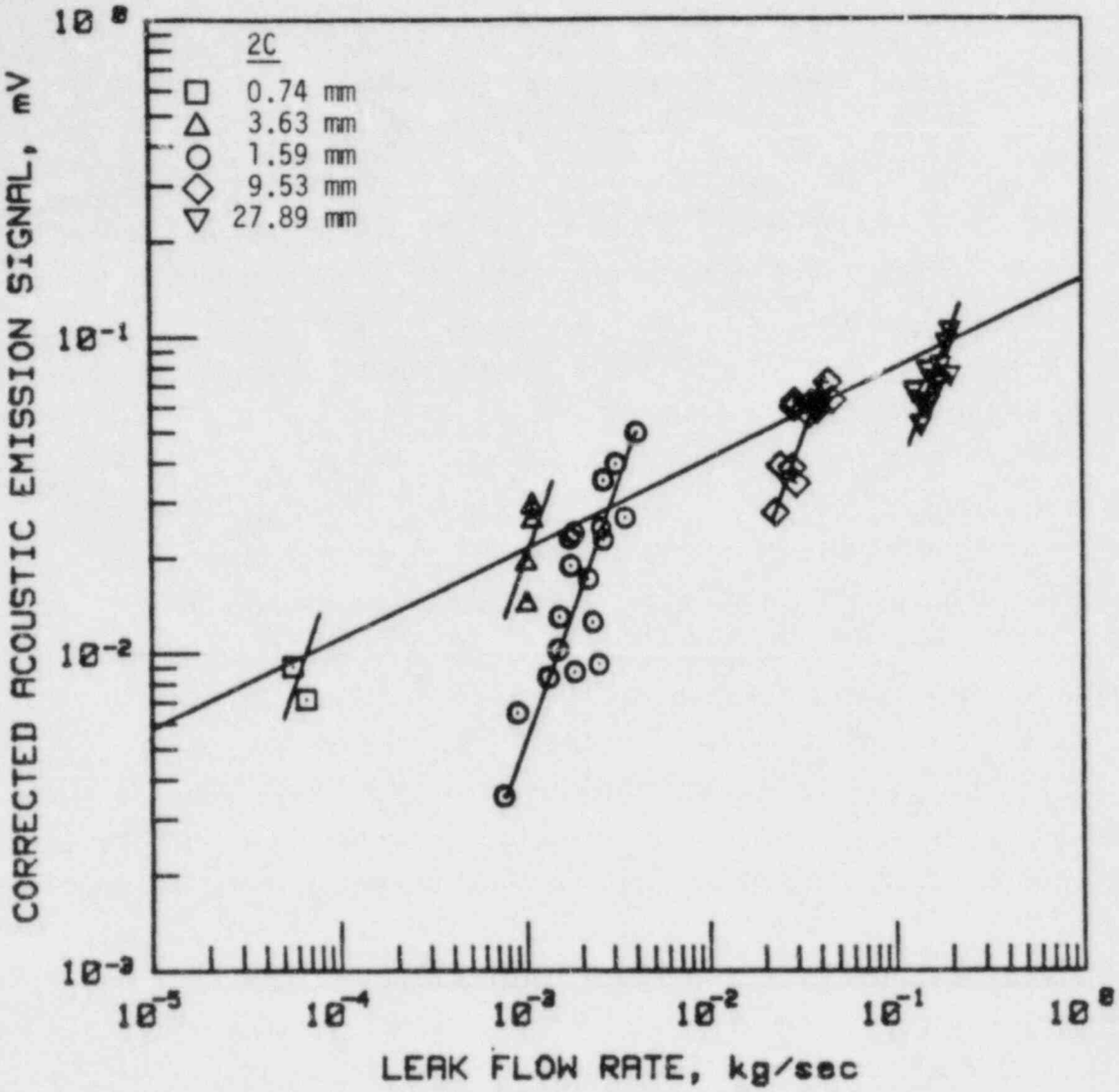

FIGURE 5. AE SIGNAL AS A FUNCTION OF LEAK FLOW RATE FOR TRANSDUCER 180 MM FROM CRACK

TABLE 1. SUMMARY OF PHASE I FLOW RATE DATA

Test No.	P_o MPa	T_o C	ΔT C	κ μm	COD mm	L/D_h	W (meas) kg/s	G_c (meas) 10^4 kg/m^2-s
1	8.36	265.06	32.98	.3	1.12	30	2.03	2.86
2	9.27	186.10	119.35	.3	.25	115	.84	5.21
3	9.00	197.20	106.10	.3	.25	115	.82	5.06
4	8.35	180.12	117.85	6.2	.23	128	.90	6.21
5	8.77	199.14	102.31	6.2	.36	80	.74	3.26
6	8.51	261.56	37.74	6.2	1.09	27	3.60	5.19
7	11.53	251.23	70.37	6.2	1.09	27	3.93	5.67
8	5.81	199.17	74.25	6.2	.36	80	.43	1.91
9	5.00	178.40	85.48	6.2	.23	128	.40	2.79
10	3.96	199.97	49.78	6.2	.36	80	.46	2.05
11	3.26	227.79	10.64	6.2	1.09	27	1.35	1.95
12	10.80	234.19	82.49	6.2	.23	128	.52	3.60
13	10.65	249.01	66.62	6.2	.23	128	.48	3.30
14	9.91	212.46	97.81	6.2	.33	87	.62	2.95
15	8.68	217.92	82.82	6.2	.33	87	.49	2.34
16	9.33	234.80	71.13	6.2	.33	87	.52	2.50
17	8.80	205.80	95.88	6.2	.23	128	.51	3.53
18	8.89	230.08	72.38	6.2	.23	128	.49	3.35
19	8.52	236.05	63.35	6.2	.23	128	.46	3.16
20	8.65	192.14	108.32	6.2	.33	87	.71	3.38
21	8.94	206.56	96.28	6.2	.33	87	.86	4.10
22	4.72	195.32	65.05	6.2	1.09	27	2.16	3.11
23	8.90	205.97	96.50	10.2	.20	144	.39	3.03
24	9.02	218.85	84.61	10.2	.20	144	.40	3.11
25	8.92	223.73	78.92	10.2	.20	144	.39	3.03
26	9.46	267.83	39.12	6.2	1.09	27	3.14	4.53
27	10.31	256.14	57.09	6.2	1.09	27	3.03	4.37

roughness, κ; the crack-opening displacement, COD; the measured leak flow rate, W (meas); and the measured mass flux, G_c (meas).

Figure 6 indicates the effect of stagnation pressure with subcooling as a parameter. For a fixed geometry and surface roughness, the critical mass flux increases as stagnation pressure or subcooling increases. We note that the effect of subcooling on critical mass flux is more pronounced at high stagnation pressures. The model of Reference 1 was used to calculate the trend lines shown in this and subsequent figures.

The influence of crack depth-over-hydraulic-diameter ratio is demonstrated by Figure 7 for two different stagnation conditions. The critical mass flux decreases uniformly with increasing crack depth-over-hydraulic-diameter ratios.

Figure 8 presents the effect on critical mass flux of surface roughness, with the subcooling as a parameter. The critical mass flux decreases smoothly with increasing surface roughness.

The effect of subcooling is illustrated as a parameter in Figures 6 and 8, and directly in Figure 9. In the latter figure, the effect of low subcooling at pressures similar to BWR operating conditions is shown.

Flow Rate Results - Phase II

The flow rate data from the Phase II experiments are tabulated in Table 2. Data include the stagnation pressure and temperature, P_o and T_o; the initial subcooling ΔT; crack length, 2C; crack-opening displacement, COD; crack-opening area, COA; and the measured leak flow rate, W (meas).

Figure 10 compares measured leak flow rates for Phase II with predicted values using the model of Reference 1. Measured flow rates varied over more than four orders of magnitude, from a measured low of 1.34×10^{-5} kg/s (2.86×10^{-4} gpm at 1000 psia and 500 F) to a measured high of 0.199 kg/s (4.24 gpm). Overall agreement between predicted and measured values is reasonable, but there is substantial scatter in the data for a given crack length.

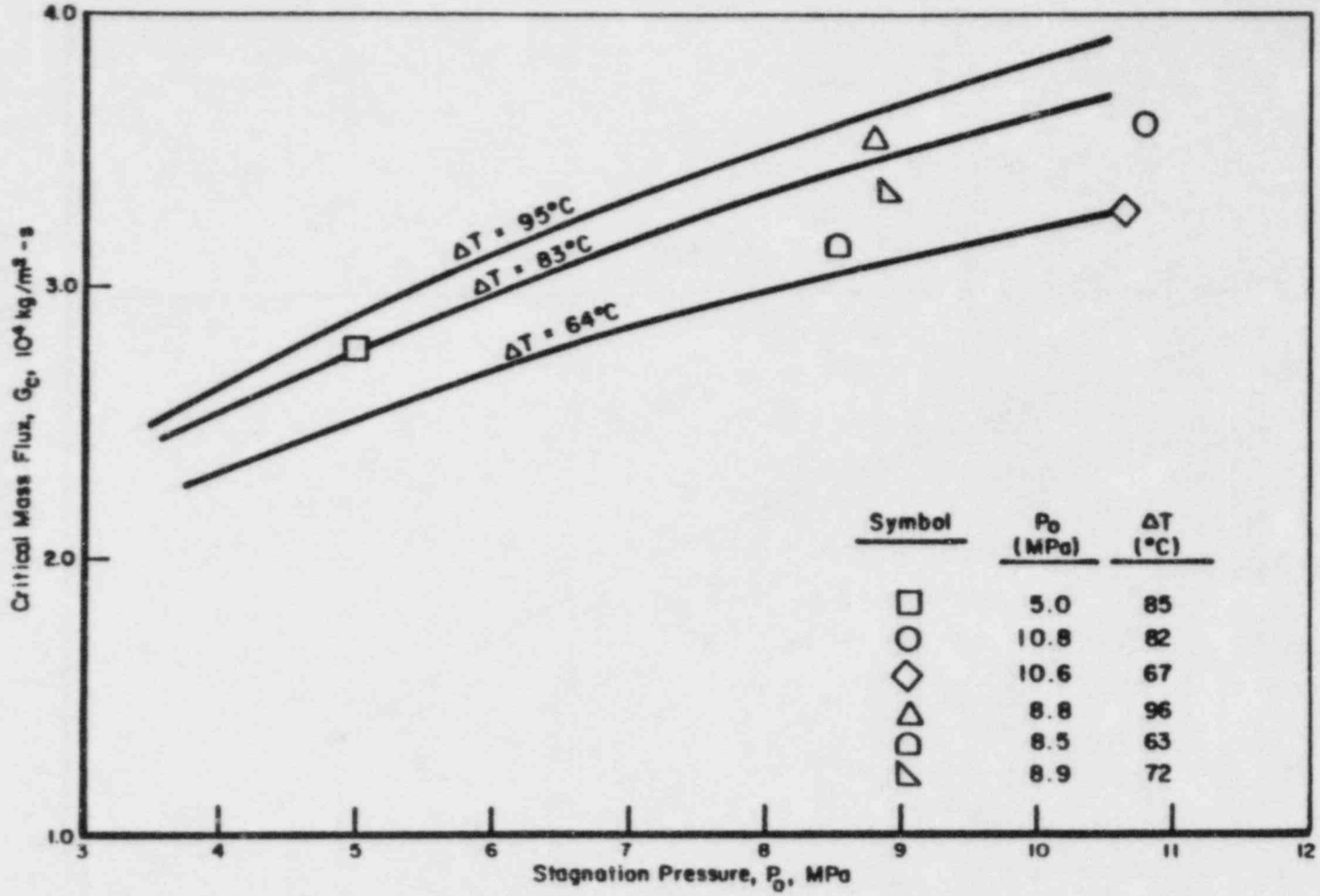

FIGURE 6. VARIATION OF CRITICAL MASS FLUX AS A FUNCTION OF STAGNATION PRESSURE WITH SUBCOOLING AS A PARAMETER

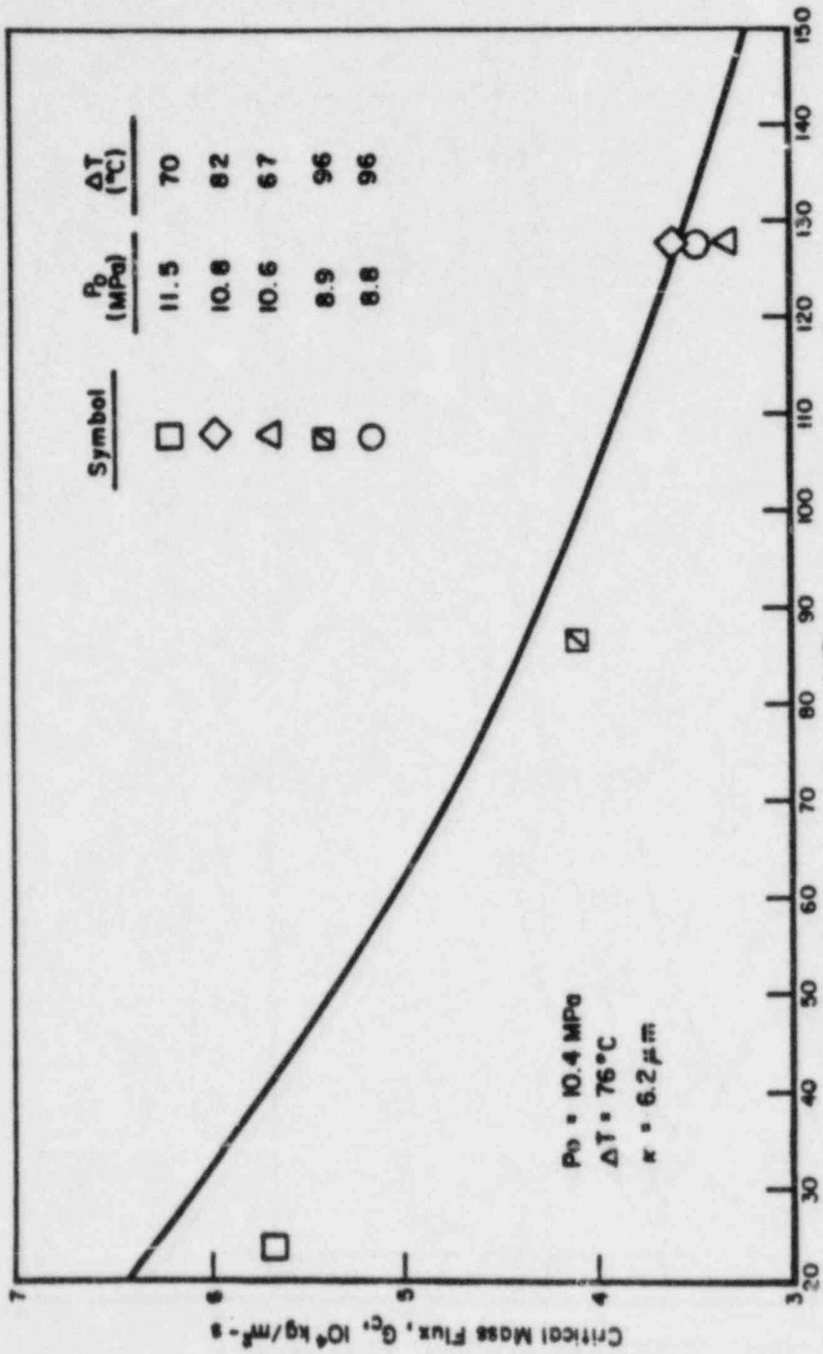

FIGURE 7. VARIATION OF CRITICAL MASS FLUX AS A FUNCTION OF L/D_h

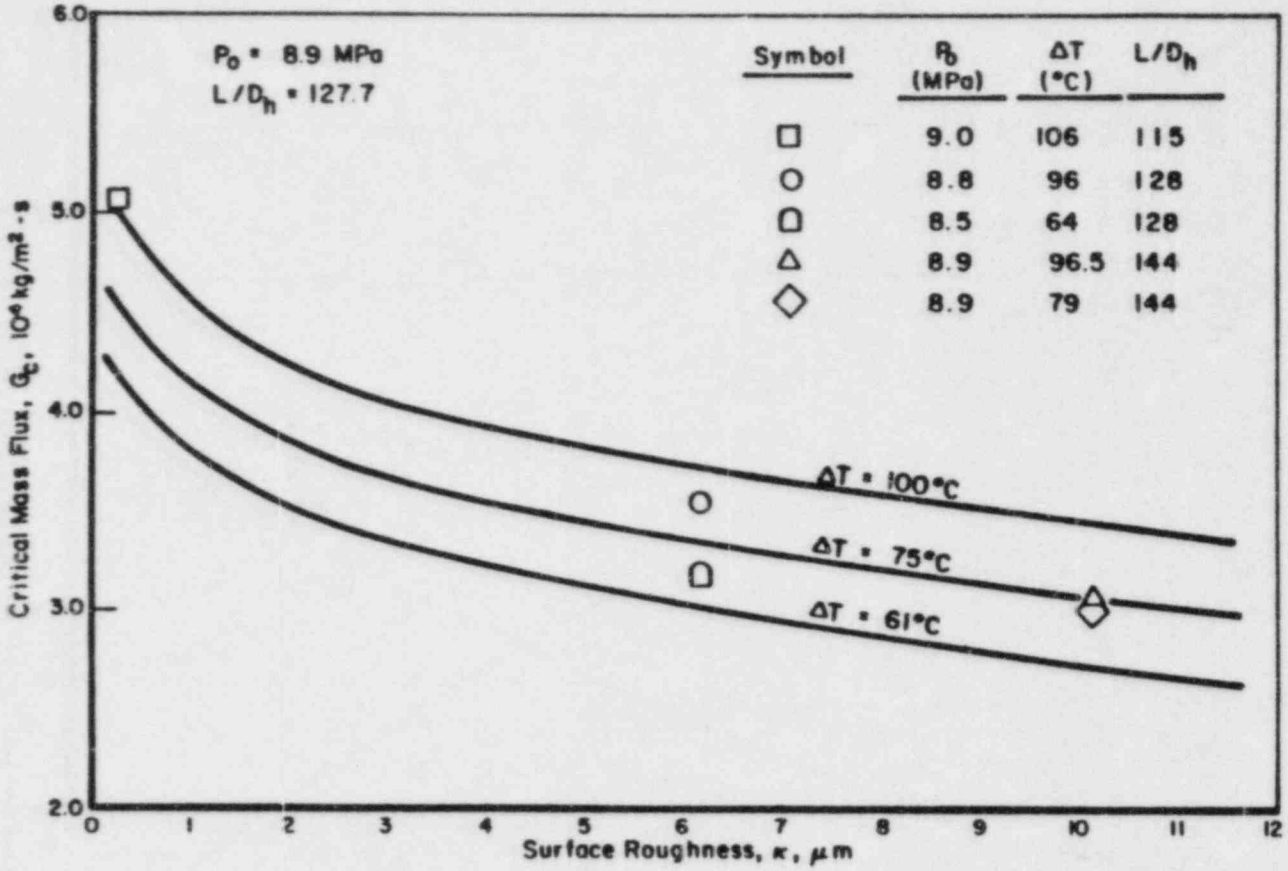

FIGURE 8. VARIATION OF CRITICAL MASS FLUX AS A FUNCTION OF SURFACE ROUGHNESS WITH SUBCOOLING AS A PARAMETER

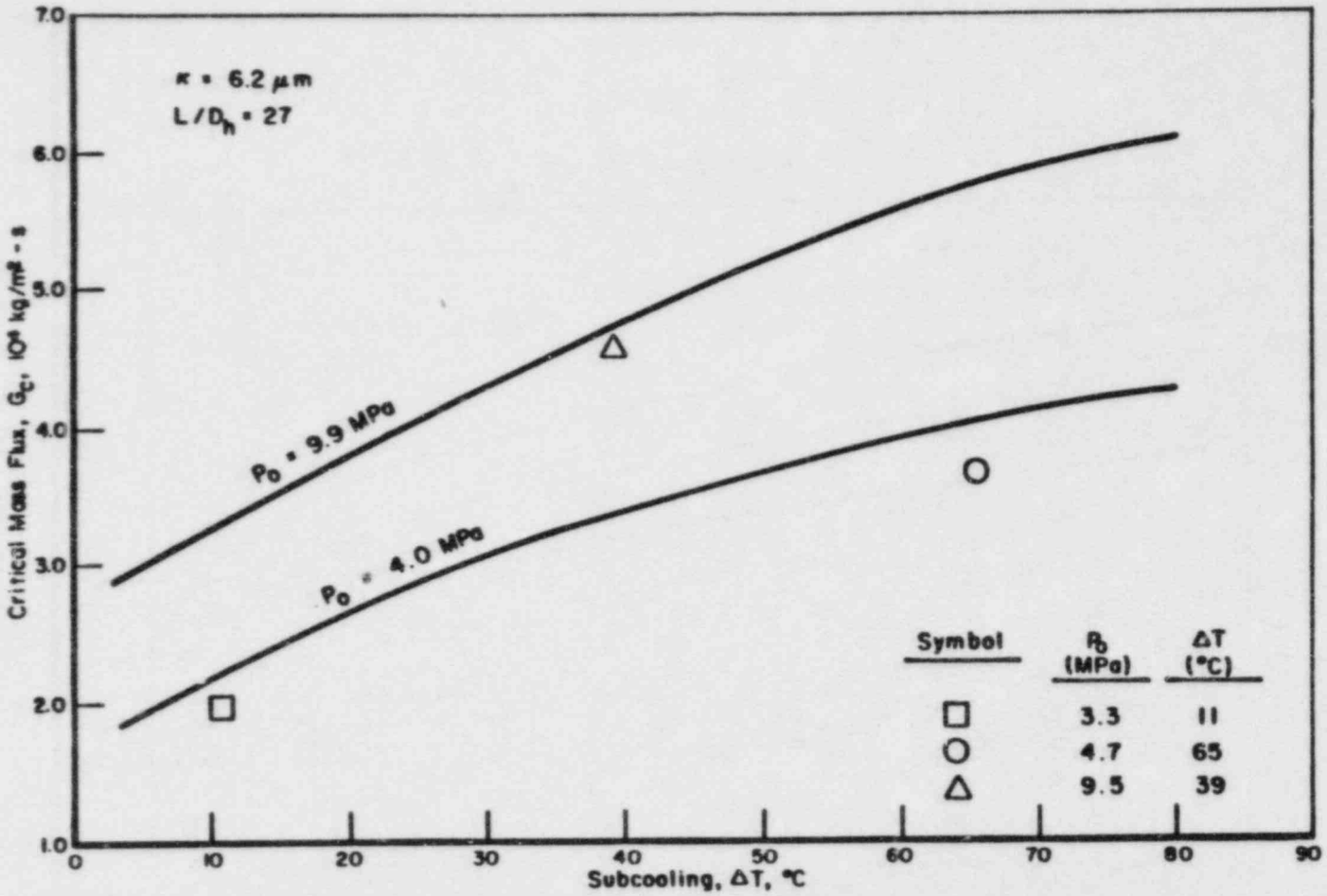

FIGURE 9. VARIATION OF CRITICAL MASS FLUX AS A FUNCTION OF SUBCOOLING WITH STAGNATION PRESSURE AS A PARAMETER

TABLE 2. SUMMARY OF PHASE II FLOW RATE DATA

Run No.	P_o MPa	T_o C	ΔT C	2C mm	COD mm	COA mm^2	W (meas) kg/s
1	7.417	272.8	18.4	3.63	0.074	0.268	1.02×10^{-3}
2	7.417	272.8	18.4	"	"	"	"
3	8.768	267.2	34.2	"	"	"	1.10×10^{-3}
4	9.513	260.6	46.8	"	"	"	"
5	9.513	260.6	46.8	"	"	"	"
6	9.423	267.8	38.8	"	"	"	"
7	9.402	284.4	22.1	0.74	0.0220	0.0162	5.49×10^{-5}
8	9.547	281.7	25.9	"	0.0218	0.0161	6.66×10^{-5}
9	9.568	278.3	29.4	"	0.0216	0.0159	5.67×10^{-5}
10	5.803	273.3	.1	"	0.0208	0.0153	3.08×10^{-5}
11	6.072	262.8	13.6	"	0.0201	0.0148	1.34×10^{-5}
12	5.969	260.0	15.2	"	0.0199	0.0146	1.09×10^{-4}
13	5.955	268.3	6.7	"	0.0205	0.0151	1.51×10^{-4}
14	5.969	272.8	2.4	"	0.0208	0.0153	1.01×10^{-4}
15	3.624	251.7	-7.1	"	0.0190	0.0140	9.30×10^{-5}
16	3.480	241.1	1.1	"	0.0183	0.0135	1.05×10^{-4}
17	5.782	278.9	-5.7	"	0.0212	0.0156	1.01×10^{-4}
18	7.182	260.0	27.6	"	--	--	6.21×10^{-5}
19	7.410	273.9	15.8	9.53	0.108	1.026	3.04×10^{-2}
20	7.410	282.2	7.4	"	"	"	2.90×10^{-2}
21	9.106	280.0	24.2	"	"	"	4.85×10^{-2}
22	9.106	273.3	30.8	"	"	"	4.62×10^{-2}
23	9.065	256.7	39.3	"	"	"	4.52×10^{-2}
24	8.989	256.7	36.3	"	"	"	4.44×10^{-2}
25	7.265	256.1	32.2	"	"	"	3.67×10^{-2}
26	7.265	256.7	31.7	"	"	"	3.59×10^{-2}
27	5.672	260.6	11.4	"	"	"	2.51×10^{-2}
28	5.727	267.8	4.8	"	"	"	2.35×10^{-2}
29	5.693	241.7	30.5	"	"	"	3.01×10^{-2}
30	5.693	243.9	28.3	"	"	"	2.98×10^{-2}
31	7.320	242.8	46.1	"	"	"	3.96×10^{-2}
32	7.320	238.3	46.6	"	"	"	3.94×10^{-2}
33	8.913	241.7	60.9	"	"	"	4.51×10^{-2}
34	8.913	235.0	67.6	"	"	"	4.73×10^{-2}
35	7.230	226.1	61.9	"	"	"	3.84×10^{-2}
36	7.230	222.8	65.2	"	"	"	3.92×10^{-2}
37	5.693	220.0	52.2	"	"	"	3.84×10^{-2}
38	5.541	223.2	47.1	"	"	"	2.97×10^{-2}
39	4.038	230.6	20.3	"	"	"	2.62×10^{-2}
40	4.038	232.8	18.1	"	"	"	1.57×10^{-2}

TABLE 2. SUMMARY OF PHASE II FLOW RATE DATA (CONTINUED)

Run No.	P_o MPa	T_o C	ΔT C	2C mm	COD mm	COA mm^2	W (meas) kg/s
41	7.410	278.9	10.8	1.59	0.0535	0.0849	1.81×10^{-3}
42	8.161	277.2	19.2	"	0.0534	0.0848	1.98×10^{-3}
43	8.823	276.7	25.2	"	0.0535	0.0850	2.19×10^{-3}
44	9.478	274.4	32.6	"	0.0533	0.0847	2.37×10^{-3}
45	7.451	278.3	11.9	"	0.0534	0.0848	3.62×10^{-4}
46	8.168	275.0	21.4	"	0.0530	0.0842	5.26×10^{-4}
47	8.858	275.0	27.2	"	0.0533	0.0845	3.91×10^{-3}
48	9.533	272.2	35.3	"	0.0530	0.0841	4.37×10^{-3}
49	7.451	276.1	13.9	"	0.0530	0.0841	3.22×10^{-3}
50	8.168	274.4	20.3	"	0.0529	0.0840	3.59×10^{-3}
51	5.314	258.3	9.4	"	0.0490	0.0778	2.51×10^{-3}
52	7.024	253.9	32.1	"	0.0487	0.0773	3.54×10^{-3}
53	8.747	252.8	48.5	"	0.0491	0.0779	4.11×10^{-3}
54	5.314	256.7	11.1	"	0.0487	0.0773	2.20×10^{-3}
55	7.003	254.4	31.4	"	0.0488	0.0775	2.61×10^{-3}
56	8.747	253.3	47.9	"	0.0492	0.0781	3.17×10^{-3}
57	3.514	233.9	8.9	"	0.0438	0.0696	7.57×10^{-4}
58	5.272	232.8	34.5	"	0.0442	0.0711	9.03×10^{-4}
59	7.024	231.1	54.9	"	0.0445	0.0706	1.50×10^{-3}
60	8.747	228.9	72.4	"	0.0446	0.0708	1.85×10^{-3}
61	8.747	231.7	69.6	"	0.0451	0.0717	1.75×10^{-3}
62	7.134	228.3	58.0	"	0.0440	0.0698	1.76×10^{-3}
63	5.307	225.0	42.7	"	0.0428	0.0679	1.53×10^{-3}
64	3.549	222.8	20.6	"	0.0415	0.0663	1.33×10^{-3}
65	3.562	235.0	8.6	"	0.0441	0.0700	1.84×10^{-3}
66	5.286	232.2	35.3	"	0.0441	0.0700	2.32×10^{-3}
67	6.996	230.0	55.8	"	0.0443	0.0703	2.69×10^{-3}
68	8.747	228.3	71.8	"	0.0445	0.0707	2.69×10^{-3}
69	8.727	241.7	59.4	27.89	0.235	6.547	1.51×10^{-1}
70	7.037	236.8	49.5	"	0.227	6.338	1.39×10^{-1}
71	6.962	236.7	48.8	"	0.227	6.334	1.57×10^{-1}
72	8.637	241.1	59.3	"	0.234	6.528	1.75×10^{-1}
73	5.210	252.8	13.7	"	0.178	4.952	1.41×10^{-1}
74	6.962	253.9	31.6	"	0.243	6.787	1.69×10^{-1}
75	8.706	254.4	46.5	"	0.247	6.882	1.91×10^{-1}
76	8.699	250.6	50.3	"	0.243	6.779	2.00×10^{-1}
77	6.962	248.3	37.1	"	0.238	6.641	1.78×10^{-1}
78	5.293	246.1	21.4	"	0.173	4.828	1.51×10^{-1}
79	4.038	240.6	10.3	"	0.144	4.024	1.28×10^{-1}
80	5.190	236.1	30.2	"	0.166	4.633	1.55×10^{-1}
81	6.872	237.2	47.3	"	0.228	6.345	1.76×10^{-1}
82	8.678	234.4	66.3	"	0.228	6.355	1.99×10^{-1}

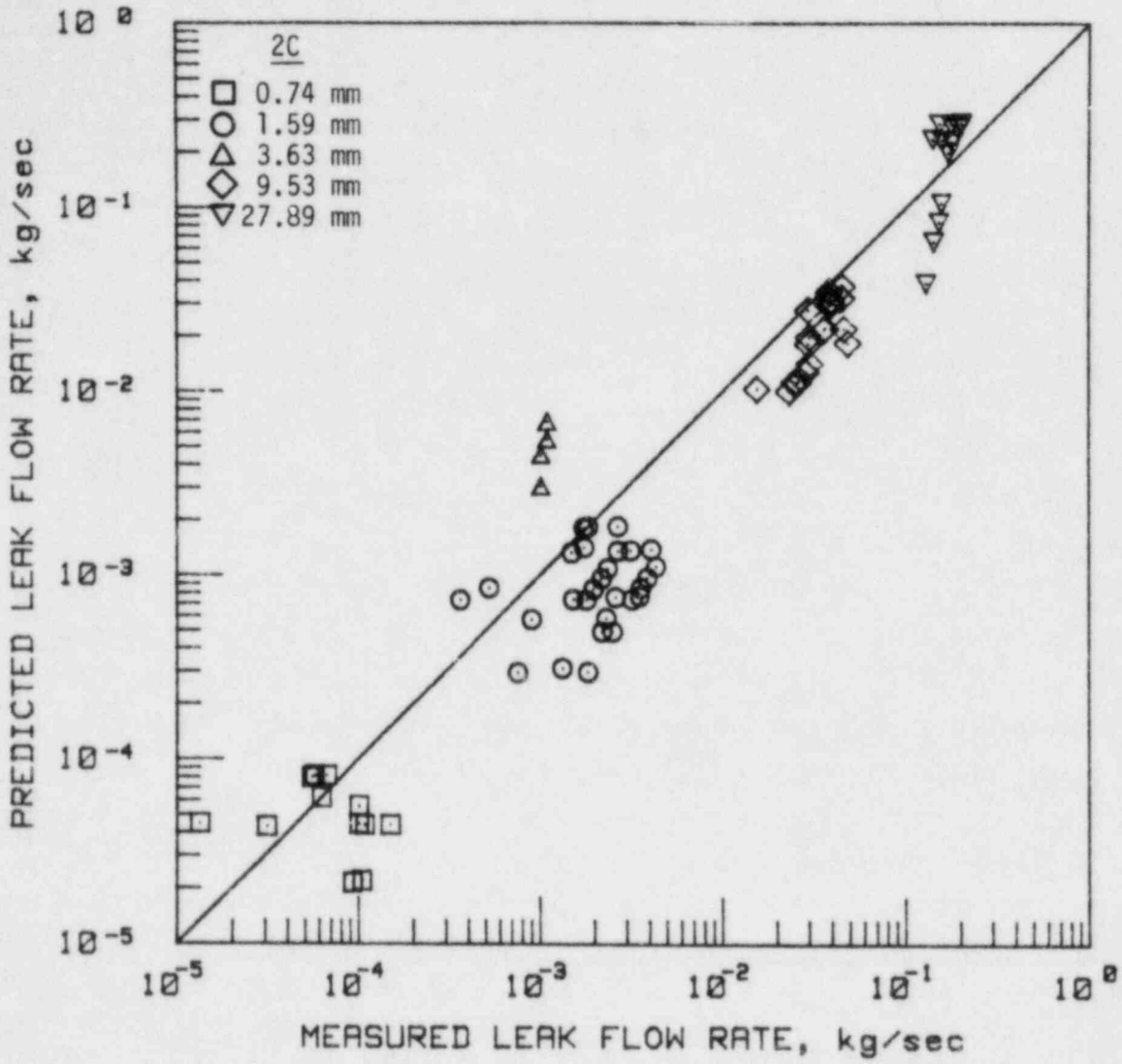

FIGURE 10. COMPARISON OF PREDICTED AND MEASURED LEAK FLOW RATE

The flow model requires flow area, number of equivalent bends in the flow path, surface roughness of the crack, and inlet area/outlet area ratio as input. In all cases shown in Figure 10, we assumed the exit flow area, COA, to be equal to the product of the crack length, 2C, and the crack-opening displacement, COD. The surface roughness was assumed to be 1.78 μm (7×10^{-5} in.), and six 45-degree turns in the flow path were assumed. The included convergence angle of the flow was assumed to be 90 degrees. These assumptions were consistent with the objective of developing a model which could be used in the reverse direction, that is to estimate flow area if leak flow rate were known. In such a case, simple, empirically validated relationships between 2C, COD, typical surface roughness, and area ratio for IGSCC's would have to be assumed.

Figure 11 presents flow rate data from run numbers 41-62 in more detail. This figure shows that the data tend to fall into groups, depending on test sequence. Within any one group, the data tend to show a linear relation between predicted and measured flow rate. One possible cause for this behavior would be partial plugging of the flow area by particulate, with a change in the amount of blockage between sequences. Thus, the flow area assumed in predicting the flow rate would be incorrect. To test this hypothesis, we adjusted the flow area for one point in each sequence to match predicted and measured leak flow rates. This area was then used to calculate a revised prediction for the other data points in the test sequence. The revised predictions for run numbers 41-62 are compared with measured results in Figure 12. Substantial improvement in agreement and reduction in data scatter is seen. Maximum reduction in flow area was by about 50 percent.

A Comment on Plugging

We believe partial plugging of cracks with particulate and the consequent reduction in leak flow rate for a given size crack should be considered for application of these data or the analytical model to reactor conditions.

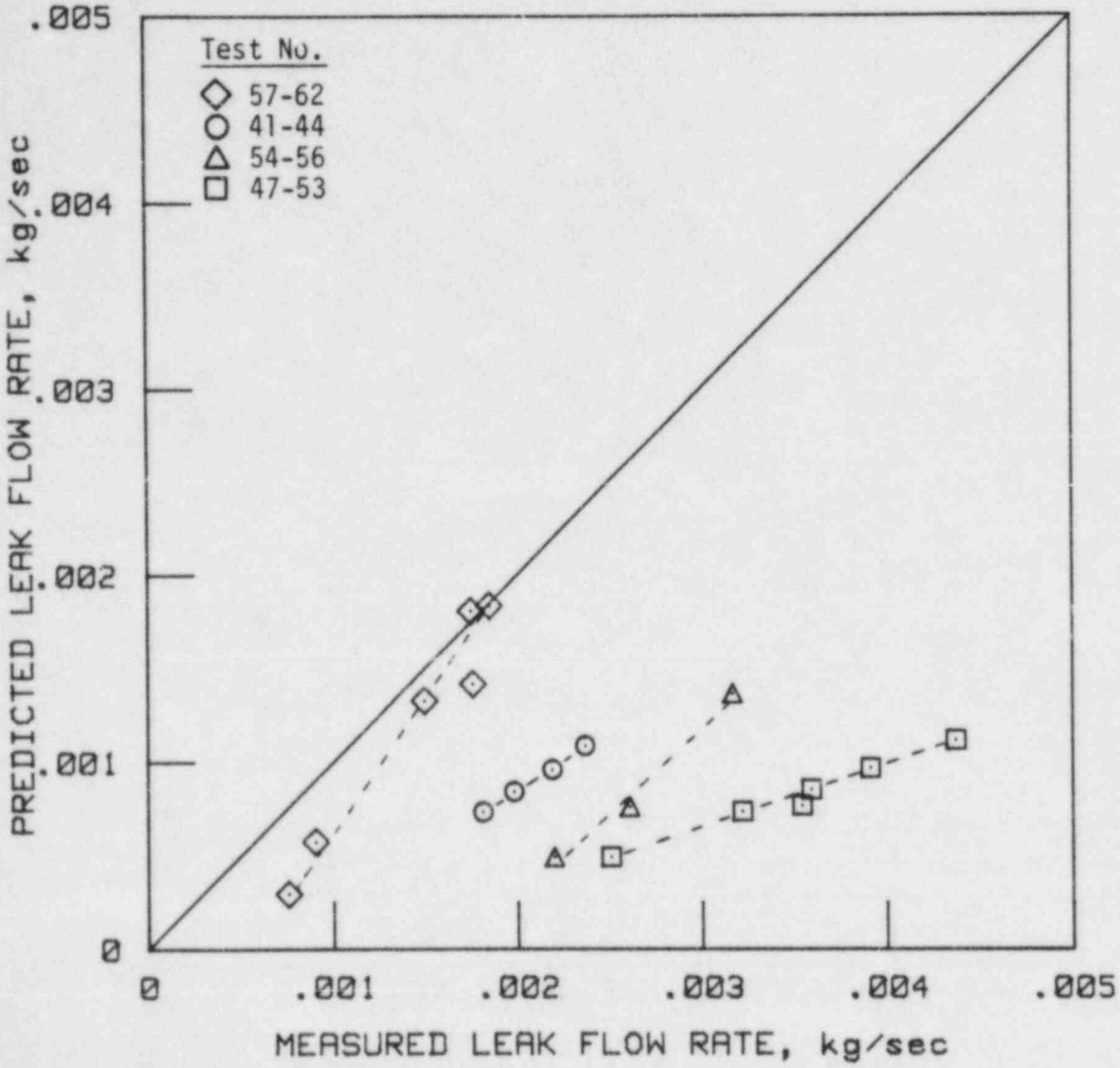

FIGURE 11. DETAILED COMPARISON OF PREDICTED AND MEASURED LEAK FLOW RATE

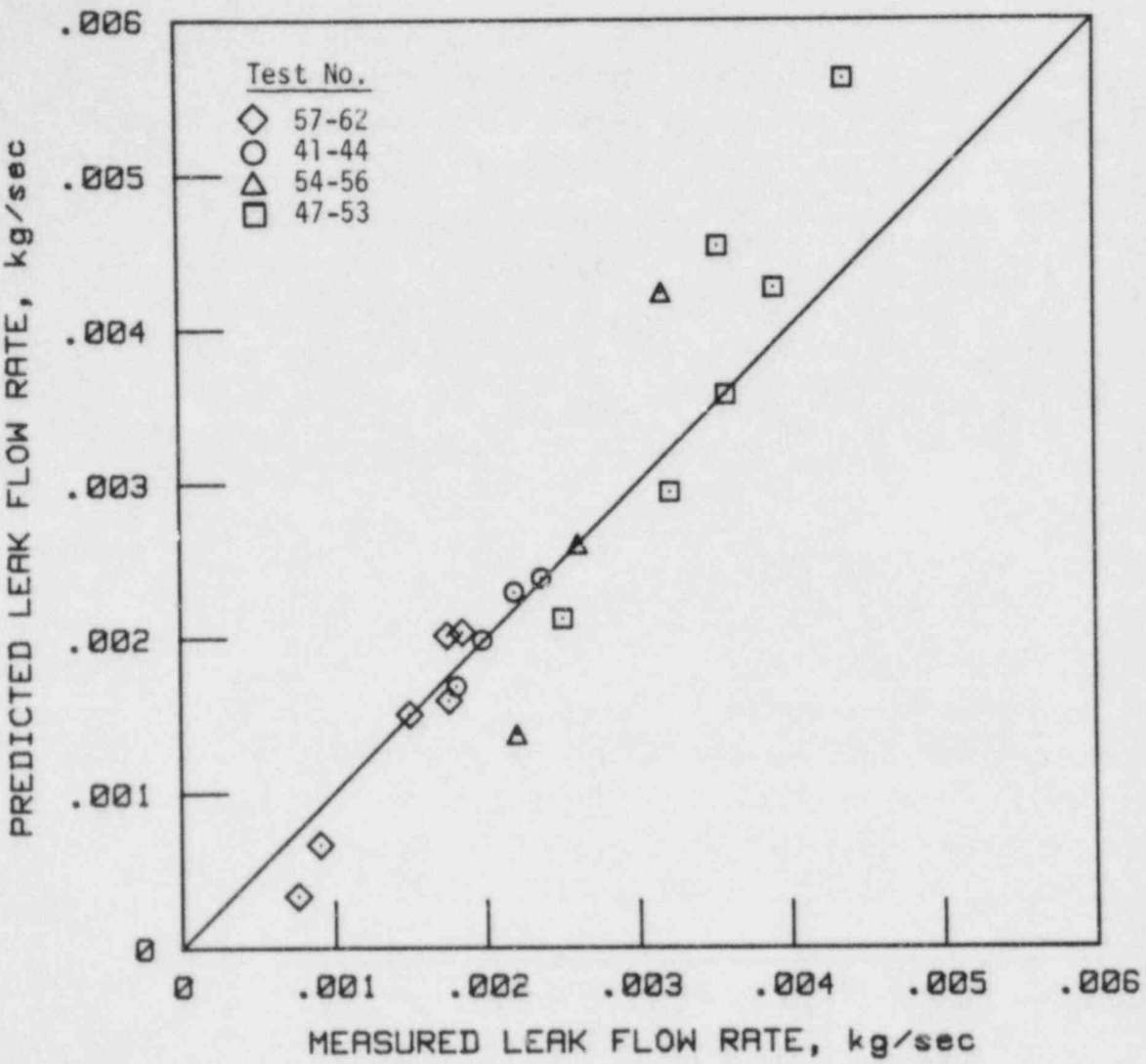

FIGURE 12. DETAILED COMPARISON OF REVISED PREDICTION AND MEASURED LEAK FLOW RATE

In this study, we used a commercial water supply system which delivered the equivalent of doubly-distilled water to the supply vessel. The water quality specifications for this purification system were similar to those typical of BWR's. The test facility was fabricated from both carbon and stainless steels and was purged with nitrogen, both during shutdown and operation. In addition to the variation in flow rate under otherwise fixed conditions, which suggested the possibility of partial plugging, we observed dark red, dark brown, and black deposits on the crack surfaces when we broke open one of the test vessels.

The effect of this partial plugging would be to reduce the flow area, and hence, leak flow rate for a given crack size. The calculations above indicate that a reduction in flow area of up to 50 percent, in a few instances, may have occurred in these experiments.

NOMENCLATURE

A	Flow area
C	Half crack length
COA	Crack Opening Area
COD	Crack Opening Displacement
D_h	Hydraulic diameter
f	Friction factor
G	Mass flux
L	Flow path length, or crack depth
P	Pressure
T	Temperature
W	Mass flow rate
κ	Roughness grain height

Subscripts

c	Critical or choked
e	Exit
o	Entrance or stagnation

REFERENCES

1. D. Abdollahian and D. M. Norris, "Prediction of Leak Rates through Intergranular Stress Corrosion Cracks", CSNI Special Meeting on Leak-Before-Break, Monterey, CA, September 1983.

2. M. E. Mayfield and R. P. Collier, "Leak-Before-Break Due to Fatigue Cracks in the Cold Leg Piping System", CSNI Special Meeting on Leak-Before-Break, Monterey, CA, September 1983.

3. G. B. Wallis, "Critical Two-Phase Flow", International Journal of Multiphase Flow, Vol. 6, 1980, pp 97-112.

4. H. S. Isbin, "Some Observations on the Status of Two-Phase Critical Flow Models", International Journal of Multiphase Flow, Vol. 6, 1980, pp 131-137.

5. J. A. Bourne, "The Critical Flow Phenomenon with Reference to Two-Phase Flow and Nuclear Reactor Systems", ASME Symposium on the Thermal and Hydraulic Aspects of Nuclear Reactor Safety, Vol. 1, 1977, pp 195-216.

6. J. Weisman and A. Tenter, "Models for Estimation of Critical Flow in Two-Phase Systems", Progress in Nuclear Energy, Vol. 2, 1978, pp 183.

7. K. H. Ardron and R. A. Furness, "A Study of the Critical Flow Models Used in Reactor Breakdown Analysis", Nuclear Engineering and Design, Vol. 39, 1976, pp 257-266.

8. P. Saha, "A Review of Two-Phase Steam-Water Critical Flow Models with Emphasis on Thermal Nonequilibrium", NUREG/CR-0417, Brookhaven National Laboratory, 1978.

9. B. L. Button, et al, "Gas Flow Through Cracks", Journal of Fluids Engineering, Vol. 100, 1978, pp 453-458.

10. A. Agostinelli and V. Salemann, "Prediction of Flashing Water Flow Through Fine Annular Clearances", ASME Transactions, Vol. 80, 1958, pp 1138-1142.

11. D. J. Ryley and G. J. Parker, "Two-Phase Critical Flow Through Suction Slots in Low Pressure Steam Turbine Blades", Journal of Mechanical Science, Vol. 10, 1968, pp 337-345.

12. R. J. Simoneau, "Two-Phase Choked Flow of Sub-Cooled Nitrogen Through a Slit", NASA Technical Memorandum, NASA TM X-71516, NASA Lewis Research Center, 1974.

13. R. E. Henry, "The Two-Phase Critical Discharge of Initially Saturated or Sub-Cooled Liquid", Nuclear Science and Engineering, Vol. 41, 1970, pp 336-342.

14. R. E. Henry and H. K. Fauske, "The Two-Phase Critical Flow of One-Component Mixtures in Nozzles, Orifices, and Short Tubes", Journal of Heat Transfer, Vol. 93, 1971, pp 179-187.

15. M. E. Mayfield, et al, "Cold Leg Integrity Evaluation - Final Report", NUREG/CR-1319, Battelle, Columbus Laboratories, 1980.

16. R. P. Collier, F. B. Stulen, M. E. Mayfield, and P. M. Scott, "Study of Critical Two-Phase Flow through Intergranular Stress Corrosion Cracks", EPRI Final Report in preparation.

PREDICTION OF LEAK RATES THROUGH INTERGRANULAR STRESS CORROSION CRACKS

D. Abdollahian
S. Levy Incorporated
Campbell, California

and

B. Chexal
D. M. Norris
Electric Power Research Institute
Palo Alto, California

ABSTRACT

The critical flow model developed at Battelle Columbus Laboratories, Ref. 1, and the computer program, LEAK, written to utilize this model were used to predict leak rates through simulated and actual intergranular stress corrosion cracks (IGSCC).

Following a review of the theoretical basis and the method of solution in LEAK, a set of modifications were suggested, and it was shown that the new model (LEAK-01) resulted in better agreement with experimental data. In addition, a simple model, based on homogeneous equilibrium assumptions, was developed which resulted in a closed form relation for the critical mass flux. The predictions using this simplified model, which is applicable for subcooled upstream conditions, were close to the predictions by the LEAK-01 code.

The critical flow model developed in this study is recommended for predicting the leak rates through IGSCC's. The simplified homogeneous equilibrium model is recommended for quick calculation if the upstream conditions are expected to remain in a subcooled state during the depressurization transient.

1. INTRODUCTION

The presence of cracks in BWR piping has attracted considerable attention because of safety considerations and the impact of cracks on plant availability. As part of the EPRI/BWR Owners Group sponsored program to study Intergranular Stress Corrosion Cracking (IGSCC) in BWRs, an experimental and analytical effort was carried out by Battelle Columbus Laboratories (BCL). The general objective of this program was the evaluation of acoustic emission (AE) techniques in leak detection and development of a relation between crack size and the flow rate through a tight crack. The experimental program consisted of testing simulated and actual cracks and measuring the leak rates and the acoustic spectra associated with the two-phase critical flow. An analytical critical flow model was used to predict the measured flow rates. The detail of the experimental facility and the results of this study can be found in Refs. 1, 2.

The objectives of the present study were to evaluate the BCL critical flow model and suggest recommendations for improving the modeling assumptions or calculational scheme. The original model was first used to reproduce BCL Phase I and Phase II predictions. The suggested improvements to this critical flow model are given in the next section. Due to the particular geometry and expected flow evolution in tight cracks, certain simplifying assumptions are justified. These assumptions were used to develop a simplified homogeneous equilibrium model as a quick check for the leak rates under subcooled upstream conditions.

For a given set of stagnation conditions, there is a maximum for the rate of flow of a compressible fluid through a pipe or an aperture which is generally called critical or choked flow rate. The flow through a crack connecting a high pressure reservoir to a low pressure environment is expected to be choked except for highly subcooled upstream conditions. The problem of critical flow for a single-phase fluid has been studied

extensively and flow rate can be predicted using single-phase compressible flow relations. For liquid upstream conditions, flow will be choked if liquid flashes within the flow path and a two-phase critical flow model should be used. The two-phase critical flow is different from its single-phase counterpart due to the influence of two characteristics, namely, slip and thermal non-equilibrium between the phases. The degree of slip and non-equilibrium is dictated by the thermodynamic stagnation conditions and geometry of the fluid flow path. Generally, these phenomena are introduced in the critical flow models through empirical relations developed for specific geometries and fluid conditions. Therefore, there are numerous models each of which is applicable to a particular geometry. Their range of applicability to different conditions depend on the detail of the governing equations used for development of the model and the degree of empiricism used for the interfacial transfer terms.

Selection of an appropriate model for prediction of critical flow through a crack depends on the fluid conditions and size of the crack. For tight cracks, where the pipe wall thickness is of the same order of magnitude or larger than the crack opening size, the detail of the flow within the pipe wall has to be studied. Generally, the ratio of flow path length to a characteristic opening dimension, L/D, is used to specify the degree of slip and thermal non-equilibrium. Except for the recent studies at Battelle Columbus Laboratories, Refs. 1, 2, no experimental or analytical work for critical flow through such tight cracks (crack width of less than 1 mm) was found in the literature. Due to the complicated geometry within the flow path, some approximations and empirical factors enter the model which can only be confirmed by comparison against test data.

The experimental program carried out at BCL was aimed at generating a data base for confirming the critical flow models in predicting the leak rates through cracks. These tests included simulated cracks in which the major parameters, namely, crack size, L/D, upstream conditions and sur-

face roughness were varied in a controlled manner. The BCL Phase II experiments were performed on two stainless steel pipes which contained approximately 90% through-the-wall circumferential cracks. In these tests a portion of the pipe surface was removed to expose the tip of the IGSCC and progressively wider cuts resulted in the variation of the L/D parameter.

In the present study, the LEAK model developed at BCL was used to reproduce the predictions for the above data. A collection of steam property subroutines was attached to the program; corrections to coding and method of solution was made; and the revised predictions were compared to the test results. The version of LEAK used to generate the reported predictions, the modifications made to the method of solution, and the predictions are presented in the next sections.

2. DESCRIPTION OF THE CRITICAL FLOW MODEL IN LEAK AND COMPARISON WITH DATA

Henry's homogeneous non-equilibrium critical flow model (3) was developed for subcooled and saturated liquid discharge through sharp-edged ducts. The flow is assumed to be homogeneous and the non-equilibrium effects are introduced through one parameter, N, which is a function of equilibrium quality and the flow path length to diameter ratio. The critical flow model in the LEAK code uses the same assumptions but includes friction and acceleration pressure drops within the flow path. The detail of this model is given in Refs. 1 and 4 and following is a brief description of the modeling assumptions.

The general features of the discharge of initially subcooled or saturated liquid through a crack are shown in Figure 1 and the configuration of a convergent crack is shown in Figure 2. For this type of geometry a hydraulic diameter, D, is defined as

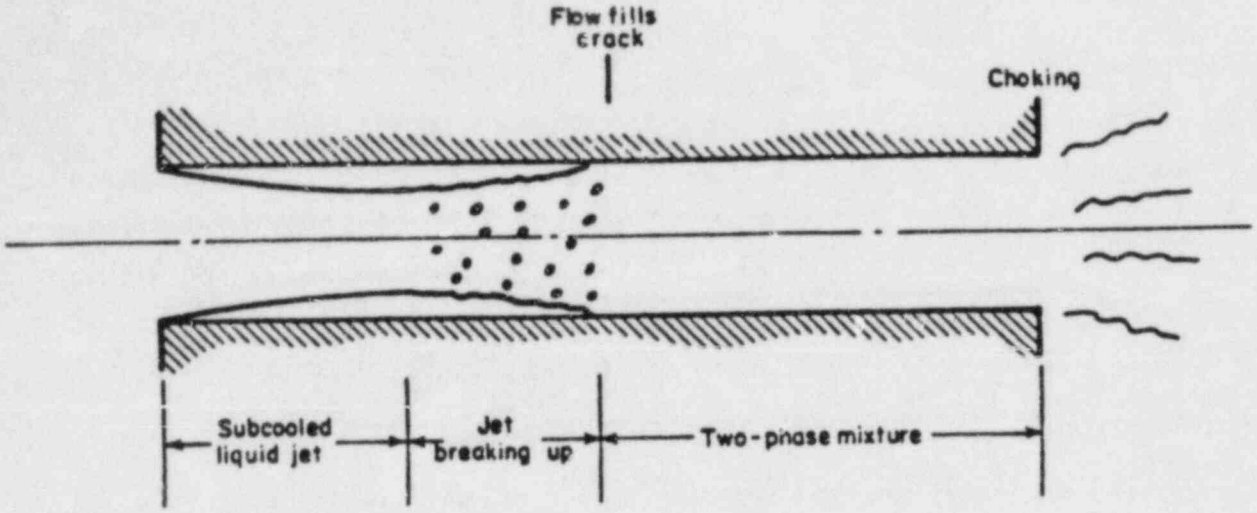

Figure 1 Two-Phase Flow Through a Long, Narrow Crack

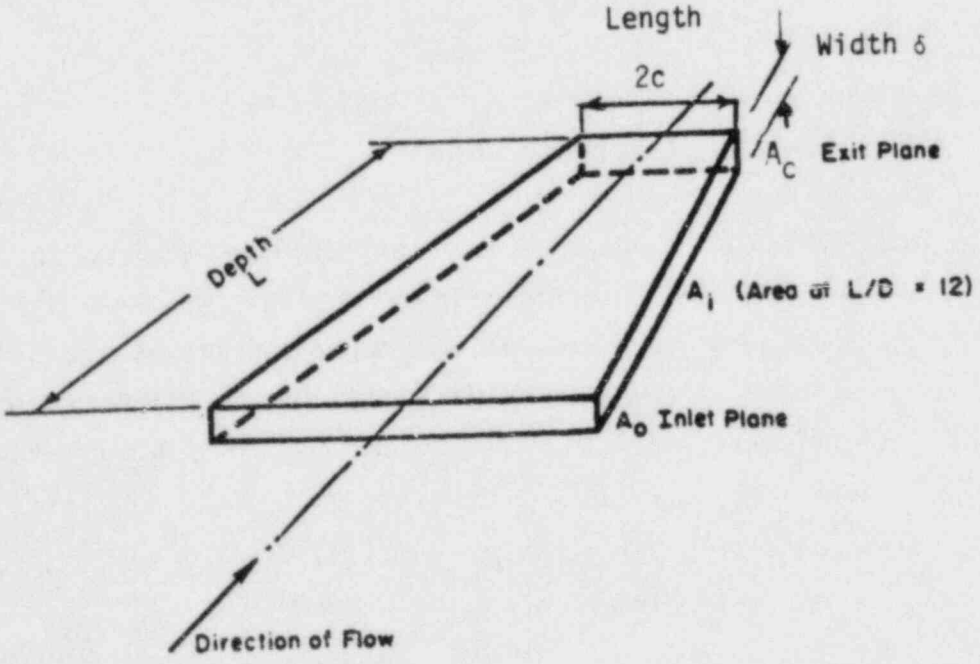

Figure 2 Geometry of a Convergent Crack

$$D = 4 \frac{A}{Pe}$$

A = Crack opening area = $2c\delta$

Pe = Opening perimeter = $2\ (2c + \delta)$

In the region $0 < L/D < 3$, a liquid jet surrounded by a vapor annulus is formed. For lengths between $L/D = 3$ and $L/D = 12$ the liquid jet breaks up into droplets at the surface, and small bubbles are entrained within the jet. It is assumed that no mass or heat transfer takes place between entrance and $L/D = 12$, and also the friction pressure drop in this region is negligble.

The one dimensional mixture mass and momentum conservation equations are used to evaluate the pressure drop components as follows:

Continuity:

$$\frac{dG}{dZ} + \frac{G}{A}\frac{dA}{dZ} = 0 \qquad (1)$$

Momentum:

$$-\frac{dP}{dZ} = \frac{1}{g_c}\left[\frac{1}{A}\frac{d}{dz}\left(\frac{G^2A}{\rho'}\right)\right] + \frac{f}{2D}\frac{G^2}{\rho_m} \qquad (2)$$

ρ' is the momentum density which is equal to mixture density, ρ_m for homogeneous flow assumption. The first term on the right hand side of the momentum equation is the acceleration pressure drop and the second term is the friction pressure drop. The acceleration pressure can be expanded into the component due to area changes and the component due to phase change.

$$\frac{1}{A}\frac{d}{dZ}\left(\frac{G^2A}{\rho_m}\right) = \frac{G^2}{\rho_m} A \frac{d}{dZ}\left(\frac{1}{A}\right) + G^2 \frac{d}{dZ}\left(\frac{1}{\rho_m}\right)$$

Equation 2 can be integrated along the flow path to evaluate the overall pressure drop across the crack as the sum of pressure drop components.

$$\Delta P_{total} = \Delta P_e + \Delta P_{ae} + \Delta P_{aa} + \Delta P_f \tag{3}$$

ΔP_e = Entrance pressure loss

$$\Delta P_e = \frac{G_c^2 v_{\ell o}}{2C^2} \left(\frac{A_c}{A_o} \right)^2 \tag{4}$$

where C is the orifice contraction coefficient, assumed to be 0.61.

ΔP_{ae} = Acceleration pressure drop due to phase change.

$$\Delta P_{ae} = \overline{G^2} \left[x_c \left(v_{gc} - v_{\ell o} \right) \right] \tag{5}$$

where $\overline{G^2}$ is the average mass flux defined below

$$\overline{G^2} = \frac{G_i^2 + G_c^2}{2} = \frac{G_c^2}{2} \left[1 + \left(\frac{A_c}{A_i} \right)^2 \right]$$

ΔP_{aa} = Acceleration pressure drop due to area change

$$\Delta P_{aa} = \frac{G_c^2}{2} \left[v_{\ell o} \left(1 - \frac{A_c^2}{A_i^2} \right) + \overline{x} \left(\overline{v}_g - v_{\ell o} \right) \left(1 - \frac{A_c^2}{A_i^2} \right) \right] \tag{6}$$

where the average quality and vapor specific volume are defined as:

$$\overline{x} = \frac{\int_{12D}^{L} x \, dZ}{L - 12D} \qquad \overline{v}_g = \frac{v_{gc} + v_{gi}}{2}$$

ΔP_f = Friction pressure drop

$$\Delta P_f = f\left(\frac{L}{D} - 12\right) \frac{\overline{G^2}}{2} \left[(1 - \overline{x}) v_{\ell o} + \overline{x}\, \overline{v}_g\right] \tag{7}$$

f is the friction factor and is calculated from the modified Von Karman relation given below where K is the average roughness height.

$$f = \frac{1}{\left(2 \log \frac{D}{2K} + 1.74\right)^2}$$

The pressure at the exit is a function of the critical mass flux, G_c

$$P_c = P_o - \Delta P_{total} = f\,(G_c) \tag{8}$$

The critical mass flow relation developed by Henry (3) for homogenous flow is used here. This relation was developed from liquid and vapor mass conservation and mixture momentum equation and is given below

$$G_c^2 = -\left[x \frac{dv_g}{dP} + (v_g - v_\ell) \frac{dx}{dP} \right]_c^{-1} \tag{9}$$

The subscript c indicates that all the enclosed parameters are evaluated at the critical section. The vapor compressibility term is calculated from ideal gas relation with isentropic assumption

$$\frac{dV_g}{dP} = -\frac{1}{\gamma} \frac{v_g}{P}$$

The nonequilibrium mass transfer rate is calculated from the correlation developed by Henry for constant area ducts

$$\frac{dx}{dP} = N \frac{dx_E}{dP} \tag{10}$$

$$N = 20\, x_E \quad \text{if } x_E < 0.05$$

$$N = 1.2 \qquad \text{if } x_E > 0.05$$

x_E is the equilibrium quality calculated from

$$x_E = \left[\frac{S_o - S_\ell}{S_g - S_\ell} \right]_E$$

The quality relation given by equation (10) and the assumption of isentropic expansion for vapor are used to simplify the mass flux relation to

$$G_c^2 = \left[x \frac{v_g}{\gamma P} - (v_g - v_{\ell o}) N \frac{dx_E}{dP} \right]_c^{-1} \tag{11}$$

The quality for a long tube is given by $x_{LT} = N x_E$ and it is assumed that within the length of the crack the quality approaches the long tube value in an exponential manner correlated as

$$dX = 0.0523 (x_{LT} - x) d \left(\frac{Z}{D} - 12\right)$$

$$x_c = x_{LT} \{ 1 - \exp [-0.0523 (L/D - 12)] \} \tag{12}$$

For given stagnation conditions and crack geometry, the leak rate and exit pressure can be evaluated by iterative solution of equation 8 and 11.

For situations where the flow is not choked, the leak rate is calculated from single phase relations with friction included:

$$G = 2g_c \sqrt{\frac{P_o - P_B}{v_o}}$$

The LEAK code which contained the critical flow model described above was used to predict the flow rates for the BCL experiments. A set of steam

property subroutines which consisted of RETRAN-02 Ref. 6, fits to 1967 ASME tables Ref. 7 and other exact fits to the steam tables were added to the code. Predicted versus measured flow rates for simulated cracks are shown in Figure 3.

For the IGSCC's an exit to entrance area ratio had been approximated by measuring the slope of crack covergence following the phase II tests. The surface roughness used for IGSCC's was 1.78 μm which actually corresponds to a relatively smooth surface but the flow path was assumed to contain six 45 degree turns. The predictions using LEAK are compared to the Phase II experimental flow rates in Figures 4 and 5. The large deviations from measured values as shown in Figure 4 are better presented in Figure 5 where the ratio of predicted to measured flow rates for IGSCC's are shown against the measured leak rates. The variation of this ratio demonstrates that for the complicated flow path geometries of actual IGSCC's the model can best predict the order of magnitude of the experimental results.

Study of the reported leak rates for phase II tests showed trends contrary to those expected under critical flow conditions. Partial plugging of the cracks has been reported in Ref. 2 which can be the reason for the erroneous trends of mass flow rate and the deviations shown in Figures 4 and 5.

3. MODIFICATIONS TO THE LEAK CODE

Following a review of the assumption in the LEAK Code and the characteristics of flow through tight cracks, several areas which required improvements were recognized. Modifications were made to improve both the theoretical basis and the method of solution in the code. These modifications are listed below and incorporated in LEAK-01 computer code.

1. Isenthalpic rather than isentropic flow evolution should be used for the pressure drop calculations. Since the non-equilibrium

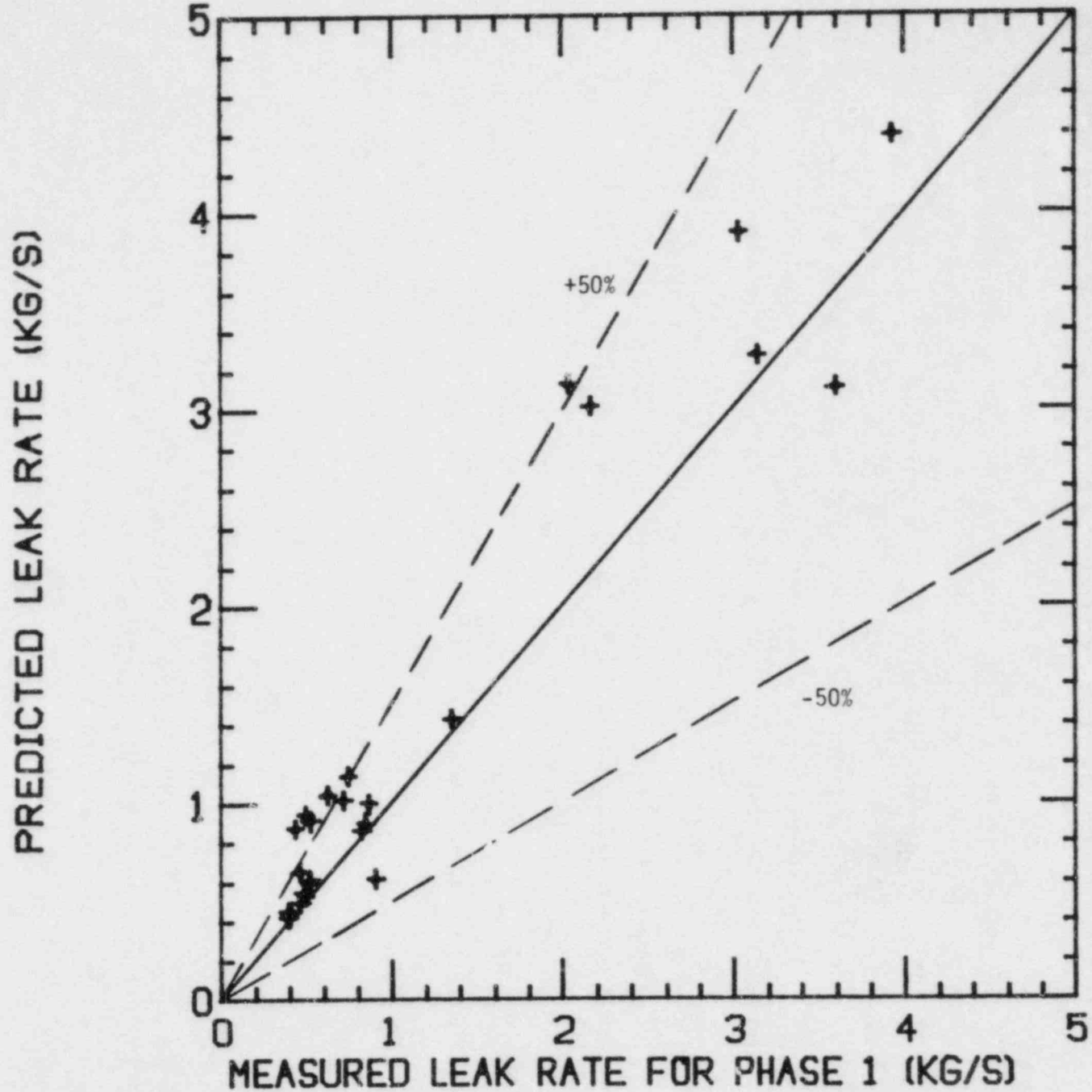

Figure 3 Comparison of Mass Flow Rate Predictions Using LEAK with Measured Flow Rates Through Simulated Cracks

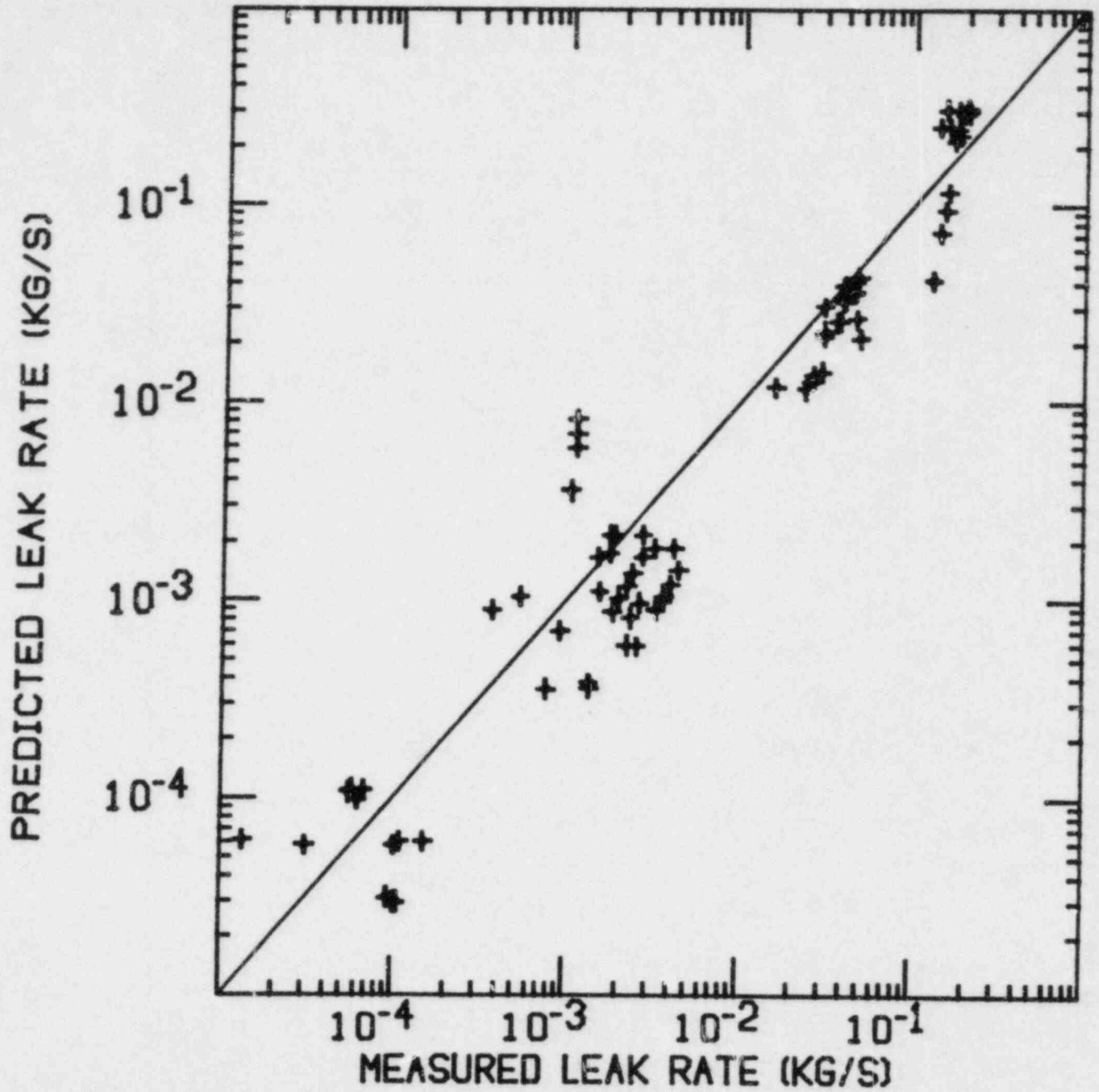

Figure 4 Comparison of Mass Flow Rate Predictions Using LEAK with Measured Flow Rates Through IGSCC's

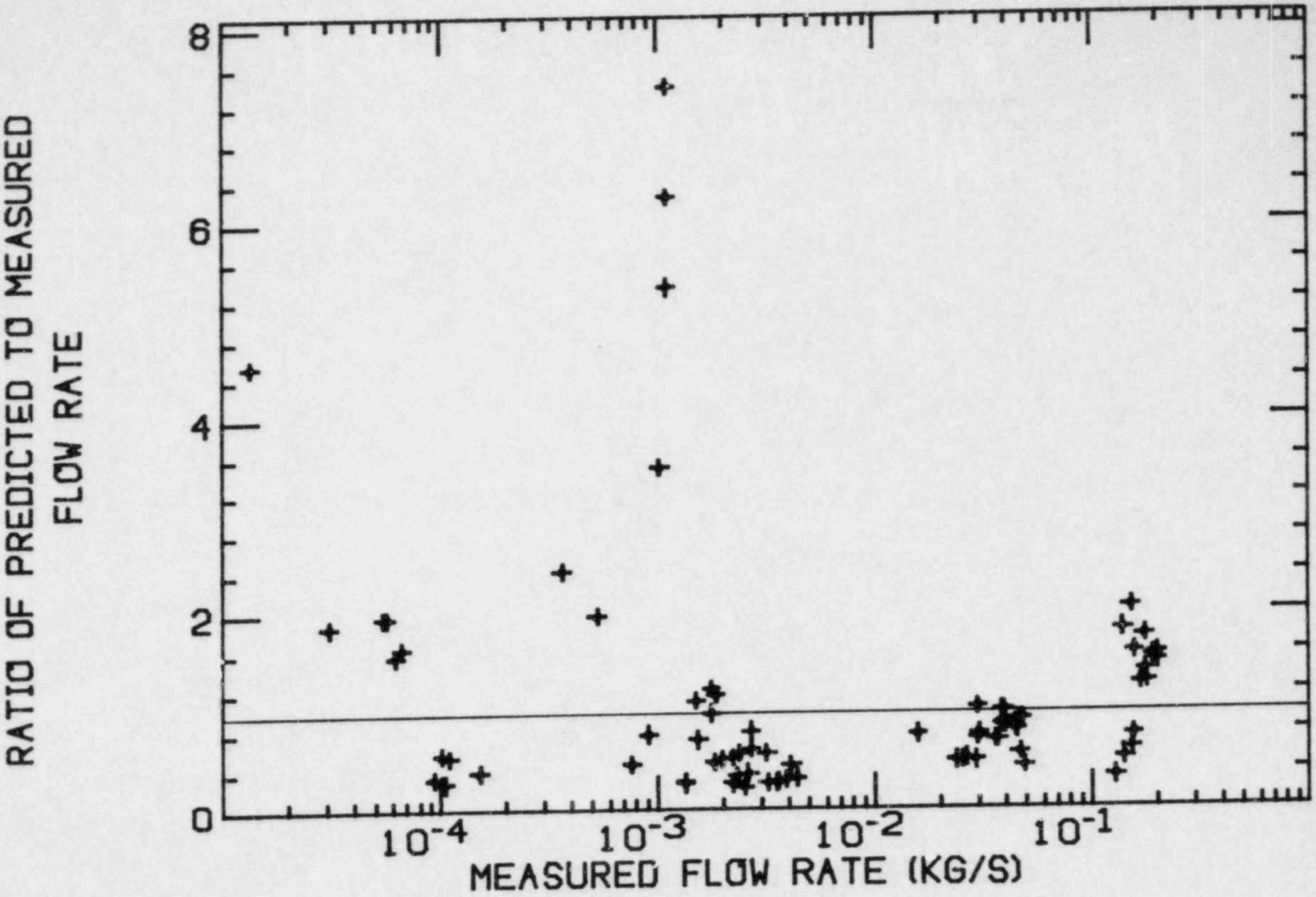

Figure 5 Ratio of Predicted to Measured Mass Flow Rate Using LEAK for Battelle IGSCC Tests

parameter in Henry's model was developed empirically based on isentropic equilibrium quality, the same quality was used in the mass flux equation. All the other terms needed for pressure drop evaluations were calculated based on isenthalpic assumption.

2. The average mass flux between sections 1 and 2 was defined in LEAK as

$$\overline{G^2} = \frac{G_1^2 + G_2^2}{2} = \frac{G_2^2}{2}\left[1 + \left(\frac{A_2}{A_1}\right)^2\right]$$

This average mass flux was used to simplify the integration of differential pressure loss terms.

Since a linear area variation along the flow path is assumed, it is more appropriate to derive an average mass flux consistent with this assumption as follows:

$$\overline{G^2} = \frac{1}{Z_2 - Z_1} \int_{Z_1}^{Z_2} G^2 \, dZ$$

$$= \frac{G_2^2 A_2^2}{Z_2 - Z_1} \int_{A_1}^{A_2} \frac{1}{A^2} \frac{dZ}{dA} \, dA$$

$$\frac{dA}{dZ} = \frac{A_2 - A_1}{Z_2 - Z_1}$$

$$\overline{G^2} = G_2^2 \frac{A_2}{A_1} = G_1^2 \frac{A_1}{A_2}$$

3. The single phase friction pressure drop in LEAK is neglected and the two phase pressure drop is calculated by assuming a constant specific volume for liquid. The overall friction pressure drop is modified as follows:

$$\frac{dP}{dZ} = \frac{f}{2D} G^2 v_m$$

$$\Delta P_f = \int_0^{12D} \frac{f}{2D} G^2 v_{\ell_o} dZ + \int_{12D}^{L} \frac{f}{2D} G^2 [v_\ell + x(v_g - v_\ell)] dZ$$

$$= \frac{12}{2} f \overline{G_1^2} v_{\ell_o} + \frac{f (L/D-12)}{2} \overline{G_2^2} [\overline{v}_\ell + \overline{x} (\overline{v}_g - \overline{v}_\ell)]$$

$\overline{G_1^2}$ and $\overline{G_2^2}$ are the averages of G^2 between entrance and L=12D, and L=12D and exit respectively. According to the averaging method described above they became:

$$\overline{G_2^2} = \overline{G_c^2} \frac{A_c}{A_i}$$

$$\overline{G_1^2} = G_i^2 \frac{A_i}{A_o} = \frac{G_c^2 A_c^2}{A_i A_o} = G_c^2 \frac{A_c}{A_i} \frac{A_c}{A_o}$$

$$\frac{A_i}{A_c} = [1 - \frac{12}{L/D} (1 - \frac{A_c}{A_o})] \frac{A_o}{A_c}$$

$\bar{v}_\ell$ and $\bar{v}_g$ are the average specific volumes evaluated at an average pressure

$$P_{AVG} = \frac{P_o - \Delta P_e + P_c}{2}$$

where ΔP_e is the entrance pressure loss. The average quality, x, is calculated from isenthalpic assumptions as follows

$$\bar{x} = \frac{h_o - (h_f)_{P_{AVG}}}{(h_{fg})_{P_{AVG}}}$$

4. The acceleration pressure drop is calculated from the following relation

$$\Delta P_{ae} = \int_o^L G^2 \frac{dv_m}{dZ} \, dZ$$

$$\Delta P_{ae} = \overline{G_1^2} \left[v_\ell + x(v_g - v_\ell)\right]_o^i + \overline{G_2^2} \left[v_\ell + x(v_g - v_\ell)\right]_i^c$$

$$= \overline{G_2^2} \left[v_{\ell c} + x_c \, (v_{gc} - v_{\ell c}) - v_{\ell o}\right]$$

5. The acceleration pressure drop due to area changes is evaluated as given below:

$$\Delta P_{aa} = - \int_{A_o}^{A_c} G^2 \, v_m \, \frac{dA}{A}$$

$$= - G_c^2 A_c^2 \int_{A_o}^{A_i} \frac{v_{\ell o}}{A^3} \, dA - G_c^2 A_c^2 \int_{A_i}^{A_c} \frac{v_m}{A^3} \, dA$$

$$= \frac{G_c^2 v_{\ell o}}{2} \left[\left(\frac{A_c}{A_i}\right)^2 - \left(\frac{A_c}{A_o}\right)^2 \right] + \frac{G_c^2}{2} \left[\overline{v}_\ell + \overline{x}(\overline{v}_g - \overline{v}_\ell) \right] \left(1 - \frac{A_c^2}{A_i^2}\right)$$

6. The method of solution in LEAK consisted of an iterative search for a critical pressure to satisfy equations 8 and 11. The iteration started from back pressure and the no choke situation was encountered when no solution was found or in case of abnormal program termination. The method of solution was changed to start the iteration from saturation pressure corresponding to the upstream temperature. The no choke situation was encountered when the critical pressure was lowered to the back pressure without finding a solution for the critical mass flux.

   The equation used for calculating the leak rate with no choking was changed to account for entrance and single phase friction losses as follows:

$$G_c = \sqrt{2g_c \frac{(P_o - P_B)}{V_o \left(1 + \frac{1}{C^2} + f\frac{L}{D}\right)}}$$

In view of the experimental trends observed fir the BCL phase II test results, it is more appropriate to evaluate the predictive capability of the critical flow models against the controlled experiments of phase I. The selected model can then be used to approximate the flow rates through IGSCC's. The leak rate predictions for the simulated cracks using the above model are shown in Figure 6. In comparison to LEAK predictions, Figure 3, the new model results in better agreement with data and it is recommended for calculating the flow rates through IGSCC's.

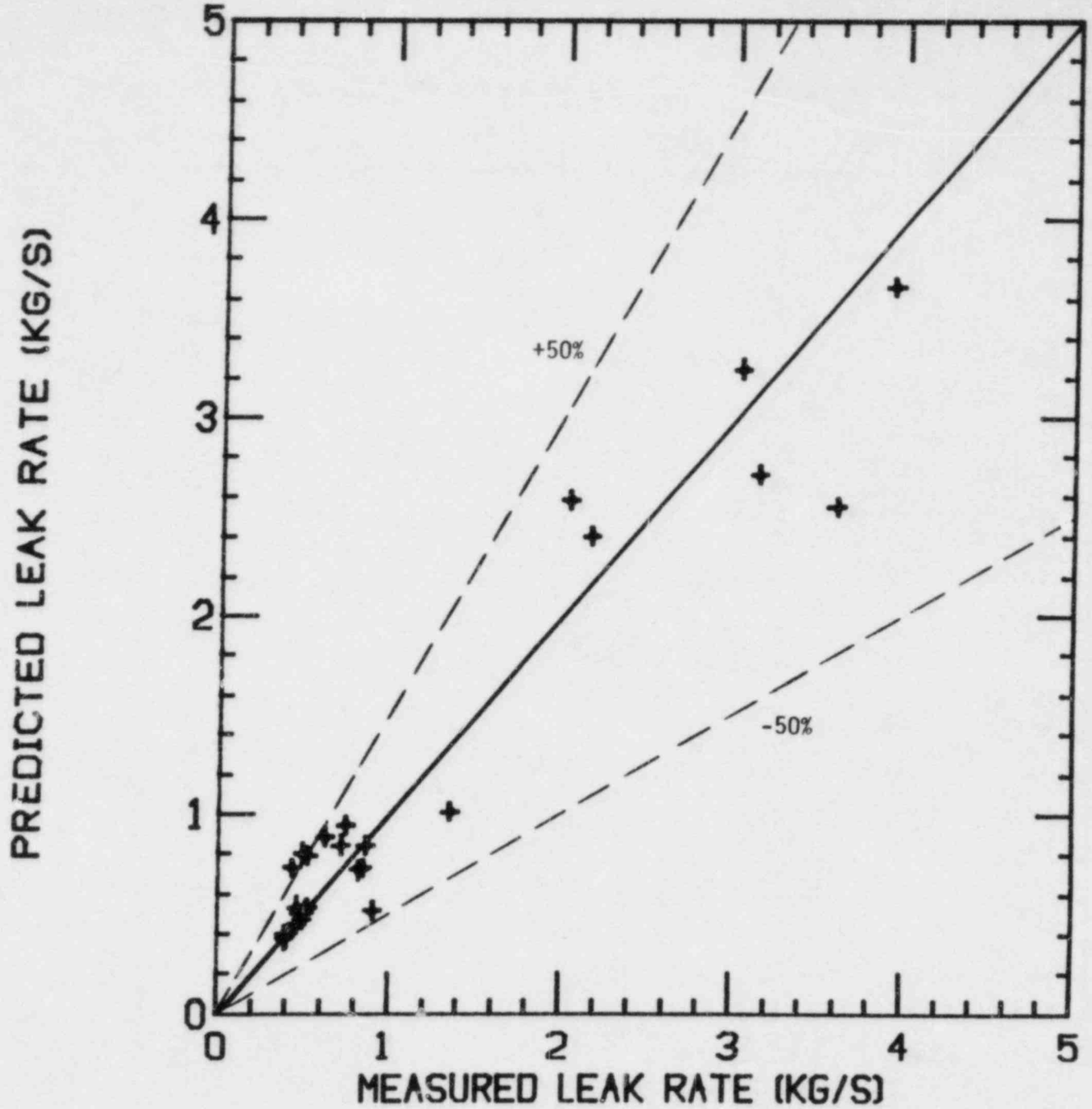

Figure 6 Comparison of Mass Flow Rate Predictions Using LEAK-01 with Measured Flow Rates Through Simulated Cracks

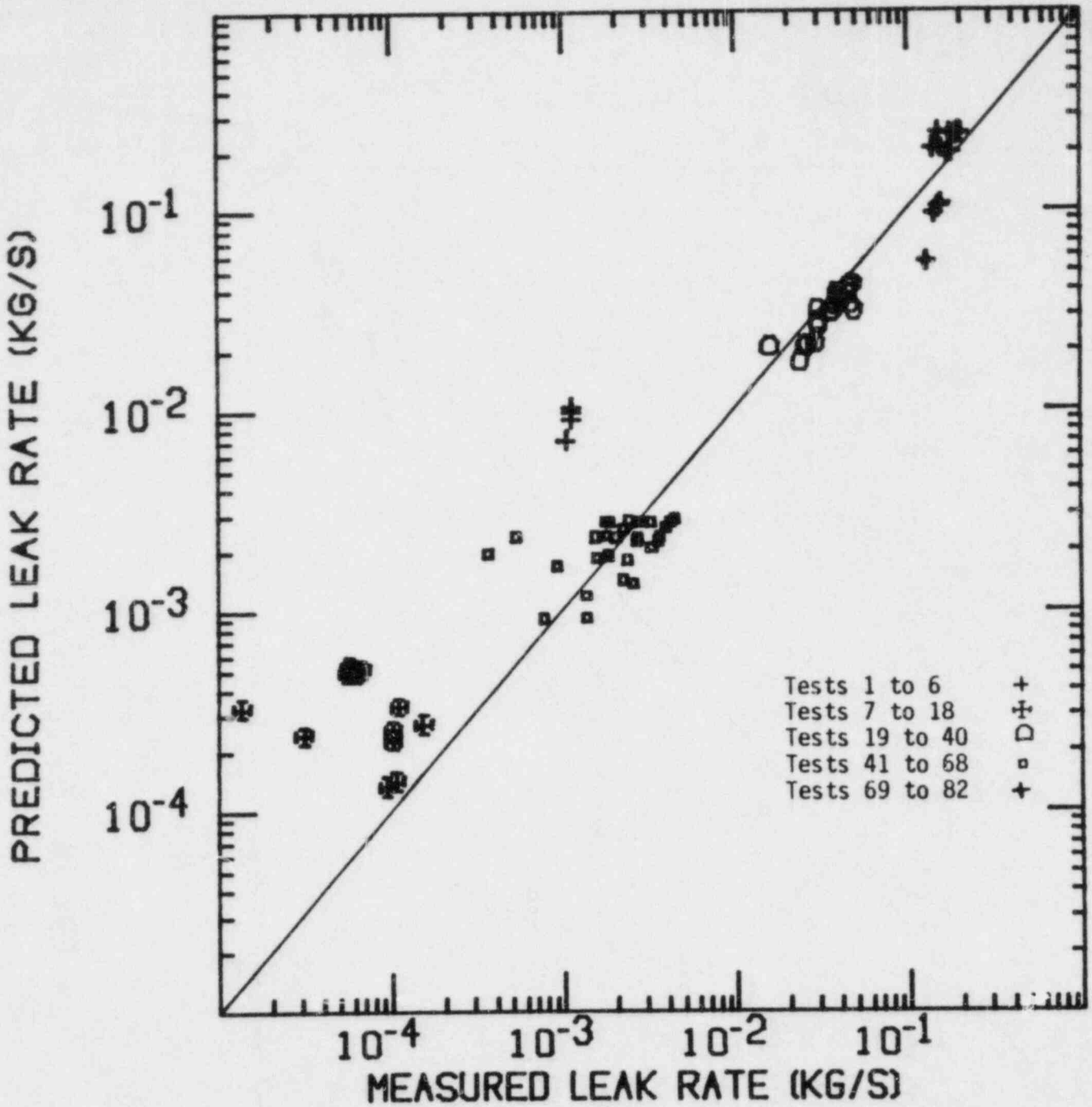

Figure 7 Comparison of Mass Flow Rate Predictions Using LEAK-01 with Measured Flow Rates Through IGSCC

As mentioned earlier, the model requires the detail of flow path geometry for calculating the pressure losses. During the BCL phase II tests, the pipes were destructively tested and the flow path was approximated to contain six 45 degree turns. A very smooth surface was assumed for the crack walls to calculate the friction pressure drop. In LEAK-01, a crack wall surface roughness of K=0.0002 in was used and the flow path was assumed to contain twenty 45 degree turns. The number of turns was selected to give the best agreement for phase II results and can be used as a guideline for predicting leak rates through IGSCC's when using LEAK-01. Figure 7 shows that LEAK-01 results in good agreement with measured leak rates for tests 19 to 81. The leak rates for very narrow cracks (tests 7 to 18, δ = .02 mm) are overpredicted. In view of the possibility of partial plugging (Ref. 2) which is more probable for narrower cracks this overprediction is plausible.

4. A SIMPLIFIED MODEL FOR SUBCOOLED UPSTREAM CONDITIONS

It is known that the two-phase flow, following a sudden depressurization, will approach the homogeneous and equilibrium conditions if the channel is long enough. Generally, the ratio of flow path length to hydraulic diameter (L/D) is used as the parameter to specify the degree of slip and thermal non-equilibrium. Different values for the characteristic L/D beyond which homogeneous equilibrium assumptions can be made have been reported in the literature. These values vary from 1.5 for reactor scale pipe breaks (Ref. 5) to 25 for 4 mm diameter tubes with sharp entrance geometry. The length to diameter ratio for tight cracks is expected to be larger than 25 and the flow can be assumed to be homogeneous and in equilibrium condition.

An attempt was made to use homogeneous equilibrium critical flow model (HEM) with both isentropic and isenthalpic assumptions for the flow evolution. In both cases the predicted critical pressure for subcooled upstream conditions was very close to saturation pressure corresponding to upstream temperature. Assuming

$$P_c \approx P_{sat}\ (T_o)$$

and considering only entrance and friction losses, the critical mass flux can be obtained from the following relations

$$P_o - P_c = P_o - P_{sat}\ (T_o) = f \frac{L}{D} \frac{G_c^2}{2} v_m + \frac{G_c^2 v_o}{2C^2} + \frac{G_c^2 v_m}{2}$$

$$G_c = \left\{ \frac{2[P_o - P_{sat}(T_o)]\, g_c}{v_m + v_m f \frac{L}{D} + \frac{v_o}{C^2}} \right\}^{1/2}$$

where

$$C = 0.61$$

$$v_m = \bar{v}_\ell + x\ (\bar{v}_g - \bar{v}_\ell)$$

$\bar{v}_\ell$ and $\bar{v}_g$ are the liquid and vapor specific volumes at

$$P_{AVG} = \frac{P_o + P_{SAT(T_o)}}{2}$$

and x is the isenthalpic quality at P_{AVG} i.e.,

$$x = \frac{h_o - h_f\ (P_{AVG})}{h_{fg}\ (P_{AVG})}$$

The predictions using this simplified homogeneous equilibrium model for phase I Battelle tests are shown in Figure 8 where very good agreement with data is obtained. This is a simplified closed form relation and does not require detail of flow path geometry. It can be used for quick calculation of leak rates under subcooled upstream conditions. The predictions for phase II BCL tests using a friction factor calculated for a very rough surface ($\frac{D}{2k} = 5$) are shown in Fig. 9.

Figure 8 Comparison of Mass Flow Rate Predictions Using Simplified Homogeneous Equilibrium Model With Measured Flow Rates Through Simulated Cracks

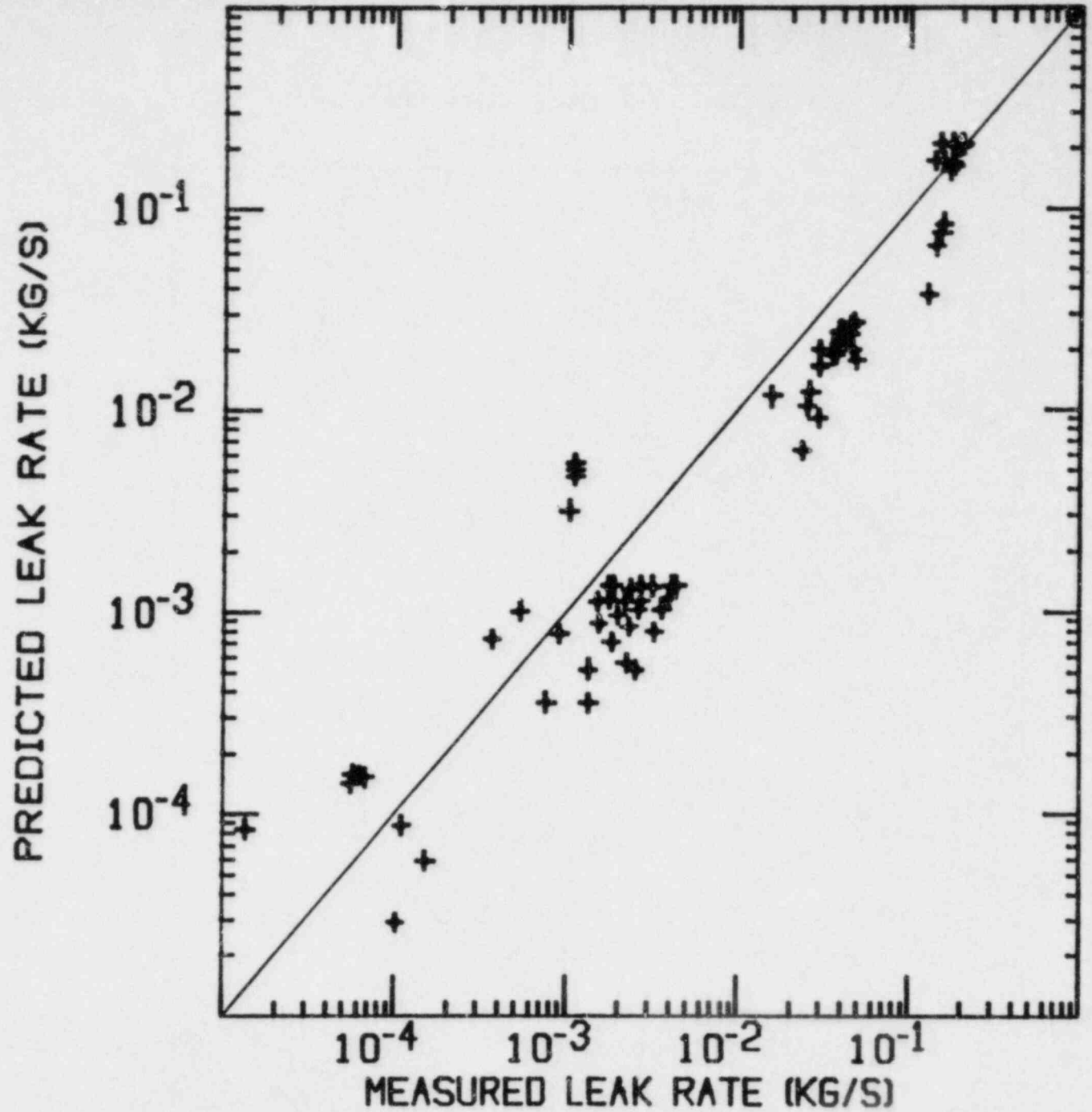

Figure 9 Comparison of Mass Flow Rate Predictions Using Simplified Homogeneous Equilibrium Model with Measured Flow Rates Through IGSCC's

5. CONCLUSIONS

The critical flow model used in the LEAK code was reviewed and the predictions of flow rate for Battelle test results were compared to the reported predictions. Study of the IGSCC data showed some inconsistencies which could have been a result of flow blockage during the tests. The critical flow models can at best predict an order of magnitude for this type of data. Several modifications, to the theoretical basis and the method of solution in LEAK were made and the new model, LEAK-01, showed better agreement with leak rates through simulated cracks. A simplified homogeneous equilibrium model which reduced to a closed form relation applicable for subcooled upstream conditions was developed. This model resulted in very good agreement with Battelle test results.

The critical flow model contained in LEAK-01 is recommended for predicting the leak rates through IGSCC's. When the detail of flow path is not known the surface roughness of a commercial steel pipe with a flow path containing 15 turns can be used. If the upstream conditions during depressurization transient is expected to remain in subcooled state, the simplified HEM relation can be use for predicting the leak rates.

NOMENCLATURE

A	Crack Opening Area, Cross Sectional Area
C	Entrance Loss Coefficient
D	Hydraulic Diameter
f	Friction Factor
g_c	Gravitational Acceleration
G	Mass Flux
h	Enthalpy
k	Average Roughness Height
L	Length
N	Non-Equilibrium Parameter
Pe	Perimeter
P	Pressure
P_B	Back Pressure
ΔP_e	Entrance Pressure Loss
ΔP_{ae}	Acceleration Pressure Loss
ΔP_{aa}	Area Change Pressure Loss
ΔP_f	Friction pressure Loss
S	Entropy
T	Temperature

v	Specific Volume
x	Quality
Z	Axial Length
ρ	Density
γ	Isentropic Exponent
δ	Width

Subscripts

o	Stagnation, Entrance
c	Critical Section
i	Section of L=12D
ℓ	Liquid
g	Vapor
m	Mixture
AVG	Average
Sat	Saturation

REFERENCES

1. R. P. Collier, J. S. K. Liu, M. E. Mayfield, F. B. Stulen, "Study of Critical Two-Phase Flow Through Simulated Cracks", Battelle Columbus Laboratories, Interim Report BCL-EPRI-80-1, November 1980.

2. R. P. Collier and D. M. Norris, "Two-Phase Flow Experiments Through Intergranular Stress Corrosion Cracks," CSNI Specialist Meeting on Leak-Before-Break, Monterey, CA, September 1982.

3. R. E. Henry, "The Two-Phase Critical Discharge of Initially Saturated or Subcooled Liquid", Nuclear Science and Engineering, Vol. 41, 1970.

4. D. Abdollahian, B. Chexal, "Calculation of Leak Rates Through Tight Cracks," EPRI Report to be published.

5. D. Abdollahian, et al., "Critical Flow Data Review and Analysis", EPRI Report NP-2192, January 1982.

6. J. H. McFadden, et al, "RETRAN-02 A Program for Transient Thermal-Hydraulic Analysis of Complex Fluid Flow Systems, Volume 1: Equations and Numerics," EPRI Report NP-1850, May 1981.

7. C. A. Meyer, et al, "Thermodynamic and Transport Properties of Steam," ASME Publication, Fourth Edition.

Leak Rate Measurements and Detection Systems*

by

D. Kupperman, W. J. Shack, and T. Claytor**

Argonne National Laboratory
9700 South Cass Avenue
Argonne, Illinois 60439

Materials Science and Technology Division

Leak Rate Measurements and Detection Systems*

by

D. Kupperman, W. J. Shack, and T. Claytor**

Materials Science and Technology Division
Argonne National Laboratory
Argonne, Illinois 60439

INTRODUCTION

Early detection of leaks in nuclear reactors is desirable in order to detect deteriorating or flawed components and to minimize the release of radioactive materials. The installation of leak detection systems in accordance with USNRC Regulatory Guide 1.45 is necessary before a nuclear power facility can be placed into operation. However, currently available systems provide little capability for leak location or for source discrimination so that leakage from, say, valve packing can be distinguished from leakage from a crack.

A research program is under way at the Argonne National Laboratory under the sponsorship of the USNRC Office of Nuclear Regulatory Research to evaluate and develop improved leak detection systems. The primary focus of the work has been on acoustic emission detection of leaks. Leaks from artificial flaws, laboratory-generated IGSCCs and thermal fatigue cracks, and field-induced intergranular stress corrosion cracks (IGSCCs) from reactor piping have been examined. The effects of pressure, temperature, and leak rate and geometry on the acoustic signature are under study. The use of cross-correlation techniques for leak location and pattern recognition and autocorrelation for source discrimination is also being considered.

---

*Work supported by the USNRC Office of Nuclear Regulatory Research (FIN NO. A2212, Program Manager, J. Muscara).

**Components Technology Division, Argonne National Laboratory.

TEST FACILITY AND LEAK RATE MEASUREMENTS

A schematic of the leak test facility is shown in Fig. 1. It contains a thirty foot run of 10-in. Schedule 80 piping formed in a "U" shape. The IGSCCs or other flaws are welded into the piping. Water at high temperature and pressure is supplied to a small pressure vessel which is welded to the inner surface of the pipe behind the crack or flaw. Hydraulic jacks are used to load the pipe and vary the crack opening.

Leak rates through two IGSCC and a thermal fatigue crack are shown as a function of applied stress in Figs. 2-4. As expected from fracture mechanics, the flow rate is in most cases proportional to the applied stress. This linear dependence breaks down for low stresses. We speculate that the residual stresses produced when the crack is welded into the piping system may tend to hold the crack shut until a certain threshold level of stress is reached. In the case of IGSCC No. 1, the crack was subjected to very high applied loads and the residual stresses were relieved. The two-phase flow model developed by Henry (1) and modified at Battelle (2) to include the effects of area change and friction was used to calculate flows through the flaws and cracks. The "averaging" used in the Battelle model to account for the effects of friction and area change was replaced by direct numerical integration of the one-dimensional flow equations. However, the uncertainties in flow geometry and friction factors involved in flow through real cracks overshadow any differences between the two models. The crack length on the inner and outer surfaces is fairly well known. The size of the crack opening is difficult to determine. Direct measurement of the crack opening on the outer surface using an optical microscope is possible, but it is clear that the size of the crack opening is a strong function of the crack depth (it is typically much wider at the outer surface), and the choice of an appropriate value based on the observed outer-

surface values is unclear. An indirect aproach was used to obtain values for fluid-flux/unit-crack-opening-area to compare with the values predicted by the model. The area of the crack opening was calculated using the measured crack length and a fracture mechanics estimate of the crack opening displacement δ:

$$\delta = 2\sigma L(1 - \nu^2)/E$$

where σ is the applied stress, L is the crack length, ν is Poisson's ratio and E is Young's modulus. The fluid flux through the crack then was determined using the measured leak rate Q and the calculated area of the crack opening. The resulting flux was then compared to the flux predicted by the Henry model for frictionless flow. For the three cracks considered the comparison indicates that the actual flux is approximately 1/6 that of the frictionless flux. Similar calculations for the data obtained by Collier et al. (3,4) on an IGSCC and simulated flaws indicate that the real flux in most cases is from 1-1/10 of the corresponding frictionless flux predicted by the Henry model. The limited data base and the uncertainty about crack length, opening, crud deposition and roughness make it difficult to make more refined predictions of the flow through an IGSCC.

This uncertainty has surprisingly little effect on the assessment of the leak-before-break margin in piping with IGSCCs. Figure 5 shows a typical case for a 10-in. pipe. It is assumed that the crack can grow completely around the pipe circumference before a throughwall crack occurs. The largest combined 360-degree part-through crack and throughwall crack that the pipe can sustain under the applied stress can be determined from a net section flow stress criterion. (The collapse curve shown in Fig. 5 was obtained with the assumption that the flow stress equals 3 S_m). The crack opening area is obtained from a simple calculation using linear fracture mechanics. The observed variations in flux are used to estimate upper and lower bounds on the crack sizes necessary to

obtain a 5 gal/min leak rate. There is a significant leak-before-break margin unless the circumferential crack is quite deep. Because of the steep nature of the collapse curve for deep circumferential cracks, the size of the crack that can be postulated before violation of the leak-before-break margin is not very dependent on the value chosen for the fluid flux.

ACOUSTIC EMISSIONS FROM IGSCC

The basic nature of the acoustic emission signals from IGSCCs has been studied using standard resonant transducers and a very broadband transducer developed by NBS. As shown in Fig. 6, acoustic signals are generated by the crack primarily over the frequency range of 0-400 kHz. Although the strongest signals are at relatively low frequencies, the available data on background noise in reactors suggests that the most practical range for leak detection is 200-400 kHz. In most cases the transducers will have to be mounted on wave-guides, owing to the relatively high temperature of the piping system. This produces some signal loss, but, as shown in Fig. 7, a 0.004 gal/min (0.014 L/min) leak from a field-induced IGSCC can produce a signal 10 dB above the electronic background noise.

A local leak detection system is currently installed at the Hatch reactor. Measurements were made on the system at the plant to determine the background noise levels at full reactor power. A similar system was then installed on our laboratory test facility, and electronic noise designed to mimic the background noise measured at the plant was added to the signal. With this background noise level the system was able to detect a 0.002 gal/min leak from an IGSCC at a distance of about 50 cm from the crack. This type of system is quite sensitive compared to other leak detection methods. However, because the system is not capable of locating or discriminating between leak sources in other ways, it is considered likely that local leak detection systems which are sensitive at such

distances may be prone to false alarms triggered by leakage from valve packing, etc., located relatively far from the leak detector. The particular system installed at the Hatch reactor also has a very low dynamic range, and tests indicate it would become saturated at a leak rate of 0.006 gal/min. Thus, it would be incapable of detecting any increase in leakage as a crack grows, and a similar system installed at a noisy location, such as near a recirculation pump (as is the case at Watts Bar, where we are currently making background noise measurements) would simply become saturated.

To overcome such problems, the use of cross-correlation techniques for leak location and pattern recognition and autocorrelation techniques for source discrimination are being investigated. The cross-correlation as a function of time lag τ is defined as

$$R_{xy}(\tau) = \lim_{T\to\infty} \int_0^T x(t)y(t + \tau)dt,$$

where x(t) and y(t) are the input time domain signals over record length T. If x(t) and y(t) are nominally the same signal differing only in phase and amplitude, the cross-correlation enables one to determine the time delay (or phase difference) between signals. Since in the leak detection case the two signals emanate from the same leak, the phase difference is proportional to the difference in distance of the leak from the two detectors. Thus the cross-correlation can be used to locate the leak. The cross-correlation of signals from an artificial leak located midway between two detectors is shown in Fig. 8. As expected the peak in the cross-correlation occurs at a slight shift from zero; this is consistent with the relative position of the source and the detectors.

The above techniques have not yet been successfully applied to actual leaks. A sequence of cross-correlations of signals from a leak is shown in Fig. 9. In each case a peak corresponding to the actual leak can be seen. However, spurious peaks are also present. It appears that signal averaging over a sequence of cross-correlations may yet yield the desired result, since the peak corresponding to the leak always occurs at the same phase shift, while the peaks corresponding to the noise occur at random and should average to zero. The software for the actual implementation of the averaging scheme is being developed.

The autocorrelation function of a signal is defined in a somewhat similar manner:

$$R_{xx}(\tau) = \lim_{T\to\infty} \int_0^T X(t)X(t+\tau)dt.$$

Preliminary investigations of the autocorrelation function show that different leak sources exhibit quite different autocorrelations, as shown in Fig. 10. Thus, this may be a promising approach for source discrimination.

ACKNOWLEDGMENT

We wish to thank Rich Groenwald of GARD, Inc. for his contribution to the correlation work.

REFERENCES

1. R. E. Henry, "The Two-Phase Critical Discharge of Initially Saturated or Sub-Cooled Liquid," Nuclear Science and Engineering, Vol. 41, 1970, pp. 336-342.

2. M. E. Mayfield et al., Cold Leg Integrity Evaluation, NUREG/CR-1319, Battelle Columbus Laboratories, 1980.

3. R. P. Collier et al., Study of Critical Two-Phase Flow Through Simulated Cracks, Interim Report BCL-EPRI-80-1, Battelle Columbus Laboratories, 1980.

4. R. P. Collier et al., Study of Critical Two-Phase Flow Through Intergranular Stress Corrosion Cracks, Draft Report to the Electric Power Research Institute, Battelle Columbus Laboratories, 1982.

LIST OF FIGURES

1. Laboratory Leak Test Facility.
2. Leak Rate for the First Field-induced IGSCC as a Function of Applied Stress.
3. Leak Rate for the Second Field-induced IGSCC as a Function of Applied Stress.
4. Leak Rate for a Thermal Fatigue Crack as a Function of Applied Stress.
5. Leak-Before-Break Margins for Piping with Combined Part-Through Circumferential Cracks and Throughwall Cracks.
6. Frequency Spectrum for a Field-induced IGSCC.
7. Effect of a Waveguide on the Acoustic Emission Signal.
8. Cross-Correlation for an Artificial Signal Source.
9. Sequence of Cross-Correlations for Signals from a Leak.
10. Autocorrelation Signals for a Variety of Leak Sources.

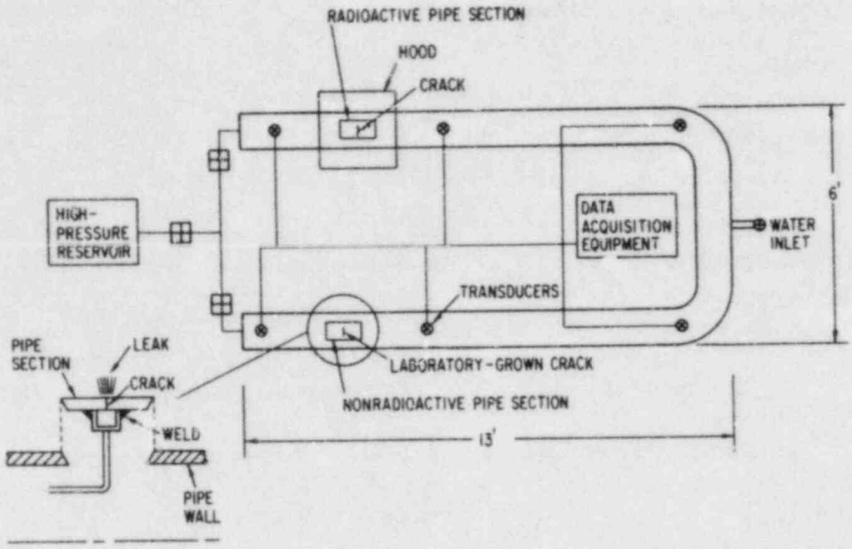

Fig. 1. Laboratory Leak Test Facility.

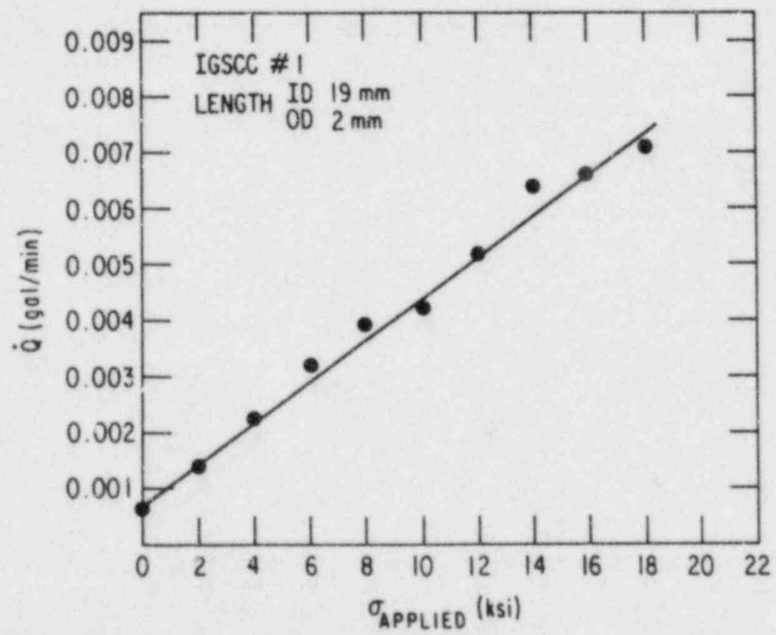

Fig. 2. Leak Rate for the First Field-induced IGSCC as a Function of Applied Stress.

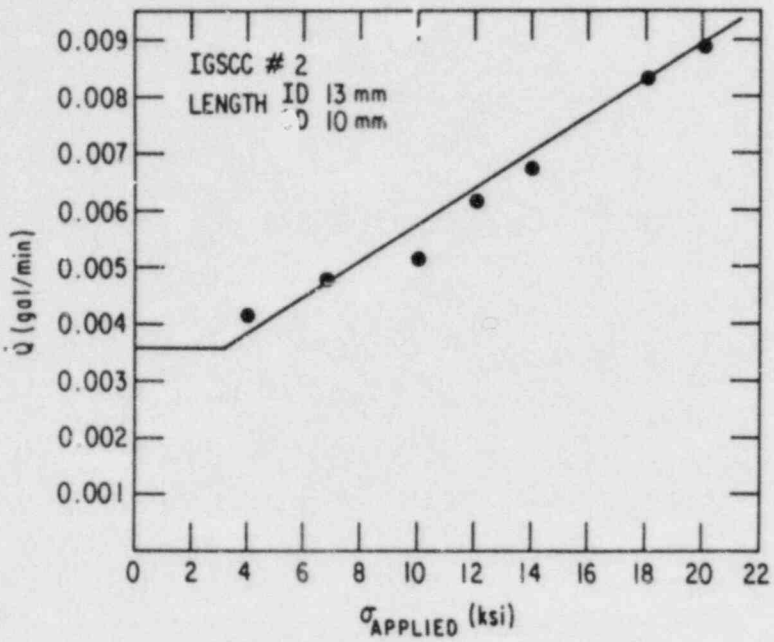

Fig. 3. Leak Rate for the Second Field-induced IGSCC as a Function of Applied Stress.

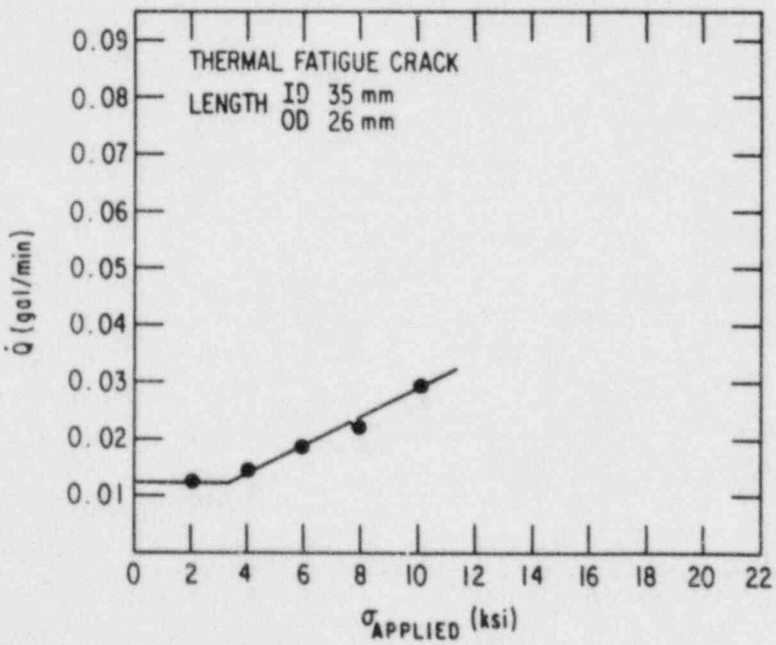

Fig. 4. Leak Rate for a Thermal Fatigue Crack as a Function of Applied Stress.

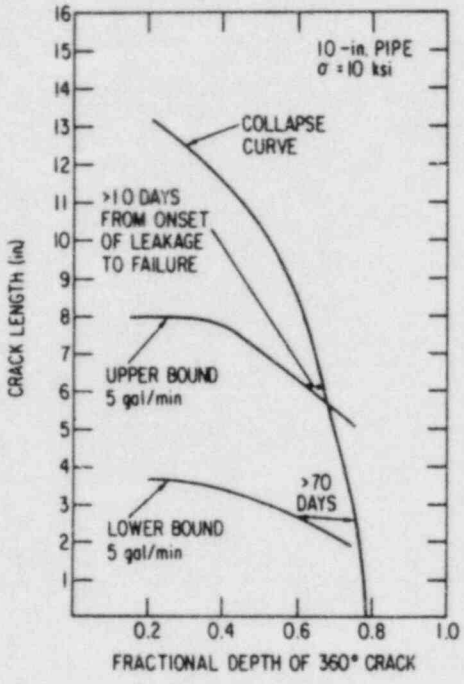

Fig. 5. Leak-Before-Break Margins for Piping with Combined Part-Through Circumferential Cracks and Throughwall Cracks.

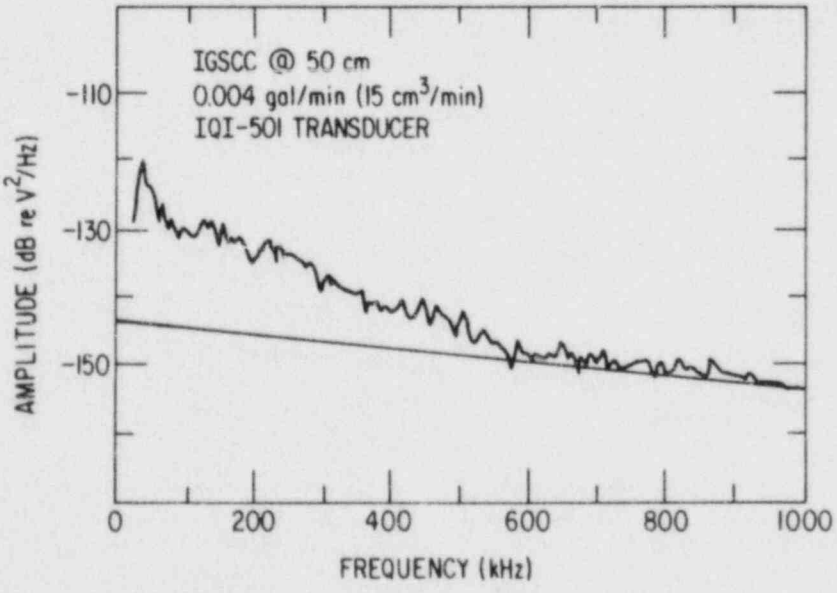

Fig. 6. Frequency Spectrum for a Field-induced IGSCC.

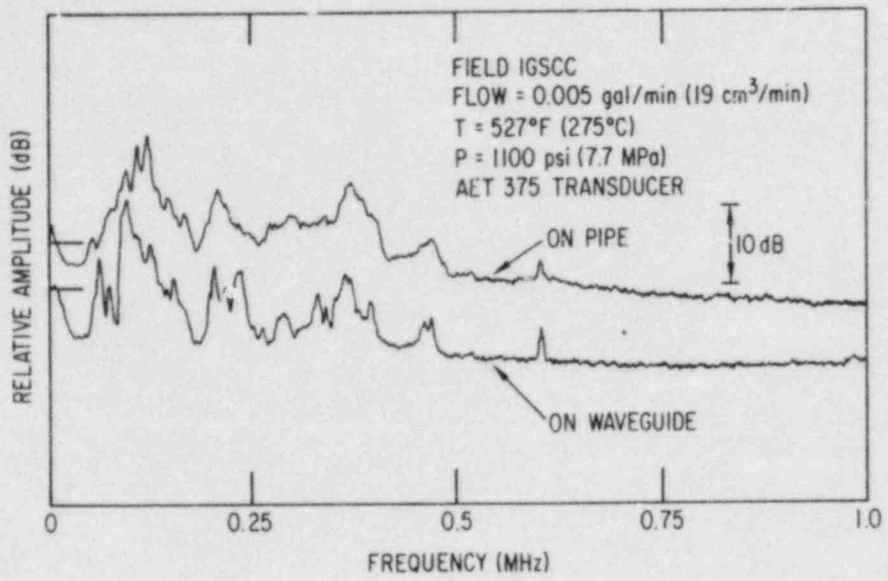

Fig. 7. Effect of a Waveguide on the Acoustic Emission Signal.

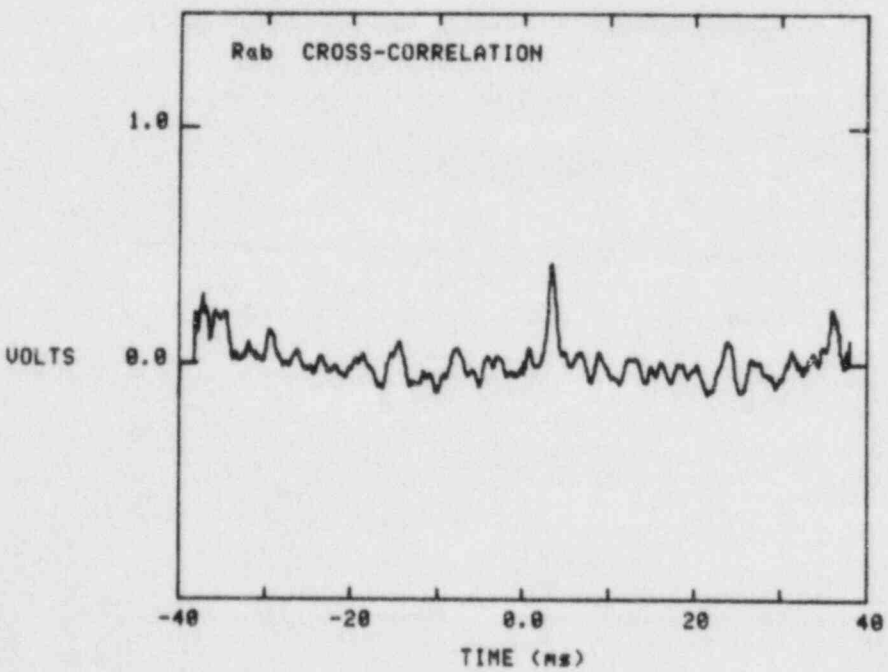

Fig. 8. Cross-Correlation for an Artificial Signal Source.

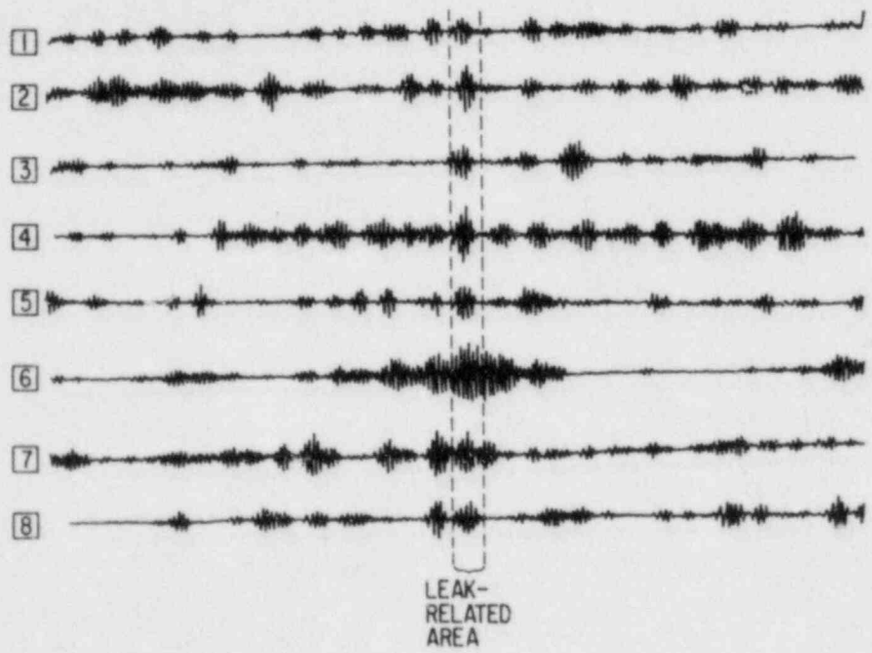

Fig. 9. Sequence of Cross-Correlations for Signals from a Leak.

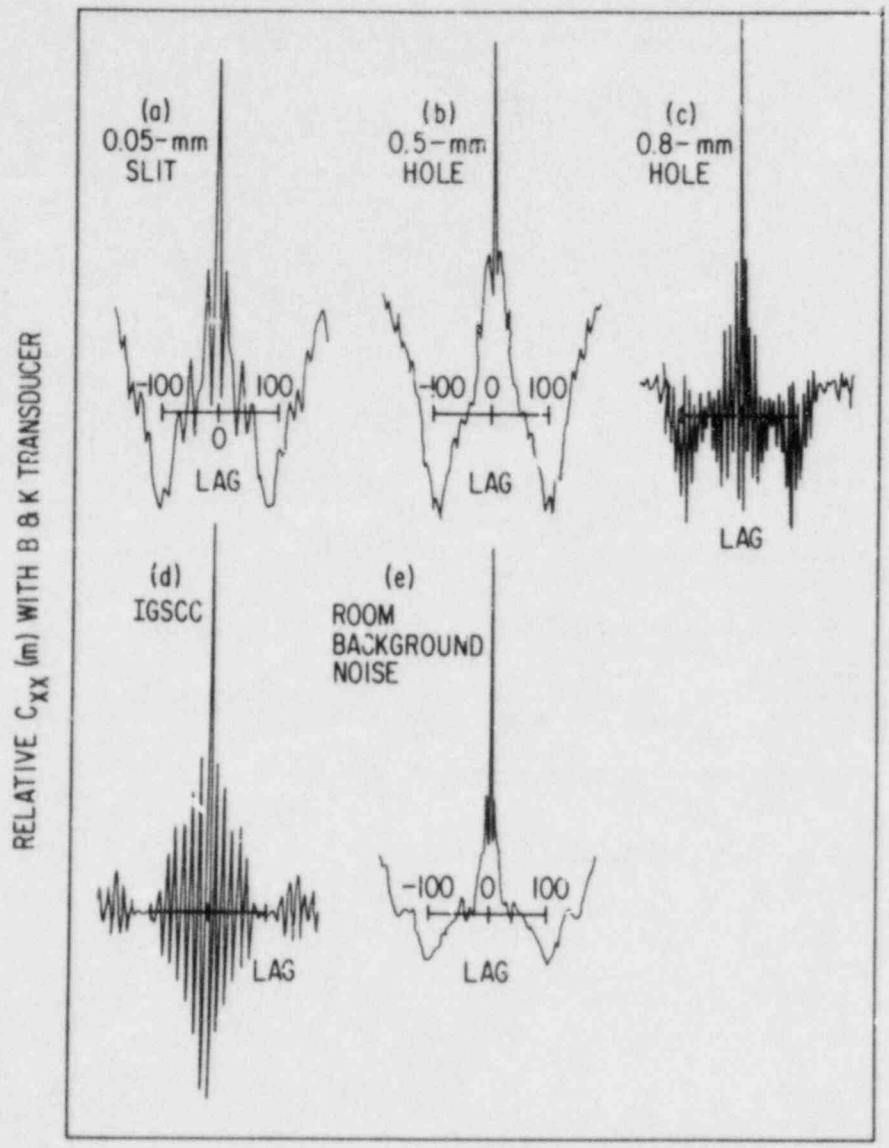

Fig. 10. Autocorrelation Signals for a Variety of Leak Sources.

THE OPENING OF THROUGH-WALL CRACKS IN BWR COOLANT LINES DUE TO THE APPLICATION OF SEVERE OVERLOADS II: A SIMPLE APPROACH

by

E. SMITH

(Joint Manchester University/UMIST Metallurgy Department, Grosvenor Street, Manchester M1 7HS, United Kingdom).

ABSTRACT

A simple theoretical analysis gives an estimate of the opening area associated with a through-wall crack in a pipe when this is subject to an imposed rotation at its ends. The crack-opening area is expressed in terms of the crack size, and the plastic rotation at the cracked cross-section, where plastic deformation is assumed to be confined. The results are relevant to the integrity of Boiling Water Reactor coolant systems during accident conditions.

NOMENCLATURE

A	Crack Area.
R	Pipe radius.
t	Pipe thickness.
L	Pipe length.
θ	Crack angle.
θ_o	Initial crack angle.
σ_o	Flow stress.
α	Defines neutral axis position.
χ	Crack tip opening angle.
ϕ_{PL}	Plastic rotation.
δ_{IC}	Crack tip opening displacement at onset of crack extension.
ϕ_{IN}	Plastic rotation at onset of crack extension.
M_P	Plastic limit moment.
E	Young's modulus.
I	Second moment of area.
ϕ	Total rotation.

I. INTRODUCTION

Intergranular stress corrosion cracking of Type 304 stainless steel Boiling Water Reactor (BWR) coolant piping is a major technological problem, because of the inspection and repair costs involved, and also concerns that there might be large radioactive coolant releases due to a loss of piping integrity. Most of the cracks have been observed in the heat-affected zones of girth welds, with the cracks forming at the inner surface of a pipe, and being oriented circumferentially. The cracks are able to grow slowly through the pipe thickness by an environmentally assisted mechanism, and a central question is whether unforeseen loads that might arise, for example, from an exceptionally severe earthquake, will convert a part-through stress corrosion crack into a through-wall crack. This might then open so that there is a significant loss of coolant or, worse still, extend unstably and cause complete pipe severance.

Against this background, Tada, Paris and Gamble[1], in their pioneering study of this type of situation, showed that circumferential growth of a through-wall crack in a pipe subject to bending loads should be stable for pipe run lengths that are typical of BWR reactor systems, in the sense that an increasing pipe deflection is required for a crack to grow at the onset of crack extension. This result demonstrates the essential stability of cracks in 304 stainless steel pipes, and strongly suggests that complete pipe severance should not occur. Nevertheless there is the possibility that a pipe might be subjected to sufficiently large deformations during an accident that a crack will open and maybe grow sufficiently that there will be a major loss of coolant. An earlier paper[2], hereafter referred to as I, has addressed this problem using the general model approach employed by Tada, Paris and Gamble[1]. Thus the material is elastic-perfectly plastic, with the plastic deformation being confined to the fully yielded cross-section

which contains the through-wall crack. Crack growth is assumed to be governed by the material's tearing modulus, i.e. the rate of increase of the J integral with crack extension is presumed to have a constant value which is independent of geometrical parameters. With this model approach Part I investigated the behaviour of a 28 in. (∿70cm) diameter pipe, containing through-wall cracks with subtended angles of 50° or 100°, and clearly showed that increasing the pipe deflection leads to an increase in the crack opening area, and that this area increases with the crack length for a given pipe deflection.

The present paper extends the earlier study in several respects. Firstly it is not assumed that the J-crack growth resistance curve is independent of geometrical parameters; e.g. crack size and pipe diameter; instead crack growth is presumed to proceed with a constant crack tip opening angle, which is in accord with experimental results[3]. Secondly, whereas in I the crack-opening area was regarded as being equal to the product of the crack tip displacement and the crack length, account is now taken of the fact that the displacement discontinuity across the crack is always greater than the crack tip opening displacement. Thirdly, and most importantly, the present paper's approach is sufficiently simple that the crack opening area results are expressed in a more general and more usable way than in I.

II. THEORETICAL ANALYSIS

The geometry of the cracked section of the pipe is shown in Figure 1; the section contains a through-wall crack with contained angle 2θ, the pipe radius as measured to the middle of the wall is R, and the pipe thickness is t. It is assumed that plastic deformation is confined to the cracked cross-section which is presumed to be fully yielded; the yielded material is perfectly plastic while the remainder of the pipe behaves elastically. The cracked cross-section is therefore subject

to the plastic limit moment M_p, and the stress distribution across this section can be described by a tensile stress σ_o acting within the region above the neutral axis, while a compressive stress of similar magnitude acts in the region below the neutral axis. σ_o is the material's tensile yield stress with a non-hardening material, but if the model is applied to a work-hardening material, with plasticity still being confined to the cracked cross-section, then a more appropriate value for σ_o would be the average of the yield and ultimate stresses. With $t/R \ll 1$, the location of the neutral axis, defined by the angle α (Figure 1), is readily shown by balancing forces to be given by $\alpha = \theta/2$ if there are no tensile forces acting perpendicular to the cracked cross-section.

It has been shown experimentally[3] that circumferential growth of a through-wall crack proceeds in such a way that a constant crack tip opening angle (CTOA) is maintained at the growing crack tip. A value of $\sim 20^{\circ}$ ($\sim$ 0.3 radians) has been measured for different sized cracks in 4 in. ($\sim$ 10cm) diameter pipes, and for one crack in a 16 in. ($\sim$ 40cm) diameter pipe; this angle is maintained even after substantial amounts of stable crack growth. With the present model, the pipe rotates about the neutral axis, which moves as the crack grows. In accord with a CTOA growth criterion, it is then argued that circumferential growth proceeds in such a way that as a crack tip moves an incremental distance δs, the opening at the position of the crack tip at the beginning of this increment increases by an amount $\chi\delta s$ where χ is the CTOA. Thus if the crack angle increases from 2θ to $2(\theta + \delta\theta)$ with the neutral axis changing correspondingly, and if the plastic rotation about this axis increases from ϕ_{PL} to $(\phi_{PL} + \delta\phi_{PL})$, simple trigonometry gives the growth condition as

$$\left[\cos\theta + \sin\frac{\theta}{2}\right]\frac{d\phi_{PL}}{d\theta} + \frac{\phi_{PL}}{2}\cos\frac{\theta}{2} = \chi \qquad (1)$$

Again, on the basis that the plastic deformation of the pipe is due to a rotation about the neutral axis, it follows that the crack opening area A when the crack angle is 2θ and the plastic rotation is ϕ_{PL}, is given by simple trigonometry as

$$A = 4R^2\phi_{PL}\left[1 - \cos\frac{\theta}{2} + \frac{1}{2}\sin\theta\right] \tag{2}$$

Equations (1) and (2), taken together, give the crack opening area when a crack grows from an initial angle $2\theta_o$ to an angle 2θ due to a plastic rotation ϕ_{PL}, noting that growth commences at a plastic rotation ϕ_{IN} given by the relation

$$\delta_{IC} = R\left[\cos\theta_o + \sin\frac{\theta_o}{2}\right]\phi_{IN} \tag{3}$$

with δ_{IC} being the crack tip opening displacement at the onset of crack extension. Of course if $\phi_{PL} < \phi_{IN}$, the crack opening area is given by relation (2) with $\theta = \theta_o$, assuming that the elastic contribution to the crack opening area can be neglected (this is an assumption thoughout this paper).

Determination of the crack opening area A is very simple if the plastic rotation is sufficiently small that the crack extension produced by this rotation can be disregarded, for equation (2) may then be used to give A with 2θ replaced by the initial crack angle $2\theta_o$. Thus, if it can be demonstrated that the crack extension is indeed small, one can proceed in this manner. To make this demonstration, the plastic rotation ϕ_{PL} is expressed in terms of the crack growth increment by the Taylor series expansion

$$\phi_{PL} = \phi_{IN} + \lambda\,(\theta-\theta_o) \tag{4}$$

where λ is a constant. Substitution for ϕ_{PL} in the differential equation (1), and equating terms that are independent of $\Delta\theta = (\theta-\theta_o)$, then gives λ as

$$\lambda = \left[\chi - \frac{\phi_{IN}}{2} \cos \frac{\theta_o}{2} \right] \Big/ \left[\cos \theta_o + \sin \frac{\theta_o}{2} \right] \qquad (5)$$

whereupon relations (3) and (4) give

$$\Delta\theta = \frac{(\phi_{PL} - \phi_{IN})}{\left[\chi - \frac{\delta_{IC}}{2R} \cdot \frac{\cos (\theta_o/2)}{\left(\cos \theta_o + \sin \frac{\theta_o}{2} \right)} \right]} \cdot \left[\cos \theta_o + \sin \frac{\theta_o}{2} \right] \qquad (6)$$

Since δ_{IC} is typically 10^{-1} in. (2.5×10^{-1} cm) and the CTOA χ is 0.3[3], for a wide range of crack sizes, i.e. $0<\theta_o<120^o$, and for pipe diameters in excess of 4 in. ($\sim$ 10cm), the second term in the denominator is small in comparison with the first term χ and may be neglected. It follows that $\Delta\theta<\phi_{PL}/\chi$, and since $\chi = 0.3$, then $\Delta\theta<0.3$ if $\phi_{PL}<0.1$, i.e. if the plastic rotation is less than $\sim 6^o$. Thus, provided the initial crack size is not too small, e.g. not less than $\theta = 30^o$, and provided the plastic rotation is less than 6^o, it is reasonable to use the zero growth formulation.

It therefore follows that, provided the plastic rotation ϕ_{PL} is less than 0.1 (6^o), then for a wide range of initial crack sizes, i.e. $30^o<\theta_o<120^o$, a usable expression for the crack opening area is obtained by taking the final plastic rotation and using the initial crack angle, i.e. relation (2) with $\theta=\theta_o$. The estimate for the crack opening area is then

$$A = 4R^2\phi_{PL} \left[1-\cos \frac{\theta_o}{2} + \frac{1}{2} \sin \theta_o \right] \qquad (7)$$

this expression being valid both before and after the onset of crack extension; Figure 2 shows a plot of A against θ_o. Relation (7) and Figure 2 are useful if the plastic rotation is specified; for example in the BWR piping system instability analysis of Cotter, Chang and Zahoor[4], ϕ_{PL} is given a bounding value of 1^o. Thus if a consideration of piping systems, taking into account the presence of supports etc.,

reveals a maximum value for the plastic rotation, then substitution of this maximum value for ϕ_{PL} in relation (7) gives an upper bound to the crack opening area.

Expression (7) is in terms of the plastic rotation ϕ_{PL}, but to put the situation in perspective, it is instructive to relate the crack opening area to the total rotation. This can be done by considering the case where a pipe of length L is subject to an imposed rotation at its ends (Figure 3). Moment equilibrium provides the relation:

$$\frac{M_P}{4\sigma_o R^2 t} = \cos\alpha - \frac{1}{2}\sin\theta = \cos\frac{\theta}{2} - \frac{1}{2}\sin\theta \qquad (8)$$

and since the elastic component ϕ_{EL} of the total rotation $\phi = (\phi_{EL} + \phi_{PL})$ is given by the relation

$$\phi_{EL} = \frac{M_P L}{EI} \qquad (9)$$

where I is the second moment of area ($=\pi R^3 t$), the elastic contribution is therefore

$$\phi_{EL} = \frac{4\sigma_o L}{\pi E R}\left[\cos\frac{\theta}{2} - \frac{1}{2}\sin\theta\right] \qquad (10)$$

To be consistent with the earlier development of the A-ϕ_{PL} relation (7), θ in relation (10) should be given the initial value θ_o. Thus equations (7) and (10) give the crack opening area as

$$A = 4R^2\left[1 - \cos\frac{\theta_o}{2} + \frac{1}{2}\sin\theta_o\right]\left[\phi - \frac{4\sigma_o L}{\pi E R}\left\{\cos\frac{\theta_o}{2} - \frac{1}{2}\sin\theta_o\right\}\right] \qquad (13)$$

a relation that gives the crack opening area A when the total rotation ϕ is specified. (In this case it should be noted that A depends on the pipe length L). Results for a 28 in. ($\sim$ 70cm) diameter pipe and a crack angle $2\theta_o = 100^o$ are shown in Figure 3 for the case L/R = 10; to obtain these values it has been assumed that $\sigma_o = 50 \times 10^3$ psi (345 MPa) and $E = 30 \times 10^6$ psi (2×10^5 MPa). The results are compared with those in

I, which concentrated specifically on the case $2\theta_o = 100^o$ and also the case $2\theta_o = 50^o$ (for which the present paper's simple analysis is not strictly applicable). The two sets of results are in excellent accord. The earlier approach (I), though accounting for crack growth, regarded the crack opening area as being the product of the crack tip opening displacement and the crack length; these factors act in opposite directions when related to the present paper's estimate, and is probably the reason why there is such good agreement between the two sets of results. The present paper's results are not compared with those obtained (for the case of $2\theta_o = 45^o$) by German and Kumar[5], since this crack angle is again beyond the scope of the present analysis. They combined a fully plastic solution, obtained by modifying the fully plastic solution for a single edge-cracked tension panel, with the elastic solution, to obtain an estimate of the crack opening area.

III. DISCUSSION

The present paper has developed a very simple analysis which gives an estimate of the crack opening area produced when a pipe containing a through-wall crack is subject to bending deformation. The dependence of the crack opening area on both the plastic rotation and the initial crack angle has been clearly demonstrated (Figure 2). These results are valid for a wide range of initial crack angles ($2\theta_o = 60^o$ to 240^o), and for plastic rotations up to ~ 0.16 (6^o); within these ranges the crack-opening area can be estimated to a sufficient accuracy without accounting for crack growth, and this enables a simple expression to be obtained for the crack opening area. To give a quantitative idea of the crack opening area: with a 28 in. (70cm) diameter pipe, the area produced by a plastic rotation of 0.1 (6^o), is 40 sq. in. ($\sim$ 250 sq. cm) when the initial crack angle is 120^o.

Important consequences follow from the result that the crack opening area is a linearly increasing function of the plastic rotation, and an increasing function of the initial crack angle. If a piping system has more than one crack, and is subject to excessive loadings, an upper bound for the total crack-opening area, which governs the amount of coolant emitted, can be obtained by assuming that the plastic rotation is confined entirely to the cross-section containing the largest crack. In other words, as far as the crack-opening area is concerned, the presence of multiple cracks does not have an adverse effect.

ACKNOWLEDGMENTS

The work described in this paper has been performed as part of the Electric Power Research Institute Programme on Pipe Cracking. The author thanks Dr. D.M. Norris for many valuable discussions in this general problem area.

REFERENCES

1. H. Tada, P.C. Paris and R.M. Gamble, Proceedings of the Twelfth National Symposium on Fracture Mechanics, ASTM STP 700, July (1980) 296.

2. E. Smith, "The Opening of Through-Wall Cracks in BWR Coolant Lines Due to the Application of Severe Overloads", International Jnl. Press. Vessels and Piping, 11 (1983) 19.

3. A. Zahoor, G. Wilkowski, I. Abou-Sayed, C. Marschall, D. Broek, S. Sampath, H. Rhee and J. Ahmad, "Instability Predictions for Circumferentially Cracked Type 304 Stainless Steel Pipes under Dynamic Loading", EPRI Report Number NP-2347, April (1982).

4. K.H. Cotter, H.Y. Chang and A. Zahoor, "Application of Tearing Modulus Stability Concepts to Nuclear Piping", Electric Power Research Institute Research Project T118-9, NP-2261, February, 1982.

5. M.D. German and V. Kumar, Aspects of Fracture Mechanics in Pressure Vessles and Piping, ASME Pressure Vessels and Piping Conference, Orlando, Florida, U.S.A. (1982) p.109.

FIGURE CAPTIONS

FIGURE 1 The geometry of the cracked section of the pipe; the section contains a through-wall crack with contained angle 2θ, the pipe radius as measured to the middle of the wall is R, and the pipe thickness is t.

FIGURE 2 The crack opening area A expressed in terms of the initial crack angle $2\theta_o$.

FIGURE 3 A pipe of length L is subject to an imposed rotation at its ends, and contains a crack of initial angle $2\theta_o$.

FIGURE 4 The crack opening area A expressed in terms of the total rotation ϕ for $2\theta_o = 100^o$, a pipe diameter 28 in. (70cm), and L/R = 10. The results are shown by the full line and are compared with the results (crosses) obtained in I.

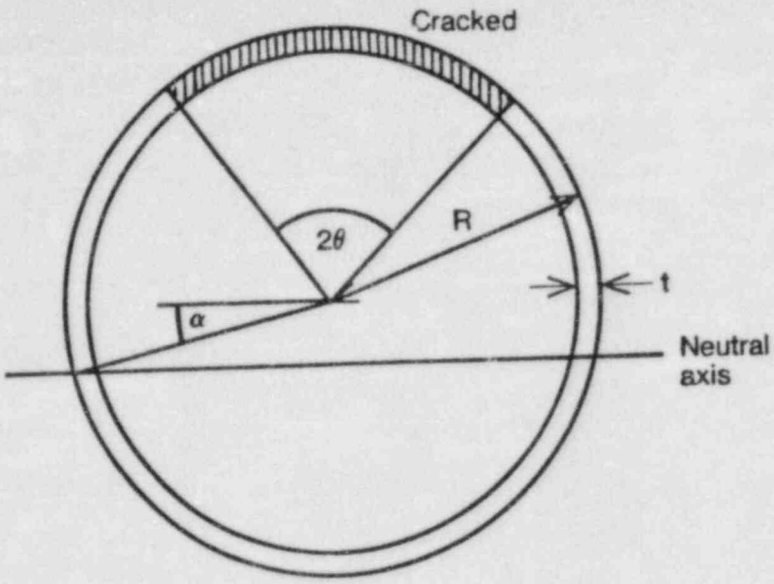

FIG. 1

FIG. 2

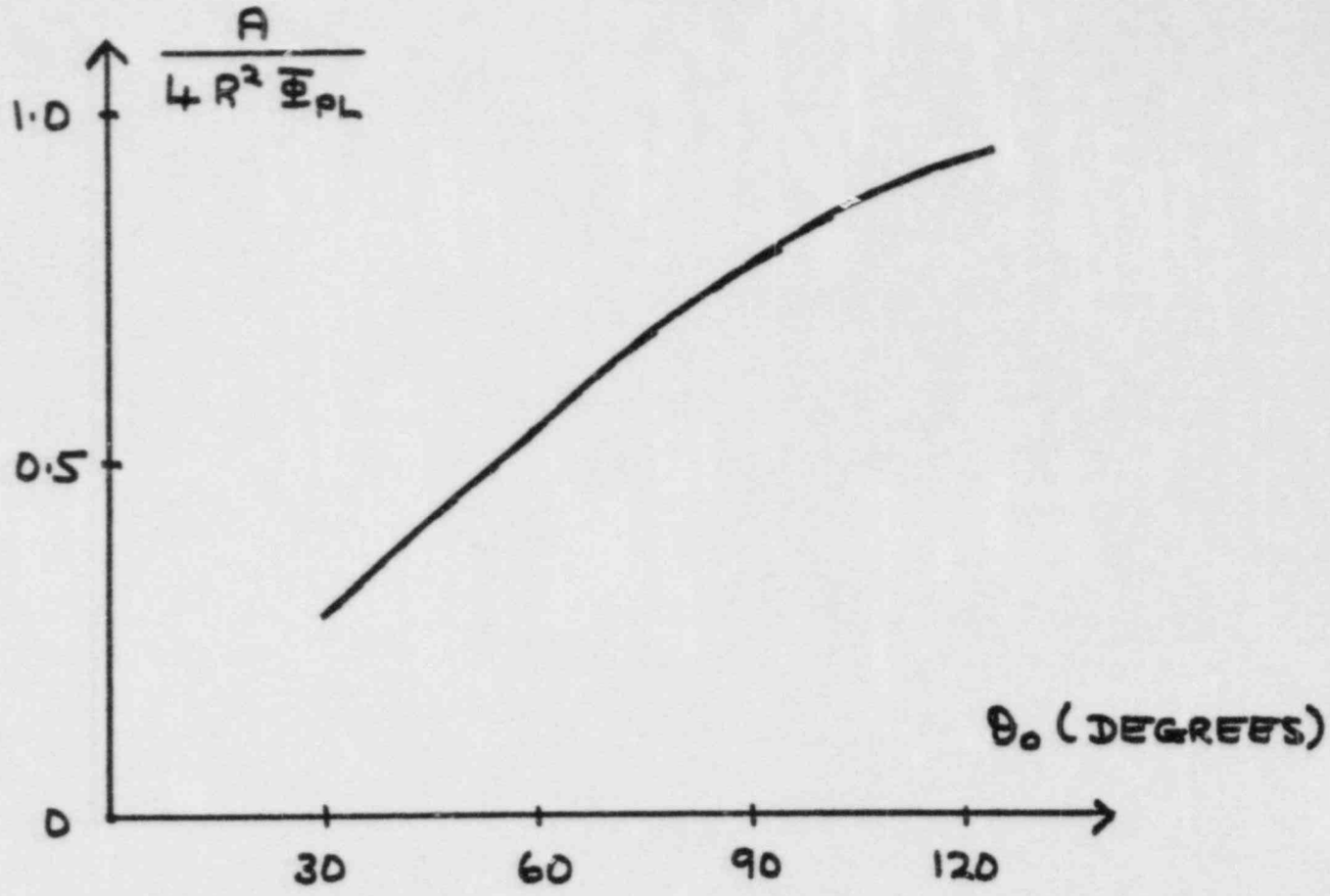

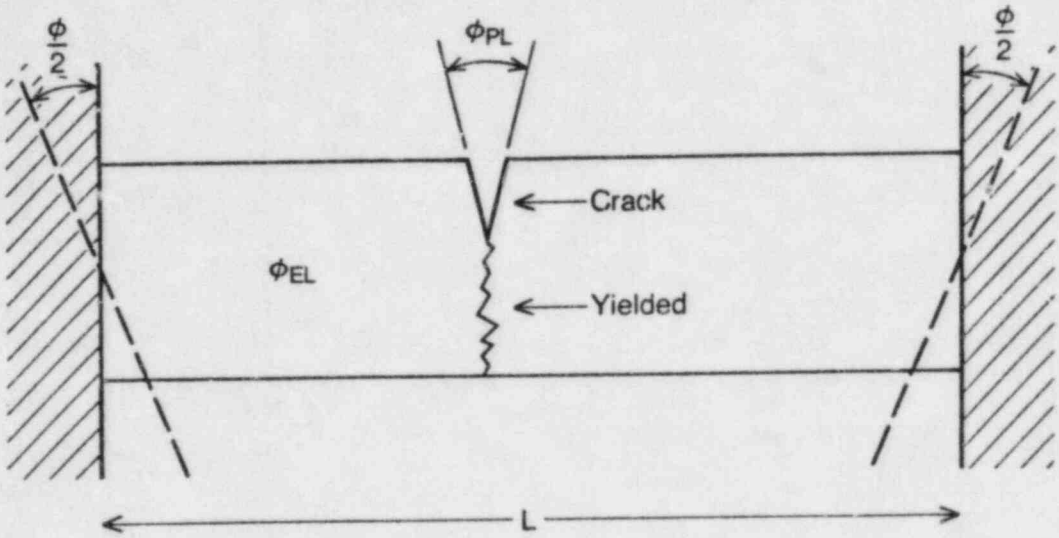

FIG. 3

FIG. 4

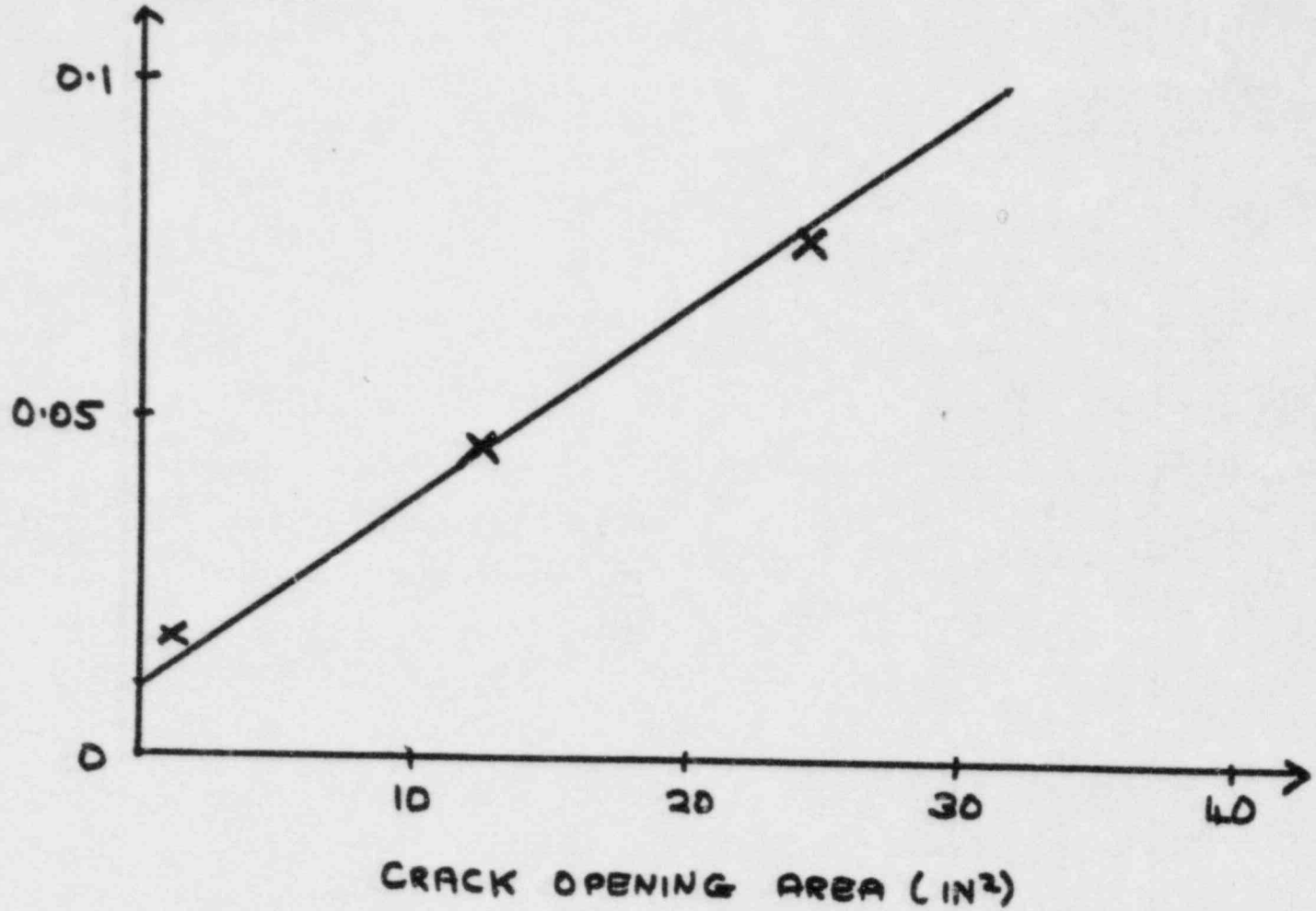
PIPE ROTATION
(RADIANS)
0·1
0·05
0
10
20
30
40
CRACK OPENING AREA (IN²)

LEAK-BEFORE-BREAK DUE TO FATIGUE CRACKS IN THE COLD LEG PIPING SYSTEM

by

M. E. Mayfield
Materials Engineering Associates
9700-B George Palmer Highway
Lanham, Maryland 20706 USA

and

R. P. Collier
Battelle Columbus Laboratories
505 King Avenue
Columbus, Ohio 43201 USA

Presented at:

CSNI Meeting on
Leak Before Break in Nuclear
Reactor Piping Systems
Monterey, California
1-2 September 1983

ABSTRACT

This review paper presents the results of a deterministic assessment of the margin of safety against a large break in the cold leg piping system of Pressurized Water Reactors. The paper focuses on the computation of leak rates resulting from fatigue cracks that penetrate the full wall thickness.

Results are presented that illustrate the sensitivity of the leak rate to stress level, crack shape and crack orientation. Further, the leak rates for specific conditions are contrasted to detection levels, shutdown criteria, make-up capacity and the leak rate associated with final failure of the piping system.

The results of these computations indicate that, in general, leaks far in excess of the present detection sensitivities would result at crack sizes well below the critical crack sizes for the upset loadings on the cold leg piping system.

INTRODUCTION

Structural integrity assessments for light water reactor (LWR) piping systems typically concentrate on the size of crack that would result in a large break if subjected to upset loading (earthquake for example). In a 1979 study, Mayfield, et al., (Ref.1) performed a deterministic study of the margin of safety against large breaks in the cold leg piping system of three pressurized water reactors (PWRs). As part of that study, a mathematical model was derived for predicting the two-phase flow rate through tight cracks. The flow rate model was coupled with fracture mechanics models for predicting crack shape and crack opening areas, and, in turn, the leak rates were computed for all through-wall cracks considered in the integrity analysis.

At the time the original study results were reported, the leak rate model had not been experimentally verified and conclusions based on the model were considered tentative. Subsequent experimental verification of the model (Ref. 2) lends credence to the results presented in Ref. 1.

This paper outlines the fracture mechanics and leak rate models and then reviews the results of the leak rate computations for a generic PWR cold leg piping system.

Review of the Cold Leg Analysis

The following review is provided to illustrate the analysis methodology. No attempt has been made to provide a comprehensive review. The reader is referred to Ref. 1 for a complete description of the work. The original study addressed the need to postulate a large break of the cold leg piping system of a pressurized water reactor. It was assumed that cracks existed in the piping system at various locations and that fatigue crack growth was the dominant damage mechanism. The analysis employed Linear

Elastic Fracture Mechanics (LEFM) technology in predicting the crack extension per reactor design lifetime.

It was assumed that the inital defect size was the largest crack that could be missed by non-destructive examination. Cracks were assumed in both the axial and circumferential orientations. Three depth-to-length ratios (a/2C) were considered, i.e., 0.1, 0.3 and 0.5. These ratios were chosen based on review of service cracking coupled with the "worst case analysis" philosophy that was adcpted throughout the study.

The stress spectrum used in the analysis was based on a review of the stress report and design specification for the three plants considered. It was assumed that the postulated transients occurred with a uniform distribution throughout the design life. Beyond the vendor postulated transients, the analysis assumed a continuous stress variation of 1000 psi range (axial and hoop directions) at a frequency of 1000 cycles per minute (2.1×10^{10} cycles during a 40-year plant life) which was also uniformly distributed throughout the design life.

The stress cycle for each transient was composed of global terms (pressure and moment) and local terms which included temperature gradient stresses, out-of-roundness induced stresses and various other displacement related stresses. This stress cycle was used in the fatigue crack growth analyses. However, owing to the ductile nature of the cold leg materiale, significant plastic deformation would occur as the cracks approached critical size, and the differential displacements (thermal gradient, out-of-roundness, etc.) would be accomodated. Thus, only the pressure and moment terms were included in evaluating the failure criteria.

The material properties needed in the analysis were obtained from the technical literature. When appropriate properties could not be found,

values were assumed based on engineering judgment coupled with the "worst case analysis" philosophy.

As noted earlier, the fatigue crack growth analysis employed LEFM-based technology. The analysis predicted the number of plant design lives for the assumed initial surface cracks to propagate through the wall thickness. It was assumed that the depth-to-length ratio was a constant. The analysis was conducted on a cycle-by-cycle basis and various failure criteria were checked on each cycle to determine breakthrough. Once a flaw was calculated to penetrate the wall thickness, the leak-versus-rupture criteria were examined. If the resulting through-wall crack was stable, the analysis was continued and the cracks were "grown" until they reached a critical size. This assessment was again made on a cycle-by-cycle basis.

As a separate yet related effort, leak rates were computed for each of the through-wall cracks from the point of breakthrough to the point of instability. It was necessary to develop a mathematical model to describe the two-phase flow through the cracks. The model coupled the fluid mechanics aspects and the fracture mechanics aspects such that leak rate could be determined as a function of fluid conditions, crack size and shape, crack face roughness and structural loading.

Two-Phase Flow Model

The two-phase flow model derivation and model assumptions have been discussed in Ref. 1 and 2 and in another paper presented at this conference (Ref. 3) and will not be repeated here. There are, however, some features of the model that bear directly on its application and warrant discussion here.

Crack Face Roughness

To illustrate the effect of crack face roughness it is convenient to consider the behavior of two-phase flow through a long, narrow crack.

Figure 1 schematically illustrates the flow behavior. It has been assumed that the flow behavior would be dictated primarily by the crack path length-to-hydraulic diameter ratio (L/D_h). With reference to Fig. 1, for the region $0 \leq L/D_h < 3$, a liquid jet is formed, surrounded by a vapor layer. For the region $3 \leq L/D_h \leq 12$, the liquid jet breaks up by shedding large globules at the surface and by forming vapor bubbles in the middle of the jet. In the vicinity of $L/D_h \sim 12$, the mixture takes on a thoroughly dispersed configuration.

The crack face roughness contributes to the two-phase flow behavior in terms of a pressure drop across the two-phase regime. This pressure drop is related to the height of protrusion of the fracture surface from a mean surface.

Figure 2 illustrates the effect of crack face roughness by plotting mass flux (leak rate per unit area) versus L/D_h with the friction factor (related to surface roughness) as a parameter. For a crack in a given pipe, L is fixed as the wall thickness. As the crack opening (length, width or both) increases, L/D_h decreases, resulting in higher mass flux for a given roughness. For small cracks (large L/D_h), the effect of an order of magnitude increase in the friction factor results in approximately a 40% decrease in the mass flux. The relative effect becomes very small as the crack opening increases (small L/D_h).

Fracture surface morphology is strongly governed by the micro-mechanisms that controlle' the cracking. For example, Intergranular Stress Corrosion Cracking (IGSCC) results in a macroscopically very rough surface. However, on a microscopic scale the surface of individual grain facets is often very smooth. Fatigue cracks, on the other hand, produce a relatively

smooth macroscopic surface while on the microscopic scale individual features tend to be rougher than the IGSCC grain facets.

The microscopic roughness would be a factor for crack openings in the micro-inch range. However, the openings of interest to this application were in the thousandths of an inch range. Thus, macroscopic roughness measurements were more pertinent.

In determining the appropriate roughness values, the surface roughness of a fatigue crack in A 106B carbon steel pipe material was measured using a surface profilometer. The average value of 366 micro-inches was used in all of the leak rate calculations.

Crack Opening Geometry

Figure 1 illustrates an assumed crack with constant flow cross-section. In the original model development it was assumed that the crack was long relative to its opening width and that the ends were parallel. The geometry was idealized as a rectangular slit of constant length and width.

While this idealization was convenient for the initial development work, it is not a very realistic description of a typical fatigue crack. Figure 3 shows the shape for an axially oriented crack that was allowed to propagate through the wall of a test pipe (Ref. 4). The ends of the crack are clearly not parallel nor are they straight. The actual shape at breakthrough is dependent on initial shape, the micro-mechanisms controlling the crack growth, the material behavior and the applied loading. Considering only the initial shape, the flaws that are long compared to the depth and wall thickness will generally result in a relatively sharp taper at the ends. Flaws that are short will have less taper, coming closer to the rectangular slit approximation.

The flow model was modified to account for what was described as

convergent crack geometry. Figure 4 illustrates the assumed crack geometry. The long crack faces were still assumed to be parallel to each other. However, the length of the crack was forced to linearly vary through the wall thickness.

The convergent flow was described in terms of the ratio of exit area to inlet area (A_e/A_o). Figure 5 illustrates the effect of area ratio on exit mass flux. In this figure the exit area was fixed and the inlet area was adjusted to achieve the desired ratios. Note that as the area ratio decreases (inlet area increases) the mass flux increases. The relative effect is essentially constant over a wide range of L/D_h.

Determination of Crack Opening Areas and Area Ratio

In determining crack opening area and the area ratio it was necessary to approximate the crack length on the outer surface just after breakthrough. The approach chosen was to use the surface crack area just prior to breakthrough to compute an equivalent through crack length. Mathematically this becomes

$$2C_{eq} = \frac{\text{Surface Crack Area}}{\text{Wall Thickness}} \ .*$$

Recalling that the fracture mechanics analysis assumed the crack depth to length ratio (a/2C) was a constant, the final inner surface crack length could be determined from

$$2C_o = \frac{\text{Wall Thickness}}{(a/2C)} \ .$$

In determining the distance between the crack faces it was necessary to employ fracture mechanics concepts of crack opening displacement (COD)

---

* The total length for a crack is 2C or $2C_{eq}$ for the equivalent crack.

and crack tip opening displacement (CTOD) along with an understanding of the intent of the analysis. The intent was to provide a conservative assessment of the leak rate, where, in this case, conservative implies underpredicting the actual leak rates. Figure 6 illustrates the intent of the analysis. It was assumed that plant leak detection and sizing systems would result in a shutdown once specific leak rate levels were reached. As such, a conservative analysis would underpredict the actual leak rate so that larger crack sizes than would actually be present in service would be associated with the shutdown criteria in the analysis.

Recognizing the intent, the COD calculations for pipe would result in larger openings than for flat plate. Further, COD calculations in general reflect the opening at the center of the crack which is larger than the "tip" opening. Therefore, the analysis employed a calculation of the CTOD for a centrally cracked flat plate in determining the distance between the crack faces. The CTOD computation used the same stress as used in evaluating the failure criteria, i.e., only the pressure and moment terms.

The area ratio (A_e/A_o) is computed as

$$A_e/A_o = [(2\ C_{eq})(CTOD_e)] \ / \ [(2C_o)(CTOD_o)].$$

Applications of the Leak Rate Analysis

There are two leak rate ranges of particular interest in the context of structural integrity analysis for LWR systems. The first is the 1 - 5 gpm leak rate range. Leak rates in this range would attract the operator's attention but would not necessarily result in a shutdown. It is possible for relatively large cracks to result in leak rates in this range. For example, the now famous 1978 Duane Arnold pipe cracking incident resulted in ~ 3 gpm leakage for a through wall crack extending one-quarter of the circumference.

The second range is for leak rates above the 5 gpm rate but less than the "normal" make-up capacity of the PWR systems. The exact upper limit on make-up capacity is system dependent but is typically on the order of 50 - 100 gpm.

There are two aspects of leak rates in this range that are particularly important. The first is the margin of safety against catastrophic failure for crack sizes resulting in leak rates in this range, i.e., if an earthquake occurred would the leaking cracks become unstable.

The second important aspect of leak rates in the 5 - 100 gpm range relates to the time rate at which the leak rate increases. The fundamental assumption here is that the through-wall fatigue cracks will continue to propagate and will eventually result in catastrophic failure. As a crack propagates the leak rate increases and the question becomes how much time does the operator have to bring the plant to a safe shutdown condition.

Results of the Integrity Evaluation

The results of the Ref. 1 integrity evaluation were presented in rather large and complex figures and tables. For the sake of brevity the results for only one location from one of the three plants are presented here. The results for all three plants are similiar to those presented.

Figure 7 presents the analysis results for an axially oriented crack with an initial depth of 10% of the wall thickness and a length ten times its depth ($a/2C = 0.1$). The analysis predicted a leak in less than one design life. The flaw was stable at breakthrough, i.e., leak-before-break. The leak rate at breakthrough was ~ 200 gpm. The flaw was calculated to propagate for an additional ~ 2 inches before becoming unstable. Just prior to failure the leak rate was computed as ~ 300 gpm.

It is important to note that variation of the axial crack analysis assumptions for this plant produces calculated life times ranging from virtually zero to nearly three design lifetimes. However, in all cases examined for all three plants, the flaws were stable at breakthrough (leak-before-break was confirmed) and the initial leak rates were in the 50 - 200 gpm range. Further, there was an appreciable amount of crack extension prior to failure with corresponding increases in leak rate.

Figure 8 presents the analysis results for circumferentially oriented cracks with initial depths of 25% of the wall thickness. Three different a/2C ratios were examined, i.e., 0.1, 0.3 and 0.5. For the a/2C = 0.1 flaw the analysis predicted just over 1 design life before a leak developed. The a/2C = 0.5 flaw analysis predicted over 26 design lives before a leak developed. The three cracks were stable at breakthrough, i.e., leak-before-break. The leak rate predicted for the a/2C = 0.1 crack was ~ 50 gpm while the predicted leak rate for the a/2C = 0.5 crack was ~ 1 gpm.

The a/2C = 0.1 flaw propagated an additional 45 inches before becoming unstable. After the flaw had propagated ~ 33 inches beyond the break through length an SSE would have resulted in catastrophic failure. The final predicted leak rate and the leak rate at the safe shutdown earthquake (SSE) critical size were the same as for the a/2C = 0.1 flaw. However, due to the extensive crack growth, the leak rate had increased by a factor of ~ 500 over the leak rate at breakthrough before the SSE could have caused failure.

On the basis of these results it appears that leak-before-break is credible. Further, there is an appreciable margin between the leak initiation condition and final failure. The leak rates at breakthrough for the axial cracks are at or slightly above the make-up capacity of the plants. The leak rates at breakthrough for the circumferential cracks range from ~ 1

gpm to ~ 50 gpm depending on the a/2C ratio. The leak rates are be discussed again below.

Figure 9 presents detailed results of the crack growth and leak rate analyses for the through-wall crack growth of the a/2C = 0.1 crack shown in Fig. 8. Recall that a vibratory stress of 1 ksi range and 1000 cpm frequency was assumed. The analysis results indicated that this vibration loading dominated the crack growth. In terms of time, the a/2C = 0.1 flaw would propagate from its breakthrough size to failure in slightly over 1 day. Note that the time between the SSE critical size and the final failure is quite short (less than 1 hour).

While detailed results are not available for the a/2C = 0.5 flaw, we estimate the time between breakthrough and the SSE critical size to be in the 5 - 10 day range, again assuming that the vibration experienced during steady state operation is the only loading.

In considering the through-wall crack extension for the axial crack of Fig. 7, we have assumed that the steady-state vibration was the only loading. This assumption results in a time between leak and break of ~ 1 day. However, the predicted leak rates were at or above the make-up capacity which would have initiated a reactor scram at breakthrough or shortly thereafter.

We emphasize that the time estimates are based solely on the assumed vibration loading. In the event that the vibration does not occur, occurs at a different range and/or frequency, or the plant experiences other transients, the time estimates may be completely erroneous. Based on the conservative nature of the analysis, we believe that the time estimates represent the minimum time available between leak and break.

Discussion

The original integrity evaluation (Ref. 1) indicated disturbingly short "lives" to failure. Depending on the choice of assumptions, the predicted lives range from virtually zero to almost 30 design lives. Review of the results indicates that the vibration loading assumption has an "all or nothing" effect. Once a crack had grown to a critical depth (determined by the threshold stress intensity factor, ΔK_{th}), where the initial growth was due to the other loading transients, the vibrational stress produced very rapid crack growth, resulting in failure of the pipe.

Simonen, Mayfield, Forte and Jones (Ref. 5) re-evaluated many of the plants and locations considered in the original study. They based their study on "best estimate" assumptions and removed the vibration loading assumptions. Depending on the particular location being considered, the re-evaluation predicted design lives to leakage ranging from over 4 design lives to over 100 design lives. Clearly, the predicted life is strongly dependent on the analysis assumptions.

The analysis supported the concept of leak-before-break in every case studied. However, in some cases the predicted leak rates were very large, exceeding the make-up capacity of the systems. This was observed for through-wall cracks resulting from long surface cracks ($a/2C = 0.1$).

For shorter initial surface cracks ($a/2C = 0.5$), the breakthrough leak rates were above the detectable limit of 1 gpm, yet below the shutdown limit of 5 gpm. The time rate at which the leak rate increases is dependent on the time rate at which the crack size increases and the stress level. Figure 10 illustrates the dependence of leak rate on crack size and stress level. It is apparent that the absolute leak rate is dependent on stress level, i.e., larger stresses result in larger leak rates. It is also apparent

that the leak rate increases with increasing crack length and that the increase per unit crack length increase is higher for higher stresses.

If one assumes a constant time rate of crack length increase, the leak rate will increase exponentially in time with the rate of increase dependent on stress level and absolute crack size. For the a/2C = 0.5 curve in Fig. 8, the inital leak rate is ~ 1 gpm. The leak rate increases to 5 gpm by the time the crack has doubled in size, whereupon shutdown procedures would be implemented. At this point, the crack is ~ 6 inches long while the SSE critical crack length is ~ 37 inches. For this particular example, the crack length at which the leak rate exceeds an assumed make-up capacity of 100 gpm is ~ 20 inches. Clearly, there is an appreciable margin of safety between leak and break in terms of both crack size and leak rate.

Based on the crack growth analyses discussed in Ref. 1 and 5, it appears that the margin of safety against a large break in the cold leg piping system is appreciable. In every case examined a leak was predicted to form before a large break. Further, the predicted leak rates were significantly greater than the shutdown limit (5 gpm) prior to reaching critical crack sizes.

The results indicate that requirements to postulate an instantaneous guillotine break in the cold leg are overly conservative, i.e., there is a significant margin of safety against such a break. However, the results also indicate that when long surface cracks break through, the leak rates can be in excess of the make-up flow capacity even though the crack is stable. Thus, while it appears unnecessary to postulate an instantaneous large break, one must consider the possibility of a large leak.

Commentary

The analyses discussed here were intentionally very conservative. As such, crack sizes, crack growth rates, material properties and stresses were

used which represent worst case assessments. The conservatisms included in each of the analysis inputs interact such that the results are certainly conservative but by an unknown margin.

The assumption of long surface cracks was made in an attempt to include the largest crack size that might be missed by pre-service and in-service inspections. The assumption that the inital crack shape did not change was chosen for conservatism and computational convenience. Actual fatigue crack growth tests using long axial cracks in pipe (Ref. 4) indicates that while limited axial growth was observed, the through thickness growth dominated.

The assumption that the crack shape did not change caused the resulting predicted through crack lengths to be artificially high compared to what we believe to be more realistic crack sizes. This in turn caused the predicted leak rates at breakthrough to be significantly higher than what might be reasonably expected. Figure 10 illustrates the dependence of leak rate on crack size. It is clear that even relatively modest overestimates of through crack length drastically increase the predicted leak rate.

The need to postulate a leak in LWR piping systems is evident from both the analysis results and service experience. However, the magnitude of the leak rates and the rate at which they increase should be considered open issues. The leak rate and rate of change of leak rate depend strongly on crack geometry and structural loadings. The geometries and loadings assumed in this study force the predicted leak rates and rate of increase of leak rate to be higher than what might be realistically expected. Improvements in crack geometry and structural loading descriptions would allow prediction of more realistic leak rates and increases in the leak rate.

References

1. M. E. Mayfield, et al., "Cold Leg Integrity Evaluation," USNRC Report NUREG/CR-1319, U. S. Nuclear Regulatory Commission, Feb. 1980.

2. R. P. Collier, F. B. Stulen, M. E. Mayfield, and P. M. Scott, "Study of Critical Two-Phase Flow Through Intergranular Stress Corrosion Cracks," EPRI Final Report in preparation. See also R. P. Collier, et al., "Study of Two-Phase Flow Through Simulated Cracks," Interim Report BCL-EPRI-80-1, Battelle Columbus Laboratories, Nov. 1980.

3. D. Abollahaian and D. M. Norris, "Prediction of Leak Rates Through Intergranular Stress Corrosion Cracks," CSNI Special Meeting on Leak-Before-Break, Monterey, CA, Sep. 1983. See also R. P. Collier and D. M. Norris, "Two-Phase Flow Experiments Through Intergranular Stress Corrosion Cracks, CSNI Special Meeting on Leak-Before-Break, Monterey, CA, Sep. 1983.

4. M. E. Mayfield and W. A. Maxey, "ERW Weld Zone Characteristics," NG-18 Report No. 130, A.G.A. Catalog No. L51427, American Gas Association, Jun. 1982.

5. F. A. Simonen, M. E. Mayfield, T. P. Forte, and D. Jones, "Crack Growth Evaluation for Small Cracks in Reactor Coolant Piping," USNRC Report NUREG/CR-3176, U. S. Nuclear Regulatory Commission, Apr. 1983.

MEM:lh/jp:32-9

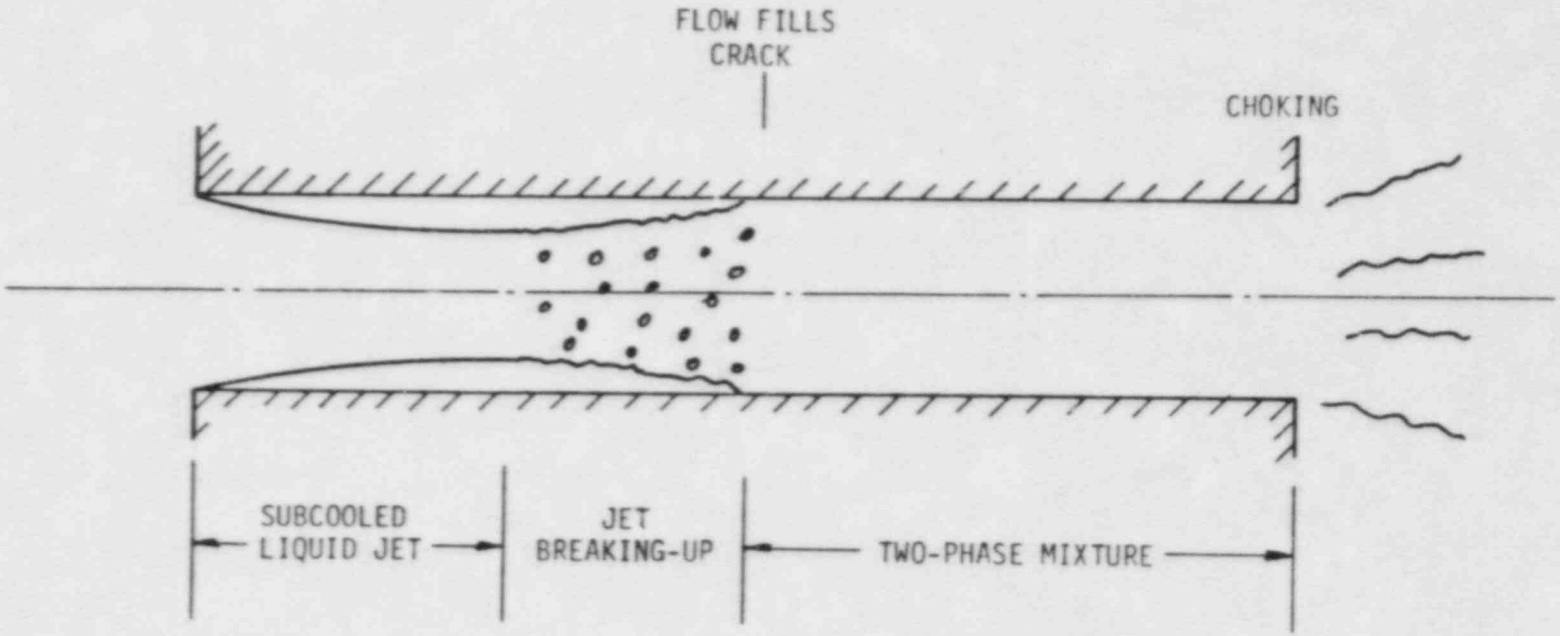

FIGURE 1. TWO-PHASE FLOW THROUGH A LONG, NARROW CRACK (Ref. 1)

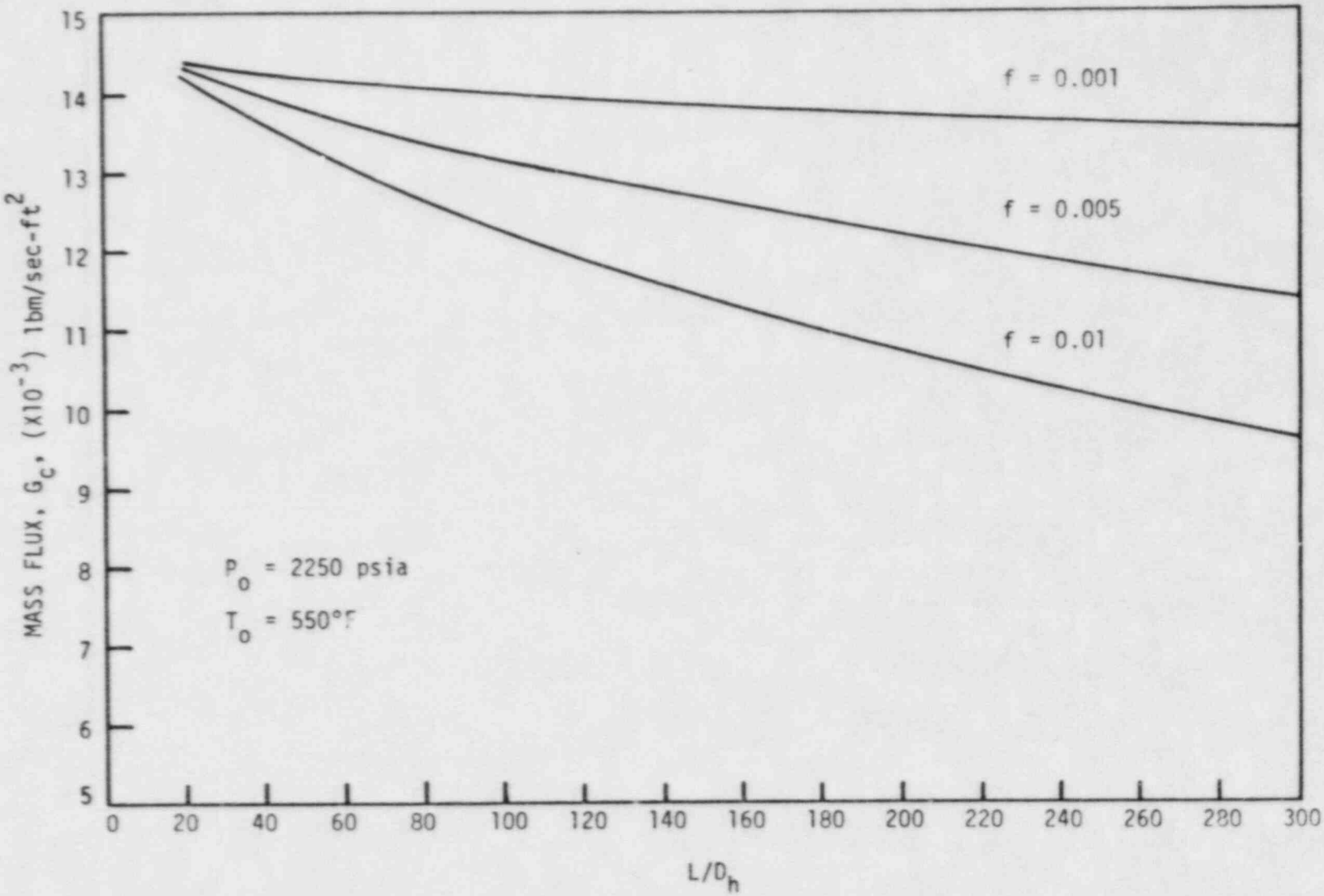

FIGURE 2. VARIATION OF MASS FLUX AS A FUNCTION OF L/D_h WITH FRICTION FACTOR AS A PARAMETER (Ref. 1)

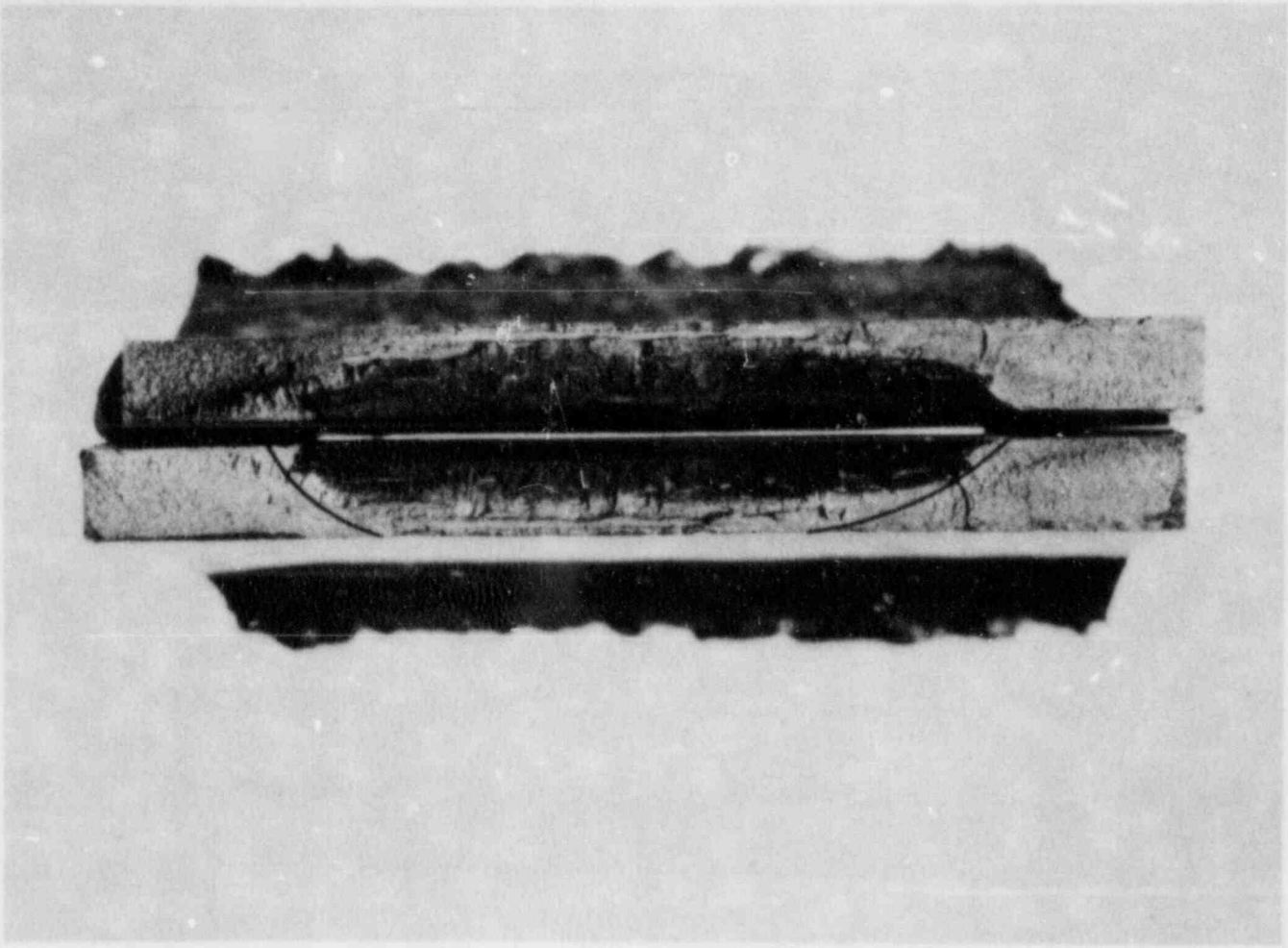

2X

FIGURE 3. FRACTURE SURFACE FROM THIRD CYCLIC PRESSURE TEST (Ref. 4)

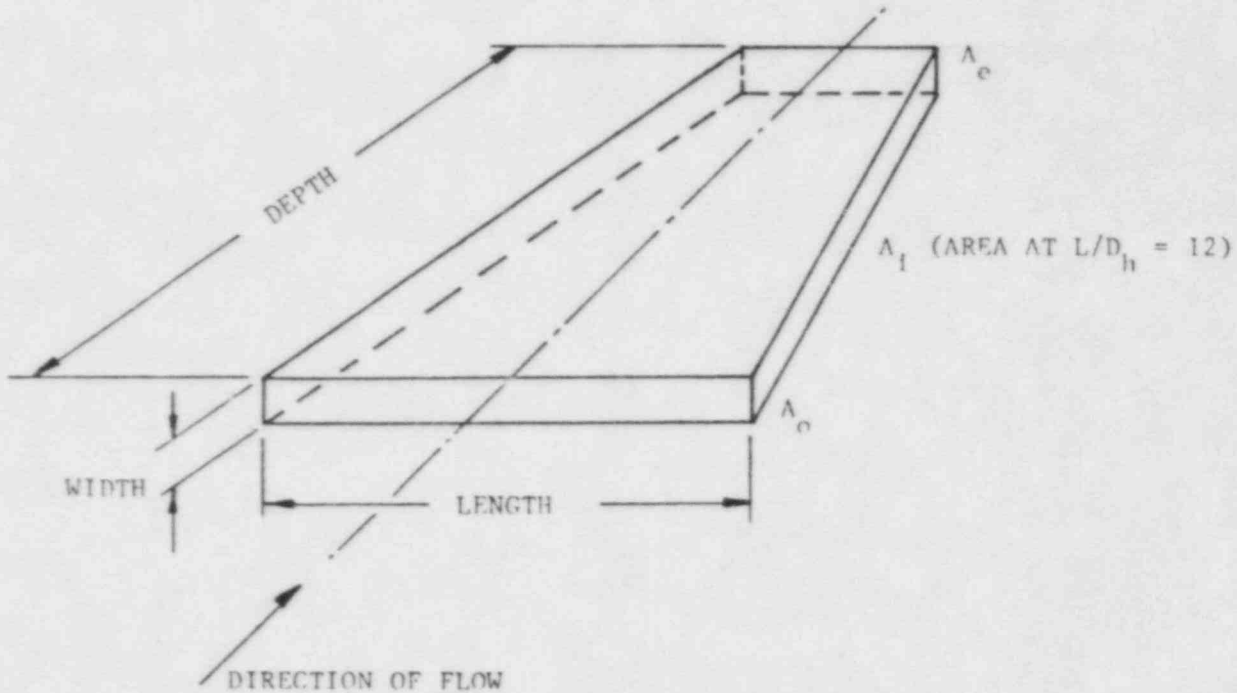

FIGURE 4. GEOMETRY OF CONVERGENT CRACKS (Ref. 1)

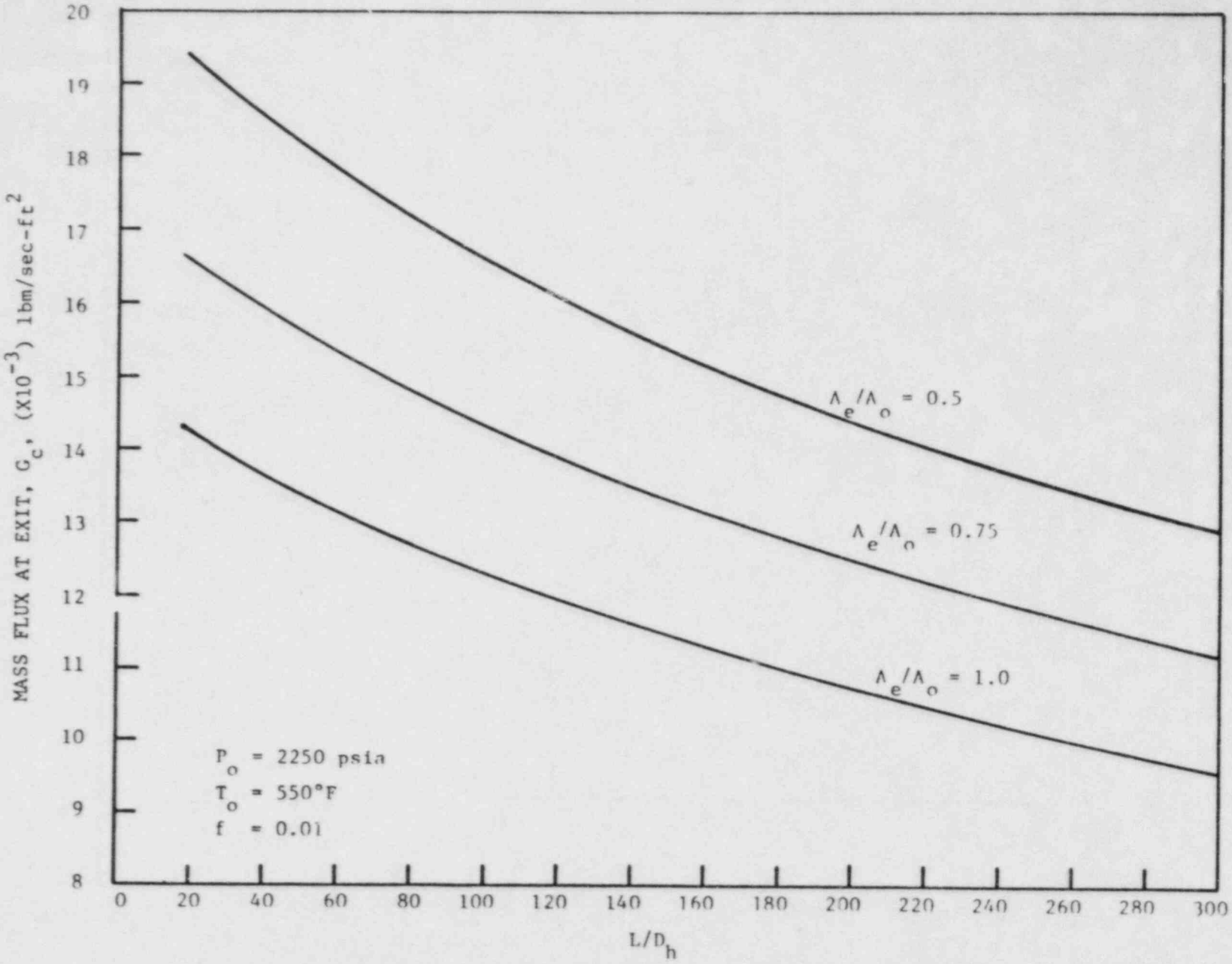

FIGURE 5. VARIATION OF MASS FLUX AS A FUNCTION OF L/D_h WITH AREA RATIO AS A PARAMETER (Ref. 1)

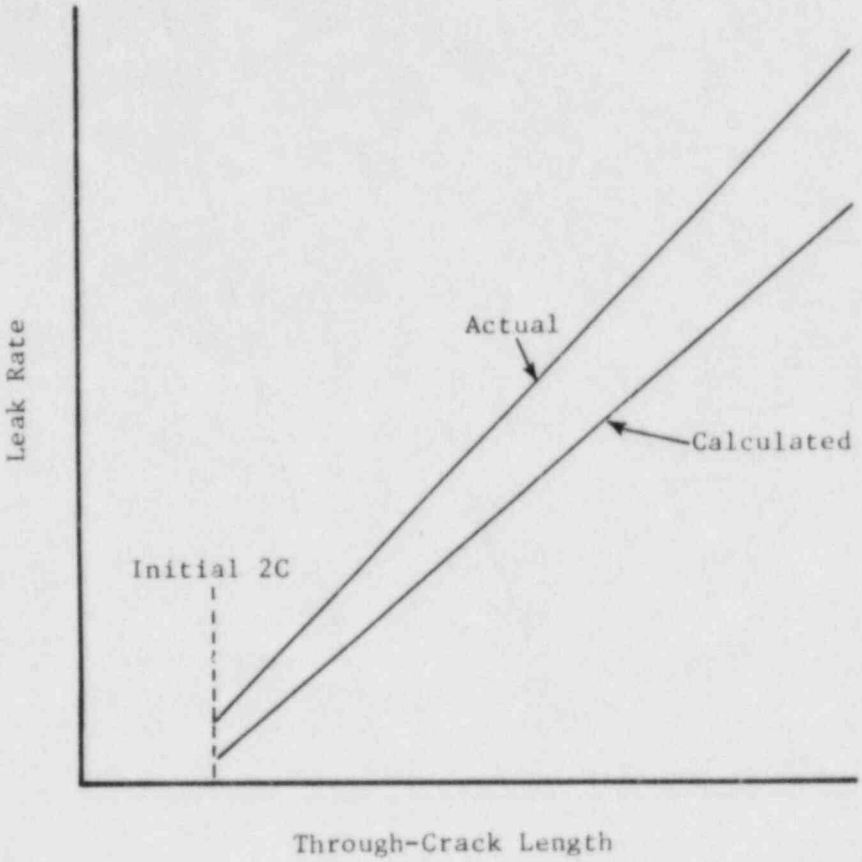

FIGURE 6. SCHEMATIC REPRESENTATION OF CALCULATED LEAK RATE CONTRASTED TO ACTUAL LEAK RATE FOR A CONSERVATIVE ANALYSIS (Ref. 1)

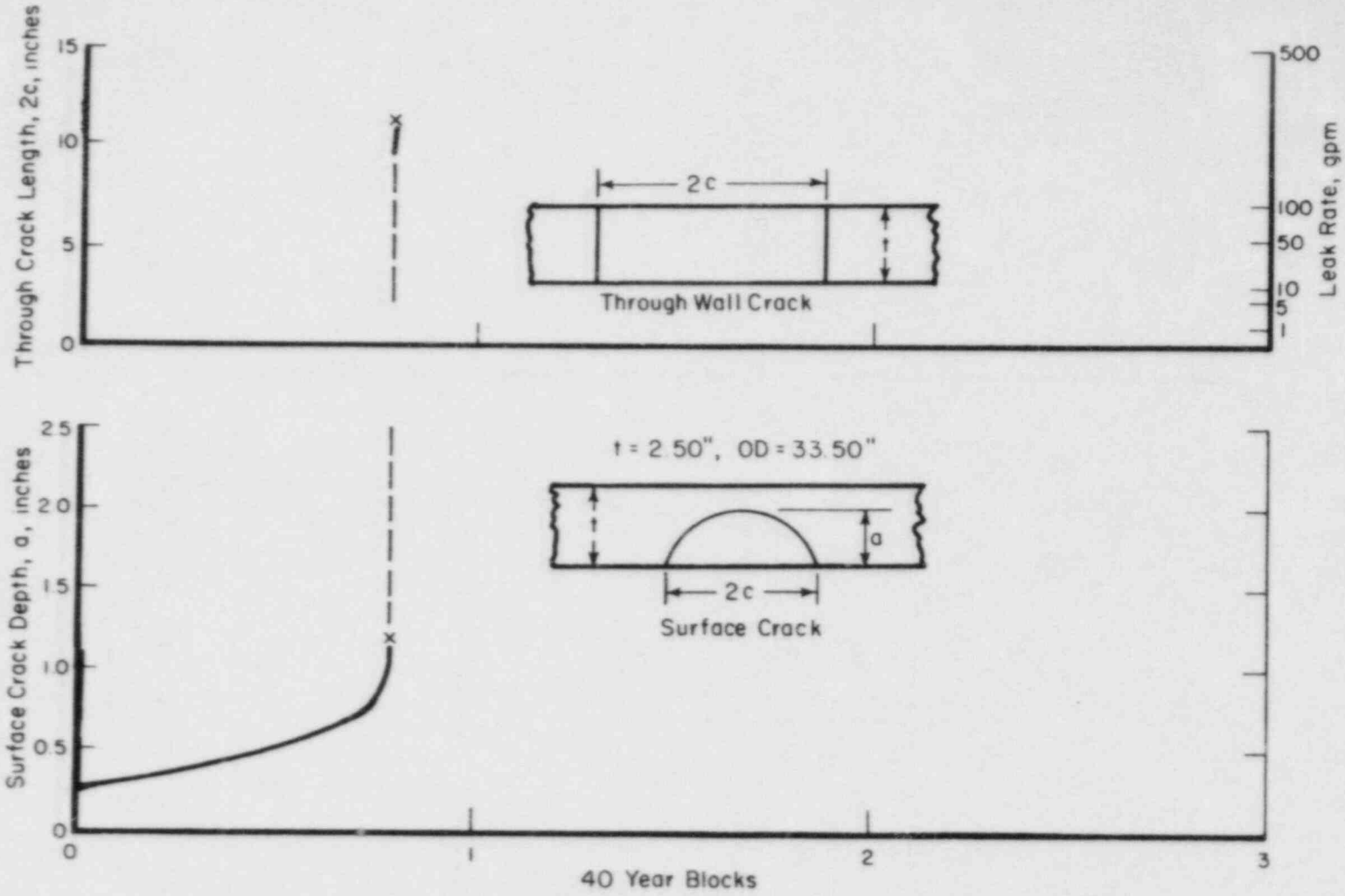

FIGURE 7. RESULTS OF SENSITIVITY STUDY ON VIBRATION, THRESHOLD, GROWTH RATE AND INITIAL FLAW SIZE FOR AXIAL CRACKS WITH a/2c = 0.1 (Ref. 1)

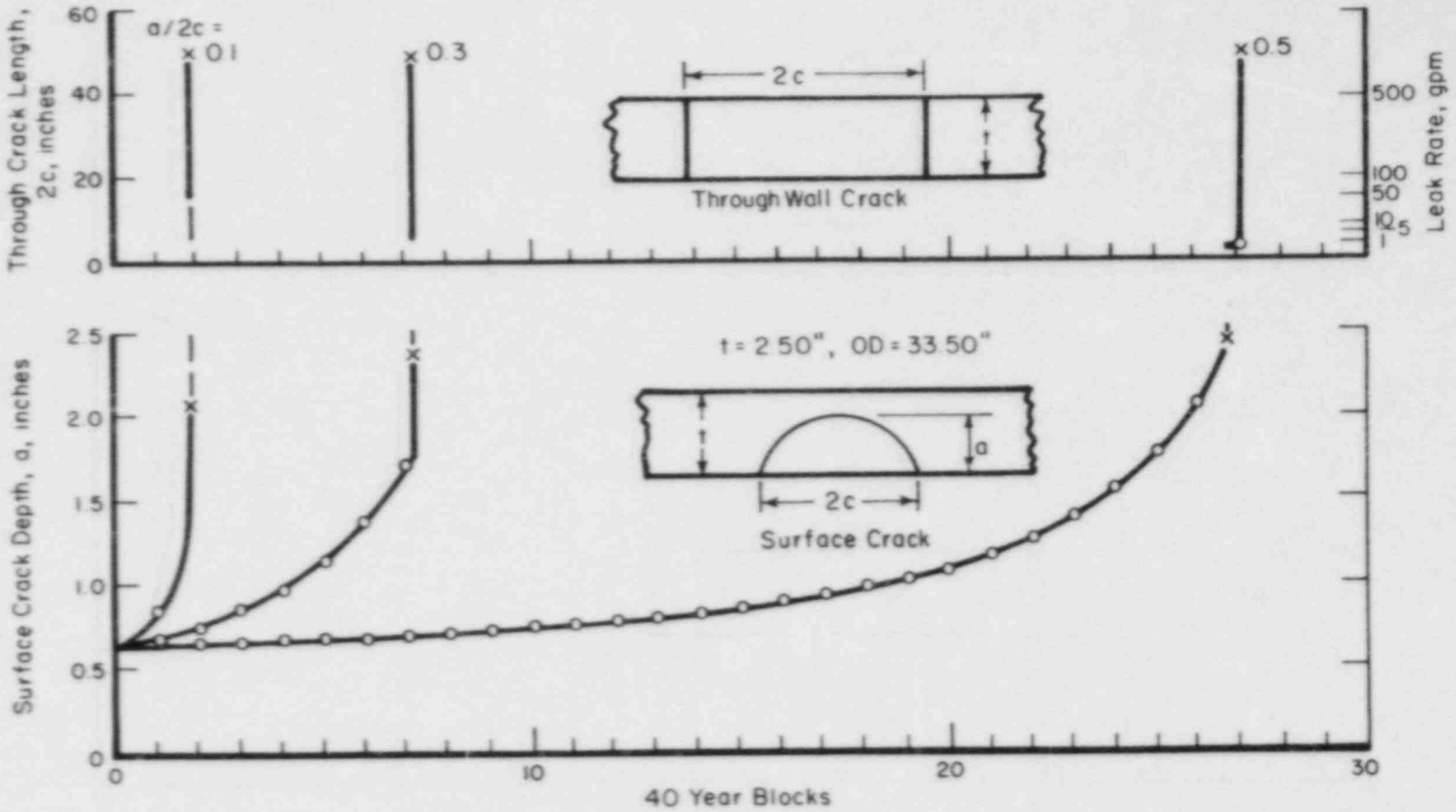

FIGURE 8. RESULTS OF SENSITIVITY STUDY ON a/2c FOR CIRCUMFERENTIAL CRACKS (Ref. 1)

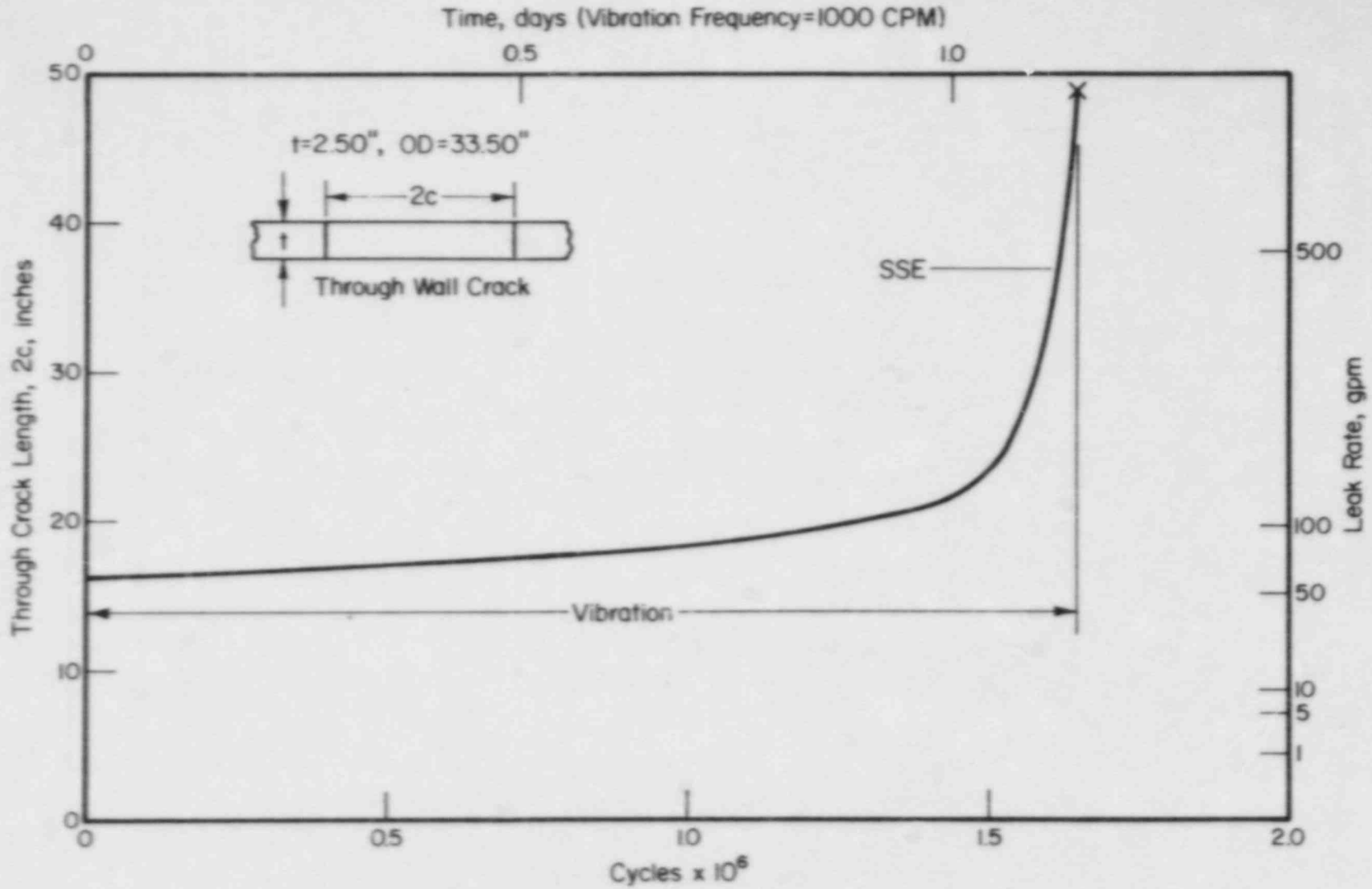

FIGURE 9. RESULTS OF THE DETAILED STUDY OF THE LEAK, TO LARGE BREAK BEHAVIOR OF CIRCUMFERENTIAL CRACKS WITH a/2c = 0.1 (Ref. 1)

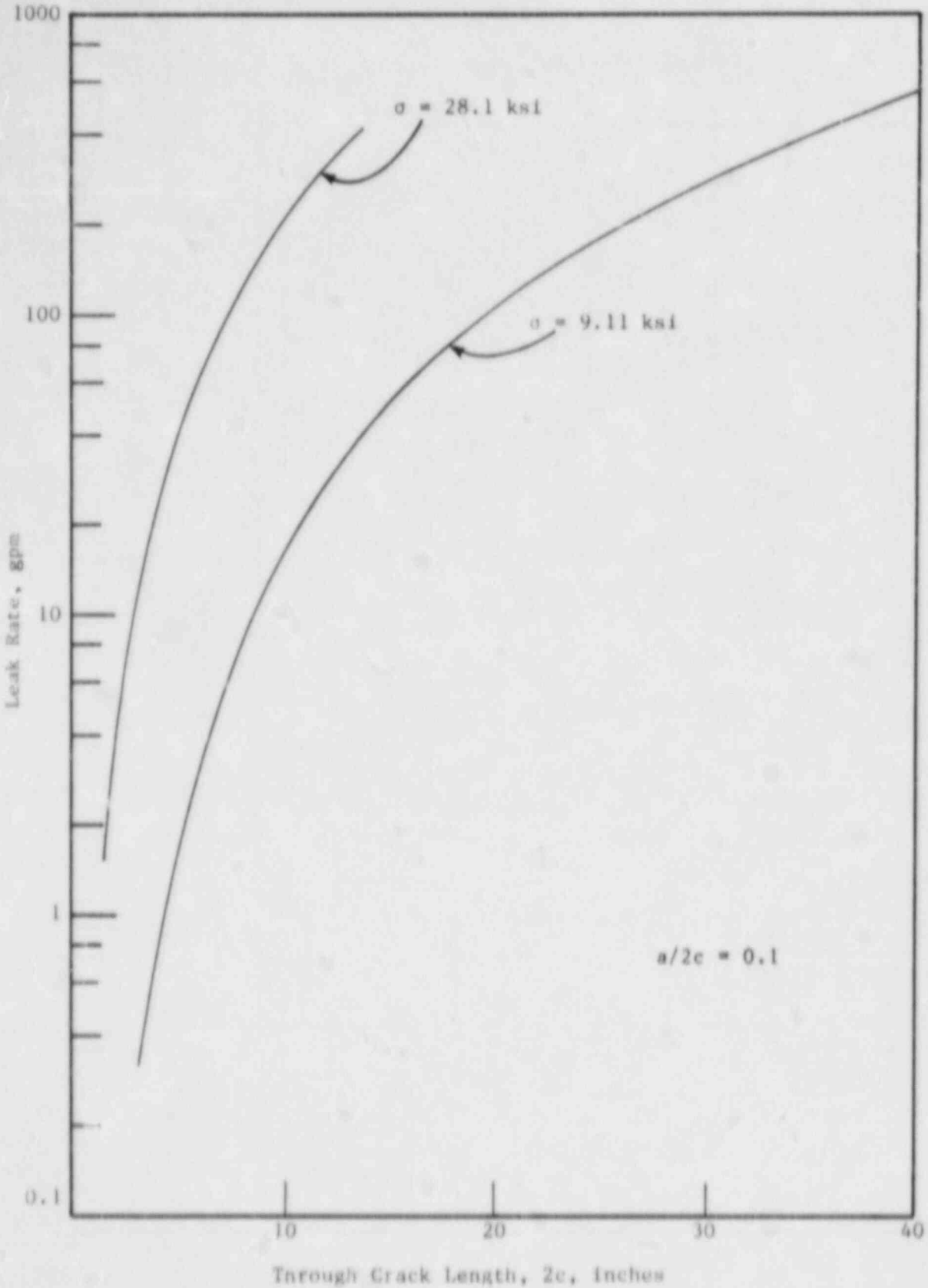

FIGURE 10. EFFECT OF THE APPLIED STRESS ON THE LEAK RATE THROUGH A FATIGUE CRACK UNDER PWR CONDITIONS (Ref. 1)

SESSION III

LEAK-BEFORE-BREAK STUDIES, METHODS AND RESULTS

SESSION CHAIRMEN

Dr. Douglas M. Norris
Electric Power Research
Institute, U.S.A.

Dr. Johann Blauel
Fraunhofer-Institut Fur
Werkstoffmechanic, FRG

SOME RESEARCH IN THE FIELD OF LEAK BEFORE BREAK CRITERIA FOR PIPING

by

L. LAZZERI

ANSALDO IMPIANTI SPA

CSNI MEETING, MONTEREY (CAL.)

Sept. 1983

Abstract

Ansaldo Impianti has begun a research activity in the field of leak before break, which should be applied to the reactors of new design. The activity has lead to the following basic results:

a) From an extensive analysis of the available experimental data it is concluded that the concept of "net section collapse" is a simple, reliable, valid tool in the case of very ductile materials. Elaborations of the data has lead to correlations to predict the collapse of circumferential and langitudinal through cracks, based on flow theory. Such correlations are a modification of existing ones for longitudinal cracks and a strain hardening approach for the collapse of circumferential cracks (SHA).

b) The analysis of some experimental data has lead to the conclusion that for partially ductile materials mixed ductile, fragile conditions may be present. A critical examination of the existing formulations (R6 and EPRI reelaborations) has lead to a simplified formulation of the fracture assessment diagram, however for very ductile material the use of such techniques is considered pleonastic.

c) From the analyses at a), b) criteria have been established in order to compute collapse conditions for through cracked pipes as a function of the applied load (moment and axial load) in term of net section collapse. Typical cases have been analyzed and are presented leading to the conclusions that even for incredibly long cracks the actual loads give still a reasonable safety margin.

The formulation favourably compares with experimental data and other available sources mainly of German origin. A special computer code (DUPIC) has been elaborated and it is intended as a postprocessor of standard pipe stress analysis codes.

d) The role of the thermal and secondary self equilibrating loads is discussed; while in the computations, which are referred to in c) the secondary loads are considered as equal to primary loads, the problem is considered in terms of overall instability of the piping.

This method originally suggested as a basic tool in the field of tearing instability, is revisited in terms of alternative parameters J, and collapse load. In order to perform such analyses a finite element model of the cracked pipe is analyzed in the elasto-plastic field by means of PAULAS code. The stiffness and overall J integral value at the crack tip are then computed and considered together with the overall model of the piping.

e) The leak areas are often evaluated on the basis of the 0.1 Aflow criterion, i.e. somewhat arbitrarily assuming a leak area equal to 10% the pipe flow area. However such an assumption is excessively conservative in most of the cases, as it corresponds to an excessively long crack (many times the thickness), alternative criteria are proposed, which correspond to much more realistic assumptions.

They are based on classical fracture mechanics criteria with plasticity corrections and a large safety factor equal to 10.

f) The 0.1 Aflow criteria is applied to typical lines, and it is concluded that such loads can be taken without using the classical pipe whip restraints, even if some increase in the size of the snubbers might be necessary, particularly if the peak loads due to the postulated break and seismic loads are directly summed, what is overly conservative.

I N D E X

1. INTRODUCTION

2. MATERIALS REQUISITES

3. APPLICATION OF THE NET SECTION COLLAPSE THEORY

3.1 General criterion

3.2 Axial cracks

3.3 Circumferential cracks

4. BRITTLE-DUCTILE INTERACTION DIAGRAM

5. TEARING INSTABILITY AND RELATED CONCEPTS

6. LEAK AREAS

7. DESIGN PROCEDURE

8. EVALUATION

9. CONCLUSION

10. REFERENCES

1. INTRODUCTION

The design of piping systems in nuclear power stations is currently done in Italy postulating the double guillotine type of break in the primary circuits, namely R.G. 1.46 and the associated SRP rules are followed.However while it may be possible to license a plant according to these procedures, some new trends and possibilities have been envisaged in the last few months as a consequence of the increasing concern about the presence of the massive structures necessary to cope with the postulated pipe whip loads. It is the aim of this paper to give a brief description of a new design procedures for the analysis of piping under the extreme loading conditions consequent to a postulated pipe break; this procedure is applicable for the design of new plants. Basically the procedure is based on the "leak before break" criterion i.e. on the assumption that in no case a break can propagate in a catastrophic manner, as local stress relieve consequent to leak can forbid a large crack extension.

2. MATERIALS REQUISITES

The basic assumption about the material is that it is ductile in all the conditions; similar assumptions have been made in the German rules /1/ and it is expected that the requisites for the material properties, inspection should be quite similar. Basically the material should have

a) upper shelf energy larger than 100 J as measured in Charpy tests

b) transition temperature below room temperature

c) energy at transition temperature plus 60°F not less than 68 J

Such requisites should be applied to the basic material (in both rolling and transverse direction), welds and HAZ Extensive volumetric ultrasonic tests must be performed on the material prior and during serivces.
While the ductility requirements do not generally present a problem for austenitic steels (which however may have some difficulties in terms of reproducibility as far as inspection are concerned), the ferritic steels might present the necessity of some changes (in general A333 gr.6 should replace A 106). However even for ferritic steels such requirements can be met without difficulties, as shown by preliminary analyses of the Italian vendor data.

3. APPLICATION OF THE NET SECTION COLLAPSE THEORY

3.1 General Criterion

As a consequence of the postulated high degree of ductility of the material, the failure of the pipe does not occur as a consequence of instability at the crack tip, as postulated in the classical fracture mechanics theory, but rather as a consequence of section collapse . Under these conditions the collapse can be described by the simple correlation :

(1) $\sigma = \sigma^* / M$

where σ = nominal gross stress

M = local magnification factor, a function of geometry

σ^* = flow stress, as described by Hahn et al /2/

The flow stress is somewhat intermediate between yield σ_{ys} and ultimate σ_{ult} stresses

(2) $\sigma^* = (\sigma_{ys} + \sigma_{ult})/n$

n is a numerical factor, which was originally postulated to be n = 2.4; subsequent studies have shown that such value may be very conservative if crack propagation is taken into consideration, being somewhat characteristic of the mechanism of crack initiation.

However it is envisaged to use n = 2.4, even if it is explicitly recognized that the procedure may be too conservative, hence

(1') $M = (\sigma_{ys} + \sigma_{ult})/2.4$

3.2 Axial cracks

Many correlations have been proposed for axial through cracks in order to compute the M factor (/2,6/) generally in terms of the λ factor

(3) $\lambda = C/(Rt)^{1/2}$

where C = half crack length
R = pipe radius
t = pipe thickness

The following correlation is proposed, based on a conservative evaluation of the experimental data

(4) $M = 1 + 0.50\,\lambda + 0.16\,\lambda^2$

For partial cracks a correlation has been proposed /6/ in terms of λ factor and remaining ligament dimension, however in this analysis the crack will always be supposed to be a through crack.

Experimental data on the behaviour of axial partial cracks have been reported by Kussmaul et al /7,8/, who have proposed a correlation for the transition between leakage and catastrophic failure. However the use of

formulae (1',4) has been demonstrated to prevent always catastrophic failure with large margin particularly in the case of very ductile material and short cracks.

3.3 Circumferential cracks

The case of circumferential cracks is somewhat more difficult due to the presence of moments, which are generally far more important than pressure loads.Three different approaches have been considered :

a) a quasi elastic stress distributio QESP has been suggested by Kastner et al /9/ and extensively used in the German letterature (see as an example ref./10,11).

b) a fully plastic approach FPA, where it is assumed that the axial stress is equal to $\neq \sigma^*$ in the net section

c) the strain hardening approach (SHA), which assumes linear strain distribution in the section, Ramber-Osgood correlation between stress and strain and maximum stress in the section equal to σ^*

Data have been reviewed in ref./9/,/10/ showing that the QESD is generally very conservative particularly in the case of pressure only loads, additional data on superimposed pressure and bending load can be found in ref./12/. An independent review of the experimental data has shown that :

a) QESD approach is generally very conservative

b) SHA approach is generally somewhat conservative particularly in the case of pressure only data

c) FPA procedure may be slightly unconservative particularly for the case of bending.

Even if it is recognized that FPA may represent, as an overall, a consistent picture of available experimental data , it is suggested to use the SHA procedure for design purposes.

4. BRITTLE-DUCTILE INTERACTION DIAGRAM

An examination of experimental data clearly shows that the correlations in paragraph 3 are unconservative if the behaviour of the material is not fully ductile; mixed brittle ductile conditions are taken into consideration by means of the so called R6 diagram, first introduced by Dowling and Townley /13/ and subsequently modified by Bloom /14/ to account for the effect of strain hardening In this case a simplified interaction formula has been considered :

$$(5) \qquad (1/Sd)^3 + (1/Sb)^3 = 1$$

where $Sd = \sigma^*/(M\sigma)$

$Sb = K_{Ic}/K$

where Kic and K are the critical and current value of the fracture toughness factor. This formulation is a simplified, somewhat conservative, evaluation of R6 diagram. It should be stressed however that in the practical cases, as fully ductile behaviour is postulated, the use of R6 diagram is somewhat pleonastic.

5. TEARING INSTABILITY AND RELATED CONCEPTS

In Usa many analyses about piping are performed according to the concept of tearing instability as introduced by Paris and coworkers /15,16/. Basically the method recognizis the fact that in ductile materials, even after fracture initiation, the crack may not propagate as a consequence of local stress relieving, in turn caused by local stiffness reduction consequent to the crack propagation itself. The material properties under consideration is the J, T diagram.

It should be stressed that the method strongly relies on the fact that in piping most of the stresses are due to thermal restrained movements and to incompatible displacements of the restraints.

Even if the methods outlined in paragraph 3 do not explicitly recognize the need for this type of analysis it is felt that some investigation in this area may be useful particularly in order to clarify the mechanism of superposition between displacement controlled and loads controlled stresses. In this connection however, other basic parameters different from J,T diagram might be used as an example the collapse load as a function of crack size.

A limited research program is under way to study the instability conditions for a pipe by means of the non linear pipe and shell code PAULA /17/ to ascertain safety margins and load combination rules.

6. LEAK AREAS

As it has been widely mentioned a leak before break criterion may be insufficient for an evaluation of the safety of the pipeline, if some evaluation is not made about the crack area and crack locations.
While the problem is still under discussion, it is envisaged that the leak areas should be evaluated as follows :

- fitting and high stress regions :

(6) $A_{leak} = 0.1\ A_{flow}$

where A_{flow} is the flow area of the pipe

- circumferential welds

(7) $A_{leak} = 10\ A_{FM}$

where A_{leak} is equal to 10 times the area evaluated on the basis of fracture mechanics computations /18/; actual computations show that :

a) formula (7) generally leads to areas seldom in excess of 1-2% of the pipe flow area, if the crack length is not larger than 2-3 times the thickness

b) comparisons with actual data /8,9,19/ show that such formulations is conservative by at least a factor 3 as compared with tests results.

7. DESIGN PROCEDURE

While some justifications and confirmations are under way, which might slightly effect the results, the following design procedure is envisaged :

a) assume a reference crack size equal to three times the pipe thickness

b) evaluate the safety coefficients for axial and circumferential cracks according to (1), (4) formulae and SHA procedure respectively

c) in the analysis in b) the maximum pressure and total sum of the gross moments should be considered; it is stressed that a direct sum of the load controlled and displacement controlled moments may be overly conservative and that a reduction factor for displacement controlled quantities should be applied.

If the safety factor is larger than one, then no crack should be postulated, however in accordance with the principle of defense in depth, an analysis of the pipe and restraints behaviour should be done, postulating a leak area as discussed in section 6.

In practice a postprocessor to a stress analysis computer code, named DUPIC /20/ has been written, which automatically performs all the mentioned checks and evaluations.

8. EVALUATIONS

The procedure outlined in section 7 has been applied to some BWR 6 piping, the basic results are as follows:

a) if one considers the direct sum of the gross moments on a piping (i.e. direct sum of the load controlled and displacement controlled quantities), the minimum safety factor found is larger than 1.4 in terms of applied load and around 3 in terms of crack length

b) the leak areas evaluated according to the precedent procedures are less than 1% of the total flow area

c) assuming that a sudden force equal to

$$F = 0.1 \; P \; Aflow$$

where P is pressure, is dynamically applied to the pipe (in this case MS line of a BWR 6) the following results are found

- ca) stresses on the lines are low so that no secondary break needs be postulated
- cb) snubbers loads are within allowables, even if direct superposition with seismic may present some problems
- cc) pipe whip restraints are not necessary

9. CONCLUSION

The elimination of the hypothesis of a double end guillotine type break is presently considered in Italy. A design procedure (still under discussion) has been presented in the hypothesis of a fully ductile behaviour of the material and leak before break assumptions. Preliminary results would indicate that the elimination of pipe whip restraints is feasible under the conditions mentioned herein.

10. REFERENCES

/1/ RSK Leitlinien fur druckwasser reaktoren, 3 Ausgabe Okt 1981

/2/ Hahn G., Sarate, Rosenfield "Criteria for crack extensions in cylindrical pressure vessels" Int J Fract Mechs, 5, 1969

/3/ Folias E.S. "On the effect of initial curvature on cracked sheets" UTEC-CE, 69-002, 1969

/4/ Parry G.W., Lazzeri L. "The application of fracture mechanics to the assessment of failure of cylindrical pressure vessels under yielding" Eng Fract Mechs, 1969

/5/ Bodman E., Fuherott H. "Investigation of critical crack geometries in pipes" 6 SMiRT Conf, L6/6, 1981

/6/ Kiefner J.F., Maxey W.A., Eiber R.J., Duffy A.R. "Failure stress levels of flaws in pressurized cylinders" ASTM, STP 539 (1978)

/7/ Kussmaul K, Sturm D., Stoppler W., Muller-Ecker D. "Experimental investigation on the crack opening behaviour of cylindrical vessels under light water reactor service conditions" - Reliability and Safety of Press Vessel Components, PVP 62

/8/ Kussmaul K., Sturm D., Stoppler W., Julisch P. "Exclusion of fracture in piping of pressure boundary - Part I: experimental investigation and their interpretation" IAEA-SM-269/7

/9/ Kastner W., Rohrich E., Schmitt W., Steinbuch R. "Critical crack size in ductile piping" Pressure vessel and piping, 9/3, 1981

/10/ Bartholomé G., Steinbuch R., Wellein R., "Ausshcluss des doppel endigen rundabrisses der Hauptkuhlmitteldeitung" 7 MPA Seminar, 1981

/11/ Bartholomé F., Kastner W., Keim E., Wellein R. "Esclusion of failure of the pressure retaining coolant system" IAEA-SM-269/7

/12/ Keim E., Steinbuch R.H., "Unfangdurchrisse in rohrleitungen unter innerdruck mit uberlagerter biegebelastung" 14 Sitzung des Arbeitskreises bruchvorgange, 1982

/13/ Dowling A.R., Townley CHA "Effects of defects on structural failure: a two criteria approach" Int.J.Press Vessel Piping (3) 77-107

/14/ J.M. Bloom "A procedure for the assessment of the structural integrity of nuclear pressure vessels" J.Press.Vess.Techn. Febr.1983

/15/ Paris P.G. et al "A treatment of the subject of tearign instability" NUREG-0311 - 1977

/16/ Tada H., PaRIS P.G., Gamble K. "Stability analysis of circumferential cracks in reactor piping systems" NUREG-CR-0838, June 1979

/17/ Lazzeri L. "PAULA 82 : a code for the non linear analysis of piping and shells" 7 SMiRT, L6/7, 1983

/18/ Erdogan F., Kibler "Cylindrical and spherical shells with cracks" Int J. Fracture Mechs., 1969

/19/ Steinbuch R., Bartholomé G., Felski N., Kastner W. "Experimental and theoretical investigation of cracks in primary piping" 6 SMiRT, F7/5, 1981

/20/ Lazzeri L. "DUPIC : a code for the analysis cracks in a ductile pipe" 160-RG-5002, 1983

A PROBABILISTIC STUDY OF LEAK-BEFORE-BREAK CONCEPT[1]

H.H. Woo
Lawrence Livermore National Laboratory
Livermore, California

Prepared for:
Specialist Meeting on Leak-Before-Break in Nuclear Piping Systems
Monterey, California

ABSTRACT

The purpose of this presentation is to assess the leak-before-break[2] concept for nuclear piping systems from the standpoint of the probabilistic approach. The approach is based on the probabilistic fracture mechanics theory. The models used to assess the piping reliability in the analyses have been tested against two real failure incidents. The incidents were (1) PWR feedwater line steam generator nozzle cracking incident, and (2) BWR recirculation safe end cracking incident. The predicted leak results showed high probabilities for leaking (order of 10^{-1}) for both lines. Analyses on three other piping lines, (1) PWR reactor coolant loops, (2) PWR pressurizer surge lines, and (3) PWR main steam line inside containment subjected to design fatigue loading, were also made. All the results indicated that the probabilities for leak are several orders of magnitude higher than those for DEGB. This finding agrees with the experience that no pipe "break" incident has ever happened in nuclear operating history.

---

[1] This work was supported by the United States Nuclear Regulatory Commission under a Memorandum of Understanding with the U.S. Department of Energy.

[2] Break refers to double-ended guillotine break.

S83-236/0536G:tld

NSSP
NUCLEAR SYSTEMS SAFETY PROGRAM
S83-236/0353G

A PROBABILISTIC STUDY OF "LEAK BEFORE BREAK" CONCEPT

PRESENTED BY:

HOWARD H. WOO
LAWRENCE LIVERMORE NATIONAL LABORATORY

PRESENTED TO:

SPECIAL MEETING ON LEAK BEFORE BREAK IN NUCLEAR REACTOR PIPING SYSTEMS
COMMITTEE ON THE SAFETY OF NUCLEAR INSTALLATIONS

MONTEREY, CALIFORNIA
SEPTEMBER 1 AND 2, 1983

PRESENTATION OUTLINE

- PROBABILISTIC VIEW ON "LEAK BEFORE BREAK" CONCEPT
- METHODOLOGY DESCRIPTIONS
- EXAMPLES AND RESULTS
- SUMMARY AND CONCLUSIONS

INITIAL FLAWS HAVE SIX CRACK PROPAGATION SCENARIOS TO FOLLOW DURING PLANT LIFE

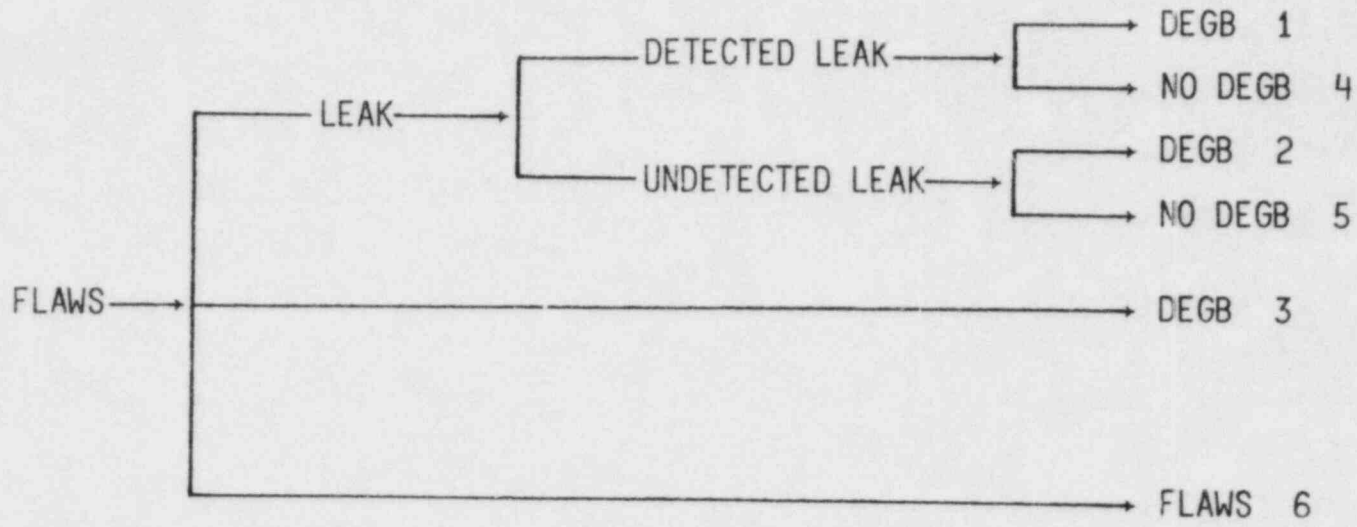

DEGB: DOUBLE-ENDED GUILLOTINE BREAK

WE CAN STUDY "LEAK BEFORE BREAK" CONCEPT FROM PROBABILISTIC STANDPOINT

LET

$$P[\text{DETECTED LEAK} \mid \text{DEGB}] = P[(1)]$$
$$P[\text{UNDETECTED LEAK} \mid \text{DEGB}] = P[(2)]$$
$$P[\text{NO LEAK PROCEEDING DEGB} \mid \text{DEGB}] = P[(3)]$$

THEN

"LEAK BEFORE BREAK" CONCEPT APPLICABLE TO A NUCLEAR PIPING SYSTEM

IF

$$P[(1)] >> P[(2)] + P[(3)]$$

PRAISE* COMPUTER CODE CAN BE USED TO ASSESS THE "LEAK BEFORE BREAK" CONCEPT

- WAS BASED ON PROBABILISTIC FRACTURE MECHANICS THEORY
- HAS BEEN VALIDATED BY COMPARING THE PREDICTIONS WITH REAL FAILURE DATA
  - -- PWR FEEDWATER STEAM GENERATOR NOZZLE CRACKING INCIDENT
  - -- BWR RECIRCULATION SAFE END CRACKING INCIDENT
- HAS BEEN USED TO ASSESS THE RELIABILITY OF VARIOUS PIPING SYSTEMS
  - -- WESTINGHOUSE PWR REACTOR COOLANT LOOP
  - -- COMBUSTION ENGINEERING PWR REACTOR COOLANT LOOP
  - -- PWR PRESSURIZER SURGE LINE
  - -- PWR MAIN STEAM LINE

* PIPING RELIABILITY ANALYSIS INCLUDING SEISMIC EVENTS

PRAISE IS BASED ON PROBABILISTIC FRACTURE MECHANICS CONCEPT

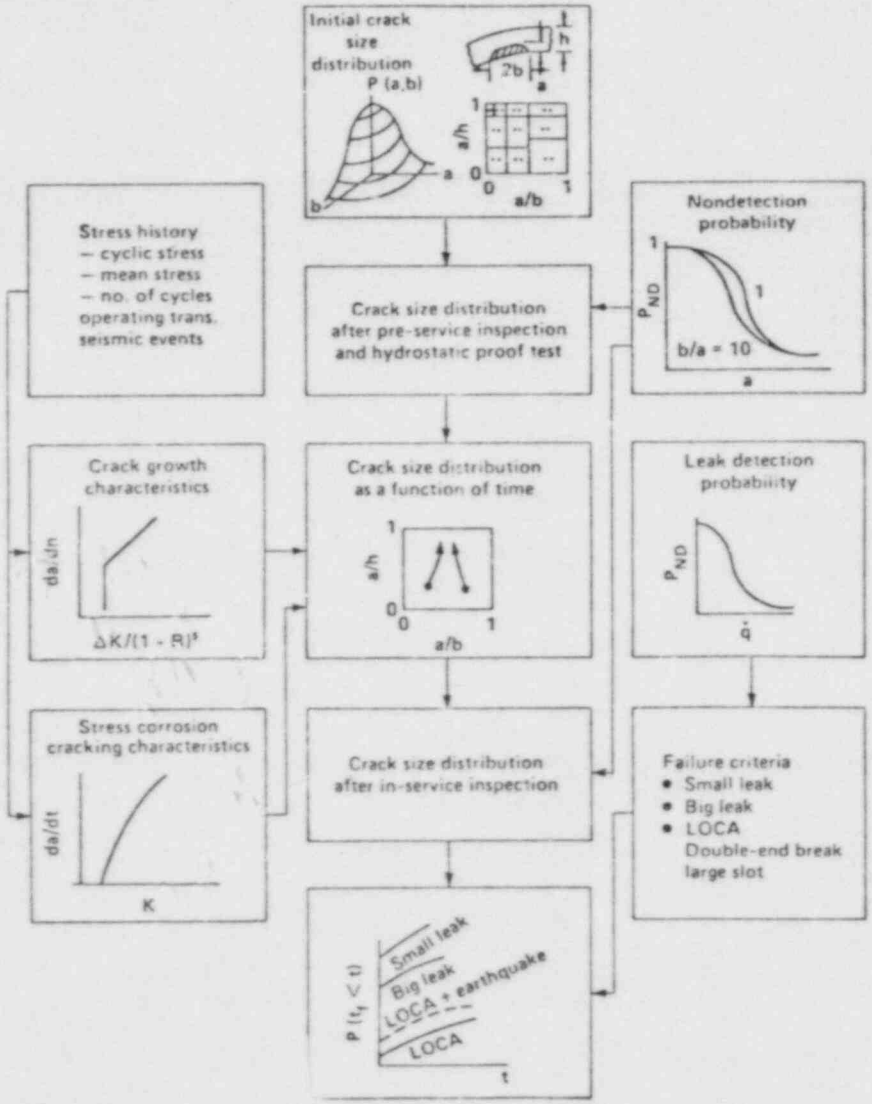

TWO DIMENSIONAL CRACK

CRACK GROWTH
- -- FATIGUE
- -- STRESS CORROSION

CYCLIC LOADS
- -- OPERATING TRANSIENTS
- -- SEISMIC & VIBRATORY STRESSES

PRE-SERVICE AND IN-SERVICE INSPECTIONS

LEAK DETECTION

LEAK AND DEGB PROBABILITIES

WE CONSIDER A SEMI-ELLIPTICAL CRACK IN TUBE INTERIOR SURFACE

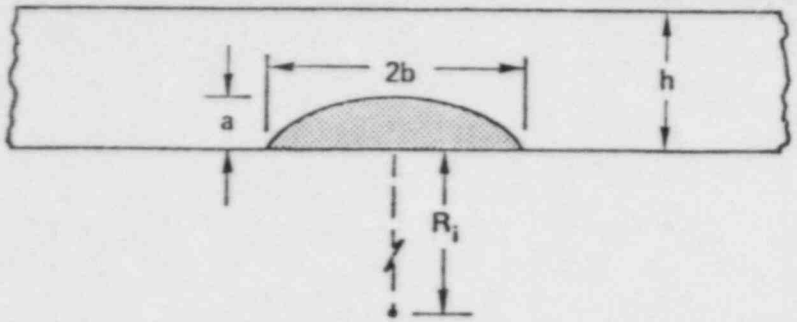

a. Tube longitudinal direction

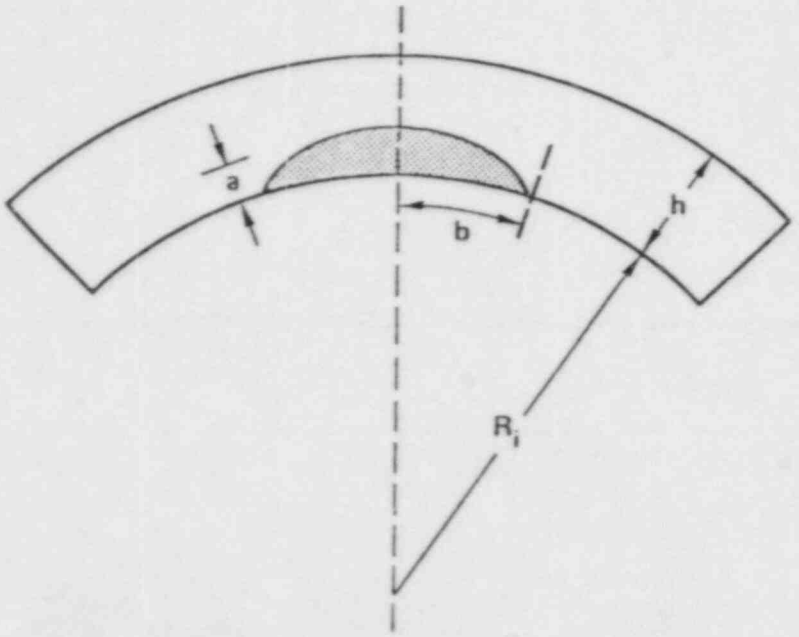

b. Tube circumferential direction

- CRACK ORIENTATION
  - -- LONGITUDINAL
  - -- CIRCUMFERENTIAL
- CRACK GROWTH DIRECTION
  - -- DEPTH
  - -- LONGITUDINAL OR CIRCUMFERENTIAL

DISTRIBUTIONS FOR INITIAL CRACK DEPTH AND CRACK ASPECT RATIO

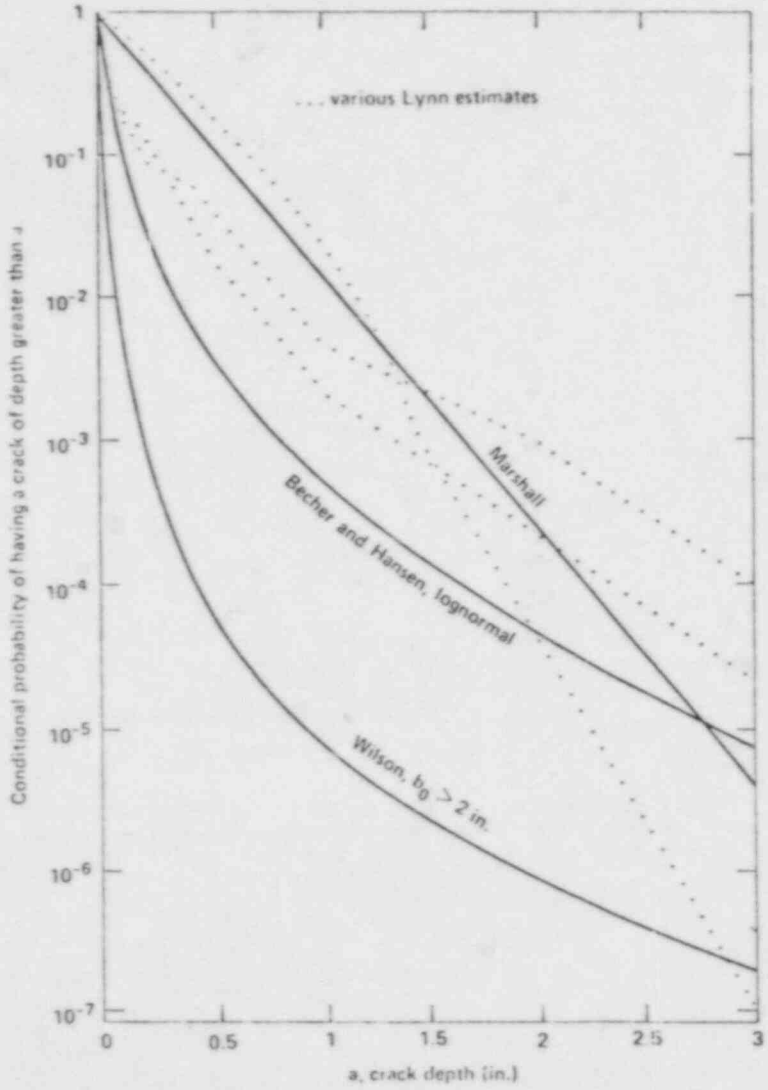

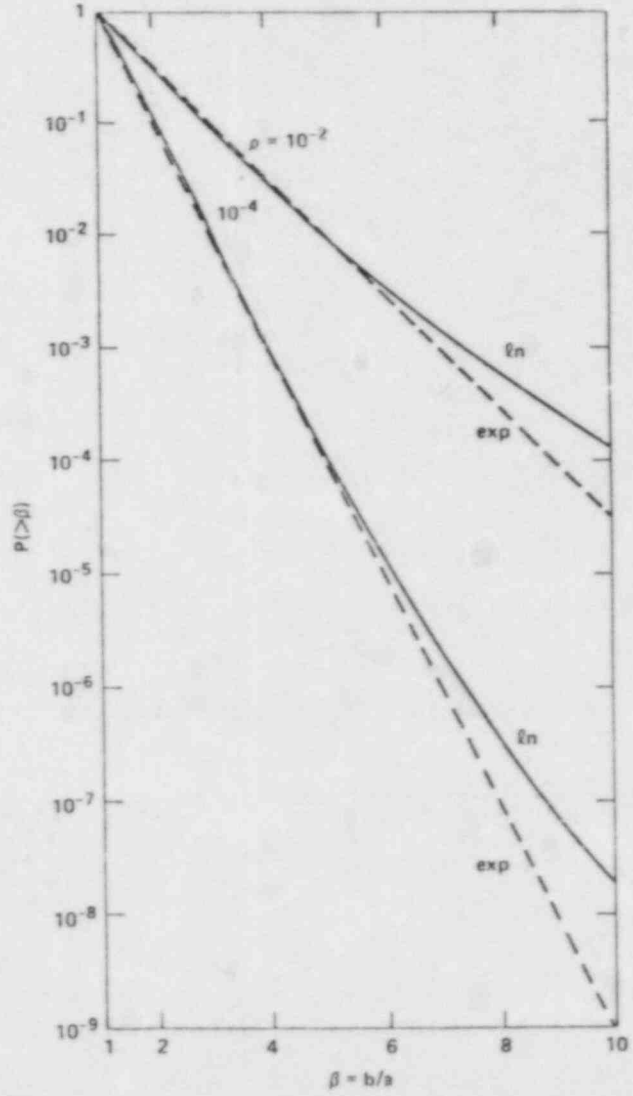

STATISTICAL FATIGUE CRACK GROWTH LAW AND CRACK NON-DETECTION PROBABILITY

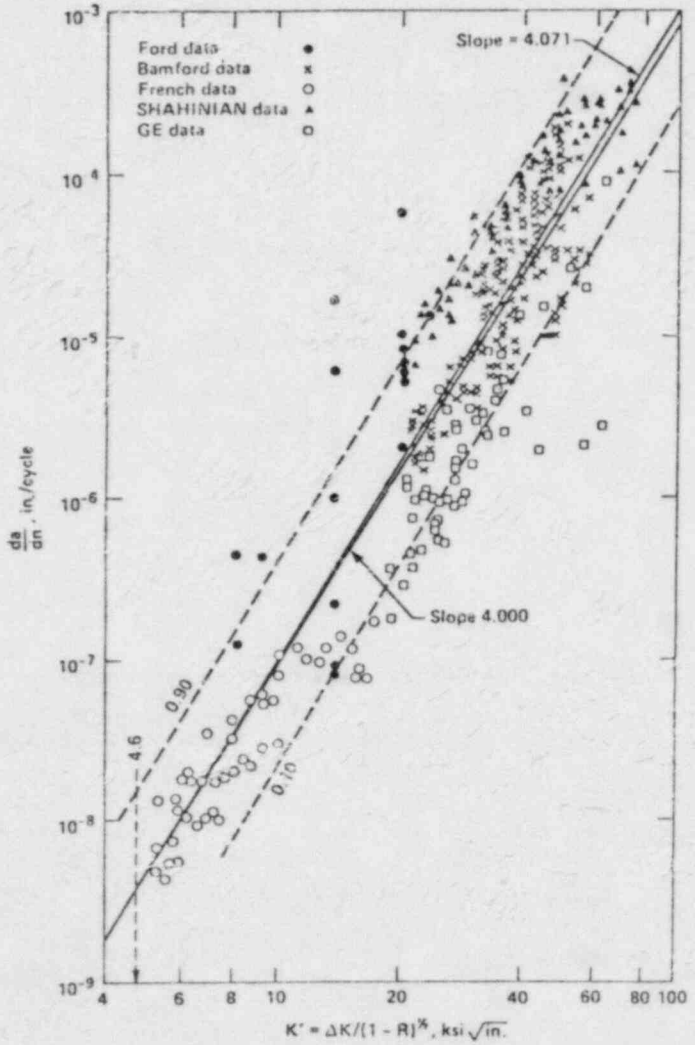

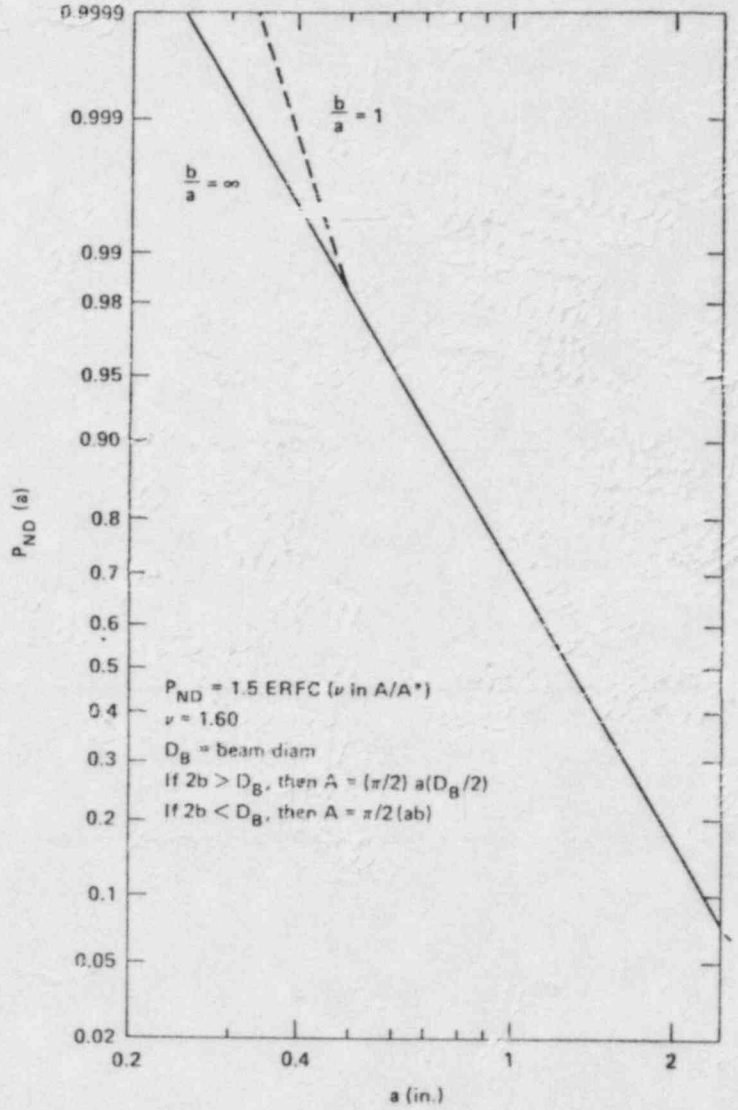

MANY PARAMETERS ARE REQUIRED FOR "PRAISE" INPUTS

- CRACK DEPTH
- CRACK ASPECT RATIO
- SEISMIC LOADS
- THERMAL EXPANSION LOAD
- SEISMIC HAZARD CURVE
  - -- EARTHQUAKE OCCURRENCE RATE
  - -- EARTHQUAKE INTENSITY
- CRACK EXISTING PROBABILITY
- CRACK NON-DETECTION PROBABILITY
- NUMBER OF GIRTH BUTT WELDS
- PRE-SERVICE AND IN-SERVICE INSPECTION
- FATIGUE CRACK GROWTH LAW
- FLOW STRESS
- LOADINGS
  - -- DEAD WEIGHT, PRESSURE
- TRANSIENT CONDITIONS
  - -- TEMPERATURE AND PRESSURE VARIATIONS
  - -- OCCURRENCE RATES
- PIPE GEOMETRY
- NUMBER OF LOOPS

ESTIMATED LEAK AND DEGB PROBABILITIES FOR WELD JOINTS AT THE PWR REACTOR COOLANT LOOPS OVER 40-YEAR PLANT LIFE

WELD JOINT	PROBABILITY OVER PLANT LIFE	
	LEAK	DEGB
1	6.4×10^{-8}	7.9×10^{-13}
2	1.6×10^{-8}	1.9×10^{-16}
3	1.7×10^{-9}	5.1×10^{-15}
4	1.9×10^{-9}	5.3×10^{-14}
5	1.5×10^{-9}	1.5×10^{-14}
6	1.1×10^{-8}	7.1×10^{-17}
7	1.3×10^{-8}	5.1×10^{-17}
8	1.1×10^{-8}	0.
9	1.1×10^{-8}	2.9×10^{-15}
10	1.7×10^{-9}	1.1×10^{-14}
11	1.0×10^{-10}	9.4×10^{-15}
12	2.1×10^{-8}	1.2×10^{-13}
13	2.1×10^{-8}	7.1×10^{-14}
14	3.0×10^{-8}	1.7×10^{-14}

O.D.: 32" - 38" THK: 13.7" - 15.5"
MAT'L: SA-376 TYPE 316

ESTIMATED LEAK AND DEGB PROBABILITIES FOR A PWR PRESSURIZER SURGE LINE OVER 40-YEAR PLANT LIFE

WELD JOINT	PROBABILITIES OVER PLANT LIFE	
	LEAK	DEGB
1	5.0×10^{-8}	5.6×10^{-13}
2	2.6×10^{-7}	3.5×10^{-12}
3	5.4×10^{-7}	2.4×10^{-10}
4	2.4×10^{-7}	8.5×10^{-12}
5	4.9×10^{-7}	1.8×10^{-10}
6	4.8×10^{-8}	1.1×10^{-12}

O.D.: 12.75" THK = 1.312"
MAT'L: SA-376 TYPE 304

ESTIMATED LEAK AND DEGB PROBABILITY FOR A PWR MAIN STEAM LINE INSIDE CONTAINMENT OVER 40-YEAR PLANT LIFE

	PROBABILITIES OVER PLANT LIFE	
WELD JOINT	LEAK	DEGB
1	1.6×10^{-8}	5.9×10^{-16}
2	1.6×10^{-8}	8.1×10^{-16}
3	1.4×10^{-8}	4.3×10^{-16}
4	1.9×10^{-8}	9.4×10^{-16}
5	1.4×10^{-8}	5.4×10^{-16}
6	1.6×10^{-8}	2.8×10^{-15}
7	6.1×10^{-8}	1.1×10^{-14}

O.D.: 28" THK = 1.75"
MAT'L: SA-155 GR. KCF 70

ALL RESULTS INDICATED THAT PROBABILITIES FOR LEAK ARE SEVERAL ORDERS OF MAGNITUDE HIGHER THAN THOSE FOR DEGB

TYPE OF LINES	PROBABILITIES OVER PLANT LIFE	
	LEAK	DEGB
RCL	10^{-10} ~ 10^{-8}	10^{-17} ~ 10^{-12}
PRESSURIZER SURGE LINE	10^{-8} ~ 10^{-7}	10^{-10} ~ 10^{-12}
MAIN STEAM INSIDE CONTAINMENT	10^{-8}	10^{-16} ~ 10^{-14}

SUMMARY AND CONCLUSIONS

- DETERMINISTIC ANALYSIS RESULTS ARE THE FOUNDATION OF PROBABILISTIC APPROACH
- DEGB IS AN EXTREMELY LOW PROBABILITY EVENT UNDER FATIGUE LOADING FOR THREE LINES STUDIED
- WE SHOULD POSTULATE LEAK IN THE DESIGN INSTEAD OF DEGB
  -- NO DEGB FAILURE INCIDENTS
- "LEAK BEFORE BREAK" IS NOT AN ISSUE FOR PIPING SYSTEMS WHOSE LEAK PROBABILITIES ARE VERY LOW
- "LEAK BEFORE BREAK" CONCEPT CANNOT STAND ALONE WITHOUT RELIABLE LEAK DETECTION DEVICES
- OUR RESULTS OF LEAK AND DEGB PROBABILITIES FOR WESTINGHOUSE RCL BASED ON PROBABILISTIC APPROACH HAVE BEEN ACCEPTED BY ACRS IN JUNE 1983
  -- WESTINGHOUSE DEGB DESIGN REQUIREMENT WILL BE RELAXED

CURRENT AND FUTURE WORK

- WE WILL MODIFY PRAISE COMPUTER CODE TO GAIN MORE INFORMATION FOR "LEAK BEFORE BREAK" STUDY

- IMPLEMENTING "LEAK BEFORE BREAK" CONCEPT IN PIPING RELIABILITY ASSESSMENT

  -- COMBUSTION ENGINEERING RCL SYSTEM
  -- GENERAL ELECTRIC BWR PRIMARY PIPING SYSTEM
  -- BABCOCK & WILCOX RCL SYSTEM
  -- ASME CLASS 2 AND 3 PIPING

- PLANNING TO STUDY THE RELIABILITY OF VARIOUS LEAK DETECTION DEVICES

NSSP
NUCLEAR SYSTEMS SAFETY PROGRAM

S83-236/0353G

NUREG REPORTS AND DOCUMENTS GENERATED BY LLNL IN THE AREA OF PIPING RELIABILITY STUDY

- PROBABILITY OF PIPE FRACTURE IN THE PRIMARY COOLANT LOOP OF A PWR PLANT (9 VOLUMES) NUREG/CR-2189
- FRACTURE MECHANICS MODELS DEVELOPED FOR PIPING RELIABILITY ASSESSMENT IN LIGHT WATER REACTORS NUREG/CR-2301
- PIPING RELIABILITY MODEL VALIDATION AND POTENTIAL USE FOR LICENSING REGULATION DEVELOPMENT NUREG/CR-2801
- PIPING RELIABILITY ANALYSIS FOR PRESSURIZED WATER REACTOR FEEDWATER LINES. RELIABILITY AND SAFETY OF PRESSURE COMPONENTS. ASME. PVP-62. 1982
- A PROBABILISTIC ASSESSMENT OF THE PRIMARY COOLANT LOOP PIPE FRACTURE DUE TO FATIGUE CRACK GROWTH FOR A TYPICAL COMBUSTION ENGINEERING PLANT. 7TH SMIRT. CHICAGO. IL. AUGUST 1983
- DUANE ARNOLD STRESS CORROSION CRACKING ANALYSIS. 7TH SMIRT . CHICAGO. IL. AUGUST 1983
- PIPING RELIABILITY MODEL DEVELOPMENT. VALIDATIONS. AND ITS APPLICATIONS TO LIGHT WATER REACTORS. 4TH NATIONAL CONGRESS ON PRESSURE VESSEL AND PIPING TECHNOLOGY. PORTLAND. OREGON. JUNE 1983

LEAK-BEFORE-BREAK DEMONSTRATION FOR A TYPICAL PWR MAIN STEAM PIPE

S. A. Swamy

Westinghouse Electric Corporation
Nuclear Energy Systems
Pittsburgh, Pennsylvania 15230

ABSTRACT

Currently the main steam line break (MSLB) evaluations of pressurized water reactor (PWR) coolant systems are performed for postulated circumferential (guillotine) breaks . This results in overly conservative loading conditions. The objective of this paper is to study the local and global stability of a postulated through wall circumferential flaw in the main steam pipe of a typical pressurized water reactor. Steam leak rates are estimated and are examined in light of currently available leak rate criteria to demonstrate the leak-before-break condition. The need for additional criteria for detection of steam leaks is identified.

1.0 INTRODUCTION

Presently, the Main Steam Line Break (MSLB) evaluation of the Pressurized Water Reactor (PWR) system is carried out by postulating non-mechanistic circumferential guillotine breaks in which the pipe is assumed to rupture along the full circumference of the pipe. This can result in overly conservative support loads. It is therefore, highly desirable to be realistic in the postulation of main steam line breaks. Presented in this report are the results of an analytical study carried out toward establishing that a non-mechanistic type break will not occur within the main steam line inside containment.

The general purpose of this investigation is to show that a circumferential flaw which is very much larger than any flaw that could be present in the main steam line is stable under the worst combination of plant loadings. The fracture criteria proposed for the analysis will examine the local and global stability. A static elastic-plastic finite element analysis of a straight piece of the main steam line pipe containing a circumferential flaw and subjected to internal pressure and external loading is performed. Global stability is demonstrated by using the finite element results and by performing a limit load evaluation. Leak rate through the crack is estimated for normal operating pressure loading. The leak rate prediction is made for a crack of length equal to half of the postulated crack length used in the crack stability evaluation. Figure 1 describes the different steps involved in the leak-before-break demonstration.

A necessary ingredient in the concept of fracture mechanics is knowledge of the present crack size. A fatigue crack growth evaluation will determine the growth of a surface flaw (either postulated or discovered during in-service inspection) through end-of-life from the initial state.

Crack stability analyses and leak rate estimates are performed by postulating large through wall cracks.

2.0 FATIGUE CRACK GROWTH EVALUATION

The fatigue crack growth analyses presented herein were conducted in the same manner as suggested by Section XI, Appendix A of the ASME Boiler and Pressure Vessel Code[1]. The analysis procedure involves assuming an initial flaw exists at some point and predicting the growth of that flaw due to an imposed series of stress transients. The growth of a crack per loading cycle is dependent on the range of applied stress intensity factor ΔK_I, by the following relation:

$$\frac{da}{dN} = C_o(\Delta K_I)^n \qquad (1)$$

where "C_o" and the exponent "n" are functions of material properties.

The input required for a fatigue crack growth analysis is basically the information necessary to calculate the parameter ΔK_I, which depends on crack and structure geometry and the range of applied stresses in the area where the crack exists. Once ΔK_I is calculated, the growth due to that particular cycle can be calculated by equation (1). This increment of growth is then added to the original crack size, and the analysis proceeds to the next transient. The procedure is continued in this manner until all the transients known to occur in the period of evaluation have been analyzed.

Crack tip stress intensity factors are calculated using semi-elliptic surface flaw expressions. Mechanical stresses and the thermal stress distribution through the thickness of the pipe are used in the calculation of the stress intensity factor K_I.

2.1 Thermal Stress Analysis

The heat transfer analysis for each of the transients was carried out by an explicit finite difference heat transfer analysis[2]. The temperature profiles generated by this analysis were then used to calculate thermal stresses. The equations for thermal stress in a hollow cylinder from Timoshenko and Goodier[3] were used:

$$\text{radial stress} = \sigma_r = \left(\frac{\alpha E}{1-\nu}\right)\frac{1}{r^2}\left(\frac{r^2 - a^2}{b^2 - a^2}\int_a^b Trdr - \int_a^r Trdr\right) \quad (2)$$

$$\text{tangential stress} = \sigma_\theta = \left(\frac{\alpha E}{1-\nu}\right)\frac{1}{r^2}\left(\frac{r^2 + a^2}{b^2 - a^2}\int_a^b Trdr + \int_a^r Trdr - Tr^2\right) \quad (3)$$

$$\text{axial stress} = \sigma_Z = \left(\frac{\alpha E}{1-\nu}\right)\left(\frac{2}{b^2 - a^2}\int_a^b Trdr - T\right) \quad (4)$$

where
- r = radial position
- T = temperature as function of r; T→T(r)
- a = inner radius of the pipe
- b = outer radius of the pipe
- ν = Poisson ratio
- αE = the product of the coefficient of thermal expansion and the modulus of Elasticity

The integrals in equations (2) through (4) were evaluated numerically to provide the necessary thermal stresses for each of the transients analyzed.

2.2 Mechanical Stress Analysis

The mechancial loading for the pipe results only from internal pressure, and since this is not a discontinuity region, the resulting stresses in the steam line were calculated in closed form:

$$\sigma_{h_i} = P\,\frac{(b^2 + a^2)}{(b^2 - a^2)} \quad (5)$$

$$\sigma_{h_o} = P\,\frac{2a^2}{(b^2 - a^2)} \quad (6)$$

$$\sigma_{a_i} = \sigma_{a_o} = P\,\frac{a^2}{(b^2 - a^2)} \quad (7)$$

where
- P = internal pressure
- a = inner wall radius
- b = outer wall radius
- σ_h = hoop stress
- σ_a = axial stress
- i = inside surface
- o = outside surface

The thermal and mechanical stresses are combined, and then linearized through the steam line thickness to allow for calculation of the applied stress intensity factor at any given time in a transient.

2.3 Stress Intensity Factor

The stress intensity factor K_I at the point of maximum depth is calculated from the membrane and bending stresses using the following equation from Section XI of the ASME Code[1]:

$$K_I = \sqrt{\frac{\pi a}{Q}} \left(\sigma_m M_m + \sigma_b M_b\right) \qquad (8)$$

The symbols have their usual meaning (see Reference 1 for details).

2.4 Design Transients

The transient conditions selected for this evaluation are based on conservative estimates of the magnitude and frequency of the temperature and pressure transients resulting from various operating conditions in the plant. These are representative of transient conditions which are considered to occur during plant operation and are sufficiently severe or frequent to be of significance to component cyclic behavior. Further, these are regarded as a conservative representation of transients which, when used as a basis for component fatigue evaluation, provide confidence that the component is appropriate for its application over the design life of the plant. The total number of cycles for each operating transient exclusive of the preoperational test cycles has been assumed to be evenly divided over the 40-year operating life of the plant.

2.5 Crack Growth Results

The reference crack growth curve for water reactor environment (ASME Section XI) was considered applicable. The postulated initial crack depths ranged from 0.125 in. to 0.375 in. and were considered to realistically encompass the range of flaws that could be present. Results of the analysis indicated negligible crack growth by fatigue.

3.0 MECHANISTIC PIPE BREAK EVALUATION

A through wall crack 3.35" long (4 times the wall thickness) was postulated for crack stability analysis even though the results of fatigue crack growth indicate that such a flaw cannot result. Both global and local failure criteria were employed to study the crack stability.

3.1 Global Failure Mechanism

A schematic description of the plastic behavior and the definition of plastic load is shown in Figure 2. For a given geometry and loading, the plastic load is defined to be the peak load reached in a generalized load versus displacement plot and corresponds to the point of instability. A simplified version of this criterion, namely, net section yield criterion has been successfully used in the prediction of the load carrying capacity of pipes containing gross size through-wall flaws and was found to correlate well with experiment. This criterion can be summarized by the following relationship:

$$W_a < W_p \tag{9}$$

where W_a = applied generalized load

W_p = calculated generalized plastic load

3.2 Local Failure Mechanism

The local mechanism of failure is primarily dominated by the crack tip behavior in terms of crack-tip blunting, initiation, extension and finally crack instability. Depending on the material properties and geometry of the pipe, flaw size, shape and loading, the local failure mechanisms may or may not govern the ultimate failure.

The stability will be assured if the crack does not initiate at all. It has been accepted that the initiation toughness, measured in terms of J_{IN} from a J-integral resistance curve is a material parameter defining the crack initiation. If, for a given load, the calculated J-integral value is shown to be less than J_{IN} of the material, then the crack will not initiate.

If initiation criterion is not met, one can calculate the tearing modulus as defined by the following relation.

$$T_{app} = \frac{dJ}{da} \left(\frac{E}{\sigma_f^2} \right) \tag{10}$$

where T_{app} = applied tearing modulus

E = modulus of elasticity

σ_f = flow stress = $(\sigma_y + \sigma_u)/2$

a = crack length

σ_y, σ_u = yield and ultimate strength of the material, respectively.

In summary, the local crack stability will be established by the two step criteria:

$$J < J_{IN} \tag{11}$$

$$T_{app} < T_{mat}, J \geq J_{IN} \tag{12}$$

3.3 Finite Element Analysis of Main Steam Pipe

The objective of the finite element analysis was to compute the response due to applied load on the main steam line pipe. The geometry of the pipe and the loadings are shown in Figure 3. The loadings consisted of internal pressure, external bending moment and axial force due to internal pressure acting on the closed end of the pipe.

A circumferential through wall 3.35 inches long crack was postulated and used in the model. Taking advantage of the symmetry, one quarter of the pipe was modeled. Three dimensional variable node isoparametric shell elements were used to model the pipe. Elements were defined by the mid surface node specification. Figure 4 shows the finite element model used in the analysis. The material representing the model pipe was assumed to obey von Mises yield condition and isotropic hardening law. The ADINA[4] computer code was used for this analysis.

The finite element elastic-plastic calculations show that the moment carrying capacity of the main steam line pipe containing a 4T through wall circumferential flaw is greater than 16400 in-kips. The generalized plastic load W_p is then at least 16400 in-kips. The maximum applied generalized load W_a is 10450 in-kips. Therefore the global criterion given by equation 9 is satisfied. The local stability criteria require that $J < J_{IN}$. Based on available data [5] the lower bound value of J_{IN} is 1320 in-lb/in^2 for the temperature of interest. The finite element elastic-plastic solution was post processed to compute the J-integral corresponding to each load step. The method of computing the J-distribution used in this analysis is based on the Virtual Crack Extension method introduced by Parks[6]. In this method the energy perturbation associated with a specified geometric perturbation is evaluated for a given loading. Since the J-integral value is related to the energy perturbation, it can be calculated once energy perturbation resulting from an applied loading is evaluated. A J-integral value of 260 in-lb/in^2 was calculated corresponding to the maximum applied load of 10450 in-kips. Since this calculated J value (260 in-lb/in^2) is lower than J_{IN} (1320 in-lb/in^2) the local stability criterion defined by equation 11 is satisfied.

3.4 Critical Flaw Size Calculation

The critical flaw size can be calculated using the net-section collapse technique. This technique has been applied successfully to predict the behavior of stainless steel pipes.

Based on this method the limit moment is calculated to be:

$$M_b = 2\sigma_f R_m^2 t (2 \cos\beta - \sin\alpha) \qquad (13)$$

and the angle β, which identifies the point of stress inversion (see Figure 5) is given by:

$$\beta = \frac{\alpha}{2} + \frac{(\pi R_i^2 P + F)}{4\sigma_f R_m t} \qquad (14)$$

Where: α = half-angle of crack, in radians

P = internal pressure

R_m = mean pipe radius, inches

t = pipe thickness, inches

σ_f = $.5\ (\sigma_{ys} + \sigma_u)$ (flow stress)

σ_{ys} = yield stress

σ_u = ultimate tensile strength

R_i = pipe inner radius, inches

Limit moment predicted by this approach has been shown to be in good agreement with the experimental results of 304 stainless steel pipe tests[7].

The pipe limit moment for several postulated flaw lengths could be calculated using equations 13 and 14. A plot of the limit moment versus postulated through wall circumferential flaw length was generated as shown in Figure 6. Based on the maximum load on the main steam pipe, the critical flaw size was calculated to be greater than 27 inches using Figure 6.

4.0 LEAK RATE PREDICTION

The NRC has given guidelines on mechanistic fracture requirements for Systematic Evaluation Program plants (Cf. SEP Topic III-5.A). In accordance with these guidelines, the crack opening area was calculated for the steam pipe subjected to the normal operating pressure load. An initial through wall circumferential crack of length equal to two times the wall thickness was postulated for the leak rate calculation. The calculated crack opening area was 0.001 in^2. The following assumptions were made for determining the steam flow rate:

(i) Flow is 1D

(ii) Adiabatic flow condition exists

(iii) Flow is steady

(iv) The flow is single phase and can be treated as an ideal gas

(v) No irreversible effects present

(vi) Flow is choked

Based on these assumptions, the steam leak rate was calculated as 5.4 gpm.

5.0 CONCLUSIONS

A mechanistic fracture evaluation of a typical PWR main steam pipe containing a postulated circumferential flaw was performed. A circumferential flaw of length equal to four times the wall thickness was postulated for stability calculations. Both local and global stabilities were addressed. The results indicated that a 4T circumferential flaw is stable when subjected to maximum loading conditions. Limit moment calculations were performed to determine the critical flaw size based on net section collapse criterion. Results indicated large critical flaw size (27 inches). Leak rate was estimated for a through-wall flaw of length equal to two times the wall thickness. The steam leak rate was calculated to be 5.4 gpm. The equivalent condensed water resulting from this leak is very small compared to the leak detection criterion of 1 gpm (Reg. Guide 1.45). Therefore, a local detection system may be required to detect such a leak. Alternately, since the critical flaw size is very large, one may calculate the leak rate through a larger flaw and show that it is detectable (using Regulatory Guide criteria) while maintaining a safety margin between the size of flaw for which the leak rate is detectable and the critical flaw size. A fatigue crack growth evaluation of the pipe with postulated surface flaws indicated negligible crack growth. Thus, no known mechanism exists that could cause the large through-wall flaws of the size assumed in the mechanistic pipe break calculations.

ACKNOWLEDGEMENT

The author would like to acknowledge the invaluable contribution of his co-workers at Westinghouse - particularly Drs. Y. S. Lee, C. Y. Yang and Messrs. W. T. Kaiser, J. F. Petsche. The encouragement and active support offered by Dr. J. N. Chirigos is gratefully acknowleged.

REFERENCES

1. ASME Boiler and Pressure Vessel Code, Section XI, Appendix A, "Analysis of Flaw Indications", American Society of Mechanical Engineers, New York, 1980 Edition.

2. Holman, J. P., Heat Transfer, McGraw Hill Book Company, New York, 1963.

3. Timoshenko, S. P. and Goodier, J. N., Theory of Elasticity, 3rd Edition, McGraw Hill Book Company, New York, 1970.

4. ADINA - A Finite Element Program for Automatic Dynamic Incremental Nonlinear Analysis, MIT Report 82448-1.

5. Gudas, J. P. and Anderson, D. R., "J_I - R Curve Characteristics of Piping Material and Welds", U. S. NRC 9th Water Reactor Safety Research Information Meeting, Washington, D.C., October 1981.

6. Parks, D. M., "Virtual Crack Extension: A General Finite Element Technique for J-Integral Evaluation, Num. Methods in Fracture Mech., Eds. A. R. Luxmoor and Dr. J. Owne, Swansea, 1978, pp. 464-478.

7. Mechanical Fracture Predictions for Sensitized Stainless Steel Piping with Circumferential Cracks, EPRI NP-192, Project 585-1, Final Report, September 1976.

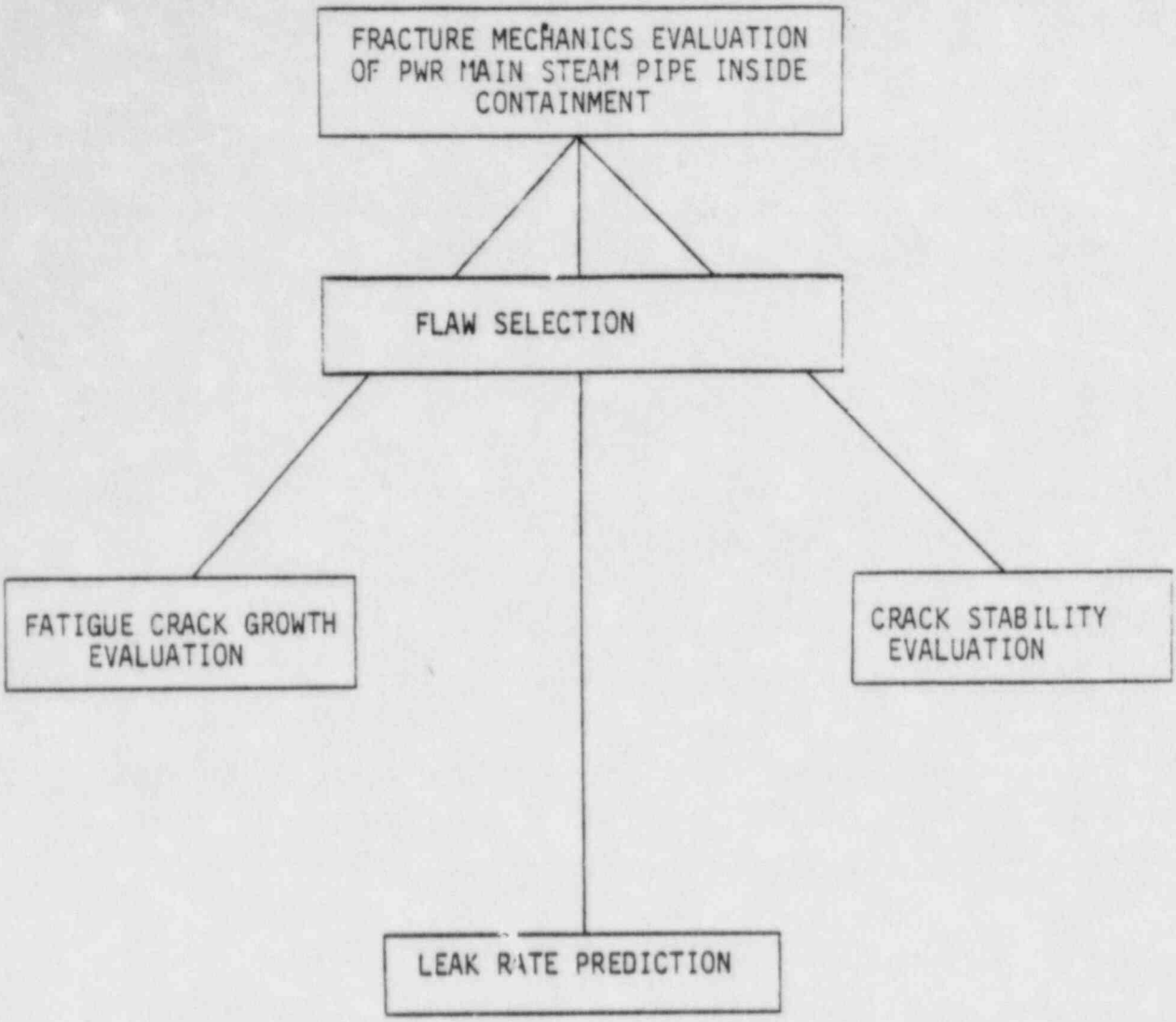

FIGURE 1 LEAK-BEFORE-BREAK METHODOLOGY

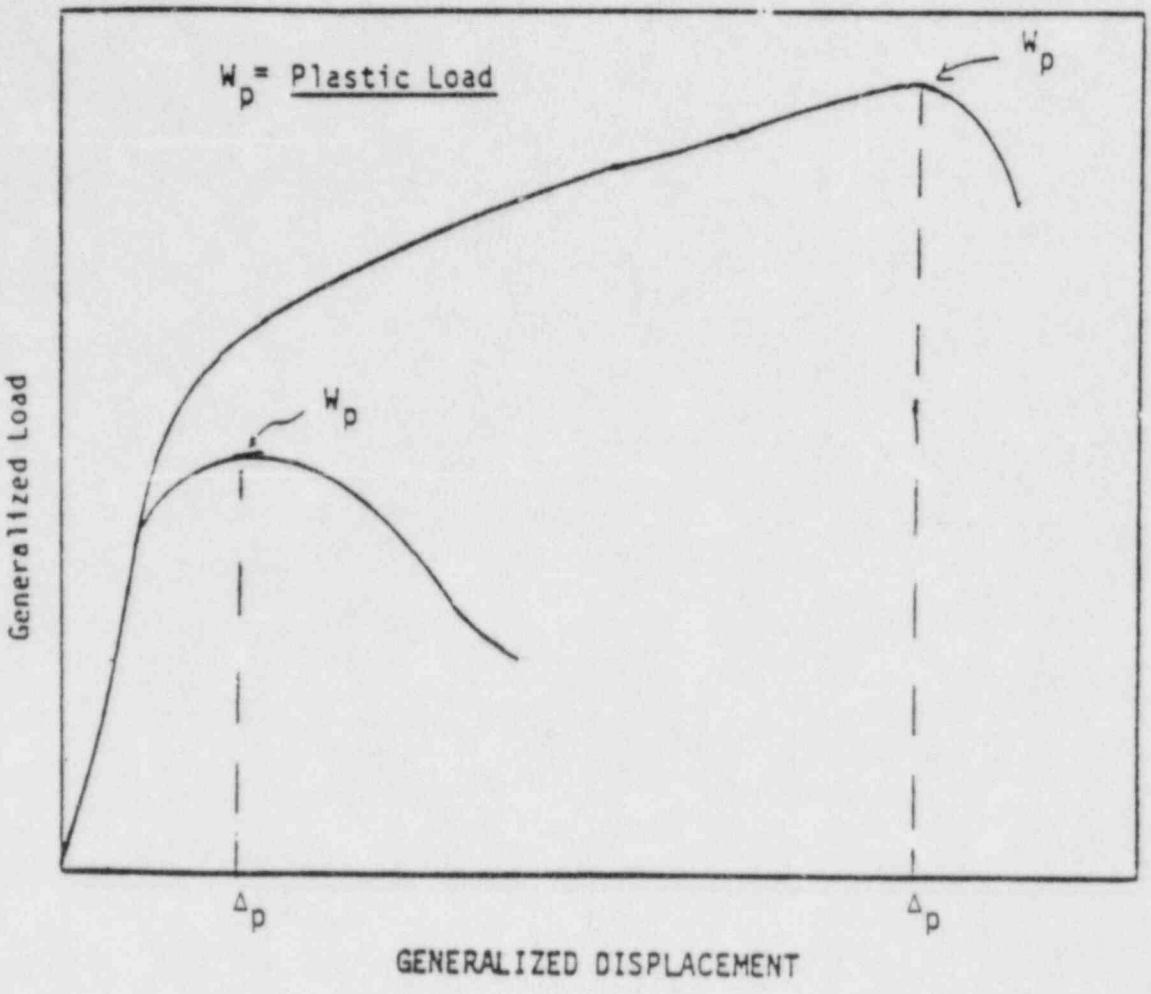

FIGURE 2 Typical Load - Deformation Behavior

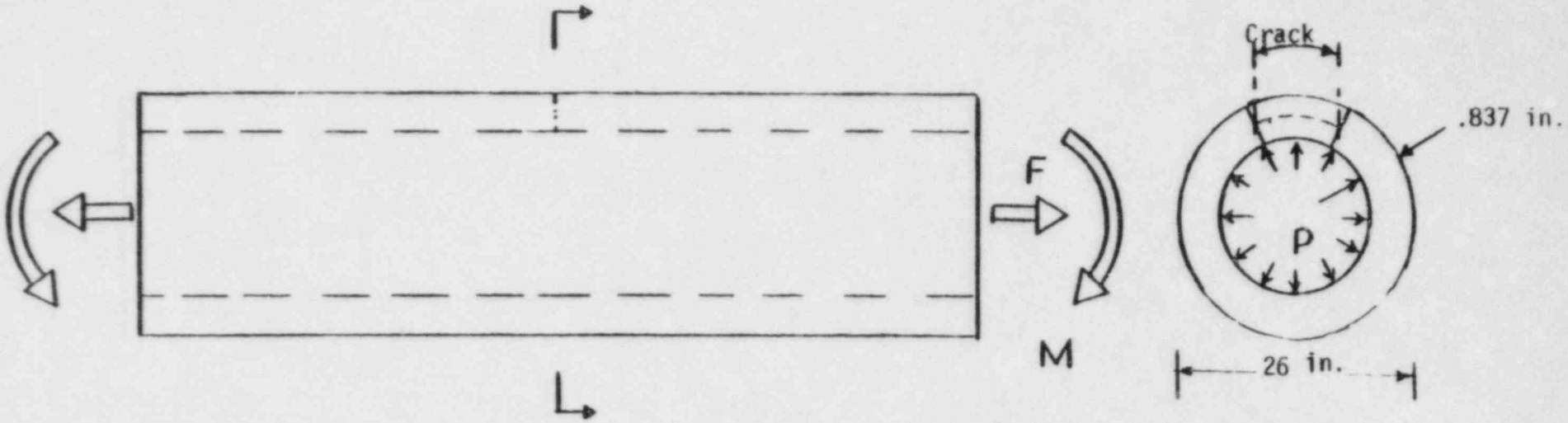

P= 785 psi

F= .39 x 10^6 lbs

M= 10.45 x 10^6 in-lbs

FIGURE 3 Main Steam Line Pipe

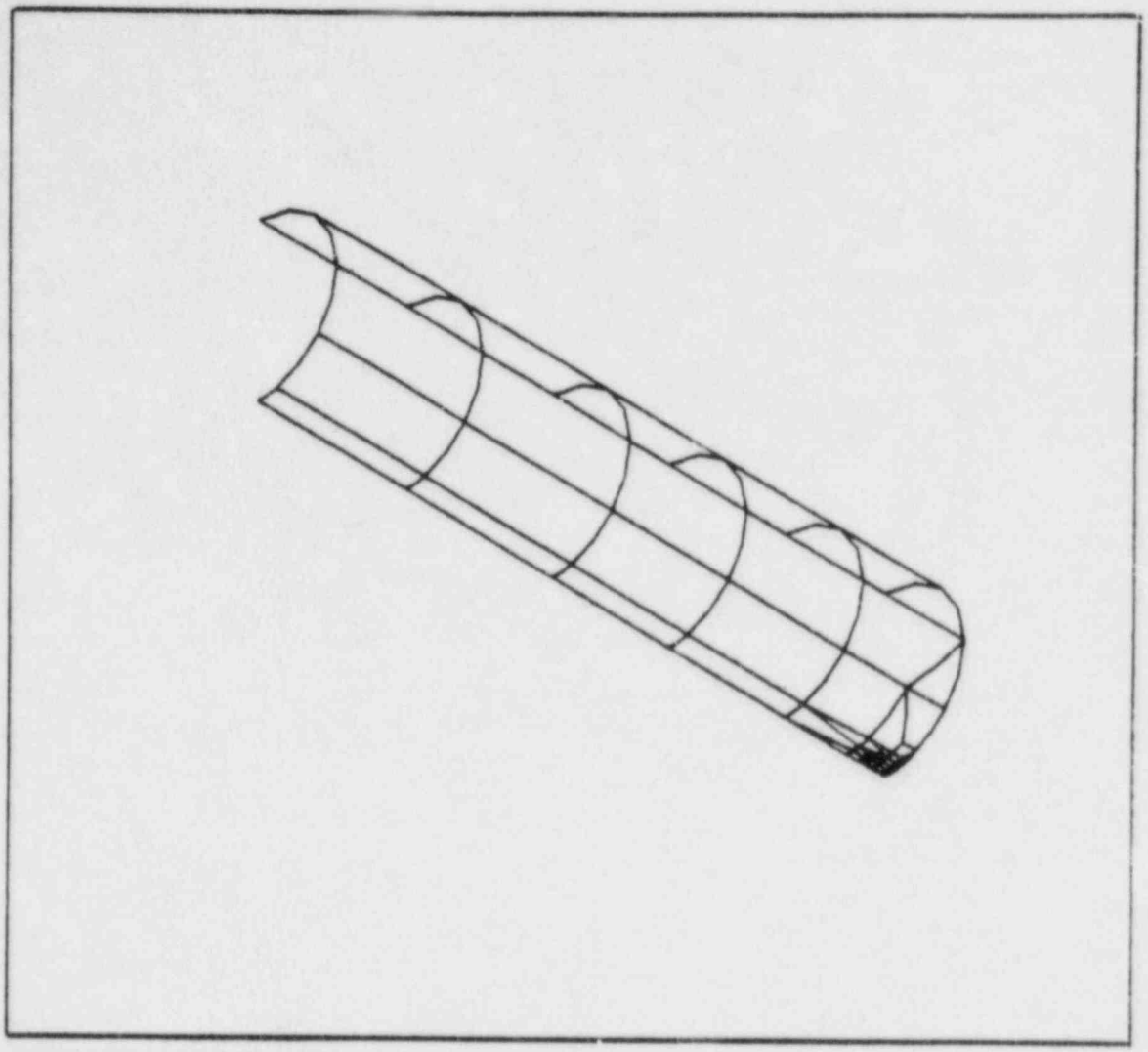

FIGURE 4 Finite Element Model

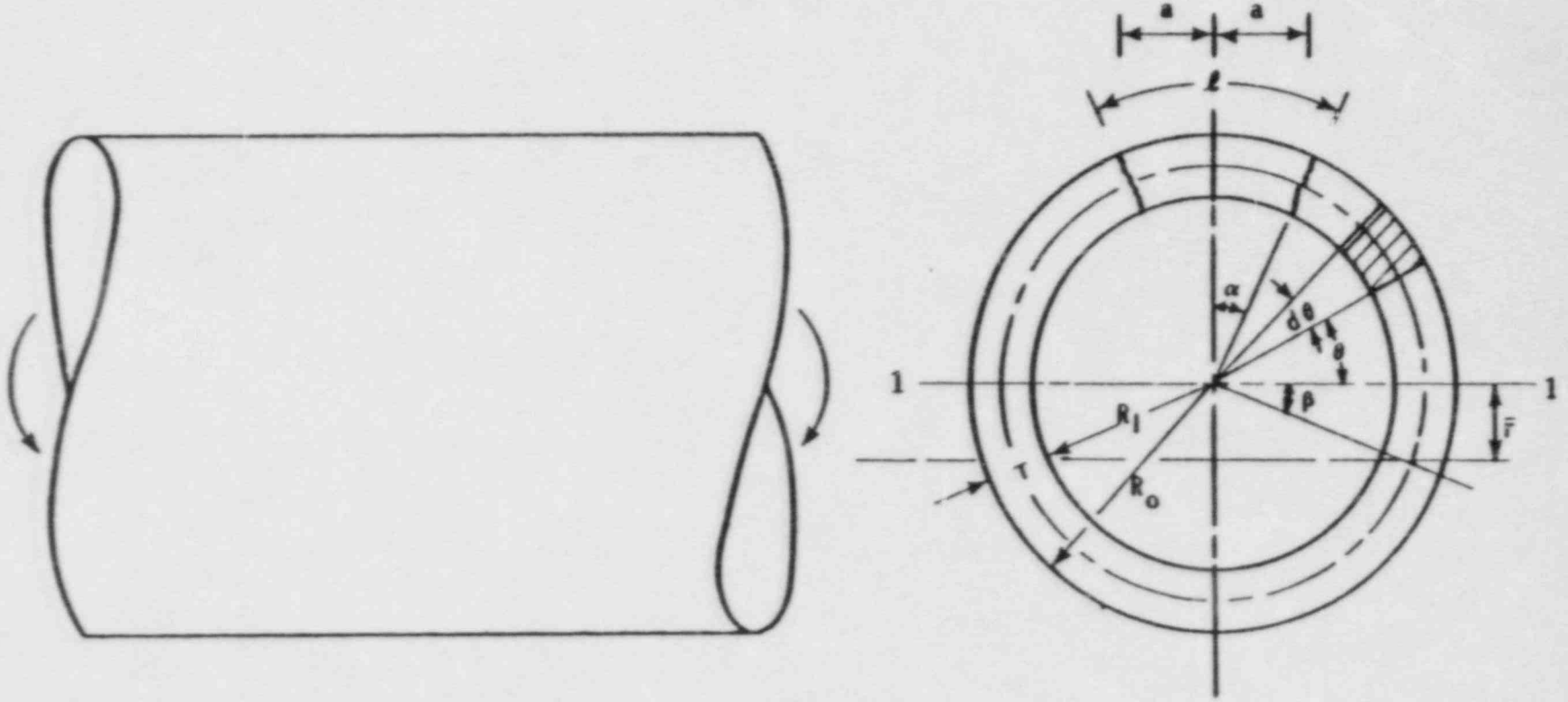

FIGURE 5 Pipe with a Through Wall Crack in Bending

FIG. 6 , CRITICAL FLAW SIZE FOR MAIN STEAM PIPE
OD = 26 IN. , T = 0.837 IN.

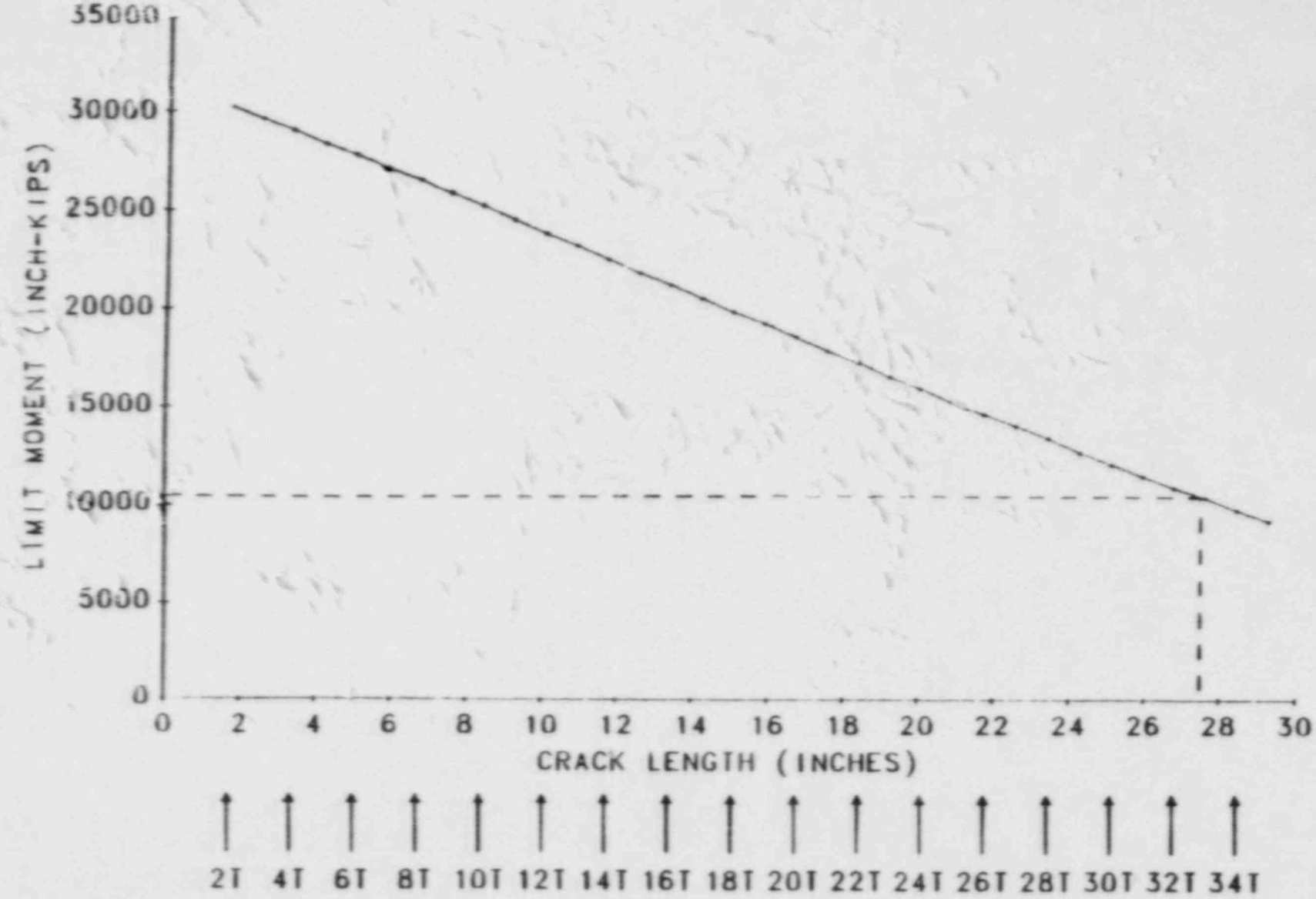

THE CASE FOR ELIMINATING INSTANTANEOUS PIPE BREAK AS A DESIGN BASIS FOR WESTINGHOUSE MAIN COOLANT PIPING

BY

W. H. Bamford, S. A. Swamy and E. R. Johnson

Westinghouse Electric Corporation
Pittsburgh, Pennsylvania

Abstract

A detailed series of studies were carried out to demonstrate the structural integrity of the stainless steel main coolant piping for Westinghouse Pressurized Water Reactors. The purpose of the work was to demonstrate that the primary coolant piping was extremely unlikely to fail due to any of the conditions for which it was designed, and that therefore the design postulate that the pipe fail instantaneously is unrealistic and unnecessary. This paper will present the details of the investigation.

THE CASE FOR ELIMINATING INSTANTANEOUS PIPE BREAK AS A DESIGN BASIS FOR WESTINGHOUSE MAIN COOLANT PIPING

W. H. Bamford
S. A. Swamy

INTRODUCTION

Primary coolant piping for Westinghouse pressurized water reactors is fabricated of stainless steel, either forged or cast. These materials provide superior fracture resistance throughout the entire temperature range of operation of the plant, and the purpose of this presentation is to document that conclusion for all Westinghouse plants.

An extensive survey has been conducted of all Westinghouse plants to determine the range of piping geometry and materials used, and to document the worst case piping loads for each plant. These loads were then compared, to develop a set of umbrella piping loads for all plants and these loads were in turn used to calculate the critical flaw size for the piping system, using a plastic instability calculation method. Both elbows and straight pipe sections were included.

The primary goal of the work reported here is to support the elimination of the large loss of coolant accident as a structural design basis. This includes the postulation of both longitudinal and circumferential breaks. This report documents a presentation made to an ACRS meeting held on March 29, 1983.

MATERIAL PROPERTIES

An in-depth survey was carried out to determine the range of materials in all Westinghouse main coolant loops. All the piping and fittings were fabricated of either Type 316 or Type 304 stainless steel, and the specific materials are listed below:

SA 376-316
SA 376-304N
SA 351-CF8A
SA 351-CF8M
SA 430-316

Although there are a number of different designations here, the actual materials are very similar in both quality and material properties. For example, the survey revealed a range of yield stress for the plants of 32 to 39.6 ksi, and a range of ultimate strength of 75 to 84.7 ksi. The ASME Code specified minimum values are yield stress equal 30 ksi and ultimate strength equal 75 ksi, at room temperature. At 600F the specified minimum values are 17 ksi and 71.8 ksi, and these values were used in the plastic instability analysis. The tensile properties of the welds in the system are required to be greater than or equal to those of the base metal.

An extensive series of fracture toughness tests have been conducted on these materials,[1,2] and results are available for all the material types listed above, including six different weld types. Tests were conducted with both static and dynamic loading rates [2] and results showed excellent fracture toughness values for all heats tested, in terms of both the J_{Ic} values and the R-curves which were obtained. Examples of the J_{Ic} results obtained for the base metal are shown in Table 1, where the lowest value of J_{Ic} at 600F was found to be 2400 in-lb/in^2. The toughness properties for the six weld types tested are also very good, and are within the scatterband of the base metal properties.

ENVELOPING PIPE LOADS

The survey of piping for Westinghouse plants included consideration of the dimensions as well as the loads imposed on each of the segments of the main coolant system. The piping dimensions showed some variations in thickness from plant to plant, but the inside diameter was constant for each segment. The detailed results are shown below:

	Inside Diameter	Wall Thickness
Hot Leg	29 in.	2.43 - 2.80 in.
Crossover Leg	31	2.6 - 3.0
Cold Leg	27.5	2.31 - 2.7

Piping loads were available for 56 of the 59 Westinghouse plants, and results cover the range of plants from coast to coast.

The loads tabulated for these plants, and the enveloping loads used in the analysis, included thermal, deadweight and SSE loads.

The three plants for which results were not available are in the eastern region of the United States, in relatively low seismic areas, so the umbrella loads are expected to be applicable to all plants. The umbrella laods are summarized below, and have been provided in two sets, the first applicable to all the pipe-to-vessel connections and elbow connections and the second for the mid-elbow region at the steam generator inlet. This second region was singled out for attention because it is the only location where a longitudinal split pipe break is postulated in the design process. Critical flaw sizes will be calculated and presented for both cases, and the umbrella loads are provided below:

Umbrella loads - Pipe-to-vessel connections and Elbow connections

Axial force	2910 kips
Bending moment	48425 in-kips

Umbrella loads - Mid-elbow location for Steam Generator inlet elbow

Axial force	2840 kips
Bending moment	37920 in-kips

FRACTURE ASSESSMENT METHODOLOGY AND EXPERIMENTAL BASIS

Determination of the conditions which lead to failure in stainless steel must be done with plastic fracture methodology because of the large amount of deformation accompanying fracture. The state of the art in plastic fracture prediction is such that several viable methods are available, including:

- Tearing instability
- R-6 failure assessment method
- Direct application of J-R curves

All of these methods include some method of dealing with the stable crack growth which precedes final failure in ductile materials. This sub-critical extension of the crack is accomplished by an increasing toughness of the material, as displayed graphically in the J-integral R curves discussed in the previous section.

A conservative method for predicting the failure of ductile material is the plastic instability method, based on traditional plastic limit load concepts, but accounting for strain hardening and taking into account the presence of a flaw. The flawed pipe is predicted to fail when the remaining net section reaches a stress level at which a plastic hinge is formed. The stress level

at which this occurs has come to be called the flow stress, termed σ_f. The flow stress is generally taken as the average of the yield and ultimate tensile strength of the material at the temperature of interest. This methodology has been shown to be applicable to ductile piping through a large number of experiments, and will be used herein to predict the critical flaw size in the primary coolant piping, to be discussed in the following section.

The failure criterion has been obtained by requiring force and moment equilibrium of a flawed pipe, as shown in Figure 1, using an adaption of the plastic analysis of an unflawed pipe given recently by Gerdeen [3]. The detailed development is provided in the appendix, for through-wall circumferential flaw in a pipe with internal pressure, axial force, and imposed bending moments. The limit moment for such a pipe is given by:

$$M_b = 2\sigma_f R_m^2 t (2\cos\beta - \sin\alpha) - 2PR_m^3 \cos\beta$$

where

α = half-angle of crack in radians (refer to Figure A-1, Appendix)
P = internal pressure
R_m = mean pipe radius inches
t = pipe thickness, inches
σ_f = $0.5\ (\sigma_{ys} + \sigma_u)$ (flow stress)
σ_{ys} = yield stress
σ_u = ultimate tensile strength
F = axial force
β = angular location of neutral axis (refer to Figure A-1)

$$\beta = \frac{\sigma_f t \alpha + 0.5 F/R_m}{2\sigma_f t - PR_m}$$

Several experiments were completed recently at Battelle Memorial Institute to consider this type of loading, and a prediction method similar in form to the above equation was used. The above method accurately accounts for the piping internal pressure as well as imposed axial force as they affect the limit moment. The results of the Battelle experiments [4] are plotted along with the predicted limit moments using this method for 304 stainless steel forged pipe in Figure 2. Good agreement was found in this case, as well as in a second set of experiments conducted by Watanabe, et. al. [5], as shown in Figure 3.

The prediction equation for a uniform circumferential flaw at the inside diameter is a simplication of the above equation where the flaw length α is set at zero, and the thickness is adjusted for the presence of the flaw.

The equivalent prediction for a through wall longitudinally oriented flaw was suggested by Eiber et. al. [6], and shown to be applicable to a number of piping geometries and materials in a sizeable number of tests. Similar predictions have been developed more recently by Paris[7] and others. Axially flawed pipes are largely unaffected by imposed bending moments and the limit pressure is given by:

$$P_{LIM} = \sigma_L t/R_m$$

where

$$\sigma_L = [1.28 - 1.4\lambda + 0.809\lambda^2 - 0.219\lambda^3 + 0.0217\lambda^4]\,\sigma_f \qquad \text{(curve-fit from ref. [6])}$$

$$\lambda = a/\sqrt{Rmt}$$

a = crack length

This prediction method was applied to experimental data obtained by Zeibig and Fortman [8] as an illustration, and the results are very good, as shown in Figure 4. Another example of the accuracy of the methodology is seen in its application to the tests of Reynolds [9] on flawed carbon steel pipes, as shown in Figure 5.

A large number of experimental results could be cited to demonstrate the utility of the plastic instability approach in predicting the critical flaw size for ductile piping material. However, for purposes of brevity here reference can be made to previous publications such as references [10] and [11].

The experimental work of [11] was particularly noteworthy in that it showed that crack initiation in the four inch stainless steel pipes tested occurred consistently at maximum load, or slightly below it. Thus it may be seen that more margin could be shown by use of the more complex and rigorous methods mentioned at the beginning of this section. From the comparisons with experimental results which have been cited, however, it hardly seems worth the extensive effort required.

A measure of the conservatism in this prediction method was obtained in the recent work of Zahoor [12]. Postulating an initial surface flaw in the circumferential direction, Zahoor set out to answer the question of whether such a surface crack would continue to propagate once it broke through the wall, leading to a guillotine break. His calculations showed that such large rotations would be required for instability, that the piping would have to be unsupported for very long distances, and free to displace (and rotate) tremendous amounts to achieve a complete break. Piping support systems now in use in light water reactors would not allow such displacements. Therefore, the probability of achieving a full burst, even should the loading be high enough, is very low.

The plastic instability methodology has been shown to be applicable for stainless steel piping in general, because of its extreme ductility. The impact of thermal aging on the cast stainless steel is to reduce the material ductility, and so the question arises as to whether thermal aging will cause a change in the failure mode of this material. This subject was investigated through several experimental programs to be summarized below.

THERMAL AGING EFFECTS ON CAST PIPING MATERIALS AND WELDS

Cast stainless steels have long been known to be sensitive to thermal aging as a result of long time service at temperatures around 885°F. Recent experimental work has shown that thermal aging can occur at temperatures as low as 550F.

Recent experimental work [13, 14] has been conducted to study the effects of long time thermal service on the properties of cast stainless steel reactor coolant piping. Results of these studies show that the flow properties are not strongly affected at all; the ultimate strength is slightly elevated and the yield strength is unchanged. The ductility is slightly reduced, as measured by the elongation and reduction in area from Tensile tests. The Charpy impact energy and J_{Ic} properties of the steel are measureably changed, however, and this information elicits the question of impact of this effect on the integrity of the piping. This question has been addressed in some detail in a recent paper [15], whose results are summarized here.

As reported in detail in [15], a heat of cast stainless steel piping was aged for 2000 hours at a temperature of 800F to study the aging effect. Charpy, tensile, and compact specimens were cut from the pipe to characterize the properties before and after aging, and whole pipe sections were tested with circumferential flaws to characterize the impact of aging on piping integrity.

The Charpy impact energy of the material was reduced by approximately 45% due to the aging process, but the other properties were not strongly affected. Tests of the 4 inch schedule 80 flawed pipe sections before and after aging showed essentially no effect of the aging process on the failure mode of the pipe, and the results are summarized in Figure 6, along with plastic instability predictions using the method described earlier. Two different prediction curves were developed for the aged and unaged pipes, due primarily to a slight difference in internal pressure for the test of the aged piece. Agreement with the predictions was excellent, and the results confirm the conclusion that there is no direct relationship between Charpy energy and failure mode or load for stainless steel, where the flow properties govern failure.

The question which then arises is what level of degradation would be enough to cause concern that the flow properties would no longer govern failure. This question has been addressed in the liquid metal breeder reactor design, where both irradiation and thermal aging are of concern, and the measure of ductility which has been imposed as a design limit is 10 percent total elongation. The use of this threshold level is supported by the work of Fish et. al. [16] on highly irradiated stainless steel.

Results to date for thermal aging of cast stainless steels have shown that the differences between the yield strength and tensile strength have been maintained, i.e. the uniform elongation is essentially not degraded. A summary of available data is given in Table 2, and shows a minimum total elongation of 25 percent after 10,000 hours at 752°F (400°C). This value is clearly far away from the level of engineering concern.

The discussions here have centered on base metal properties. The effect of thermal aging on stainless steel pipe welds has also been studied in reference 14, and results show there is little or no effect. This conclusion holds for virtually all the properties, including tensile as well as charpy energy, which as been seen previously to be the most sensitive indicator. Aging times have exceeded 10000 hours.

Thus it can be seen that the impact of thermal aging on the integrity of primary coolant piping is not of significant engineering concern, based on presently available data.

RESULTS OF CRITICAL FLAW SIZE CALCULATIONS

The plastic instaiblity methodology was used in conjunction with the umbrella loads obtained from the survey of individual plants to develop a prediction of the critical flaw size for a circumferential flaw in the main coolant loop. Both the straight pipe connections and elbows were considered, and separate consideration was given to longitudinal flaws in the steam generator inlet elbow, since that is the only place where a longitudinal split break is postulated in the Westinghouse main coolant loop.

Circumferential Flaws in Straight Pipe and Connections

Figure 7 shows a plot of the plastic limit moment as a function of through-wall circumferential flaw length in main coolant piping of nominal dimensions. This limit moment was calculated for a pressurized pipe at 2250 psi with an aixal force of 2910 kips, operating at 600F with code minimum tensile properties. The umbrella moment for all Westinghouse plants, 48425 in-kips can be plotted on this figure, and used to determine the critical flaw length, which is shown to be approximately 25 inches.

Longitudinal Flaws in Elbows

A longitudinal split break is postulated in the steam generator inlet elbow, and this is the only location in the main coolant loop where a longitudinal break is postulated. The steam generator inlet elbow is a 50 degree elbow, and the likelihood of a split there is very low, for a number of reasons, one of which is the fact that it is seamless. The break is postulated in the elbow because it is the most highly stressed elbow. Even though the loads in this elbow are the highest of all elbows, they are still below the governing terminal connection, as shown earlier in the section on enveloping pipe loads.

The prediction methods for failure in elbows are virtually the same as those for straight pipes; that is the plastic instability predictions for straight pipes are directly applicable to elbows of the same nominal pipe size.

Over 20 experiments have been carried out to study the failure of stainless steel pipe elbows, and the results have confirmed the applicability of straight pipe limit load predictions for longitudinal flaws [17]. It will be useful to examine some of the results shown in reference 17 in more detail. Tests were run on scale model elbows of Type 304 stainless steel, with flaws located at the crown of the elbow as well as the intrados and extrados locations. Results for the longitudinally oriented flaws are summarized in Figure 8.

Recalling that piping bending moments have little or no influence on the failure of longitudinally flawed piping, it is somewhat intuitive that the additional moments which result in the elbow because of its geometry do not affect longitudinal flaws there. Figure 4 shows a plot of hoop stress at failure σ_H non-dimensionalized with the flow stress, and this may be visualized as a dimensionless failure pressure. This parameter is plotted aginst a dimensionless measure of the through-wall flaw length, a. The parameters r = mid-radius of the pipe, and t = wall thickness of the pipe.

This figure shows that the plastic instability model for limit pressure discussed earlier does an excellent job of predicting the failures of all of these elbows. The elbows tested had a ratio of diameter to bend radius of between 0.67 and 0.75 which compares to a ratio of about 0.70 for Westinghouse primary coolant piping.

This is the key parameter for comparing elbow behavior, and so the test results should be directly applicable to the Westinghouse primary coolant system. The second parameter of interest is the radius to thickness ratio, and here we find the primary coolant elbows to be somewhat stiffer than the model elbows, having a ratio of about 7 compared with the value of 15-16 for the test elbows. This difference is probably not significant, but would indicate that the main coolant elbows would be slightly more resistant to failure, if there were any effect at all.

Limit pressure predictions were carried out for the Westinghouse steam generator inlet elbows in the presence of longitudinal flaws, and the results are shown in Figure 9. As discussed earlier these predictions also apply to longitudinal flaws in straight pipes, and indicate a critical flaw length of about 26 inches for a through-wall flaw.

SUMMARY AND CONCLUSIONS

An extensive study of Westinghouse main coolant piping materials has been carried out, and confirmed excellent fracture resistance. Enveloping pipe loads were determined from detailed study of 56 of the 59 plants. (The others are expected to fall within the envelope obtained).

Analytical methods were presented for prediction of piping failure in the presence of either axial or circumferential flaws. These methods, based on plastic instability, were shown to be applicable to both straight piping and elbows through presentation of extensive experimental results.

Application of these methods to Westinghouse primary coolant piping showed that the critical length of a through-wall flaw is at least 25 inches, so the likelihood of a pipe rupture is very remote. Flaws smaller than 25 inches will be stable, because the materials fracture resistance is greater than the driving force. Flaws less than one third this length will produce detectable leakage, and so leak before break can be demonstrated. Therefore the postulation of instantaneous full area pipe breaks is unrealistic, and should be eliminated for the main loop.

REFERENCES

1. Bamford, W. H. and Bush, A. J., "Fracture of Stainless Steel", in Elastic Plastic Fracture, ASTM STP 668, 1978.

2. Palusmay, S. S. and Houtman, A. J., "Mechanistic Fracture Evaluation of Reactor Coolant Pipe Containing a Postulated Circumferential Through-wall Crack" Westinghouse Electric Corp., Report WCAP 9570, June 1981.

3. Gerdeen, J. C., "A Critical Evaluation of Plastic Behavior Data and a Unified Definition of Plastic Loads for Pressure Components" in Welding Research Council Bulletin 254, November 1979.

4. Kanninen, M. F., Broek, D., Marschall, C. W., Rybicki, E. F., Sampath, S. G., Simonen, F. A., and Wilkowski, G. M., "Mechanical Fracture Predictions for Sensitized Stainless Steel Piping with Circumferential Cracks", EPRI-NP-192, September, 1976.

5. Watonabe, M., Mukai, Y., Kaga, S. and Fujihara, S., "Mechanical Behavior on Bursting of Longitudinally and Circumferentially Notched 304 Stainless Steel Pipes by Hydraulic and Explosion Tests" in Proceedings Third International Conference on Pressure Vessel Technology, Tokyo, April 19-22, 1977, pp. 677-683, ASME, New York, 1977.

6. Eiber, R. J., Maxey, W. A., Duffy, A. R., and Atterbury, T. J., "Investigation of the Initiation and Extent of Ductile Pipe Rupture", BMI 1866, July 1969.

7. Vasquez, J. A. and Paris, P. C., "A Plastic Zone Instability Phenomenon Leading to Crack Propagation and its Application to Pressure Vessel Failure", Journal of Testing and Evaluation (to be published).

8. Zeibig, H. and Fortmann, F., "Fracture Behavior of Ferritic and Austenitic Steel Pipes", Procedings Second Conference on Structural Mechanics in Reactor Technology", Berlin 1973, F4/8.

9. Reynolds, M. B., "Failure Behavior of ASTM A1063 Pipes Containing Axial Through-Wall Flaws" General Electric Corp., Report GEAP 5620, April 1968.

10. Norris, D. M., Marston, T. U., and Taggart, S. W., "Acceptance Criteria for Circumferential Flaws in Stainless Steel Piping", in Aspects of Fracture Mechanics in Pressure Vessels and Piping, ASME Publication PVP Vol. 58, June 1982.

11. Ranganath, S. and Metha, H. S., "Engineering Methods for the Assessment of Ductile Fracture Margin in Nuclear Power Plant Piping, in Proceedings Second International Symposium on Elastic Plastic Fracture Mechanics, ASTM STP, 1981.

12. "Instability Predictions for Circumferentially Cracked Pipe", M. F. Kanninen, et. al., Electric Power Research Institute Project T118-2 Final Report.

REFERENCES (cont'd)

13. Landerman, E. I. and Bamford, W. H., "Fracture Toughness and Fatigue Charateristics of Centrifugally Cast Type 316 Stainless Steel Piping After Simulated Thermal Service" in Ductility and Toughness Considerations in Elevated Temperature Service, ASME Publication MPC-8, New York 1978.

14. Slama, G., et. al. "Influence of Aging on the Mechanical Properties of Austenitic Stainless Steel Casting and Welds" in Proceedings Seventh Conference on Structural Mechanics in Structural Mechanics in Reactor Technology, August 1983 (to be published).

15. Bamford, W. H., et. al., "Thermal Aging of Cast Stainless Steel, and Its Impact on Piping Integrity" ASME, Journal of Pressure Vessel Technology (to be published).

16. Fish, R. L., Cannon, N. S. and Wire, G. L., "Tensile Property Correlations for Highly Irradiated 20 Percent Cold-Worked Type 316 Stainless Steel" in Effects of Radiation and Structural Materials, ASTM STP 683, 1979, pp. 450-465.

17. Begley, J. A., et. al., "Crack Propagation Investigation Related to the Leak Before Break Concept for LMFBR Piping" in Proceedings, Conference on Elastic Plastic Fracture, Institution of Mechanical Engineers, London 1978.

TABLE 1

FRACTURE TOUGHNESS TEST RESULTS

(ALL TESTS AT 600F)

HEAT	MATERIAL TYPE	CONDITION	J_{Ic} STATIC	J_{Ic} DYNAMIC
C1488	A351-CF8M	CENT. CAST	4500	4000
C2375	A351-CF8M	CENT. CAST	3500	4500
154581	A351-CF8M	CENT. CAST	5200	8500
D8770	A376TP316	WROUGHT	2400	5000
D8771	A376TP316	WROUGHT	9300	6000
156576	A351-CF8A	CENT. CAST	5998	-

TABLE 2 SUMMARY OF AGING DATA FOR CASTINGS STUDIED IN DETAIL [1,2]

Material (Water Quenched)	RT Yield Strength As Rec'd	RT Yield Strength 10,000 hrs. at 400°C	RT-Tensile Strength As Rec'd	RT-Tensile Strength 10,000 hrs. at 400°C	RT-Elongation - % As Rec'd	RT-Elongation - % 10,000 hrs at 400°C	Ferrite	Carbon	RT - CV As Rec'd	RT - CV 10,000 hrs. at 400°C
	(MPa)		(MPa)						(dJ/cm^2)	
CF8 473BC	225	250	510	550	62	47	5.5	.021	25	17.5
CF8M 472V	275	300	550	660	53	36	10.6	.026	27	6
CF8 167	260	275	530	620	45	44	16.2	.041	27	7
CF8M 166CN	250	287*	525	643	40	28	12	.050	24	4
CF8M 166CN	250	313**	550	750	43	30/25				
CF8M 1488	290	390***	571	691	52	52	17.5	.06	27	5

*5000 hours

**7500 hours

***3000 hours, at 427°C

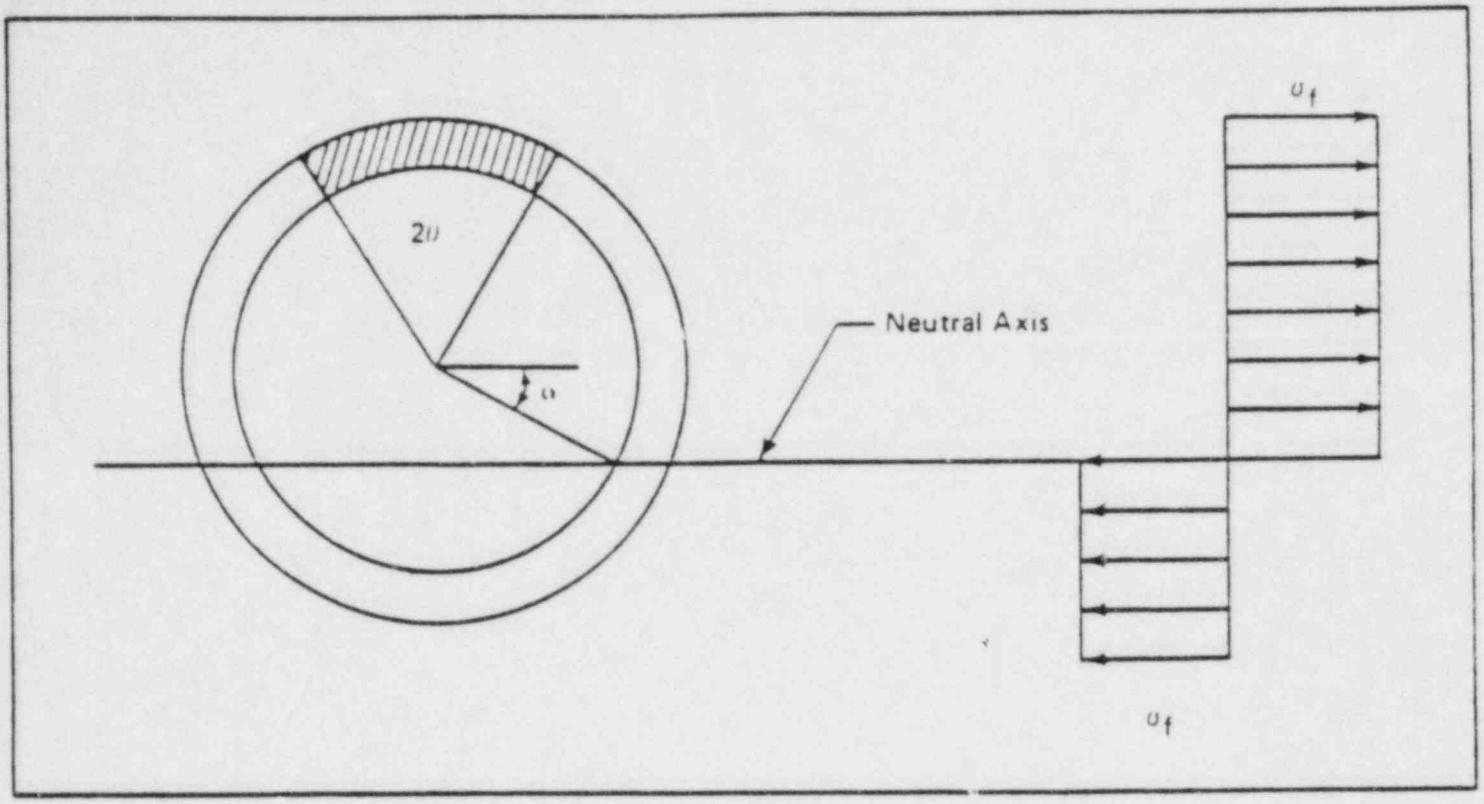

Figure 1 Fully Plastic Stress Distribution

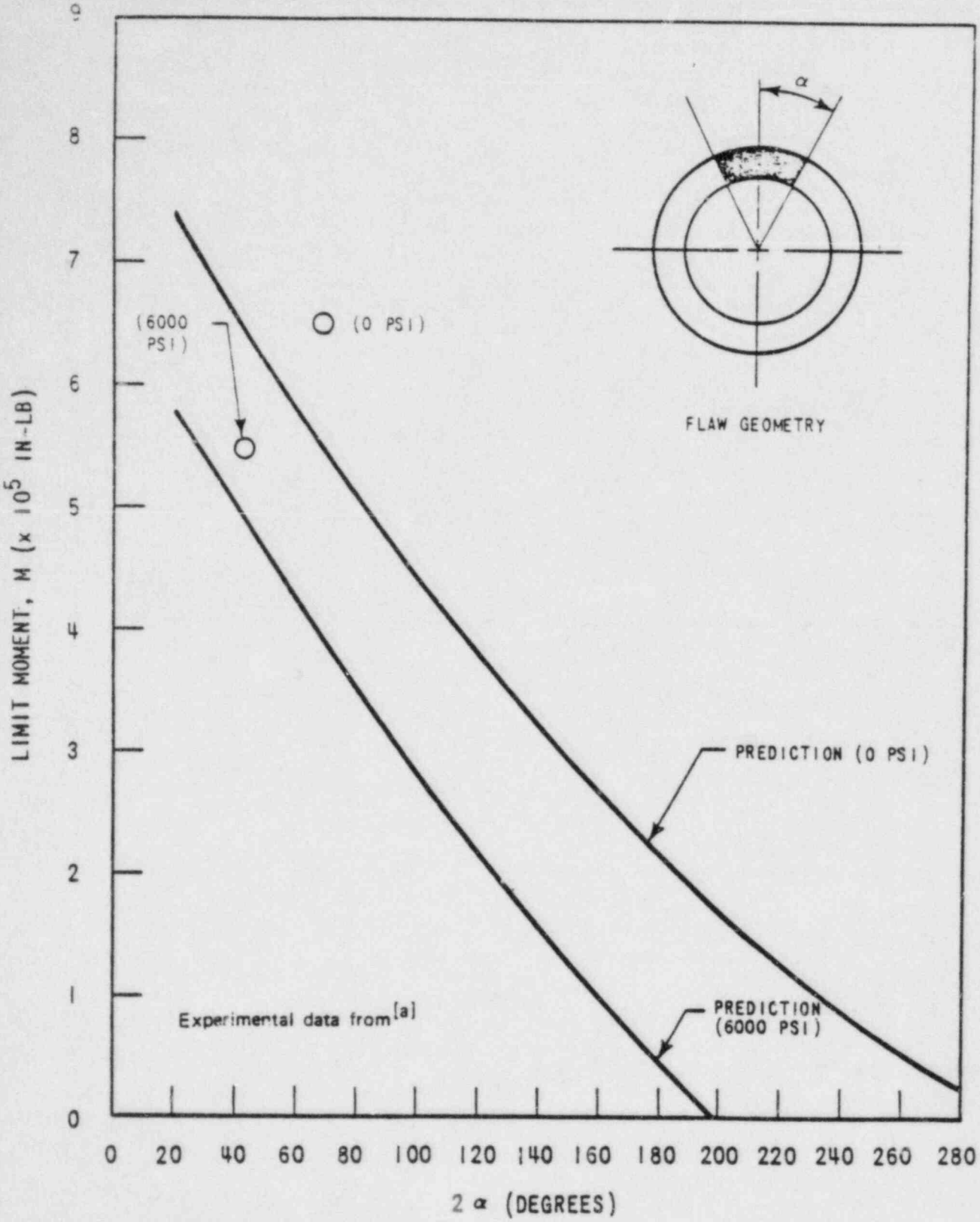

a. Kanninen, M. F., et. al., "Mechanical Fracture Predictions for Sensitized Stainless Steel Piping With Circumferential Cracks," EPRI-NP-192, September 1976

Figure 2 Comparison of Limit Moment Predictions With Experimental Results

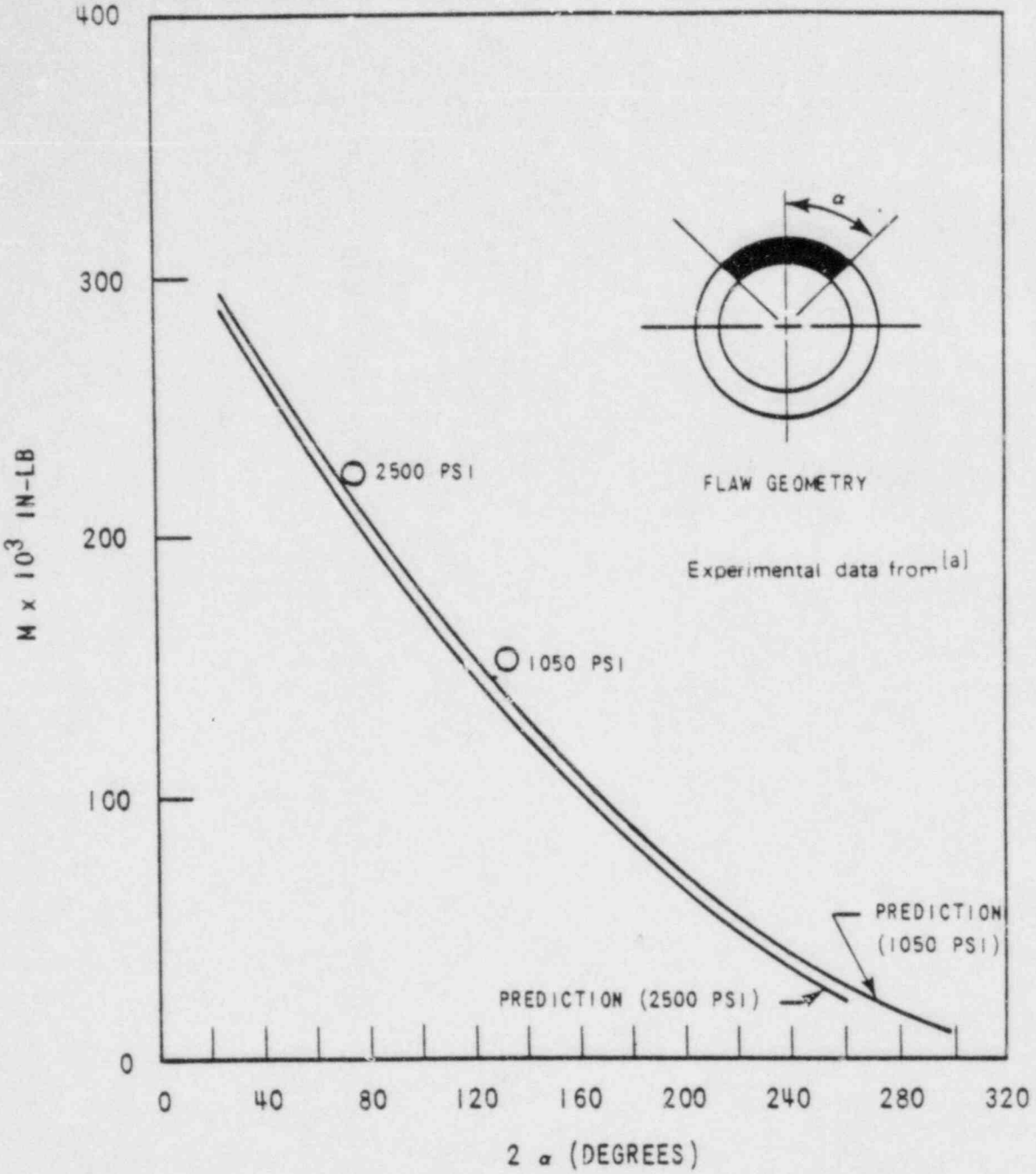

a. Watanabe, M., Mukai, Y., Kaga, S., and Fujihara, S., "Mechanical Behavior on Bursting of Longitudinally and Circumferentially Notched AISI 304 Stainless Steel Pipes by Hydraulic and Explosion Tests," Proceedings of Third International Conference on Pressure Vessel Technology, Tokyo, April 19-22, 1977, 677-683, ASME, NY, 1977.

Figure 3

COMPARISON OF LIMIT MOMENT PREDICTIONS WITH EXPERIMENTAL RESULTS - AISI 304 PIPING

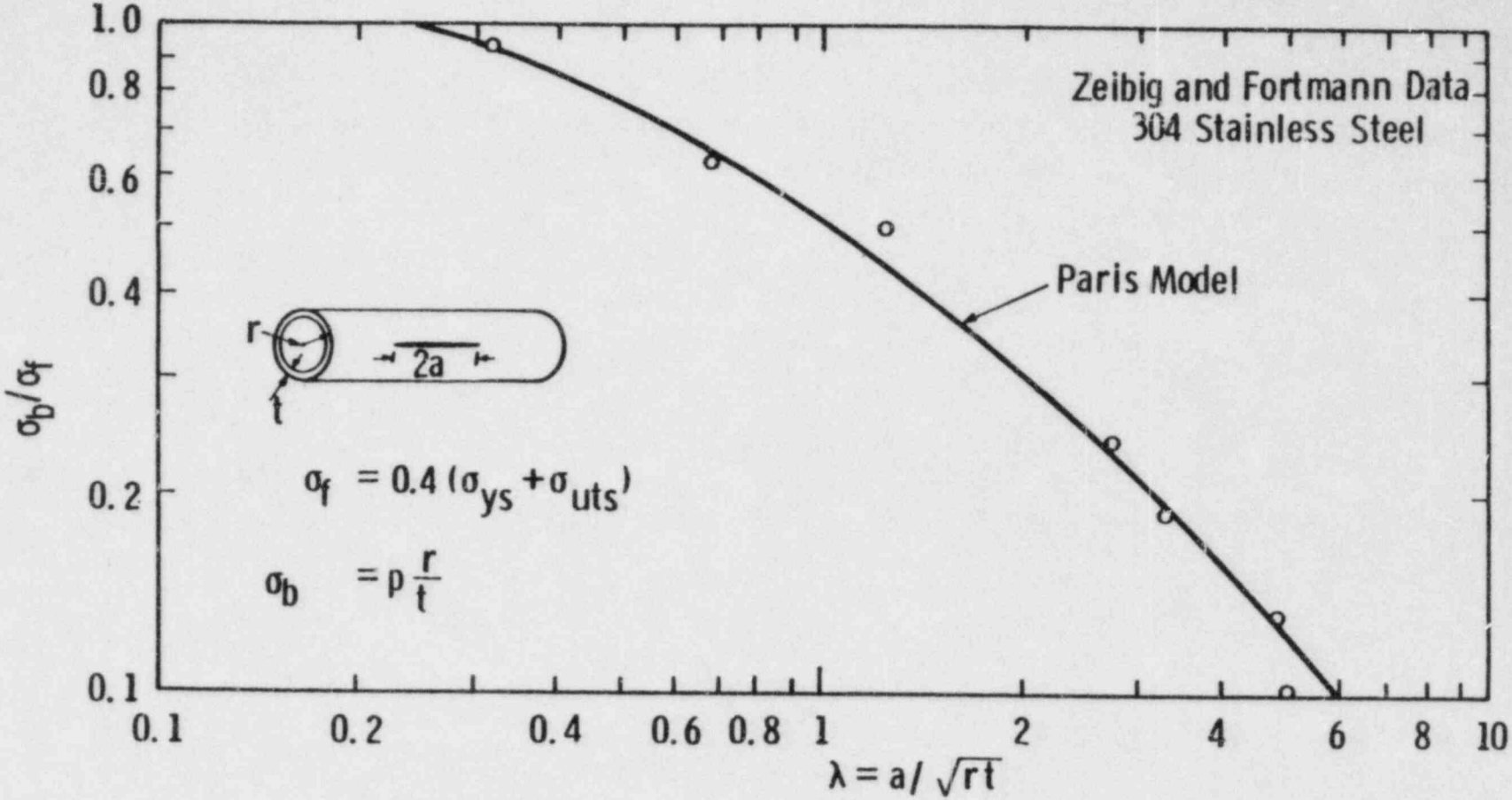

FIGURE 4—Correlation between the burst test data of Zeibig and Fortmann and the Paris model

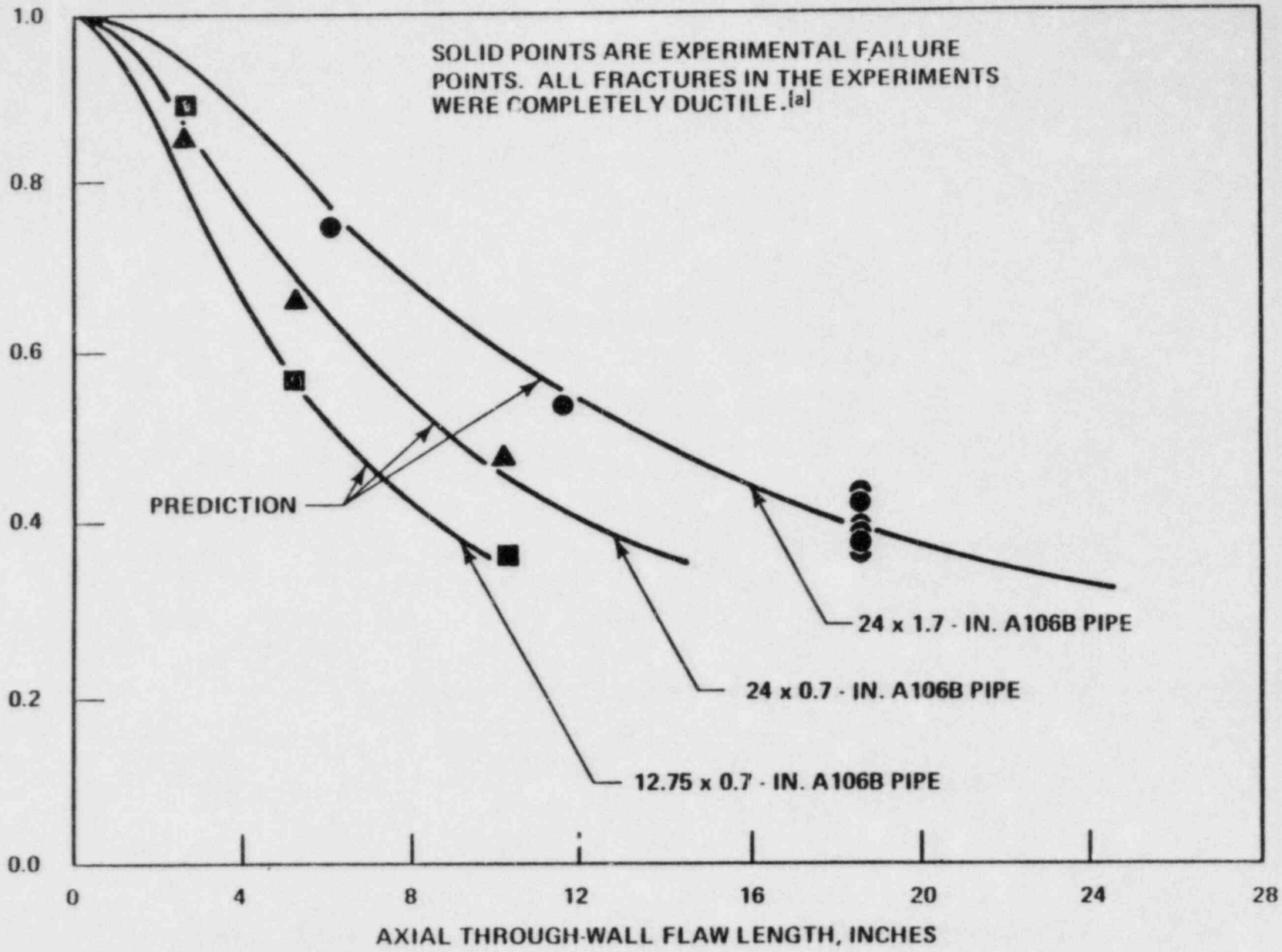

a. Reynolds, M. B., "Failure Behavior in ASTM A 1068 Pipes Containing Axial Through-Wall Flaws," GEAP-5620, April 1968.

Figure 5 Comparison of Experimental Critical Flaw Size Data

FIGURE 6

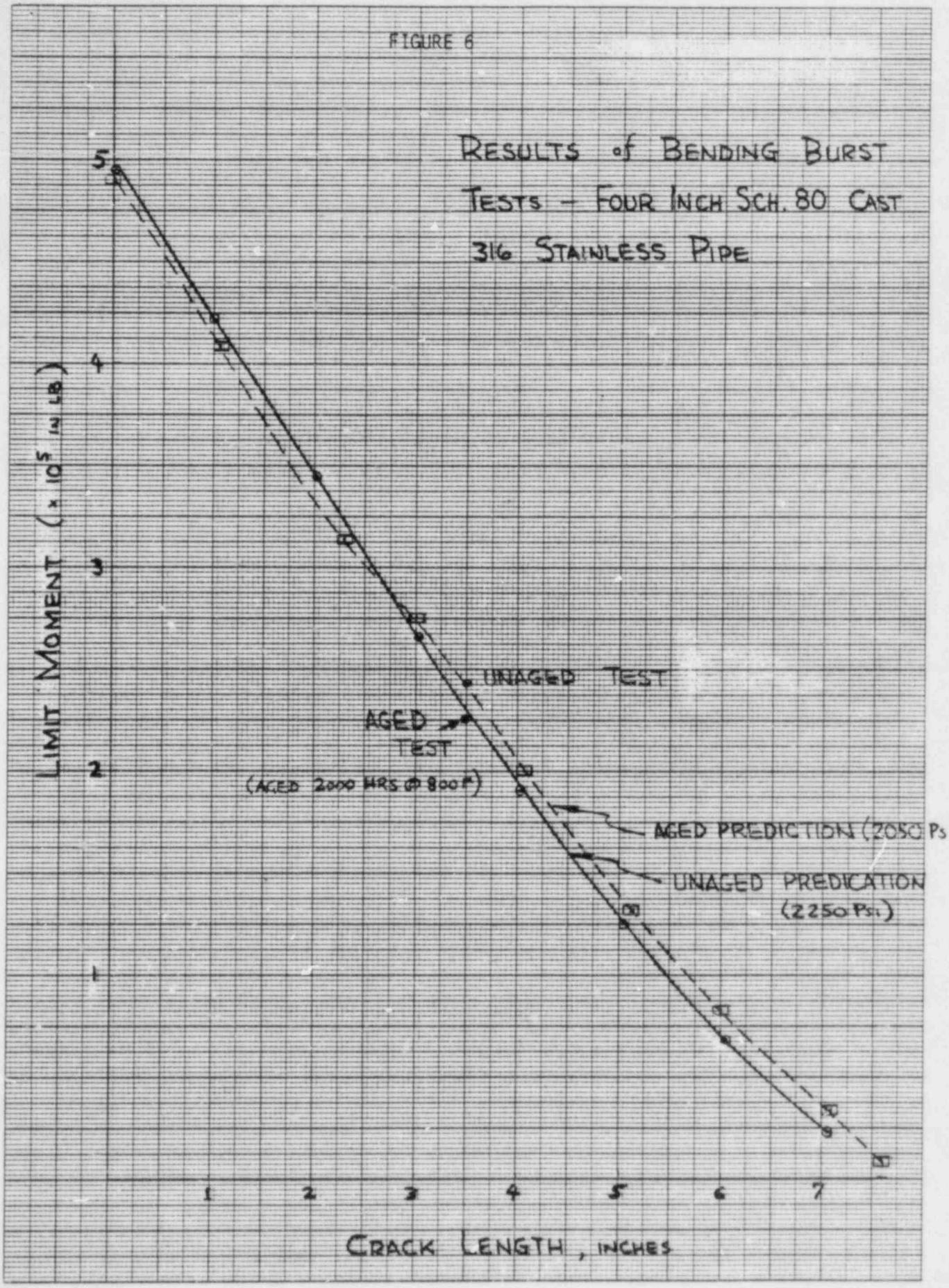
RESULTS of BENDING BURST TESTS - FOUR INCH SCH. 80 CAST 316 STAINLESS PIPE
LIMIT MOMENT (x 10^5 IN LB)
5
4
3
2
1
UNAGED TEST
AGED TEST
(AGED 2000 HRS @ 800°F)
AGED PREDICTION (2050 Ps
UNAGED PREDICATION (2250 Ps.)
1
2
3
4
5
6
7
CRACK LENGTH, INCHES

FIGURE 7

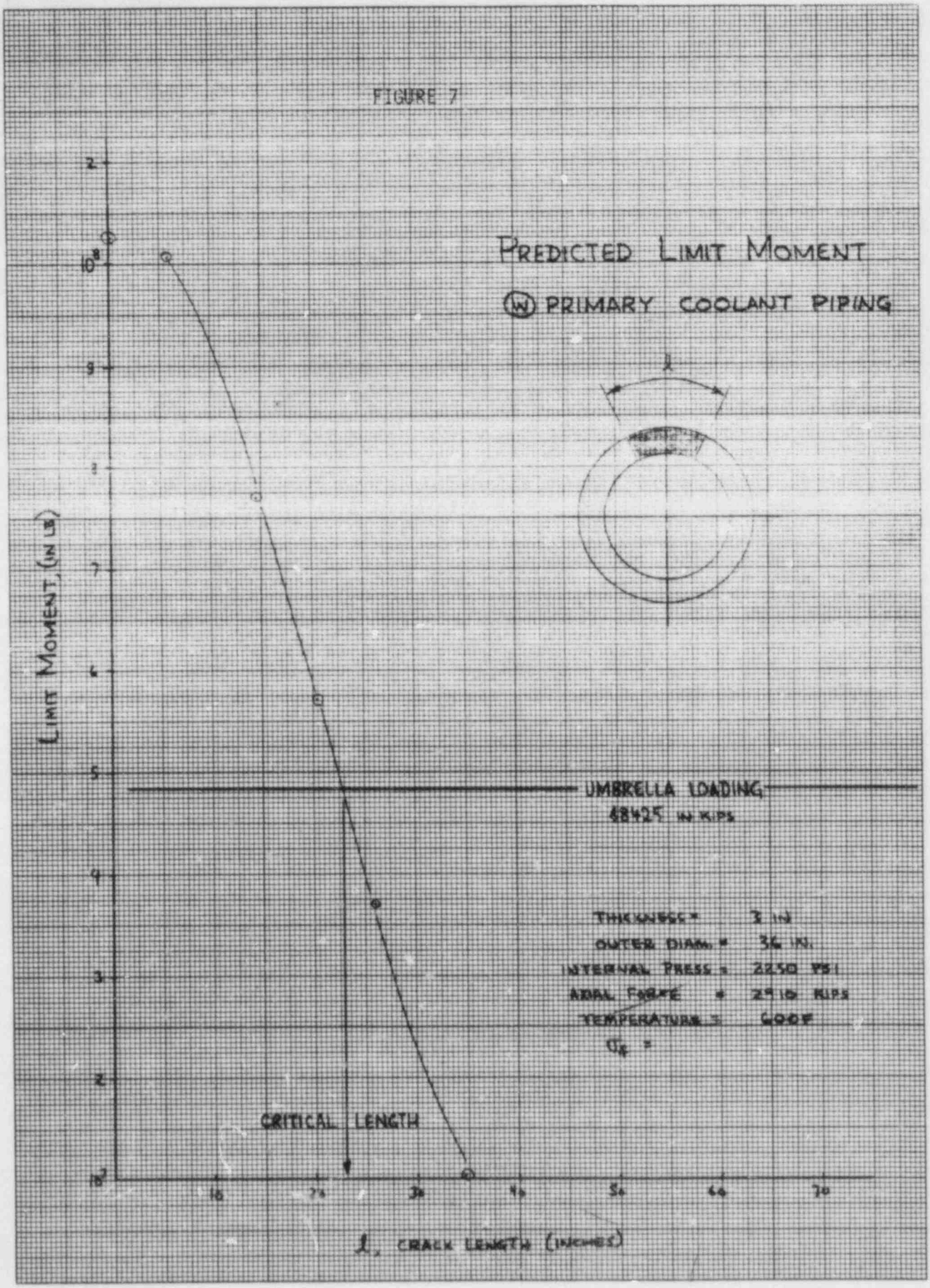
PREDICTED LIMIT MOMENT
(W) PRIMARY COOLANT PIPING
UMBRELLA LOADING
48425 IN KIPS
THICKNESS = 3 IN
OUTER DIAM. = 36 IN.
INTERNAL PRESS = 2250 PSI
AXIAL FORCE = 2910 KIPS
TEMPERATURE = 600F
CRITICAL LENGTH
LIMIT MOMENT, (IN LB)
l, CRACK LENGTH (INCHES)

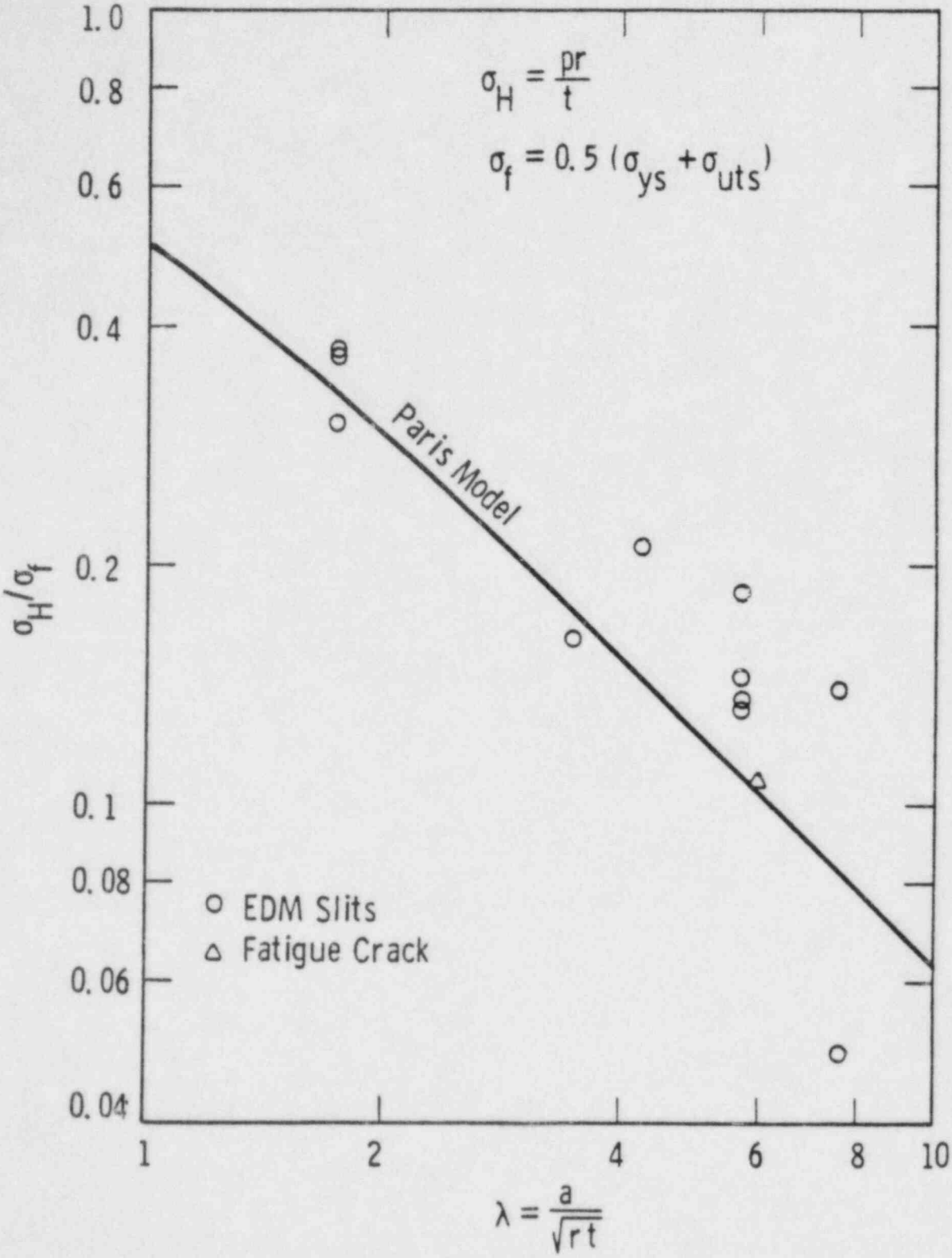

FIGURE 8 - Comparison of the burst test data for scale-model elbows with the Paris model for longitudinal cracks [17]

FIGURE 4

CRITICAL FLAW LENGTH PREDICTIONS

(W) MAIN COOLANT PIPING, LONGITUDINAL FLAWS

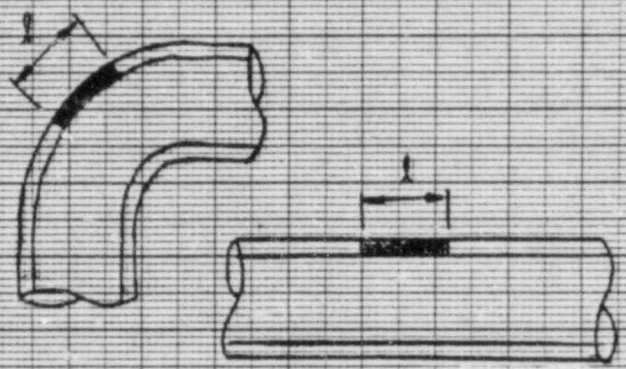

FLAW GEOMETRIES

APPENDIX A

DETERMINATION OF THE MOMENT CAPACITY OF PRESSURIZED PIPING WITH CIRCUMFERENTIALLY-ORIENTED FLAWS

A straight section of pipe with a circumferentially-oriented through-wall flaw; as shown in Figure A-1, is considered. It is assumed that plane sections remain plane during deformation, and that the flaw is not too large in comparison with the pipe circumference. For flaw lengths which approach one-half of the circumference, the present method is not accurate.

The pipe is loaded by internal pressure, P, an axial force, F, and a bending moment, M. Because of the bending moment the axial stress will be compressive somewhere in the cross section. The point of demarcation between tensile and compressive stresses is the neutral axis, as shown in Figure A-1. To determine the location of the neutral axis, the axial force on the pipe from the internal pressure and other loads, N, is equated to the integrated stresses over the cross-sectional area of the pipe. On the top part the pipe yields with $\sigma_\theta - \sigma_x = \sigma_y$, according to the Tresca maximum shear stress criterion. The strain hardening is accounted for by replacing the yield stress σ_y with the flow stress σ_f. The axial force can then be expressed as

$$N = P\pi R^2 + F \tag{A-1}$$

where

P = internal pressure
R = mean radius of the pipe
F = other axial force (if any)

$$N = 2 \int_{-\beta}^{\frac{\pi}{2} - \alpha} \sigma_f \, Rt \, d\theta + 2 \int_{\frac{-\pi}{2}}^{-\beta} (\sigma_\theta - \sigma_f) \, Rt \, d\theta \tag{A-2}$$

where

σ_θ = PR/t
t = pipe thickness
σ_f = flow stress = 0.4 $(\sigma_{ys} + \sigma_u)$
α = crack angle as shown in Figure A-1
β = angle to located neutral axis, Figure A-1

Equating the quantities in (A-1) and (A-2) leads to the definition of the neutral axis which is:

$$\beta = \frac{\sigma_f t \alpha + \frac{F}{2R}}{2 \sigma_f t - PR} \tag{A-3}$$

Figure A-1 also illustrates that the angles α and β are related at the limit moment; therefore, equating areas above and below the neutral axis results in the following:

$$\alpha = 2\beta \tag{A-4}$$

The fully-plastic limit moment capacity, M_ℓ, is obtained by taking moments about the neutral axis as follows:

$$M = 2 \int_{-\beta}^{(90 - \alpha)} R^2 t \sigma_f \sin\theta \, d\theta + 2 \int_{\frac{-\pi}{2}}^{-\beta} (\sigma_\theta - \sigma_f) R^2 T \sin\theta \, d\theta$$

where σ_f = 0.5 $(\sigma_{ys} + \sigma_u)$, that is, σ_f is the flow stress.

σ_θ = pressure stress = PR/t

After integration and subsitution of the limits, the moment capacity of the pressurized pipe is found to be:

$$M = 2\sigma_f R^2 t (2 \cos \beta - \sin \alpha) - 2PR^3 \cos \beta \qquad \text{(A-6)}$$

This expressions is valid for through wall cracks in pressurized pipes, with or without axial loads (F). The axial loadings are accounted for in calculation of the angle β.

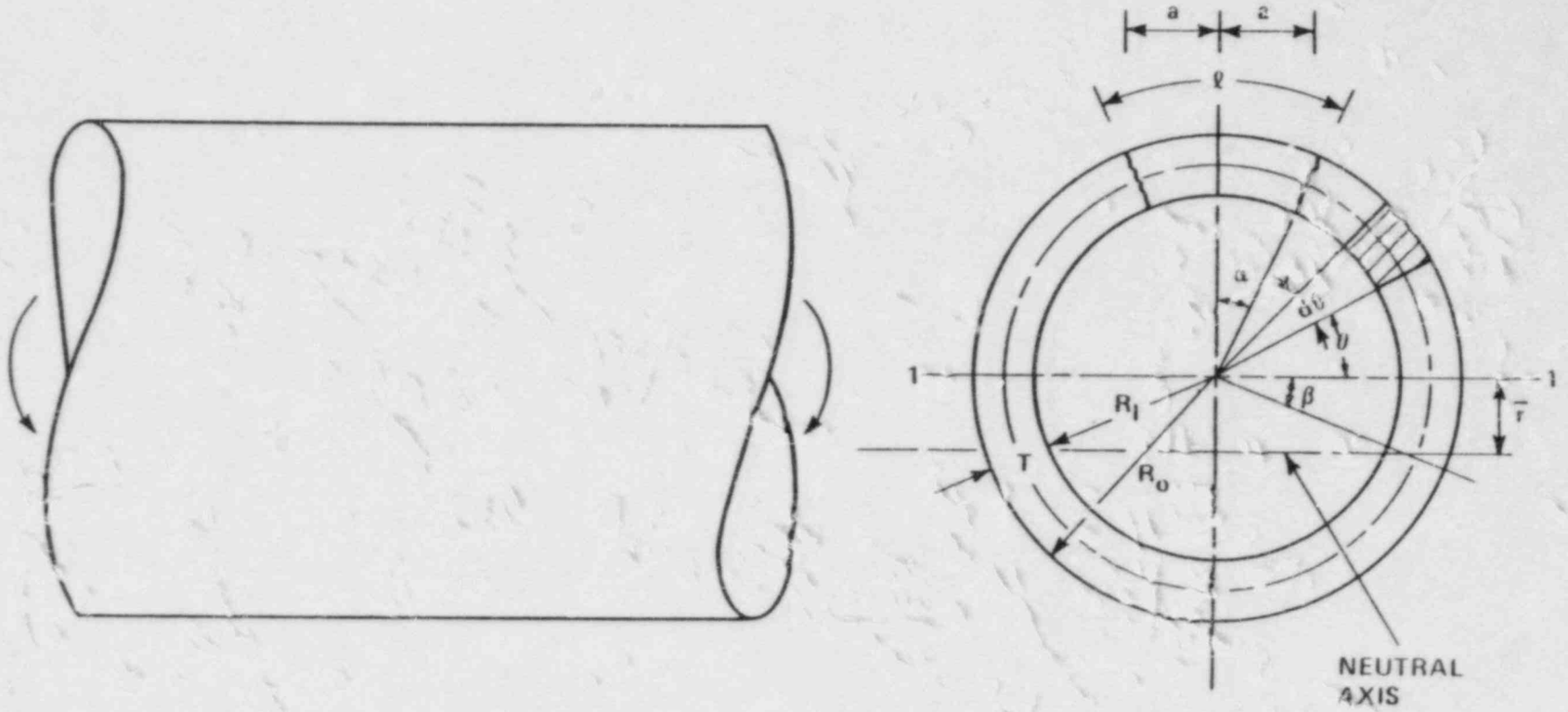

Figure A-1. Pipe with a Through-Wall Crack in Bending

THE APPLICATION OF FRACTURE MECHANICS LEAK-BEFORE-BREAK ANALYSES FOR PROTECTION AGAINST PIPE RUPTURE IN SEP PLANTS

Presented at the CSNI Specialist Meeting
September 1-2, 1983
Monterey, CA

by
J. F. Copeland
P. C. Riccardella
Structural Integrity Associates
San Jose, CA

INTRODUCTION

Current designs protect engineered safety features against the consequences of high energy line breaks (HELBs) through the use of pipe whip restraints, jet impingement shields, physical separation and other methods. However, plants designed before the existence of current requirements generally do not have such features. Furthermore, in many cases modifications to incorporate these features may be impractical due to physical plant configurations or other considerations. Therefore, the NRC has given guidance on other acceptable methods for the resolution of this Systematic Evaluation Program (SEP) Topic III-5.A, for High Energy Line Breaks Inside Containment.

One approach which has gained acceptance for protecting against postulated pipe ruptures is leak-before-break analysis, as shown in Figure 1. It is based on a combination of augmented inservice inspection (ISI) and local leak detection, to detect the presence of cracks, and a fracture mechanics analysis to assure that pipe rupture will not occur for cracks smaller than those detectable by these methods. In this way, crack detection and corrective actions will precede any chance of HELB and its subsequent postulated effects on engineered safety features.

These detection methods complement each other, since ISI is especially suited to finding long cracks, and leak monitors detect short, through-thickness cracks, shown schematically in Figure 2. Crack opening areas and the resultant leak rates are computed for comparison with detection limits. The augmented ISI involves volumetric inspection in accordance with ASME Section XI for a Class 1 system, regardless of actual system classification. The goal is to detect and limit any service induced flaws to allowable sizes prescribed by the ASME Code, Section XI (crack depth limited to less than approximately 10% of pipe wall thickness). Fracture mechanics subcritical crack growth analyses are employed to assure that this goal for limiting crack growth is met. These limits on crack size imposed by leak monitors and ISI are compared to the critical crack sizes predicted for instability and pipe rupture. Adequate margin between crack detection and the crack size for rupture must exist.

RESULTS

In accordance with the latest NRC guidance, the leak-before-break technique was evaluated for high energy piping systems in a nuclear power plant. The elements of this evaluation (Figure 3) include the determination of the following:

a) Largest crack size which will remain stable

b) Leak rate resulting from a crack of length 2t (twice the pipe wall thickness)

c) Size of crack which will leak at a rate greater than 1 gpm, if b) results in less than 1 gpm.

d) Analysis of part-through-thickness cracks for subcritical crack growth rates to establish ISI intervals.

Conservative analyses were performed to predict the largest stable crack sizes, by using ASME Code maximum allowable stresses. In this way, one set of analyses was performed to envelope all locations in these lines, as well as to compensate for potential future load increases. The subcritical crack growth rate analyses were also enveloped in a similar manner, by using a conservative load cycling spectrum based on design transients and the most severe transient loads in the stress reports. The loads considered for each evaluation

are shown in Figure 4.

The leak-before-break approach is shown to be practical and effective. Large critical crack sizes are computed for the stainless steel piping studied, using the methods of fracture mechanics from NRC guidance, net section plastic collapse, and tearing modulus analysis (Figures 5, 6, and 7). Furthermore, a very large effective unsupported piping length, L, is required for plastic instability, even with large through wall flaws (Figure 8). Conservative leak rates are computed as shown in Figure 9, for normal operating pressure stresses. The minimum crack lengths resulting in leak rates of 1 gpm (Figure 10) are shown to be significantly smaller than the critical crack sizes for both circumferential and longitudinal cracks. Subcritical crack growth rate analyses (Figure 11) show that ISI intervals of 10 years are appropriate to detect part-through-thickness cracks before they approach instability (rupture). Thus, ISI and leak detection give substantial margins against pipe rupture, even for these conservative analyses, and are an effective means to resolve the HELB issue for the piping lines investigated.

SUMMARY

1. The fracture mechanics leak-before-break approach is shown as a viable option to prevent pipe rupture.

2. Austenitic stainless steel pipes possess significant toughness, and large cracks are required for rupture, based on tearing modulus and net section plastic collapse evaluation.

3. The net section plastic collapse analysis is more conservative than tearing modulus evaluations.

4. Leak rates are large enough to assure detection well before cracks reach a critical size.

5. In the case studied, subcritical crack growth is slow enough to require inservice inspection intervals of about 10 years to detect part-through-wall cracks.

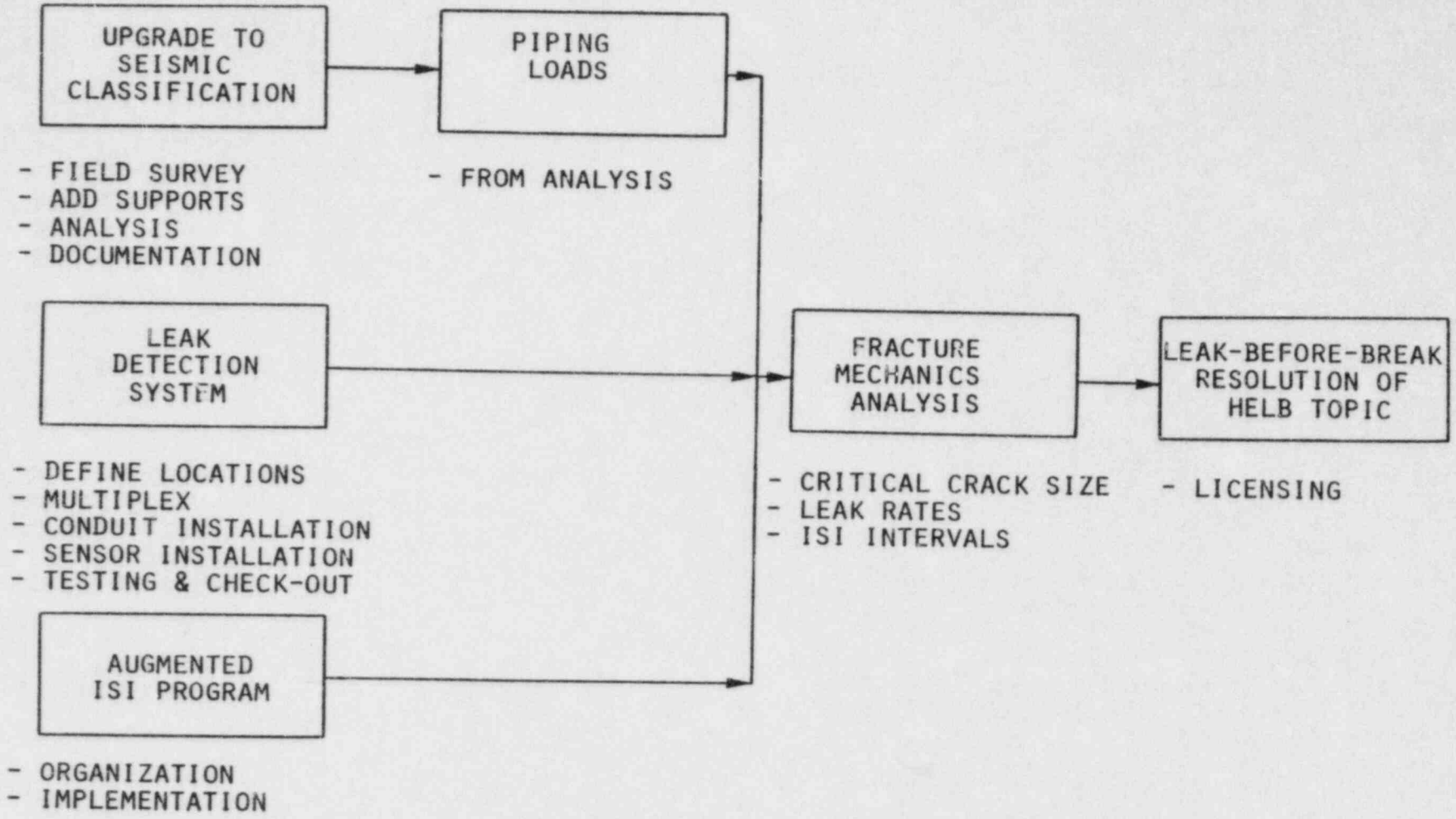

Figure 1
LEAK-BEFORE-BREAK APPROACH BASED ON FRACTURE MECHANICS ANALYSIS WITH AUGMENTED INSERVICE INSPECTION (ISI) AND LEAK DETECTION

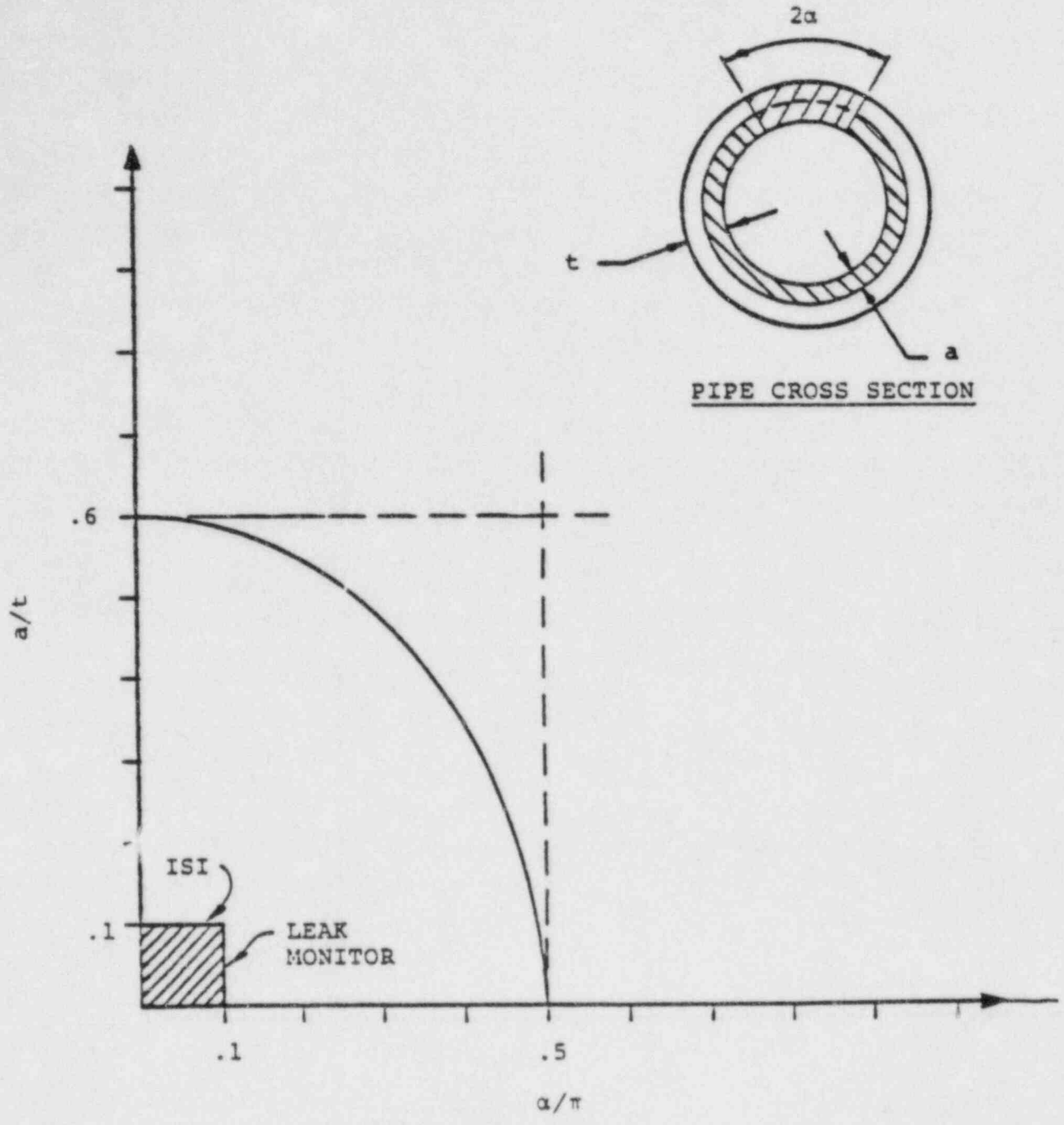

Figure 2
ILLUSTRATION OF PROPOSED ISI/LEAK DETECTION
APPROACH TO PROTECTION AGAINST PIPE RUPTURE

Figure 3

LEAK-BEFORE-BREAK

FRACTURE MECHANICS APPROACH

- DEMONSTRATE NO SUBSTANTIAL CRACK GROWTH ($J \leq J_{IC}$) OR PLASTIC INSTABILITY UNDER THE FOLLOWING CONDITIONS:
  - FAULTED (LEVEL D) SERVICE CONDITION
  - THROUGH-WALL CRACK OF LENGTH EQUAL TO FOUR TIMES WALL THICKNESS
- ADDRESS SUBCRITICAL CRACK GROWTH DEVELOPMENT IN SERVICE TO SHOW:
  - TENDENCY IS TO DEVELOP THROUGH-WALL CRACKS
  - IF LONG CRACKS DO DEVELOP, THEY WILL REMAIN SHALLOW (OPTIMIZE ISI INTERVALS)
- DEMONSTRATE THE CIRCUMFERENTIAL THROUGH-WALL CRACKS WILL REMAIN STABLE FOR LOADS APPROACHING GROSS PLASTIC COLLAPSE CONDITIONS FOR PIPING SYSTEM
- COMPUTE LEAK RATE RESULTING FROM A CRACK OF LENGTH EQUAL TO TWICE THE PIPE WALL THICKNESS
  - ADDRESS ABILITY TO DETECT LEAK RATE

Figure 4

LOADINGS CONSIDERED

- PLASTIC INSTABILITY OF CRACK
  - PRIMARY MEMBRANE AND BENDING LOADS (PRESSURE, SEISMIC, WEIGHT)
- SUBCRITICAL CRACK GROWTH
  - ALL PRIMARY AND SECONDARY LOADS, AND WELD RESIDUAL STRESSES
- LEAK RATES (CRACK OPENING AREA)
  - PRESSURE STRESS (CONSERVATIVE)

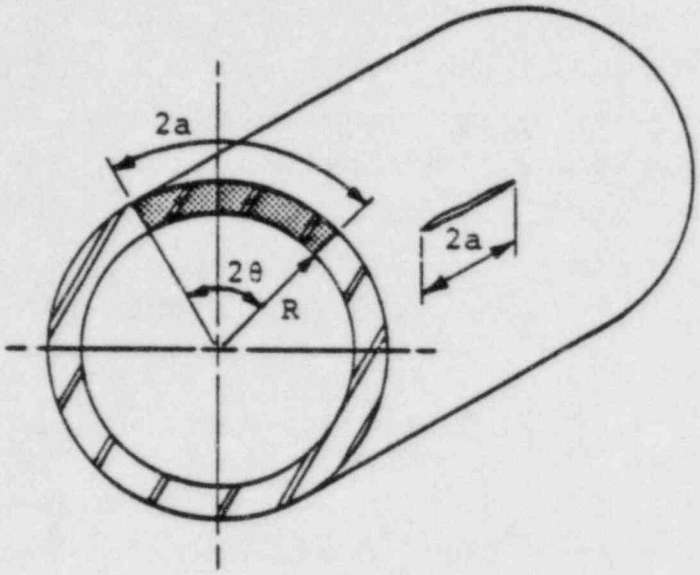

a) THROUGH-THICKNESS CIRCUMFERENTIAL AND LONGITUDINAL CRACKS OF LENGTH 2a.

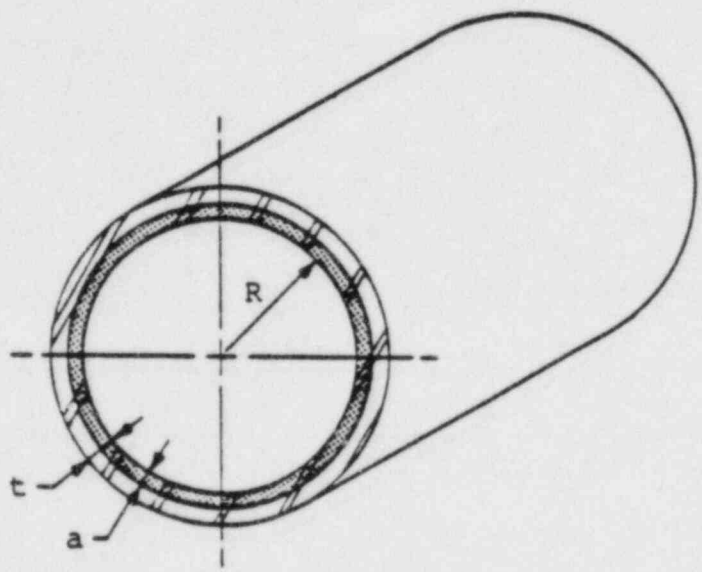

b) PART-THROUGH THICKNESS CIRCUMFERENTIAL CRACK OF DEPTH a.

Figure 5

REPRESENTATION OF POSTULATED CRACKS IN PIPES FOR FRACTURE MECHANICS LEAK-BEFORE-BREAK ANALYSIS

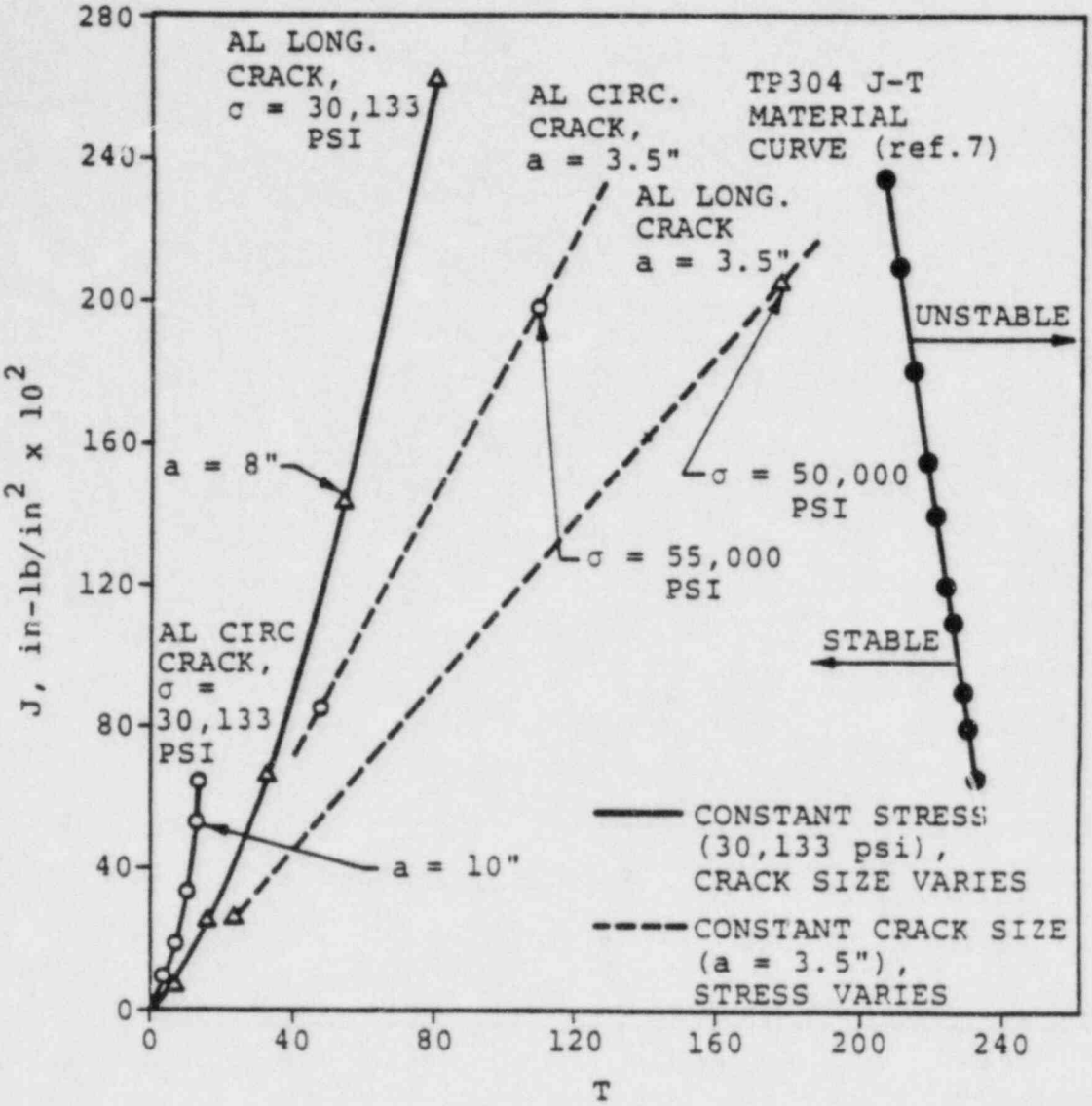

Figure 6

J-INTEGRAL/TEARING MODULUS STABILITY DIAGRAM FOR ACCUMULATOR LINE WITH THROUGH-WALL CRACKS

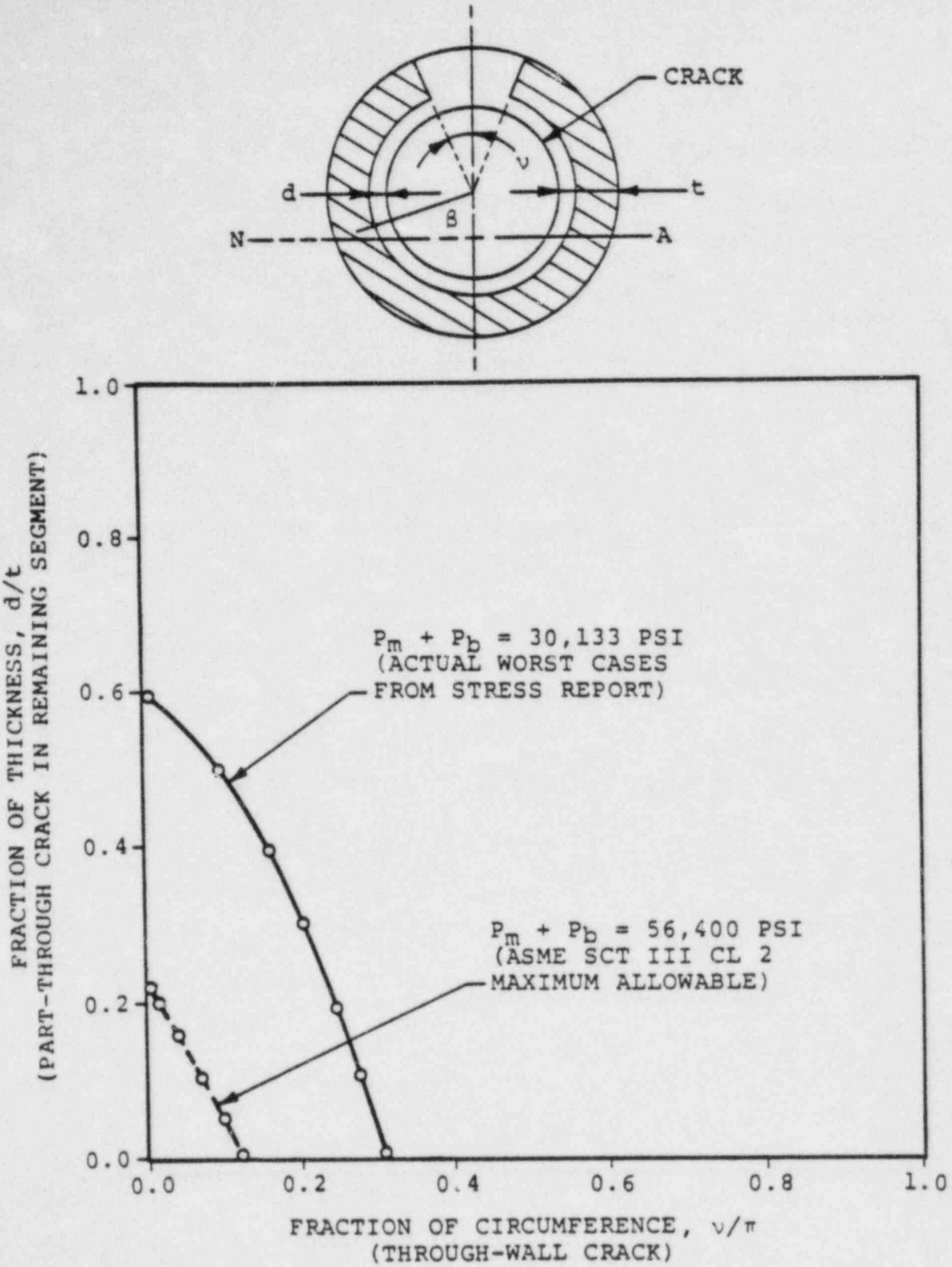

Figure 7

FAILURE ANALYSIS DIAGRAM FOR POSTULATED COMPOUND CRACK IN ACCUMULATOR LINE, BASED ON NET SECTION PLASTIC COLLAPSE CRITERION

Figure 8

TEARING STABILITY OF CIRCUMFERENTIAL THROUGH-WALL FLAWS IN STAINLESS STEEL PIPES (REFERENCE NUREG / CR-0830, TADA, PARIS, GAMBLE)

- FOR A 10" DIAMETER LINE:

  $R = 5"$ $\qquad \bar{P} = \frac{1}{2}\left(\frac{R}{t}\right)\frac{P}{\sigma_0}$

  $t = 1"$ $\qquad = 0.15$

  CRACK LENGTH = 7.8" ($2\theta = 90°$) $\qquad \bar{a} = a/t = 0$

  $\sigma_0 = 50{,}000$ PSI

  $E = 27.5 \times 10^6$ PSI

- FROM THE REFERENCE NUREG / CR-0838:

  $$T_{APP} = F_1 \, L/R + F_2 \left(\frac{JE}{\sigma_0^2 R}\right)$$

  $F_1 = 0.668$

  $F_2 = -0.198$

  $T_{APP} = 0.688 \; L/R - 0.00044 \; J$

  $T_{APP} \approx 0.67 \; L/R$

- FOR PREDICTED INSTABILITY:

  FOR $T_{MAT} = 200$

  CRICITAL $L/R \geq 300$

  $L_{CRIT} \geq 125$ FEET

Figure 9

LEAKAGE VERSUS CRACK OPENING

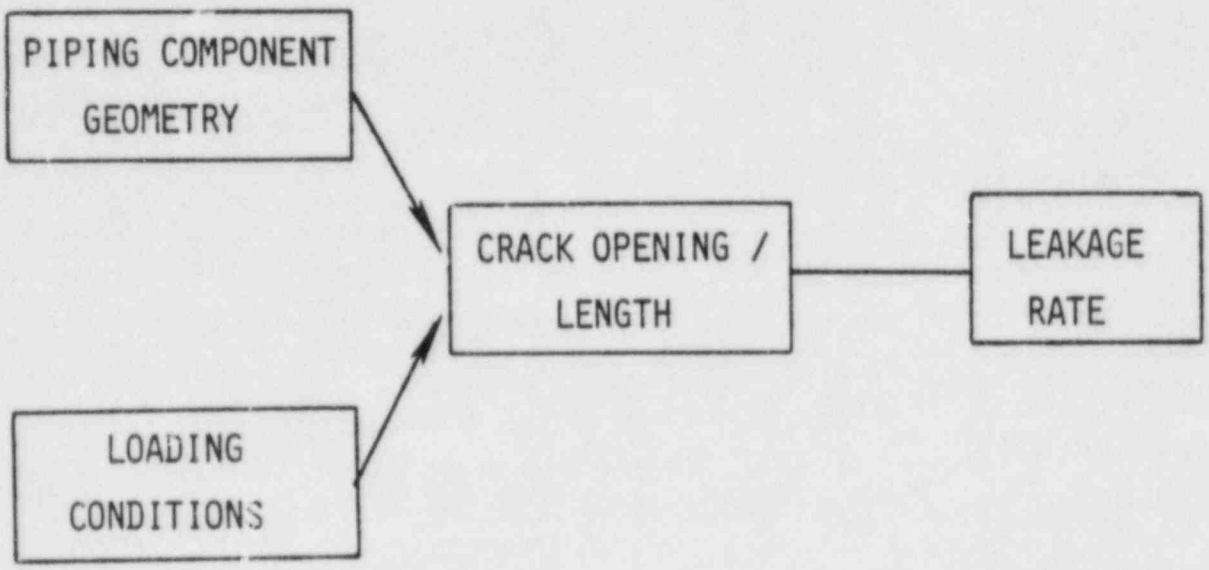

EXAMPLE:

4" SCHEDULE 80 WATER LINE 1200 PSI DESIGN PRESSURE → CIRCUMFERENTIAL CRACK OPENING 0.006" CRACK LENGTH 5.9" → LEAKAGE RATE 5 GPM

Figure 10

CRACK LENGTH FOR 1GPM LEAKAGE

CRACK ORIENTATION	PRESSURE STRESS (S_M = 16.7 KSI)	CRACK LENGTH FOR 1GPM LEAK (IN.)
CIRCUMFERENTIAL	.3 S_M	2.5
LONGITUDINAL	.6 S_M	1.8
CIRCUMFERENTIAL	.1 S_M	3.5
LONGITUDINAL	.2 S_M	2.5

Figure 11

SUBCRITICAL CRACK GROWTH OF PART-THROUGH-WALL CRACKS

- PREDICTED GROWTH DEPENDS ON ASSUMED INITIAL FLAW SIZE
  - INITIAL FLAW OF DEPTH EQUAL TO 2% OF PIPE WALL GIVES INSIGNIFICANT GROWTH FOR PLANT LIFE FOR THE CASE CONSIDERED
  - INITIAL FLAW OF DEPTH EQUAL TO 10% OF PIPE WALL INDICATES ISI INTERVAL SHOULD BE 10 YEARS FOR THE CASE CONSIDERED
- ISI INTERVAL OF 10 YEARS GIVES AMPLE MARGIN AGAINST REACHING THE CRITICAL CRACK DEPTH IN THIS CASE

SESSION IV

CURRENT AND PROPOSED POSITIONS ON LEAK-BEFORE-BREAK

SESSION CHAIRMEN

Dr. C. K. Chou
Lawrence Livermore National Laboratory, U.S.A.

Mr. Jack Strosnider
U.S. Nuclear Regulatory Commission, U.S.A.

SOME CONSIDERATIONS IN THE APPLICATION OF FRACTURE MECHANICS TO DELIMIT LEAK-BEFORE-BREAK CONDITIONS IN NUCLEAR POWER PLANT PIPING

by

M. F. Kanninen
Institute Scientist
Engineering and Materials Sciences Division
Southwest Research Institute
San Antonio, Texas 78284

October, 1983

Submitted for the proceedings of the CSNI Special Meeting on Leak-Before-Break held in Monterey, California, 1-2 September 1983.

INTRODUCTION

One of the most likely causes of a loss of coolant accident in a nuclear power plant is a rupture in the piping system caused by stress corrosion. Many incidents of stress corrosion cracking have been reported, particularly in smaller diameter stainless steel pipes; e.g., see reference [1]. Consequently, there is a great need for a quantitative understanding of the behavior of cracked pipes under normal operating and postulated accident conditions such as seismic events. In most instances, concern is for surface cracks that initiate at the inner surface of the pipe in the heat affected zone around a girth weld. Assisted by the weld-induced residual stress, these cracks tend to grow circumferentially and radially, sometimes attaining a size that is a significant fraction of the pipe wall area.

A prime consideration in analyzing cracked nuclear plant pipes is to determine, if failure actually occurs, whether it will lead to a "leak-before-break" condition. The leak-before-break concept generally refers to a pressure containment system failure event in which a part-through-wall crack extends to become a through-wall crack, thus allowing the contained fluid to escape, but with no further crack growth. Then, the loss of fluid can presumably be detected in one way or another in time for the system to be shut down safely. The alternative--where the through-wall crack does not arrest upon break-through but instead continues to propagate along the wall-is likely to lead to a catastrophic event that, obviously, must be avoided. Hence, if failure occurs, it is essential that it will be of the leak-before-break type. Indeed, in nuclear power plant applications it is legally necessary to show that the leak-before-break concept is applicable. In critical piping systems where cracking has occurred, or even could occur, it must be established that a pipe crack will be revealed by leak detection techniques before it reaches a condition where fracture could occur under normal operating or postulated accident conditions.

It is also important to be able to anticipate how cracking will occur in connection with subsequent events that would be triggered by a pipe failure. The design basis accident used in nuclear plant regulation around the world is the so-called full guillotine offset break; i.e., an instantaneous circumferential fracture. This extreme condition has resulted in the incorporation of massive pipe whip restraints into the piping system. These are not only very expensive to design and install, but they can reduce the reliability of inservice inspection while increasing the radiation hazard in the inspection process. The necessity for such devices in the design stage and as modifications in operating plants would be substantially relieved if leak-before-break conditions could be demonstrated. Consequently, there is currently a great deal of research interest in developing more precise fracture mechanics analysis methods for this purpose.

In applying fracture mechanics techniques for leak-before-break assessments, it should be recognized that the entire range of crack enlargement processes can be involved. These range from subcritical crack growth by fatigue and/or stress corrosion, through slow stable ductile crack growth, to rapid unstable crack propagation and arrest. Fracture in a pressure containment component very often emanates from defects in or around welds. Yet, the presence of the residual stress and deformation fields induced by the welding process are nearly always treated in a simplistic way, if not ignored, in applying fracture mechanics analysis of crack growth processes. This paper presents computational results contrasting crack growth predictions in which residual stresses are included with those in which they have been ignored. Both fatigue and dynamic crack propagation are addressed. The implications of the significant differences that are found on leak-before-break assessments are examined.

FACTORS AFFECTING LEAK-BEFORE-BREAK

Leak-before-break can be simply viewed as one possible outcome of a sequence of crack extension events. For a ductile material, a general sequence of events might be one in which a weld defect or other intrinsic flaw enlarges in service through the following series of events:

1. Subcritical crack growth by fatigue and/or corrosion to a critical crack depth
2. Stable crack growth under operating or accident loads
3. Fracture instability and subsequent rapid crack growth through the wall
4. Arrest of the through-thickness crack (leak)
5. Reinitation of the through-thic! ss crack and subsequent stable growth along the wall
6. Fracture instability and rapid crack growth (break)

Leak-before-break occurs when events 4 and 5 are well separated in time or when events 5 and 6 are precluded.

It can be seen from the above list that several factors will affect the occurrence of leak-before-break. These include, (1) the orientation of the initial flaw, (2) the size and shape of the crack at the onset of stable crack growth, (3) the type, intensity and duration of the applied loads, (4) the distribution of any residual stresses that might be present, and (5) the mechanical and fracture properties of the pressure boundary material. Two particular cases are of most interest for nuclear plant piping applications. Table 1 summarizes these.

Of the two sets of conditions displayed in Table 1, owing to the stress corrosion cracking problems experienced in BWR plants, circumferentially-cracked stainless steel piping has received by far the most attention in leak-before-break assessments. Kanninen et al. [2, 3] were among the first to address this problem area. They developed a net-section collapse load approach that permitted the applied loads required for leak and break to be calculated explicity. The boundary between the "leak" and "break" regimes could then be portrayed in the form of a leak-before-break assessment diagram. A typical result is shown in Figure 1. While this approach was subsequently

TABLE 1. TYPICAL CONDITIONS FOR LEAK-BEFORE BREAK ASSESSMENTS IN NUCLEAR PLANT PIPING SYSTEMS

	Pipe Material	
	Stainless Steel	Carbon Steel
Crack Location	Girth Weld	Longitudinal weld
Crack Orientation	Circumferential	Axial
Subcritial Crack Growth Mechanism	Stress Corrosion	Fatigue
Critical Applied Loading Type	Bending	Pressure
Condition At Fracture	Net Section Yielding	Small Scale Yielding

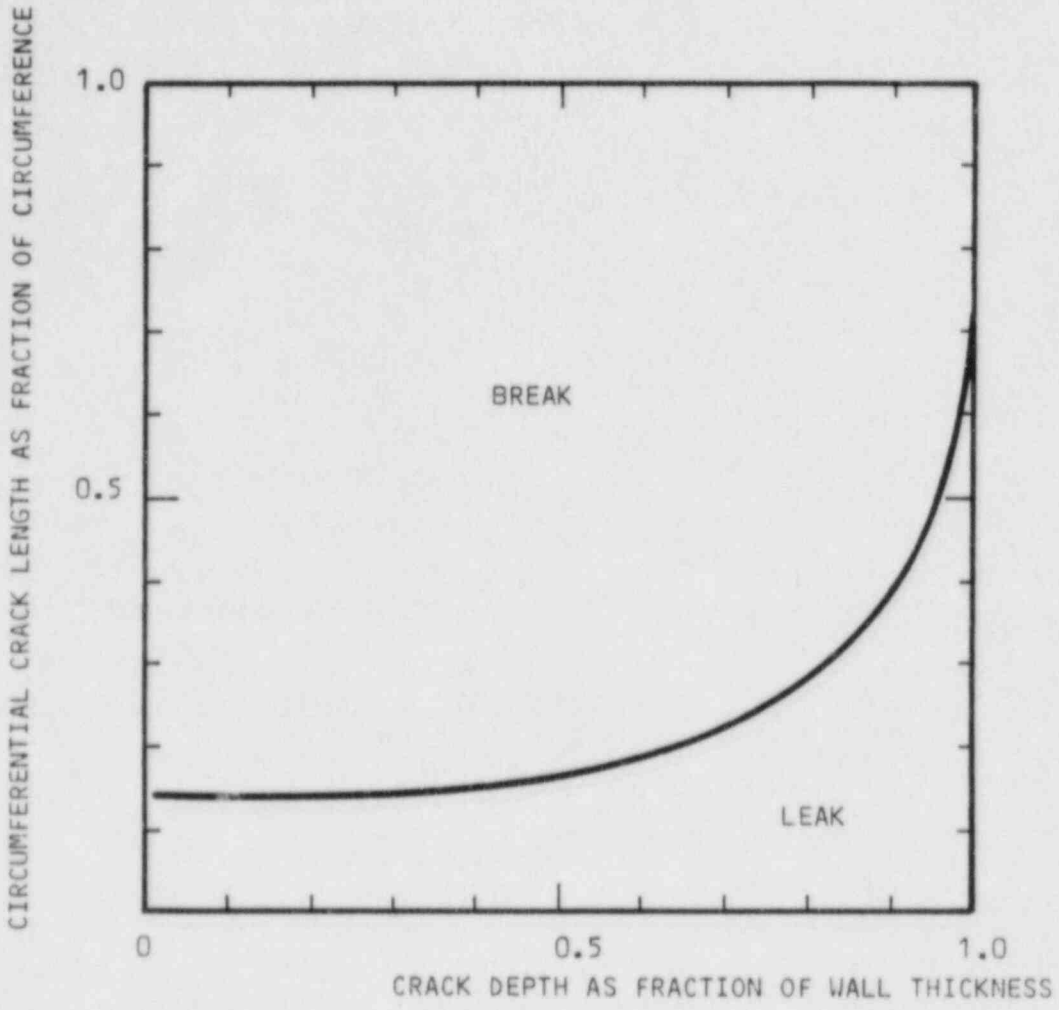

FIGURE 1. LEAK-BEFORE-BREAK ASSESSMENT DIAGRAM FOR CIRCUMFERENTIALLY-CRACKED 28-INCH DIAMETER STAINLESS STEEL PIPES IN BENDING

advanced by many others - for example, see reference [4] - the type of results shown in Figure 1 remains one of the more useful ways to delineate this condition.

Because stainless steel is highly ductile and tough, nonlinear fracture mechanics approaches generally must be applied. Kanninen et al [5] later developed and applied a tearing instability theory, for example. However, this technology is complex and has not yet been developed to the point where routine assessments can be made of leak-before-break in a realistic manner. To help illuminate the basic considerations involved in leak-before-break, it might therefore be useful to turn to the second of the two sets of conditions displayed in Table 1. This case can be treated in a simple way for heuristic purposes, as follows.

Consider that a part-through-wall axial crack exists in a pressurized pipe under conditions such that a linear elastic fracture mechanics approach is applicable. Further, suppose that the length of the crack along the surface is long in comparison to the crack depth; NB, this will lead to a conservative prediction for all crack aspect ratios. Then, the initiation of unstable crack propagation will occur in the radial direction when

$$1.12 \frac{p_0 R}{h} \left[\pi a \sec \left(\frac{\pi}{2} \frac{a}{h} \right) \right]^{1/2} = K_{Ic} \qquad (1)$$

where p_0 is the internal pressure, K_{IC} is the plane strain fracture toughness, while a, c, R and h are the geometric parameters shown in Figure 2.

It is likely that the nature of the unstable crack propagation event that follows the satisfaction of equation (1) will result in a through-wall crack of length equal to the surface length of the original part-through crack. It can be assumed that this state will exist, momentarily at least, before the crack continues to grow along the wall. The critical condition for reinitiation of crack growth to occur is given by

$$\frac{p_1 R}{h} \left[\pi c \left(1 + 1.61 \frac{c^2}{Rh} \right) \right]^{1/2} = K_C \qquad (2)$$

where p_1 is the internal pressure at the onset of longitudinal crack instability and K_C is the fracture toughness that corresponds to the wall thickness.

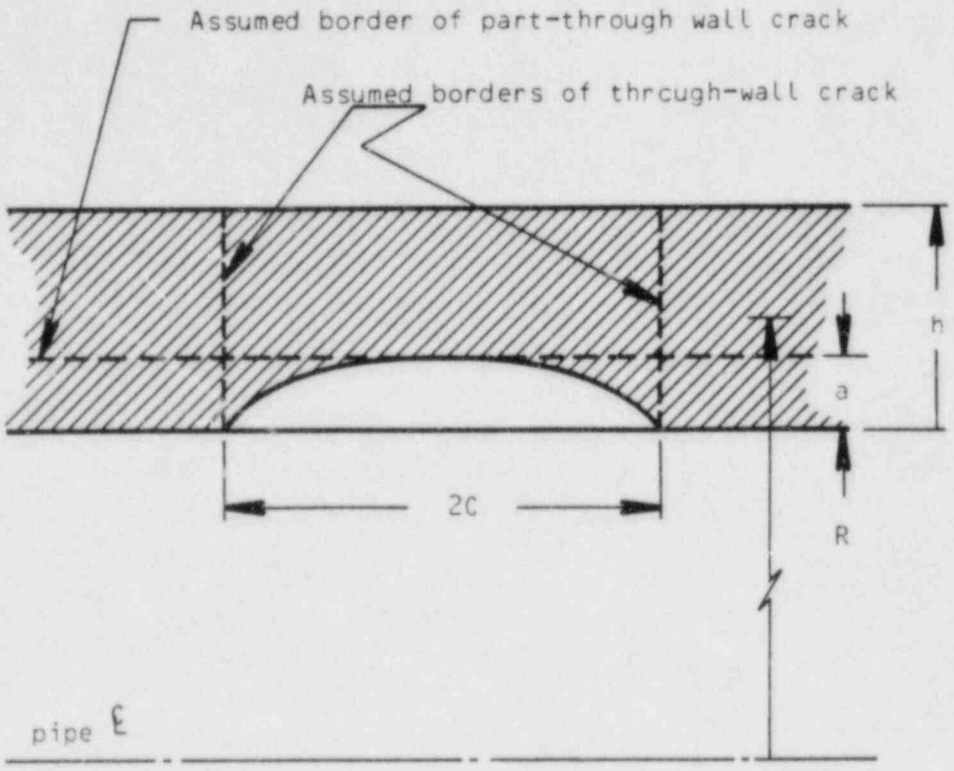

FIGURE 2. AXIAL SURFACE CRACK IN A PIPE

A relation that provides the boundary between leak and break behavior in an analogous fashion to that shown in Figure 1 can be obtained by combining equations (1) and (2). This is

$$\left(1 + 1.61 \frac{h}{R}\left(\frac{c}{h}\right)^2\right) \frac{c}{h} = 1.25 \left(\frac{K_c}{K_{IC}}\right)^2 \left(\frac{p_o}{p_1}\right)^2 \frac{a}{h} \sec\left(\frac{\pi}{2} \frac{a}{h}\right) \qquad (3)$$

which provides a leak-before-break delimitation for axial cracks in pressurized pipes. Equation (3) can be solved numerically (e.g., by Newton's method) for c/h as a function of a/h, provided the remaining parameters are specified. To illustrate, by taking $K_c = K_{IC}$ and $p_o = p_1$, equation (3) can be solved for different pipe geometries. The results are shown in Figure 3.

A useful connection between K_c and K_{IC} is the semi-empirical relation developed by Irwin and subsequently given a theoretical basis by Merkle [6]. This is

$$K_c = K_{IC} \left[1 + \frac{1.4}{h}\left(\frac{K_{IC}}{\sigma_Y}\right)^2\right] \qquad (4)$$

where σ_Y is the material yield stress. It can be seen from equation (3) that K_c will generally differ from K_{IC}. Of equal importance to this discussion, p_1 also can differ from p_o. In the case of fluid leakage, it would be expected that $p_1 < p_o$. However, if the fracture is caused by a waterhammer or other dynamic loading, it is entirely conceivable that $p_1 > p_o$. Thus, it is of interest to explore the effect of variations in these parameters. Figure 4 shows the set of results obtained for R/h = 10.

Figure 4 reveals the important (albeit intuitive) conclusion that the differences in the fracture properties and the change in applied stress during the fracture event can have a significant effect on the leak-before-break delimitation. For example, accounting for the greater toughness that generally confronts a through-wall crack and admitting a reduction of the pressure due to fluid leakage would shift the boundary so as to enlarge the "leak" zone. But, in contrast, should an escalation in the pressure overcome the increased toughness, it would be the "break" region which enlarges. Clearly, considerations of this kind should enter into any leak-before-break assessment procedure.

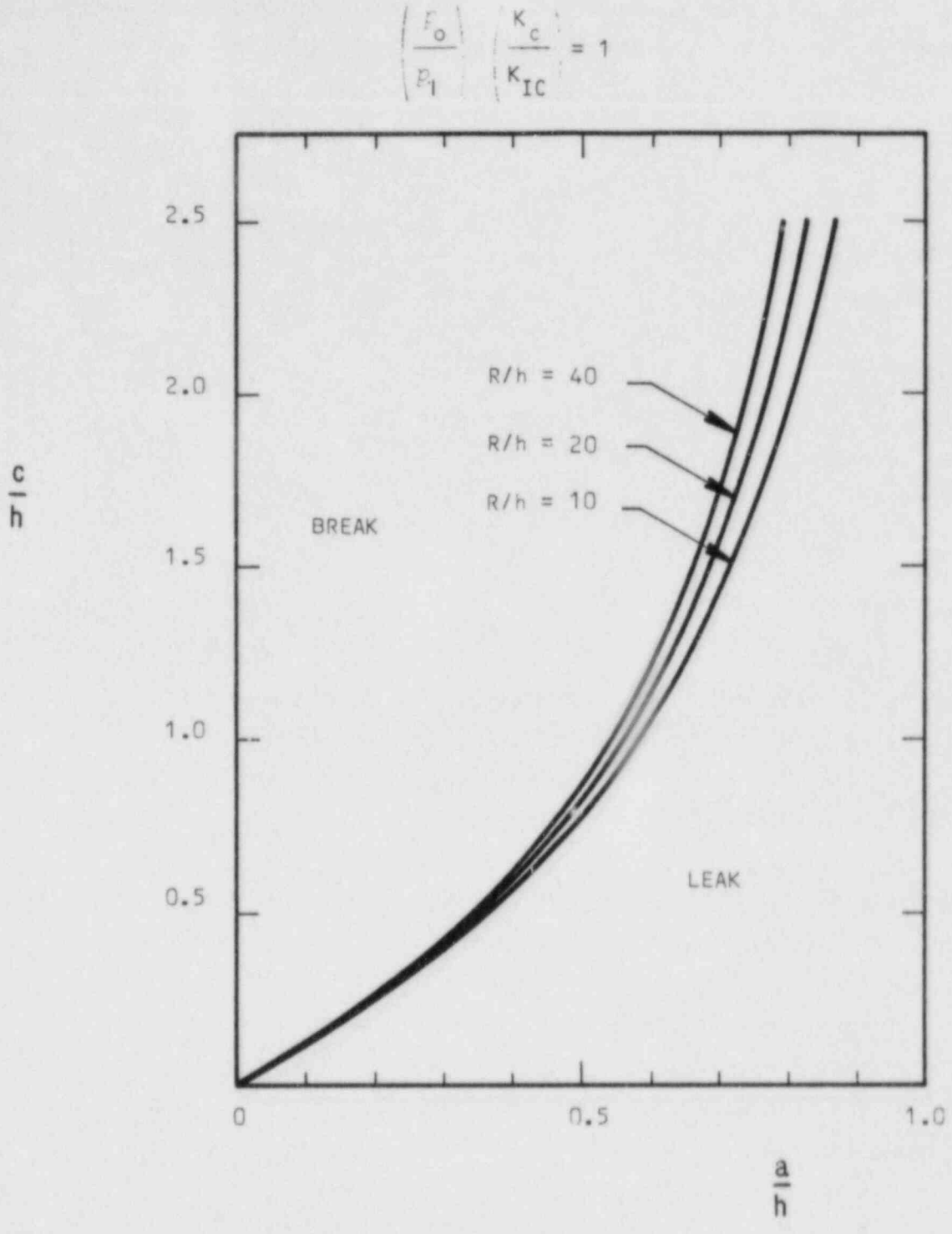

FIGURE 3. LEAK-BEFORE-BREAK ASSESSMENT DIAGRAM FOR AXIAL CRACKS IN PRESSURIZED PIPES

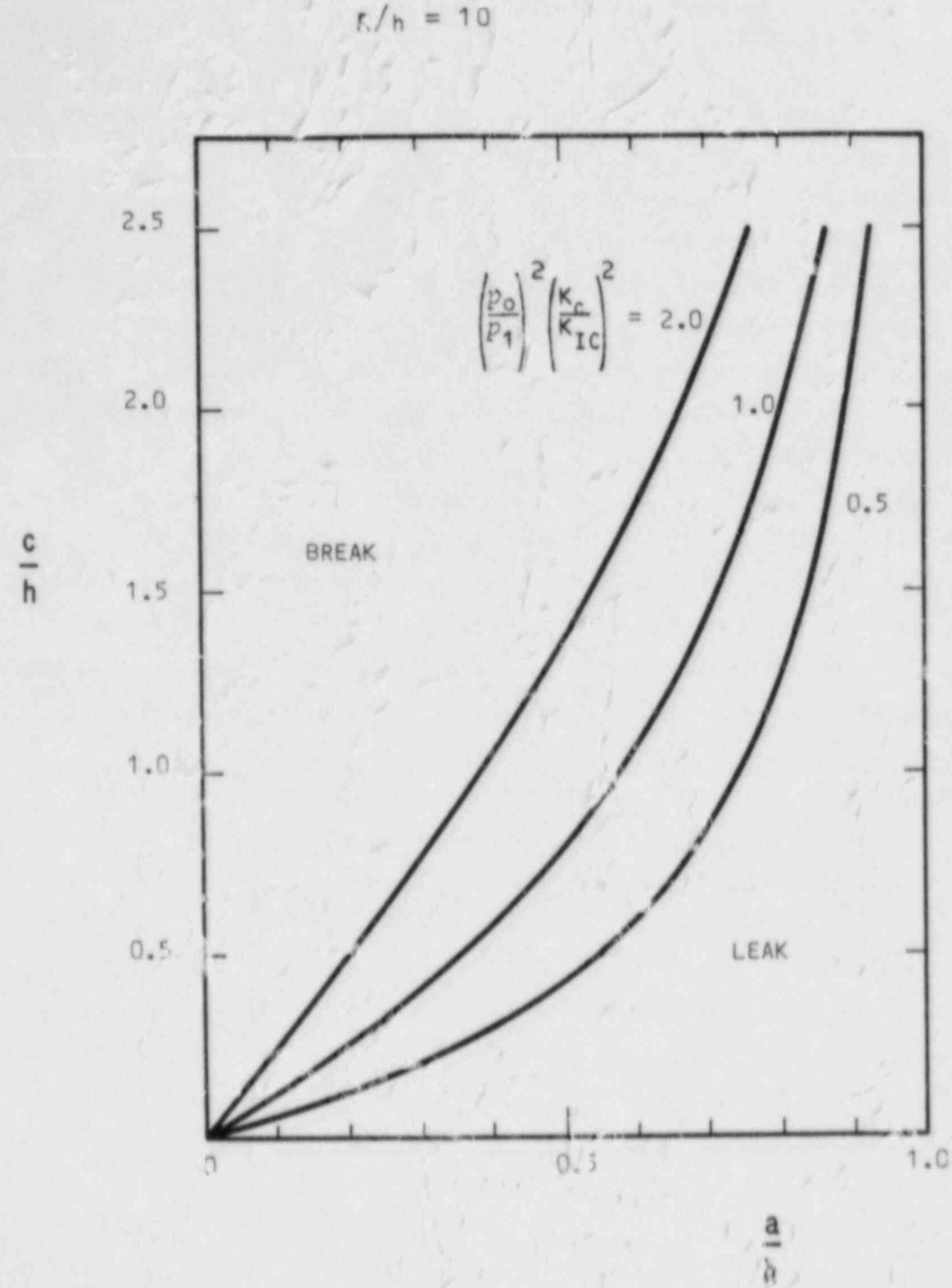

FIGURE 4. LEAK-BEFORE-BREAK ASSESSMENT DIAGRAM FOR AXIAL CRACKS IN PRESSURIZED PIPES

THE EFFECT OF RESIDUAL STRESSES

For the purpose of illuminating some key aspects of leak-before-break behavior, the preceding discussion was presented in terms of linear elastic fracture mechanics. However, nuclear plant piping materials are generally very ductile and tough. In the materials selected for such service, crack growth is generally preceded by substantial crack tip blunting with significant amounts of stable crack growth occurring prior to fracture instability. Linear elastic fracture mechanics techniques can lead to predictions that are very conservative in such instances; conservatism that could prompt unnecessary remedial action.

This fact has motivated the development of elastic-plastic fracture mechanics techniques. While these have indeed improved the accuracy of the predictive methods, one complexity of the problem has not yet been fully addressed. This is due to the fact that pipe cracks tend to be located within weld-induced residual stress and deformation fields. The importance of this fact will be briefly examined in two areas - fatigue and rapid as follows.

Kanninen, et al [7] studied the effect of weld-induced residual stresses on fatigue crack propagation through a two-part computation. In the first part, the pass-by-pass welding process was simulated with an elastic-thermoplastic finite element model. The weld geometry and the residual stresses acting on the prospective crack line that resulted from this computation are shown in Figure 5. These residual stresses then formed the initial conditions for an elastic-plastic fatigue crack growth analysis. In this analysis the crack advance criterion was taken as the local crack opening displacement. The fatigue "law" then took the form of a generalized Paris law. This is

$$\frac{da}{dN} = C\left(\delta^{1/2}_{max} - \delta^{1/2}_{min}\right)^{m} \qquad (5)$$

To compare with the elastic-plastic prediction, a linear elastic analaysis was also obtained. The two results are shown in Figure 6.

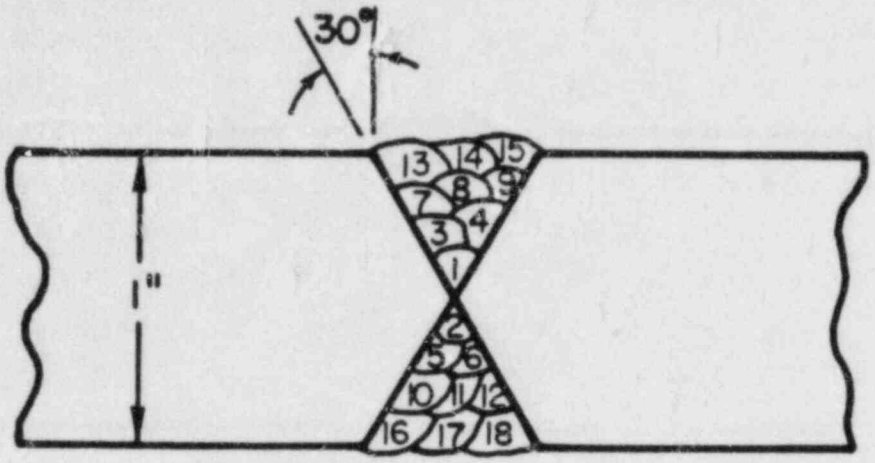

CROSS SECTION OF AN 18-PASS WELD

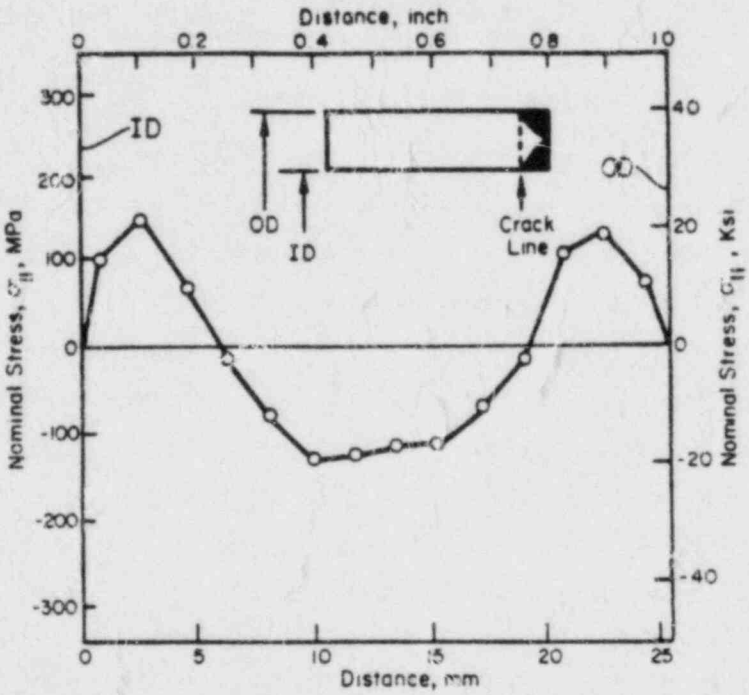

CALCULATED RESIDUAL STRESSES ON CRACK LINE

FIGURE 5. RESULTS OF A WELD SIMULATION COMPUTATION

It can be seen in Figure 6 that there is a significant difference between the elastic and the elastic-plastic results. In particular, the former is found to give anti-conservative predictions. This, of course, may depend upong the nature of the residual stress distribution that is being considered. Regardless, it appears that weld-induced residual stresses have a definite affect on fatigue crack growth predictions.

Turning to dynamic crack propagation and crack arrest in the presence of weld-induced residual stress fields, the work of Barnes et al. [8] may be of interest. They also used a local COD criterion for crack growth. But, they were able to show that such a criterion has a basis. Their key result, which stems from a generation-phase computation on 4340 steel, is shown in Figure 7.

To establish the initial conditions for their computations, Barnes et al. first computed the residual stress field by a computational simulation of the multi-pass welding process. A comparison with the experimentally-measured values (obtained by trepanning) is shown in Figure 8. It can be seen that the agreement is entirely reasonable. A more basic difficulty was that the precise numerical value of the critical CTOA for unstable crack propagation in an HY80 weldment was not known. As their

In order to compare computational techniques to ascertain the importance of residual stresses, they adopted an expedient. This was to choose a $(CTOA)_c$ value such that the computation that including residual stresses predicted crack arrest correctly. As shown in Figure 9, the parallel computations (i.e., without residual stresses) predicted complete penetration of the specimen. Note that, in their experimental work, crack arrest occurred after approximately 14 mm of crack growth (blast loading experiment). It might be noted that the $(CTOA)_c$ selected in this way corresponds roughly to $K_{ID} = 84\ MPa\sqrt{m}$; a value that is in reasonable accord with the limited data available for HY80 weldments reported by Hahn and Kanninen [9].

Taken together, these two sets of results clearly indicate that residual stresses can exert a strong influence on crack growth in welds. They further indicate that, although uncertainties do exist (e.g., in regard to the crack advance criterion), the computational methods needed for treating residual stresses exist. However, these techniques have not generally been used in leak-before-break assessments as yet.

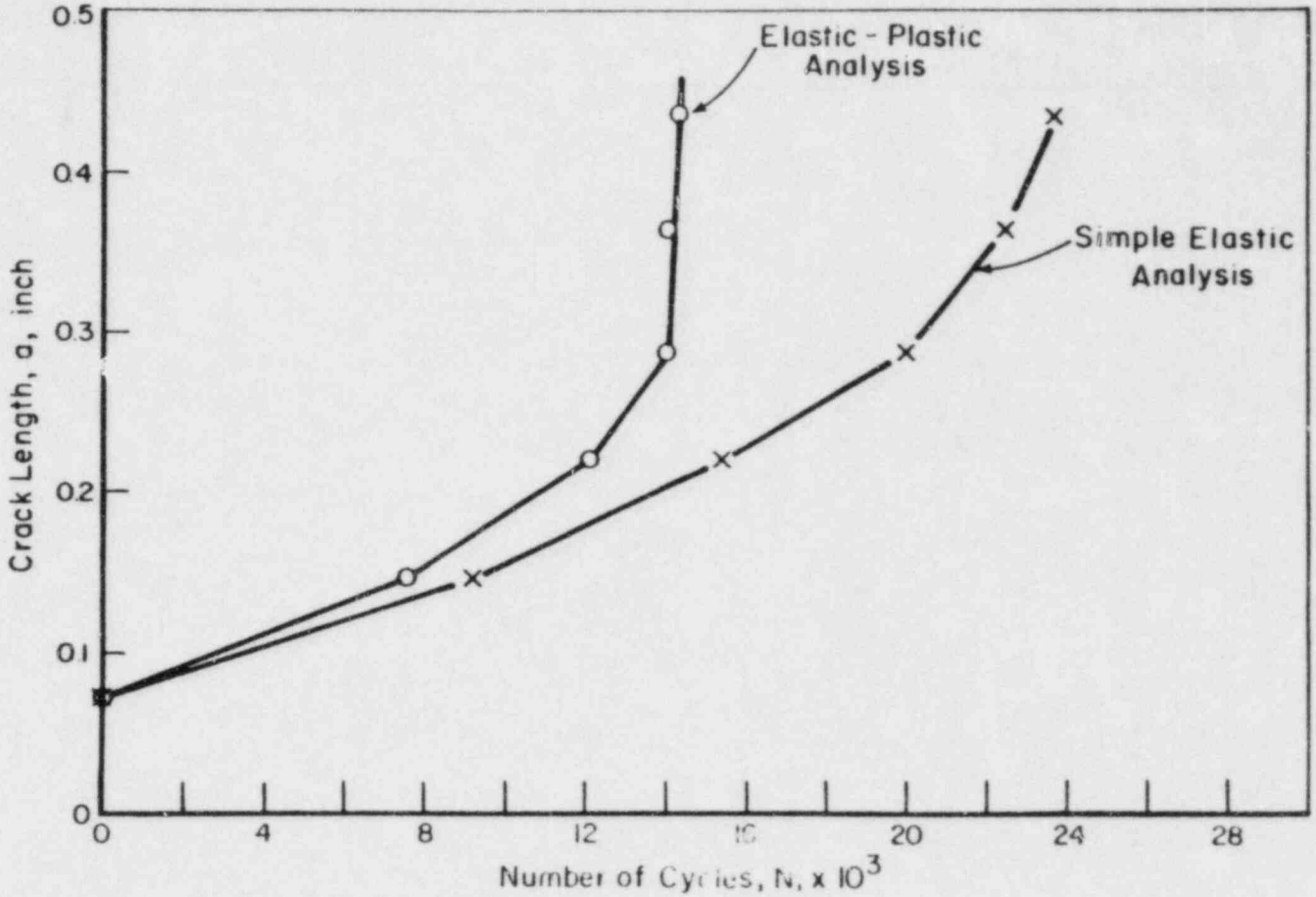

FIGURE 6. COMPARISON OF ELASTIC AND ELASTIC-PLASTIC COMPUTATIONS FATIGUE CRACK GROWTH IN A BUTT-WELDED PLATE (Maximum Load = $0.67\sigma_o$, Minimum = 0)

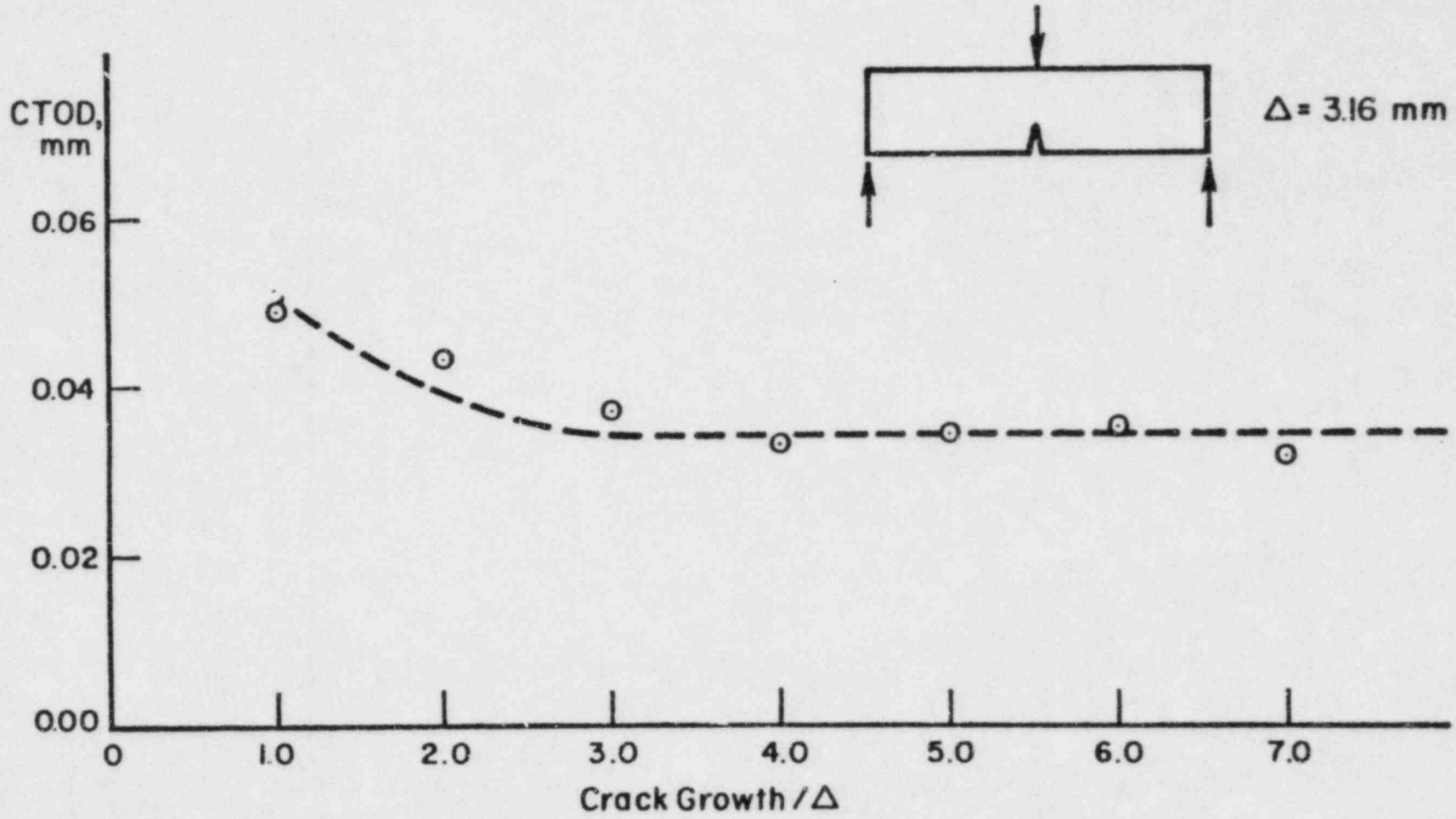

FIGURE 7. ELASTIC-PLASTIC DYNAMIC ANALYSIS OF DYNAMIC CRACK PROPAGATION IN A SIDE GROOVED AISI 4340 STEEL BEND SPECIMEN SUBJECTED TO A QUASI-STATIC LOAD

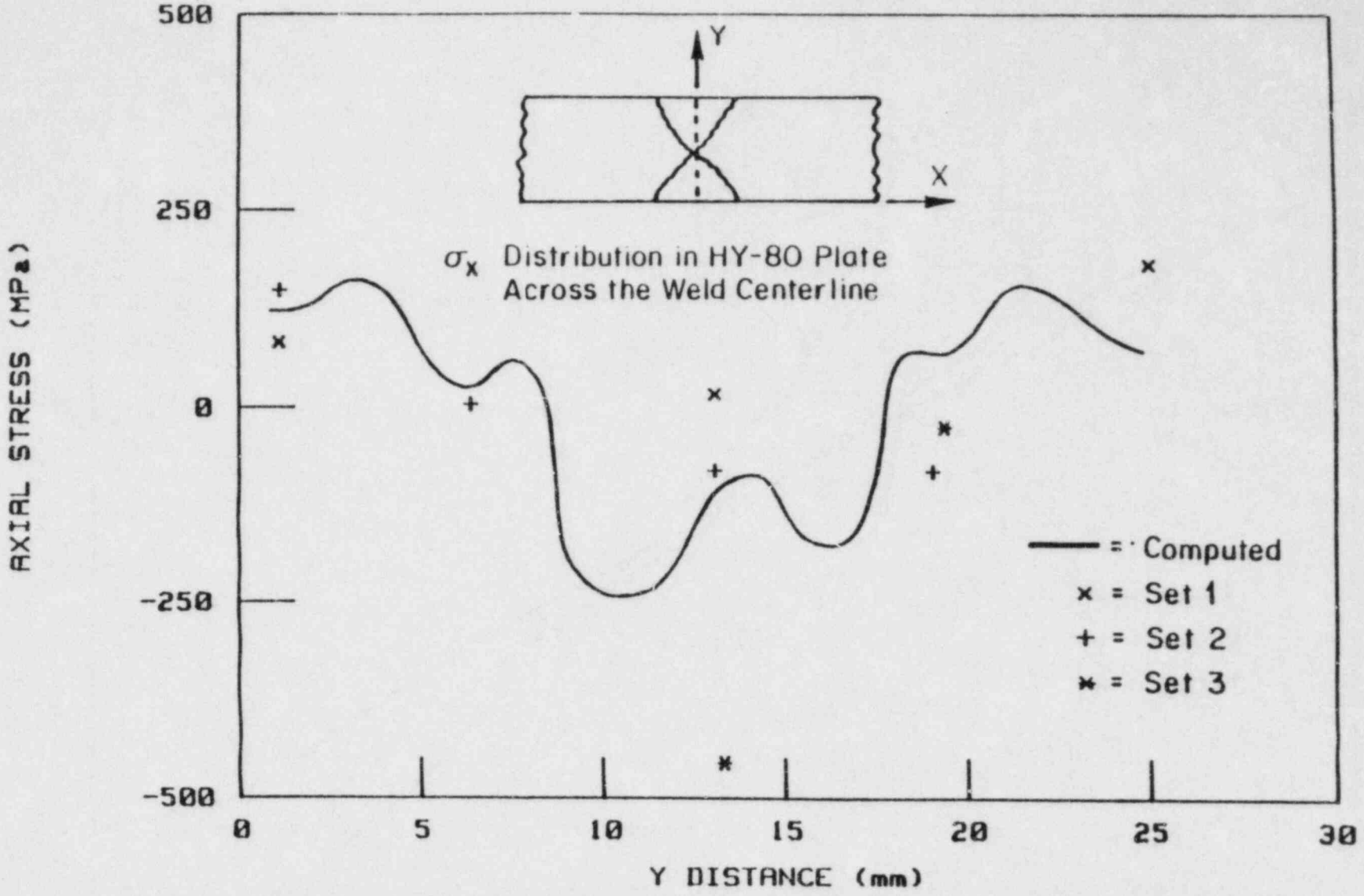

FIGURE 8. COMPARISON OF COMPUTED AND MEASURED WELD-INDUCED RESIDUAL STRESSED IN WELDED HY-80 SPECIMENS

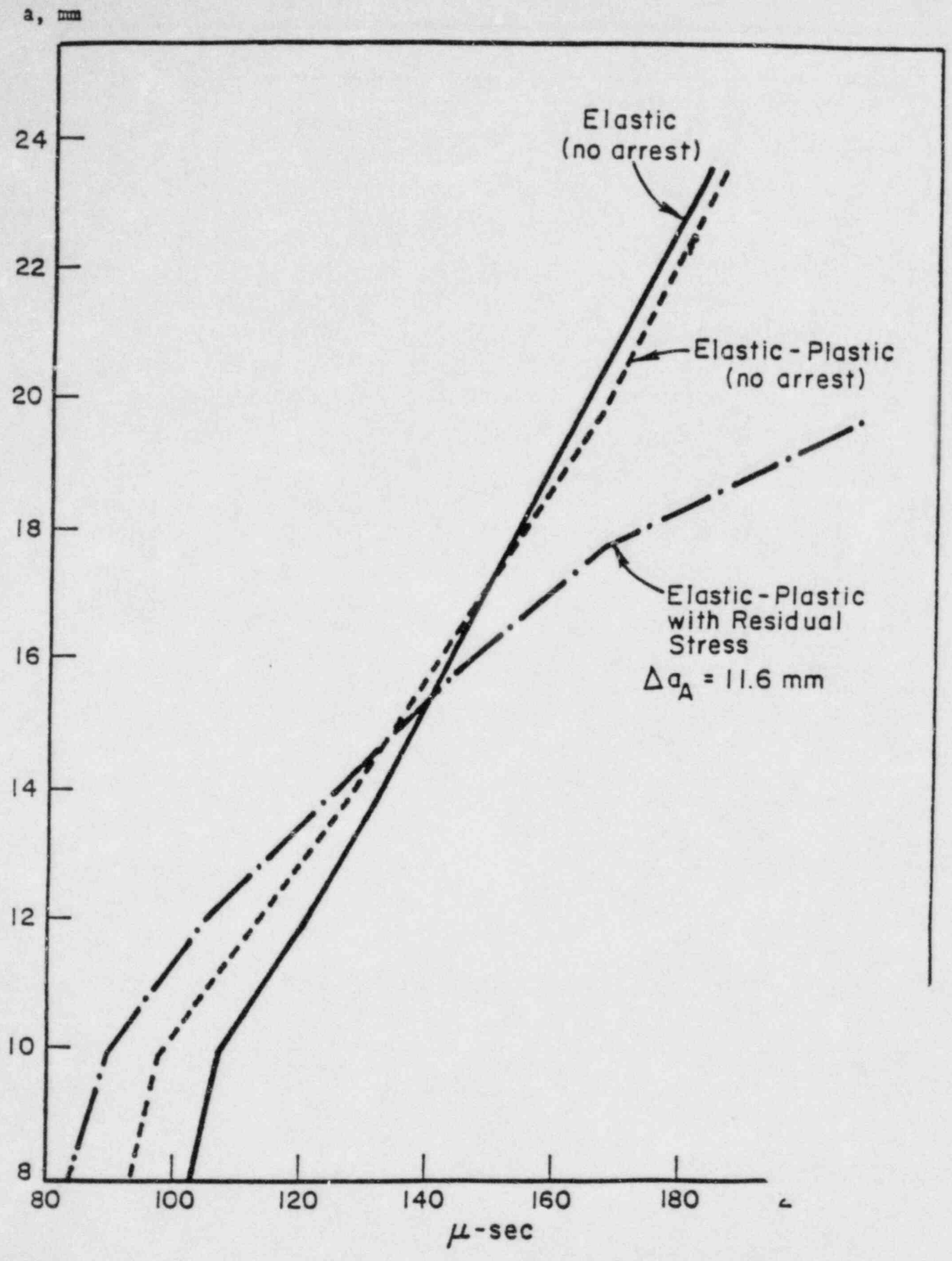

FIGURE 9. PREDICTION OF CRACK LENGTH HISTORY FOR A WELDED HY-80 SPECIMEN UNDER BLAST LOADING

CONCLUSIONS

The determination of precise delimitations of leak-before-break conditions is of vital importance for nuclear plant piping systems. Because the manner in which pipe fracture occurs is influenced by subcritical and rapid crack propagation, fracture mechanics applications must be made to quantify both aspects. The intial flaws that trigger fracture in nuclear piping systems generally occur in or near a weld. Among other considerations, weld-induced residual stresses are present. Residual stresses have been shown to affect crack growth in all its stages. Consequently, there would appear to be a definite need for more rigourous elastic-plastic fracture mechanics techniques to treat residual stresses in order to provide more realistic leak-before-break assessments.

REFERENCES

[1] Kanninen, M. F., Popelar, C. H. and Broek, D., "A Critical Survey on the Application of Plastic Fracture Mechanics to Nuclear Pressure Vessels and Piping", Nuclear Engineering and Design, vol. 68, pp 27-55, 1981.

[2] Kanninen, M. F., Broek, D., Marschall, C. W., Rybicki, E. F., Sampath, S. G., Simonen, F. A., and Wilkowski, G. M., Mechanical Fracture Predictions for Sensitized Stainless Steel Piping with Circumferential Cracks, Battelle's Columbus Laboratories Report to the Electric Power Research Institute, NP-192, September, 1976.

[3] Kanninen, M. F., Broek, D., Hahn, G. T., Marschall, C. W., Rybicki, E. F., Wilkowski, G. M., "Towards an Elastic-Plastic Fracture Mechanics Predictive Capability for Reactor Piping", Nuclear Engineering and Design, vol. 48, pp 117-134, 1978.

[4] Hale, D. A., et al., The Growth and Stability of Stress Corrosion Cracks in Large-Diameter BWR Piping, General Electric Company Report to the Electric Power Research Institute, NP-2472 (in two volumes), July, 1982.

[5] Kanninen, M. F. et al., Instability Predictions for Circumferentially Cracked Type 304 Stainless Steel Pipes Under Dynamic Loading, Battelle's Columbus Laboratories Report to the Elastic Power Research Institute, NP-2347 (in two volumes), April, 1982.

[6] Merkle, J. G., "New Method for Analyzing Small Scale Fracture Specimen Data in the Transition Zone", Tenth Water Reactor Safety Meeting, October, 1982.

[7] Kanninen, M. F., Brust, F. W. Ahmad, J. and Papaspyropoulous, V., "An Elastic-Plastic Fracture Mechanics Prediction of Fatigue Crack Growth in the Heat-Affected Zone of a Butt-Welded Plate", Fracture Tolerance Evaluation, T. Kanazawa et al., editors, Toyoprint Co., Ltd., Tokyo, p 113, 1982.

[8] Barnes, C. R., Ahmad, J. and Kanninen, M. F., "Dynamic Crack Propagation Through Welded HY80 Plates Under Blast Loading", Sixteenth ASTM National Symposium on Fracture mechanics, Columbus, Ohio, 15-17 August 1983.

[9] Hahn, G. T. and Kanninen, M. F., "Dynamic Fracture Toughness Parameters for HY-80 and HY-130 Steels and Their Weldments", Eng. Fracture Mech., vol. 14, p 725, 1981.

CURRENT POSITION AND ACTUAL LICENSING DECISIONS

ON LEAK-BEFORE-BREAK

IN THE

FEDERAL REPUBLIC OF GERMANY

H. SCHULZ

GESELLSHAFT FÜR REAKTORSICHERHEIT

ABSTRACT

In the updating of the Guidelines for PWR's of the "Reaktorsicher-heitskommission" (RSK) /1/ in 1981 the requirements on the design have been changed with respect to the postulated leaks and breaks in the primary pressure bounday. The major change is a revision in the requirements for pipe whip protection. As a logical consequence of the "concept of basic safety" /2/ a guillotine type break or any other break type resulting in a large opening is not postulated any longer for the calculation of reaction and jet forces.

As an upper limit for a leak an area of 0,1 f (F = open cross section of the pipe) is postulated. This decision is based on a general assessment of the present PWR system design in Germany.

Regarding the design of the emergency core cooling system (ECCS) and the containment the requirements are unchanged. For the design of the strength and stability of the component support the requirements were simplified.

The paper presents the

- details of the change in the RSK Guidelines
- the reasoning behind it
- actual application in present PWR- and BWR licensing cases.

1. INTRODUCTION

In the design of nuclear power plants with light-water reactors a high quality standard is required /1, 3/ for the pressure retaining walls of the components of the primary pressure boundary. This general requirement, established first in the "General Design Criteria" /4/ has been adopted by all countries. However there is no common understanding what a "high quality standard" means in terms of qualitative and quantitative requirements. Independent of the high quality standard of the primary pressure boundary a failure of the primary piping up to a "guillotine" type break was postulated to design engineered safeguards for all kinds of loss-of-coolant accidents.

Historically the postulated piping failure was first the design basis for the containment. Then the emergency core cooling systems where designed according to this postulate. This development was followed by a steadily increasing effort to analyse the system behaviour in case of a pipe rupture with respect to the reaction forces and mechanical damage due to pipe whip as well as the pressure differentials between the compart- ments of the containment internal structures. This resulted in an enforcement of the internal structure of the containment as well as the internal structure of the primary pressure boundary. To avoid mechanical damage of the whipping pipe restraints were designed and applied at several locations of the primary piping. These engineered safeguards were extended to all high energy piping wherever safety related items had to be protected.

Parallel to this development a huge amount of research and development funds were devoted to the understanding of fracture phenomena. Most of them have been focused on thick-walled structures of ferritic steels e.g. the "HSST-Program" and the German program on "component-safety"/9/. The results of these research programs are applicable to ferritic piping to some extend and have led to a better understanding of material behaviour in general.

For german light-water reactor systems which use ferritic steels for the vessels as for the piping we found ourselves in a situation that we required an increasing amount of engineered safeguards against the postulated double-ended pipe rupture at a time where we have gained a better understanding and increasing knowledge of the influencing factors to produce a high quality product and to analyse the system behaviour.

2. DEVELOPMENTS IN REGULATORY REQUIREMENTS

Starting with the problems of underclad cracking and reheat cracking in nuclear components /5,6/ a continuous development has taken place to improve the requirements regarding the quality of the components of the primary pressure boundary. The first approach was to strenghten the requirements on fracture toughness of the heat-affected-zones of welds, tighten up the manufacturing control and to apply more sophisticated ultrasonic testing methods /7/. In the next development stages of the RSK-guidelines /1,8/ and KTA-rules /10-13/ the objective was to give preference to all measures which increase the quality of the product and thus to become more independent of the effectiveness of the administrative and control measures of the quality assurance system. The supporting research work sponsored by the Federal Ministry of Science and Technology, the Federal Ministry of the Interior, Industry and Utilities has been presented mainly at the MPA-Seminars /9/ and elsewhere.

With the 2nd edition of the RSK-guidelines /8/ the concept of basic safety was established which is determined by:

- high grade material properties;
  major emphasis is placed on chemical composition, fracture toughness, processiblity and testability
- conservative limitation of stresses and reduction of peak stresses;
  that means a sufficient load-bearing margin in relation to the entire of loads that may occur and a preference that must be given to certain forms of design and construction so that stress concentrations at welds are minimized

- assurance of the application of optimized manufacturing and testing technologies;
  preference must be given to certain semi-finished products (forged rings for vessels, seamless tubes and pipe elbows with extended ends),
  tight tolerances to achieve a small edge displacement
- the ability of finding defects and assessing them properly;
  experience has shown that the improved testability of the base material and the welds (less indications from nonmetallic inclusions or geometrical imperfections) results in a higher reliability of the results of the nondestructive testing,
  advances in fracture mechanics as well as experimental investigations have improved the understanding of fracture behaviour
- control of the operating medium and system behaviour.

For components which are designed and manufactured to these principles a instantaneous failure is excluded.
For an adequate surveillance during the life-time of the plant leak-detection systems as well as recurring inspections are required /1,13/.
The detailed requirements on the primary pressure boundary are laid down in the KTA-Rules (10,11,12,13/.
Fig. 1 gives an impressive example how the principles of basic safety were applied to the primary circuit of a PWR. As far as the primary coolant piping is concerned, the number of welds could be reduced from about 250 to about 60 by using forged parts with integrated nozzles /14/.

3. CURRENT POSITION ON LEAK-BEFORE-BREAK

The experimental and analytical work on leak-before-break in the F.R.G. is summarized in /15,16/ to a certain extent. More work is still going on devoted to a better understanding of fracture behaviour in ductile materials /17/. From the results of the research and development work finished so far it can be concluded that leak-

before-break behaviour is given for circumferential cracks as well as for longitudinal cracks in pipes which are built to the quality standard required by the basic safety concept /15,16/.
For a general application with respect to the exclusion of piping failures the following questions have to be taken into account:

1. possibility of multiple cracking
2. corrosive influence
3. validity of fatigue design curves
4. reliability of defect detection and sizing
5. applicability of fracture mechanics to degraded material conditions

Of equal importance as these questions are is the need to evaluate the operating experience also. Up to now the primary piping of the PWR's using ferritic steel and stainless steel cladding show an excellent performance.
Due to the improvements in the primary pressure boundary built to the standard of the basic safety concept, instantaneous failure of components can be excluded. The resistance of the weld connections to fatigue cracking has been enhanced by applying optimized manufacturing technology and reduction of peak stress, this covers point 1 and 3. The testability has been improved and therefore reliability of defect detection and sizing increased, point 4. A significant degradation of the material over the lifetime ist not to be expected. This judgement is based on the relatively low fatigue usage factor calculated as well as the excellent operating record, so point 5 has no importance. Ferritic steel piping in BWR-systems which had been questioned with respect to their resistance to unstable crack growth have been replaced during the last 2 years by pipes of ferritic steels to a comparable quality standard as the piping of the PWR's /18, 19/. Corrosion problems (point 2) on stainless-steel clad ferritic piping have not been detected in German PWRs.

For these reasons it has been decided that engineered safeguards as pipe whip restraints to protect against a postulated pipe break are not justified. The abandonment of pipe whip restraints on the main primary coolant piping allows a simpler layout of the system with easier access for inspection and surveillance.

If any crack growth might occur only minor leakage is expected. For design purposes it has been decided that a leak area of 0,1 F (F = open cross section of the pipe) is chosen as an upper value to calculate reaction and jet forces.
The design requirement for the strength and stability of the component support has been simplified, an equivalent static force is used.
The requirements for the design of the containment and the emergency core cooling systems have been maintained for several reasons.
A translation of the relevant chapter of the RSK guidelines is given in Appendix A.

4. PWR- AND BWR LICENSING DECISIONS WITH RESPECT TO BREAK ASSUMPTIONS

With the revision of the RSK-guidelines in 1981 all license applications for construction of PWR's which abandoned the pipe whip restraints on the main primary coolant piping have been accepted by the licensing authorities.
For PWRs already under construction where the license part concerning the primary circuit was still under consideration the abandonment of the pipe whip restraints was accepted if the applicant could demonstrate that the achieved quality of the main primary coolant piping complied with the requirement of the basic safety concept.
The exclusion of pipe break for pipes made of austenitic steel, like the surge-line of the German PWR-system, is not yet decided. There are still questions if a sufficient reliability of the nondestructive testing and surveillance during operation can be achieved, in particular for the dissimilar metal welds (connections to the pressurizer and main coolant pipe).
For PWRs licence applications which abandoned the pipe whip restraints on the main steam and feedwater line inside the containment up to the first closure valve outside the containment have

also been accepted if the applicant had demonstrated that the principles of basic safety were met equally to the primary piping. A corresponding amendment to the RSK guidelines has been published in 1983 /20/.

For BWR systems equivalent decisions are taken in some license applications concerning the replacement of ferritic piping in the main coolant system.

5. REFERENCES

/1/ RSK-Guidelines for Pressurized Water Reactors,
3rd Edition, Oct. 14. 1981;
Gesellschaft für Reaktorsicherheit (GRS) mbH

/2/ Kussmaul K., Blind D.
"Basic Safety - A Challenge to Nuclear Technology"
IAEA Specialist Meeting, Madrid, 5-8 March 1979

/3/ Sicherheitskriterien für Kernkraftwerke,
Der Bundesminister des Innern
Ausgabe Oktober 1979

/4/ General Design Criteria
10 CFR 50, Appendix A

/5/ Statusreport on Reactor Pressure Vessels
Volume 2, December 1976
Institut für Reaktorsicherheit

/6/ BMFT-TB RS 101
Forschungsprogramm "Reaktordruckbehälter"
1. Technischer Bericht Oktober 1973
MPA-Stuttgart

/7/ RSK-Guidelines for Pressurized Water Reactors,
April 24. 1974
Gesellschaft für Reaktorsicherheit (GRS) mbH

/8/ RSK-Guidelines for Pressurized Water Reactors,
2nd Edition, Jan. 24. 1979
Gesellschaft für Reaktorsicherheit (GRS) mbH

/9/ MPA-Seminars, Safety of the Pressure Boundary of
Light Water Reactors
Seminar 1-8 1974-1982
Staatliche Materialprüfungsanstalt
Universität Stuttgart

/10/ Sicherheitstechnische Regel des KTA
KTA 3201.1 - Komponenten des Primärkreises
von Leichtwasserreaktoren, Teil: Werkstoffe

/11/ Sicherheitstechnische Regel des KTA
KTA 3201.2 - Komponenten des Primärkreises
von Leichtwasserreaktoren, Teil: Auslegung,
Konstruktion und Berechnung

/12/ Sicherheitstechnische Regel des KTA
KTA 3201.3 - Komponenten des Primärkreises
von Leichtwasserreaktoren, Teil: Herstellung

/13/ Sicherheitstechnische Regel des KTA
KTA 3201.4 - Komponenten des Primärkreises
von Leichtwasserreaktoren, Teil: Wiederkehrende
Prüfungen und Betriebsüberwachung

/14/ H. Dorner: Grundlagen zur weiteren Verbesserung
von Primärkreis-Komponenten
Tagung Reaktorsicherheitsforschung Köln,
17.05.1982
GRS-45 September 1982

/15/ K. Kussmaul et. al.: Exclusion of Fracture in
Piping of Pressure Boundary
Part 1: Experimental Investigations and Their
Interpretation
International Symposium on Reliability of Reactor
Pressure Components, IAEA - SM - 269/7
Stuttgart, 21-25 March 1983

/16/ G. Bartholome´et. a.: Exclusion of Fracture in
Piping of Pressure Boundary
Part 2: Application to the Primary Coolant Piping
International Symposion on Reliability of Reactor
Pressure Components, IAEA - SM - 269/7
Stuttgart, 21-25 March 1983

/17/ Gesellschaft für Reaktorsicherheit (GRS) mbH
Annual Report on Reactor Safety Research Projects
Sponsored by the Ministry for Research and Technology of the Federal Republic of Germany
1982
GRS-F-124 (June 1983)

/18/ Stäbler K.: Nachrüstung von Kernkraftwerken aus der Sicht des Betreibers
Atomwirtschaft Oktober 1982

/19/ Bieselt et. a.: Nachrüstung der druckführenden Umschließung von Siedewasserreaktoren unter Berücksichtigung des Leck-vor-Bruch Kriteriums.
Jahrestagung Kerntechnik
Berlin, Juni 19-16, 1983

/20/ Bundesanzeiger Nr. 106 vom 10.06.1983
Empfehlungen der Reaktor-Sicherheitskommission auf ihrer 181. Sitzung am 15.12.1982.

Reaktorkühlkreislauf des KWU Druckwasserreaktors
Reactor Coolant System of KWU Pressurized Water Reactor

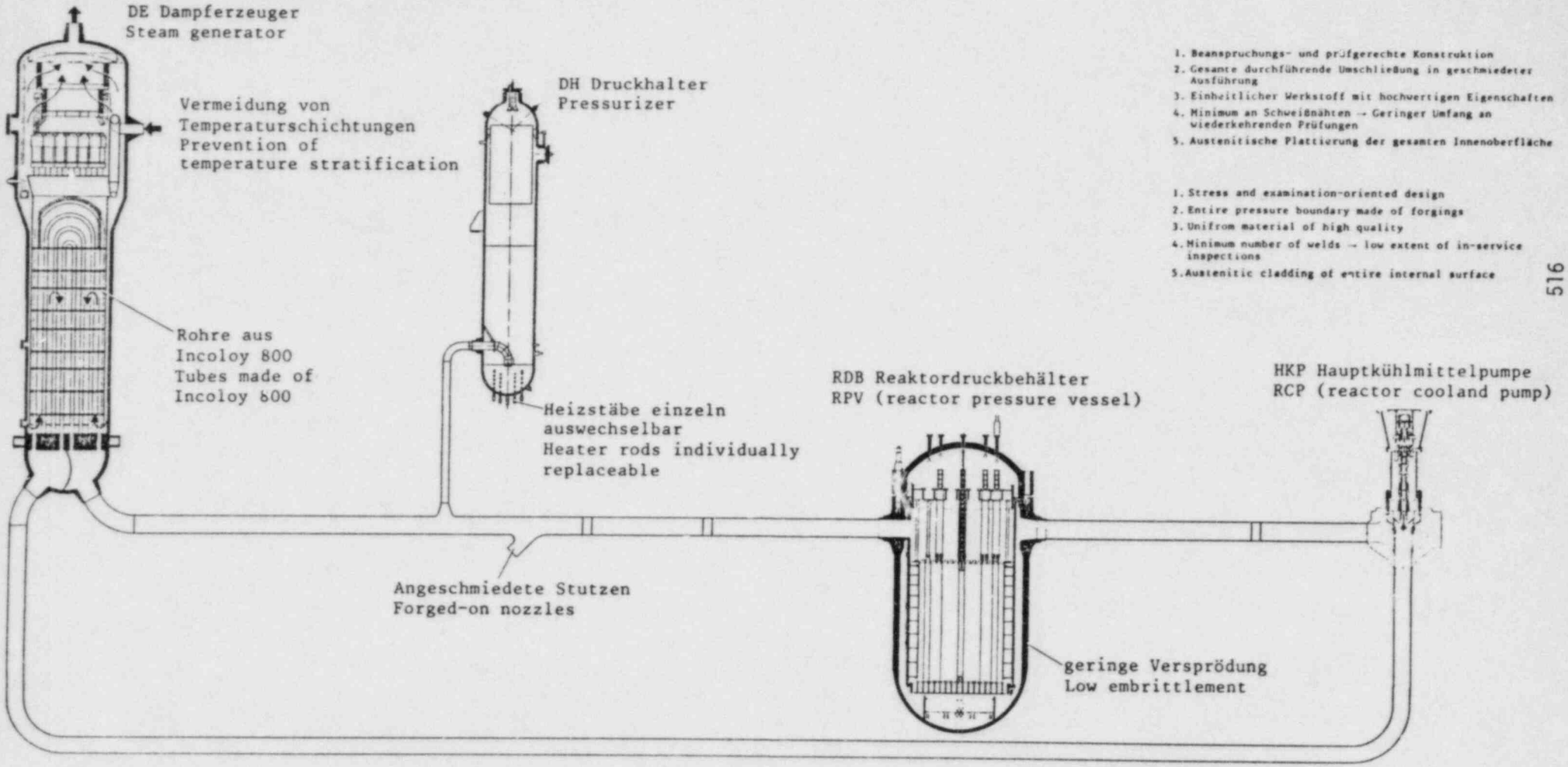

1. Beanspruchungs- und prüfgerechte Konstruktion
2. Gesamte durchführende Umschließung in geschmiedeter Ausführung
3. Einheitlicher Werkstoff mit hochwertigen Eigenschaften
4. Minimum an Schweißnähten → Geringer Umfang an wiederkehrenden Prüfungen
5. Austenitische Plattierung der gesamten Innenoberfläche

1. Stress and examination-oriented design
2. Entire pressure boundary made of forgings
3. Unifrom material of high quality
4. Minimum number of welds → low extent of in-service inspections
5. Austenitic cladding of entire internal surface

516

FIG. 1: REACTOR COOLANT SYSTEM OF KWU PRESSURIZED QUELLE KWU

Appendix A

TRANSLATIONS-
SAFETY CODES AND GUIDES

Edition 5 / 82

Contents

RSK Guidelines for Pressurized Water Reactors, 3rd Edition, October 14, 1981

RSK Leitlinien für Druckwasserreaktoren 3. Ausgabe, 14. Oktober 1981

Chapter 21: Postulated Leaks and Breaks

21.1: Postulated Leak Cross Sections in the Main Cooland Pipe and in the Reactor Pressure Vessel

Editor: Gesellschaft für Reaktorsicherheit (GRS) mbH
Glockengasse 2 · D-5000 Köln 1 · Telefon (0221) 2068-1 · Telex 8881807 GRS D

(1) Reaction and jet forces acting on pipes, components, component internals, and buildings.[1)]

1. Concerning the load assumptions for reaction and jet forces on pipes, components, component internals, and buildings a spontaneously opening leak (linear opening behaviour, opening time 15 ms) with a cross section of 0,1 F (F = open cross section) shall be postulated for different break positions.

2. In order to cope with the consequences (pressure increase of in the reactor pit, release-pressure-wave acting on the reactor pressure vessel internals) of a postulated leak with a cross section of 0,1 F between the reactor pressure vessel and the biological shield, measures shall be taken, e.g. double pipes in the area of the main coolant pipe penetrations through the biological shield.

(2) Presumptions for the design and the safety demonstration of the emergency core cooling systems, the containment vessel and its internals as well as the supports of the reactor coolant system components.

For the design and examination by calculation the following postulates are relevant:

1. The analysis of the emergency core cooling efficiency (reference to Sec. 22.1.1) shall be based on leak cross sections in the main coolant pipes up to 2 F. The emergency core cooling systems shall be designed accordingly.

---

1) Note: This definition is relevant for the design requirements in Sec.

3.3	(1)	Reactor pressure vessel internals
5.1	(5)	Containment internals
5.2	(1),(5)	Electrical equipment inside the containment

2. The determination of the containment vessel design pressure as well as the determination of pressure differences inside the containment vessel shall be based on leak cross sections up to 2 F.

   The determination of design pressure and design temperature for incident resistant electrical equipment shall be based on leak cross sections of 2 F as well.

3. For the demonstration of stability of components reactor pressure vessel, steam generators, main coolant pumps, and pressurizer the following assumtions shall be made:

   The stability of the components shall be assured for a static force P_{ax} with

   magnitude: $P_{ax} = p \times F \times S$
   p = nominal operation pressure
   F = open cross section
   S = 2 (safety margin)

   origin of force: middle of the pipe cross section in the area of the nozzle circum ferential weld

   direction of force: middle line of the nozzle acting towards the component.

   This force acts only on one nozzle for the time being. The stability shall be demonstrated for each nozzle separately.

   Note: with respect to the steam generator the stability shall be assured for the connection to the secondary circuit in the same way.

(3) Deterministic postulated leak cross section in the reactor pressure vessel

1. In view of the restraints of the reactor pressure vessel, the stresses acting on the reactor pressure vessel internals and the design of the emergency core cooling system, a leak of about 20 cm^2 (geometric cross section: circular) shall be also postulated below the reactor core upper edge. Prior defects of the reactor pressure vessel which might lead to a leak size of more than 20 cm^2 shall be detectable in time by means of suitable monitoring measures.

2. The design shall also be based on the consequences of the sudden break of a control assembly nozzle involving the maximum possible leak cross section as well as the postulated leaks in the reactor pressure vessel.

(4) Pressure barrier of the low-pressure system towards the high-pressure system.

Provisions shall be made against pressurizing of the low-pressure system as a result of a failure of the pressure barrier towards the high-pressure system (pressure-retaining boundary). The provisions may include recurrent tests of valve functions, measurements of the pressure between two successive valves and the indication of leaks in the control room).

21.2 Postulated Leaks and Breaks in the Main Steam and/or Feedwater Pipe

(1) The loads acting on the steam generator heating tubes as a result of the static and transient stresses (pressure-surge, flow forces, static pressure differences along the steam generator heating tubes) in case of a main steam and/or feedwater pipe break or remaining open of a secondary safety valve shall be determined. It shall be demonstrated that the steam generator heating tubes will cope with these stresses. In principle,

however, in this incident analysis the failure of a few steam generator heating tubes shall be postulated as a single failure wich shall be considered by the assumption of a total break (2F) of a steam generator heating tube in the concerned steam generator comprehensively. For the case of a main steam pipe break outside the outer isolating valve an additional "isolating valve nonclosure" single failure, a steam generator heating tube failure need not be postulated if the above demonstration has had a positive result.

(2) The effects of a main steam pipe break and of a cold water transient on the reactivity behavior and on the changes in pressure and temperature in the reactor as well as the resulting stresses on the reactor pressure vessel and its internals shall be kept under control.

22. Systems for Post-Incident Heat Removal

22.1 Emergency Core Cooling and Residual Heat Removal System

(1) A reliable and efficient redundant emergency core cooling and residual heat removal system shall be available for the removal of heat after loss-of-coolant accidents. The system shall be capable of keeping core temperatures at long-term low values in case of an occurrence of leaks and breaks in the pressure-retaining boundary as specified in Sec. 21.1.

22.1.1 Requirements

(1) The emergency core cooling system shall assure that

1. the calculated maximum fuel rod cladding temperature will not exceed 1 200 °C;

PROPOSED CHANGES IN INTERMEDIATE PIPE BREAK CRITERIA

R. P. SCHMITZ

CHIEF NUCLEAR ENGINEER

BECHTEL POWER CORPORATION

PROPOSED CHANGES IN INTERMEDIATE PIPE BREAK CRITERIA

For Presentation September 2, 1983

Committee on the Safety of Nuclear Installations
Meeting on Leak Before Break in Nuclear Reactor Piping Systems

by R.P. Schmitz, Chief Nuclear Engineer
Bechtel Power Corporation

Progress is being made in making the overall U.S. criteria for nuclear plants more rational. Hopefully, this will lead to better and safer plants for the future. These improvements are resulting from the increased use and understanding of risk assessment techniques and safety goals, as well as evaluation of the impressive operating experience being accumulated.

An important part of this effort is the review of criteria for nuclear plant piping systems and the development of more realistic safety-effective and cost-effective criteria for design. Our organization is giving this subject a very high priority. Improvements in pipe break criteria are a key part of this effort.

Pipe breaks have always been considered to some degree in commercial nuclear power stations in the U.S. At first, there was consideration only of potential radioactive releases. Next, emergency core cooling systems were added to replace the primary system coolant lost through the break. Later, criteria were developed for pipe whip restraints to protect against pipe movement. A detailed definition of break locations was required. Every year we added some detail to the definition of pipe breaks and their effects, including jet impingement loads, compartment pressurization, asymmetric loading on the reactor vessel, pump overspeed, effects on equipment supports, pipe dynamic impact loads, potential effects of pipes impacting smaller or larger pipes, formation of secondary missiles and formation of plastic hinges in the ruptured pipe. These effects are constantly being evaluated in greater and greater detail and presumably with greater accuracy. This progression has resulted from the tendency of engineers to achieve perfection, along with the reaction of engineers to the legalistic and adversarial atmosphere surrounding many projects. The regulators have encouraged this entire process, but industry must assume responsibility also.

The impact of these developments is just now being fully appreciated. A typical PWR now can have about 300 pipe whip restraints. The engineering effort on the part of the architect engineer required to deal with the entire problem can range up to 250,000 person-hours, more than was required for the entire balance-of-plant design work for many operating 500-600 MWe nuclear plants. Estimated costs for the design and construction work associated with pipe break effects for a typical unit are 30 to 50 million dollars. The design features included to protect against pipe whip clearly complicate the

overall plant design, make access for maintenance and inservice inspection more difficult, and add to the dose accumulated by the plant operators for the life of the plant. These are real incentives to review, change and improve the pipe break criteria and practices now being used.

Regulatory criteria relating to piping design were essential for the design and construction of nuclear power plants but were promulgated prior to having the experience, analyzed data and detailed knowledge of the impact of the criteria that we have today.

Detailed analyses were recently completed to resolve NRC Generic Issue A-2 on asymmetric loads on the reactor vessel resulting from PWR main coolant pipe ruptures near the reactor vessel. Work by Westinghouse (WCAP No. 9570 - "Mechanistic Fracture Mechanics Evaluation of Reactor Coolant Pipe Containing a Postulated Circumferential Through-Wall Crack"), Lawrence Livermore National Laboratory (LLNL) under contract to the NRC, and others has provided substantially convincing conclusions that, at least for the main cooling loop piping covered by these analyses, undetected defects that could cause guillotine and full size longitudinal breaks are incredible. The Lawrence Livermore work has also supported the argument that there is negligible safety benefit in combining pipe break and seismic loads. Combustion Engineering also participated in this review and recently formally requested changes on their docket for CESSAR Systems 80 to eliminate pipe breaks in the primary loop piping.

The NRC sponsored the LLNL work and closely monitored the work by others. They reviewed the results with the Advisory Committee on Reactor Safeguards sub- committee on March 29, 1983 and with the full committee on June 10, 1983. The NRC staff reported that they are technically satisfied with the arguments presented and that they plan to recommend appropriate changes to the current NRC criteria to eliminate mechanistic treatment of PWR primary loop breaks. They also plan to allow use of these criteria before the formal changes are implemented on a case by case basis.

Although the discussions to date relate specifically to the PWR primary loop, the technology and principles obviously apply to many other piping systems. There is a need to develop definitive criteria so that similar analyses can be made to attain the substantial benefits of this approach for other piping and locations.

These are important changes. However, there are a large number of other documents and criteria related to pipe breaks, such as containment design, emergency core cooling systems, equipment qualification, load combination equations, flooding, shielding, and jet impingement protection. The Atomic Industrial Forum's Subcommittee on Load Combinations is actively discussing proposed criteria changes for many of these subjects with the NRC. The NRC is considering forming a task force to make recommendations for all resulting changes. Hopefully, implementation of these changes can be completed in a year or less.

In order to attain a substantial and more immediate benefit, Bechtel proposed in a letter to the NRC on April 25, 1983 that the NRC eliminate from their criteria all intermediate breaks. The basic criteria for determining high energy line break locations are contained in Regulatory Guide 1.46 and Branch Technical Positions MEB 3-1 and ASB 3-1. These documents require that breaks be considered at terminal ends and at points where stresses or cumulative usage factors exceed specified limits or at the two highest intermediate stress points. On a typical PWR, breaks required at the two highest stress points represent more than half of the 300 break points, compared with 10 to 20 primary loop restraints.

We believe that current knowledge and experience indicate that assuming intermediate breaks at locations where stresses do not exceed ASME Code allowables is not justified and that, except for branch connections, this requirement should be deleted. There is now extensive operating experience with piping in over 80 operating U.S. plants and a number of additional similar plants overseas. We are not aware of any failure which indicates that designing for the intermediate breaks is necessary.

In addition, reason and logic indicate that postulating breaks based on the highest stress is not justified. These intermediate breaks are most often at locations where stresses are well below those susceptible to crack propagation. The present approach requires protecting against breaks at certain points but not at other points in the same system where stress levels may be only a few percent less. It also results in inconsistent approaches from system to system. In fact, the number of breaks in branched piping systems depends more on the capability of the computer program used to handle all the branches in a single analysis than on the physical conditions occurring within the piping systems.

While the restraints associated with intermediate breaks represent more than half of the restraints, these restraints represent a disproportionately high percentage of the cost of the overall restraint design and installation effort. The location of terminal end breaks, and hence the location of their associated pipe whip restraints, is known as soon as piping layout and preliminary stress analyses are completed. This allows structural embeds to be located and placed before pouring concrete, space to be allocated for restraints and supporting steel, and safety-related targets to be routed away from the vicinity of the postulated break. The locations of intermediate breaks, on the other hand, are not known until detailed piping and hanger design and subsequent stress analyses are completed. Even then, the addition of new piping system tie-ins or modifications to piping or hanger details due to field interferences and other reasons can change the stress at different points in the line requiring changes in the location of intermediate breaks. The impact that changes of this nature have on the construction schedule during the latter stages of construction and startup is substantial.

Access during plant operation for maintenance and/or inservice inspection is hampered due to the congestion created by these restraints and the supporting structural steel, and due to the need to remove some restraints to gain access to welds. In addition to the increased work load, a significant increase in man-rem exposure is involved. Also, the need to verify adequate cold and hot clearances between pipe and restraint during initial heatup requires additional hold points during this already critical startup phase.

Recovery from unusual plant conditions would also be hampered by this congestion. In the event of a radioactive release or spill inside the plant, decontamination operations would be much less effective due to the complex shapes represented by the structural framework supporting the restraints. These effects would work to increase man-rem exposures associated with decontamination and restoration activities. Access for control of fires within these areas of the plant would be more difficult, especially under low visibility conditions. Substantial overall benefits in these areas would be realized by reducing the number of whip restraints required.

By design, whip restraints fit closely around the high energy piping with gaps typically on the order of half an inch. These restraints and their supporting steel significantly increase the heat loss to containment. Also, since thermal movement of the piping system during startup and shutdown could deform the piping insulation against the fixed whip restraint, the insulation must be cut back in these areas, creating convection gaps adjacent to the restraint, also increasing heat loss to containment. This effect is particularly pronounced with metal reflective insulation. The heat loss from 1 foot of uninsulated pipe is equivalent to the heat loss from approximately 200 feet of completely insulated pipe. Thus, the addition of whip restraints yielding a net increase in heat loss equivalent to 6 inches of uninsulated pipe per 100 feet of pipe would double the piping heat loss inside containment. This is a major contributor to the tendency of many containments to operate at temperatures very near technical specification limits. The elimination of whip restraints associated with intermediate breaks would assist in controlling the containment temperatures.

There is a small but finite possibility that installation, inspection or maintenance procedures involving whip restraints would not leave proper clearances between the restraints and the pipe, thus causing higher stresses in the pipe. Reducing the number of restraints decreases the chances of this happening.

Some consideration is being given to continuing the requirement for environmental qualification of equipment, protection against flooding and possibly some other effects of leaks in place of these intermediate breaks.

Overall, we are extremely pleased with the progress being made on improving the criteria for pipe breaks in light water plants. We have very actively supported this effort and will continue to work toward complete implementation of new criteria because we believe that substantially better future plants will be the result.

A PROBABILISTIC ASSESSMENT OF LEAK-BEFORE-BREAK

S. H. Bush

INTRODUCTION

Probabilistic fracture mechanics can be used to assess both failure modes and failure mechanisms of nuclear piping systems. In turn, such assessments can be used in the decision process for licensing and regulation. This paper outlines one possible approach applicable to leak-before-break and asks the questions that must be answered before leak-before-break can become a viable alternative.

The following questions need to be answered in pursuing the probabilistic approach:

- Can pipes fail?
- What is connoted by failure?
- What are the probabilities of failure?
- What is the probability of catastrophic failure?
- Where does leak-before-break fit in between failure and catastrophic failure?
- What factors contribute to failure, or to leak-before-break versus catastrophic failure?

A system that is of current interest and amenable to probabilistic modeling is the BWR recirculation piping using IGSCC as the failure mechanism. Typical parameters requiring evaluation in a probabilistic model are discussed in the next section.

Parameters in the Probabilistic Model

Although the ASME Code deterministic approach establishes conservative load limits and property levels, factors outside the scope of both code and designer may lead to failures so that failure probability plays a role even in

the so-called deterministic approach. The following paragraphs simplistically discuss the key parameters of loads, material properties, and flaw geometry as they relate to failure of structures.

Figure 1 uses a stress-strain diagram to portray load thresholds and failure mechanisms. Zone I failures occur when the ultimate strength is exceeded. In this mode, if one assumes that code maximum loads remain the same, failure will occur through a loss of section such as may occur with gross cracking. Zone II represents elastic-plastic or general yield failure where the flaw contributes to failure at stresses below the ultimate. Zone III is the region where linear elastic fracture mechanics controls and failure will occur without perceptible deformation.

Factors outside the scope of design rules or codes such as ASME can lead to failure. Also, probabilities of failure may vary widely even when a system operates within the bounds of load and material properties set by the code.

The deterministic approach to such behavior as component failure has proven satisfactory and relatively straightforward, given that the relevant data base is sufficiently large to permit meaningful predictions. Generally, with a large data base, a direct relationship can be established with actual field experience. Unfortunately, the deterministic approach becomes less effective as the data base decreases, or when one wishes to extrapolate beyond the data base. For example, predicting failure behavior at higher stresses, pros and cons of modified nondestructive examination techniques, behavior near end of design life, etc.

The probabilistic approach involves the development and application of engineering models based on an understanding of failure modes and on the statistical distribution of the various controlling parameters. Basically, one analyzes failure by interrogation from the inside rather than from the outside of the system. Even so one starts with a deterministic model of one or more system failure modes, then modifies them appropriately to the probability format. Such physical models include fracture mechanics, fatigue life analyses, static stress strength analyses, etc. Probability is applied by combining known, assumed or proposed statistical variations of the various controlling parameters to predict the statistical variations in structural performance.

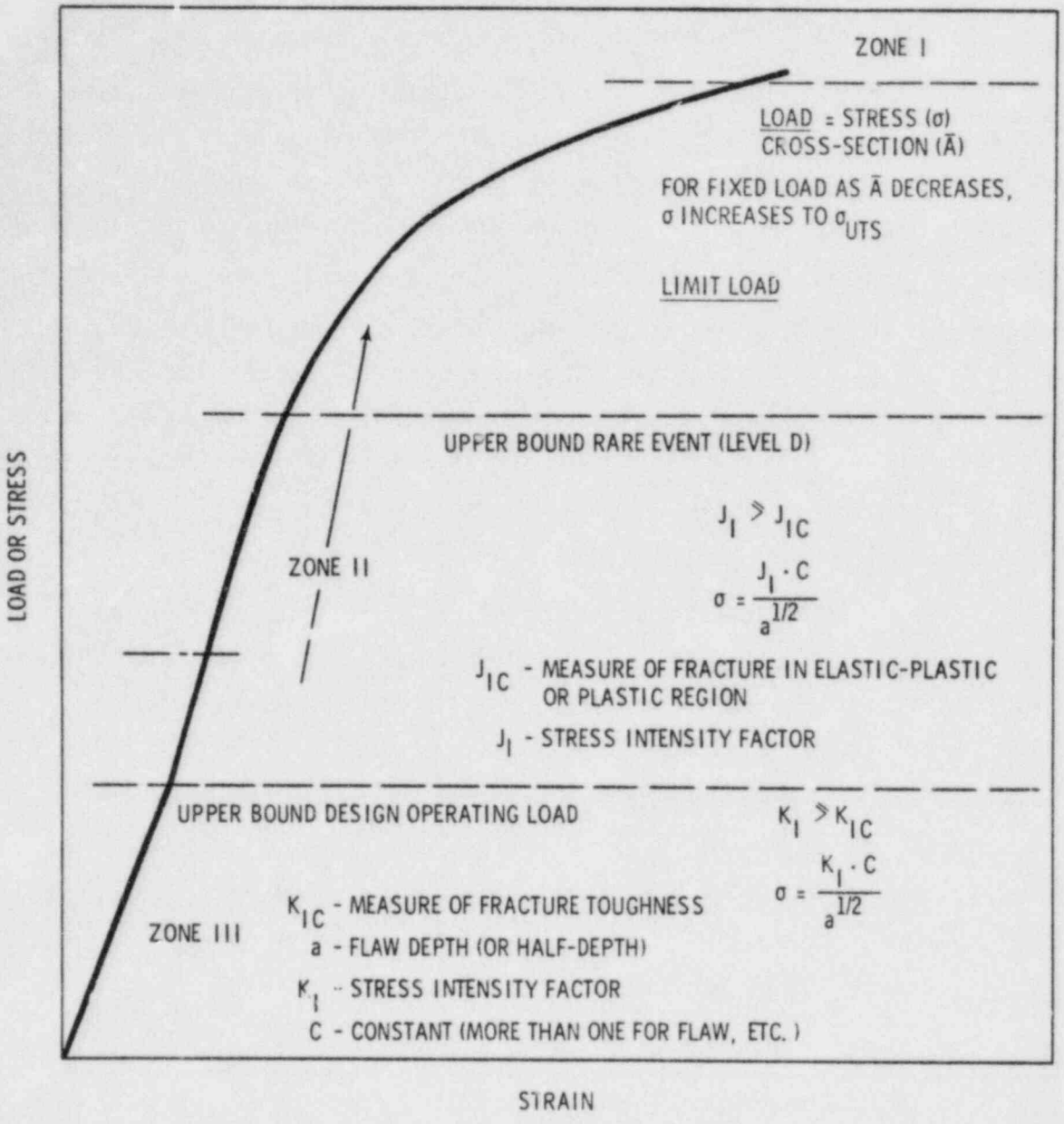

FIGURE 1. Simplified Stress-Strain Diagram Illustrating Failure Regions for Net Section Failure (I); Elastic-Plastic or General Yield (II); and Linear-Elastic (III); Assumes Membrane (Tensile) Load

The following sections will deal with the specific case of piping in the context of flaw-size distribution, loads, and mechanical properties. Flaw distribution at any time, transients affecting flaw growth, loads, stress intensities, and fracture toughness are tied together to yield failure probability. Figure 2 is an excellent presentation of the parameters affecting probability of failure.

One of the most critical input parameters, and the one we know the least about, is the flaw-size distribution probability density function at any time (T). Figure 3 is an attempt to represent schematically the time-dependent effects relevant to piping fracture. The use of a population of cracks initiated and grown exclusively during the operating life T_{OP} is justified on the basis of observed plant behavior.

Table 1 gives some idea of the sensitivity of pipe size and fabrication conditions to failure rate in the case of IGSCC in BWR primary coolant systems. Such defects in almost all cases are operationally initiated requiring no prior fabrication crack.

The statement of the flaw-size distribution problem is relatively straightforward; unfortunately, this is not true with the answer. Basically, the problem is--how well can we define the shape and dimensions of the probability density function for the flaw-size distribution at any time (T)? The answer depends on the following factors at a minimum:

- original flaw-size distribution if any
- accuracy of the fatigue crack growth equation used
- correct definition and applications of all transients causing crack growth
- effects leading to the initiation and propagation of new cracks by mechanisms such as IGSCC, corrosion-fatigue, thermal fatigue, etc. (Such effects may include but not be limited to the environment seen by the system, material properties, type of alloy, degree of sensitization, condition of surface, level of residual stress, existence of crevices, etc.)

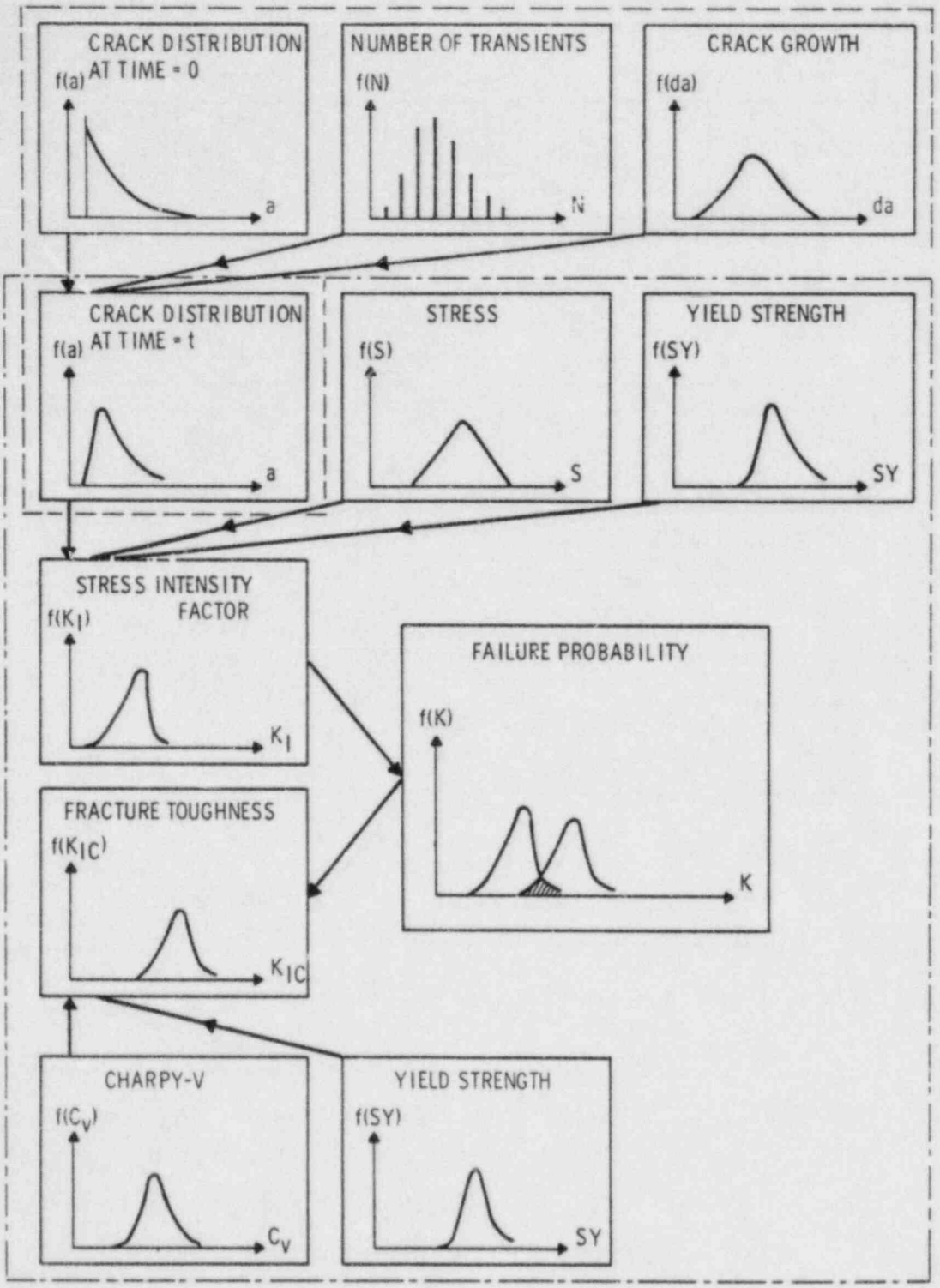

FIGURE 2. General Procedure for Calculating Time-Dependent Failure Probability

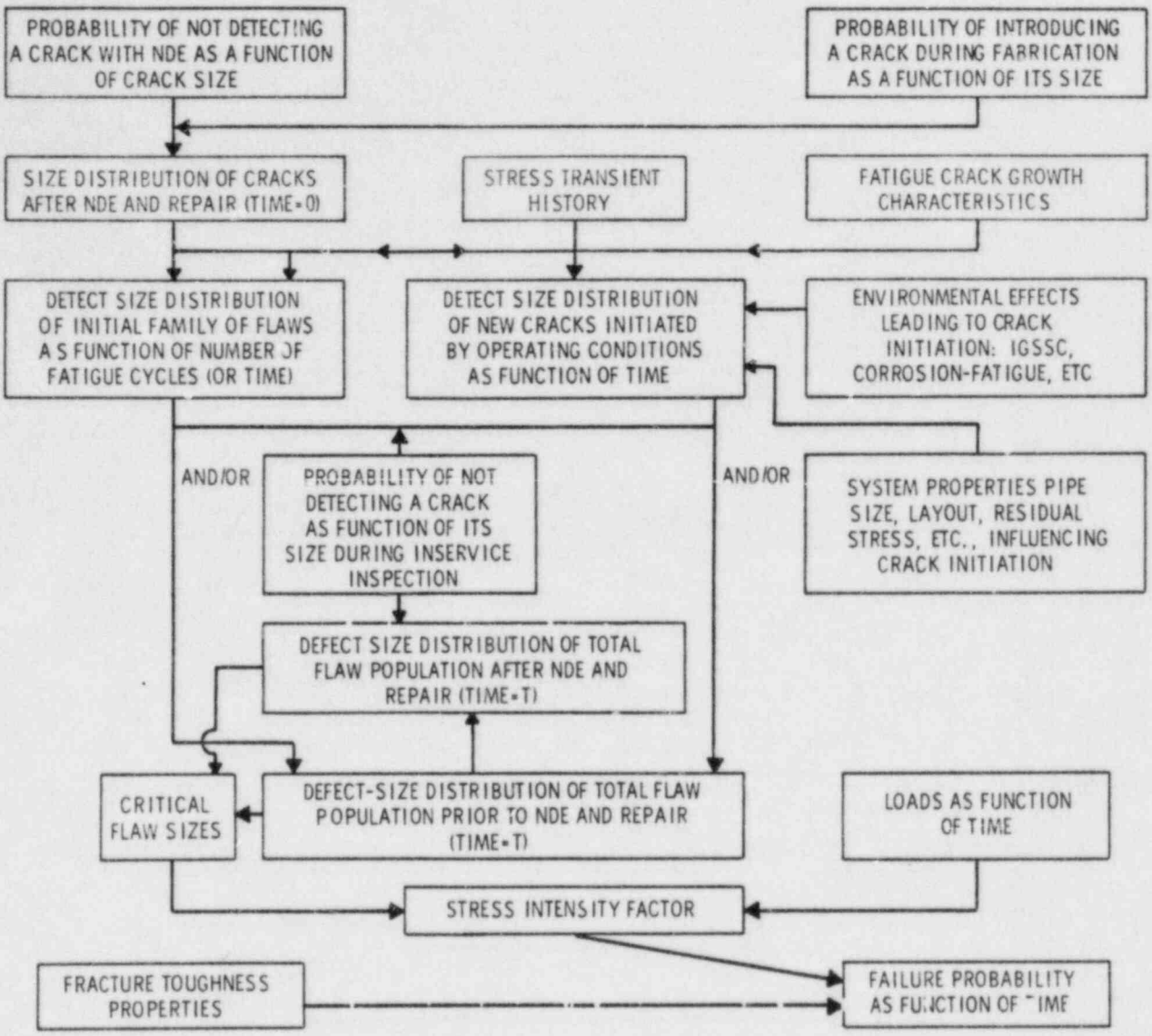

FIGURE 3. Schematic Diagram of Time-Dependent Effects Relevant to Piping Fracture

- adequacy of NDE techniques to detect both fabrication and operationally initiated flaws. (This is better defined as the probability of detection as a function of flaw size, location and orientation.)
- degree of corrective action taken to repair defects
- time since last NDE permitting further growth of existing flaws or initiation and growth of new flaws.

TABLE 1. Failure Rates Due to IGSCC in Weld Heat-Affected Zones of BWRs (Multiply all values by 10^{-4})

Failures	Dresden 1		BWR Mark 1 and 2		BWR Mark 3 and 4	
	Per Weld	Per Weld-Year	Per Weld	Per Weld-Year	Per Weld	Per Weld-Year
All welds	395	25.1	22.0	2.59	60.3	15.1
2-in. (51-mm) line welds			30.5	3.59		
4-in. (102-mm) line welds	345	53.9	50.5	5.94	251.6	62.9
6-in. (152-mm) line welds	1684	106.8	40.7	4.79		
8-in. (204-mm) line welds	909	57.7	40.2	4.73	141	35.3
10-in. (254-mm) line welds					125	31.2

Presumably, if one can correctly define all of the above, one can define the flaw-size distribution at time (T).

If we assume the existence of cracks, we need to assess the probability of detection and of sizing such cracks. As an input into our fracture mechanics model Figure 4 is a generalized model while Figure 5 contains actual detection probabilities for IGSCC, confirming the shape of and band width illustrated in Figure 4.

Several factors influence the reliability of flaw detection. Figure 6 presents those internal and external factors significant to such reliability.

The external and internal factors cited vary in relative significance; however, any one of them can reduce reliability to zero under a given set of circumstances. This is particularly true for flaw characteristics. Several of the factors are interactive. For example, varying the equipment may substantially improve or reduce the reliability as influenced by flaw characteristics.

With data concerning the probability of detection and of sizing of IGSCC, it is possible to establish factors of improvement in failure probability assuming corrective actions or replacement. These factors are inputs leading to overall reductions in the probability of failure.

The significance of initial flaw-size distribution in piping welds probably has been exaggerated, particularly when the flaws usually occur between 1/4t and 3/4t (the central half of section thickness). The driving forces for

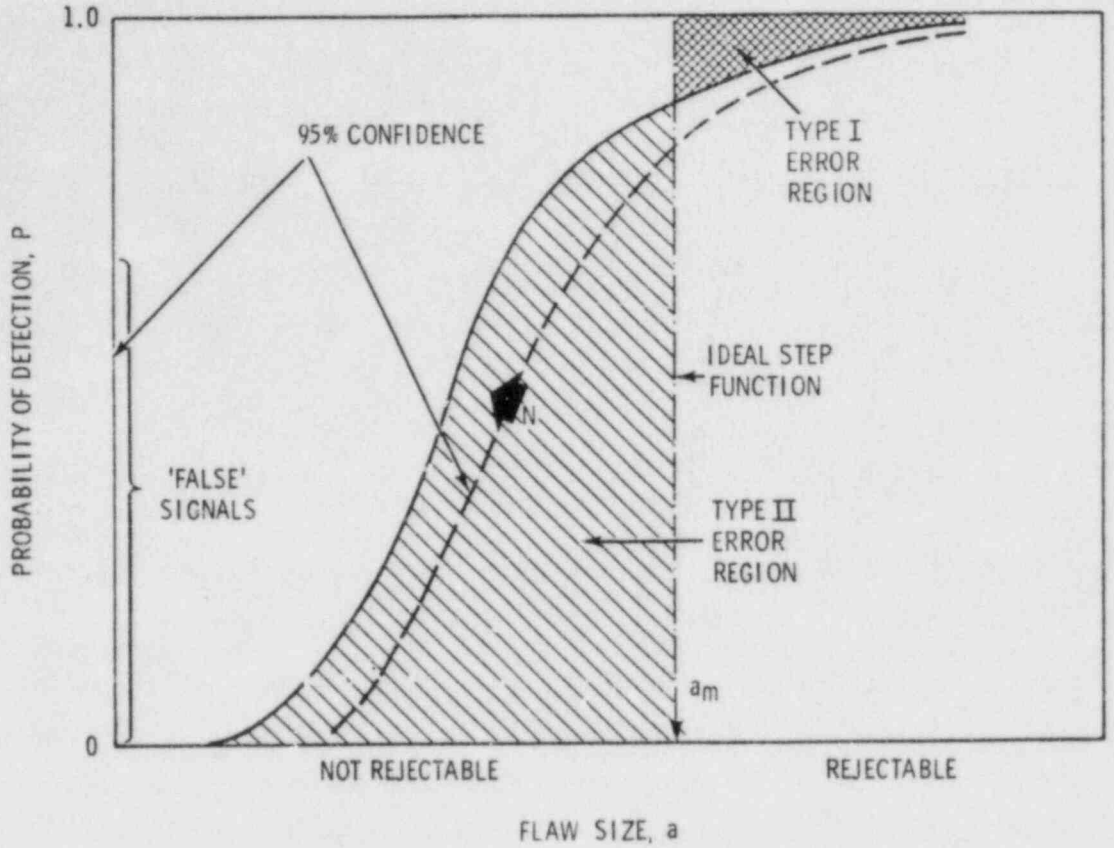

FIGURE 4. Hypothetical Curve of Probability of Rejection Versus Imperfection Size. "False" signals and 95% confidence levels shown.

crack propagation are relatively low for small deeply embedded flaws, not exposed to the coolant. The situation is different for surface or near-surface flaws, particularly those distributed around the inner surface. In such flaws it may not be necessary to assume a prior flaw-size distribution. Under certain circumstances, the driving forces are sufficiently high to result in both crack initiation and crack growth with the cumulative time for both stages less than predicted for the growth of embedded flaws when the two processes are compared against the same final flaw size.

Three mechanisms leading to crack initiation and growth are cited. The following are three mechanisms, all of which have resulted in piping failures in operating BWRs and/or PWRs:

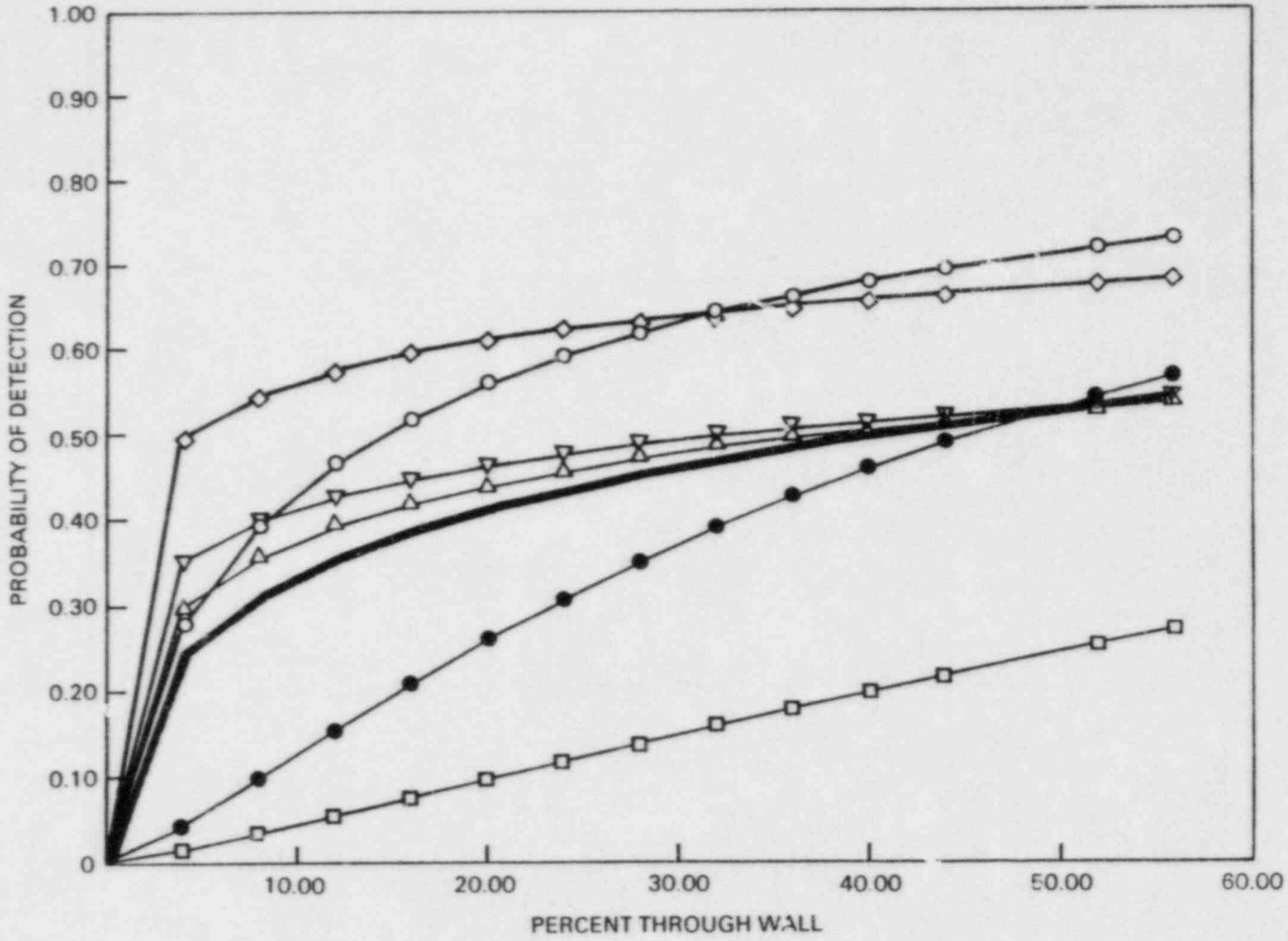

FIGURE 5. Probability of Detection (POD) of IGSCC in 10 inch Stainless Steel Pipe Limited to Near Access Side of Weld Using ASME XI Code Ultrasonic Procedure

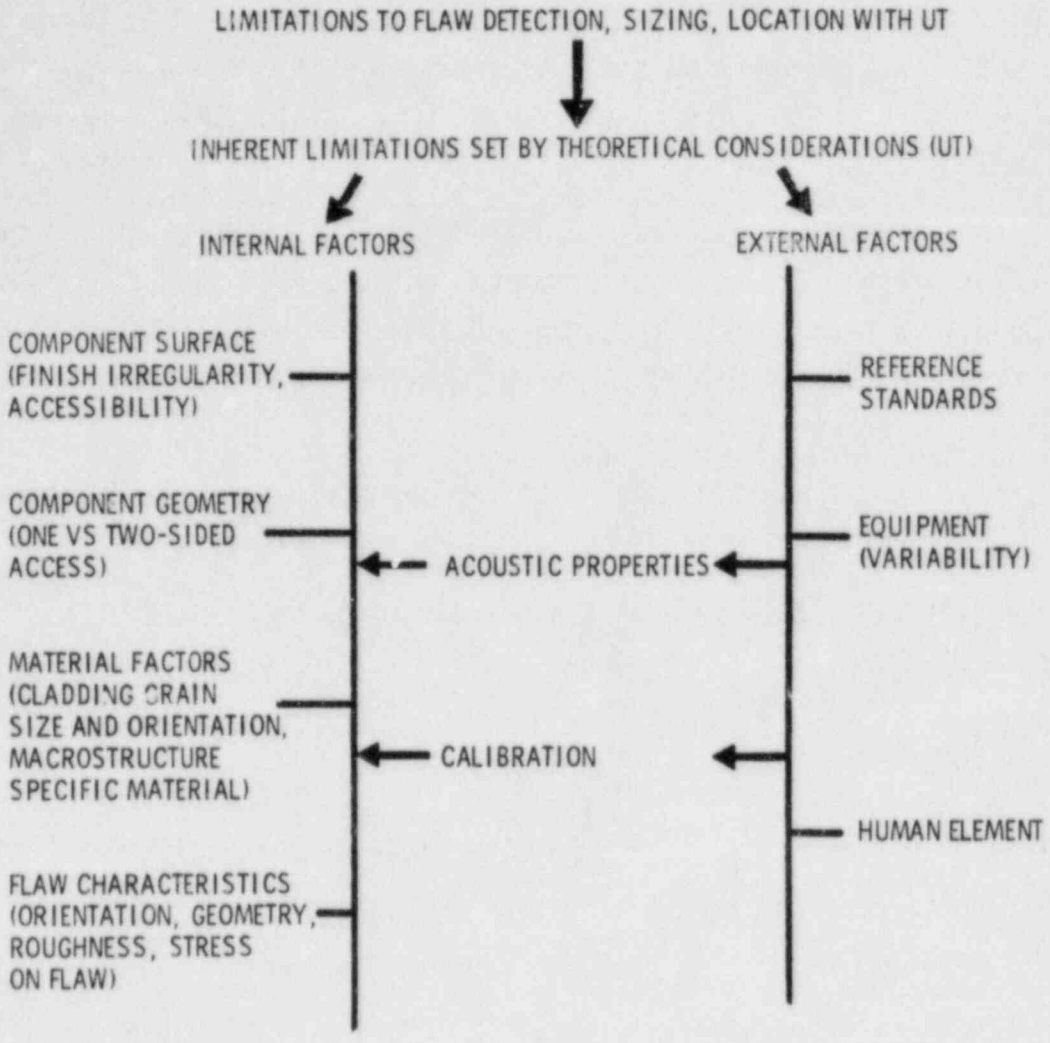

FIGURE 6. Limitations to Flaw Detection, Sizing, Location

1. stress corrosion cracking, primarily intergranular stress corrosion cracking (IGSCC). (This is predominantly but not exclusively a BWR problem occurring in austenitic weldments.)
2. fatigue cracking, initiated by thermal-transients and continued by combined thermal and pressure loads.
3. corrosion-fatigue, where cracks initiate and grow from the inner surface due to a combination of the environment and the cyclic loads.

Relatively little has been reported relevant to incorporating IGSCC into a probability failure model. A recent study attempts to attack the problem;

however, that study begins with the a priori assumption of a flaw population so that the system is propagation controlled. In my opinion this introduces undue restrictions into the model.

The crack growth by IGSCC can be divided into two stages--the initiation or nucleation period, and the crack propagation period. While a microscopic model probably is better for describing crack nucleation, a deliberate decision was made to use a macroscopic model to be consistent with the crack-growth models used in most probability studies.

Extensive studies in BWRs and simulated BWR environments indicate that the following parameters are controlling for austenitic weldments:

1. the environment (E) with the level of oxygen in the coolant (at temperature) usually controlling
2. the degree of sensitization (S) in the wrought structure (heat affected zone)
3. the level of stress (σ) at the inner surface (σ_{res}, $\sigma_{D.W.}$, σ_{p}, etc.)
4. the condition of the internal surface (γ) in the region of stress and sensitization

The time-to-crack nucleation or initiation will be a complex function of these and possibly other parameters. For example, the process has been arbitrarily limited to austenitic alloys even though it is known that certain austenitic alloys are relatively insensitive to IGSCC while some of the high nickel alloys are relatively susceptible. Times of initiation may range from days to months, or even years, based both on experimental evidence and observations with operating reactors. We can define this initiation as

$$T_{init}(hrs) = f\ (E, S, \sigma, \gamma)$$

where stress may be steady state plus transient, and may consist of residual, dead weight, pressure, bending, etc. With regard to surface condition γ, one could argue that a rough surface corresponds to a population of small cracks, thus shortcutting the initiation stage.

The preceding relationship could be defined in terms of a probability relationship; however, no analytic procedure is known for quantifying the relationship, primarily because of the very limited data on initiation of IGSCC and equally limited information concerning the interaction of E, S, σ, γ. One can infer that the presence of some level of oxygen in the water at 250 to 300°C and a nominal level of sensitization both represent plateaus where further increases of E or S are relatively unimportant. With this assumption, σ and γ effectively control T_{init}. The relative contributions of σ and γ are difficult to assess.

The post-initiation step is followed by crack growth with the same parameters controlling, or

$$\text{Crack growth rate} = a = f'(E, S, \sigma, \gamma),$$

where a is a rate function which probably is not uniform and may be discontinuous. For example, the effective E will be that at the crack tip; however, that E will be influenced by the macroscopic E, the level of oxygen in the coolant. Typically BWR's start with fairly high levels of oxygen at startup with these levels reduced markedly before reaching operating (P, T).

It has been postulated that the crack growth occurs primarily during startup and shutdown. The suggested mechanism particulary relevant to startup is that oxygen is present, and loads during heatup may be substantial, particularly bending loads that could open the cracks permitting access of coolant. If such is true, one might have 90 to 95% of the crack growth in <1% of the time during a 300-day operating cycle.

The preceding is conjecture; it would be beneficial to have definitive data confirming or denying the postulate.

The effect of loads is two-fold. They, in combination with other factors such as the environment, are responsible for the propagation of cracks to a greater or lesser degree. Ultimately, a load is necessary to result in failure either due to leakage, or catastrophically.

In the crack initiation and propagation stage, the probability of crack growth is sensitive not only to f (E, S, σ, γ) for IGSCC, but also to piping diameter and to piping subsystems. It is necessary to examine a spectrum of piping size to meaningfully predict crack growth as Figure 7 illustrates the contribution of primary and secondary stresses to relative probability of failure, and Figure 8 examines geometric and size factors influencing probability of failure. Both support the significance of pipe size and of subsystem to failure.

Another factor influencing probability of failure is the rate of loading as well as the maximum load. For example, faulted loads predicted by one mechanism may be quasi-static while faulted loads predicted by another may be dynamic. A specific example might be certain seismic loads where the ramp approximates quasi-static conditions and a region of high-stress intensity such as a discontinuity might yield but not fail. A dynamic faulted load might be the opening of safety relief valves or water slugging.

There has been substantial work in probabilistic modeling of structures; however, the information available on the modeling of loads in piping systems is quite limited.

Examples of factors to be considered are:

1. The designer or reviewer should only have to combine peak responses from individual loads.
2. The response combinations in requirements in 1 should be specified in simple deterministic terms.
3. For mechanical components the ASME code stress limit and service level (A, B, C, D) philosophy should be used.

Particular attention needs to be given to the specification of loads, load combinations and load factors. The following questions were asked:

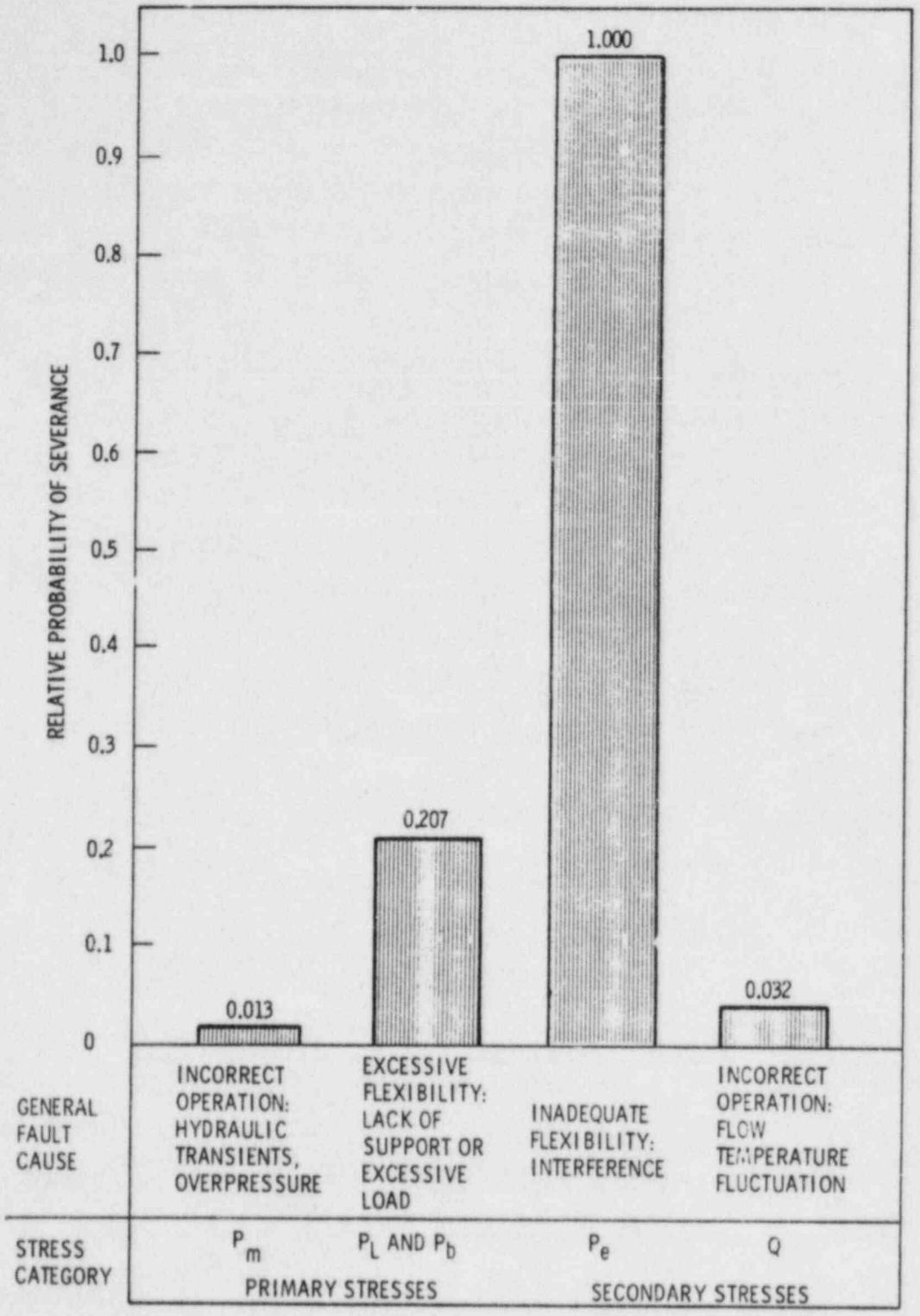

FIGURE 7. Relative Probability of Severance by General Fault Cause (Stress Category)

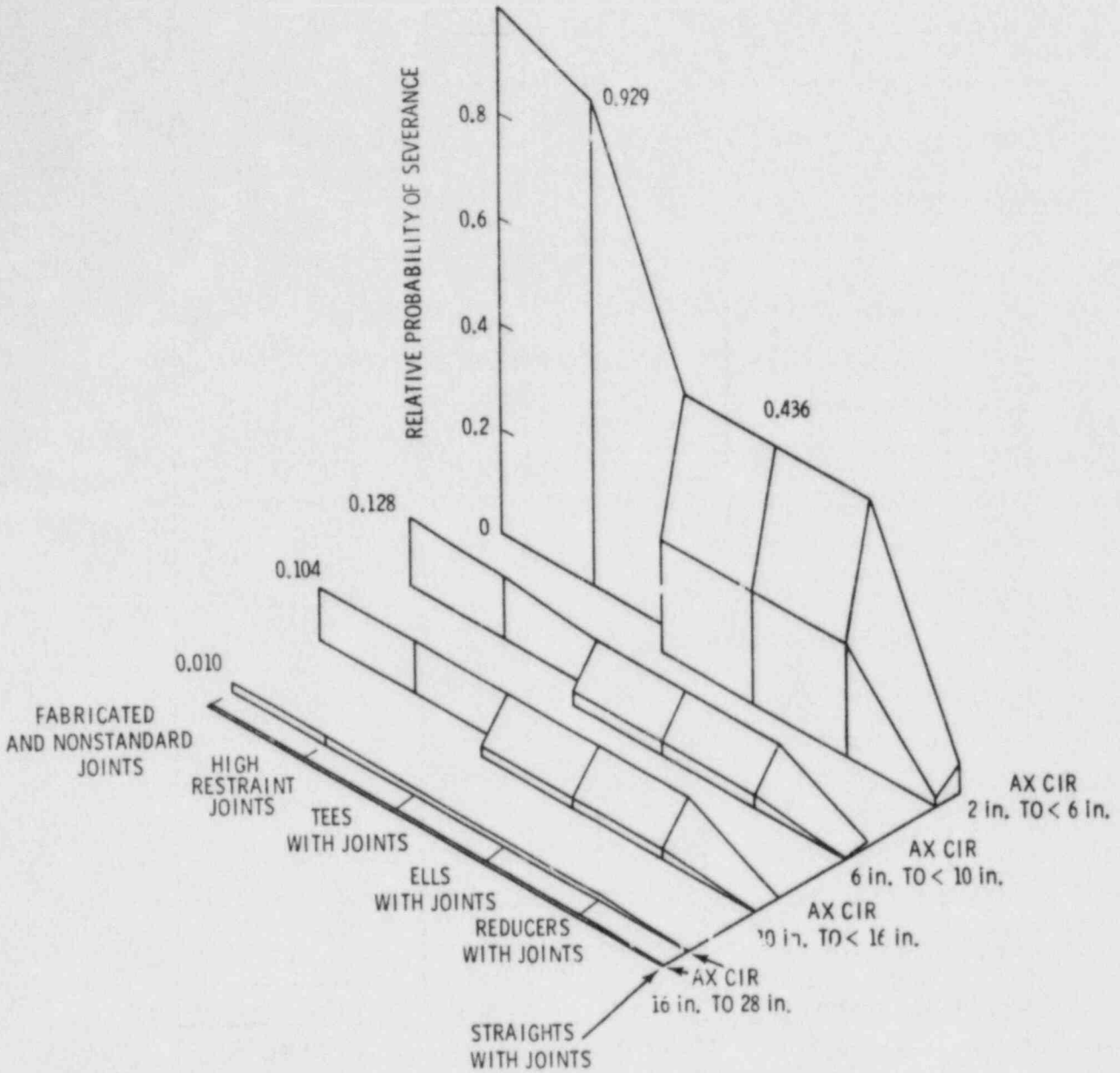

FIGURE 8. Relative Probability of Severance by Component-With-Joint Pipe Size and Crack Orientation

- Loads
  - What are the sources of and uncertainties in the loads?
  - What are the probabilities of occurrence of different load intensities?

- What are the durations of the loads?
- Is the loading function or displacement controlled?
- What are the dynamic characteristics of the loads?

- Load Combinations
  - What is the probability of two or more concurrent loads?
  - What consequences can be allowed due to concurrent loads? (This determines the equipment service level or structural load acceptance criteria.)
  - What is the probability that the specified consequences (deformation, cracking, etc.) would be exceeded with the specified load combination?
  - What is the effect on safety for the specified load combinations (sensitivity of overall risk)?
  - What response combination criteria is to be associated with the selected load combination criteria?

- Load Factors
  - What is the nature and mode of the load; i.e., is it static, vibratory, pulsatory, load controlled, displacement controlled?
  - What are the dynamic characteristics of the structure?
  - What factors for combined loads will result in the code intended "safety margins?"
  - What effect do the factors have on the probability of failure (sensitivity of risk)?

All these issues must be addressed to develop a rational and uniform basis for combining loads.

Crack growth can be approximated by a fatigue model based on linear elastic fracture mechanics. Loads for both crack growth and possible failure can

be postulated. The third parameter influencing failure will be the relevant mechanical properties. A simplistic approach would be to relate flaw size to K_{IC}; e.g.,

$$a_{max} = \text{const} \left(\frac{K_{IC}}{\sigma} \right)^2$$

Since the failures of interest are after pressurization and heatup, the meaningful fracture toughness properties for typical reactor piping more realistically are characteristic of elastic-plastic rather than linear-elastic properties. If we had the relevant fracture toughness data (which rarely is the case), we could evaluate

$$a_{max} = C_o \frac{J_{IC}}{\sigma^2}$$

where this a_{max} should be substantially larger than the a_{max} as a function of K_{IC}.

The third possibility is a general yield model where the remaining ligament is assumed to fail by ductile tearing.

There are some experimental data relating flaw size to stress (usually flow stress) and to toughness properties; however, the data are rather limited with regard to developing a probability model inter-relating flaw size, stress and toughness properties. In terms of probability density functions, the following is my best estimate as to where the state of knowledge is:

- There is no meaningful model available for the PDF of flaw-size distribution in typical nuclear piping.
- Fracture toughness values are sensitive both to prior history and to operational history; for example, there is evidence of long-term reduction in upper shelf toughness in cast austenitics that could be significant. Degradation mechanisms exist for ferritic materials so time of operation could be significiant.

- Real versus postulated transients differ widely, as do postulated faulted conditions versus the probability of their occurrence. The uncertainty in loads at any given time will be very high.

The failure load-temperature relationship is illustrated schematically in Figure 9.

At this stage, we should have all the necessary inputs to permit the prediction of failure. Given a system or subsystem made up of components having a defined range of mechanical properties and operating under a defined set of temperatures and loads, the problem is to determine the probability of failure if one or more of the components contain a spectrum of flaws. Basically the solution is one of load versus strength with the flaws decreasing the effective strength. We can define loads in terms of stress, stress intensity factor or J, and strength in terms of strength, K_{IC}, or J_{IC}.

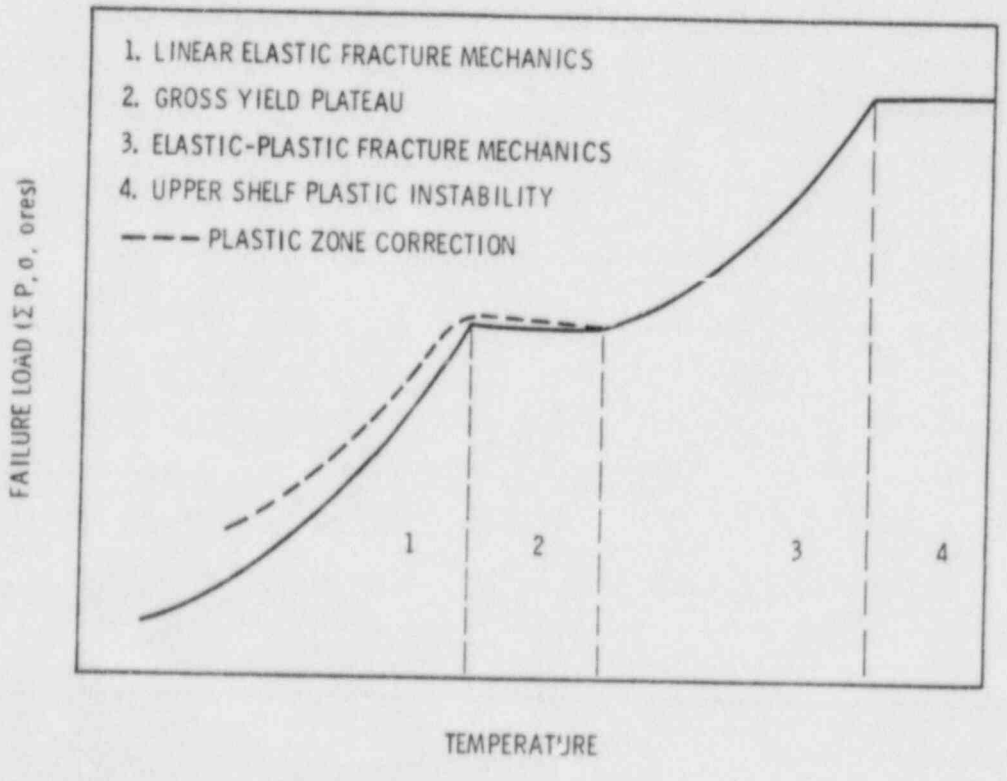

FIGURE 9. Failure Load-Temperature Relationship Schematically Displayed Illustrating Various Toughness Regions for a Typical Primary Pipe

1. The crack distribution in terms of shape, size, location and orientation. This distribution may be modified by NDE and subsequent repair as well as by growth through mechanisms such as fatigue.

2. The statistical distribution of strength. This might be the upper-shelf fracture toughness such as $f(K_{IC})d\,K_{IC}$, which will give the probability that the toughness in any component in any location lies between K_{IC} and $K_{IC} + dK_{IC}$ which can be normalized to this equation:

$$\int_0^\infty f(K_{IC})d\,K_{IC} = 1$$

recognizing that the values of K will vary with time, so we are considering a three-dimensional diagram.

3. The design transients for normal, upset and test conditions (which can be extended to emergency and faulted). These transients are assumed to occur regularly in time at the design frequency. They will influence both flaw growth and ultimate failure probability.

INPUTS INTO PROBABILISTIC MODEL

An analysis of the types and numbers of various piping failures permits a benchmarking of our probabilistic model. The following represent somewhat random examples of input information. If one uses non-nuclear failure data, there is a problem in assessing its pertinence. An example is given in Table 2 on an original analysis followed by a reanalysis, illustrating this subjectively.

An example of early failure data comparing pipe size failure locations and failure causes is given in Table 3 for 1 year.

Water hammers represent one of the most severe loading conditions. Some data relevant to water hammer in BWRs is given as an example of potential inputs into our probabilistic model. Tables 4 to 7 contain such information. For example, Table 4 cites instances of cracking, permitting a gross correlation with water hammers cited in Tables 6, 7, and 8.

TABLE 2. Distribution of Failures for Piping During Service

Failures	Catastrophic (C)	Noncatastrophic (NC)		Relevance to Nuclear	
		Leak	Nonleak	C	NC
Prior to service[a]	1[a]	2[a]			
During service					
Fatigue	2	17	24	1(1)[b]	14(12)
Corrosion	0	0	14	0 0	11 (4)
Preexisting defect	1	1	7	1(0)	8 (3)
Not determined	0	14	11	0 0	15 (4)
Miscellaneous	0	1	1	0 0	0 (0)
Maloperation	0	1	0	0 0	0 (0)
Creep	0	1	0	0 0	0 (0)
Total	3	35	57	2(1)	48(23)

(a) Preservice failures; not considered of safety significance.
(b) Independent evaluation of nuclear relevance by Bush.

TABLE 3. Distribution of Reported Licensing Event Reports in Piping Systems (1976)

Pipe Size		Location			Causes	
<1 (<25 mm)	28	Weld		22	Fatigue	25
		Socket	10			
≥1 <2 (≥25 <51 mm)	4	Socket-elbow	7		Fitup	1
		Other	5			
>2 ≤4 (>51 ≤102 mm)	3	HAZ		6	Stress corrosion cracking	10
>4 ≤6 (>102 ≤152 mm)	1	Tee		2	Erosion	4
>6 ≤8 (>152 ≤203 mm)	1	Reducer		2	Wrong thickness	1
>8 ≤10 (>203 ≤254 mm)	1	Cold bend		1	Slag inclusion	1
>10 <20 (>254 <508 mm)	2	U-bend		1	Weld leak	1
≥20 (≥508 mm)	0	Threaded connection		1	Leaking thread	1
Unknown	11	Elbow		3	Internal corrosion	2
		Other		9	Other	5
Total	51			47		51

Materials	
Stainless steel	23
Carbon steel	3
Unknown	25

At this time we somewhat superficially have the various pieces necessary to conduct a probabilistic analyses. Table 8 is a distillation of results yielding failure probabilities based on statistics as well as the most probable mechanisms. Unfortunately, the message is that failure rates are reasonably comparable, with the notable exception of failures due to IGSCC. These may not be catastrophic in nature but they represent a much higher failure rate and one cannot reject the possibility of pipe severance under certain conditions.

The factors contributing to failure cited in Table 8 appear to be generally applicable; however, they do not cover the environmental aspects leading to rapid IGSCC.

TABLE 4. Instances of Cracking and Leaking in LWR Safety-Related Piping Systems Relevant to BWRs (through 1980)

Piping System	Nominal Pipe Size(s), in. (mm)		IGSCC	Other
Feedwater	12-18	(305-457)	0	14
Recirculation	10-14	(305-356)	18	1
Recirculation bypass	4-6	(102-152)	42	4
Steam	26	(660)	6	0
Reactor water cleanup	3-10	(76-254)	45	4
Reactor heat removal	12-14	(305-356)	1	4
Core spray	6-12	(152-305)	7	5
Control rod drive	3-4	(76-102)	3	7
Isolation condenser	10-14	(254-356)	5	0
High pressure coolant injection	10-14	(254-356)	0	4
Low pressure coolant injection	16	(406)	1	0

Inspection techniques will be of value for many of the failure mechanisms but are of little benefit for such events as water hammer or major design and construction errors leading to abrupt failures. Inspection is beneficial in cases of IGSCC but is not completely reliable; therefore, additional work is required to improve inspection of stainless steel by ultrasonics.

TABLE 5. BWR Water Hammers by Year and System

System	1969	1970	1971	1972	1973	1974	1975	1976	1977	1978	1979	1980	Total
Steam		3	3	4		1		3	2		1		17
Isolation condenser (IC)			1								1		2
Feedwater (FW)					3	6	3	2					14
RCIC			1	1		1	2	4	1				10
RHR	1		1	2		2	11	2	9	3	1	2	34
HPCI		2	2	2	1	4	7	5	3	2		4	32
Core spray			4			2	1	1	2	1		1	12
LPCI													0
Containment spray (CS)													0
Service water (SW)				1	4	5	2	3	1			1	17
ECCS											2		2
Miscellaneous	—	—	—	—	—	—	—	—	1	—	—	1	2
Total	1	5	12	10	8	21	26	20	19	6	5	9	142

NOTE: Probably not a complete listing of incidents.

System	1969	1970	1971	1972	1973	1974	1975	1976	1977	1978	1979	1980
BWR reactor-years per year	3.5	6.5	7.5	9	12.5	14.5	19	22.5	23.5	23.5	23.5	24
Frequency	0.28	0.76	1.46	1.11	0.64	1.44	1.26	0.88	0.80	0.25	0.17	0.25

NOTE: Domestic only.

TABLE 6. Assessment of Severity of Failure by System for BWRs

Class of Damage	Safety Related System							
	Main Steam	Feed Water	RCIC	Core Spray	RHR	HPCI	Service/ Cooling Water	Total
Supports								
Damaged	1	2	-	-	11	1	-	18
Failed	1	2	-	1	1	3	3	11
Snubbers								
Damaged	1	-	-	2	8	5	1	17
Failed	1	-	-	1	9	4	1	17
Pipe								
Overstressed	2	2	-	1	3	4	3	20
Cracked	1	1	-	-	1	-	2	5
Leaked	3	1	-	-	2	-	-	6
Failed	2	1	-	-	-	1	4	8
Small Lines (inst., etc.)								
Failed	2	3	-	-	-	-	-	5
Valve								
Operator damage/failure	2	-	-	1	1	1	-	5
Yoke failure	1	1	-	1	-	-	2	5
Body cracked	-	1	-	-	1	-	-	2
Body failure	-	1	-	-	-	-	1	2
Stem broken/ejected	-	3	-	-	-	-	1	4
Disc failure	-	-	5	-	-	4	1	10
Electrical failure	-	-	-	4	1	1	-	6
Pump								
Impeller damage	-	1	1	-	-	-	-	2
Body failure	-	-	-	-	-	-	1	1
Miscelleneous								
Broken sparger	1	-	-	-	-	-	-	1
Damage to condenser/HX	1	-	-	-	1	-	-	2
Electrical failure	-	1	-	-	-	-	-	1
Rupture disc failed	-	-	-	-	-	3	-	3
Instrument damage	-	-	-	-	-	2	-	2
Gasket failure	-	-	-	-	-	1	1	2
Cracked concrete	-	2	-	-	1	2	1	6
Total	19	22	6	13	44	35	22	161

TABLE 7. Hierarchy of Damage to Systems Relevant to BWRs

System	Reactor	Date	Mechanism	Damage
Feedwater	Dresden	6/23/74	Control malfunction; valve partial closure	Failed air and electric lines; piping supports; cracked concrete; bent pipe
	Nine Mile Point	12/74	Valve instability; vibration	Broken valve stem; damaged pump impeller
	Pilgrim-1	1/6/76	Valve instability; vibration	Failed valve yoke, ejected steam; cracked valve body; damaged hangers
	Quad Cities-2	8/31/75	Valve instability	Cracked/leaking pipe
	Vermont Yankee	7/20/73	Valve closure; vibration	Broken/damaged hangers/ snubbers; dented pipe
HPCI	Browns Ferry-1	4/14/74	Valve opening entrainment	Failed valve switch; broken/damaged snubbers/ supports; cracked concrete; bent pipe
	Brunswick-1	3/28/81	Valve opening entrainment?	Damaged 29 snubbers/ supports
	Brunswick-2	9/76	Valve opening entrainment	Damaged snubbers/supports; overstressed pipe
	Dresden-2	5/29/70	Valve opening entrainment	Broken/damaged snubbers/ supports; dented pipe
RHR	Millstone-1	2/12/76	Bubble Collapse or Entrainment	Damaged condenser; overstressed pipe
	Peach Bottom-2	11/75	Valve instability; vibration	Cracked/leaking pipe; cracked valve
Service Water	Fitzpatrick	4/10/74	Flow into voided line	Failed restraints; damaged snubbers; cracked concrete; overstressed pipe

TABLE 7. (contd)

System	Reactor	Date	Mechanism	Damage
Cooling Water	Peach Bottom-2 and 3	5/76	Column separation	Cracked pipe; failed bolts on pump casing
Feedwater	Beaver Valley-1	11/5/76 12/17/76 1/5/77	Valve chatter	Failed instrument lines, fittings; snubbers; damaged valves
Steam Line	H. B. Robinson	4/70	Dynamic load on valves; design error	Blew off valve
	Turkey Point-3	1972	Dynamic load on valves; design error	Blew off valve and header
RHR	H. B. Robinson	5/8/79	Undefined water hammer	Failed 6 of 10 supports in 130 ft (39.7 m) line

TABLE 8. Comparison of Failure Rates, Failure Probabilities, and Failure Mechanisms for Major Failures (large pipe only)

Rupture probabilities per year (basically per component-year)	10^{-4} to 10^{-6}
Rupture probability per year per foot (meter) of pipe	1.8×10^{-5} (5.9×10^{-5})
Failure (not rupture) rate per FS component-year (on low side)	~100 to 300 $\times 10^{-4}$
Failure (not rupture) rate per weld-year (IGSCC)	6 to 60 $\times 10^{-4}$
Failure rates per year per foot (meter) of pipe	1.3×10^{-5} (4.3×10^{-5})

Factors and Their Relevance

Inadequate flexibility	Yes (IGSCC)
High incidence for nonstandard joints	Not certain
Rate highest in small pipe sizes	Yes
Axial cracking due to excessive flexibility	Not certain
Secondary stresses, control	Yes
Stainless steel analogous to carbon steel	Worse (IGSCC)
Fatigue significant in nuclear	Yes (smaller sizes)

CONCLUSIONS

A distillation of results illustrating what might be derived from a probabilistic risk assessment (PRA) study follows

- The failure probabilities for larger sizes of nuclear piping are considered to be in the range of 10^{-4} to 10^{-6} per reactor-year (exclusive of IGSCC).
- Smaller pipe sizes, of lesser safety significance, have much higher failure rates.
- In BWRs, IGSCC can cause failure rates much higher than 10^{-4} (e.g., 10^{-2}) in piping 4 to 10 in. (102 to 250 mm) in size.
- Suggested failure mechanisms apply in most instances, exclusive of IGSCC.
- Catastrophic failures would appear more likely from operator error or design and construction errors (water hammer, improper handling of dynamic loads, and undetected fabrication defects) rather than conventional flaw initiation and growth by fatigue.

POSTLUDE

The preceding illustrates a probabilistic approach that might help in the licensing and regulatory process. Obviously the interest here is the relevance to leak-before-break. The somewhat out-of-date information does not appear to support leak-before-break on probabilistic grounds. Possibly a more refined model with up-to-date inputs might be more optimistic. There are straws in the wind indicating that the PRA approach is becoming more acceptable and is an element in relaxation of criteria on a case-by-case or a generic basis. These apply to PWR piping more than BWR piping, at least for the present. Some examples are:

- ACRS letter concerning fracture mechanics approach to postulated pipe failure
- Executive Director of Operations response to ACRS letter
- relaxation of generic issue A-2 on asymmetric blowdown loads and some Westinghouse plants and one Combustion Engineering plant
- positive response to LLNL piping study regarding failure probabilities in Westinghouse plants
- PVRC/NRC programs on piping criteria emphasizing seismic and dynamic loads and leading to relaxation of criteria
- German action regarding PWR leak-before-break
- planned NRC program at LLNL on probability of failure of Babcock and Wilcox and Combustion Engineering primary piping; also on BWR piping with IGSCC failure mechanism. This latter program may or may not resolve the concern of IGSCC in BWR recirculation lines.

NRC FORM 335 (2-84) NRCM 1102, 3201, 3202

U.S. NUCLEAR REGULATORY COMMISSION

BIBLIOGRAPHIC DATA SHEET

SEE INSTRUCTIONS ON THE REVERSE

1. REPORT NUMBER (Assigned by TIDC, add Vol. No., if any)

NUREG/CP-0051
CSNI Report No. 82

2. TITLE AND SUBTITLE

Proceedings of the CSNI Specialist Meeting on Leak-Before-Break in Nuclear Reactor Piping

3. LEAVE BLANK

4. DATE REPORT COMPLETED

MONTH	YEAR
July	1984

5. AUTHOR(S)

6. DATE REPORT ISSUED

MONTH	YEAR
August	1984

7. PERFORMING ORGANIZATION NAME AND MAILING ADDRESS (Include Zip Code)

Division of Engineering Technology
Office of Nuclear Regulatory Research
U.S. Nuclear Regulatory Commission
Washington, D.C. 20555

8. PROJECT/TASK/WORK UNIT NUMBER

9. FIN OR GRANT NUMBER

10. SPONSORING ORGANIZATION NAME AND MAILING ADDRESS (Include Zip Code)

Same as 7 above.

11a. TYPE OF REPORT

Collection of Conference Papers

b. PERIOD COVERED (Inclusive dates)

September 1-2, 1983

12. SUPPLEMENTARY NOTES

13. ABSTRACT (200 words or less)

On September 1 and 2, 1983, the CSNI Subcommittee on Primary System Integrity held a special meeting in Monterey, California, on the subject of Leak-Before-Break in Nuclear Reactor Piping Systems. The purpose of the meeting was to provide an international forum for the exchange of ideas, positions, and research results; to identify areas requiring additional research and development; and to determine the general attitude toward acceptance of the leak-before-break concept. This report documents the presentations made at the meeting in the areas of (1) application of piping fracture mechanics to leak-before-break; (2) leak rate and leak detection; (3) leak-before-break studies, methods, and results; and (4) current and proposed positions on leak-before-break.

14. DOCUMENT ANALYSIS – a. KEYWORDS/DESCRIPTORS

piping
fracture mechanics
leak-before-break

b. IDENTIFIERS/OPEN-ENDED TERMS

15. AVAILABILITY STATEMENT

Unlimited

16. SECURITY CLASSIFICATION

(This page) Unclassified

(This report) Unclassified

17. NUMBER OF PAGES

18. PRICE

UNITED STATES
NUCLEAR REGULATORY COMMISSION
WASHINGTON, D.C. 20555

OFFICIAL BUSINESS
PENALTY FOR PRIVATE USE, $300

FOURTH CLASS MAIL
POSTAGE & FEES PAID
USNRC
WASH. D. C.
PERMIT No. G-67

120555078877 1 1AN
US NRC
ADM-DIV OF TIDC
POLICY & PUB MGT BR-PDR NUREG
W-501
WASHINGTON DC 20555